



Deliverable 6.3: Training materials of the 1st GAS/HITEC Joint training course

Work Package **GAS**

The project leading to this application has received funding from the European Union's Horizon 2020 research and innovation programme under grant agreement No 847593.



<http://www.ejp-urad.eu/>

Document information

Project Acronym	EURAD
Project Title	European Joint Programme on Radioactive Waste Management
Project Type	European Joint Programme (EJP)
EC grant agreement No.	847593
Project starting / end date	1st June 2019 – 30 May 2024
Work Package No.	6
Work Package Title	Mechanistic understanding of gas transport in clay materials
Work Package Acronym	GAS
Deliverable No.	D6.3
Deliverable Title	Training materials of the 1st GAS/HITEC joint training course
Lead Beneficiary	32 – ONDRAF/NIRAS[ULiège]
Contractual Delivery Date	November 2019
Actual Delivery Date	February 2020
Type	Report
Dissemination level	PU
Authors	Frédéric COLLIN (ULIEGE), Robert CHARLIER (ULIEGE).

To be cited as:

Collin F., Charlier R. (2020): Training materials of the 1st GAS/HITEC joint training course. Final version as of 24.02.2020 of deliverable D6.3 of the HORIZON 2020 project EURAD. EC Grant agreement no: 847593.

Disclaimer

All information in this document is provided "as is" and no guarantee or warranty is given that the information is fit for any particular purpose. The user, therefore, uses the information at its sole risk and liability. For the avoidance of all doubts, the European Commission has no liability in respect of this document, which is merely representing the authors' view.

Acknowledgement

This document is a deliverable of the European Joint Programme on Radioactive Waste Management (EURAD). EURAD has received funding from the European Union's Horizon 2020 research and innovation programme under grant agreement No 847593.

Status of deliverable		
	By	Date
Delivered (Lead Beneficiary)	ONDRAF/NIRAS[ULiège]	21 February 2020
Verified (WP Leader)	ONDRAF/NIRAS	24 February 2020
Reviewed (Reviewers)	ONDRAF/NIRAS	24 February 2020
Approved (PMO)	Rob WISLEY on behalf of the PMO	9 April 2020
Submitted to EC (Coordinator)	Coordinator	15 May 2020

Executive Summary

The first GAS/HITEC Joint training course is a Doctoral School entitled “Multiphysical Couplings in Geomechanics, a focus on thermal effect and gas transfer impact on the behaviour of geomaterials”.

The school was organized from 22 to 24 January 2020 at Liège University, within the framework of EURAD, the European Joint programme on Radioactive waste management (grant agreement No 847593). Objectives of EURAD include the development of new knowledge and consolidation of existing knowledge for the safe start of operation of the first geological disposal facilities for spent fuel, HLW, and other long-lived radioactive waste, and supporting optimization linked with the step wise implementation of disposal.

This doctoral school is related to two of the WPs of the EURAD Joint Programme, namely the GAS and HITEC WPs. In both WPs, geomechanics plays a significant role in the understanding of the relevant thermo-hydro-mechanical couplings taking place around the disposal area. The objectives of the school is therefore to present the students with the state-of-the-art on basic concepts related to the thermo-hydro-mechanical (multi-physical) couplings, the physical impacts of thermal loading and a mechanistic understanding of gas migration.

This school allows the attendees to improve their understanding of heat transfers, water and gas migration, stress and strain evolution in a repository. The school addresses both experimental and numerical investigations, at small (lab) and large (in situ) scale. These investigations involve geomaterials such as the host rock, either clayey or crystalline rock, but also bentonite which is typically used in engineered barriers for its sealing capacity. The provided lecture notes are based on key references in these fields (e.g. state-of-the-art, scientific reports and papers). A selection of this material was made available from the beginning of the school.

The school was organized firstly for people coming from institutions active in EURAD, including staff members from agencies as well as young researchers, involved or interested in the geomechanics field. The school also offered a limited number of places to people from institutions not directly participating in EURAD. The attendance was limited to 80 people. The number of registered participants was about 70. The number of attendees (including the teachers) was 70 on Wednesday, 65 on Thursday and 55 on Friday. During the feedback organized at the end of the school, almost half of the participants were PhD students, about one-quarter were researchers in a research entity and 7 were members of agency (both WMOs and regulators).

At the end of the school, the final presentations of the lecturers and the related reference papers have been sent to all the participants. For the members of the EURAD project, these files are permanently available on Projectplace:

<https://service.projectplace.com/#project/1763332387/documents/813993294>

The feedback showed that the participants appreciated the content of the school and especially the fact that the lecturers provided a critical view of the current state-of-the-art on the multiphysical couplings in geomechanics. The program of the school was well foreseen, even if modelling lectures were delivered before the presentation of the in situ experiment, and in hindsight they may have been of more value afterwards. In terms of improvement for the next school, some participants indicated that they would have further benefited if they could have observed the equipment used in the laboratory and in situ. Combining the next doctoral school with a visit to a laboratory in a research centre and an Underground Research Laboratory should be considered.

Table of content

Executive Summary	4
Table of content	5
List of figures	7
List of Tables	8
1. Introduction	9
1.1 Topics and target audience	9
1.2 Learning outcomes	10
2. School program	10
2.1 Wednesday 22/1	10
2.2 Thursday 23/1	11
2.3 Friday 24/1	11
3. List of participants	12
4. Synopsis of the lectures	15
4.1 Scientific challenges addressed by HITEC WP (M. Olin)	15
4.2 Scientific challenges addressed by GAS WP (S. Levasseur)	15
4.3 Fundamentals on geomechanics and multi-physical couplings (A. Gens)	15
4.4 Experimental evidences of high temperature effect, at lab scale (P. Delage)	16
4.5 Constitutive modelling for thermomechanical behavior of geomaterials (D. Masin)	17
4.6 FE numerical modelling of THM couplings in geomaterials (F. Collin)	17
4.7 Microstructure of bentonites: characterisation and evolution under mechanical and environmental loads (A-C. Dieudonné)	18
4.8 Experimental evidences of advective gas transfers at lab scale (E. Romero & L. Gonzalez Blanco)	18
4.9 Modelling for gas transfers in geomaterials (S. Olivella)	19
4.10 In situ thermo-hydro-mechanical experiment on poorly indurated clays (A. Dizier)	20
4.11 In situ testing of gas transfer in clayey rocks (J. Talandier & R. de la Vaissière)	20
4.12 In situ testing of gas transfer in crystalline rocks (P. Sellin)	21
4.13 In situ testing of EBS in crystalline rock (E. Bohner)	21
5. Feedback of the participants at the end of the school	22
References	23
Appendix A. Scientific challenges addressed by HITEC WP (M. Olin)	26
Appendix B. Scientific challenges addressed by GAS WP (S. Levasseur)	31
Appendix C. Fundamentals on geomechanics and multi-physical couplings (A. Gens)	37
Appendix D. Fundamentals on geomechanics and multi-physical couplings - Application (A. Gens)	91
Appendix E. Fundamentals on geomechanics and multi-physical couplings - Paper (A. Gens)	132

Appendix F.	Experimental evidences of high temperature effect, at lab scale (P. Delage)	155
Appendix G.	Constitutive modelling for thermomechanical behavior of geomaterials (D. Masin)	190
Appendix H.	FE numerical modelling of THM couplings in geomaterials (F. Collin).....	282
Appendix I.	Numerical modelling of coupled transient phenomena (F. Collin).....	335
Appendix J.	THM behaviour of engineered and natural clay barriers (F. Collin)	359
Appendix K.	Microstructure of bentonites: characterisation and evolution under mechanical and environmental loads (A-C. Dieudonné)	372
Appendix L.	Microstructure of bentonites : characterisation and evolution under mechanical and environmental loads (A-C. Dieudonné) - Paper	392
Appendix M.	Experimental evidences of advective gas transfers at lab scale (E. Romero & L. Gonzalez Blanco)	414
Appendix N.	Modelling for gas transfers in geomaterials (S. Olivella).....	464
Appendix O.	In situ thermo-hydro-mechanical experiment on poorly indurated clays (A. Dizier)	512
Appendix P.	In situ testing of gas transfer in clayey rocks (J. Talandier & R. de la Vaissière)	545
Appendix Q.	In situ testing of gas transfer in crystalline rocks (P. Sellin)	581
Appendix R.	In situ testing of EBS in crystalline rock (E. Bohner).....	603

List of figures

No table of figures entries found.

List of Tables

Table 1 – List of participants..... 14

1. Introduction

The first GAS/HITEC Joint training course is a Doctoral School entitled “Multiphysical Couplings in Geomechanics, a focus on thermal effect and gas transfer impact on the behaviour of geomaterials”.

This school is organized within the framework of EURAD, the European Joint programme on Radioactive waste management (grant agreement No 847593). Objectives of EURAD include the development of new knowledge and consolidation of existing knowledge for the safe start of operation of the first geological disposal facilities for spent fuel, HLW, and other long-lived radioactive waste, and supporting optimization linked with the step wise implementation of disposal.

This doctoral school is related to two of the Work Packages of the EURAD Joint Programme, namely the GAS and HITEC WPs.

The main objectives of the GAS WP are to improve the mechanistic understanding of gas transport processes in natural and engineered clay materials, their couplings with the mechanical behaviour and their impact on the properties of these materials; to evaluate the gas transport regimes that can be active at the scale of a geological disposal system and their potential impact on barrier integrity and repository performance.

The main objectives of the HITEC WP are to evaluate whether an increase in temperature limits is feasible/safe considering existing and newly produced knowledge about the behaviour of clay materials at elevated temperatures; to deploy knowledge on mechanics of clay in order to better evaluate and model possible damage during the temperature transient and assess the consequence for the host rock; to deploy knowledge on mostly mechanical, but also chemical and transport changes of bentonite (buffer).

In both GAS and HITEC WPs, geomechanics plays a significant role in the understanding of the relevant thermo-hydro-mechanical couplings taking place around the disposal area. The objectives of the school is therefore to present the students with the state-of-the-art on basic concepts related to the thermo-hydro-mechanical (multi-physical) couplings, the physical impacts of thermal loading and the mechanistic understanding of gas migration.

1.1 Topics and target audience

The HITEC WP deals with thermal impact and the GAS WP concerns gas transfer, both in the context of geological disposal of radioactive waste. This school allows the attendees to improve their understanding of heat transfers, water and gas migration and stress and strain evolution in a repository. The school addresses both experimental and numerical investigations, at small (lab) and large (in situ) scale. These investigations involve geomaterials such as the host rock, either clayey or crystalline rock, but also bentonite which is typically used in engineered barriers for its sealing capacity.

The provided lecture notes are based on key references in these fields (state-of-the-art scientific papers etc.). A selection of this material was made available from the beginning of the school.

The school was organized firstly for people coming from institutions active in EURAD, including staff members from agencies as well as young researchers, involved or interested in the geomechanics field. The school also offered a limited number of places to people from institutions not directly participating to EURAD. The attendance was limited to 80 people. The number of registered participants was about 70.

1.2 Learning outcomes

At the end of the school, participants had a broad view of the state-of-the-art and of the challenges related to the GAS and HITEC WP research programme. They met a number of key researchers on THM and gas transport in the context of geological disposal, fostering information exchange and cooperation within the geomechanics community.

In particular, the attendees were able to:

- Understand the basics of the thermo-hydro-mechanical (multi-physical) couplings in geomaterials;
- Perceive the experimental evidences and figure out the physical processes at the laboratory scale and from in situ tests;
- Capture the fundamentals on constitutive modelling of the relevant phenomena;
- Identify the challenges in numerical modelling of these physical processes;
- Appreciate/better appreciate the application of THM (multi-physical) couplings in geomaterials within geological disposal facility post-closure safety cases (e.g. claims arguments and Evidence).

2. School program

The school was organized from 22 to 24 January 2020 at the “Institut de Mathématique” of the Liège University. The 3-day school was divided into lectures that include a Q/A part organised at the end of each lecture. Here is the list of the lecturers:

Markus Olin, VTT Technical Research Centre of Finland (Finland)

Séverine Levasseur, ONDRAF/NIRAS (Belgium)

Antonio Gens, Universitat Politècnica de Catalunya (Spain)

Pierre Delage, École des Ponts ParisTech (France)

David Masin, Charles University in Prague (Czech)

Frédéric Collin, Université de Liège (Belgium)

Anne-Catherine Dieudonné, TU Delft (Nederland)

Enrique Romero, CIMNE, Universitat Politècnica de Catalunya (Spain)

Laura Gonzalez-Blanco, CIMNE, Universitat Politècnica de Catalunya (Spain)

Sebastia Olivella, Universitat Politècnica de Catalunya (Spain)

Arnaud Dizier, ESV Euridice (Belgium)

Edgar Bohner, VTT Technical Research Centre of Finland (Finland)

Patrik Sellin, Svensk Kärnbränslehantering AB (Sweden)

Rémi de la Vaissière, ANDRA (France)

Xavier Sillen, ONDRAF/NIRAS (Belgium)

Robert Charlier, Université de Liège (Belgium)

2.1 Wednesday 22/1

9h00 Welcome, registration and coffee

9h30 Introduction

General aspects (school organizers)

Challenges addressed by HITEC WP (Markus Olin)

Challenges addressed by GAS WP (S everine Levasseur)

10h00 Coffee break

10h30 **Fundamentals on geomechanics and multi-physical couplings** (A Gens)

12h30 Lunch

13h30 **Experimental evidences of high temperature effect, at lab scale** (P Delage)

15h00 Coffee break

15h30 **Constitutive modelling for thermomechanical behavior of geomaterials** (D Masin)

17h00 Closure

19h00 Diner at Labo 4

2.2 Thursday 23/1

9h00 **THM coupling and FE numerical modelling** (F Collin)

10h30 Coffee break

11h **Microstructure of bentonites: characterisation and evolution under mechanical and environmental loads** (AC Dieudonn e)

12h Lunch

13h **Experimental evidences of advective gas transfers at lab scale** (E. Romero & L. Gonzalez Blanco)

14h30 Coffee break

15h **Modelling for gas transfers in geomaterials** (S Olivella)

16h30 Closure

2.3 Friday 24/1

9h00 **In situ testing at high temperature 1. Poorly indurated clays** (A Dizier)

10h00 **In situ testing of gas transfer 2. Clayey rocks** (R de la Vaissiere)

11h00 Coffee break

11h30 **In situ testing of gas transfer 1. Crystalline rocks** (P Sellin)

12h30 Lunch

13h30 **In situ testing at high temperature 2. Crystalline rocks** (E Bohner)

14h30 Challenges and open questions – Numerical and experimental investigations on gas and high temperature (X Sillen & R Charlier)

15h00 Feedback of the participants at the end of the school

15h30 School closure

3. List of participants

Last name	First name	Company
Ait Mouheb	Naila	Forschungszentrum Juelich GmbH
Amri	Abdellah	IRSN
Awarkeh	May	ESV EURIDICE / ENPC
Bertrand	François	Université de Liège
Bésuelle	Pierre	Laboratoire 3SR
Bohner	Edgar	VTT, teacher
Bolleni	Sai Charan	SCK•CEN
Burlaka	Victoria	BGE
Canak	Mirta	Fund for financing the decommissioning of the Krsko NPP
Cardoso	Rafaela	Instituto Superior Técnico
Cernochova	Katerina	Czech Technical University
Chaaya	Roy	BRGM
Charlier	Robert	Université de Liège
Chaves Deptulski	Rafael	IRSN
Coene	Emilie	Amphos 21 Consulting S.L.
Collin	Frédéric	Université de Liège, teacher
Conde Perez	Patrick	BEL V
Corman	Gilles	Université de Liège
Dal Pont	Stefano	Université Grenoble-Alpes
Daniels	Katherine	BGS
Darde	Benjamin	ENPC
De La Vaissière	Rémi	ANDRA, teacher
de Lesquen	Christophe	ANDRA
Delage	Pierre	ENPC, teacher
Dieudonné	Anne-Catherine	TU Delft, teacher
Dinc Gogus	Ozge	NA

Dizier	Arnaud	ESV EURIDICE, teacher
Ferrucci	Barbara	ENEA
Gbewade	Coffi Agbégmigan Fabrice	GeoRessources
Gens	Antonio	UPC, teacher
Gonzalez-Blanco	Laura	CIMNE, teacher
Govers	Kevin	FANC
Gramegna	Liliana	Université de Liège
Gupta	Abhishek	Aalto university
Haimour	Sultan	Poole Hospital NHS Trust
Hasanpour	Rohola	NA
Hassanzadegan	Alireza	BGE
Hoyer	Eva-Maria	BGE
Jacops	Elke	SCK•CEN
Justinavicius	Darius	Lithuanian Energy Institute
Kašpar	Vlastislav	ÚJV Řež, a.s.
Khadivipanah	Peiman	CIMNE
Lamouchi	Takoua	Ecole Centrale de Lille
Lemy	Frank	BEL V
Levasseur	Séverine	ONDRAF/NIRAS
Maes	Norbert	SCK•CEN
Masin	David	Charles University, teacher
Mélot	Geoffroy	EDF
Mendoza	Angela	ÚJV Řež a. s.
Mesa Alcantara	Arisleidy	UPC
Molnár	László	PURAM
Montoya	Vanessa	Helmholtz Centre for Environmental Research (UFZ) GmbH
Müller	Christian	BGE
Olin	Markus	VTT

Olivella	Sebastia	UPC, teacher
Pitz	Michael	BGR
Pont Ribas	Arnau	Amphos 21
Poonoosamy	Jenna	Forschungszentrum Juelich GmbH
Poskas	Gintautas	LEI
Pouya	Julie	IRSN
Rackstraw	David	Radioactive Waste Managment
Romero Morales	Enrique	CIMNE
Šachlová	Šárka	Nuclear Research Institute
Sau Valenzuela	Nuria	CIMNE
Scaringi	Gianvito	Přírodovědecká fakulta Univerzity Karlovy
Seetharam	Suresh	SCK•CEN
Sellin	Patrick	SKB, teacher
Sillen	Xavier	ONDRAF/NIRAS
Simo	Eric	BGE mbH
Song	Hangbiao	Université de Liège
Sun	Zhao	Charles University
Tourchi	Saeed	CIMNE
Verstricht	Jan	ESV EURIDICE
Wessely	Ola	Swedish Nuclear Fuel and Waste Management Co
Yang	Jinwen	ENPC
Yara	Barakat	IRSN
Yuan	Tao	Helmholtz-Zentrum Dresden-Rossendorf
Zalamea	Nicolas	CNRS Laboratoire 3SR- UMR 5521
Zengin	Enes	NA
Zhang	Aoxi	Delft University of Technology
Ziefle	Gesa	BGR

Table 1 – List of participants

4. Synopsis of the lectures

The school has been divided into lectures given by the academic members and people from national agencies, e.g. WMOs, TSOs/Regulators, national RE representatives. For each lecture, a synopsis is provided as well as a list of references that are available on Projectplace: <https://service.projectplace.com/#project/1763332387/documents/813993294>. Some of the lecturers have proposed in addition a specific paper for the school (see Appendix). A copy of the presentations given by the lecturers is provided in Appendices A to R.

4.1 Scientific challenges addressed by HITEC WP (M. Olin)

Both clay host rock and bentonite buffers, and their behaviour at high temperature are included. For clay host rock temperatures under 120°C and for bentonite buffer temperatures under 150°C (even 200°C) are considered. Mechanical behaviour is the focus area, while chemical conditions will be taken care of whenever possible by some simplified couplings. Clay host rock: Formation of overpressure, stresses caused by the overpressure, fractures caused by these stresses and propagation under thermal load, propagation of excavation induced fractures under thermal load. Clay buffer: Influence of high temperature on material: changes, characterisation, safe temperature level determination; influence of high temperature on processes inside buffer – processes at high temperature, Development of coupled THM models at high temperature. Chemical conditions will be only taken care of whenever possible by some simplified couplings.

Presentation: Appendix A

4.2 Scientific challenges addressed by GAS WP (S. Levasseur)

The WP GAS of EURAD is dedicated to the mechanistic understanding of gas transport in clay materials. The main objectives of this WP are (1) to improve the mechanistic understanding of gas transport processes in natural and engineered clay materials, their couplings with the mechanical behaviour and their impact on the properties of these materials; (2) to evaluate the gas transport regimes that can be active at the scale of a geological disposal system and their potential impact on barrier integrity and repository performance. Within this WP, knowledge gained from new and past lab and in situ experiments will be put in context for configurations that are commonly found in current repository designs with the aim to address the key questions from the end-users: How could gas migrate within the repository and which water soluble and volatile radionuclide transport could be associated with it? How and to what extent could the hydro-mechanical perturbations induced by gas effect barrier integrity and long-term repository performance?

Presentation: Appendix B

4.3 Fundamentals on geomechanics and multi-physical couplings (A. Gens)

The basic thermo-hydro-mechanical (THM) phenomena occurring in saturated and unsaturated porous media are reviewed, with special attention to their interactions. A theoretical formulation that encompasses the most relevant THM phenomena and their couplings is developed. The description of the formulation is divided into balance equations, constitutive equations and equilibrium restrictions. Governing equations include solid mass balance, water mass balance, air mass balance, energy balance and momentum balance (equilibrium). Constitutive equations are proposed for the various THM phenomena that are deemed most relevant. The specific form of each constitutive equation generally includes information on the nature of the interactions between different phenomena.

Equilibrium restrictions provide conditions for processes that are considered fast with respect to the characteristic times of the overall THM problem, notably phase changes. Examples of application to field cases related to radioactive waste disposal are described.

Presentation: Fundamentals – Appendix C

Application – Appendix D

Specific Paper:

Fundamentals on geomechanics and multiphysical couplings – Appendix E

Reference:

1. *Soil–environment interactions in geotechnical engineering (47th Rankine Lecture)*

4.4 Experimental evidences of high temperature effect, at lab scale (P. Delage)

Since the pioneering work of Mitchell and Campanella (1968), further attention has been given with the seminal experimental and theoretical contributions of Hueckel and co-workers in the 90's, who evidenced the change in volume, under constant stress, of clays specimens submitted to temperature elevation. They showed for first time the thermo-elastic response of over-consolidated clays and the thermo-elasto-plastic one of normally consolidated clays, also extended to the thermal response of compacted bentonites and claystones, with, in the last case, the evidence of a thermal hardening phenomenon based on the maximum temperature supported by the claystone during its geological history. Temperature elevation also appeared to have little effects on elastic properties, and to reduce a little bit the shear resistance of clays and claystones. Another important aspect is linked to the THM coupling that governs, in clay and claystones, both thermal consolidation and thermal pressurisation, that results from the large difference in thermal expansion coefficient between water and minerals. All these features are important for better understanding and modelling the effects of temperature in the near-field in radioactive waste disposal.

Presentation: Appendix F

References:

2. *Thermal volume changes and creep in the Callovo-Oxfordian claystone (2017)*
3. *The thermo-mechanical behaviour of the Callovo-Oxfordian claystone (2015)*
4. *On the thermal impact on the excavation damaged zone around deep radioactive waste disposal (2013)*
5. *On the THM behaviour of a sheared Boom clay sample : Application to the behaviour and sealing properties of the EDZ (2012)*
6. *A laboratory investigation of thermally induced pore pressures in the Callovo-Oxfordian claystone (2012)*
7. *A laboratory investigation on thermal properties of the Opalinus claystone (2011)*
8. *Temperature effects on the volume change behaviour of Boom clay (2002)*
9. *On the thermal consolidation of Boom clay (2000)*

4.5 Constitutive modelling for thermomechanical behavior of geomaterials (D. Masin)

This lecture covers basic principles of constitutive modelling of geomaterials subject to elevated temperatures. In particular, the following concepts are covered: (1) Heating-induced compaction and heating-induced expansion, depending on the relative density of soil specimen; (2) Incorporation of volumetric response of mineral grain particles and water into constitutive models; (3) temperature-dependency of matric suction and the effect of temperature on soil water retention behaviour; (4) temperature-dependency of bentonite microstructural behaviour. Subsequently, incorporation of these concepts into two main modelling frameworks (elasto-plasticity and hypoplasticity) is explained, with examples of models from both groups. Finally modelling concepts of double (and triple) structure are introduced. Enhancement of existing models by elevated temperature are explained and model predictions are compared with experimental response of bentonite.

Presentation: Appendix G

References:

10. *A hypoplastic model for mechanical response of unsaturated soils (2008)*
11. *Predicting the dependency of a degree of saturation on void ratio and suction using effective stress principle for unsaturated soils (2010)*
12. *Modelling of thermal effects in hypoplasticity (2011)*
13. *Double structure hydromechanical coupling formalism and a model for unsaturated expansive clays (2013) Modelling of thermal effects in hypoplasticity (2011)*
14. *Coupled hydro-mechanical model for partially saturated soils predicting small strain stiffness (2014)*
15. *Modelling of shear stiffness of unsaturated fine grained soils at very small strains (2014)*
16. *Swelling phenomena and effective stress in compacted expansive clays (2016)*
17. *Coupled Thermohydromechanical Double-Structure Model for Expansive Soils (2017)*
18. *Modelling of unsaturated soils with hypoplasticity (Alert Presentation)*
19. *Constitutive modelling for expansive clay : a hypoplastic approach and numerical implementation (Beacon Presentation)*

4.6 FE numerical modelling of THM couplings in geomaterials (F. Collin)

A good understanding of the interacting thermo-hydro-mechanical phenomena (occurring in the engineered barrier and adjacent rock) is necessary in order to make robust safety case argument for the safe disposal of a range of radioactive wastes. To this end, a multiphysical formulation is described that allows the performance of coupled THM analyses capable of reproducing observed phenomena. An introduction to numerical modeling of coupled problems in geotechnical engineering is presented. It aims to provide an overview both of the techniques and the difficulties encountered when modeling this type of problems. The different couplings are introduced step by step, in the context of finite element techniques.

Presentation: Appendix H

Specific papers:

Numerical modelling of coupled transient phenomena – Appendix I

THM behaviour of engineered and natural clay barriers – Appendix J

References:

20. *3D zero-thickness coupled interface finite element : Formulation and application (2015)*
21. *Shear banding modelling in cross-anisotropic rocks (2015)*
22. *Influence of evaporation and seepage on the convergence of a ventilated cavity (2008)*
23. *Finite element analysis of non-isothermal multiphase geomaterials with application to strain localization simulation (2006)*
24. *Thermo-hydro-mechanical coupling in clay barriers (2002)*
25. *Computational Geomechanics With Special Reference to Earthquake Engineering (1999)*
26. *Multiphase flow in porous media : a numerical benchmark (1997)*
27. *A strategy for numerical analysis of the transition between saturated and unsaturated flow conditions (1997)*
28. *Numerical formulation for a simulator (CODE_BRIGTH) for the coupled analysis of saline media (1995)*
29. *A General Mass-Conservative Numerical Solution for the Unsaturated Flow Equation (1990)*

4.7 Microstructure of bentonites: characterisation and evolution under mechanical and environmental loads (A-C. Dieudonné)

Bentonites exhibit a complex behaviour under repository conditions, owing to the high sensitivity of the material to mechanical and environmental loads. This sensitivity of bentonites to external factors arises from both the mineralogical composition and the multi-scale structure of the material. This lecture aims to provide the fundamental concepts necessary to better understand the observed macroscopic behaviour of bentonites. The mineralogical composition, structure and physicochemical properties of bentonites are presented and used to explain hydration and swelling mechanisms. The effect of mechanical and environmental loads on the material structure is then described and analysed. Modelling challenges and prospects are finally addressed.

Presentation: Appendix K

Specific paper:

Microstructure of bentonites: characterisation and evolution under mechanical and environmental Loads – Appendix L

4.8 Experimental evidences of advective gas transfers at lab scale (E. Romero & L. Gonzalez Blanco)

Understanding the processes governing the advective movement of repository gas has long been the subject of debate and conjecture within the radioactive waste community, in order to define process, approach, and treatment of gas in safety assessment. Two approaches are usually proposed to describe the advective movement of gas, (i) classical two-phase flow models, where one fluid displaces another, with the process described by the water retention curve, and (ii) dilatancy flow where gas is unable to move within the original porosity because of capillary restrictions, creating new 'dilatant' features, which open and close in response to the gas pressure. This module focuses on the importance of laboratory scale measurements and their role in defining process understanding, reviews the different methods available for the determination of advective gas flow properties and examines some of the data obtained during 25 years of laboratory measurements to assess which mechanism is dominant in repository clay-based materials. This information is combined with natural

analogue studies to provide an insight into the fundamental processes governing advective gas flow in low permeability clays.

Presentation: Appendix M

References:

30. *Modeling of Gas Migration Through Low-Permeability Clay Rock Using Information on Pressure and Deformation from Fast Air Injection Tests (2018)*
31. *Exploring fissure opening and their connectivity in a Cenozoic clay during gas injection (2017)*
32. *Air injection tests in two argillaceous rock formations : experimental results and modelling (2016)*
33. *Gas migration in a Cenozoic clay : Experimental results and numerical modelling (2016)*
34. *Characterization of gas flow through low-permeability claystone : laboratory experiments and two-phase flow analyses (2014)*
35. *Gas Network Development in Compact Bentonite : Key Controls on the Stability of Flow Pathways (2019)*
36. *An experimental study of the influence of stress history on fault slip during injection of supercritical CO₂ (2018)*
37. *Gas network development in a precompacted bentonite experiment : Evidence of generation and evolution (2017)*
38. *Gas transport properties through intact and fractured Callovo-Oxfordian mudstones (2017)*
39. *An experimental study of the potential for fault reactivation during changes in gas and porewater pressure (2016)*
40. *An experimental study of the flow of gas along synthetic faults of varying orientation to the stress field : Implications for performance assessment of radioactive waste disposal (2015)*
41. *The visualization of flow paths in experimental studies of clay-rich materials (2015)*
42. *Evidence of localised gas propagation pathways in a field-scale bentonite engineered barrier system; results from three gas injection tests in the large scale gas injection test (Lasgit) (2014)*
43. *Experimental observations of mechanical dilation at the onset of gas flow in Callovo-Oxfordian claystone (2014)*
44. *Gas flow in Callovo-Oxfordian claystone (COx) : results from laboratory and field-scale measurements (2012)*
45. *Gas migration experiments in bentonite : implications for numerical modelling (2012)*
46. *Evidence for gas-induced pathways in clay using a nanoparticle injection technique (2012)*

4.9 Modelling for gas transfers in geomaterials (S. Olivella)

Basic properties of gases such as density, viscosity, diffusivity, solubility are reviewed briefly. Migration of gases in geological materials involves several transport mechanisms, and mathematical representations are required for each one. Conservation equations and the corresponding boundary conditions are presented in the context of geological materials. The theoretical and numerical approach includes saturated-unsaturated flow; multi-component mixture of gases; non-isothermal multiphase flow in deformable media; and preferential path formation. The coupling with thermo-hydro-mechanical equations is described in detail. Examples of modelling of laboratory and in situ experiments are presented and the challenges encountered discussed.

Presentation: Appendix N

4.10 In situ thermo-hydro-mechanical experiment on poorly indurated clays (A. Dizier)

In the frame of RD&D on the geological disposal of radioactive waste in Belgium, the thermo-hydro-mechanical (THM) behaviour of Boom Clay has been studied over several decades through small-scale laboratory tests and in-situ experiments at different scales in the HADES underground research laboratory (URL) in Mol (Belgium). The intermediate-scale in situ heating tests ATLAS allowed to observe the impact of the heat on the Boom Clay beyond the zone affected by the drilling of the borehole hosting the heater. In November 2014, the in situ large scale PRACLAY Heater test, carried out in the PRACLAY gallery of the HADES URL, was started. Its purpose is to ensure, on a scale representative of a geological disposal facility, that the heat released by high-level radioactive waste does not affect the favourable properties of the clay. The large scale of this experiment allows for studying the thermo-hydro-mechanical behaviour of the clay in the near field, i.e. within the excavation damaged zone, and in the far-field of a heated gallery. An extensive monitoring network installed around the PRACLAY gallery allows to observe the evolution of temperature and pore water pressure in the Boom Clay. In this lecture, the main observations that have been made within ATLAS and since the start of the heating of the PRACLAY Heater test will be presented. These observations combined with a comparison with numerical modelling generally confirm the knowledge gained previously from past experiments at different scales (laboratory and in situ).

Presentation: Appendix O

References:

General documents can be found in <http://www.euridice.be/nl/scientific-publications>

Documents for the large scale PRACLAY Heater test:

47. *The start-up phase of the PRACLAY Heater test (EURIDICE report)*

48. *The PRACLAY Heater test after two years of the stationary phase (EURIDICE report)*

Documents for the ATLAS heating test:

49. *ATLAS III in situ heating test in boom clay: Field data, observation and interpretation (2011)*

50. *The second phase of ATLAS: the continuation of a running THM test in the HADES underground research facility at Mol (2002)*

51. *Overview of in-situ thermomechanical experiments in clay : concept, results and interpretation (1996)*

Explications from EURIDICE website for ATLAS : <http://www.euridice.be/nl/content/atlas-1992-2012>

4.11 In situ testing of gas transfer in clayey rocks (J. Talandier & R. de la Vaissière)

R&D programme has been developed for more than 15 years by Andra to improve the understanding and representation of the physical processes associated with gas migration in clay environments. Andra has actively participated in the European programmes FORGE (Fate of Gas Repository) and Gasnet (A Thematic Network on Gas Issues in Safety Assessment of Deep Repositories for Radioactive Waste), in experimental programmes developed in underground laboratories (Aspö, Mont-Terri, Hades). Andra has been conducting its own experiments first in a deep borehole in 2004 and then in the Meuse/Haute-Marne underground research laboratory since 2009.

This presentation summarizes the various gas injection tests carried out in situ. The behavior of the Callovo-Oxfordian claystone under gas stress was studied at different gas injection pressure levels as well as swelling clay-based sealing plugs (compacted mixture of MX80- sand and pure MX80 in pellet and powder form).

Presentation: Appendix P

References:

52. *Fate of repository gases (FORGE)*
53. *Design and analysis of a gas threshold pressure test in a low permeability clay formation*
54. *From two-phase flow to gas fracturing into Callovo-Oxfordian claystone*
55. *Gas injection test in the Callovo-Oxfordian claystone : data analysis and numerical modelling (2014)*
56. *Gas injection tests in the Meuse/Haute Marne underground research laboratory*
57. *Effect of gas flow rate on gas fracturing in Callovo-Oxfordian claystone*
58. *Interaction between Gas and Bentonite Seals : Small Scale In-situ Test in the Meuse/Haute Marne Underground Research Laboratory*
59. *Poster : Effect of gas flow rate on gas fracturing in Callovo-Oxfordian claystone*

4.12 In situ testing of gas transfer in crystalline rocks (P. Sellin)

There are still uncertainties around the gas migration process in bentonite and the findings from the laboratory have to be verified in a large scale experiment. The objectives of the Lasgit test is to undertake a large-scale gas injection test to provide data to improve process understanding and test/validate modelling approaches which might be used in performance assessment. This relates in particular to issues relating to up-scaling and its effect on gas movement and buffer performance. The test has been in operation since 2005 and several gas injection tests have been performed. The observation so far is that gas pathways are formed in the bentonite at a gas pressure similar to the total stress in the test.

Presentation: Appendix Q

References:

60. *Evidence of localised gas propagation pathways in a field-scale bentonite engineered barrier system; results from three gas injection tests in the Large scale gas injection test (Lasgit)*
61. *Large scale gas injection test (Lasgit) performed at the Äspö Hard Rock Laboratory (Summary report 2008)*

4.13 In situ testing of EBS in crystalline rock (E. Bohner)

The safety concept of Posiva, the Finnish expert organisation responsible for the final disposal of spent nuclear fuel, is based on the KBS-3 design of the geological repository and the characteristics of the Olkiluoto site, which have been studied since the 1980's and monitored for more than 20 years. Important elements of the KBS-3 concept are engineered barriers that comprise the EBS, such as canister, buffer, backfill and deposition tunnel plugs, and closure, with its different backfill and plug types. In the lecture, three different in situ tests of EBS will be presented. Next to the design of the tests, the used materials, the different components and their manufacturing, as well as various instrumentation and monitoring systems will be discussed. The presented demonstrations allow for

identifying the trigger values for evaluating EBS performance. Therefore, they are essential tools to observe and evaluate performance and safety of EBS.

Presentation: Appendix R

References:

- 62. *Designing, Commissioning and Monitoring of 40% Scale Bentonite Buffer Test*
- 63. *Instrumentation and Monitoring of Tunnel Plug in ONKALO*
- 64. *Nordic Full-Scale Demonstrations of Tunnel Plugging Technologies for Repository Conditions*
- 65. *Designed Buffer Components for Finnish KBS-3V Concept*
- 66. *Poster Instrumentation of Posiva's Full Scale Demonstration Plug*
- 67-70. *List of related literature*

5. Feedback of the participants at the end of the school

At the end of the school, feedback from the participants was collected by the organizers. The discussion was divided into several issues and is open for debate between all the participants. The number of attendees (including the teachers) was 70 on Wednesday, 65 on Thursday and 55 on Friday. For the feedback, 48 people are present because some of them had already to return home. Among them, almost half of the participants were PhD students, about a quarter were researchers at a University and 7 were members of agency, e.g. WMOs, TSOs/Regulators, national RE representatives.

The participants appreciated the content of the school and especially the fact that the lecturers provided a critical view of the current state-of-the art on the multiphysical couplings in Geomechanics. A further suggested improvement is that it could in the future also seek to provide a critique on what evidence is actually needed in order to construct robust safety case arguments. Putting the two together gives needs driven knowledge gaps.

The program of the school was well foreseen, even if modelling lectures were delivered before the presentation of the in situ experiment, and in hindsight they may have been of more value afterwards. In terms of improvement for the next school, some participants indicated that they would have further benefited if they could have observed the equipment used in the laboratory and in situ. It appears actually that most of the attendees never visited an underground research laboratory before the school. Combining the next doctoral school with a visit to a laboratory in a research centre and an Underground Research Laboratory should be considered.

Concerning the numerical aspects, practice sessions with a finite element code would allow a deeper understanding of the capability of the numerical codes. It however requires some additional period for the school and would extend its duration.

The attendees have no special remarks on the support materials and an updated version of all the presentations has been sent to each participant few days after the school.

The last issue discussed during the feedback session is related to the logistic during the school. The point highlighted by the participants is the need of coffee break during the day and also on the morning. These interruptions are indeed useful for informal exchanges between the participants and with the teachers.

References

1. Gens A. (2010). Soil–environment interactions in geotechnical engineering. *Géotechnique* 60, No. 1, pp. 3–74 (doi: 10.1680/geot.9.P.109).
2. Belmokhtar et al. (2017). Thermal volume changes and creep in the Callovo-Oxfordian claystone. *Rock Mech Rock Eng* 50, pp. 2297–2309.
3. Menaceur et al. (2015). The thermo-mechanical behaviour of the Callovo-Oxfordian claystone *International Journal of Rock Mechanics & Mining Sciences* 78, pp. 290–303.
4. Delage P. (2013). On the thermal impact on the excavation damaged zone around deep radioactive waste disposal. *Journal of Rock Mechanics and Geotechnical Engineering* 5, pp. 179–190.
5. Monfared et al. (2012). On the THM behaviour of a sheared Boom clay sample: Application to the behaviour and sealing properties of the EDZ. *Engineering Geology* 124, pp. 47–58.
6. Mohajerani et al. (2012). A laboratory investigation of thermally induced pore pressures in the Callovo-Oxfordian claystone. *International Journal of Rock Mechanics & Mining Sciences* 52, pp. 112–121.
7. Monfared et al. (2011). A laboratory investigation on thermal properties of the Opalinus claystone. *Rock Mech Rock Eng* 44, pp. 735–747 (DOI 10.1007/s00603-011-0171-4)
8. Sultan et al. (2002). Temperature effects on the volume change behaviour of Boom clay *Engineering Geology* 64, pp. 135–145.
9. Delage et al. (2000). On the thermal consolidation of Boom clay. *Can. Geotech. J.* 37, pp. 343–354.
10. Masin et al. (2008). A hypoplastic model for mechanical response of unsaturated soils. *Int. J. Numer. Anal. Meth. Geomech.* 32, pp. 1903–1926.
11. Masin D. (2010). Predicting the dependency of a degree of saturation on void ratio and suction using effective stress principle for unsaturated soils. *Int. J. Numer. Anal. Meth. Geomech.* 34, pp. 73–90.
12. Masin at al. (2011). Modelling of thermal effects in hypoplasticity. 13th International Conference of the IACMAG – Melbourne, Australia, 9–11 May 2011.
13. Masin D. (2013). Double structure hydromechanical coupling formalism and a model for unsaturated expansive clays. *Engineering Geology* 165, pp. 73–88.
14. Wong et al. (2014). Coupled hydro-mechanical model for partially saturated soils predicting small strain stiffness. *Computers and Geotechnics* 61, pp. 355–369.
15. Wong et al. (2014). Modelling of shear stiffness of unsaturated fine grained soils at very small strains. *Computers and Geotechnics* 56, pp. 28–39.
16. Masin et al. (2016). Swelling phenomena and effective stress in compacted expansive clays. *Can. Geotech. J.* 53, pp. 134–147 (dx.doi.org/10.1139/cgj-2014-0479).
17. Masin D. (2017). Coupled Thermo-hydromechanical Double-Structure Model for Expansive Soils. *J. Eng. Mech.* 143(9), 13 p.
18. Masin D. (2015). Modelling of unsaturated soils with hypoplasticity (Alert Presentation). ALERT Olek Zienkiewicz Course, Barcelona, May 28, 2015.
19. Masin D. (2018). Constitutive modelling for expansive clay: a hypoplastic approach and numerical implementation (Beacon Presentation), BEACON Training Course, Barcelona, 18. 1. 2018.
20. Cerfontaine et al. (2015). 3D zero-thickness coupled interface finite element : Formulation and application. *Computers and Geotechnics* 69, pp. 124–140.
21. Pardoën et al. (2015). Shear banding modelling in cross-anisotropic rocks. *International Journal of Solids and Structures* 72, pp. 63–87.
22. Gerard et al. (2008). Influence of evaporation and seepage on the convergence of a ventilated cavity. *Water resources research* 44, W00C02 (doi:10.1029/2007WR006500).
23. Sanavia et al. (2006). Finite element analysis of non-isothermal multiphase geomaterials with application to strain localization simulation. *Comput Mech* 37, pp. 331–348 (DOI 10.1007/s00466-005-0673-6).
24. Collin et al. (2002). Thermo-hydro-mechanical coupling in clay barriers. *Engineering Geology* 64, pp. 179–193.
25. Zienkiewicz et al. (1999). *Computational Geomechanics With Special Reference to Earthquake Engineering*. John Wiley & Sons, Chichester.
26. Jommi et al. (1997). Multiphase flow in porous media: a numerical benchmark, *Proceedings NAFEMS World Congress Stuttgart, 1997*.


27. Vaunat et al. (1997). A strategy for numerical analysis of the transition between saturated and unsaturated flow conditions. *Numerical Models in Geomechanics*, pp. 297-302.
28. Olivella et al. (1995). Numerical formulation for a simulator (CODE_BRIGHT) for the coupled analysis of saline media. *Engineering Computations* 13(7), pp. 87-112.
29. Celia et al. (1990). A General Mass-Conservative Numerical Solution for the Unsaturated Flow Equation. *WATER RESOURCES RESEARCH*, 26(7), pp. 1483-1496.
30. Senger et al. (2018). Modeling of Gas Migration Through Low-Permeability Clay Rock Using Information on Pressure and Deformation from Fast Air Injection Tests. *Transp Porous Med.* <https://doi.org/10.1007/s11242-017-0962-5>.
31. Gonzalez-Blanco et al. (2017). Exploring fissure opening and their connectivity in a Cenozoic clay during gas injection
32. Gonzalez-Blanco et al. (2016). Air injection tests in two argillaceous rock formations : experimental results and modelling. *ICEGT (2016)*
33. Gonzalez-Blanco et al. (2016). Gas migration in a Cenozoic clay : Experimental results and numerical modelling. *Geomechanics for Energy and the Environment* 6, pp. 81–100.
34. Senger et al. (2014). Characterization of gas flow through low-permeability claystone : laboratory experiments and two-phase flow analyses. *Geological Society, London, Special Publications*, 400, <http://dx.doi.org/10.1144/SP400.15>.
35. Harrington et al. (2019). Gas Network Development in Compact Bentonite : Key Controls on the Stability of Flow Pathways. *Geofluids Volume 2019, Article ID 3815095*, 19 p., <https://doi.org/10.1155/2019/3815095>.
36. Cuss et al. (2018). An experimental study of the influence of stress history on fault slip during injection of supercritical CO₂. *Journal of Structural Geology* 109, pp. 86–98.
37. Harrington et al. (2017). Gas network development in a precompacted bentonite experiment : Evidence of generation and evolution. *Applied Clay Science* 147, pp. 80–89.
38. Harrington et al. (2017). Gas transport properties through intact and fractured Callovo-Oxfordian mudstones. *Geological Society, London, Special Publications*, 454, pp. 131–154. <https://doi.org/10.1144/SP454.7>.
39. Cuss et al. (2016). An experimental study of the potential for fault reactivation during changes in gas and porewater pressure. *International Journal of Greenhouse Gas Control* 53, pp. 41–55.
40. Cuss et al. (2015). An experimental study of the flow of gas along synthetic faults of varying orientation to the stress field: Implications for performance assessment of radioactive waste disposal. *J. Geophys. Res. Solid Earth*, 120, pp. 3932–3945. DOI:10.1002/2014JB011333.
41. Wiseall et al. (2015). The visualization of flow paths in experimental studies of clay-rich materials. *Mineralogical Magazine* 79(6), pp. 1335–1342.
42. Cuss et al. (2014). Evidence of localised gas propagation pathways in a field-scale bentonite engineered barrier system; results from three gas injection tests in the large scale gas injection test (Lasgit). *Applied Clay Science* 102, pp. 81–92.
43. Cuss et al. (2014). Experimental observations of mechanical dilation at the onset of gas flow in Callovo-Oxfordian claystone. *Geological Society, London, Special Publications*, 400, pp. 507–519. First published online May 8, 2014, <http://dx.doi.org/10.1144/SP400.26>.
44. Harrington et al. (2012). Gas flow in Callovo-Oxfordian claystone (COx) : results from laboratory and field-scale measurements. *Mineralogical Magazine*, 76(8), pp. 3303–3318.
45. Graham et al. (2012). Gas migration experiments in bentonite : implications for numerical modelling. *Mineralogical Magazine*, 76(8), pp. 3279–3292.
46. Harrington et al. (2012). Evidence for gas-induced pathways in clay using a nanoparticle injection technique. *Mineralogical Magazine*, 76(8), pp. 3327–3336.
47. Dizier et al. (2016). The start-up phase of the PRACLAY Heater test (EURIDICE report), EURIDICE Report, ref. EUR_PH_16_025.
48. Dizier et al. (2017). The PRACLAY Heater test after two years of the stationary phase (EURIDICE report). EURIDICE Report, ref. EUR_PH_17_043.
49. Chen et al. (2011). ATLAS III in situ heating test in boom clay : Field data, observation and interpretation. *Computers and Geotechnics* 38, pp. 683–696.
50. De Bruyn et al. (2002). The second phase of ATLAS : the continuation of a running THM test in the HADES underground research facility at Mol. *Engineering Geology* 64, pp. 309–316.
51. Bernier et al. (1996). Overview of in-situ thermomechanical experiments in clay : concept, results and interpretation. *Engineering Geology* 41, pp. 51-64.
52. Selling P. Eds (2014). Fate of repository gases (FORGE). Experiments and modelling on the behaviour of EBS. FORGE Report D3.38.426pp.

53. Senger et al. (2006). Design and analysis of a gas threshold pressure test in a low permeability clay formation. TOUGH Symposium 2006, Lawrence Berkeley National Laboratory, Berkeley, California, May 15–17, 2006.
54. De la Vaissière et al. (2019). From two-phase flow to gas fracturing into Callovo-Oxfordian claystone. ARMA 19–1723, 53rd US Rock Mechanics/Geomechanics Symposium held in New York, NY, USA, 23–26 June 2019.
55. De la Vaissière et al. (2014). Gas injection test in the Callovo-Oxfordian claystone : data analysis and numerical modelling. Geological Society, London, Special Publications, 400, <http://dx.doi.org/10.1144/SP400.10>.
56. De la Vaissière et al. (2013). Gas injection tests in the Meuse/Haute Marne underground research laboratory. Proceedings FORGE Symposium, Luxembourg 5 to 7 February 2013.
57. De la Vaissière et al. (2020). Effect of gas flow rate on gas fracturing in Callovo-Oxfordian claystone. Rock Mechanics for Natural Resources and Infrastructure Development, Fontura, Rocca & Pavón Mendoza (Eds), © 2020 ISRM, ISBN 978-0-367-42284-4.
58. De la Vaissière et al. (2014). Interaction between Gas and Bentonite Seals : Small Scale In-situ Test in the Meuse/Haute Marne Underground Research Laboratory. International Conference on the Performance of Engineered Barriers, February 6-7, 2014 - Hannover, Germany.
59. De la Vaissière et al. (2019). Effect of gas flow rate on gas fracturing in Callovo-Oxfordian claystone. Poster, IRSM Congress, September 13 to 18, 2019, Brazil.
60. Cuss et al. (2014). Evidence of localised gas propagation pathways in a field-scale bentonite engineered barrier system; results from three gas injection tests in the Large scale gas injection test (Lasgit). Applied Clay Science, 102, pp. 81-92.
61. Cuss et al. (2008). Large scale gas injection test (Lasgit) performed at the Äspö Hard Rock Laboratory (Summary report 2008). SKB Technical report, TR-10-38, February 2010.
62. Kivikoski et al. (2014). Designing, Commissioning and Monitoring of 40% Scale Bentonite Buffer Test. In: Final Proceedings of the 40th Waste Management Conference (WM2014), March 2-6, 2014, Phoenix, Arizona, USA, 2014. (CD-ROM, Paper Nr. 14260)
63. Hakola et al. (2014). Instrumentation and Monitoring of Tunnel Plug in ONKALO. In: Final Proceedings of the 40th Waste Management Conference (WM2014), March 2-6, 2014, Phoenix, Arizona, USA, 2014, 14 p. (CD-ROM, Paper Nr. 14261)
64. Holt et al. (2014). Nordic Full-Scale Demonstrations of Tunnel Plugging Technologies for Repository Conditions. In: Final Proceedings of the 40th Waste Management Conference (WM2014), March 2-6, 2014, Phoenix, Arizona, USA, 2014. (CD-ROM, Paper Nr. 14282)
65. Juvankoski et al. (2014). Designed Buffer Components for Finnish KBS-3V Concept. In: Final Proceedings of the 40th Waste Management Conference (WM2014), March 2-6, 2014, Phoenix, Arizona, USA, 2014. (CD-ROM, Paper Nr. 14285)
66. Bohner et al. (2016). Instrumentation of Posiva's Full Scale Demonstration Plug. In: Proceedings of the DOPAS Seminar, 25-26 May 2016, Turku, Finland, 2016 (Poster)
67. Bohner, E., Kivikoski, H., Raunio, K., Hansen, J., Niskanen, M., Rantamäki, P., Luterkort, D., Johannesson, L.-E.: EBS monitoring plan - Spent fuel disposal concept at crystalline host rock. Modern2020 Deliverable D4.1. EC Horizon2020 Contract no. 622177. 2019, 82 p. http://www.modern2020.eu/fileadmin/Deliverables/Modern2020D4.1_EBS_monitoring_plan__v7_final.pdf
68. Modern2020 Deliverable 6.3: Final conference proceedings. Second International Conference on Monitoring in geological disposal of radioactive waste: Strategies, technologies, decision-making and public involvement. EC Horizon2020 Contract no. 622177. 2019, 483 p. http://www.modern2020.eu/fileadmin/user_upload/Modern2020-_D6.3_PU_Conference_proceedings_FINAL-web.pdf
69. DOPAS Work Package 3 - Deliverable 3.30: WP3 Final Summary Report. Summary of, and Lessons Learned from, Design and Construction of the DOPAS Experiments: http://www.posiva.fi/files/4496/DOPAS_D3_30_WP3_Final_Summary_Report_B_16112016_E C.pdf
70. Holt, E., Bohner, B., Sanden, T., Malm, R., Pacovsky, J., Svoboda, J.: Instrumentation and Monitoring Systems for Evaluation of Plug Responses in Geological Disposal Demonstration. In: Proceedings of the DOPAS Seminar, 25-26 May 2016, Turku, Finland, 2016, pp. 152-158 http://www.posiva.fi/files/4528/Dopas_Deliverable_D7_3_DOPAS_2016_proceedings_final_public_ver3.pdf

Appendix A. Scientific challenges addressed by HITEC WP (M. Olin)





**WP7 - INFLUENCE OF TEMPERATURE ON
CLAY-BASED MATERIAL BEHAVIOUR
(HITEC)**
Training course at Uliège
22 January 2020 • Markus Olin

 The project leading to this application has received funding from the European Union's Horizon 2020 research and innovation programme under grant agreement n° 847593.

Date Event 1


1



HITEC - MAIN OBJECTIVES

- **Briefly:** Improved THM description of clay based materials at elevated temperatures – no C yet

1. To evaluate whether an increase of temperature is feasible and safe by applying existing and novel knowledge about clay materials at elevated temperatures:
 - a) to improve understanding of the THM behaviour of clay rock and clay buffer under high temperature and provide suitable THM models,
 - b) to better assess effect of overpressures on the THM behaviour and properties of the clay host rock, and
 - c) to identify processes at high temperature and the impact of high temperature on the THM properties of the buffer material.



2

2

HITEC - MAIN OBJECTIVES 2

2. **Host clays formations**: to deploy knowledge to mechanics of clay to better evaluate/model possible damage evolution.
3. **Buffer bentonite**: to deploy knowledge to hydro-mechanical behaviour at high T.
4. **To document all the above to be utilised in Safety Cases studies**
 - I. Mechanical properties, swelling pressure, hydraulic conductivity, while the integrity of the clay may be evaluated as changes in mineralogy, chemical content or physical integrity of the compacted blocks.
 - II. The safety functions and the overall integrity of the bentonite and/or clay host rock will be evaluated after a high temperature exposure.
5. **To assure interaction between CSO and participants of the WP**



3

HITEC - EXPECTED IMPACTS

- **Regarding RWM implementation needs**
 - Important to assess the consequences of the high T
 - Most of safety cases limit maximum temperature to 100°C: Higher temperatures can have significant advantages: higher enrichment/burn-up fuels, interim storage requirements, (re)packaging of the waste, reducing footprint of the disposal
- **Regarding safety case concerns**
 - Knowledge about utilising higher temperatures, setting up limits of temperature and which kind of overall impacts higher temperatures causes to materials and systems.
 - Proving that higher than present temperatures are acceptable is very relevant even for current concepts:
- **Regarding increasing scientific and technical Knowledge**
 - There is now only limited knowledge about the clay mechanics at higher than 100°C - increase scientific and technical knowledge.



4

WP 7 – HITEC: TASKS & (EXTENDED) BOARD

- **Task 1 – S/T coordination, State-of-the-art and training material**
 - Task Leader: VTT – Markus Olin
 - SoA: CIEMAT – Maria Villar
 - Training: Uliège – Robert Charlier
- **Task 2 - Clay host rock <120°C**
 - Task Leader: Ulorraine – Dragan Grgic
 - T2.1: Ulorraine - Dragan Grgic
 - T2.2: BGS – Katherine Daniels
 - T2.3: Andra – Gilles Armand
- **Task 3 - Clay buffers >100°C**
 - Task Leader: CTU – Jiří Svoboda
 - T3.1: SKB - Daniel Svensson
 - T3.2: BGS - Katherine Daniels
 - T3.3: CIEMAT - Maria Victoria Villar
- **Task 4 - Impacts and deployment of results**
 - Task Leader: VTT – Markus Olin
 - T4.1: NAGRA – Olivier Leupin



eurad

5

WP 7 - HITEC WHAT?: TASK 2&3

- **T2 Clay host rock**
 - **Subtask 2.1** will use lab experiments to assess a possible extension of the excavation induced fracture network, investigating the role of the fracture network on the containment properties of the host rock.
 - **Subtask 2.2** will also use lab experiments on materials at elevated temperatures, and will focus on the thermal pressurisation and the risk of damage when the effective stress increases up to the overburden weight.
 - **Subtask 2.3** will focus on the development of THM models which are able to consider processes studied in subtasks 2.1 and 2.2.
- **T3 Buffer bentonite**
 - **Subtask T3.1:** Material subjected to the high temperature will be studied and changes of properties will be determined. Both laboratory treated material and samples from (in-situ) experiments are included.
 - **Subtask T3.2:** Investigation of processes and material behaviour at higher temperatures/transients.
 - **Subtask T3.3:** Experiment designed to simulate processes in clay buffer at various level of complexity. These experiments create basis for system behaviour understanding and database for mathematical model validation. Conceptual development of mathematical models. Validation by data from T3.1 and 3.2. Benchmarking the codes in cooperation with DONUT.

eurad

6



WP 7 – HITEC: WHY?

- **T2 Clay host rock**

- The overpressure generated by the difference between thermal expansion coefficient of pore water and the solid rock skeleton may have deleterious consequences.
- In far field, this could induce rock damage and reactivate fractures/faults.
- In near field characterized by a fractured zone, this could induce fracture opening or propagation in this fractured zone, altering the permeability.

- **T3 Buffer bentonite**

- Proving that higher temperatures than presently accepted are suitable is very relevant even for current concepts.
- It increases safety margin and gives greater credibility to the design (e.g. if it is proven to work for 130°C then for 100°C it is definitely safe).

Appendix B. Scientific challenges addressed by GAS WP (S. Levasseur)




CHALLENGES ADDRESSED BY THE WP GAS

EURAD Doctoral School – WP GAS & HITEC


22 January 2020, Liège (BE) • S. Levasseur

 The project leading to this application has received funding from the European Union's Horizon 2020 research and innovation programme under grant agreement n° 847593.

1st doctoral school WP GAS & HITEC



1





WP GAS MAIN OBJECTIVE

MECHANISTIC UNDERSTANDING OF GAS TRANSPORT IN CLAY MATERIALS

- Objective 1: Improve the **mechanistic understanding of gas transport** processes in natural and engineered **clay materials**, their couplings with the mechanical behaviour and their impact on the properties of these materials;
- Objective 2: Evaluate the gas transport regimes that can be active at the scale of a **geological disposal system** and their potential **impact on barrier integrity and repository performance**

1st doctoral school WP GAS & HITEC

2

WP GAS SPECIFIC CHALLENGES

- **Transfer knowledge gained from lab and in situ experiments to configurations that are commonly found in current repository designs, to address key questions from the end-users**
 - How could gas migrate within a repository and which water soluble and volatile radionuclide transport could be associated with it?
 - How and to what extent could the hydro-mechanical perturbations induced by gas effect barrier integrity and long-term repository performance?
- **Provide results that are applicable to a wide range of national programmes**

1st doctoral school WP GAS & HITEC

euRad

3

WP GAS EXPECTED IMPACTS

- **Building confidence in and extending the scientific bases on the fundamentals of gas transport in clay materials**
- **Closing the gap between experimentalists and modellers**
- **Foster the exchange of knowledge between the scientific community (RE's) and the end-users (WMO's and TSO's)**
- **Answer the key questions that are common to all end-users**
- **Provide input to implementers that may inspire design measures to reduce impact and/or uncertainty**



1st doctoral school WP GAS & HITEC

euRad

4

WP GAS PARTICIPANTS

30 organisations from 10 countries

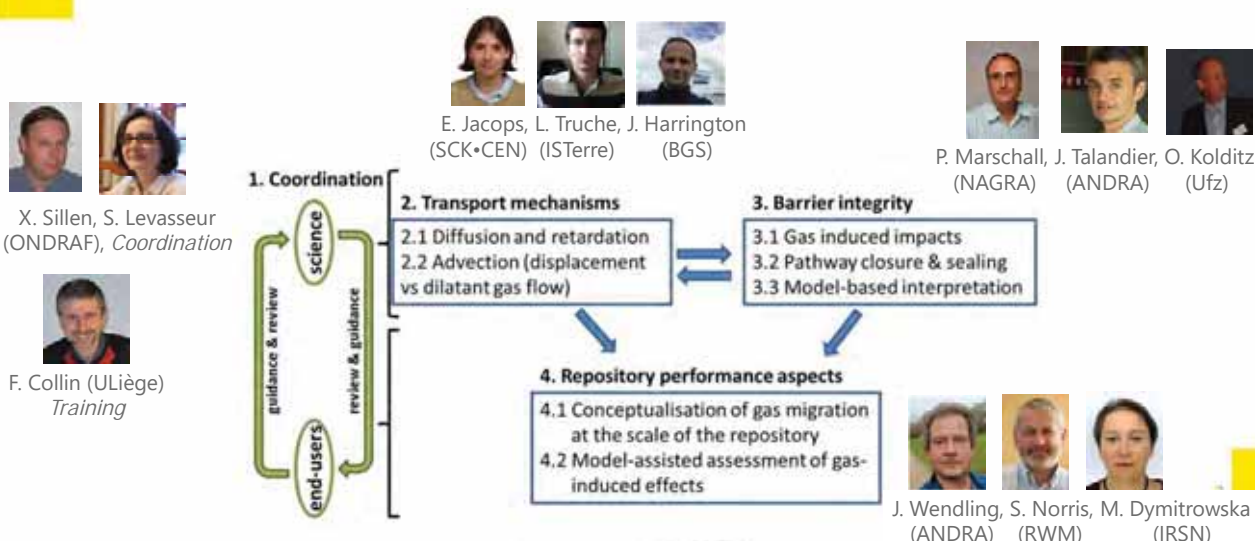



Participants of the joint WP GAS & HITEC Progress Meetings, 20-21 January 2020, Liège

Organisations		
✓ Andra (FR, WMO)	✓ CIEMAT (ES, TSO)	✓ SCK-CEN (BE, RE)
✓ CEA	• EDF (FR, RE)	• ONDRAF/NIRAS (BE, WMO)
✓ LEI (LT, RE)	• University of Helsinki	• ULiège (BE, RE)
✓ COVRA (NL, WMO)	• Aalto Uni (FI, RE)	✓ PSI (CH, RE)
• TU Delft (NL, RE)	✓ CNRS (RE, FR)	✓ NAGRA (CH, WMO)
✓ BGS (UK, RE)	• CNRS / ISTERre	• EPFL (CH, RE)
✓ RWM (UK, WMO)	• CNRS / GeoRes.	• ZHAW (CH, RE)
	• CNRS / IC2MP	• CIMNE (ES, RE)
	• CNRS / Subatech	✓ SÚRAO (CZ, WMO)
	✓ IRSN (FR, TSO)	• CTU (CZ, RE)
		• UJV (CZ, RE)
		✓ FZJ
		• UFZ (DE, RE)
		✓ KIT-PTKA
		• GRS (DE, RE)
		• BGR (DE, RE)
		✓ BGE (DE, WMO)

5

WP GAS – TASK BREAKDOWN AND WP BOARD



1. Coordination

X. Sillen, S. Levasseur (ONDRAF), *Coordination*

F. Collin (ULiège) *Training*

2. Transport mechanisms

2.1 Diffusion and retardation
2.2 Advection (displacement vs dilatant gas flow)

E. Jacobs, L. Truche, J. Harrington (SCK+CEN) (ISTERre) (BGS)

3. Barrier integrity

3.1 Gas induced impacts
3.2 Pathway closure & sealing
3.3 Model-based interpretation

P. Marschall, J. Talandier, O. Kolditz (NAGRA) (ANDRA) (Ufz)

4. Repository performance aspects

4.1 Conceptualisation of gas migration at the scale of the repository
4.2 Model-assisted assessment of gas-induced effects

J. Wendling, S. Norris, M. Dymitrowska (ANDRA) (RWM) (IRSN)

1st doctoral school WP GAS & HITEC

6

WP GAS – TASK 2 TRANSPORT MECHANISMS

OBJECTIVE: improve understanding of gas transport in clay

- **Diffusion and retardation (Subtask 2.1)**
 - Determine gas diffusion parameters on different clayey materials at different degree of saturation and support experimental data interpretation by pore network modelling
 - Understand gas physiosorption mechanisms in microporous systems
- **Advection (Subtask 2.2)**
 - Provide reference data for various natural and engineered clay materials under a sufficient broad range of conditions
 - Improve understanding of the observed gas transport modes and identifying their main control
 - Conceptualisation of transport mechanisms at micro & macro scales

1st doctoral school WP GAS & HITEC

eurad

7

7

WP GAS – TASK 3 BARRIER INTEGRITY

OBJECTIVE: improve understanding of gas impact on barriers

- **Improve the mechanistic understanding of the hydro-mechanical phenomena and processes, associated with:**
 - the gas-induced failure of clay barriers, i.e. within the engineered barrier system, within the Excavation Damage Zone and within the host rock (Subtask 3.1);
 - the effectiveness of self-sealing processes along gas-induced pathways in the clay barriers of a geological repository (Subtask 3.2).
- **Evaluate achievements by model-supported data analyses:**
 - predictive modelling and application of newly developed modelling tool on in-situ experiments (Subtask 3.3).

1st doctoral school WP GAS & HITEC

eurad

8

8

WP GAS – TASK 4 REPOSITORY PERFORMANCES

OBJECTIVE: ensure that WP is end-user oriented (with T2, T3)

- Evaluate gas transport regimes that can be active at the scale of a geological disposal system and their potential impact on repository performance

→ Conceptualizations of gas migration → storyboards (subtask 4.1) + model assisted assessment of gas induced effects (subtask 4.2) to identify:

- effects of the presence of gas and its transport on the transfer of soluble and volatile radionuclides
- consequences of gas-induced hydro-mechanical perturbations on barrier integrity and long-term performance.

WP GAS on EURAD website: <https://www.ejp-eurad.eu/implementation/mechanistic-understanding-gas-transport-clay-materials-gas>

1st doctoral school WP GAS & HITEC

eurad

9

9

WP GAS & HITEC DOCTORAL SCHOOLS

**“Multiphysical Couplings in Geomechanics,
a focus on thermal effects and gas transfer impacts on the behaviour of geomaterials”**

OBJECTIVE: Experimental characterisation and numerical analysis of thermal and gas-induced hydro-mechanical perturbations on barrier integrity and consequences for the long-term performance of a radioactive waste geological disposal

- 1st school at the beginning of the project: state-of-knowledge on the fundamentals of multiphysical couplings in geomechanics → January 22-24, 2020

→ Prerequisites for WP GAS & WP HITEC, in complement of WP SOTAs

→ Training materials: WP GAS Deliverable D6.3 (available soon)

- 2nd school on the development of these WPs

→ P

Thanks to ULiège (Profs. Charlier, Collin and their teams) for the organization of this 1st doctoral school of EURAD

Thanks to all lecturers and all participants for coming

Enjoy the school!

main results of publications in the management


eurad


10

1st doctoral school WP GAS & HITEC

10


Appendix C. Fundamentals on geomechanics and multi-physical couplings (A. Gens)





FUNDAMENTALS ON GEOMECHANICS AND MULTI- PHYSICAL COUPLINGS



January 22, 2020 • Antonio Gens (UPC)

 *The project leading to this application has received funding from the European Union's Horizon 2020 research and innovation programme under grant agreement n° 847593.*

Date

1

Introduction

EURAD SCHOOL FOR RADIOACTIVE WASTE MANAGEMENT | GAS & HITEC MULTIPHYSICAL COUPLINGS IN GEOMECHANICS: A FOCUS ON THERMAL EFFECT AND GAS TRANSFER IMPACT ON THE BEHAVIOUR OF GEOMATERIALS

January 22 - 24, 2020 | Liège University

PROGRAMME

Day 1 | Wednesday, January 22, 2020

08:30 - 09:30 h	Welcome, registration and coffee
09:30 - 12:00 h	Introduction Invited experts, Antonio Gens & Robert Charlier, Université de Liège Challenges addressed by HITEC WP: Markus Otto, VTT Technical Research Centre of Finland Challenges addressed by GAS WP: Alexander Jovanovic, Chalmers
12:30 - 13:30 h	Coffee break
13:30 - 15:30 h	Presentations on geomechanics and multiphysics coupling Antonio Gens, Universidad Politécnica de Catalunya
15:30 - 16:30 h	Lecture
16:30 - 17:30 h	Experimental analysis of high temperature effect on rock mass Pierre Deshayes, Ecole des Mines de Saint-Etienne
17:30 - 18:30 h	Coffee break
18:30 - 19:30 h	Introduction to multiphysics coupling: a focus on geomechanics Antonio Gens, Universidad Politécnica de Catalunya
19:30 - 21:00 h	Dinner

Date

Day 2 | Thursday, January 23, 2020

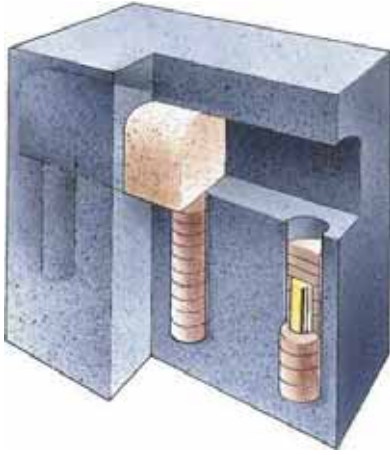
08:30 - 09:30 h	Introduction to gas transfer in geomechanics Antonio Gens, Universidad Politécnica de Catalunya
09:30 - 10:30 h	Coffee break
10:30 - 12:00 h	Introduction of gas transfer: theories & models Alexandre Gens, Universidad Politécnica de Catalunya
12:30 - 13:30 h	Lunch
13:30 - 14:30 h	Subsidence induced by gas transfer in rock mass Jianping Wang, China University of Geosciences
14:30 - 15:30 h	Coffee break
15:30 - 16:30 h	Introduction to gas transfer in geomechanics: a focus on geomechanics Antonio Gens, Universidad Politécnica de Catalunya
16:30 - 18:00 h	Dinner

Day 3 | Friday, January 24, 2020

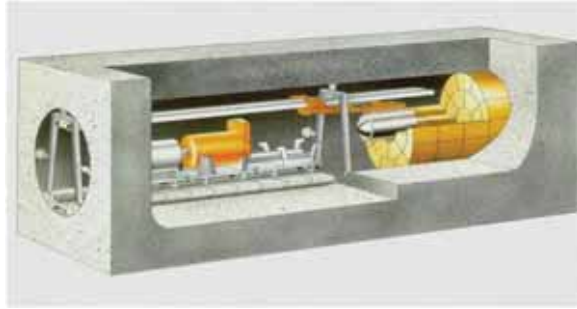
08:30 - 09:30 h	W. Wu, China University of Geosciences Multiphysics coupling Jianping Wang & Alexander Gens, China University of Geosciences
09:30 - 10:30 h	W. Wu, China University of Geosciences Multiphysics coupling Jianping Wang & Alexander Gens, China University of Geosciences
10:30 - 11:30 h	Lecture
11:30 - 12:30 h	W. Wu, China University of Geosciences Multiphysics coupling Jianping Wang & Alexander Gens, China University of Geosciences
12:30 - 13:30 h	Lunch
13:30 - 14:30 h	W. Wu, China University of Geosciences Multiphysics coupling Jianping Wang & Alexander Gens, China University of Geosciences
14:30 - 15:30 h	Challenges and next steps National and international perspectives on gas and heat transfer Antonio Gens & Robert Charlier, Université de Liège
15:30 - 16:30 h	President of the programme in the end of his lecture
16:30 - 18:00 h	Final dinner

2

Introduction



Disposal in vertical boreholes



Disposal in horizontal drifts

Date

3

Introduction



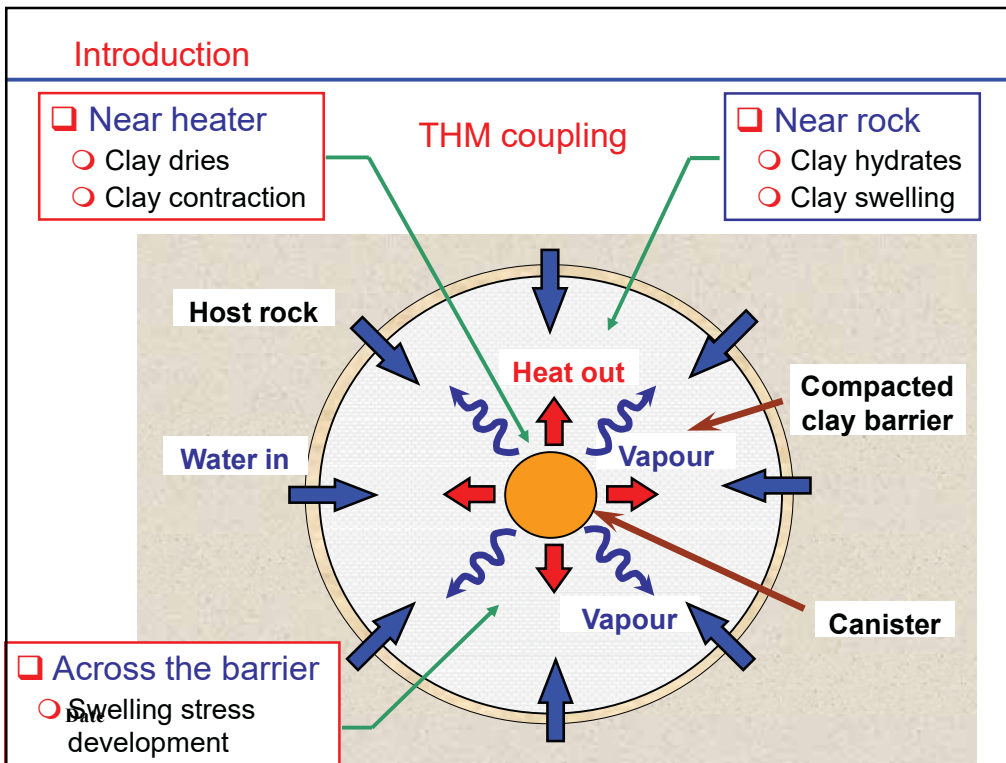
Disposal in vertical boreholes



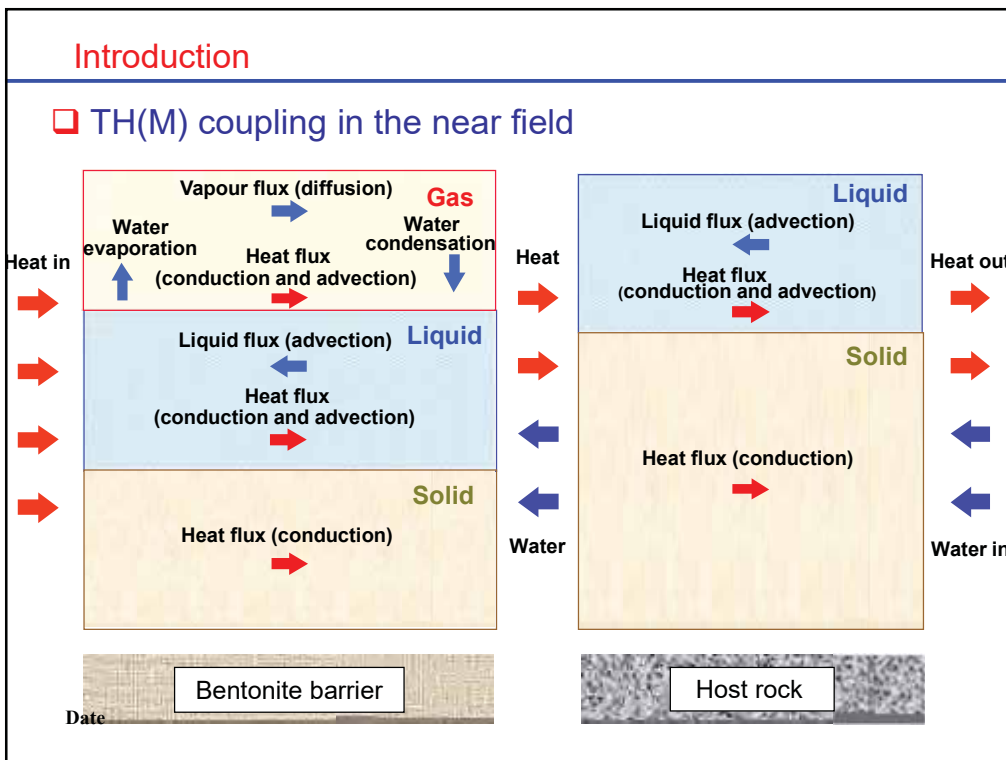
Disposal in horizontal drifts

Date

4



5



6

Introduction

Relevant phenomena

■ THERMAL

- Heat conduction
- Heat advection (liquid water and vapour)
- Phase changes

■ HYDRAULIC

- Liquid flow
- Gas flow
- Air dissolution in water
- Air diffusion in water
- Vapour diffusion
- Gas generation and transport

Date

■ MECHANICAL

- Deformation of materials (constituents and overall) caused by changes of:
 - Stresses
 - Suction/Water pressures
 - Temperatures

7

Introduction

- ❑ We deal with saturated and **unsaturated porous media**
- ❑ Coupled multi-physics (THM)
 - ❑ Temperature (T)
 - ❑ Fluid flow (may include liquid and/or gas movement) (H)
 - ❑ Mechanical (stress, deformation, strength) (M)
- ❑ We must end up with a coupled THM formulation
 - ❑ Establishing appropriate governing equations
 - ❑ Adopting constitutive relations as realistic as possible
 - ❑ Developing a numerical approximation to incorporate in a computer code
- *We will not address the geochemical and biological aspects although there are certainly part of the multi-physics domain!*

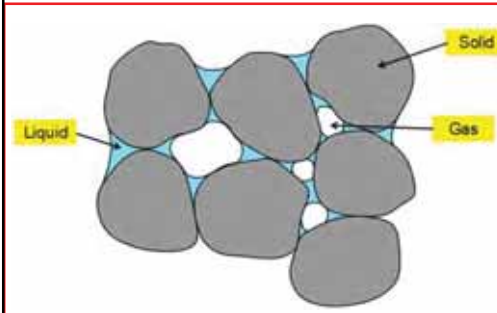
Date

8

Introduction

We deal with saturated and unsaturated porous media

A simplified picture: **Three phases:**



- **solid (s)** : mineral
- **liquid (l)** : water + air dissolved
- **gas (g)** : dry air + water vapour

Three species :

- **mineral (-)** : the mineral is coincident with solid
- **water (w)** : as liquid or evaporated in the gas phase
- **air (a)** : dry air, as gas or dissolved in the liquid phase

Volumetric mass of a species in a phase (e.g. water in gas phase θ_g^w is the product of the mass fraction of that species (ω_g^w) and the bulk density of the phase (ρ_g):

Date

$$\theta_g^w = \omega_g^w \rho_g.$$

9

Outline of the lecture

- Introduction. Relevant phenomena
- Unsaturated geomaterials and suction
- Constitutive relations
 - General
 - Thermal
 - Hydraulic
 - Mechanical
- Governing equations
- Concluding remarks

Date

10

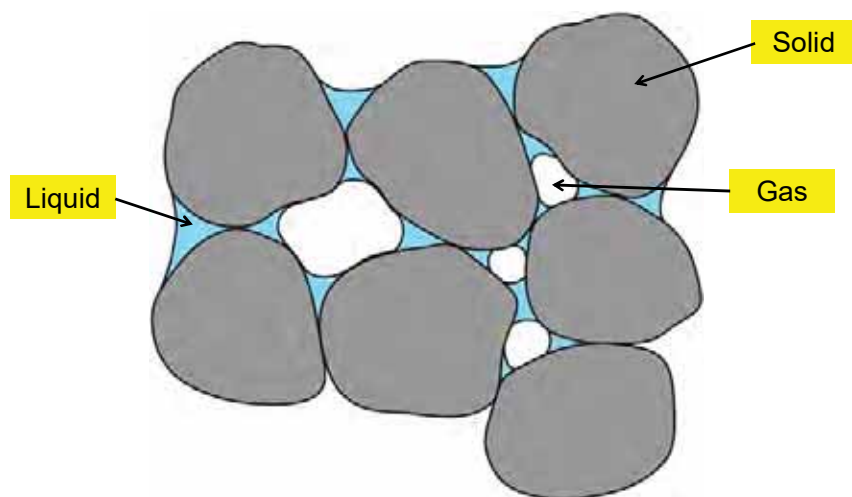
Outline of the lecture

- ❑ Introduction. Relevant phenomena
- ❑ **Unsaturated geomaterials and suction**
- ❑ Constitutive relations
 - ❑ General
 - ❑ Thermal
 - ❑ Hydraulic
 - ❑ Mechanical
- ❑ Governing equations
- ❑ Concluding remarks

Date

11

Unsaturated geomaterials and suction



$$n(\phi) = \frac{V_{pores}}{V_{total}} = \frac{V_{liquid} + V_{gas}}{V_{total}}$$

Date

Porosity

$$S_r = \frac{V_{liquid}}{V_{pores}} = \frac{V_{liquid}}{V_{liquid} + V_{gas}} = 1 - S_g$$

Degree of saturation

12

Unsaturated geomaterials and suction

Water potential, Ψ : work required to transport a unit mass from a reference pool of pure water to the soil water under consideration

$$\Psi = \Psi_c + \Psi_o + \Psi_g + \Psi_z$$

Matric
Osmotic
Gas
Gravitational

$\Psi_c = (u_w - u_a)$: Matric (capillary) potential

$\Psi_o = c_m RT$: Osmotic potential

$\Psi_g = (u_a - u_{atm})$: Gas pressure potential

$\Psi_z = \gamma_w z$: Gravitational potential

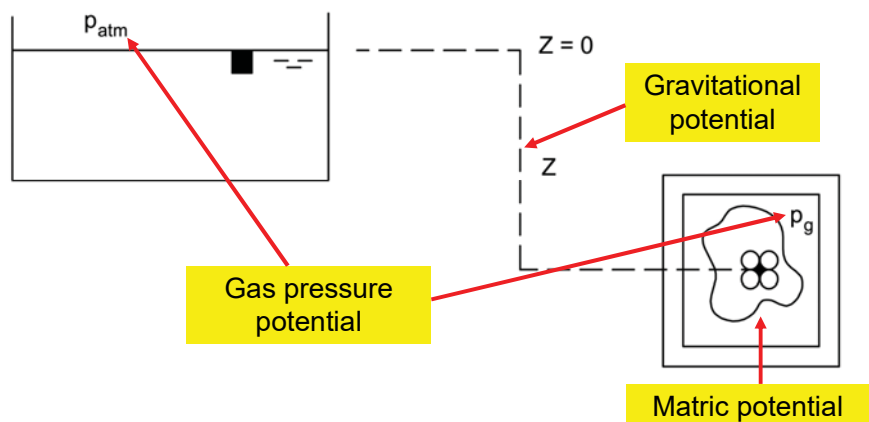
Date

Review panel (1965)

13

Unsaturated geomaterials and suction

Water potential, Ψ : work required to transport a unit mass from a reference pool of pure water to the soil water under consideration

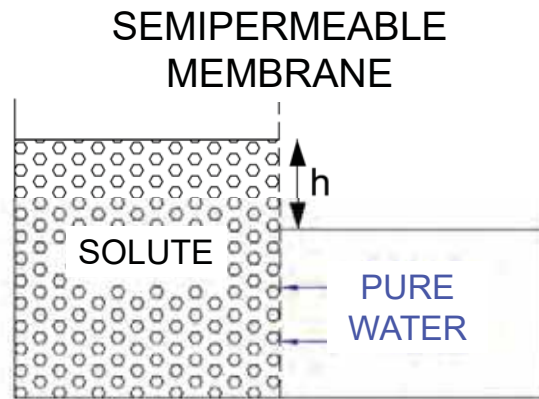


Date

14

Unsaturated geomaterials and suction

Water potential, Ψ : work required to transport a unit mass from a reference pool of pure water to the soil water under consideration



$$\pi_{os} = \frac{n_s}{V} RT$$

Date

Osmotic potential

15

Unsaturated geomaterials and suction

Water potential, Ψ : work required to transport a unit mass from a reference pool of pure water to the soil water under consideration

$$\Psi = \Psi_c + \Psi_o + \Psi_g + \Psi_z \quad (\text{Review panel, 1965})$$

Matric Osmotic Gas Gravitational

- Total water potential controls water flow
- Water potential affects mechanical behaviour. Not all potential components have, however, the same effect

$$S = -\rho_w \Psi_c : \text{Matric suction} \quad \pi = -\rho_w \Psi_o : \text{Osmotic suction}$$

$$S_t = S + \pi : \text{Total suction}$$

- Total suction is directly related to relative humidity (psychrometric law)

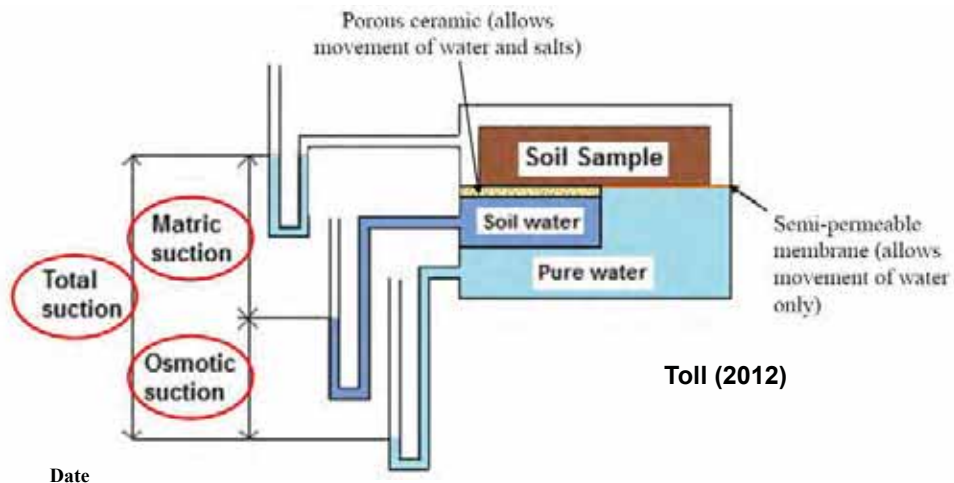
Date

16

Unsaturated geomaterials and suction

$$\Psi = \Psi_c + \Psi_o + \Psi_g + \Psi_z \quad (\text{Review panel, 1965})$$

Matric
Osmotic
Gas
Gravitational



17

Unsaturated geomaterials and suction

- Matric suction is often associated with capillary phenomena

$$s = p_a - p_w$$



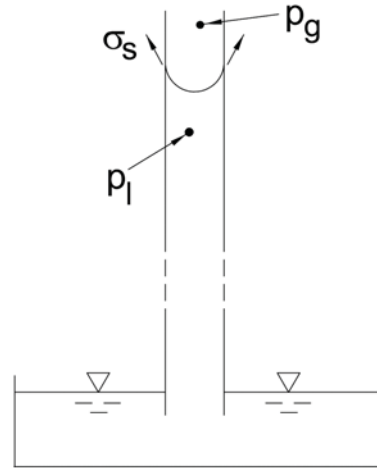
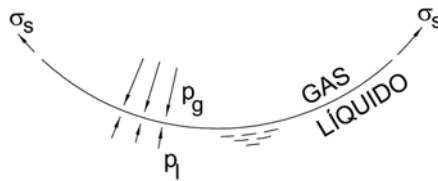
Date

18

Unsaturated geomaterials and suction

EFFECT OF SURFACE TENSION. LAPLACE'S LAW

The surface tension is able to maintain different pressures of liquid and gas in the interface



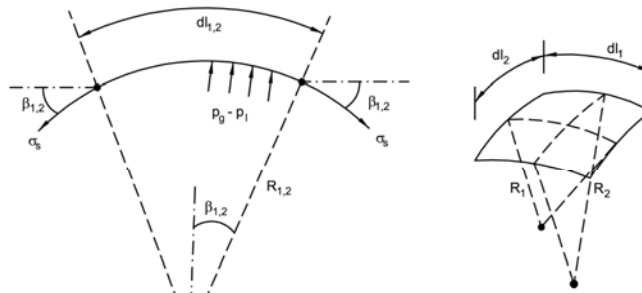
- This effect is evident in the capillary ascension of water in small diameter tubes

Date

19

Unsaturated geomaterials and suction

FORCE EQUILIBRIUM IN AN INTERFACE ELEMENT



$$(p_g - p_l) dl_1 dl_2 = \sigma_s \frac{dl_1 dl_2}{R_2} + \sigma_s \frac{dl_1 dl_2}{R_1}$$

$$p_g - p_l = \sigma_s \left(\frac{1}{R_2} + \frac{1}{R_1} \right)$$

$$\Rightarrow \frac{2}{r} = \frac{1}{R_1} + \frac{1}{R_2}$$

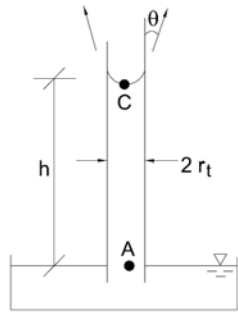
Mean radius

$$p_g - p_l = \frac{2\sigma_s}{r}$$

Date

20

Unsaturated geomaterials and suction



HEIGHT OF CAPILLARY RISE

Force equilibrium
Weight = Force exerted by the surface tension

$$\pi r_t^2 h \gamma_w = 2\pi r_t \sigma_s \cos \theta$$

$$\theta = 0^\circ; h = \frac{2\sigma_s \cos \theta}{\gamma_w r_t} \cong \frac{2\sigma_s}{\gamma_w r} = \frac{p_g - p_l}{\gamma_w} = \frac{s}{\gamma_w}$$

Example:

$$r = 0.73 \mu\text{m} ; s = 0.1 \text{MPa} ; h = 10 \text{m}$$

$$r = 1 \text{mm} ; s = 0.073 \text{kPa} ; h = 14.8 \text{mm}$$

The capillary rise height is therefore equal to the value of suction expressed in length units.

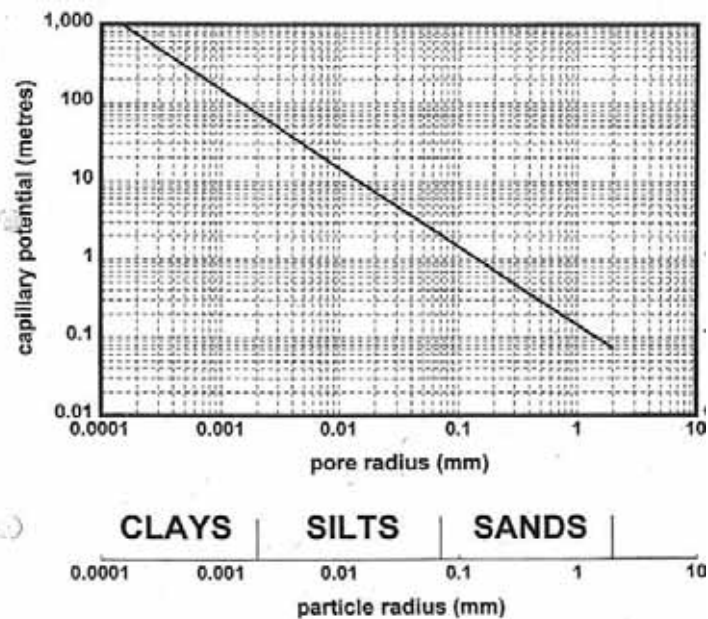
Capillary suction depends essentially on pore size and geometry

Date

21

Unsaturated geomaterials and suction

HEIGHT OF CAPILLARY RISE

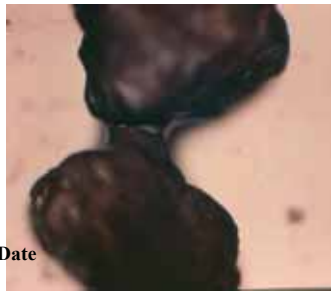


Date

22

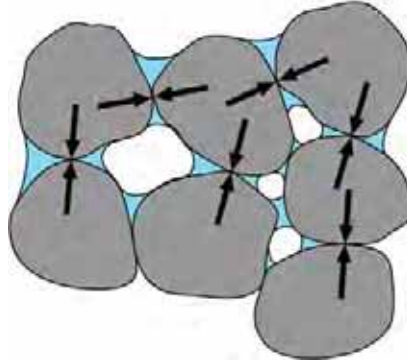
Unsaturated geomaterials and suction

- Suction in the menisci give rise to (stabilizing) intergranular capillary forces



Date

$$s = p_a - p_w$$

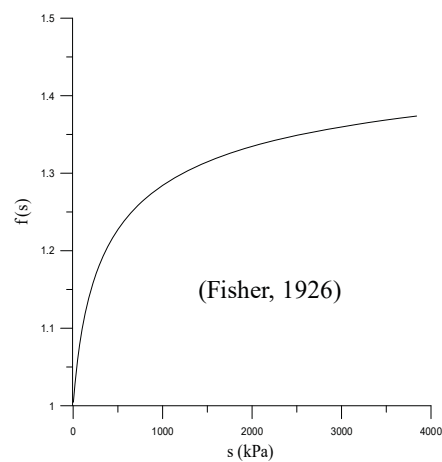
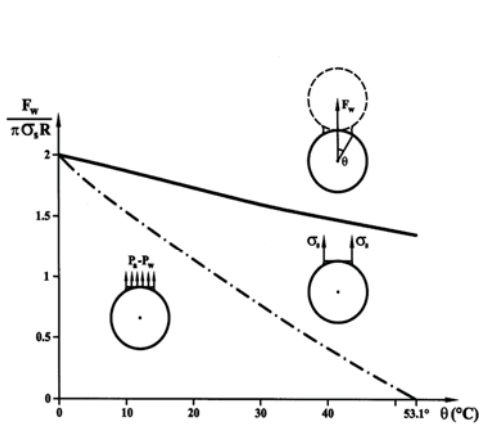


Intergranular capillary forces

23

Unsaturated geomaterials and suction

- Suction in the menisci give rise to (stabilizing) intergranular capillary forces



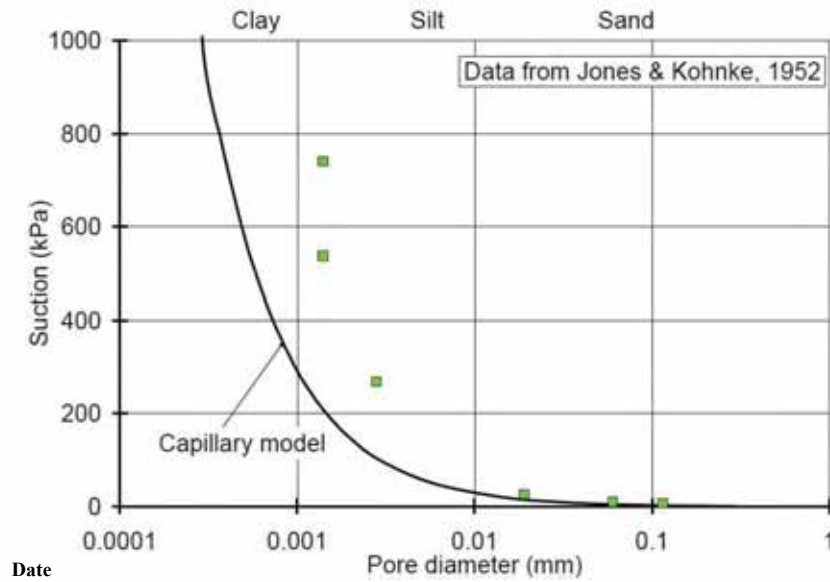
Intergranular capillary forces

Date

24

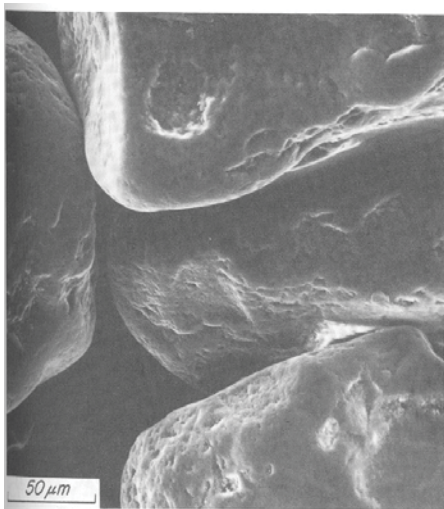
Unsaturated geomaterials and suction

➤ Suction measurements



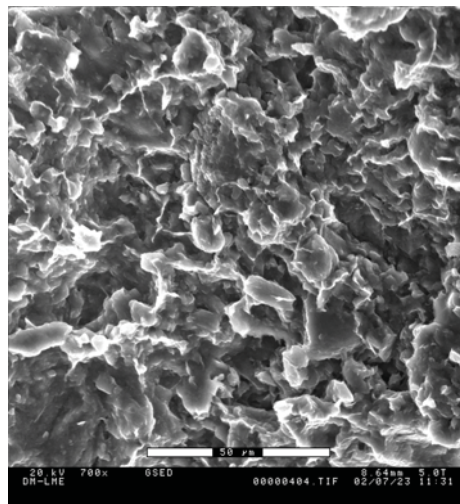
25

Unsaturated geomaterials and suction



Date

Sand



Clay

26

Unsaturated geomaterials and suction

- **Matric suction** contains a capillary component and an adsorptive component (Philip, 1977; Tuller et al., 1999)

$$\mu = \psi_m = A(h) + C(\kappa)$$

Augmented Young-Laplace (AYL) equation

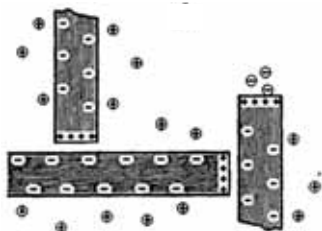
- Modern interface surface theory (Derjaguin et al., 1987)
 - The difference in chemical potentials across an interface can be expressed as an equivalent interfacial force per unit area of the interface, called *disjoining pressure*
 - It corresponds to the **matric suction!**
- Force contributions to adsorptive component (disjoining pressure)
 - Attractive
 - Van der Waals forces (< 100 Å)
 - Electrostatic (Ion-dipole, Coulomb, hydrogen bridges...)
 - Repulsive
 - Hydration repulsion (< 100 Å) (change of water structure?)
 - Electrostatic (DDL) (> 500 Å)

Date

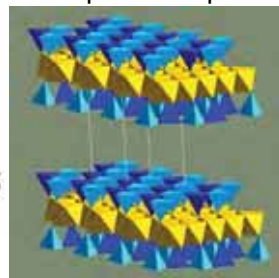
27

Unsaturated geomaterials and suction

- Force contributions to adsorptive component (disjoining pressure)



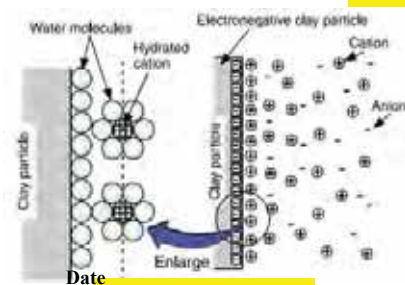
Coulomb attraction



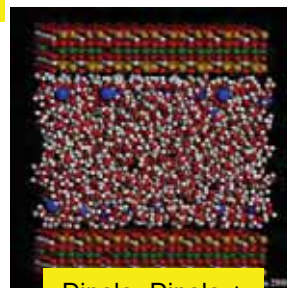
Van der Waals



Ion-Dipole



DDL



Dipole- Dipole + hydrogen bridge

28

Unsaturated geomaterials and suction

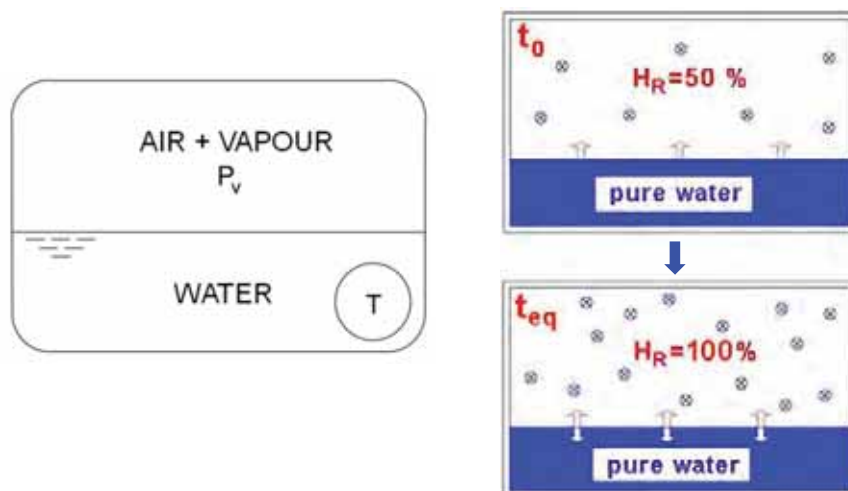
- Matric suction should be viewed as the result of the general interaction between solid surface, liquid and associated interfaces
- Adsorptive and capillary components may well cause different mechanical effects, in practice distinguishing them is not easy
- Historically, matric suction is expressed as $S = p_a - p_w$
 p_a : air pressure, p_w : water pressure
- Large (negative) potentials give rise to very large negative 'water pressures', they are just an expression of the potential. They do not correspond to the usual bulk thermodynamic pressures
- "suction must be considered merely as a convenient index of the affinity of soil for free water" (Blight, 1965)

Date

29

Unsaturated geomaterials and suction

- Suction and relative humidity
 - Vapour pressure (no solutes, no curvature)

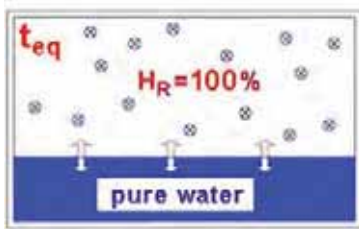
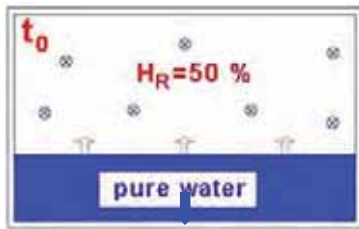


Date

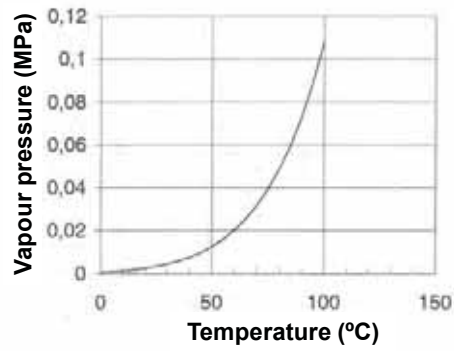
30

Unsaturated geomaterials and suction

- Vapour pressure (no solutes, no curvature)
 - Effect of temperature



Date

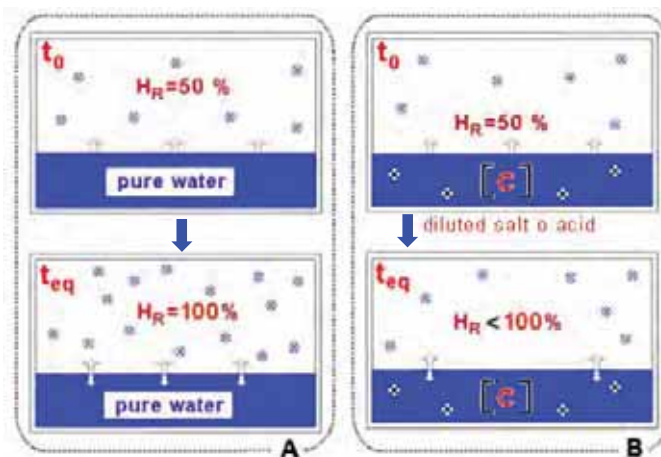


$$p_v^o \text{ (MPa)} = 136075 \exp \left(-\frac{5239.7}{273.15 + T} \right)$$

31

Suction in unsaturated soils

- Vapour pressure (solute, no curvature)



- Raoult's law:

$$\text{RH (relative humidity)} = \frac{p_v}{p_v^o} = \frac{n_w}{n_w + n_s} \text{ (solvent molar fraction)}$$

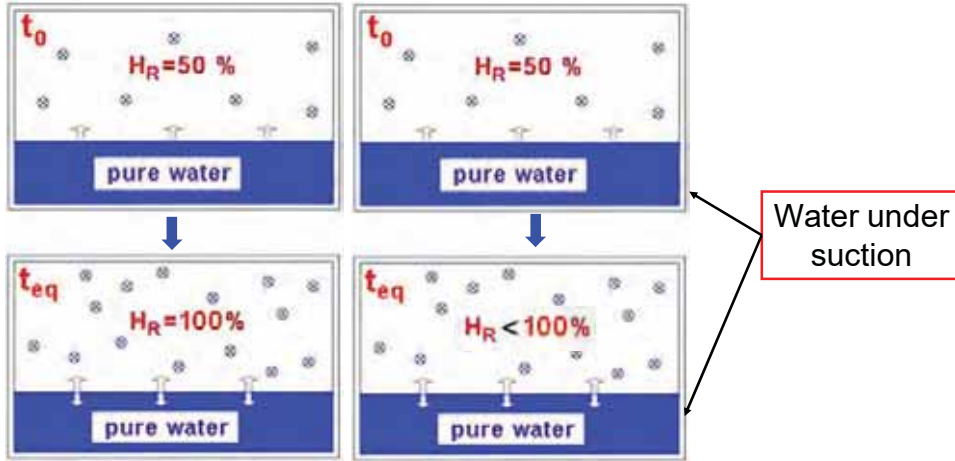
Date

- Only valid for small concentrations!

32

Suction in unsaturated soils

- Vapour pressure (no solutes, curvature)



$$RH = \frac{p_v}{p_v^0} = \exp\left(\frac{\psi M_w}{R(273.15 + T)\rho_l}\right)$$

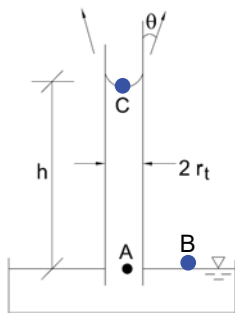
Psychrometric law or Kelvin's law

Date

33

Suction in unsaturated soils

- Psychrometric law



$$h = \frac{\psi}{\rho_l g}$$

Over a differential height

$$dp_v = -\rho_v g dy$$

$$\frac{\rho_v + dp_v}{\rho_v} dy$$

From the ideal gas law

$$\rho_v = p_v \frac{M_w}{RT}$$

Combining the two expressions

$$dy = -\frac{dp_v}{\rho_v g} = -\frac{dp_v}{p_v} \frac{RT}{M_w g}$$

Integrating from 0 (B) and h (C)

$$\int_0^h dy = h = \frac{\psi}{\rho_l g} = -\frac{RT}{M_w g} \int_{p_v^0}^{p_v} \frac{dp_v}{p_v} = -\frac{RT}{M_w g} \ln \frac{p_v}{p_v^0}$$

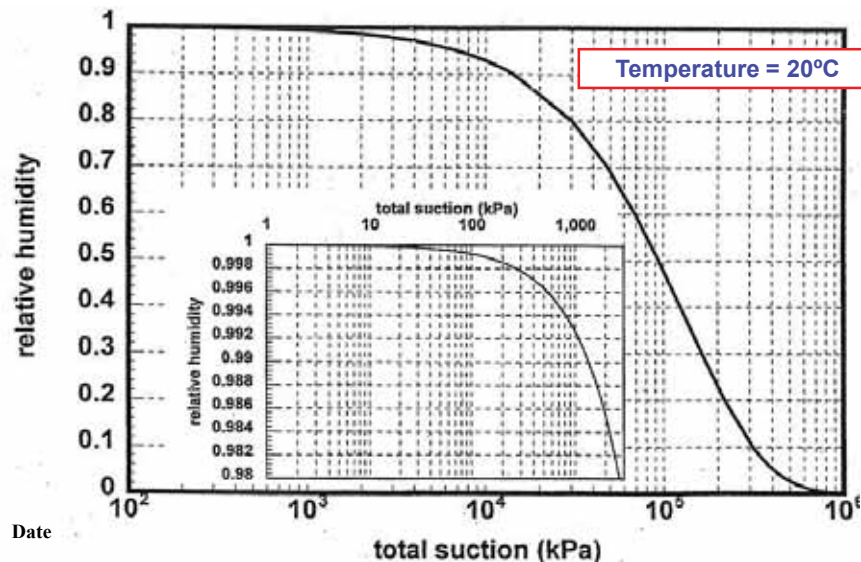
$$RH = \frac{p_v}{p_v^0} = \exp\left(\frac{\psi M_w}{R(273.15 + T)\rho_l}\right)$$

Date

34

Suction in unsaturated soils

- Psychrometric law $\frac{\rho_v}{\rho_v^0} = \frac{\rho_v}{\rho_v^0} = \frac{\theta_g^w}{(\theta_g^w)^0} = \text{RH (relative humidity)}$



35

EQUILIBRIUM RESTRICTIONS

- Concentration of water vapour (psychrometric law)

$$\theta_g^w = (\theta_g^w)^0 \exp\left(\frac{\psi M_w}{R(273.15 + T)\rho_l}\right)$$

Vapour concentration with no capillary effects (depends on temperature and concentration)

Modification of vapour concentration due to capillary effects (depends on suction and temperature)

θ_g^w : vapour density in the gaseous phase

ψ : water potential

T : temperature

$(\theta_g^w)^0$: vapour density in the gaseous phase ($P_g - P_l = 0$)

M_w : molecular mass of water (0.018 kg/mol)

R : the gas constant (8.314 J/mol^oK)

Date

- Concentration of water vapour depends on:

➤ Temperature (**Thermal**)

➤ Suction (**Hydraulic**)

36

Outline of the lecture

- ❑ Introduction. Relevant phenomena
- ❑ Unsaturated geomaterials and suction
- ❑ **Constitutive relations**
 - ❑ General
 - ❑ Thermal
 - ❑ Hydraulic
 - ❑ Mechanical
- ❑ Governing equations
- ❑ Concluding remarks

Date

37

Constitutive relations: general

- ❑ From irreversible thermodynamics, all coupled processes must exist
- ❑ Coupled processes should be distinguished from coupled phenomena

	Gradients			
Flow	Hydraulic Head	Chemical Concentration	Temperature	Electrical
Fluid	Darcy's Law (Hydraulic Conduction)	Chemical Osmosis	Thermo Osmosis	Peltier effect
Solutes	Ultra Filtration	Fick's Law (Diffusion)	Soret Effect (Thermal Diffusion)	Electrical osmosis
Heat	Thermo Filtration (Isothermal Heat Transfer)	Dufour Effect	Fourier's Law (Thermal Conduction)	Electrophoresis
Electric current	Seebeck or Thompson Effect	Rouss Effect	Diffusion and membrane potential	Electrical conduction

Date

38

Constitutive relations: general

- ❑ From irreversible thermodynamics, all coupled processes must exist
- ❑ Coupled processes should be distinguished from coupled phenomena

Flow	Gradients			
	Hydraulic Head	Chemical Concentration	Temperature	Electrical
Fluid	Darcy's Law (Hydraulic Conduction)	Chemical Osmosis	Thermo Osmosis	Peltier effect
Solutes	Ultra Filtration	Fick's Law (Diffusion)	Soret Effect (Thermal Diffusion)	Electrical osmosis
Heat	Thermo Filtration (Isothermal Heat Transfer)	Dufour Effect	Fourier's Law (Thermal Conduction)	Electrophoresis
Electric current	Seebeck or Thompson Effect	Rouss Effect	Diffusion and membrane potential	Electrical conduction

Date

39

Constitutive relations: thermal

❑ Mechanisms of heat transfer

- Conduction
 - Heat transfer by direct contact of particles of matter (elastic impact, free electron diffusion, vibration of adjacent atoms...)
- Advection
 - Heat transfer by mass movement
 - The term **convection** is used when the mass movement is driven by buoyancy (density differences) caused by the thermal field
- Radiation
 - Heat transfer by electromagnetic waves



Date

40

Constitutive relations: thermal

- Energy conservation

$$dU = \partial Q + \partial W$$

- Gases

$$dU = \partial Q - PdV$$

$$dU = TdS - PdV \quad (\text{reversible processes})$$

- General

$$dU = \partial Q + \partial W + \sum_i \mu_i dN_i$$

$$dU = \partial Q + \sum_i X_i dx_i + \sum_i \mu_i dN_i$$

$$d \left(\begin{array}{l} \text{internal energy in solid,} \\ \text{liquid and gas phases} \end{array} \right) = d(\text{supply of heat})$$

Date

41

Constitutive relations: thermal

- Heat capacity

$$\text{Constant volume} \quad C_V = \left(\frac{\partial U}{\partial T} \right)_V \quad dU = TdS - PdV$$

$$\text{Constant pressure} \quad C_P = \left(\frac{\partial H}{\partial T} \right)_P \quad dH = TdS - VdP$$

Date

42

Constitutive relations: thermal

- Internal energy per unit volume (additive)

$$E_s \rho_s (1 - n) + E_l \rho_l n S_l + E_g \rho_g n S_g \quad ; \quad S_l + S_g = 1$$

$$E_s = c_s T \quad E_l = (c_l^w \omega_l^w + c_l^a \omega_l^a) T \quad E_g = (c_g^w T + L) \omega_g^w + c_g^a \omega_g^a T$$

↑
 Phase change:
 evaporation/condensation
 latent heat

$$L = 2.26 \times 10^3 \text{ KJ/Kg}$$

- Internal energy depends on

- Degree of saturation (**Hydraulic**)
- Porosity (**Mechanical**)

Date

43

Constitutive relations: thermal

- Specific heat capacity (25°C unless otherwise specified)

Substance	c_p (kJ kg ⁻¹ K ⁻¹)
Air (sea level, dry, 0°C)	1.0035
Air (typical room conditions)	1.012
Brick	0.84
Concrete	0.88
Glass, silica	0.84
Granite	0.79
Graphite	0.84
Gypsum	1.09
Marble	0.88
Quartz	0.71
Sand	0.80
Sodium Chloride	0.85

Substance	c_p (kJ kg ⁻¹ K ⁻¹)
Stainless steel	0.51
Steel	0.42
Water vapour (25°C)	1.86
Water vapour (100°C)	1.89
Water (liquid, 25°C)	4.18
Water (ice, 0°C)	2.05
Water (ice, -10°C)	2.00
Wood	0.42

Date

44

Constitutive relations: thermal

○ Heat conduction: Fourier's law

$$i_c = -\lambda \nabla T$$

□ Heat driven by temperature gradients

➤ Thermal conductivity

λ : global thermal conductivity

$$\lambda = \lambda_s^{(1-\phi)} \lambda_l^{\phi S_l} \lambda_g^{\phi(1-S_l)} = \lambda_{sat}^{S_l} \lambda_{dry}^{1-S_l}$$

$$\lambda_{sat} = \lambda_s^{1-\phi} \lambda_l^{\phi}$$

$$\lambda_{dry} = \lambda_s^{1-\phi} \lambda_g^{\phi}$$

□ Thermal conductivity depends on

- Temperature (**Thermal**)
- Degree of saturation (**Hydraulic**)
- Porosity (**Mechanical**)

Date

45

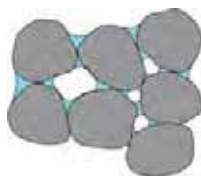
Constitutive relations: thermal

○ Heat conduction

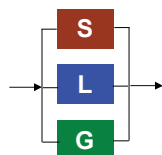
➤ Fourier's law

$$i_c = -\lambda(T) \nabla T$$

λ : Thermal conductivity



$$\text{S} \rightarrow \text{L} \rightarrow \text{G} \rightarrow 1/\lambda = 1/\lambda_s(1-n) + 1/\lambda_l n S_l + 1/\lambda_g n S_g$$



$$\lambda = \lambda_s(1-n) + \lambda_l n S_l + \lambda_g n S_g$$

- Geometric mean: $\lambda = \lambda_s^{(1-n)} \lambda_l^{n S_l} \lambda_g^{n(1-S_l)}$

$$\lambda_{sat} = \lambda_s^{1-n} \lambda_l^n$$

$$\lambda_{dry} = \lambda_s^{1-n} \lambda_g^n$$

$$\lambda = \lambda_s^{(1-n)} \lambda_l^{n S_l} \lambda_g^{n(1-S_l)} = \lambda_{sat}^{S_l} \lambda_{dry}^{1-S_l}$$

Date

46

Constitutive relations: thermal

○ Thermal conductivity of some substances

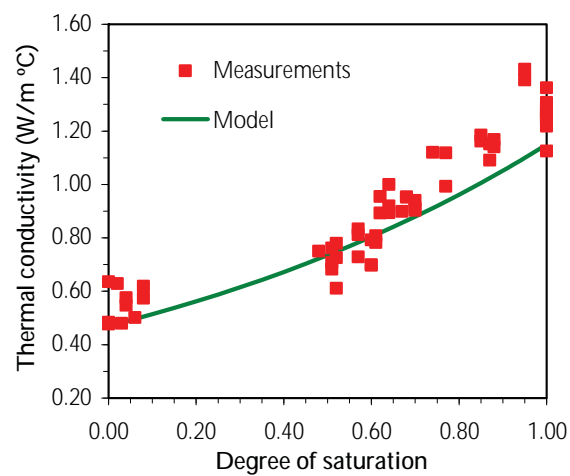
Substance	λ (W m ⁻¹ K ⁻¹)	Substance	λ (W m ⁻¹ K ⁻¹)
Air	0.024 - 0.026	Snow	0.06 - 0.59
Cement mortar	1.73	Stainless steel	150
Concrete	1.8	Steel	63
Granite	1.7 - 3.0	Water vapour (100°C)	0.016
Limestone	1.3	Water (liquid, 25°C)	0.60
Marble	2.1 - 2.9	Water (ice, 0°C)	2.22
Polysterene	0.03 - 0.06	Water (ice, -10°C)	2.30
Quartz	4 - 8	Wood	0.06 - 0.17
Sandstone	1.8 - 2.9		
Soil, saturated	1.0 - 2.7		

Date

47

Constitutive relations: thermal

Thermal conductivity of Febex bentonite



Date

48

Outline of the lecture

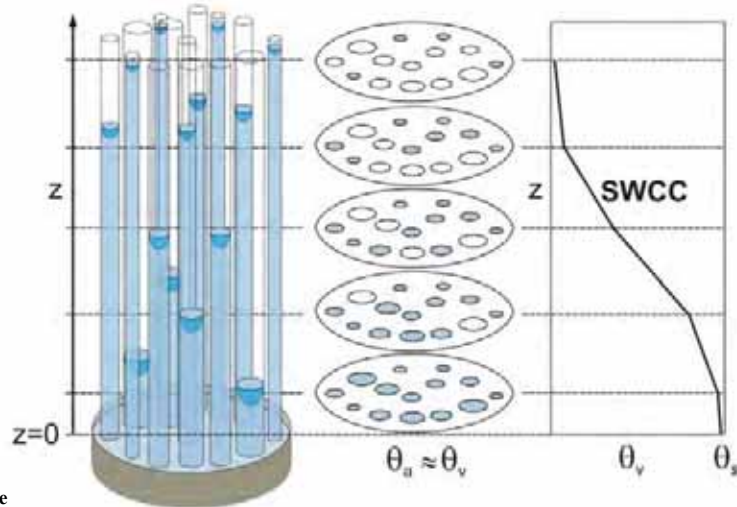
- ❑ Introduction. Relevant phenomena
- ❑ Unsaturated geomaterials and suction
- ❑ **Constitutive relations**
 - ❑ General
 - ❑ Thermal
 - ❑ **Hydraulic**
 - ❑ Mechanical
- ❑ Governing equations
- ❑ Concluding remarks

Date

49

Constitutive relations: hydraulic

- Soil water retention curve (also called soil water characteristic curve, SWCC)
 - It expresses the relationship between suction and amount of water in the porous medium

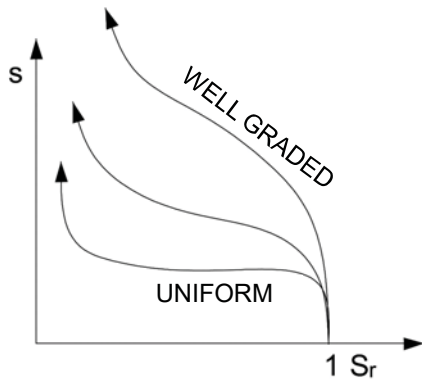


Tuller & Or (2003)

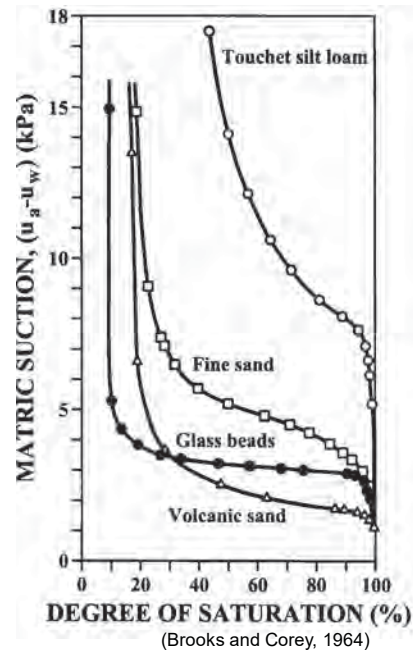
50

Constitutive relations: hydraulic

- Soil water retention curve



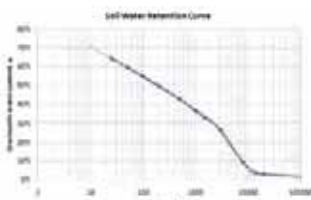
Date



51

Constitutive relations: hydraulic

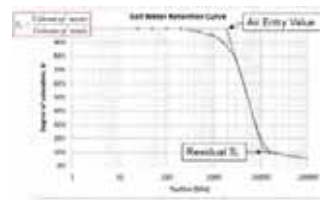
- Soil water retention curve
- Relationship between suction (water potential) and:
 - Gravimetric water content (water mass / dry soil mass)
 - Volumetric water content (volume of water / total volume)
 - Degree of saturation (volume of water / volume of voids)



Gravimetric water content



Volumetric water content



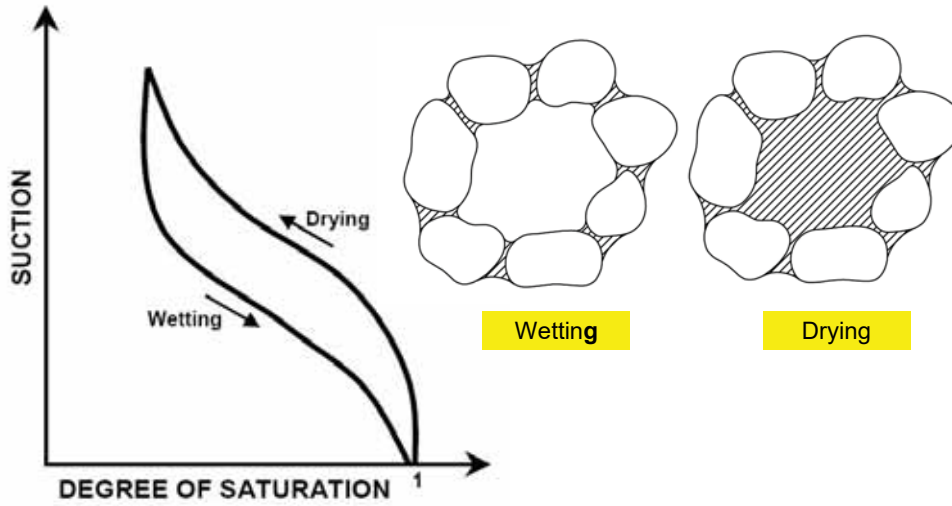
Degree of saturation

Date

52

Constitutive relations: hydraulic

- Soil water retention curve: hysteresis

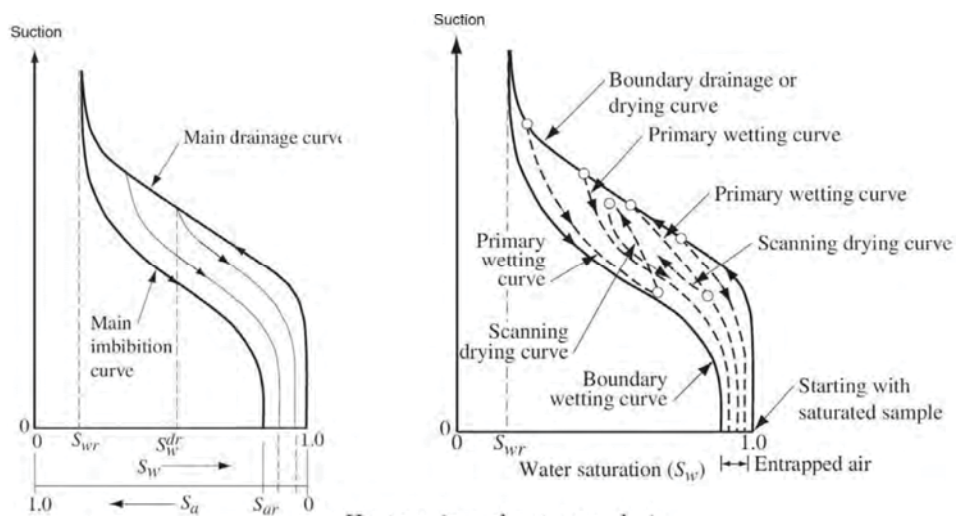


Date

53

Constitutive relations: hydraulic

- Soil water retention curve: hysteresis

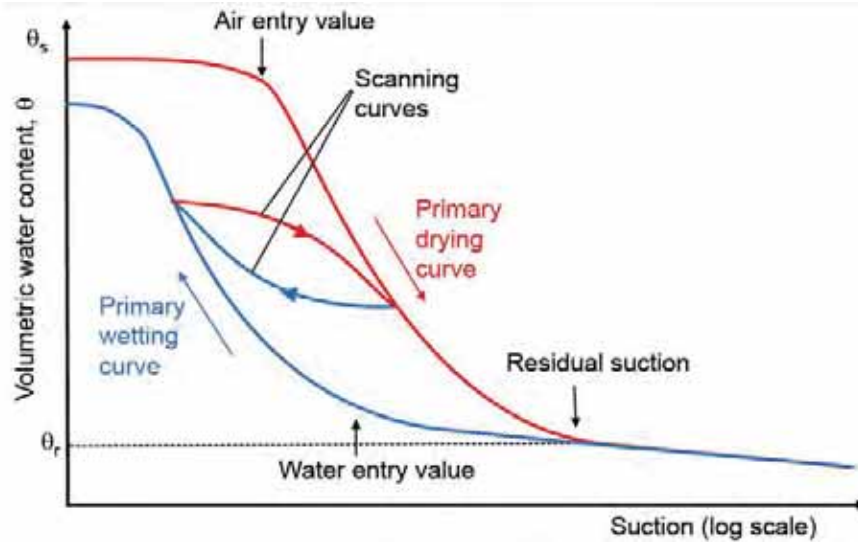


Date

54

Constitutive relations: hydraulic

- Soil water retention curve: hysteresis

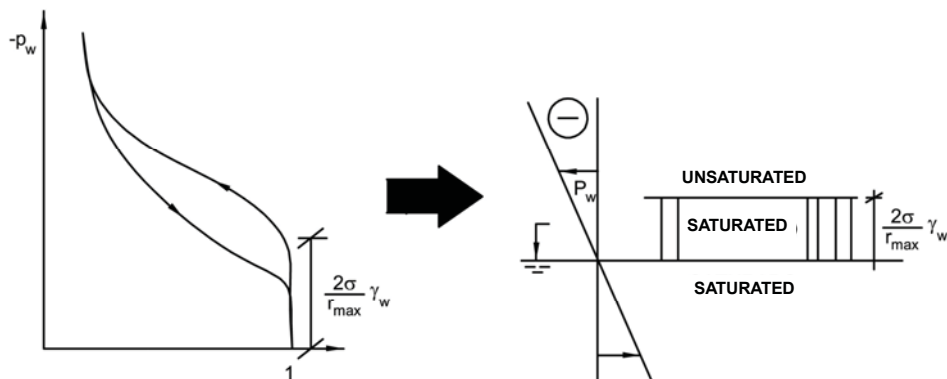


Date

55

Constitutive relations: hydraulic

- Soil water retention curve
 - An air entry value can be defined as the suction required for air to penetrate a saturated soil
 - Air entry value depends on pore size
 - Negative pore pressures can exist in saturated soils

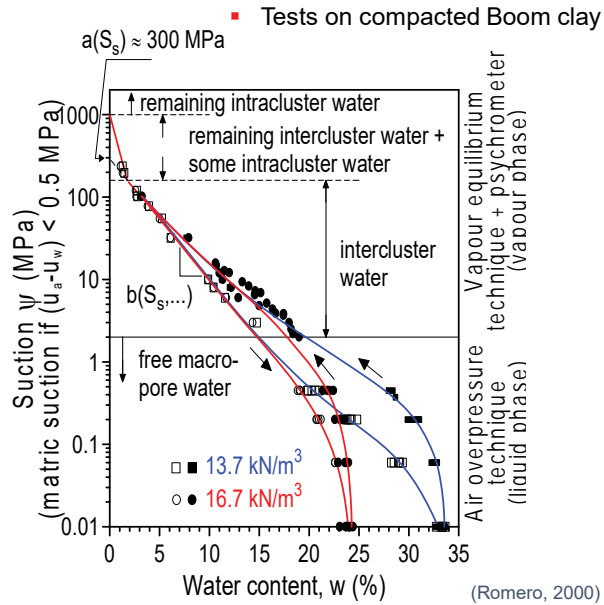


Date

56

Constitutive relations: hydraulic

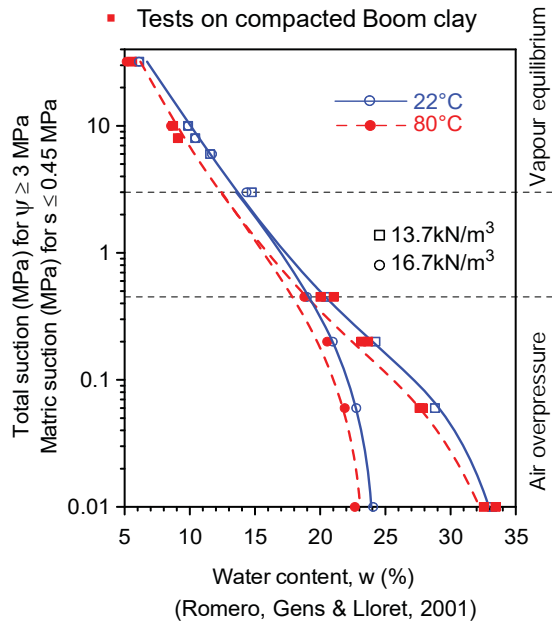
- Soil water retention curve: dependence on dry density



57

Constitutive relations: hydraulic

- Soil water retention curve: dependence on temperature



58

Constitutive relations: hydraulic

- Soil water retention curve: dependence on temperature
 - A way to introduce temperature-dependence in the retention curve

Van Genuchten expression

$$S_e = \frac{S_l - S_{\min}}{S_{\max} - S_{\min}} = \left[1 + \left(\frac{\rho_g - \rho_l}{P} \right)^{1/(1-\lambda)} \right]^{-\lambda}$$

$$\rho_g - \rho_l = P \left(S_e^{-1/\lambda} - 1 \right)^{(1-\lambda)}$$

P is related to the air entry pressure

$$\rho_g - \rho_l = \frac{2\sigma}{r} \quad \begin{array}{l} r: \text{pore radius} \\ \sigma: \text{surface tension} \end{array}$$

σ depends on temperature

$$\sigma (N/m) = 0.0359 \exp\left(\frac{252.93}{273.15 + T}\right) \quad P = P_0 \frac{\sigma(T)}{\sigma(T_0)}$$

Date

59

Constitutive relations: hydraulic

■ Liquid and gas flow: Darcy's law

$$\begin{array}{l} q_l = -K_l (\nabla P_l - \rho_l g) \\ q_g = -K_g (\nabla P_g - \rho_g g) \end{array}$$

□ Water and gas flow driven by **pressure gradients**

➤ **Permeability tensor**

$$K_\alpha = k k_{r\alpha} / \mu_\alpha$$

k : intrinsic permeability tensor

$k_{r\alpha}$: relative permeability

μ_α : dynamic viscosity

➤ **Relative permeability**

$$k_{rl} = f(S_l) \quad \text{or} \quad k_{rl} = f(P_g - P_l)$$

$$k_{rg} = 1 - k_{rl}$$

□ **Permeability depends on**

➤ Temperature (water viscosity) (**Thermal**)

➤ Degree of saturation (relative permeability) (**Hydraulic**)

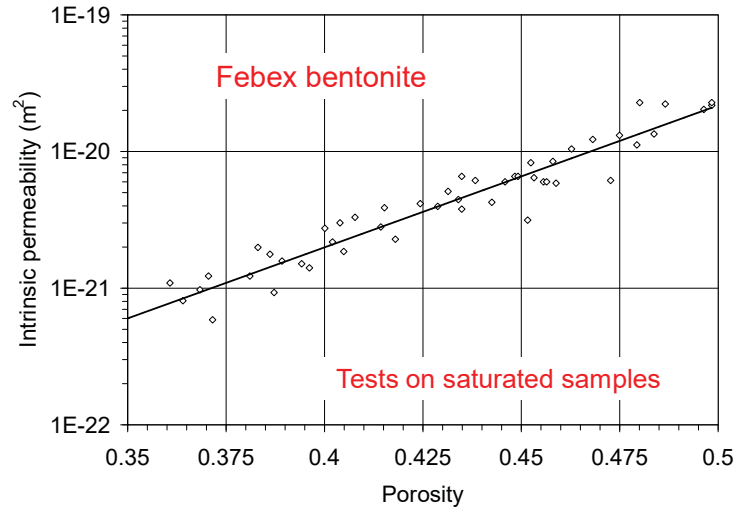
➤ Porosity (intrinsic permeability) (**Mechanical**)

Date

60

Constitutive relations: hydraulic

- Intrinsic permeability: dependence on porosity (or dry density)



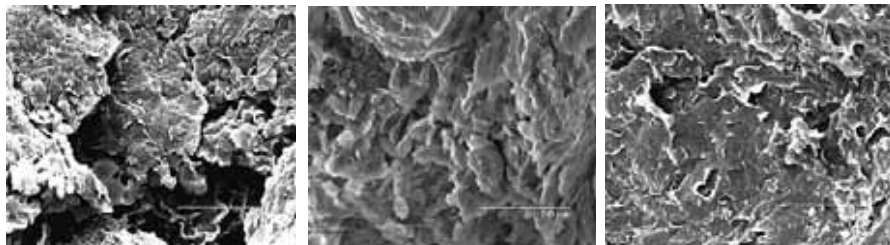
Date

Kozeny's law $k = k_0 \frac{\phi^3}{(1-\phi)^2} \frac{\phi_0^3}{(1-\phi_0)^2}$

61

Constitutive relations: hydraulic

- In fact, intrinsic permeability depends on pore size (and interconnectivity of pores)
- Pore size of expansive clays may change very significantly due to hydration (even under constant volume conditions)



Compacted (suction \approx 110 MPa)

Suction = 10 MPa

Saturated

Evolution of compacted FEBEX bentonite microstructure during hydration. Constant volume test

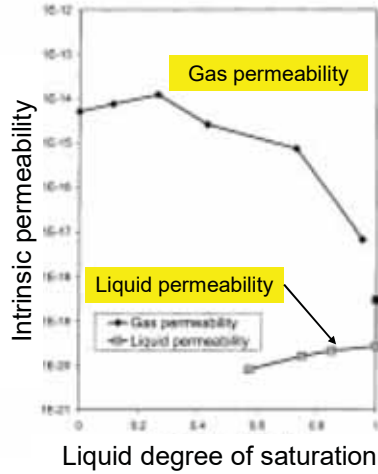
Date

62

Constitutive relations: hydraulic

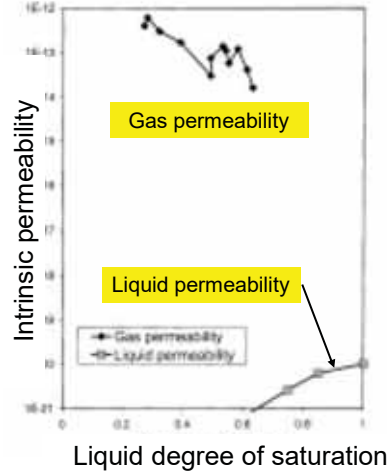
➤ Gas and liquid intrinsic permeability

- Differences cannot be accounted for by Knudsen/Klickenberg enhancement



Boom clay
(Volckaert et al. 1994)

Date



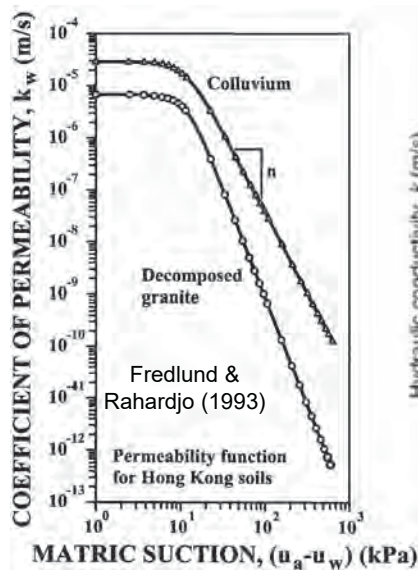
FEBEX bentonite
(Villar 1998)

63

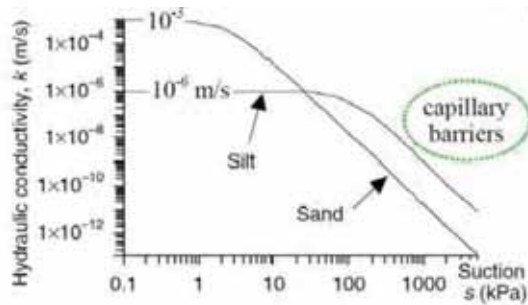
Constitutive relations: hydraulic

➤ Relative permeability

$$K_{\alpha} = k k_{r\alpha} / \mu_{\alpha}$$



Date



64

Constitutive relations: hydraulic

➤ Relative permeability

- Gardner (1958)

$$K_w = \frac{a}{b + |e|^{2m}}$$

a, b and m are constants,
 $m \approx 2$ for heavy clay soil,
 $m \approx 4$ for sand.

He also suggested the exponential model

$$K_w = K_{sat} e^{-\alpha e}$$

α is a soil index parameter,
 related to pore size distribution,

- Childs and Collis-George (1950)

$$K_w = B \frac{\theta^3}{S_e}$$

S_e is the specific surface area of the soil,
 B is a coefficient.

- Irimay (1954)

$$K_w(S_w) = K_{sat} (S_e)^3 \cong K_{sat} \left(\frac{S_w - S_r}{1 - S_r} \right)^3$$

S_e is the effective water saturation

- Corey (1957): proportional to $(S_e)^{2-2\lambda}$

- Brooks and Corey (1964, 1966)

$$k_w = k_{sat} \left(\frac{u_w - u_w}{u_w - u_w} \right)^{\frac{2+3\lambda}{\lambda}}$$

λ = index of the pore-size distribution

- Van Genuchten (1980)

$$K_w = K_{sat} S_e^3 \left[1 - (1 - S_e^{\frac{1}{m}})^m \right]^2$$

m is the same coefficient

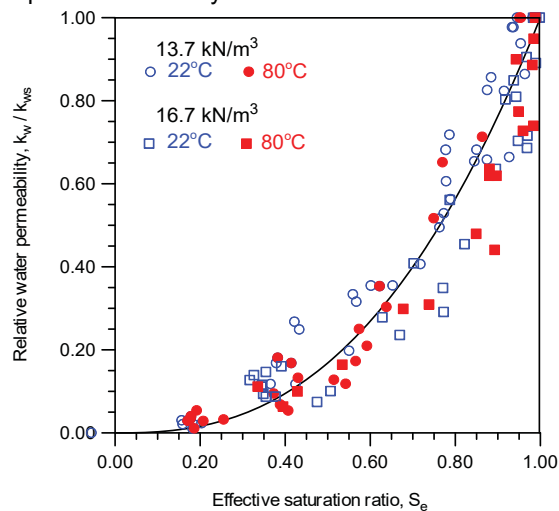
Date

65

Constitutive relations: hydraulic

○ Relative water permeability vs. degree of saturation at two different temperatures

- Tests on compacted Boom clay



Date

(Romero, Gens & Lloret, 2001)

66

Constitutive relations: hydraulic

○ Liquid flow

- Liquid permeability (hydraulic conductivity) dependence on temperature

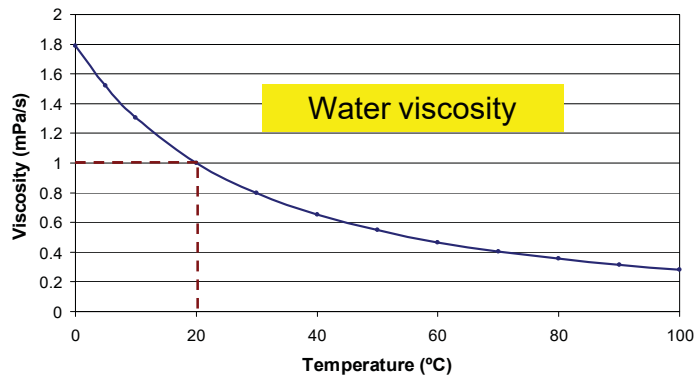
$$\mathbf{q}_l = -\mathbf{K}_l (\nabla P_l - \rho_l \mathbf{g})$$

k : intrinsic permeability tensor

Permeability tensor $\mathbf{K}_l = k k_r / \mu_l(T)$

k_r : relative permeability

μ_l : dynamic viscosity (depends on temperature)

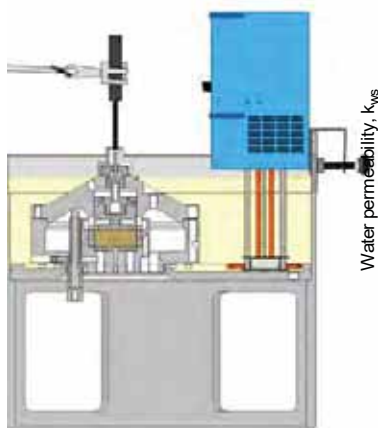


Date

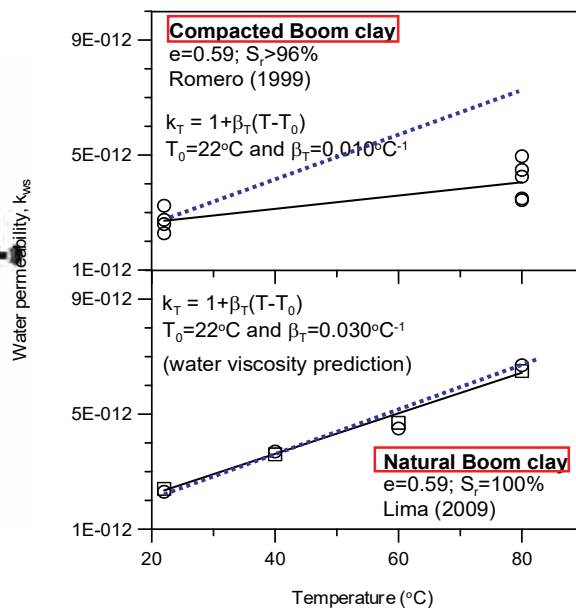
67

Constitutive relations: hydraulic

○ Dependence of water permeability on temperature



Lima (2009)
Date



68

Constitutive relations: hydraulic

○ Dependence of permeability with temperature

$$K_l(T) / K_l(T_0) = 1 + \beta_T(T - T_0)$$

Material	$\beta_T(K^{-1})$	Reference
Compacted Boom clay	0.010	Romero et al. (2001)
Natural Boom clay	0.030	Lima (2009)
Saturated kaolinite	0.042	Towhata et al., (1993)
Saturated kaolinite	0.010	Kemissa (1998)
Saturated montmorillonite	0.014	Volckaert et al. (1996)
Saturated bentonite	0.010	Cho et al. (1999)

Date

69

Constitutive relations: hydraulic

○ Gas flow

- Gas permeability (conductivity) dependence on temperature

$$\mathbf{q}_g = -\mathbf{K}_g(\nabla P_g - \rho_g \mathbf{g})$$

k : intrinsic permeability tensor

k_r : relative permeability

Permeability tensor $\mathbf{K}_l = k k_r / \mu_l(T)$

μ_l : dynamic viscosity (depends on temperature)

○ Gas viscosity

- Gas viscosity *increases* with temperature at low and moderate pressures

Gas viscosity (10^{-5} Pa s)

	Temperature				
	0°C	20°C	50°C	100°C	200°C
Water	1.73	1.82	1.96	2.20	2.61
Vapour (steam)	0.92	0.97	1.06	1.24	1.62

70

Constitutive relations: hydraulic

- Concentration of water vapour (psychrometric law)

$$\theta_g^w = (\theta_g^w)^0 \exp\left(\frac{\psi M_w}{R(273.15 + T)\rho_l}\right)$$

Vapour concentration with no capillary effects (depends on temperature and concentration)

Modification of vapour concentration due to capillary effects (depends on suction and temperature)

θ_g^w : vapour density in the gaseous phase

ψ : water potential

T : temperature

$(\theta_g^w)^0$: vapour density in the gaseous phase ($P_g - P_l = 0$)

M_w : molecular mass of water (0.018 kg/mol)

R : the gas constant (8.314 J/mol/°K)

□ Concentration of water vapour depends on:

- Temperature (water viscosity) (**Thermal**)
- Suction (**Hydraulic**)

Date

71

Constitutive relations: hydraulic

- Vapour diffusion: Fick's law

$$\mathbf{i}_g^w = -\mathbf{D}_g^w \nabla \omega_g^w = -(\tau \phi S_g \rho_g D_m^w \mathbf{I} + \rho_g \mathbf{D}'_g) \nabla \omega_g^w$$

□ Vapour diffusion driven by **concentration (partial pressure) gradients**

i_g^w : non advective flux of water in gas

D_g^w : dispersion tensor

ω_g^w : mass fraction of water in gas

τ : tortuosity

D'_g : mechanical dispersion tensor

D_m^w : dispersion coefficient corresponding to molecular diffusion of vapour in air

□ Retention curve depends on

- Temperature (**Thermal**)
- Degree of saturation (**Hydraulic**)
- Porosity (**Mechanical**)

$$D_m^w (m^2 / s) = 5.9 \times 10^{-12} \frac{(273.15 + T)^{2.3}}{P_g}$$

Date

72

Constitutive relations: hydraulic

- Solubility of air in water (Henry's law)

$$\theta_l^a = \omega_l^a \rho_l = \frac{P_a}{H} \frac{M_a}{M_w} \rho_l$$

ω_l^a : mass fraction of air in liquid ($\theta_l^a = \omega_l^a \rho_l$)

P_a : partial pressure of air

M_a : molecular mass of air (0.02895 kg/mol)

H : 10000 MPa, Henry's constant

- Air dissolved depends on air pressure

Date

73

Constitutive relations: hydraulic

○ Liquid density

- Dependence on pressure

$$-\frac{1}{\rho} \frac{d\rho}{dP} = -\beta \quad \beta = 5 \times 10^{-4} \text{ MPa}^{-1}$$

- Dependence on temperature

$$-\frac{1}{\rho} \frac{d\rho}{dT} = -\alpha$$

- Dependence on solute

$$-\frac{1}{\rho} \frac{d\rho}{dc} = -\gamma \quad \gamma = \ln 2 (\text{ClNa})$$

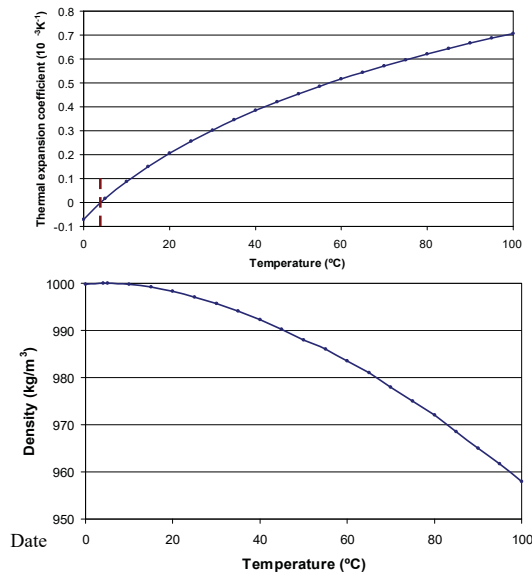
Date

74

Constitutive relations: hydraulic

○ Liquid density (dependence on temperature)

- Thermal expansion coefficient of water



$$\alpha = -\frac{1}{\rho} \frac{\partial \rho}{\partial T}$$

75

Constitutive relations: hydraulic

○ Gas density

- Ideal gas law

$$pV = NRT$$

- ❖ Neglects molecular size effects and inter-molecular attractions

$$pV = \frac{m}{M} RT ; p = \frac{mRT}{VM} ; p = \rho \frac{R}{M} T$$

$$\rho = \frac{M}{R} \frac{p}{T}$$

- N : number of moles
- R : universal gas constant (8.31446261815324 J K⁻¹ mol⁻¹, since 2019)
- M : molecular mass

Date

76

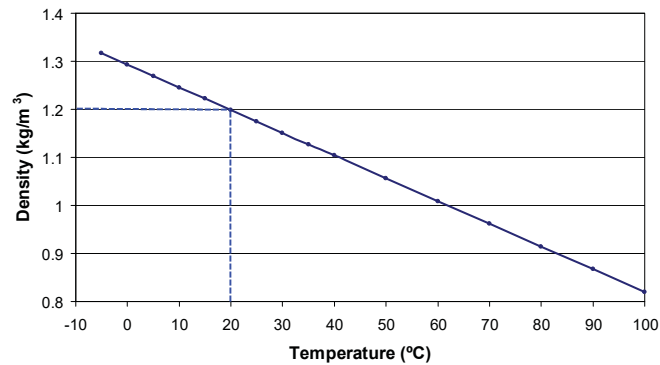
Constitutive relations: hydraulic

○ Gas density

➤ Ideal gases $pV = nRT$ $\rho_g = \frac{M p}{RT}$

P : pressure n : number of moles T : temperature

R : gas constant (8.314 J/mol K) M : molar mass



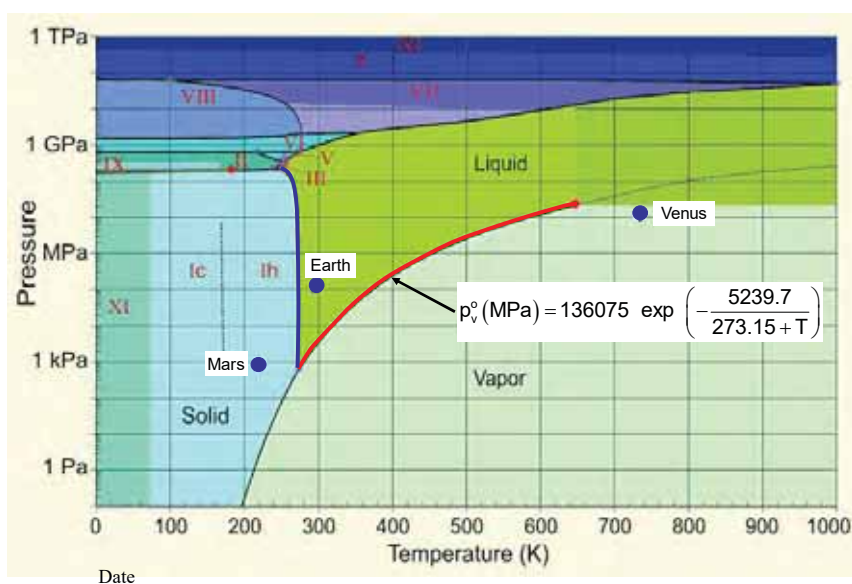
At 20°C and 101.325 kPa, dry air has a density of 1.2041 kg/m³

At 0°C and 100 kPa, dry air has a density of 1.2754 kg/m³ (IUPAC standard)

77

Constitutive relations: hydraulic

□ Phase diagram of pure water



78

Constitutive relations: hydraulic

□ What happens above 100°C?

- The formulation involves the simultaneous consideration of:
 - Retention curve
 - Vapour pressure (density) dependence on temperature (phase diagram)
 - Vapour pressure (density) dependence on water potential (psychrometric law)
 - Surface tension dependence on temperature (retention curve)

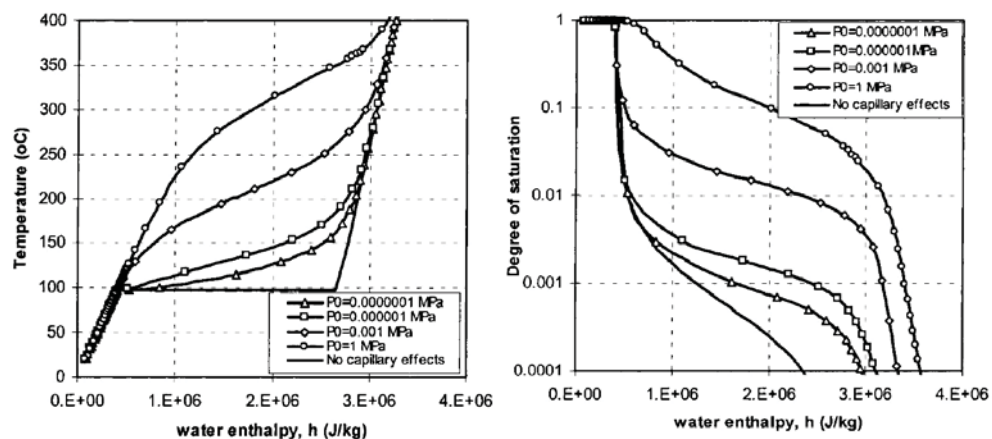
Olivella, S., Gens, A. (2000). "Vapour transport in low permeability unsaturated soils with capillary effects". *Transport in Porous Media*, 40:219-241.

Date

79

Constitutive relations: hydraulic

□ What happens above 100°C?



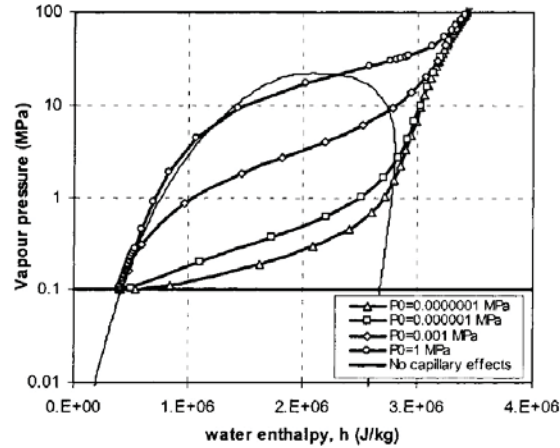
- Soil initially saturated
- Liquid pressure constant: 0.1 MPa

Date

80

Constitutive relations: hydraulic

- What happens above 100°C?



$$p_g = p_a + p_v$$

- If gas pressure is assumed constant (0.1 MPa), air pressure may become (implicitly) negative

81

Outline of the lecture

- Introduction. Relevant phenomena
- Unsaturated geomaterials and suction
- Constitutive relations
 - General
 - Thermal
 - Hydraulic
 - Mechanical
- Governing equations
- Concluding remarks

Date

82

Constitutive relations: mechanical

■ Stress/strain constitutive law

$$d\sigma = Dd\varepsilon + \beta dT + hds$$

σ : net stresses ($\sigma^* - P_g m$)

σ^* : total stresses

P_g : gas pressure

P_l : liquid pressure

T : temperature

m^T : auxiliary vector [1,1,1,0,0,0]

$s = (P_g - P_l)$: capillary suction

ε : strain tensor

D : constitutive stiffness matrix

β : constitutive vector temperature-net stresses

h : constitutive vector suction-net stresses

□ Constitutive equation:

Thermo-elasto-plastic model for unsaturated soils

□ Mechanical constitutive law depends on:

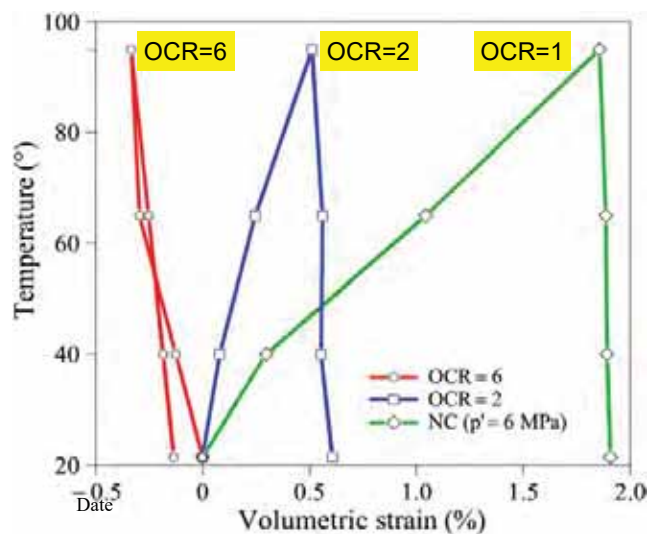
- Temperature (**Thermal**)
- Suction (**Hydraulic**)
- Stress/Strain (**Mechanical**)

Date

83

Constitutive relations: mechanical

➤ Effect of temperature and OCR on volume change



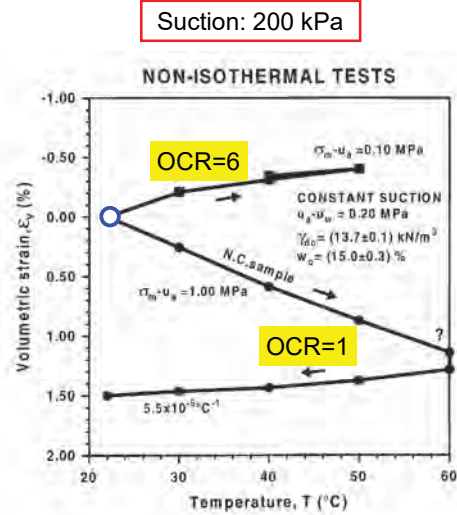
Tests on saturated Boom Clay

(Baldi et al., 1991)

84

Constitutive relations: mechanical

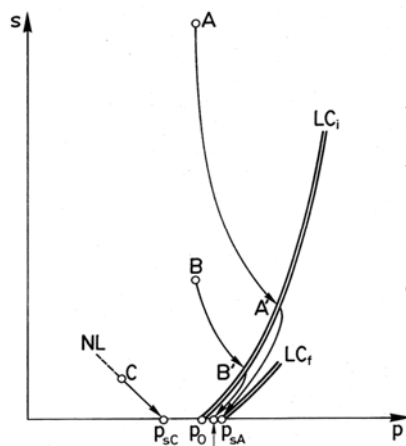
- Non isothermal test on compacted Boom clay under constant suction



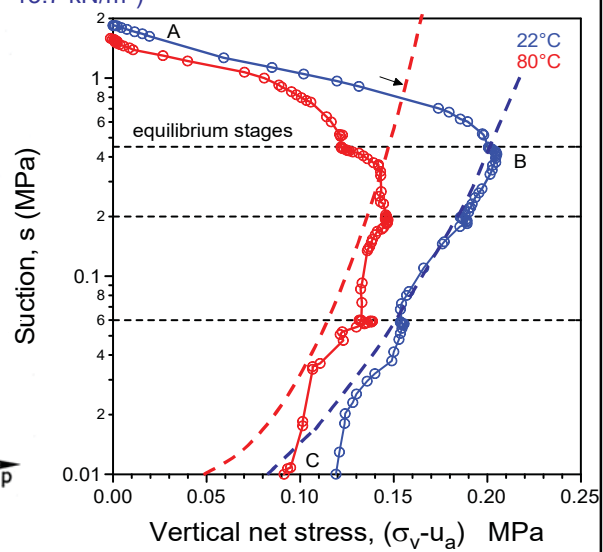
85

Constitutive relations: mechanical

- Swelling pressure tests
 - Compacted Boom clay ($\gamma_d = 13.7 \text{ kN/m}^3$)



Gens & Alonso (1992)
Date



(Romero, Gens & Lloret, 2003)

86

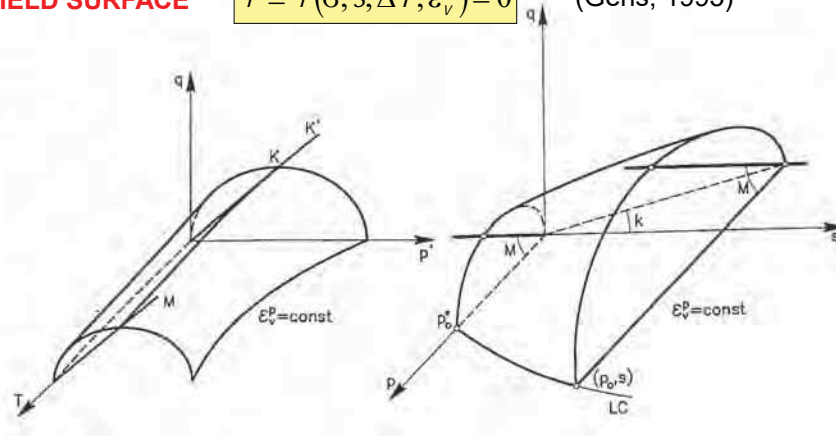
Constitutive relations: mechanical

- Thermomechanical constitutive model for unsaturated soils

YIELD SURFACE

$$f \equiv f(\sigma, s, \Delta T, \varepsilon_v^p) = 0$$

(Gens, 1995)



Section at constant suction

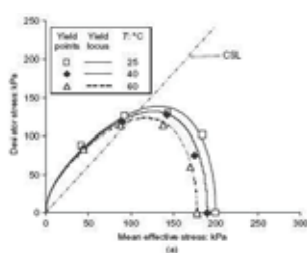
Section at constant temperature

$$d\sigma_{\text{Dare}}^* = D(\varepsilon, s, T)(d\varepsilon) + h(\varepsilon, s, T)ds + \beta(\varepsilon, s, T)dT$$

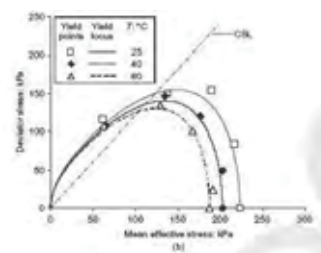
87

Constitutive relations: mechanical

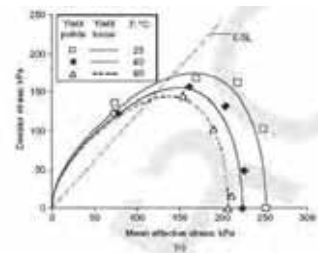
- Temperature effects in unsaturated soils
 - Tests on laboratory compacted silt



s=0 kPa



s=100 kPa



s=300 kPa

(Uchaipichat & Khalili, 2009)

Date

88

Constitutive relations: general

EQUATION	VARIABLE NAME	VARIABLE
<i>Constitutive equations</i>		
Fourier's law	conductive heat flux	i_c
Darcy's law	liquid and gas advective flux	q_l, q_g
Retention curve	liquid phase degree of saturation	S_l, S_g
Fick's law	vapour and air non-advective fluxes	i_g^w, i_l^a
Mechanical constitutive model	stress tensor	σ
Phase density	liquid density	ρ_l
Gases law	gas density	ρ_g
<i>Equilibrium restrictions</i>		
Psychrometric law	vapour mass fraction	ω_g^w
Henry's law	air dissolved mass fraction	ω_l^a

Date

89

Constitutive relations: general

○ Temperature effects are pervasive

- Heat conduction
- Retention curve
- Liquid and gas flow
- Partial density (pressure) of vapour
- Vapour diffusion
- Liquid density
- Gas density
- Mechanical behaviour (stress-strain and strength)

Date

90

Outline of the lecture

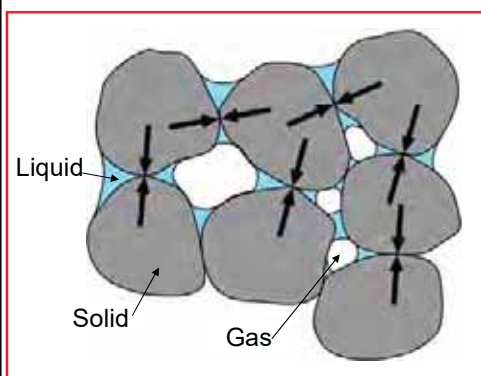
- ❑ Introduction. Relevant phenomena
- ❑ Unsaturated geomaterials and suction
- ❑ Constitutive relations
 - ❑ General
 - ❑ Thermal
 - ❑ Hydraulic
 - ❑ Mechanical
- ❑ Governing equations
- ❑ Concluding remarks

Date

91

Governing equations

Multiphase – Multispecies approach



The three **phases** are:

- **solid** (*s*) : mineral
- **liquid** (*l*) : water + air dissolved
- **gas** (*g*) : dry air + water vapour

The three **species** are:

- **mineral** (*-*) : the mineral is coincident with solid
- **water** (*w*) : as liquid or evaporated in the gas phase
- **air** (*a*) : dry air, as gas or dissolved in the liquid phase

Volumetric mass of a species in a phase (e.g. water in gas phase θ_g^w is the product of the mass fraction of that species (ω_g^w) and the bulk density of the phase (ρ_g):

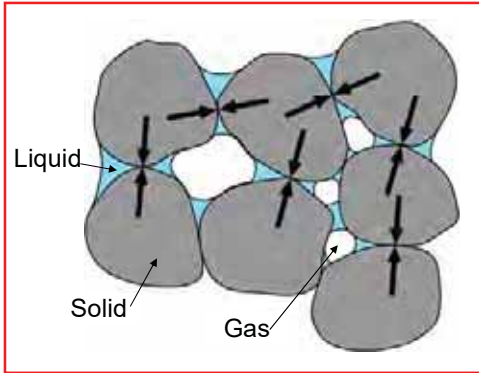
Date

$$\theta_g^w = \omega_g^w \rho_g.$$

92

Governing equations

Multiphase – Multispecies approach



The three **phases** are:

- **solid** (*s*) : mineral
- **liquid** (*l*) : water + air dissolved
- **gas** (*g*) : dry air + water vapour

The three **species** are:

- **mineral** (-) : the mineral is coincident with solid
- **water** (*w*) : as liquid or evaporated in the gas phase
- **air** (*a*) : dry air, as gas or dissolved in the liquid phase

Partial density $\rho_g = \theta_g^a + \theta_g^w$

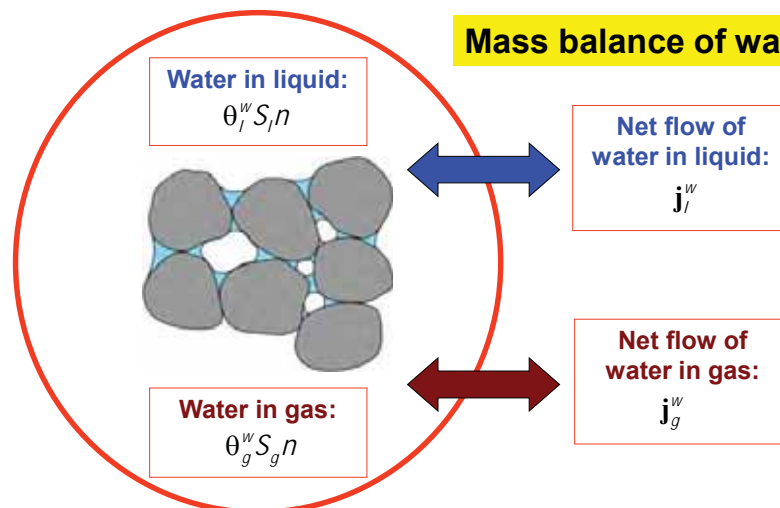
Date

Example (1% vapour): $1,200 \text{ g/m}^3 = 1,188 \text{ g/m}^3 + 12 \text{ g/m}^3$

93

Governing equations

Mass balance of water



Date
$$\frac{\partial}{\partial t} \left(\text{mass of water in liquid and gas phases} \right) + \text{divergence} \left(\text{total flows of water} \right) = \left(\text{external supply of water} \right)$$

$$\frac{\partial}{\partial t} (\theta_l^w S_l n + \theta_g^w S_g n) + \nabla \cdot (\mathbf{j}_l^w + \mathbf{j}_g^w) = f^w$$

94

Governing equations

- Energy conservation

$$dU = \partial Q + \partial W$$

- Gases

$$dU = \partial Q - PdV$$

$$dU = TdS - PdV \quad (\text{reversible processes})$$

- General

$$dU = \partial Q + \partial W + \sum_i \mu_i dN_i$$

$$dU = \partial Q + \sum_i X_i dx_i + \sum_i \mu_i dN_i$$

Date

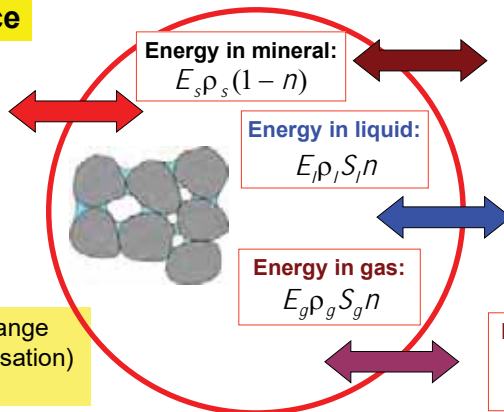
$$d \left(\begin{array}{l} \text{internal energy in solid,} \\ \text{liquid and gas phases} \end{array} \right) = d(\text{supply of heat})$$

95

Governing equations

Energy balance

Net flow of energy
by conduction
 i_c



Includes phase change
(vaporisation/condensation)
latent heat

$$\frac{\partial}{\partial t} \left(\begin{array}{l} \text{internal energy in solid,} \\ \text{liquid and gas phases} \end{array} \right) + \text{divergence} \left(\begin{array}{l} \text{total flows of} \\ \text{heat} \end{array} \right) = \left(\begin{array}{l} \text{internal/external} \\ \text{supply of energy} \end{array} \right)$$

$$\frac{\partial}{\partial t} (E_s \rho_s (1-n) + E_l \rho_l S_l n + E_g \rho_g S_g n) + \nabla \cdot (\mathbf{i}_c + \mathbf{j}_{Es} + \mathbf{j}_{El} + \mathbf{j}_{Eg}) = f^Q$$

Date

96

Governing equations

MASS BALANCE OF SOLID

$$\frac{\partial}{\partial t}(\theta_s(1-\phi)) + \nabla \cdot (\mathbf{j}_s) = 0$$

MASS BALANCE OF WATER

$$\frac{\partial}{\partial t}(\theta_g^w S_g \phi + \theta_g^w S_g \phi) + \nabla \cdot (\mathbf{j}_g^w + \mathbf{j}_g^w) = f^w$$

MASS BALANCE OF AIR

$$\frac{\partial}{\partial t}(\theta_g^a S_g \phi + \theta_g^a S_g \phi) + \nabla \cdot (\mathbf{j}_g^a + \mathbf{j}_g^a) = f^a$$

INTERNAL ENERGY BALANCE FOR THE MEDIUM

$$\frac{\partial}{\partial t}(E_s \rho_s (1-\phi) + E_l \rho_l S_g \phi + E_g \rho_g S_g \phi) + \nabla \cdot (\mathbf{i}_c + \mathbf{j}_{Es} + \mathbf{j}_{El} + \mathbf{j}_{Eg}) = f^Q$$

MOMENTUM BALANCE FOR THE MEDIUM

$$\nabla \cdot \boldsymbol{\sigma} + \mathbf{b} = \mathbf{0}$$

97

Governing equations

FLUX COMPONENTS

THE TOTAL MASS FLUX OF A SPECIES IN A PHASE (E.G. FLUX OF WATER PRESENT IN GAS PHASE, \mathbf{j}_g^w) IS, IN GENERAL, THE SUM OF THREE TERMS:

the nonadvective flux: \mathbf{i}_g^w , i.e. diffusive/ dispersive	\mathbf{i}_g^w →
the advective flux caused by fluid motion: $\theta_g^w \mathbf{q}_g$, where \mathbf{q}_g is the Darcy's flux	$\theta_g^w \mathbf{q}_g$ →
the advective flux caused by solid motion: $\phi S_g \theta_g^w \mathbf{du}/dt$ where \mathbf{du}/dt is the vector of solid velocities	$\phi S_g \theta_g^w \mathbf{du}/dt$ →
Total flux is obtained simply by:	
$\phi S_g \theta_g^w \mathbf{du}/dt \quad \theta_g^w \mathbf{q}_g \quad \mathbf{i}_g^w$	
$\mathbf{j}_g^w = \mathbf{i}_g^w + \theta_g^w \mathbf{q}_g + \phi S_g \theta_g^w \mathbf{du}/dt = \mathbf{j}_g^w + \phi S_g \theta_g^w \mathbf{du}/dt$	

Date

98

Governing equations

- The material derivative with respect to the solid velocity is very useful to obtain the final expressions of the governing equations

$$\frac{D_s(\cdot)}{Dt} = \frac{\partial(\cdot)}{\partial t} + \dot{\mathbf{u}} \nabla(\cdot)$$

- For instance, the water mass balance equation becomes:

$$\phi \frac{D_s(\theta_l^w S_l + \theta_g^w S_g)}{Dt} + (\theta_l^w S_l + \theta_g^w S_g) \frac{D_s \phi}{Dt} + ((\theta_l^w S_l + \theta_g^w S_g) \phi) \nabla \cdot \frac{d\mathbf{u}}{dt} + \nabla \cdot (\mathbf{j}_l^w + \mathbf{j}_g^w) = f^w$$

- The solid mass balance equation is removed from the system, being replaced by a porosity evolution equation:

$$\frac{D_s \phi}{Dt} = \frac{1}{\theta_s} \left[(1 - \phi) \frac{D_s \theta_s}{Dt} \right] + (1 - \phi) \nabla \cdot \frac{d\mathbf{u}}{dt}$$

Olivella, S., Carrera, J., Gens, A., and Alonso, E.E. (1994). "Non-isothermal Multiphase Flow of Brine and Gas through Saline media", *Transport in porous media*, 15: 271-293.

Date

99

Governing equations

MASS BALANCE OF WATER. Unknown: P_l

$$\phi \frac{D_s(\theta_l^w S_l + \theta_g^w S_g)}{Dt} + (\theta_l^w S_l + \theta_g^w S_g) \frac{D_s \phi}{Dt} + ((\theta_l^w S_l + \theta_g^w S_g) \phi) \nabla \cdot \frac{d\mathbf{u}}{dt} + \nabla \cdot (\mathbf{j}_l^w + \mathbf{j}_g^w) = f^w$$

MASS BALANCE OF AIR. Unknown: P_g

$$\phi \frac{D_s(\theta_l^a S_l + \theta_g^a S_g)}{Dt} + (\theta_l^a S_l + \theta_g^a S_g) \frac{D_s \phi}{Dt} + ((\theta_l^a S_l + \theta_g^a S_g) \phi) \nabla \cdot \frac{d\mathbf{u}}{dt} + \nabla \cdot (\mathbf{j}_l^a + \mathbf{j}_g^a) = f^a$$

INTERNAL ENERGY BALANCE FOR THE MEDIUM. Unknown: T

$$\phi \frac{D_s(E_l \rho_l S_l + E_g \rho_g S_g)}{Dt} + (1 - \phi) \frac{D_s(E_s \rho_s)}{Dt} + (E_l \rho_l S_l + E_g \rho_g S_g) \nabla \cdot \frac{d\mathbf{u}}{dt} + \nabla \cdot (\mathbf{i}_c + \mathbf{j}'_{Es} + \mathbf{j}'_{El} + \mathbf{j}'_{Eg}) = f^E$$

MOMENTUM BALANCE FOR THE MEDIUM. Unknown: \mathbf{u}

$$\nabla \cdot \boldsymbol{\sigma} + \mathbf{b} = \mathbf{0}$$

Date

100

Numerical implementation

CODE_BRIGHT

■ Finite elements in space

- Different types of elements available (1D, 2D, 3D)
- Element-wise, modified cell-wise and node-wise elements
- Secant method for non advective terms

■ Finite differences in time

- Storage terms (mass conservative approach)
- Implicit scheme
- Full Newton Raphson method to solve nonlinearities

■ Other numerical features

- Simultaneous solution of all THM equations
- Direct and iterative solver
- Sequential and parallel versions
- Convergence tolerance in terms of variable corrections and residuals

Olivella, S., Gens, A., Carrera, J., and Alonso, E.E. (1996). "Numerical formulation for a simulator (CODE-BRIGHT) for the coupled analysis of saline media" Engineering Computations, 13:87-112.

101

Concluding remarks

High-level nuclear waste is fun!

- Relatively abundant resources: underground laboratories, large scale in situ tests, intensive monitoring, extensive laboratory testing programmes
- Challenging problems involving a large number of coupled THM (and C and B) phenomena. Coupled formulations coupled need to be developed in a multi-physics framework
- Formulations are a combination of governing equations (establishing basic physical principles) and appropriate constitutive relations (that incorporate couplings)
- Grounded on sound physical principles and understanding (required for long term extrapolation)
- Formulations can then be introduced in computer codes to perform coupled THM analyses to simulate a wide variety of rad waste problem
- Adaptations of the formulations may be required to take into account the specific features of each particular case

Date

102

References

- Sánchez, M., Gens, A., Villar, M.V., Olivella, S. (2016). Fully Coupled Thermo-Hydro-Mechanical Double-Porosity Formulation for Unsaturated Soils. *International Journal of Geomechanics*, 16 (6), D4016015, 1-17. doi:10.1061/(ASCE)GM.1943-5622.0000728
- Garitte, B., Gens, A., Vaunat, J., Armand, G. (2014). Thermal conductivity of argillaceous rocks: Determination methodology using in situ heating tests. *Rock Mechanics and Rock Engineering*, 47 (1), 111-129.
- Sánchez, M., Gens, A., Guimaraes, L. (2012). Thermal-hydraulic-mechanical (THM) behaviour of a large-scale in situ heating experiment during cooling and dismantling. *Canadian Geotechnical Journal*, 49:(10) 1169–1195, 10.1139/t2012-076
- Zandarin M.T., Gens A., Olivella S., Alonso E.E. (2011). Thermo-hydro-mechanical model of the Canister Retrieval Test. *J. Phys. Chem. Earth*, 36, 1806-1816. doi:10.1016/j.pce.2011.10.009
- Gens, A. (2010). "Soil-environment interactions in geotechnical engineering. 47th Rankine Lecture". *Geotechnique*, 60, 3-74
- Gens, A., Guimarães, L. do N., Sánchez, M., Olivella, S. (2010). "Modelling thermo-hydro-mechanical-chemical interactions for nuclear waste disposal". *Journal of Rock Mechanics and Geotechnical Engineering*, 2, No 2, 97-102
- Gens A., Garitte, B., Olivella, S., Vaunat, J. (2009). "Application of multiphysical geomechanics un underground nuclear waste storage". *European Journal of Environmental and Civil Engineering*, 13, No 7-8, 937-962
- Gens A., Sánchez, M., Guimarães, L. do N., Alonso, E.E., Lloret, A., Olivella, S., Villar, M.V., Huertas, F. (2009). "A full-scale in situ heating test for high-level nuclear waste disposal: observations, analysis and interpretation". *Geotechnique*, 59, 377-399
- Sheng, D., Gens, A., Fredlund D.G., Sloan, S.W. (2008). "Unsaturated soils: From constitutive modelling to numerical algorithms". *Computers and Geotechnics*, 35 (6), 810-824.
- Villar M.V., Sánchez, M., Gens, A. (2008). "Behaviour of a bentonite barrier in the laboratory: Experimental results up to 8 years and numerical simulation". *Physics and Chemistry of the Earth*, 33, S476-S485.
- Gens, A., Vaunat, J., Garitte, B. & Wileveau, Y. (2007). "In situ behaviour of a stiff layered clay subject to thermal loading: observations and interpretation". *Geotechnique*, 57, 207-228.
- Guimaraes, L. do N., Gens, A., Olivella, S. (2007). "Coupled thermo-hydro-mechanical and chemical analysis of expansive clay subjected to heating and hydration". *Transport in porous media*, 66: 341-372
- Gens, A., Sánchez, M., Sheng, D. (2006). "On constitutive modelling of unsaturated soils". *Acta Geotechnica*, 1: 137-147.
- Guimaraes, L. do N., Gens, A., Sánchez, M., Olivella, S. (2006). "THM and reactive transport of expansive clay barrier". *Communications in Numerical Methods in Engineering*, 22: 849-859
- Gens, A., Guimaraes, L. do N., Olivella, S. (2005). "THMC coupling in partially saturated geomaterials". *Revue européenne de génie civil*, 9: 747-765.
- Olivella, S., Gens A. (2005). "Double structure THM analysis of a heating test in a fractured tuff incorporating intrinsic permeability variations". *International Journal of Rock Mechanics and Mining Sciences*, 42: 667-679

Date

103

References

- Gens, A., Olivella, S. (2001). "THM phenomena in saturated and unsaturated porous media". *Revue française de génie civil*, 5: 693-717.
- Gens, A., Olivella, S. (2001). "Clay barriers in radioactive waste disposal". *Revue française de génie civil*, 5: 845-856.
- Olivella, S., Gens, A. (2000). "Vapour transport in low permeability unsaturated soils with capillary effects". *Transport in Porous Media*, 40:219-241.
- Romero, E., Gens, A., Lloret, A. (1999). "Water permeability, water retention and microstructure of unsaturated compacted Boom clay" *Engineering Geology*, 54: 117-127.
- Gens, A., Garcia-Molina, A.J., Olivella, S., Alonso, E.E., Huertas, F. (1998). "Analysis of a full scale in situ test simulating repository conditions". *International Journal for Numerical and Analytical Methods in Geomechanics*, 22: 515-548.
- Olivella, S., Gens, A., Carrera, J., and Alonso, E.E. (1996). "Numerical formulation for a simulator (CODE-BRIGHT) for the coupled analysis of saline media" *Engineering Computations*, 13:87-112.
- Olivella, S., Carrera, J., Gens, A., and Alonso, E.E. (1994). "Non-isothermal Multiphase Flow of Brine and Gas through Saline media", *Transport in porous media*, 15: 271-293.

Date

104



FUNDAMENTALS ON GEOMECHANICS AND MULTI- PHYSICAL COUPLINGS

January 22, 2020 • Antonio Gens (UPC)




The project leading to this application has received funding from the European Union's Horizon 2020 research and innovation programme under grant agreement n° 847593.

Date




Appendix D. Fundamentals on geomechanics and multi-physical couplings - Application (A. Gens)




eurad
 European Joint Programme
 on Radioactive Waste Management

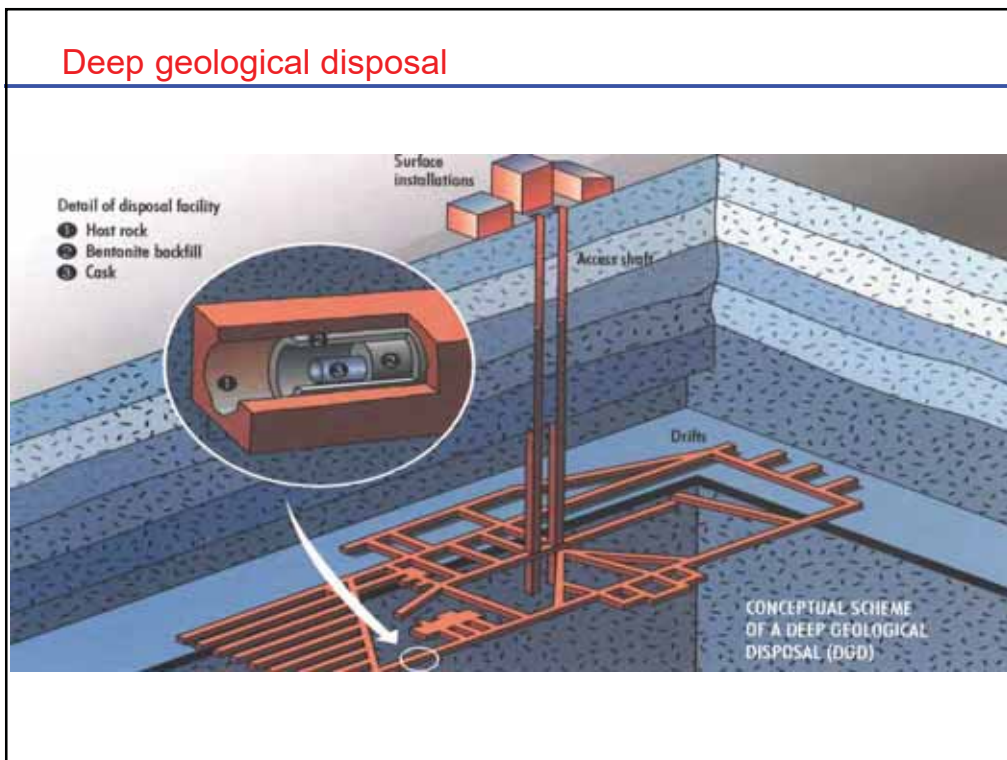
FUNDAMENTALS ON GEOMECHANICS AND MULTI- PHYSICAL COUPLINGS

January 22, 2020 • Antonio Gens (UPC)

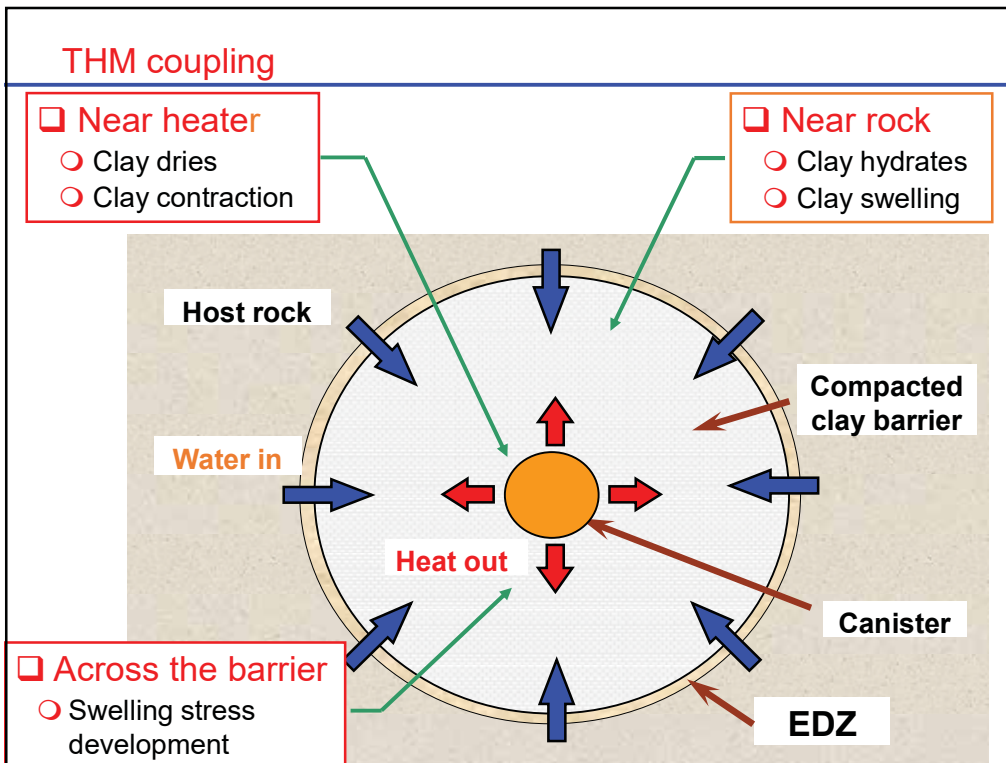

 The project leading to this application has received funding from the European Union's Horizon 2020 research and innovation programme under grant agreement n° 847593.



1



2



3

A field scale in situ heating test: FEBEX test

□ Grimsel Test Site

- Located in the Swiss Alps
- Granite
- 450 m deep
- Operating since 1983
- Generic, not purpose - built

4

A field scale in situ heating test: FEBEX test



5

A field scale in situ heating test: FEBEX test

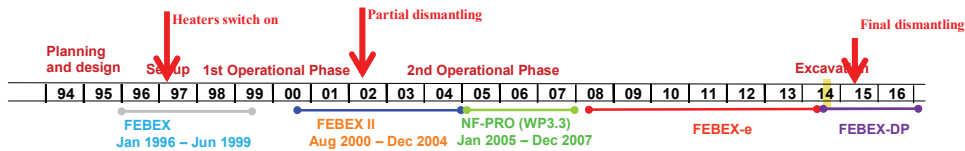


6

A field scale in situ heating test: FEBEX test

□ The FEBEX in situ Test

□ History of the test

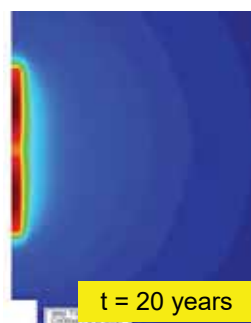
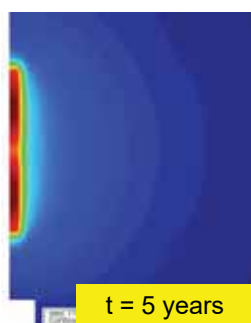
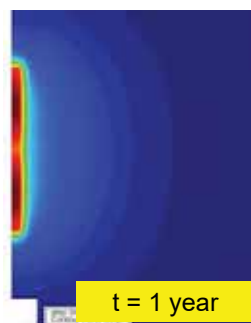


□ Important dates:

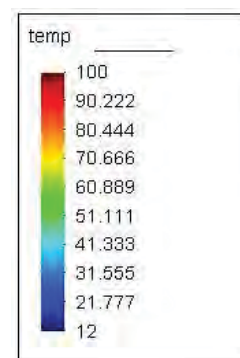
- Start of tunnel excavation: 25/09/1995
- End of tunnel excavation: 30/10/1995
- Start of installation: 01/07/1996
- End of installation: 15/10/1996
- Heaters switch on: 27/02/1997 (day zero)
- Heater #1 switch off: 28/02/2002
- End of first dismantling: 19/07/2002 (5 years)
- Heater #2 switch off: 20/04/2015
- End of final dismantling: 20/07/2015 (18 years)

7

A field scale in situ heating test: FEBEX test

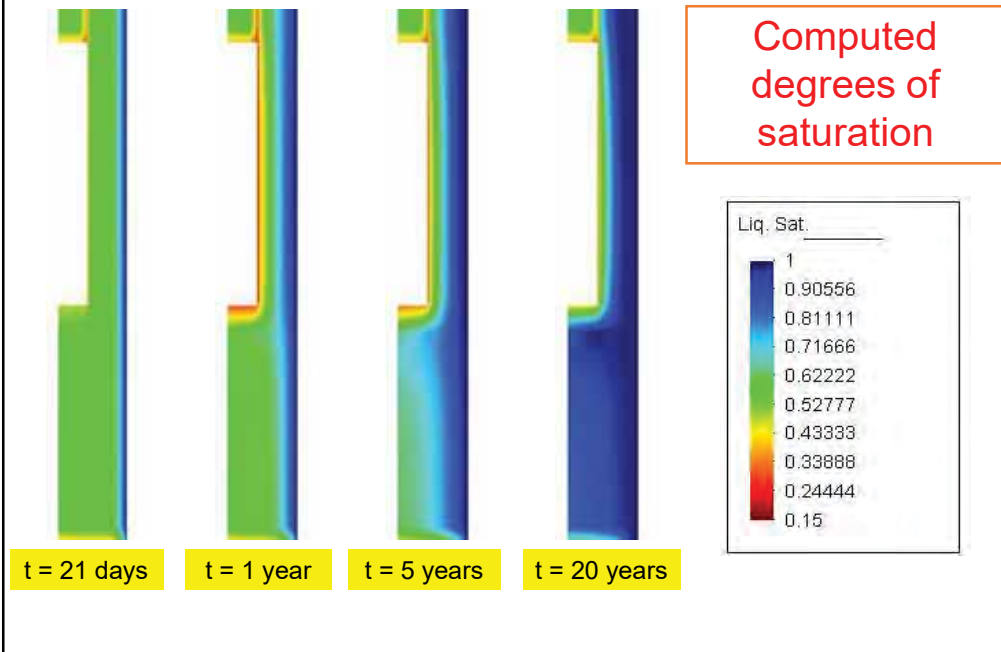


Computed temperatures



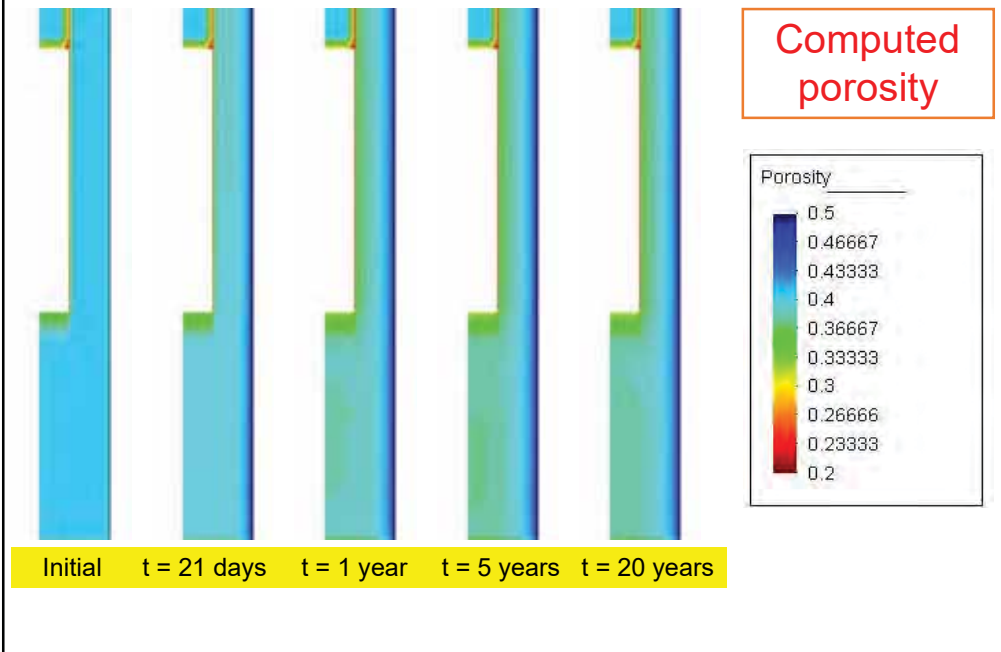
8

A field scale in situ heating test: FEBEX test

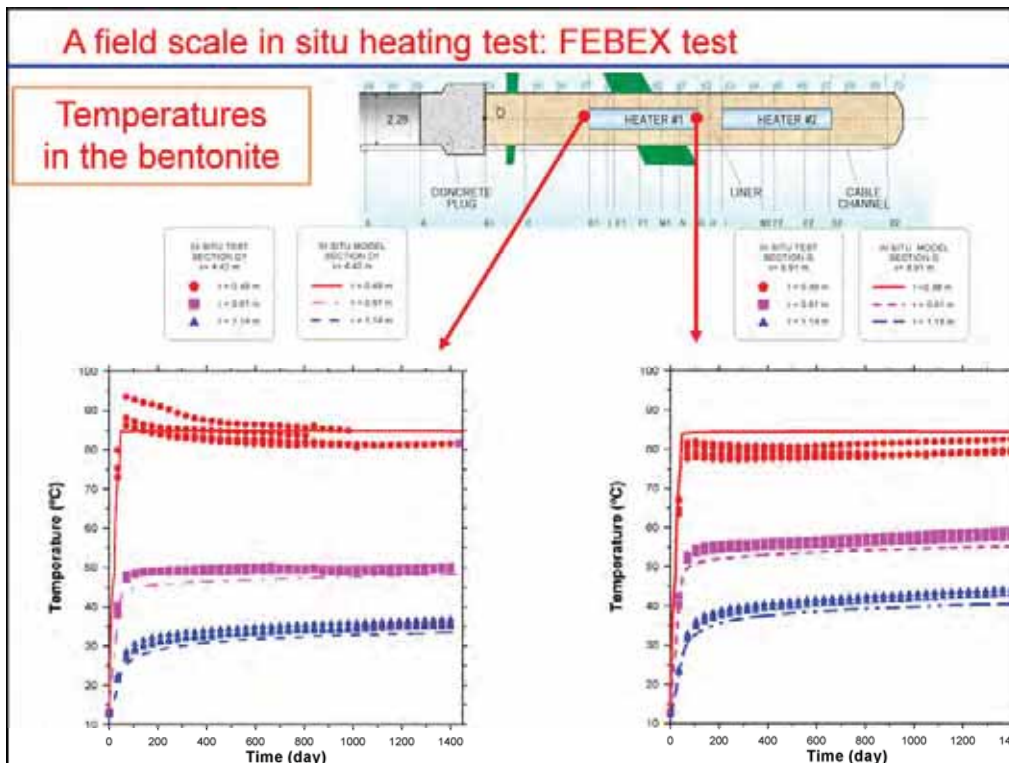


9

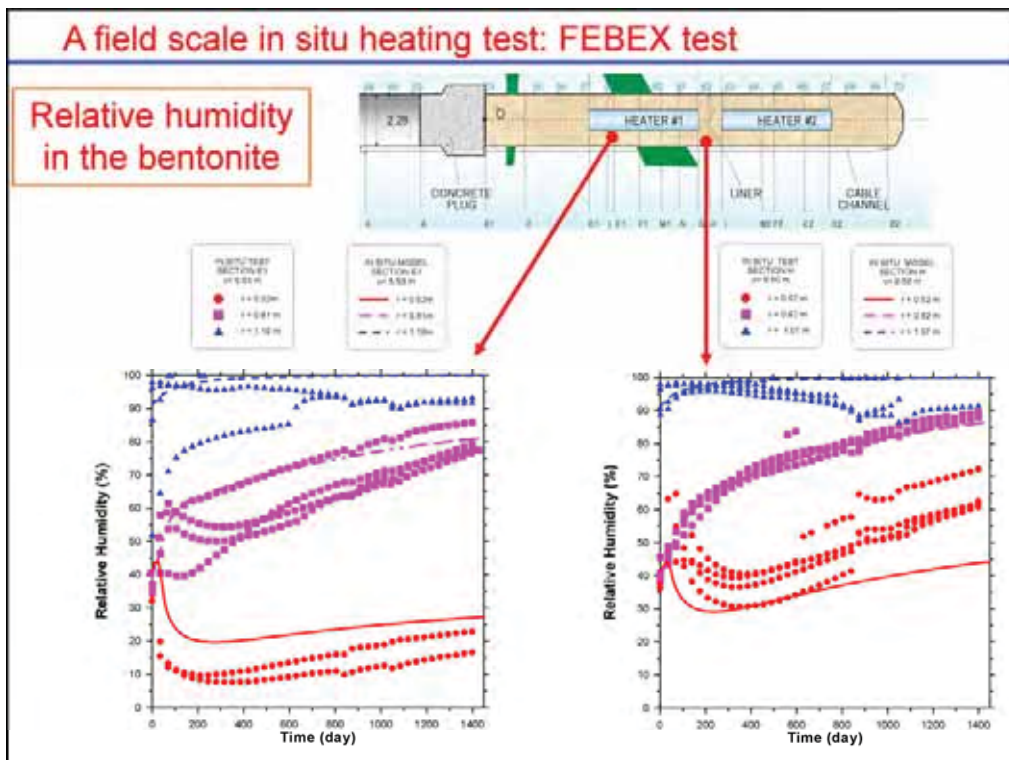
A field scale in situ heating test: FEBEX test



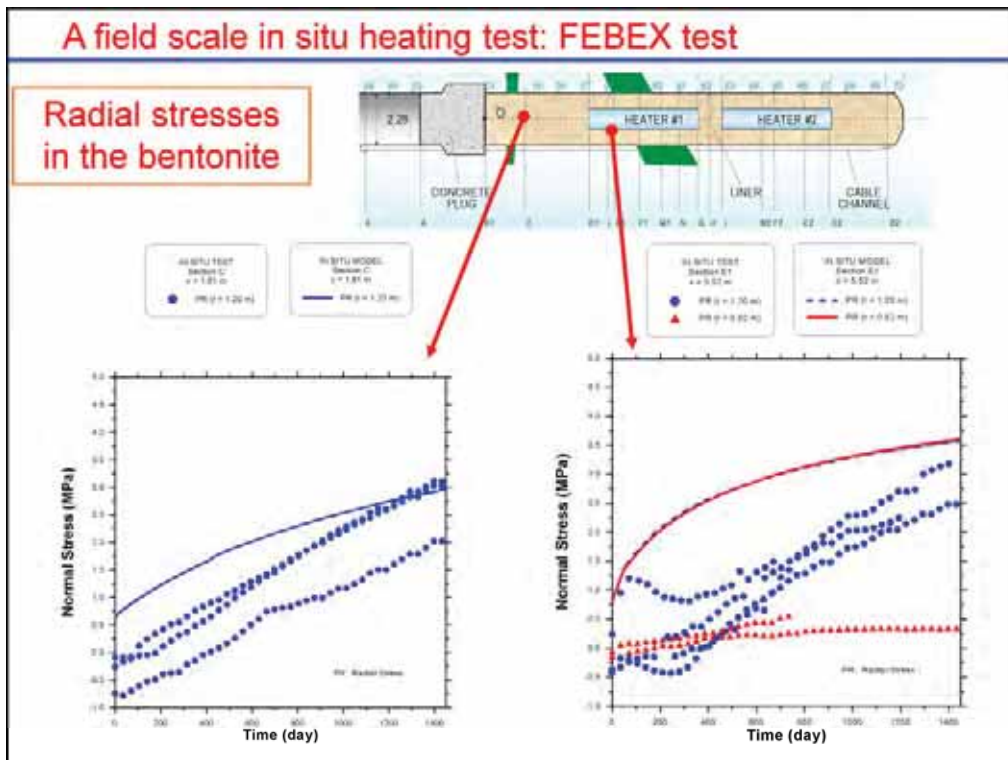
10



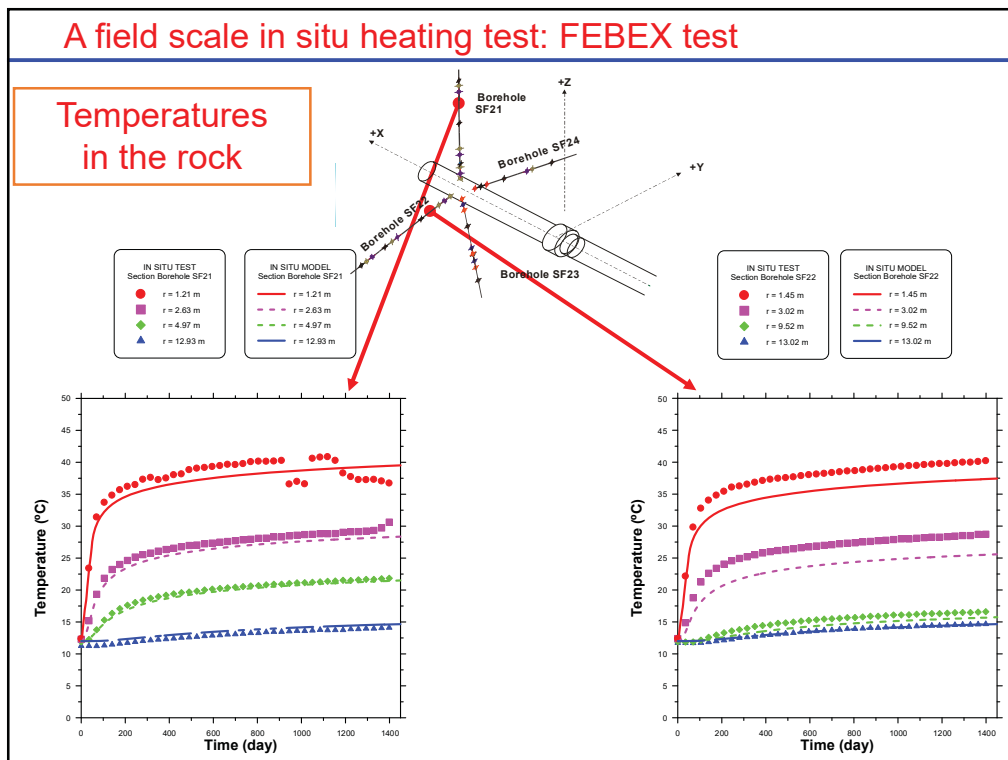
11



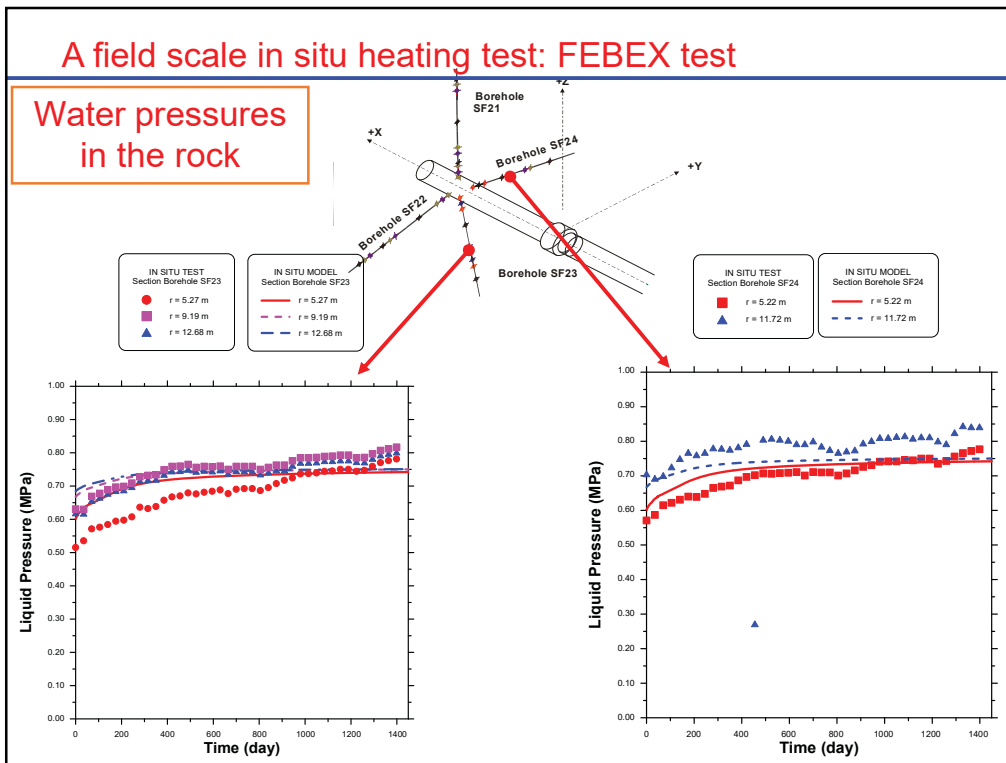
12



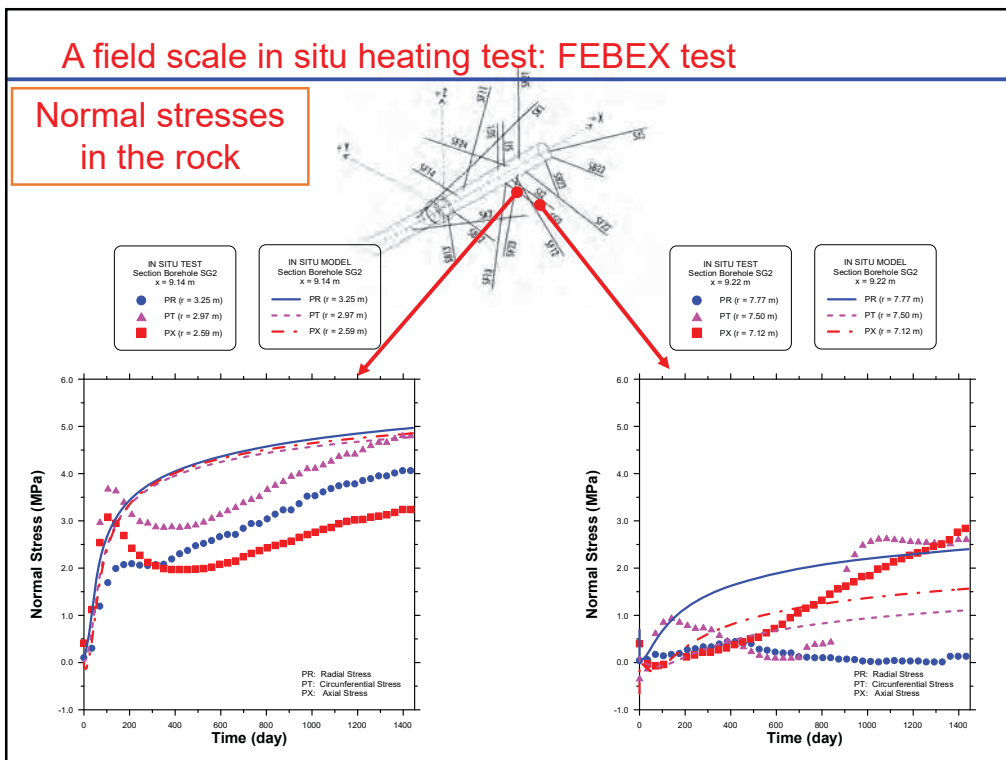
13



14



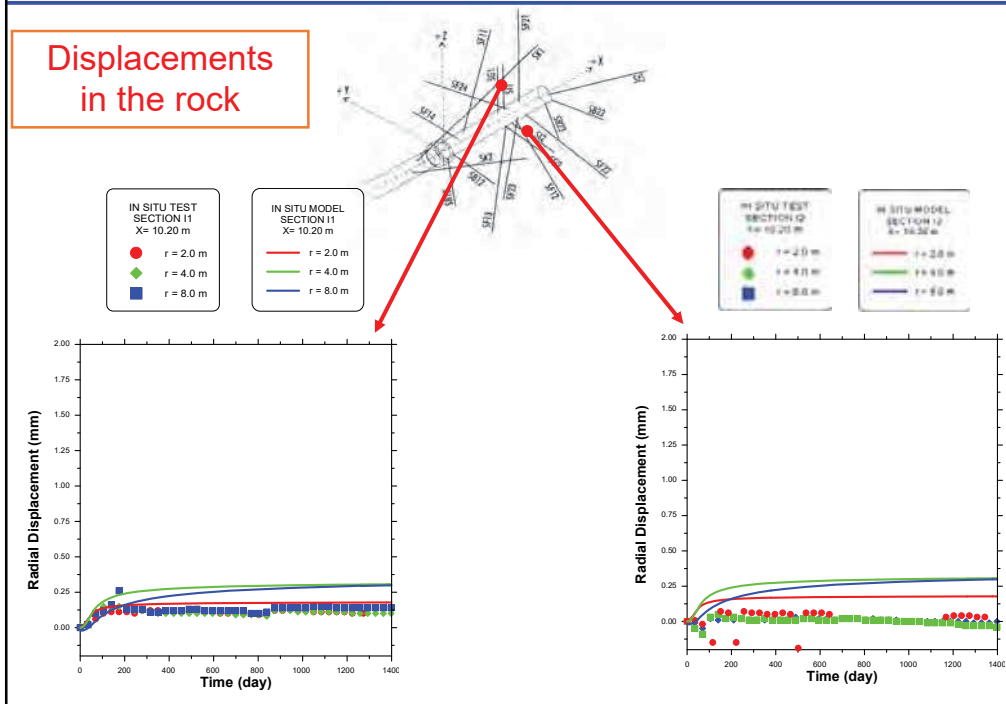
15



16

A field scale in situ heating test: FEBEX test

Displacements in the rock



17

A field scale in situ heating test: FEBEX test

□ Dismantling (partially) the test



18

A field scale in situ heating test: FEBEX test

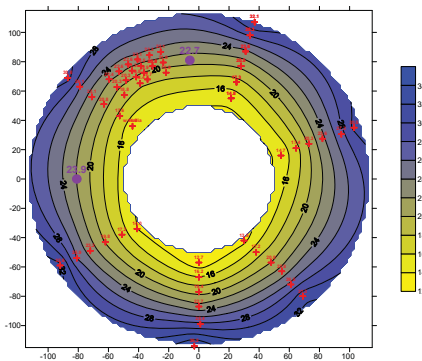
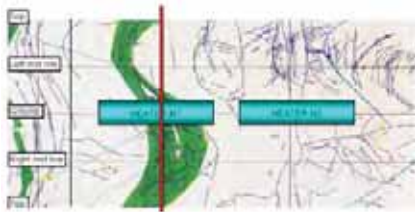
❑ Dismantling (partially) the test



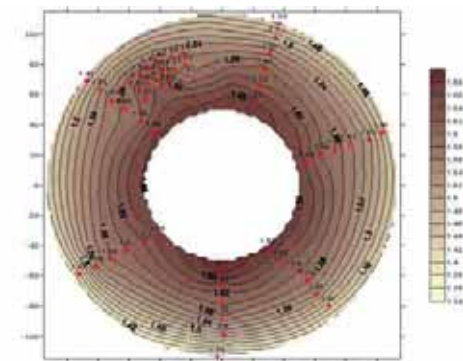
Bentonite sampling

19

A field scale in situ heating test: FEBEX test



Water content

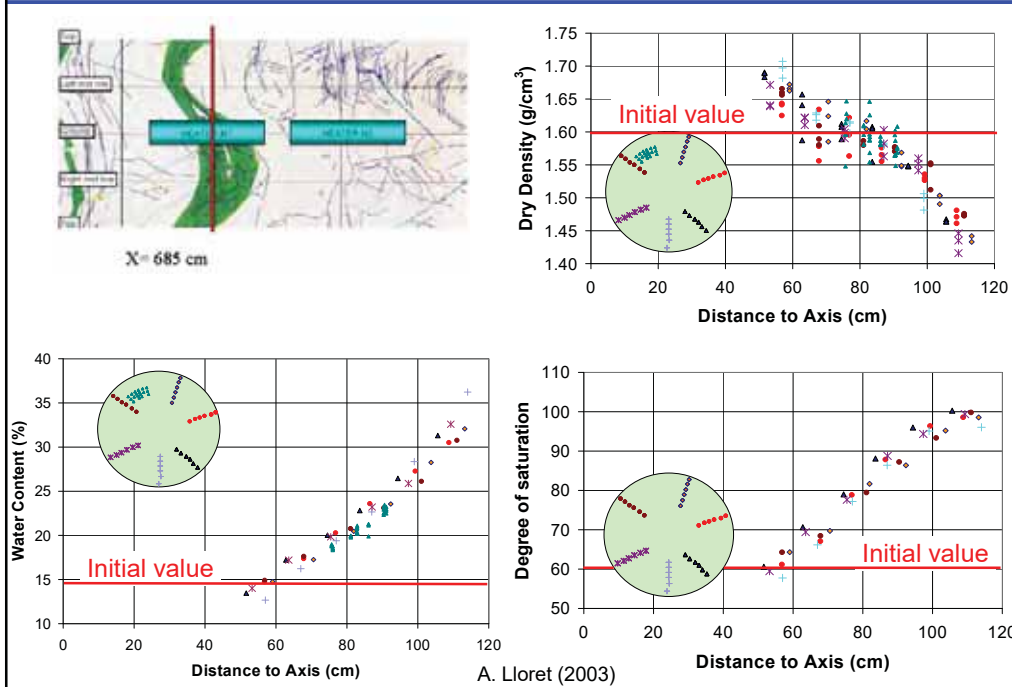


Dry density

A. Lloret (2003)

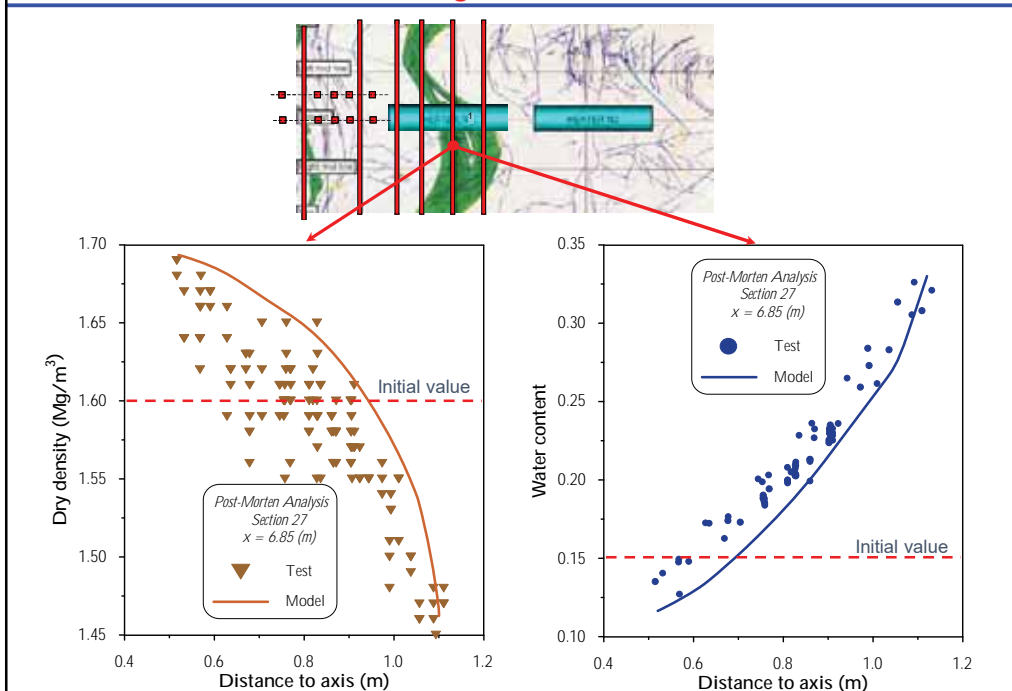
20

A field scale in situ heating test: FEBEX test



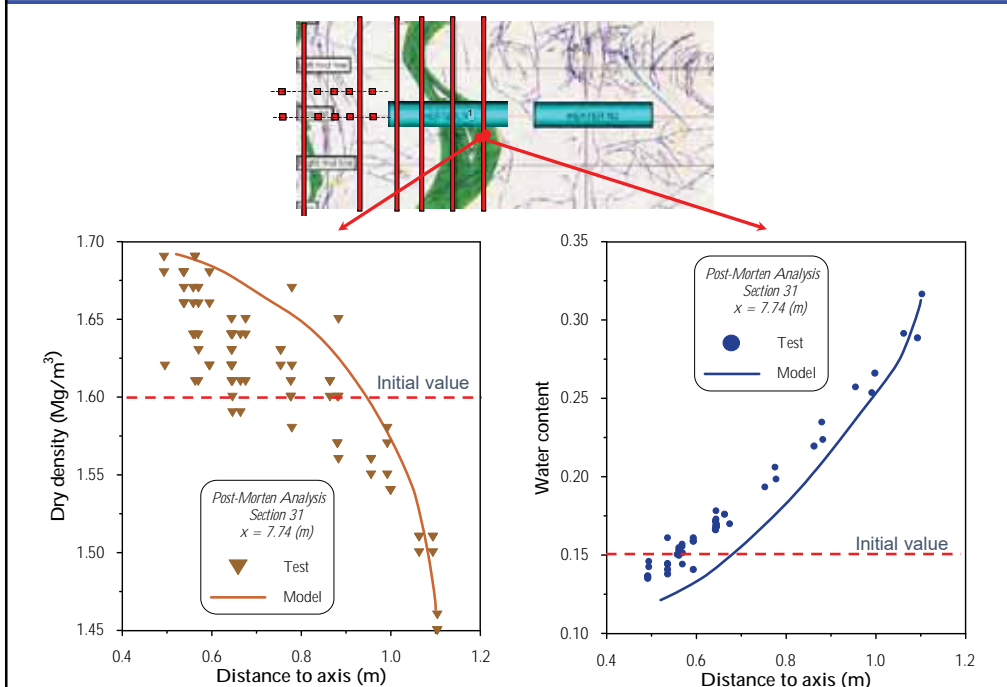
21

A field scale in situ heating test: FEBEX test



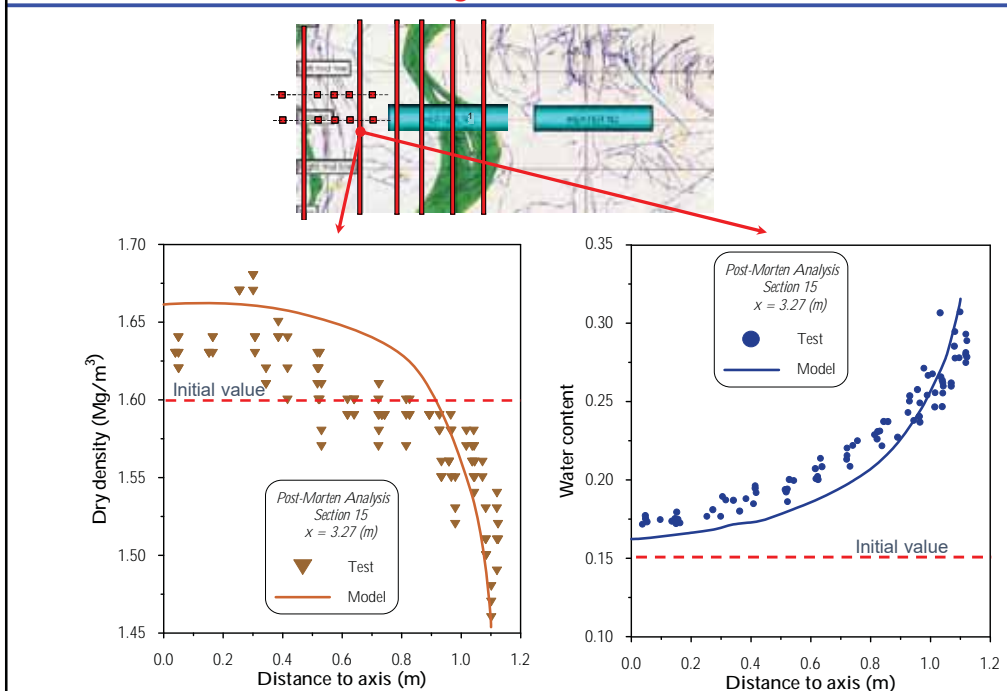
22

A field scale in situ heating test: FEBEX test



23

A field scale in situ heating test: FEBEX test

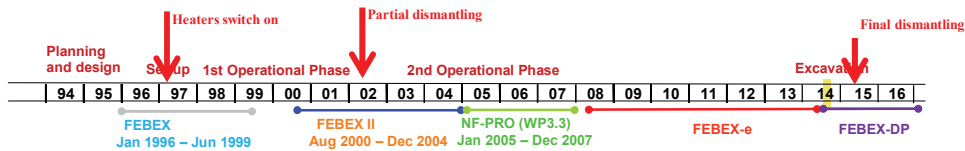


24

A field scale in situ heating test: FEBEX test

□ The FEBEX in situ Test

□ History of the test



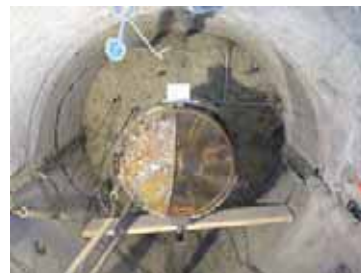
□ Important dates:

- Start of tunnel excavation: 25/09/1995
- End of tunnel excavation: 30/10/1995
- Start of installation: 01/07/1996
- End of installation: 15/10/1996
- Heaters switch on: 27/02/1997 (day zero)
- Heater #1 switch off: 28/02/2002
- End of first dismantling: 19/07/2002 (5 years)
- Heater #2 switch off: 20/04/2015
- End of final dismantling: 20/07/2015 (18 years)

25

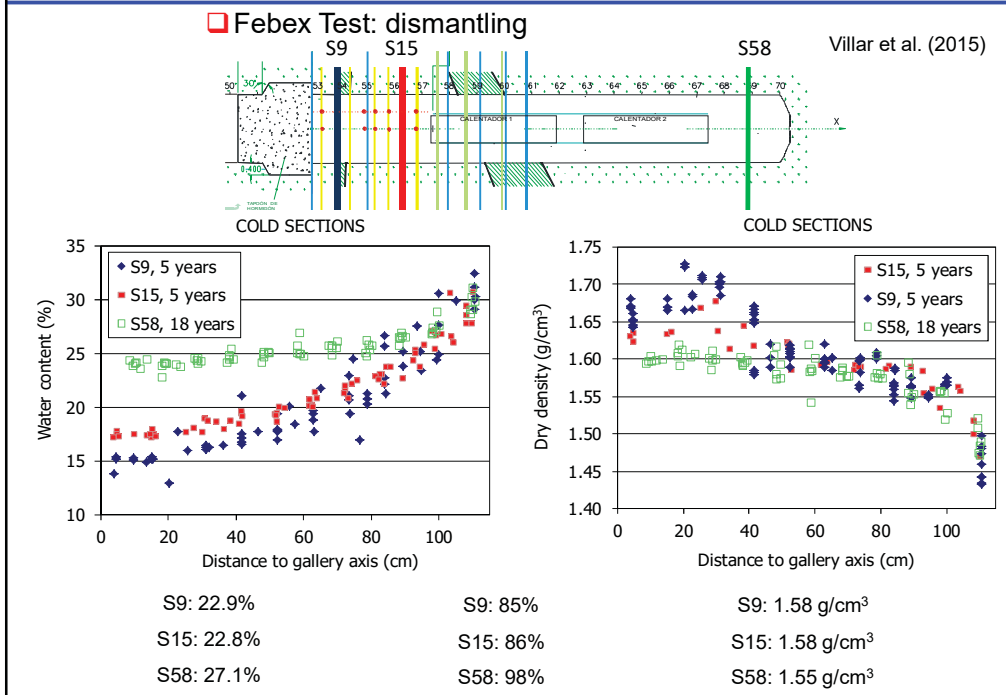
A field scale in situ heating test: FEBEX test

FEBEX test: total dismantling after 18 years



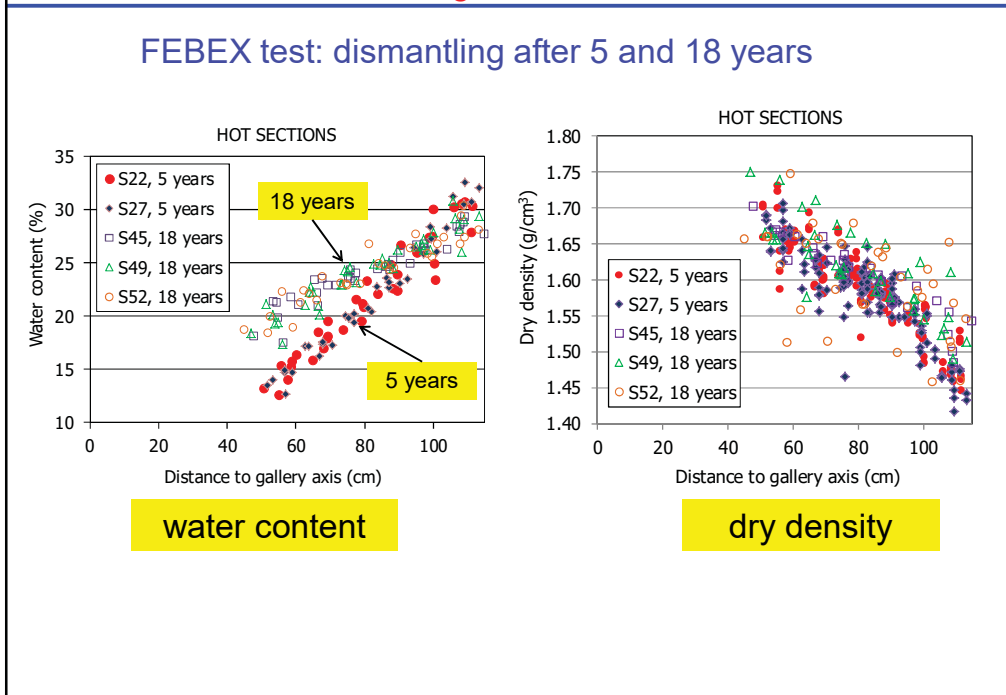
26

A field scale in situ heating test: FEBEX test



27

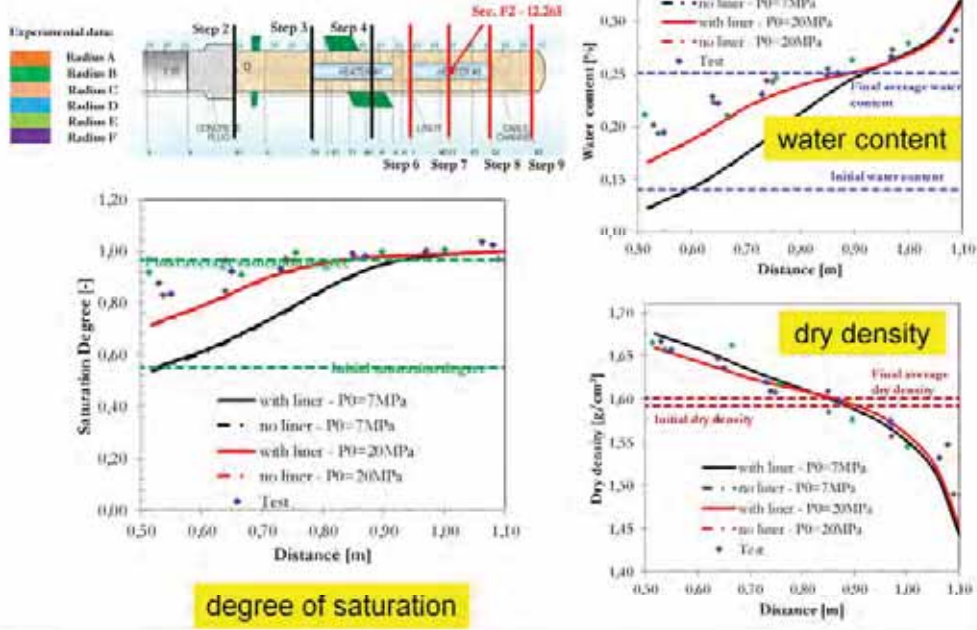
A field scale in situ heating test: FEBEX test



28

A field scale in situ heating test: FEBEX test

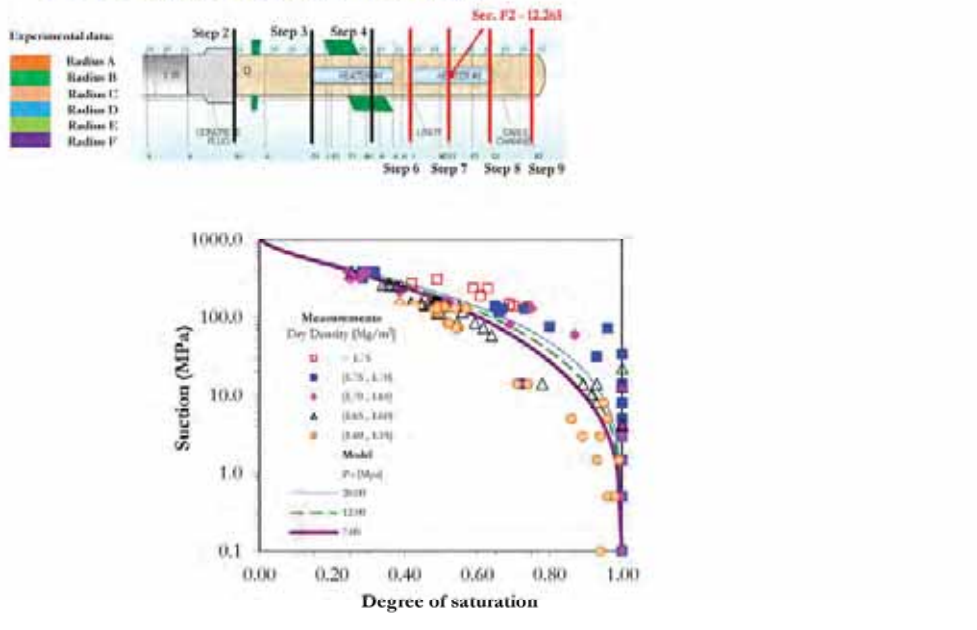
FEBEX test: total dismantling



29

A field scale in situ heating test: FEBEX test

FEBEX test: total dismantling



30

Outline of the lecture

- ❑ Introduction. Relevant phenomena
- ❑ Coupled THM formulation
 - ❑ Balance equations
 - ❑ Constitutive equations and equilibrium restrictions
 - ❑ Numerical implementation
- ❑ Applications
 - ❑ Field scale in situ test on a compacted bentonite engineered barrier
 - ❑ Field scale in situ test on a bentonite pellets engineered barrier
 - ❑ Laboratory tests on bentonite pellets/powder mixture
- ❑ Conclusions

31

A field scale in situ heating test: HE-E test

- ❑ A new generation of engineered barriers
 - Use of granular bentonite as the basic material
 - Allowance for higher temperatures (up to 140°C)
 - there is nothing especial about the 100°C mark (Olivella & Gens, 2000)

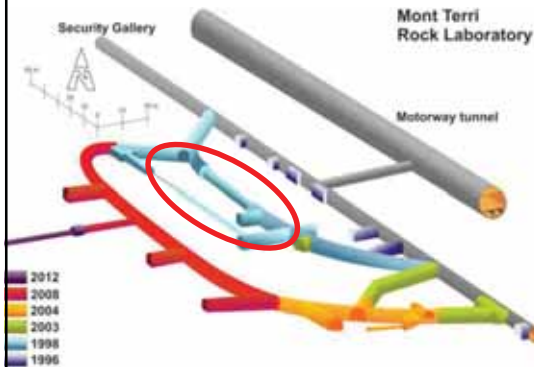


32

A field scale in situ heating test: HE-E test

Tunnel dimensions

- Diameter: 1.3 m
- Length: 10 m



6 % water content
Well graded (max size: 15 mm)

Bentonite (MX-80) pellets



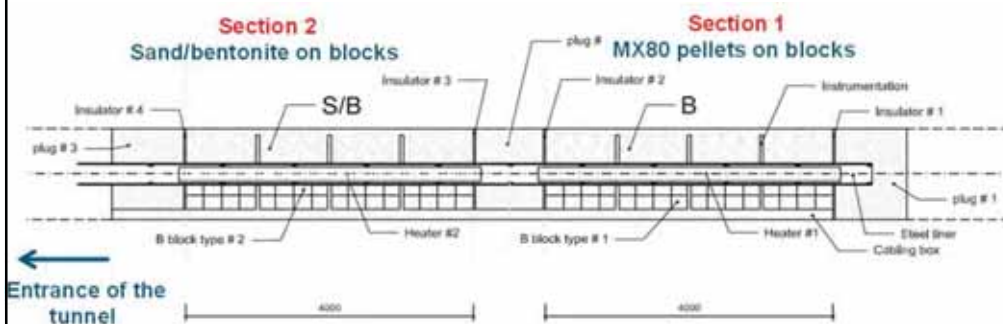
3-4 % water content
Uniform (max size: 2mm)

Sand-bentonite mixture

33

A field scale in situ heating test: HE-E test

Layout



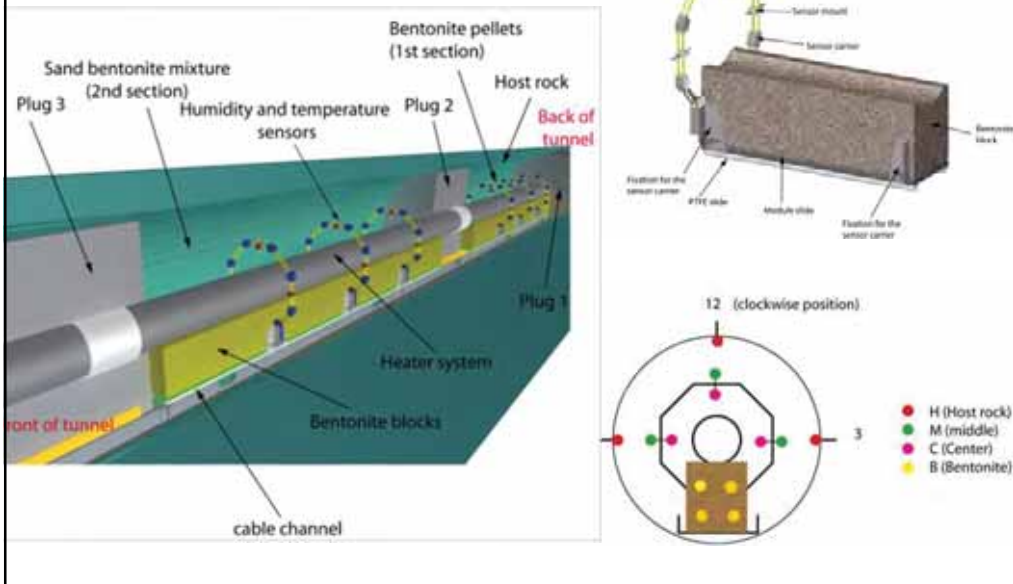
- 1:2 scale (microtunnel 1.3 m)
- Natural resaturation from clay hostrock
- Heater surface temperature: 140°C
- Duration: June 2011 - > ??
- Two symmetrical sections - different Engineered Barrier materials

(NAGRA, NAB 07-23)

34

A field scale in situ heating test: HE-E test

Instrumentation



35

A field scale in situ heating test: HE-E test

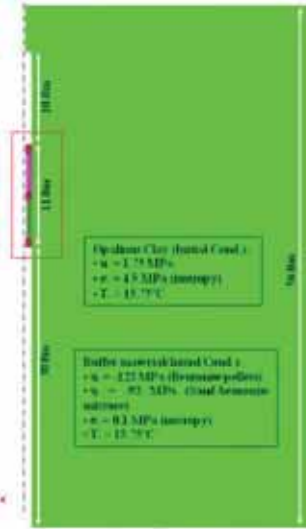
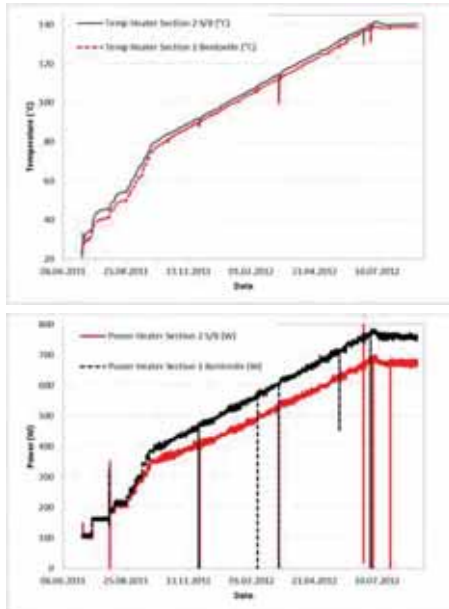


36

A field scale in situ heating test: HE-E test

Performance of HE-E Experiment

- Heating started in June 2011
- Maximum heater temperature of 140°C reached in June 2012 after 1 year of heating



37

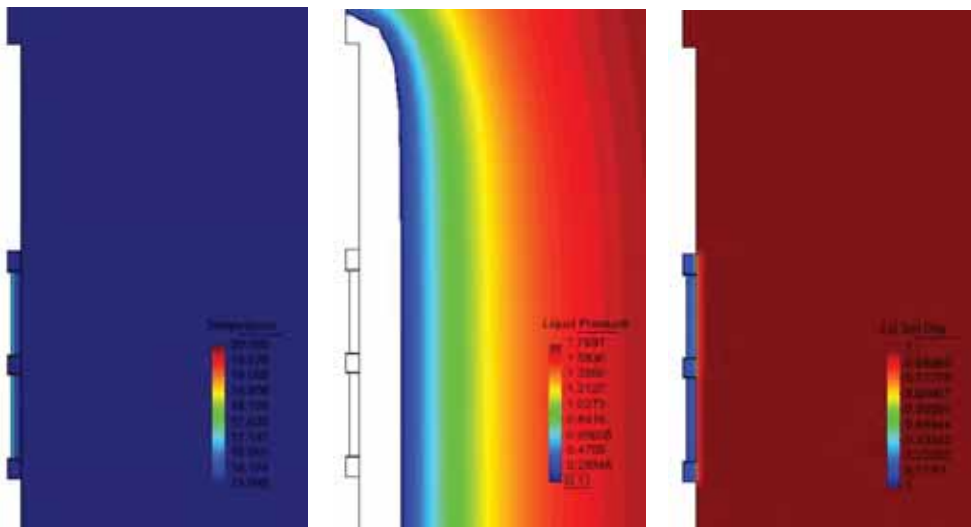
A field scale in situ heating test: HE-E test

t= 0 days (after the beginning of heating)

TEMPERATURE

LIQUID PRESSURE

DEGREE OF SATURATION

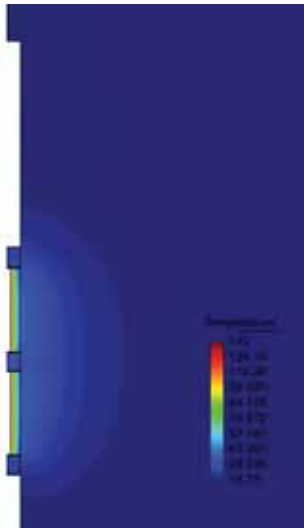


38

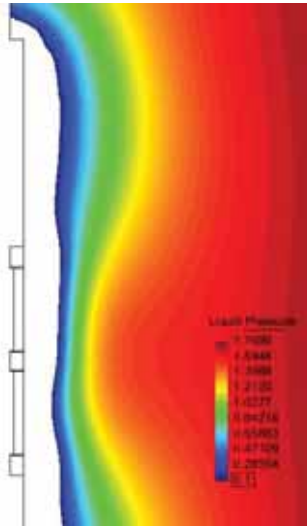
A field scale in situ heating test: HE-E test

t= 1.0 year (after the beginning of heating)

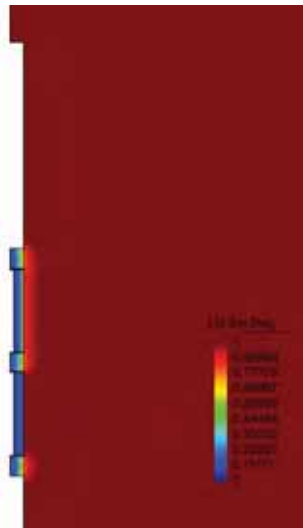
TEMPERATURE



LIQUID PRESSURE



DEGREE OF SATURATION

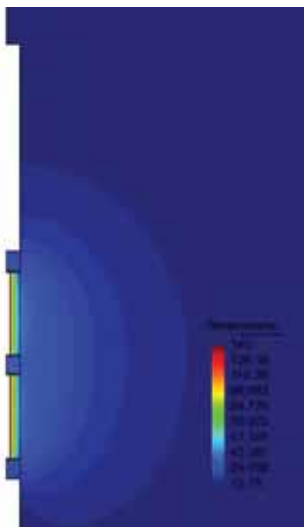


39

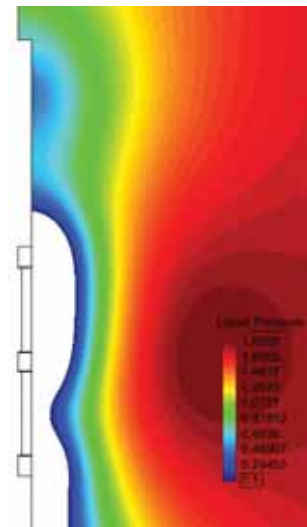
A field scale in situ heating test: HE-E test

t= 2.5 years (after the beginning of heating)

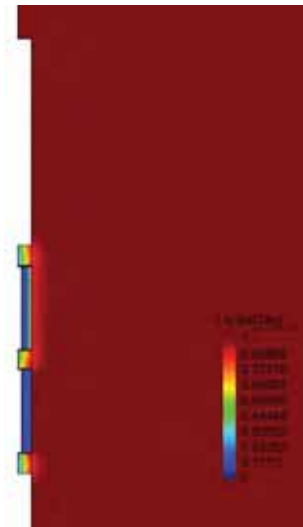
TEMPERATURE



LIQUID PRESSURE



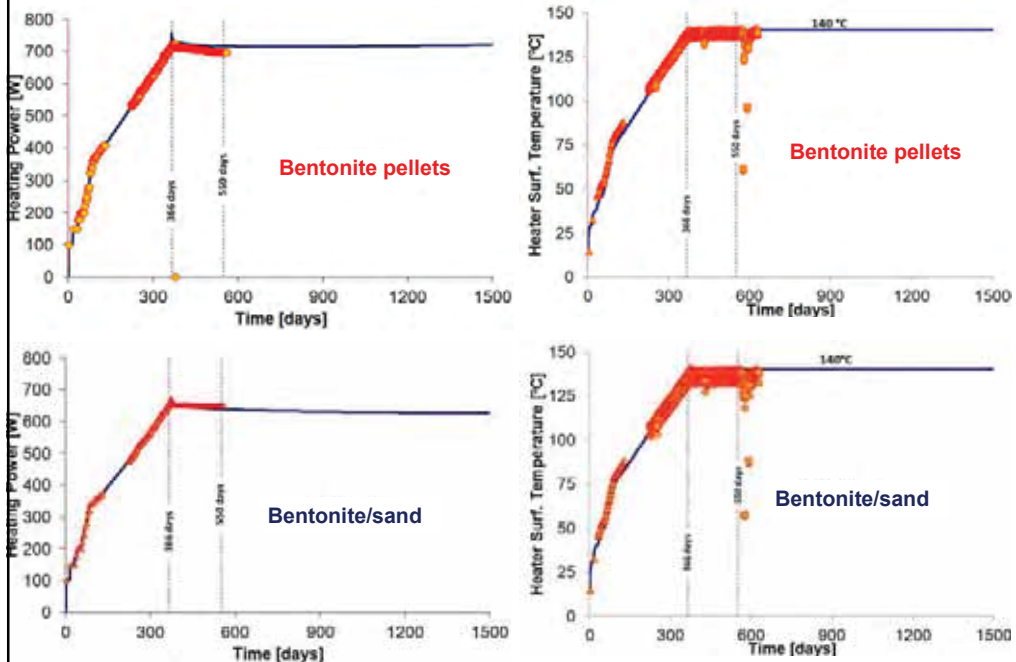
DEGREE OF SATURATION



40

A field scale in situ heating test: HE-E test

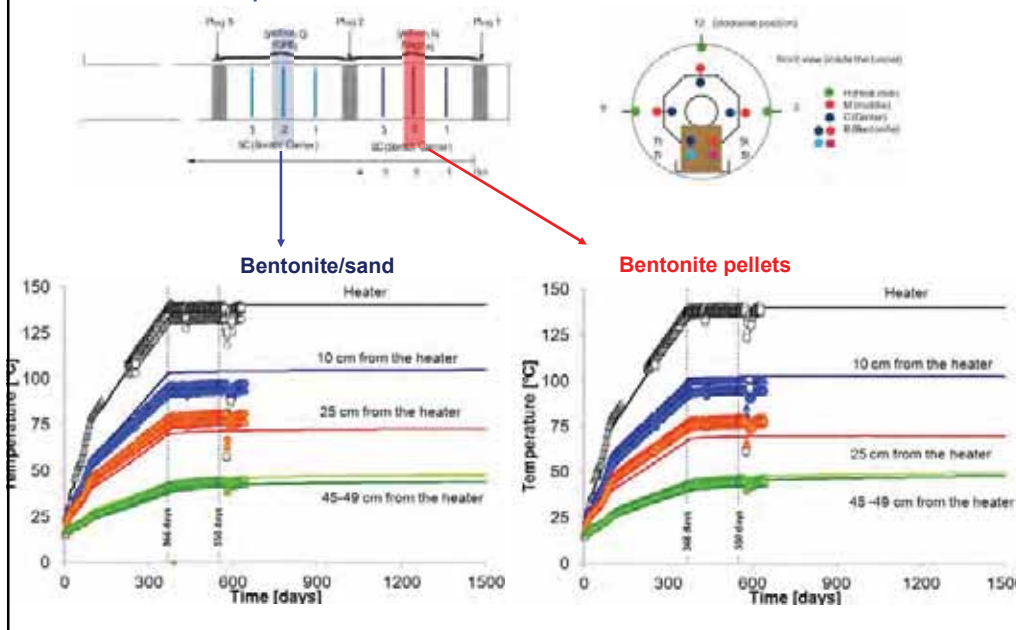
Heating power and heater surface temperature (barrier mid-section)



41

A field scale in situ heating test: HE-E test

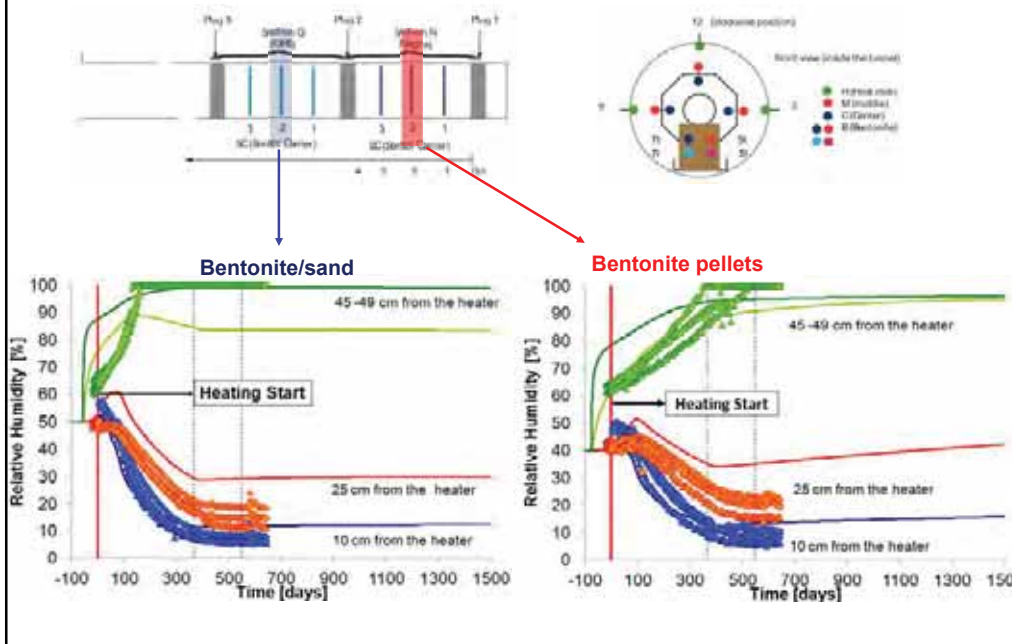
Temperature in the mid-section of the barriers



42

A field scale in situ heating test: HE-E test

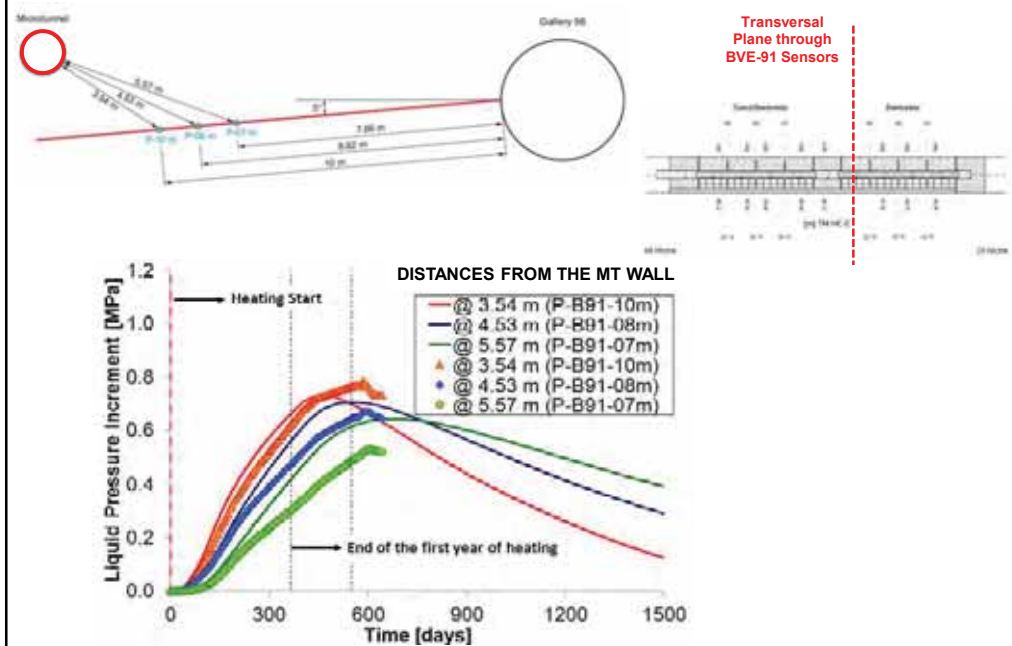
Relative Humidity in the mid-section of the barriers



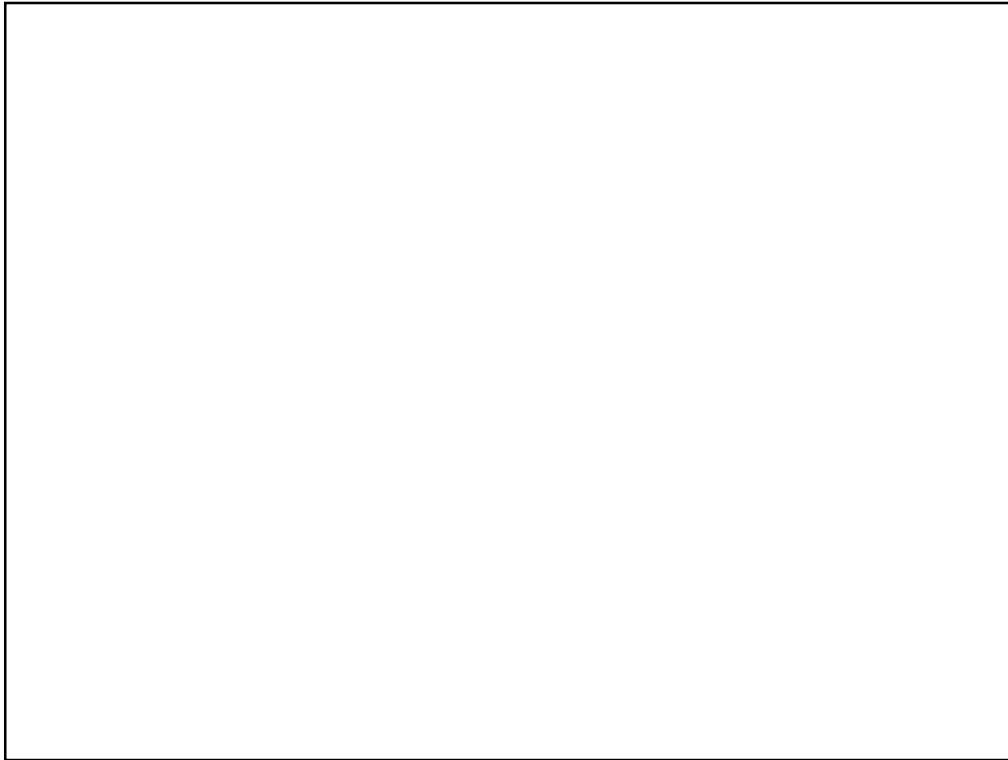
43

A field scale in situ heating test: HE-E test

Liquid Pressure in the rock: BVE-91 Borehole



44

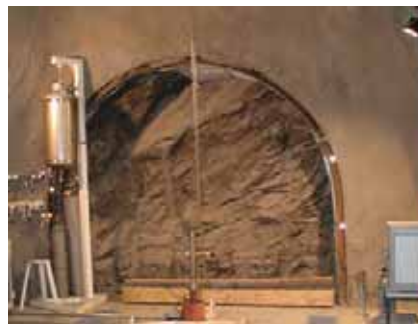


45

Deep geological disposal: host rocks

□ Argillaceous rocks: plastic clays and indurated mudrocks

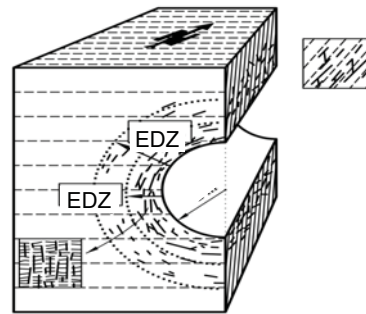
- Low permeability
- Significant retardation properties for solute transport
- No economic value
- Strength not high, support will be required
- More sensitive to chemical changes (oxidation)
- Significant self healing properties (plastic clays)
- Uncertain capacity for self healing (indurated mudrocks)



46

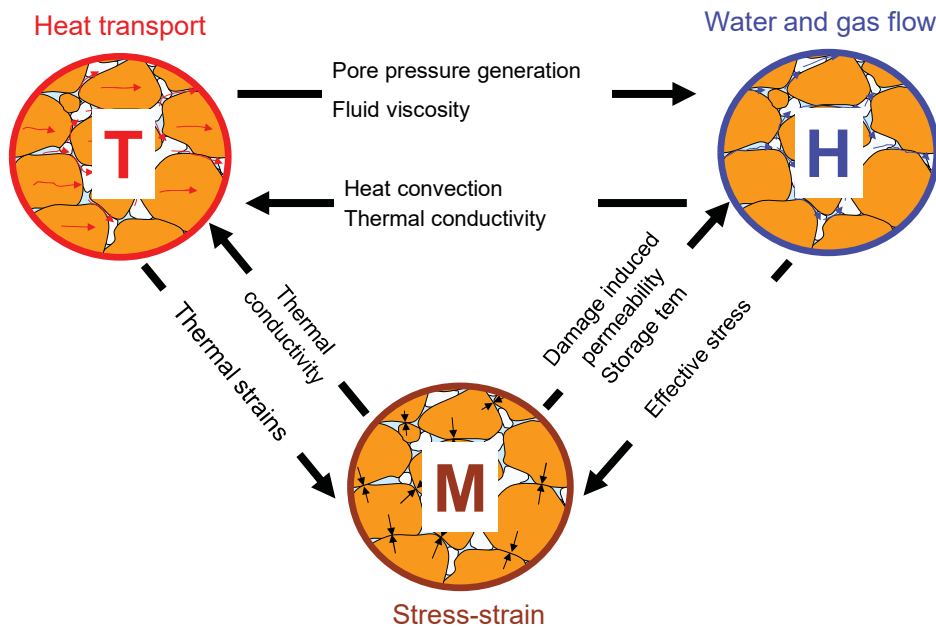
Argillaceous rocks

- ❑ Due to the relatively low strength of argillaceous rocks, damage of the material close to the excavation (EDZ) may be unavoidable
- ❑ Damage increases permeability providing a preferential path for radionuclide migration
- ❑ Damage may be induced by
 - Excavation
 - Thermal loading
 - Ventilation and chemical changes



47

THM coupling in the host rock



48

THM formulation

□ Balance equations for saturated porous media

MASS BALANCE OF SOLID

$$\frac{\partial}{\partial t}(\rho_s(1-\phi)) + \nabla \cdot (\mathbf{j}_s) = 0$$

MASS BALANCE OF WATER

$$\frac{\partial}{\partial t}(\rho_w \phi) + \nabla \cdot (\mathbf{j}_r^w) = f^w$$

INTERNAL ENERGY BALANCE FOR THE MEDIUM

$$\frac{\partial}{\partial t}(E_s \rho_s(1-\phi) + E_l \rho_l S \phi) + \nabla \cdot (\mathbf{i}_c + \mathbf{j}_{Es} + \mathbf{j}_{El}) = f^Q$$



MOMENTUM BALANCE FOR THE MEDIUM

$$\nabla \cdot \boldsymbol{\sigma} + \mathbf{b} = \mathbf{0}$$

49

THM formulation

○ Balance of solid

$$\frac{\partial}{\partial t}(\rho_s(1-\phi)) + \nabla \cdot (\mathbf{j}_s) = 0$$

• Using the definition of material derivative

$$\frac{D_s(\bullet)}{Dt} = \frac{\partial(\bullet)}{\partial t} + \frac{d\mathbf{u}}{dt} \cdot \nabla(\bullet)$$

$$\frac{D_s \phi}{Dt} = \frac{1}{\rho_s} \left[(1-\phi) \frac{D_s \rho_s}{Dt} \right] + (1-\phi) \nabla \cdot \frac{d\mathbf{u}}{dt}$$

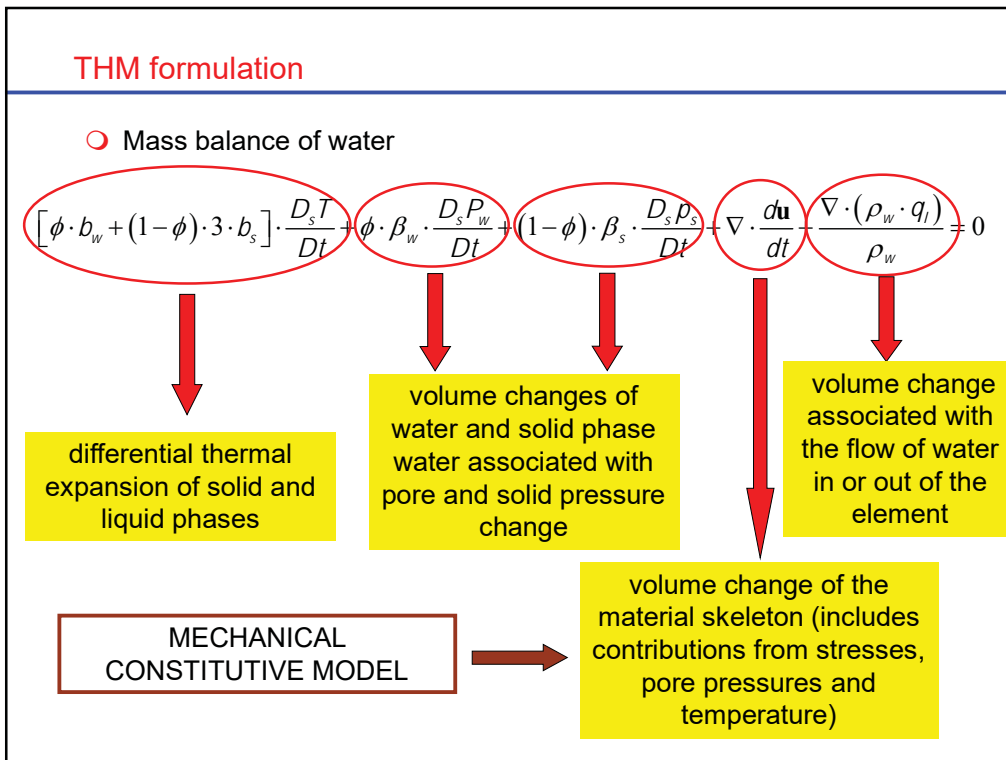
○ Mass balance of water

$$\phi \frac{D_s \rho_w}{Dt} + \frac{\rho_w}{\rho_s} (1-\phi) \frac{D_s \rho_s}{Dt} + \rho_w \nabla \cdot \frac{d\mathbf{u}}{dt} + \nabla \cdot (\rho_w \mathbf{q}_l) = 0$$

$$\rho_w = \rho_{w0} \cdot \exp[\beta_w(\rho_l - \rho_{l0}) + b_w \cdot T]$$

$$\rho_s = \rho_{s0} \cdot \exp[\beta_s(\rho_s - \rho_{s0}) + 3 \cdot b_s \cdot (T - T_{ref})]$$

50

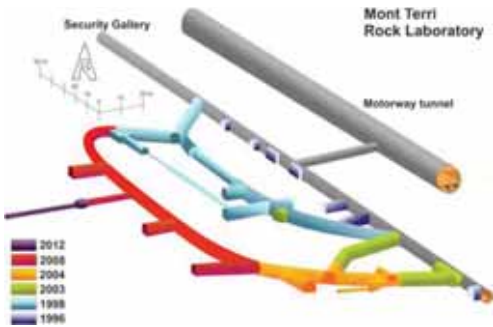



51

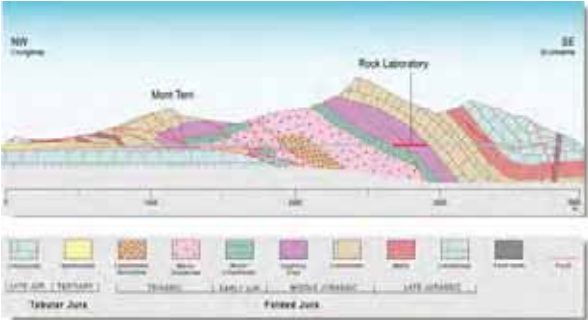
Underground Research Laboratories (URLs)

□ Mont Terri Project

- Located in Northern Switzerland
- Opalinus clay (shale)
- 400 m deep
- Operating since 1995
- Generic, not purpose - built







52

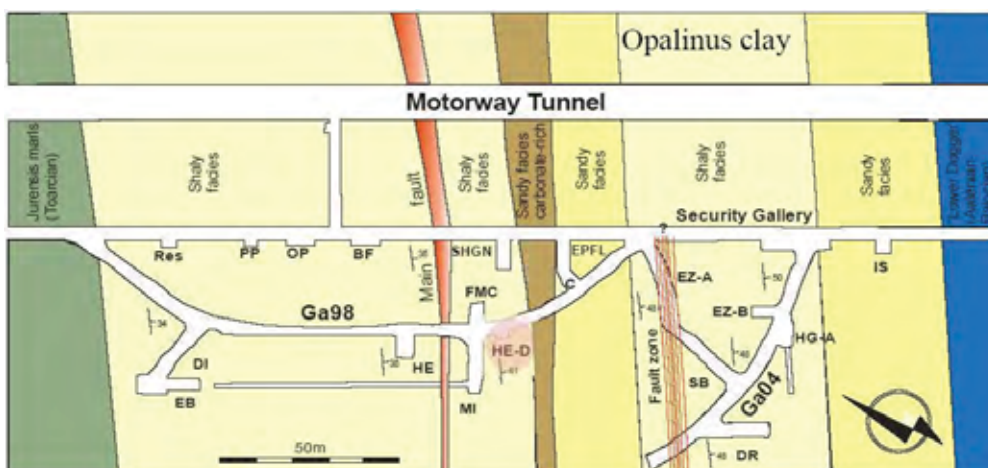
Mont Terri project



53

Mont Terri project

○ The HE-D experiment



Wileveau (2005)

54

Mont Terri Project

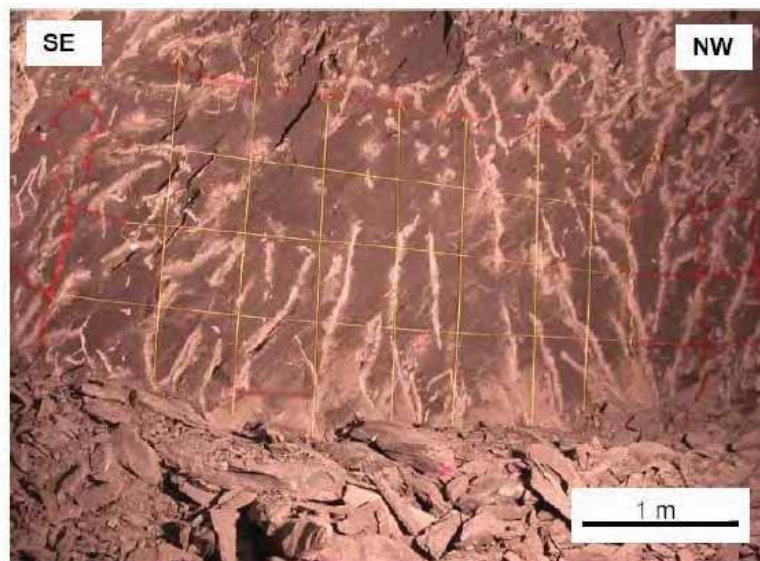
HE-D Experiment



55

Mont Terri Project

HE-D Experiment: geological mapping niche HE-D



Wileveau (2005)

56

Mont Terri Project

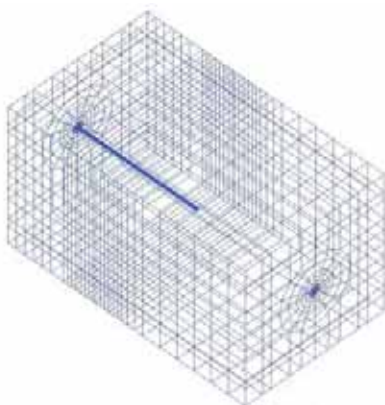
HE-D Experiment



57

HE-D heating test (Mont Terri project)

Coupled three-dimensional THM analysis



day - 29: Excavation: borehole diameter = 0.30m

day - 28: Heaters placed and pressurized (1MPa)

day 0: First heating phase: 325 W/heater

day 91: Second heating phase: 975 W/heater

day 339: Cooling phase

day 518: End of test

Day 0: 6/04/2004

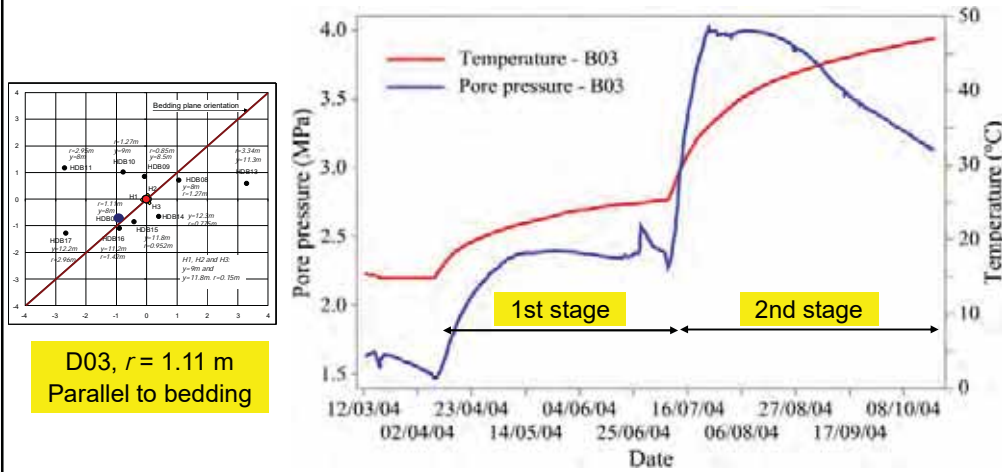
- Anisotropic thermal conductivity
- Anisotropic clay stiffness
- Anisotropic in situ stress system

Principal stress	Orientation	Azimuth	Dip	Value (MPa)
Major, σ_1	Subvertical	N210°	70°	6.0 – 7.0
Intermediate, σ_2	Subhorizontal	N320°	10°	4.0 – 5.0
Minor, σ_3	Subhorizontal	N50°	20°	2.0

58

HE-D test

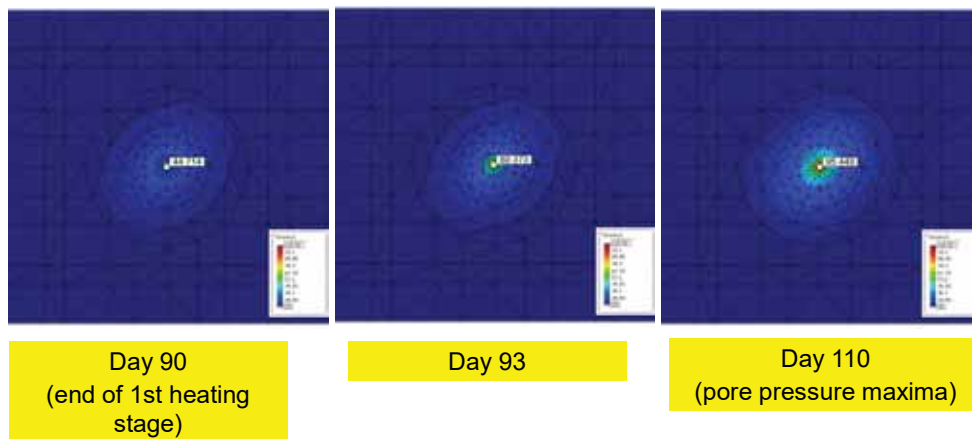
Observed evolution of pore pressure and temperature



59

HE-D test

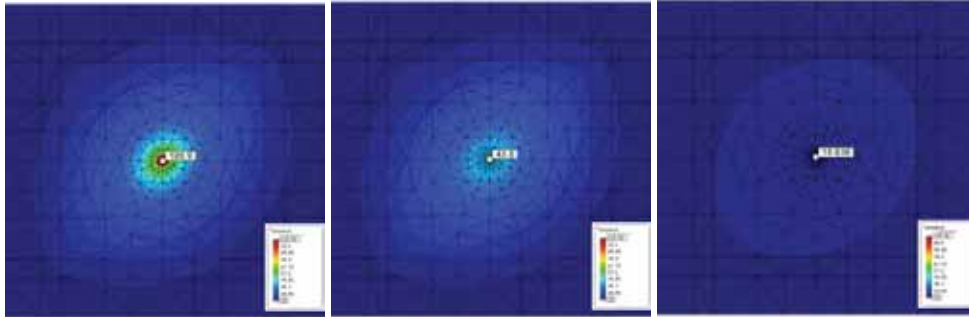
Three dimensional analysis: temperatures



60

HE-D test

Three dimensional analysis: temperatures



Day 297
(near the end of 2nd heating stage)

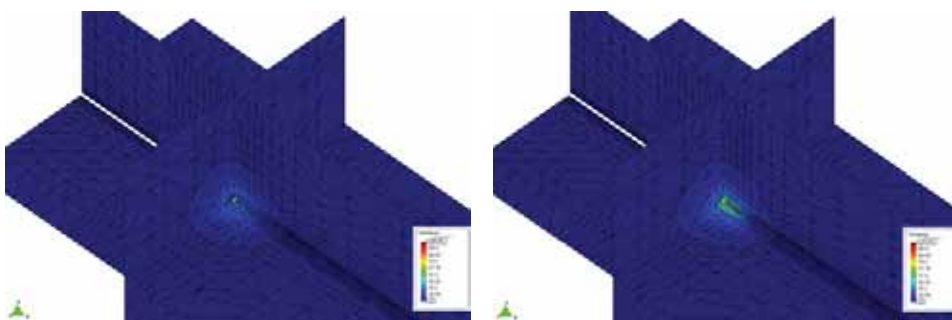
Day 346
(start of cooling phase)

Day 508
(end of test)

61

HE-D test

Three dimensional analysis: temperatures



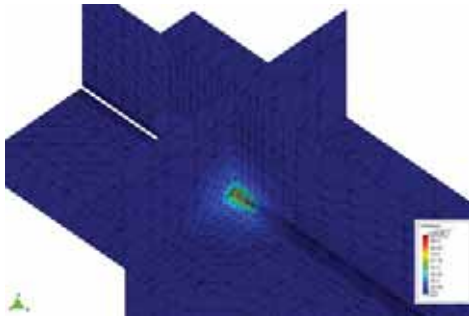
Day 90
(end of 1st heating stage)

Day 93

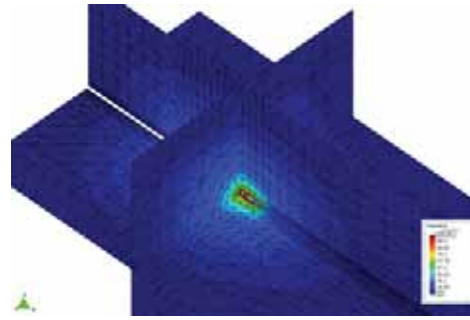
62

HE-D test

Three dimensional analysis: temperatures



Day 110
(pore pressure maxima)

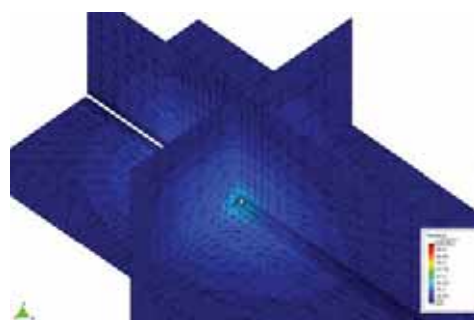


Day 297
(near the end of 2nd heating stage)

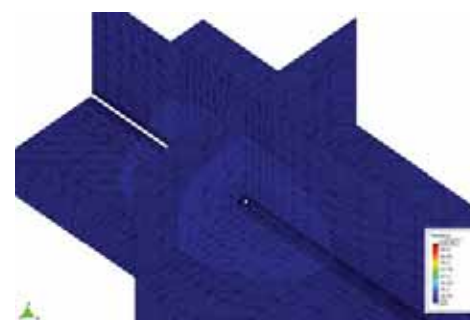
63

HE-D test

Three dimensional analysis: temperatures



Day 346
(start of cooling phase)

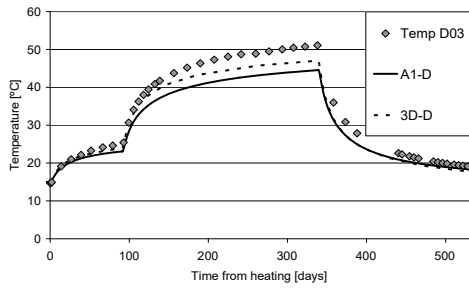


Day 508
(end of test)

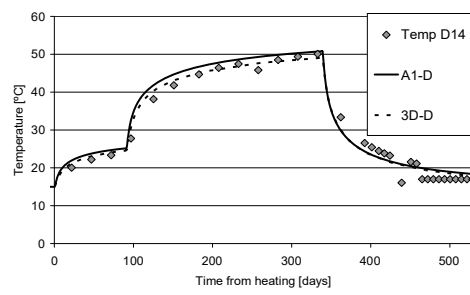
64

HE-D test

Rock temperatures



D03, $r = 1.11$ m
Parallel to bedding

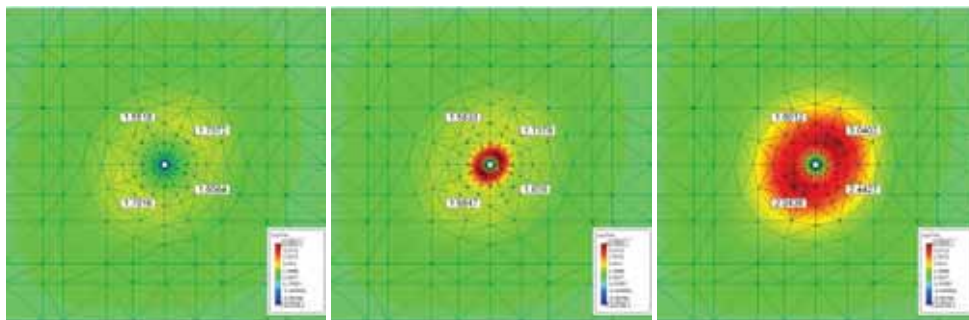


D14, $r = 0.78$ m
Perpendicular to bedding

65

HE-D test

Three dimensional analysis: pore pressures



Day 90
(end of 1st heating stage)

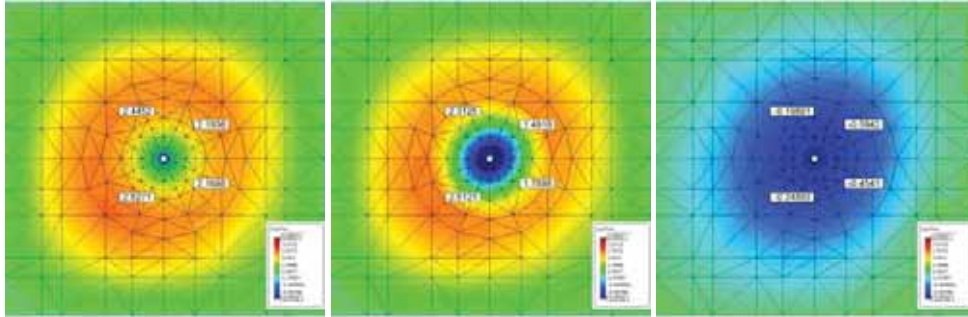
Day 93

Day 110
(pore pressure maxima)

66

HE-D test

- Three dimensional analysis: pore pressures



Day 297
(near the end of 2nd
heating stage)

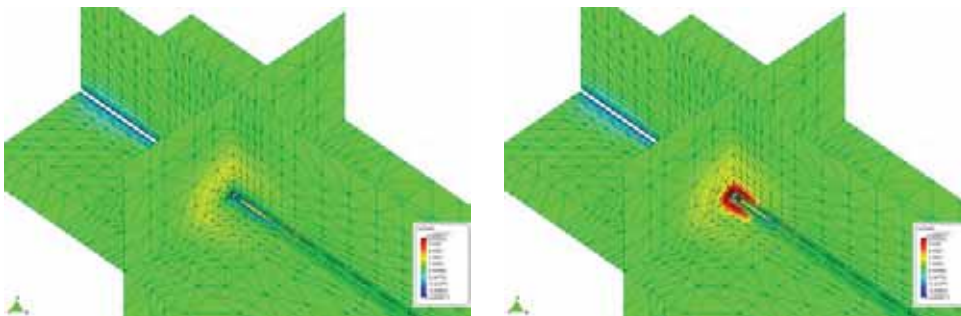
Day 346
(start of cooling phase)

Day 508
(end of test)

67

HE-D test

- Three dimensional analysis: pore pressures



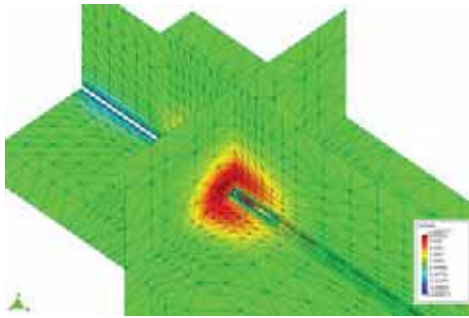
Day 90
(end of 1st heating
stage)

Day 93

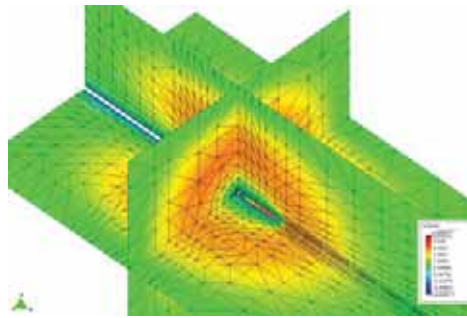
68

HE-D test

Three dimensional analysis: pore pressures



Day 110
(pore pressure maxima)

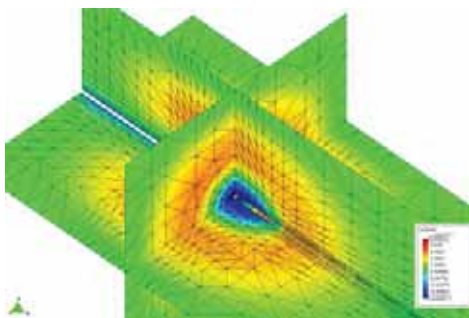


Day 297
(near the end of 2nd heating stage)

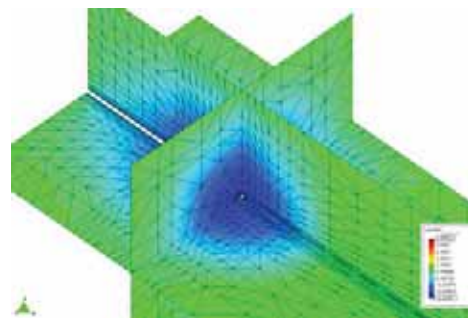
69

HE-D test

Three dimensional analysis: pore pressures

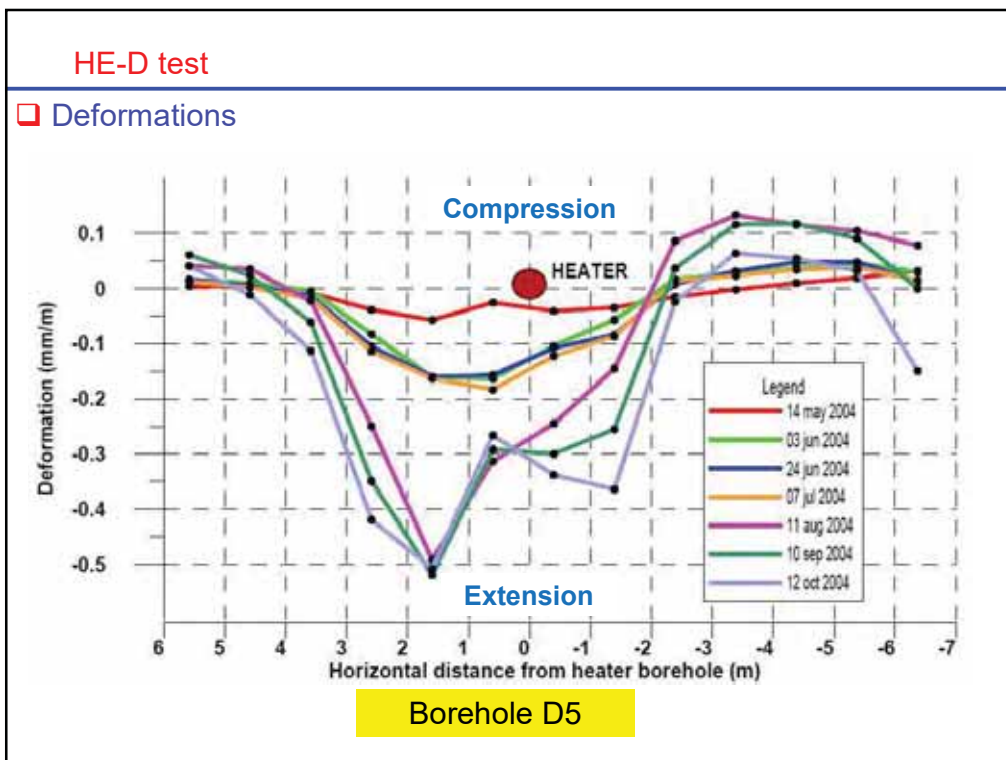


Day 346
(start of cooling phase)

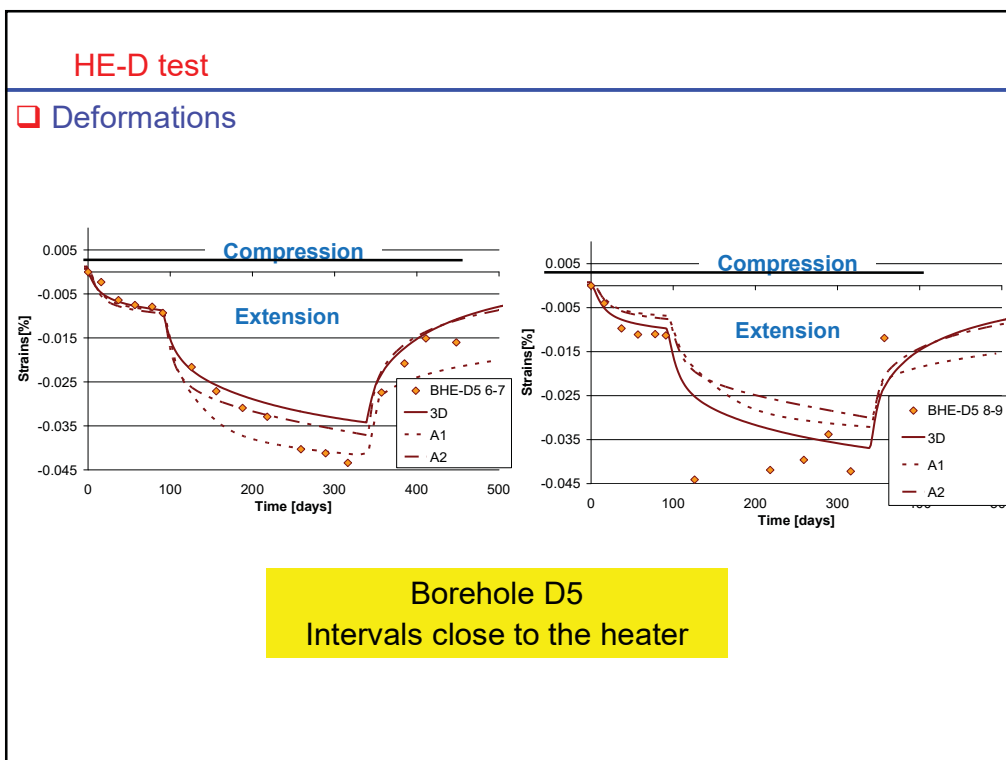


Day 508
(end of test)

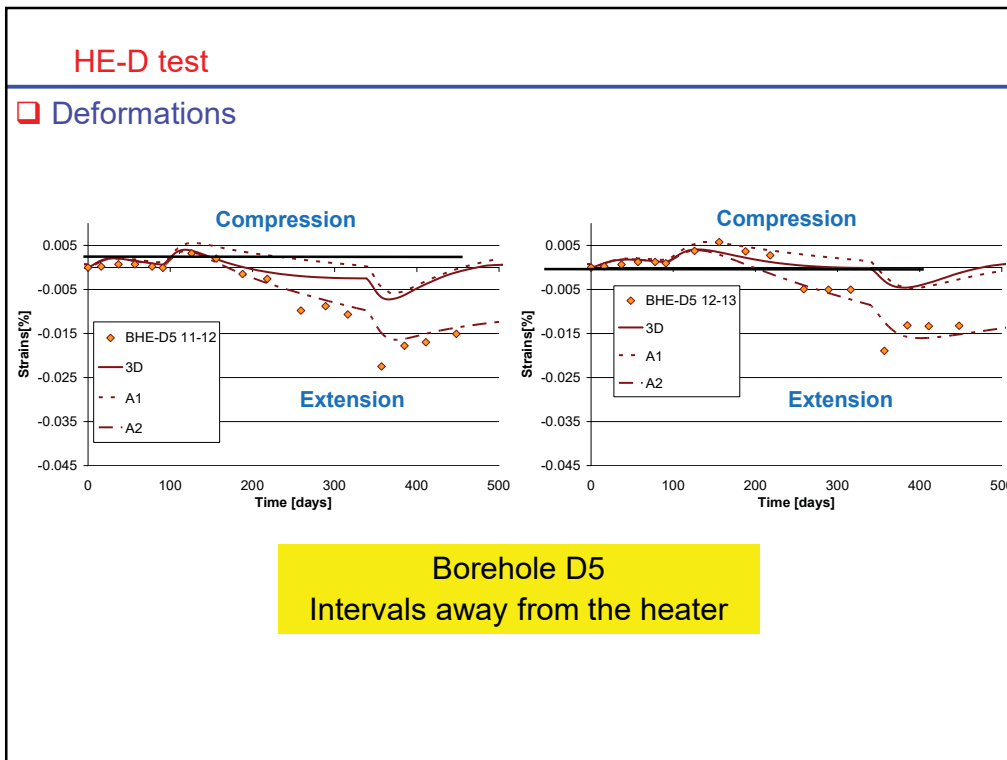
70



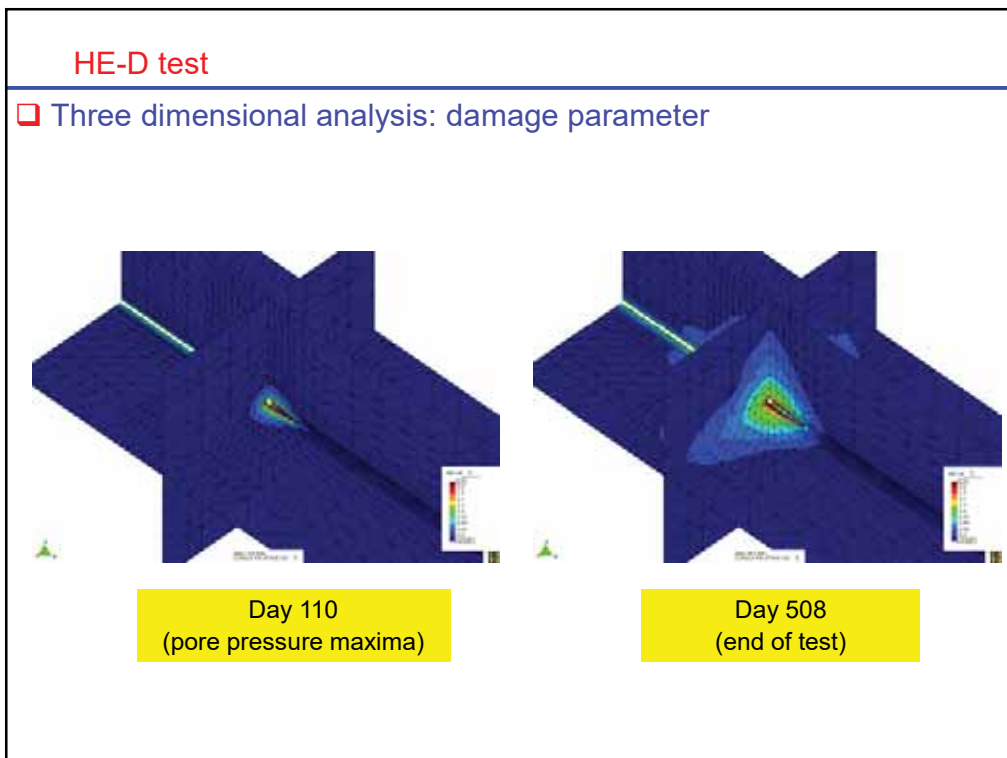
73



74



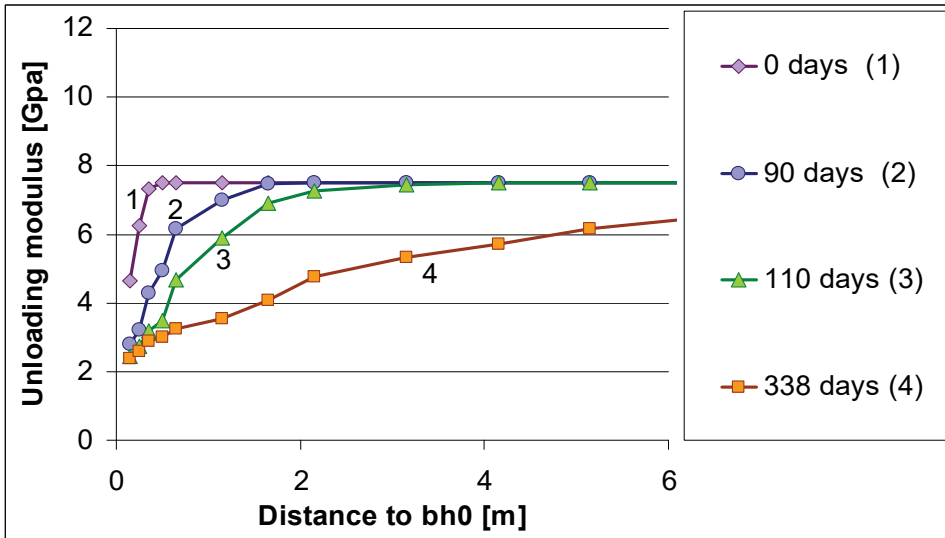
75



76

HE-D test

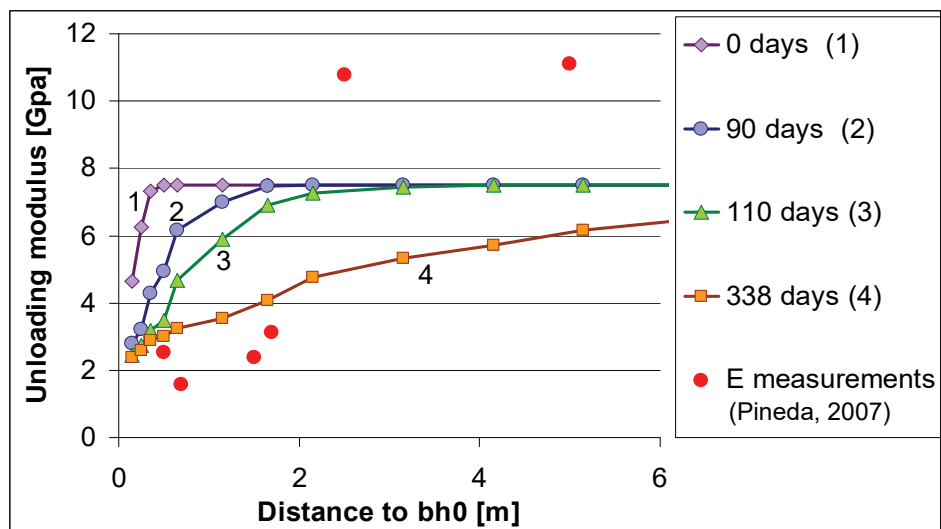
Computed damage effect on elastic modulus



77

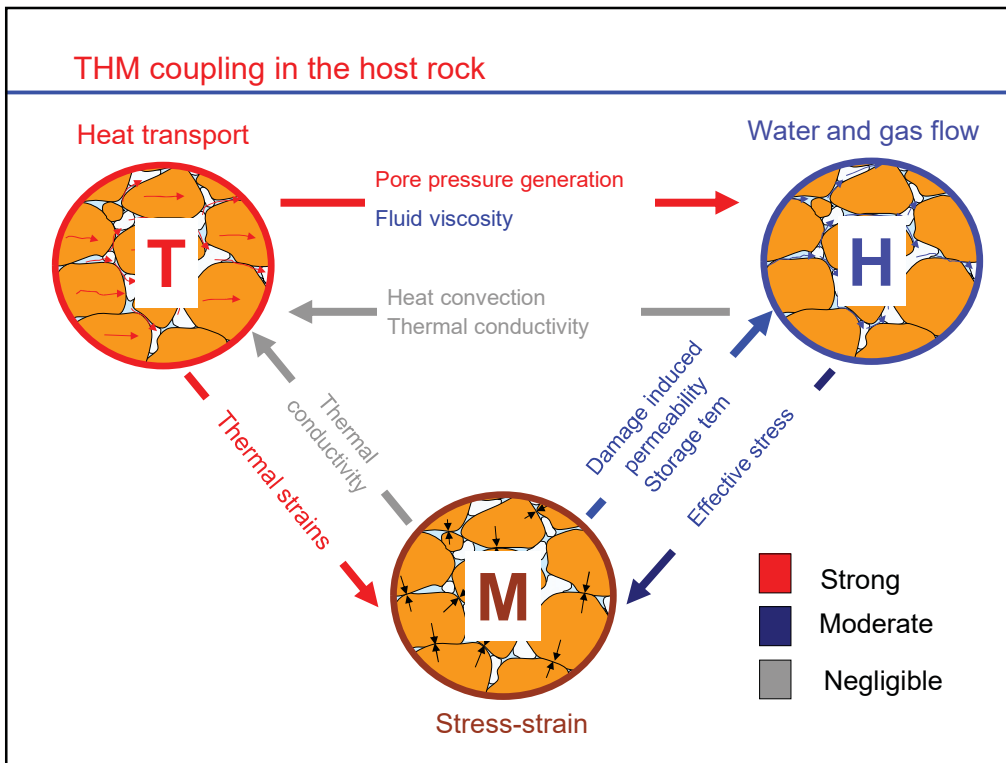
HE-D test

Computed damage effect on elastic modulus



78

THM coupling in the host rock



79

Appendix E. Fundamentals on geomechanics and multi-physical couplings - Paper (A. Gens)

Fundamentals on geomechanics and multi-physical couplings

Antonio Gens

Universitat Politècnica de Catalunya, Barcelona Tech

ABSTRACT. The basic thermohydromechanical (THM) phenomena occurring in saturated and unsaturated porous media are reviewed, with special attention to their interactions. A mechanistic theoretical formulation that encompasses the most relevant THM phenomena and their couplings is developed. The description of the formulation is divided into balance equations, constitutive equations and equilibrium restrictions. Mass balance equations are established in terms of species rather than phases. Governing equations include solid mass balance, water mass balance, air mass balance, energy balance and momentum balance (equilibrium). Constitutive equations are proposed for the various THM phenomena that are deemed most relevant. The specific form of each constitutive equation generally includes information on the nature of the interactions between different phenomena. Equilibrium restrictions provide conditions for processes that are considered fast with respect to the characteristic times of the overall THM problem, notably phase changes.

KEY WORDS: Thermohydromechanical phenomena, multiphase porous media, coupled phenomena, balance equations, constitutive equations.

1. Introduction

The engineering problems in the field of Environmental Geomechanics generally involve a variety transport phenomena occurring in porous multiphase materials. Because the phases interact with each other, coupled phenomena are a very characteristic feature of these problems. The simplest and most well-known coupling is implicit in the principle of effective stress of saturated soils where the mechanical problem (represented by stresses) and the hydraulic problem (represented by the pore pressure) interact. When the number of phases increase the quantity of possible couplings multiply. In addition, in Environmental Geomechanics, it is not uncommon to find nonisothermal situations and, therefore, attention should be given to the mechanisms involving heat transport. The incorporation of a thermal component gives rise to numerous additional interactions between phenomena. Inevitably, a high degree of complexity ensues.

Moreover, interest generally lies not only in finding what the final situation for a particular problem will be, but also in following the development of processes throughout time. In fact, events at early times may control the final state of the system under examination. For this reason, transient analyses are a typical feature of this field. In this chapter, only the THM aspects of the general problem will be considered, focussing on heat and mass transport phenomena. Contaminant transport is examined in (Thomas and Cleall 2001).

The basic concepts and most relevant phenomena in the context of thermohydronechanical (THM) behaviour of porous materials are reviewed first. The case of a porous media with two different fluids will be used as basic reference. It is more general than the single fluid one and it incorporates important additional concepts. Saturated materials can therefore be regarded as a particular instance of the two-fluid case. To focus the discussion, it is assumed that the main fluids are water and air, but the same concepts are basically applicable to other binary systems such as oil/water or oil/gas. Afterwards, a coupled THM formulation is described in some detail to approach the problem in a more rigorous manner. The formulation provides a rational framework in which the various THM phenomena and their interactions can be properly examined.

2. Basic concepts and relevant phenomena

2.1 Unsaturated porous medium: potential and suction

For the case taken as reference, a porous medium consists of three phases (solid, liquid and gas) and three species (mineral, water and air). It is postulated that the mineral species coincides with the solid phase. This is not always the case; for instance in saline materials water inclusions may be present in the solid phase (Olivella et al. 1996). The liquid phase is mainly composed of water but it may also contain dissolved air. The gas phase is a mixture of air and water vapour. Note that, for simplicity, air is considered as a single species although it is in fact a mixture of different gasses. Figure 1 depicts a schematic representation of the porous medium considered.

Dealing with unsaturated porous media, it is useful at this point to review the question of water potential and suction. The total water potential, ψ , can be defined as the variation of the Gibbs free energy of water per unit change of mass when the rest of thermodynamical variables remain constant. The same kind of definition can be made in terms of internal energy. The potential can be envisaged as the energy required (under isothermal conditions) to extract a unit mass of water and take it to a reference state. Total potential controls the mass transfer of water; water will flow from regions of high water potential towards regions of lower water potential. When two water volumes are in contact and there is no flow, it necessarily means that the water potential is the same in the two zones.

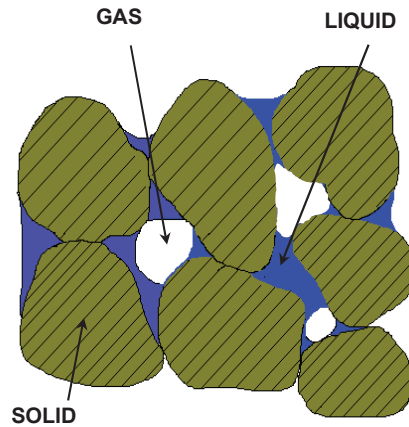


Figure 1 : Schematic representation of an unsaturated porous medium

In 1965, A Review Panel in the Symposium on Moisture Equilibrium and Moisture Changes in Soils Beneath Covered Areas (Review Panel 1965) proposed a division of the total potential into four different components: gravitational potential, ψ_g , gas pressure potential, ψ_p , matric potential, ψ_m and osmotic potential, ψ_o .

$$\psi = \psi_g + \psi_p + \psi_m + \psi_o \quad [1]$$

that has proved very useful. The gravity potential is given by the difference in elevations, the gas pressure potential is related to the applied gas pressure, osmotic potential depends on differences in solute concentrations and the matric suction reflects the attraction that a soil matrix has for liquid moisture. In Soil Science, gas pressure potential is replaced by overburden potential, a more general concept. Although this division into components is useful for a better understanding, it should be stressed that the only parameter controlling the mass transfer of water is the sum of all four components.

With respect to the mechanical behaviour of unsaturated media, the situation is more complex as it is by no means true that all potential components have a similar effect. In fact, it is obvious that the gravitational potential will not affect mechanical behaviour. In addition, experimental results (and some theoretical considerations) indicate clearly that gas pressure potential has no effect on mechanical behaviour either. Therefore, only osmotic potential and matric potential will affect the mechanical response of unsaturated soils. Again, there is no reason for the two potential components to have equivalent effects. In fact, it can be easily checked experimentally that their influence on mechanical behaviour is quite different and depends on the type of soil.

As an alternative to potential, the concept of suction is often used; suction being simply the potential with the opposite sign. Thus matric suction is $s = -\psi_m$ and osmotic suction is $s_o = -\psi_o$. The sum of matric and osmotic suctions is often called total suction. For convenience, the matric suction is frequently equated to a capillary pressure difference across a meniscus:

$$s = P_a - P_w \quad [2]$$

where P_a is the air pressure and P_w is the water pressure.

This definition has only real meaning in the framework of the capillary model of the soil. However, it is clear that the capillary approach is not applicable to many soils especially when clay fractions are significant. It is by no means certain that all soil water in an unsaturated soil is in a state of true tension, so the high negative pore pressures that frequently arise from [2] should not be taken literally. Matric suction simply reflects the degree of attraction of the water by the soil matrix and it is often more related to physico-chemical surface effects than to some virtual capillary meniscus existing in the soil. Therefore, the use of negative water pressures in the study and analysis of unsaturated porous media should always be understood in the context of these comments.

2.2 Relevant phenomena

A great number of phenomena can be potentially present in a THM problem involving unsaturated porous media. It is necessary to apply engineering judgement in order to select the most relevant phenomena so that the resulting formulation does not become too cumbersome to use.

Starting with thermal phenomena, it can be stated that in most cases the main mechanism for heat transport is heat conduction. Heat conduction responds to gradients of temperature, T . However, additional heat transfer will also be accomplished by advection due to the movement of the three phases: solid, liquid and gas. The latent heat inherent to phase changes may also have significant thermal effects.

With respect to hydraulic phenomena, two of the main ones are, naturally, the advective flow of liquid and gas. Here, the term hydraulic is used in a generalized manner, including both liquid and gas flow. In the absence of gravitational or osmotic potential gradients, advective flows are controlled uniquely by liquid and gas pressures. Note that now liquid and gas pressures are used rather than water and air pressures. This in accordance with the assumption that each phase may contain more than one species. Phases are the subjects of advective flows.

As more than one species may be present in the fluid phases, nonadvective (diffusion) flows are potentially significant. The most important one, especially in nonisothermal situations, is the diffusion of water vapour in the gas phase. The usual

conceptual understanding of this phenomenon is that of binary diffusion. For each mol of water vapour diffusing in one direction, there is another mol of air (considered as a single species) diffusing in the opposite direction. The total contribution to advective flow is therefore zero. Vapour diffusion is controlled by gradients of vapour concentration (or partial pressure). Exactly the same considerations can be made for dissolved air diffusion in the liquid phase, although its importance in practice is generally much less.

Finally, the mechanical behaviour of unsaturated porous media will be associated not only with the usual stress/strain relationship but there will be additional contributions from changes in suction (matric and, sometimes, osmotic) and changes in temperature.

Most of the phenomena outlined above are in fact strongly coupled and they must be considered as parts of a single interconnected system. As an example, Figure 2 shows the thermal and hydraulic interactions in an unsaturated soil subjected to hydration from one end and to heating from the other end. The real degree of complexity is in fact higher since, for clarity, the mechanical phenomena have not been added to the Figure.

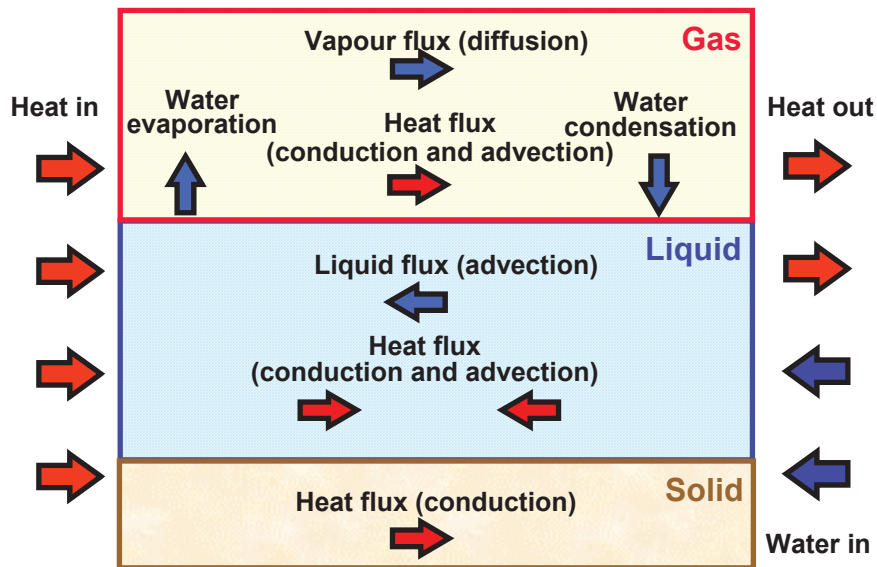


Figure 2 : *Coupled thermo-hydraulic phenomena in an unsaturated porous medium subject to heating and hydration*

A final point regarding the phenomena described. In all cases the mass or energy transfer depend only on the gradients of the thermodynamically conjugate forces.

Off-diagonal processes such as Dufour effect, Soret effect, thermal filtration or thermal osmosis are not considered. Except in very special cases, their practical significance is negligible in a THM context.

2.3 Basic features of the formulation

The formulation to be described incorporates the basic thermal, hydraulic and mechanical phenomena briefly described in the previous section, i.e.:

- Thermal: Heat conduction, heat advection for all three phases and phase changes
- Hydraulic: Liquid advection, gas advection, water vapour diffusion, dissolved air diffusion
- Mechanical: Dependence of strains on changes of stresses, suction and temperature

A variety of approaches have been proposed to establish this type of formulation on a sound basis. Some examples are: hybrid mixture theory (Hassanizadeh and Gray 1979a, 1979b, 1980), porous media theory (De Boer 1996, Ehlers and Volk 1998) or thermodynamic generalisations of Biot's theory (Coussy 1995, Coussy et al. 1999). A macroscopic mechanistic approach will be adopted herein. The aim is to achieve a formulation capable of application to engineering problems, without omitting any significant terms in the equations.

The formulation is expressed in terms of balance equations, constitutive equations and equilibrium restrictions. Each of these categories is described in turn below. The following convention is established for writing the equations: superscripts refer to species (*w* for water and *a* for air) and subscripts refer to phases (*s* for solid, *l* for liquid and *g* for gas). No symbol is attributed to the mineral species because it has been assumed that it coincides with the solid phase. Notation for some of the frequently used variables is as follows:

ϕ : porosity	ρ : density
\mathbf{i} : non-advective mass flux	\mathbf{q} : advective flux
\mathbf{j} : total mass flux	\mathbf{u} : solid displacement vector
$\boldsymbol{\sigma}$: stress tensor	\mathbf{b} : body forces vector
θ : mass content per unit volume of phase	ω : mass fraction
S_l : degree of saturation of liquid phase	S_g : degree of saturation of gas phase
\mathbf{i}_c : conductive heat flux	\mathbf{j}_E : energy fluxes due to mass motion

Volumetric mass of a species in a phase (e.g. water in gas phase θ_g^w) is the product of the mass fraction of that species, ω_g^w , and the bulk density of the phase, ρ_g , i.e. $\theta_g^w = \omega_g^w \rho_g$.

3. Balance equations

3.1 Mass balance equations

To establish the mass balance equations, the compositional approach (Panday and Corapcioglu 1989) is followed. This approach consists of balancing the species rather than the phases. Total species equations are obtained by adding over all phases the equation of balance of each species. In this way, phase exchange terms cancel out, which is particularly useful when equilibrium is assumed (Olivella et al. 1994). It should be pointed out, however, that alternative approaches based on balancing phases are equally feasible.

The macroscopic balance of any thermodynamic property π (per unit mass) in a continuum can be expressed by

$$\frac{\partial}{\partial t}(\rho\pi) + \nabla \cdot (\mathbf{j}_\pi) - f^\pi = 0 \quad [3]$$

where ρ is the mass of the species per unit volume containing π , \mathbf{j}_π is the total flux of π with respect to the reference system and f^π is the rate of production/removal of π per unit volume. It is important to stress here that \mathbf{j}_π is expressed in relation to a fixed reference system because corrections may be required to take into account that the solid phase moves. Total flux can be decomposed into two components: an advective one (phase motion) and a non advective one (motion of the species inside the phase), i.e.

$$\mathbf{j}_\pi = \rho\pi\mathbf{v}_\pi + \mathbf{i}_\pi \quad [4]$$

where \mathbf{v}_π is the mass weighted mean velocity and \mathbf{i}_π is the non advective flux. Using this decomposition, equation [3] would be the general equation given by [HAS 86].

3.1.1 Mineral mass balance equation

The mass balance of the mineral (solid phase) present in the medium is:

$$\frac{\partial}{\partial t}(\theta_s(1-\phi)) + \nabla \cdot (\mathbf{j}_s) = 0 \quad [5]$$

where θ_s is the mass of solid per unit volume of solid and \mathbf{j}_s is the total flux of solid with respect a fixed reference system.

3.1.2 Water mass balance equation

Water is the main component of the liquid phase but it is also a component of the gas phase in vapour form. The total mass of water per unit volume is expressed as:

$$\theta_l^w S_l \phi + \theta_g^w S_g \phi \quad [6]$$

where the two terms account for water in liquid and gas respectively. Note that

$$S_l + S_g = 1 \quad [7]$$

is a constraint arising from the definition of fluid phase saturation.

The water fluxes in each phase can be written as:

$$\mathbf{j}_l^w = \mathbf{i}_l^w + \theta_l^w \mathbf{q}_l + \theta_l^w S_l \phi \dot{\mathbf{u}} = \mathbf{j}'_l^w + \theta_l^w S_l \phi \dot{\mathbf{u}} \quad [8]$$

$$\mathbf{j}_g^w = \mathbf{i}_g^w + \theta_g^w \mathbf{q}_g + \theta_g^w S_g \phi \dot{\mathbf{u}} = \mathbf{j}'_g^w + \theta_g^w S_g \phi \dot{\mathbf{u}} \quad [9]$$

where \mathbf{i}_l^w and \mathbf{i}_g^w are the nonadvective fluxes of water in the liquid and gas phases. The other terms are advective and take into account the motion of the phase. The second part of the expression corresponds to the distinction between the relative motion of the species water, \mathbf{j}'_w , with respect to the solid phase and the absolute motion \mathbf{j}_w with respect to a fixed reference system.

With these definitions, the total water mass balance is expressed as:

$$\frac{\partial}{\partial t} (\theta_l^w S_l \phi + \theta_g^w S_g \phi) + \nabla \cdot (\mathbf{j}'_l^w + \mathbf{j}'_g^w) = f^w \quad [10]$$

where f^w is an external supply of water. It should be pointed out that, in this form, the dependence of the storage term on porosity variations does not appear explicitly. To do so, the equation for mineral mass balance will be resorted to, as described below.

3.1.3 Air mass balance equation

As pointed out above, dry air is considered as a single species and the gaseous phase is a mixture of air and water vapour. Air is also dissolved in the liquid phase. The total air content in the porous medium is expressed by:

$$\theta_l^a S_l \phi + \theta_g^a S_g \phi \quad [11]$$

The mass fluxes of air in each fluid phase are

$$\mathbf{j}_l^a = \mathbf{i}_l^a + \theta_l^a \mathbf{q}_l + \theta_l^a S_l \phi \dot{\mathbf{u}} = \mathbf{j}'_l^a + \theta_l^a S_l \phi \dot{\mathbf{u}} \quad [12]$$

$$\mathbf{j}_g^a = \mathbf{i}_g^a + \theta_g^a \mathbf{q}_g + \theta_g^a S_g \phi \dot{\mathbf{u}} = \mathbf{j}'_g^a + \theta_g^a S_g \phi \dot{\mathbf{u}} \quad [13]$$

where \mathbf{i}_l^a and \mathbf{i}_g^a are the nonadvective fluxes of water in the liquid and gas phases. The air mass balance equation is:

$$\frac{\partial}{\partial t} (\theta_l^a S_l \phi + \theta_g^a S_g \phi) + \nabla \cdot (\mathbf{j}'_l^a + \mathbf{j}'_g^a) = f^a \quad [14]$$

3.2 Energy balance equation

Although the energy balance reduces to enthalpy balance in most cases, it is possible to express it in terms of internal energy. If thermal equilibrium between phases is assumed, the temperature is the same in all phases and only one equation

of total energy is required. Adding the internal energy of each phase, the total internal energy per unit volume of porous medium becomes:

$$E_s \rho_s (1 - \phi) + E_l \rho_l S_l \phi + E_g \rho_g S_g \phi \quad [15]$$

where E_s , E_l and E_g are the specific internal energies corresponding to each phase, i.e. the internal energy per unit mass of phase.

The most important processes for energy transfer in a porous medium are conduction, advection and phase change (Bear et al. 1991). Using the specific internal energies and the species mass fluxes, the energy fluxes due to the motion of phases can be written as:

$$\mathbf{j}_{E_s} = E_s \rho_s (1 - \phi) \dot{\mathbf{u}} \quad [16]$$

$$\mathbf{j}_{E_l} = \mathbf{j}_l^w E_l^w + \mathbf{j}_l^a E_l^a + E_l \rho_l S_l \phi \dot{\mathbf{u}} = \mathbf{j}_{E_l}^w + E_l \rho_l S_l \phi \dot{\mathbf{u}} \quad [17]$$

$$\mathbf{j}_{E_g} = \mathbf{j}_g^w E_g^w + \mathbf{j}_g^a E_g^a + E_g \rho_g S_g \phi \dot{\mathbf{u}} = \mathbf{j}_{E_g}^w + E_g \rho_g S_g \phi \dot{\mathbf{u}} \quad [18]$$

where $\mathbf{j}_{E_l}^w$ and $\mathbf{j}_{E_g}^w$ are advective energy fluxes with respect to the solid phase.

Using those definitions, the energy balance equation is expressed as:

$$\frac{\partial}{\partial t} (E_s \rho_s (1 - \phi) + E_l \rho_l S_l \phi + E_g \rho_g S_g \phi) + \nabla \cdot (\mathbf{i}_c + \mathbf{j}_{E_s} + \mathbf{j}_{E_l} + \mathbf{j}_{E_g}) = f^Q \quad [19]$$

where \mathbf{i}_c is the heat conduction flux and f^Q is an internal/external energy supply. The internal production could include, for instance, energy dissipation due to medium deformation, but this is generally negligible.

3.3 Momentum balance equation

The balance of momentum for a porous medium reduces to the equilibrium equation for macroscopic total stresses, if inertial terms are neglected (Bear and Bachmat 1986):

$$\nabla \cdot \boldsymbol{\sigma} + \mathbf{b} = \mathbf{0} \quad [20]$$

where $\boldsymbol{\sigma}$ are total stresses and \mathbf{b} is the vector of body forces. This assumption is usually accepted because in Environmental Geomechanics problems both velocities and accelerations are small, yielding terms that are negligible in comparison with the stress terms.

3.4 Algebraic transformation of balance equations

The mass balance equations derived above can be conveniently transformed by introducing the equation for mineral mass into the other three balance equations. In this way the effect of porosity variation on the storage term is explicitly incorporated and the mineral balance equation is eliminated from the set of equations to be solved.

To perform this algebraic transformation it is useful to consider the definition of material derivative with respect to the solid velocity:

$$\frac{D_s(\bullet)}{Dt} = \frac{\partial(\bullet)}{\partial t} + \frac{d\mathbf{u}}{dt} \cdot \nabla(\bullet) \quad [21]$$

Using this definition, the mineral mass balance equation can be expressed as:

$$\frac{D_s\phi}{Dt} = \frac{1}{\theta_s} \left[(1-\phi) \frac{D_s\theta_s}{Dt} \right] + (1-\phi) \nabla \cdot \frac{d\mathbf{u}}{dt} \quad [22]$$

An explicit expression for the variation of porosity with time has been obtained. The first term refers to porosity changes due to variations in solid density and the second term reflects the porosity variations caused by volumetric soil deformation. If the first term is neglected, the expression for porosity variation, characteristic of consolidation analysis, is obtained:

$$\frac{D_s\phi}{Dt} = (1-\phi) \nabla \cdot \frac{d\mathbf{u}}{dt} \quad [23]$$

The equation of water mass balance [10], is transformed substituting definitions [8] and [9] and using the material derivative with respect to the solid velocity field [21]:

$$\begin{aligned} & \phi \frac{D_s(\theta_l^w S_l + \theta_g^w S_g)}{Dt} + (\theta_l^w S_l + \theta_g^w S_g) \frac{D_s\phi}{Dt} + \\ & (\theta_l^w S_l \phi + \theta_g^w S_g \phi) \nabla \cdot \frac{d\mathbf{u}}{dt} + \nabla \cdot (\mathbf{j}_l^w + \mathbf{j}_g^w) = f^w \end{aligned} \quad [24]$$

It can be noted that there now exists a term expressing the total variation of porosity with time. Introducing equation [23], the following is obtained:

$$\phi \frac{D_s(\theta_l^w S_l + \theta_g^w S_g)}{Dt} + (\theta_l^w S_l + \theta_g^w S_g) \nabla \cdot \frac{d\mathbf{u}}{dt} + \nabla \cdot (\mathbf{j}_l^w + \mathbf{j}_g^w) = f^w \quad [25]$$

It is also noteworthy that the fluxes that appear in the transformed equation are fluxes with respect to the solid phase, a form more convenient for applying the conventional constitutive laws.

By similar manipulations the transformed equation for the air mass balance equation can also be obtained:

$$\begin{aligned} & \phi \frac{D_s(\theta_l^a S_l + \theta_g^a S_g)}{Dt} + (\theta_l^a S_l + \theta_g^a S_g) \frac{D_s\phi}{Dt} + \\ & (\theta_l^a S_l \phi + \theta_g^a S_g \phi) \nabla \cdot \frac{d\mathbf{u}}{dt} + \nabla \cdot (\mathbf{j}_l^a + \mathbf{j}_g^a) = f^a \end{aligned} \quad [26]$$

Again resorting to [23] gives

$$\phi \frac{D_s(\theta_l^a S_l + \theta_g^a S_g)}{Dt} + (\theta_l^a S_l + \theta_g^a S_g) \nabla \cdot \frac{d\mathbf{u}}{dt} + \nabla \cdot (\mathbf{j}_l^a + \mathbf{j}_g^a) = f^a \quad [27]$$

Similarly, for the energy balance equation:

$$\begin{aligned}
& \phi \frac{D_s(E_l \rho_l S_l + E_g \rho_g S_g)}{Dt} + (1-\phi) \frac{D_s(E_s \rho_s)}{Dt} + \\
& (E_l \rho_l S_l + E_g \rho_g S_g) \frac{D_s \phi}{Dt} + E_s \rho_s \frac{D_s(1-\phi)}{Dt} + \\
& (E_s \rho_s (1-\phi) + E_l \rho_l S_l \phi + E_g \rho_g S_g \phi) \nabla \cdot \frac{d\mathbf{u}}{dt} + \\
& \nabla \cdot (\mathbf{i}_c + \mathbf{j}'_{Es} + \mathbf{j}'_{El} + \mathbf{j}'_{Eg}) = f^E
\end{aligned} \tag{28}$$

and introducing [23],

$$\begin{aligned}
& \phi \frac{D_s(E_l \rho_l S_l + E_g \rho_g S_g)}{Dt} + (1-\phi) \frac{D_s(E_s \rho_s)}{Dt} + \\
& + (E_l \rho_l S_l + E_g \rho_g S_g) \nabla \cdot \frac{d\mathbf{u}}{dt} + \nabla \cdot (\mathbf{i}_c + \mathbf{j}'_{Es} + \mathbf{j}'_{El} + \mathbf{j}'_{Eg}) = f^E
\end{aligned} \tag{29}$$

It must be noted that in these transformed equations, material derivatives can be approximated by eulerian ones if small strain rates are assumed but the variation of porosity due to volume change is not neglected. This is equivalent to the classical way of obtaining coupled flow-deformation formulation for porous media. A conceptual advantage lies in the fact that, now, the point of introduction of the assumption of small strains is precisely identified.

At this stage, it is convenient to associate each balance equation with a state variable that will play the role of main unknown of the mathematical problem to be solved. Obviously, this association is somewhat arbitrary, as every equation is related to several variables. However, it is possible to identify for all equations the variable that, in the majority of problems, is the most relevant one. Thus, state variables are selected as follows: solid velocity, \mathbf{u} for the stress equilibrium equations, liquid pressure, P_l , for the water balance equation, gas pressure, P_g , for the air balance equation and temperature, T , for the energy balance equation. These balance equations constitute the set of governing equations that must be solved simultaneously in order to take into account all the range of coupled phenomena. To this end it is necessary to use numerical methods via a suitable discretization technique. This aspect of the problem is described in detail in (Charlier et al. 2001).

4. Constitutive equations

In addition to the state variables, there are many others that affect the thermo-hydro-mechanical problem. The closure of the formulation requires, therefore, the incorporation of further equations in the form of constitutive laws and equilibrium restrictions. Here, the basic constitutive laws are presented, divided in thermal, hydraulic and mechanical. In spite of this distinction between the three basic components of the problem, the constitutive equation provide in fact the links that couple the various phenomena considered in the formulation.

4.1 Thermal constitutive equations

Heat conduction is assumed to be governed by Fourier's law:

$$\mathbf{i}_c = -\lambda \nabla T \quad [30]$$

where λ is the thermal conductivity of the whole porous media. The heat transport by conduction through a porous media is a complex phenomenon in which all three phases play a significant part. The overall thermal conductivity reduces as porosity increases and as degree of saturation decreases. Empirical observations have shown that a reasonable approximation can be obtained by adopting the geometric mean of the thermal conductivities of the three phases. In that case:

$$\lambda = \lambda_s^{(1-\phi)} \lambda_l^{\phi S_i} \lambda_g^{\phi(1-S_i)} = \lambda_{sat}^{S_i} \lambda_{dry}^{1-S_i} \quad [31]$$

where

$$\lambda_{sat} = \lambda_s^{(1-\phi)} \lambda_l^{\phi} \quad \lambda_{dry} = \lambda_s^{(1-\phi)} \lambda_g^{\phi} \quad [32]$$

It can be observed that hydraulic coupling is introduced by the dependence on degree of saturation and mechanical coupling by the influence of porosity. Sometimes, thermal conductivity may depend on temperature as well, giving rise to a nonlinear conduction law. Figure 3 shows experimental results concerning the thermal conductivity variation with degree of saturation for a compacted bentonite. A comparison with the proposed law is also provided.

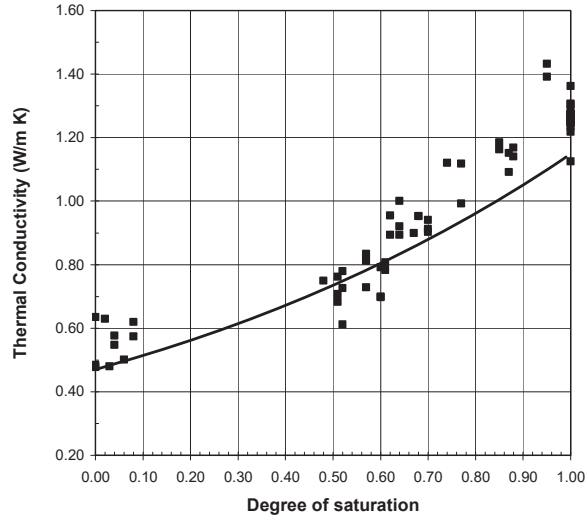


Figure 3 : Dependence of thermal conductivity on degree of saturation for a compacted bentonite

As pointed out before, the total internal energy per unit volume of a porous medium is computed by simply adding the internal energy of the three phases:

$$E_s \rho_s (1 - \phi) + E_l \rho_l S_l \phi + E_g \rho_g S_g \phi \quad [33]$$

where E_s , E_l and E_g are the specific internal energy corresponding to each phase, i.e. the internal energy per unit mass of phase.

The gas phase energy is usually expressed as:

$$E_g \rho_g = (E_g^w \omega_g^w + E_g^a \omega_g^a) \rho_g = E_g^w \theta_g^w + E_g^a \theta_g^a \quad [34]$$

where E_g^w and E_g^a are the specific internal energies of species (water and air). This additive decomposition is admissible for the gaseous phase because of the assumption of mixture of gasses.

It is not so immediate that the same decomposition is also valid for the liquid phase where there is a solution and not a mixture. However the same hypothesis will be made since the significance of the internal energy of dissolved air is small:

$$E_l \rho_l = (E_l^w \omega_l^w + E_l^a \omega_l^a) \rho_l = E_l^w \theta_l^w + E_l^a \theta_l^a \quad [35]$$

The values of the specific internal energies for the individual species are: $E_l^w = 4180.0 (T - T_o)$ (J/Kg), $E_l^a = 1006.0 (T - T_o)$ (J/Kg), $E_g^a = 1006.0 (T - T_o)$ (J/Kg) and $E_g^w = 2.5 \times 10^6 + 1900.0 (T - T_o)$ (J/Kg).

It can be noted that the specific internal energy of the vapour (water in gas phase) contains an additional term that represents the latent heat in vapour. The thermal consequences of evaporation/condensation are therefore taken into account in a straightforward manner.

4.2 Hydraulic constitutive equations

4.2.1 Advection (phase) fluxes

Balance of momenta for fluid phases are reduced to constitutive equations and advective fluxes are computed using generalized Darcy's law (Bear 1979), expressed as:

$$\mathbf{q}_l = -\mathbf{K}_l (\nabla P_l - \rho_l \mathbf{g}) \quad [36]$$

$$\mathbf{q}_g = -\mathbf{K}_g (\nabla P_g - \rho_g \mathbf{g}) \quad [37]$$

where \mathbf{K} is the permeability tensor, and \mathbf{g} the gravity vector. As pointed out above, Darcy's law refers to the relative motion of the fluid phase with respect to the solid phase.

The permeability tensor is not constant but in turn depends on other variables:

$$\mathbf{K}_\alpha = \mathbf{k} k_{r\alpha} / \mu_\alpha \quad [38]$$

where \mathbf{k} is the intrinsic permeability tensor, $k_{r\alpha}$ is the relative permeability and μ_α is the dynamic viscosity. Note that α stands for l or g depending on which phase is being considered.

Relative permeability expresses the variation of permeability with degree of saturation (or suction):

$$k_{rl} = f(S_l) \quad \text{or} \quad k_{rl} = f(s) \quad ; \quad k_{rg} = 1 - k_{rl} \quad ; \quad s = P_g - P_l \quad [39]$$

This dependence is very strong, the permeability may change orders of magnitude over limited ranges of degree of saturation or suction (Figure 4).

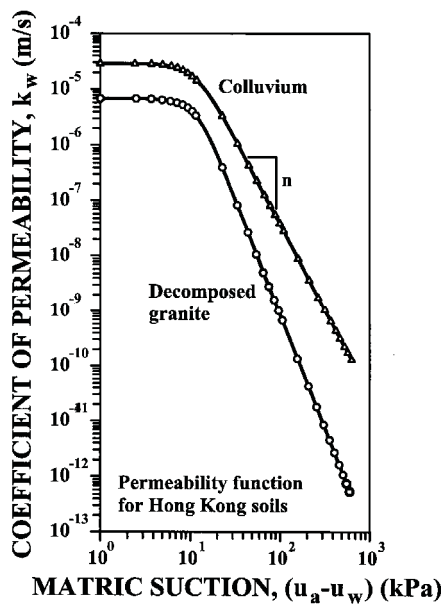


Figure 4 : Variation of permeability with suction for various materials

Intrinsic permeability is often made dependent on porosity (Figure 5). However, although porosity does indeed have an important influence on permeability, it should not be forgotten that permeability depends also on pore structure and pore size distribution. This fact is not very significant in granular materials but it may be dominant in materials that undergo important changes in fabric such as, for instance, swelling clays during hydration. Often, the intrinsic permeabilities for gas and liquid are assumed identical. However, experimental evidence demonstrates that this is by no means always the case (Villar 1998, Volckaert et al. 1994). Sometimes this is due to well-attested phenomena such as the Knudsen effect whereas in other cases simply reflect the changes in pore size distribution of the material.

Again, advective flow exhibits coupling with the thermal problem, via the variation of fluid viscosity, with the hydraulic problem through the expression for relative permeability and with the mechanical problem due to the effect of porosity (or pore structure) on intrinsic permeability.

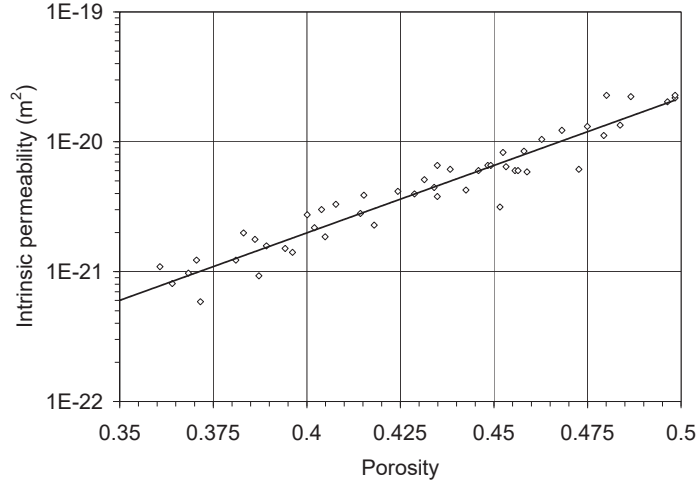


Figure 5 : Variation of intrinsic permeability with porosity for a compacted bentonite (Villar 2000)

4.2.2 Nonadvective (species) fluxes

The nonadvective fluxes of the different species in a phase are subject to the constraint:

$$\sum_i \mathbf{i}_\alpha^i = 0, \quad \alpha = l, g \quad [40]$$

where $i = \omega, a$ for $\alpha = g$ or l . Often, nonadvective fluxes are called species diffusion.

Gas phase is considered a mixture of two species. For most problems, molecular diffusion is dominant and it complies with [40]. Therefore the nonadvective flux of air is simply equal the nonadvective flux of vapour with opposite sign (Bear et al 1991). The same approach is used for the nonadvective flow of dissolved air in liquid.

Nonadvective fluxes are computed through Fick's law that expresses them in terms of gradients of mass fraction of species through a hydrodynamic dispersion tensor that includes both molecular diffusion and mechanical dispersion (Pollock 1986):

$$\mathbf{i}_\alpha^i = -\mathbf{D}_\alpha^i \nabla \omega_\alpha^i \quad i = w, a \quad \alpha = g, l \quad [41]$$

For vapour diffusion, the following expression for the hydrodynamic dispersion tensor is adopted:

$$\mathbf{i}_g^w = -\mathbf{D}_g^w \nabla \omega_g^w = -\left(\phi \rho_g S_g \tau D_m^w \mathbf{I} + \rho_g \mathbf{D}'_g \right) \nabla \omega_g^w \quad [42]$$

where \mathbf{D}_g^w is the dispersion tensor, τ is the tortuosity, D_m^w is the dispersion coefficient corresponding to molecular diffusion of vapour in air and \mathbf{D}'_g is the mechanical dispersion tensor. The value of the molecular diffusion coefficient is given by:

$$D_m^w (\text{m}^2/\text{s}) = 5.9 \times 10^{-12} \frac{(273.15 + T)^{2.3}}{P_g} \quad [43]$$

A usual expression for the mechanical dispersion tensor is:

$$\mathbf{D}'_g = d_t |\mathbf{q}_g| \mathbf{I} + (d_l - d_t) \frac{\mathbf{q}_g \mathbf{q}_g^t}{|\mathbf{q}_g|} \quad [44]$$

where d_t and d_l are the transversal and longitudinal dispersivities respectively. Generally, molecular diffusion is dominant and it will be possible to neglect mechanical dispersion of vapour unless advective velocities are very high.

It can be remarked that in vapour diffusion, the couplings with all three aspects of the formulation again appear: thermal effects through the variation of molecular diffusion with temperature, hydraulic effects through the influence of degree of saturation and mechanical effects due to porosity changes.

The same considerations can be made regarding diffusion of air in the liquid phase:

$$\mathbf{i}_l^a = -\mathbf{D}_l^a \nabla \omega_l^a = -\left(\phi \rho_l S_l \tau^a D_m^a \mathbf{I} + \rho_l \mathbf{D}'_l \right) \nabla \omega_l^a \quad [45]$$

4.2.3 Retention (characteristic) curve

The retention or characteristic curve expresses the relationship between degree of saturation and suction. This is an important law that has a crucial influence on unsaturated flow and provides useful information regarding the type of soil and the features of its pore structure (Figure 6). Generally, characteristic curves exhibit hysteresis effects with the drying curve not coinciding with the wetting curve. A number of proposals have been put forward to account for this feature of behaviour (Vaunat et al. 2000).

A widely used expression for the characteristic curve was given by (Van Genuchten 1980):

$$\frac{S_l - S_{lr}}{S_{ls} - S_{lr}} = S_e = \left(1 + \left(\frac{s}{P} \right)^{1-\lambda} \right)^{-\lambda} \quad [46]$$

where λ and P are parameters. The parameter P can be assimilated to the air entry value of the material. It is therefore reasonable to expect that P will be proportional to the surface tension, σ_o . Surface tension depends on temperature as:

$$\sigma_o(T) = 0.03059 \exp\left(\frac{252,93}{273,15+T}\right) \text{ in N/m} \quad [47]$$

By varying P in accordance with this expression, a dependence of the characteristic curve with temperature is introduced, albeit a small one. The experimental evidence, however, has shown that, in most cases, the influence of temperature on the characteristic curve is indeed small (Romero and Vaunat 2000).

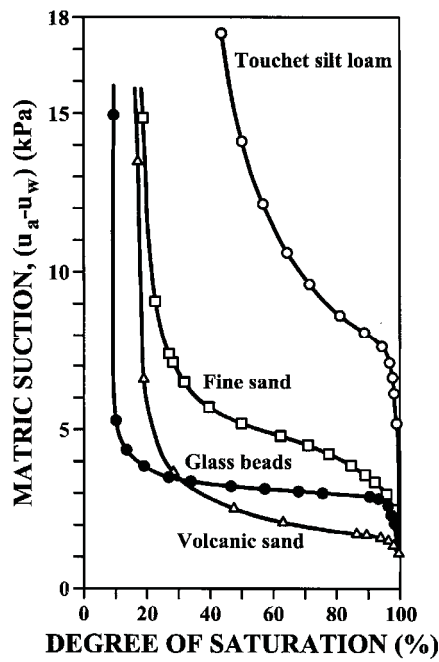


Figure 6 : Characteristic curves for various soils (Brooks and Corey, 1964)

An attractive feature of Van Genuchten expression is that an associated relative permeability relationship can be used with the same parameters:

$$k_{rl} = S_e^{1/2} \left(1 - \left(1 - S_e^{1/\lambda} \right)^\lambda \right)^2 \quad [48]$$

It should be pointed out that this expression is not very suitable for very low permeability soils where alternative functions can be adopted.

Sometimes, characteristic curves are expressed in terms of water content vs. suction, although this is less convenient for numerical analysis as the water content

of full saturation changes with porosity. An advantage is that, for clayey soils, there appears to be a unique relationship between suction and water content when suctions are high. This corresponds to the situation when most of the water occupies the very small pores where basic surface physico-chemical phenomena predominate. Figure 7 (Romero and Vaunat 2000) illustrates this fact for a bentonite compacted at two dry densities. It can be observed that the relationship suction-water content becomes quasi-unique at high suctions in spite of the difference in porosity and fabric. When saturation approaches, the effect of differing dry densities are clearly apparent. It is also noteworthy that hysteresis at high suctions is nearly absent when data is plotted in this way.

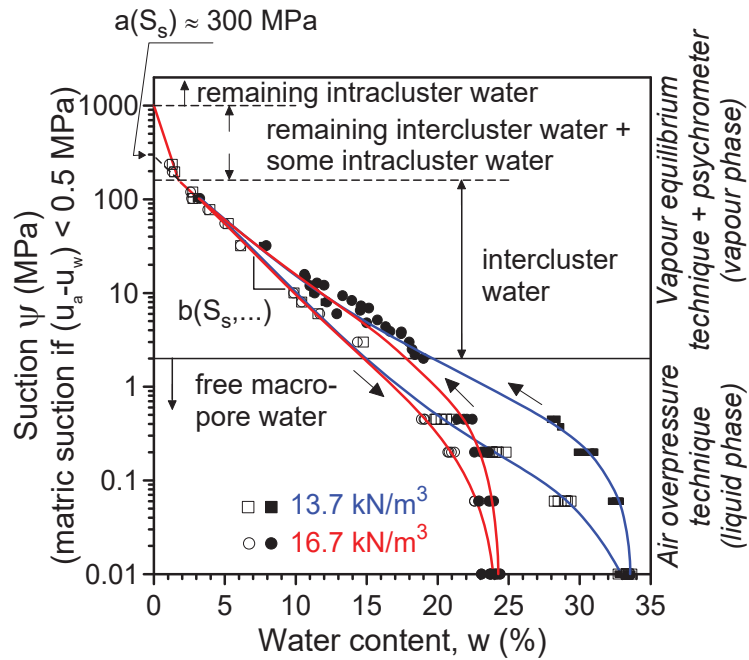


Figure 7 : Characteristic curves for bentonite compacted at two different dry densities

4.3 Mechanical constitutive equations

The mechanical behaviour of porous materials and of soils in particular is very intricate which has led to the development of mechanical constitutive models with a high degree of complexity. Naturally when dealing with the THM behaviour of soils the level of complexity increases even further. A general form of a suitable constitutive equation, showing explicitly the independent contributions of strains, temperature and suction, is:

$$d\boldsymbol{\sigma} = \mathbf{D}d\boldsymbol{\varepsilon} + \boldsymbol{\beta}dT + \mathbf{h}ds \quad [49]$$

where $\boldsymbol{\sigma}$ is the constitutive stress, $\boldsymbol{\varepsilon}$ the strains, \mathbf{D} the constitutive stiffness matrix, $\boldsymbol{\beta}$ the constitutive vector relating stresses and temperature and \mathbf{h} the constitutive vector relating stresses and suction (Gens 1995). It should be pointed out that the coupling of the mechanical behaviour with other THM phenomena is not only expressed in the fact that there are now two additional terms but it also affects the coefficients of \mathbf{D} , $\boldsymbol{\beta}$ and \mathbf{h} by making them nonlinear and potentially dependent on other mechanical, hydraulic or thermal variables. The issue of mechanical constitutive laws for saturated and unsaturated materials is dealt with in detail in (Laloui 2001, Laloui et al. 2001).

4.4 Phase physical properties

The properties of the fluid phases appear in the balance equations and in the constitutive laws. In general, they depend on the composition of the phase and on the state variables (temperatures and pressures). Some of them such as surface density and specific energy have already been defined above. It remains however to specify expressions for density and viscosity.

The function of density for the liquid phase can be expressed as:

$$\rho_l \text{ (kg/m}^3\text{)} = 1002.6 \exp(4.5 \times 10^{-4}(P_l - 0.1) - 3.4 \times 10^{-4}T) \quad [50]$$

It can be noted that the effect of presence of air is neglected. This expression must have a cut-off for significant negative liquid pressures; otherwise, unrealistic density reductions are obtained.

The air density and the vapour densities are obtained from the law of ideal gases:

$$\theta_g^a = \frac{M_a P_a}{R(273.15 + T)} \quad [51]$$

$$\theta_g^w = \frac{M_w P_v}{R(273.15 + T)} \quad [52]$$

where P_a is the partial pressure of air, M_a the molecular mass of air (0.02895 kg/mol), P_v is the partial pressure of vapour and M_w the molecular mass of water (0.018 kg/mol).

The density of the gas phase is obtained adding the partial densities of the two species:

$$\rho_g = \theta_g^a + \theta_g^w \quad [53]$$

Finally, the viscosities of the liquid and gas phase are, respectively (Hassanizadeh and Leijnse 1988):

$$\mu_l \text{ (MPa} \cdot \text{s)} = 2,1 \times 10^{-12} \exp\left(\frac{1808.5}{273.15 + T}\right) \quad [54]$$

$$\mu_g \text{ (MPa} \cdot \text{s)} = 1.48 \times 10^{-12} \frac{(273.15 + T)^{1/2}}{1 + \frac{119}{273.15 + T}} \quad [55]$$

5. Equilibrium restrictions

It is assumed that phase changes (air dissolution/exsolution and water evaporation/condensation) are rapid in relation to the characteristic times typical of this type of problems. Therefore, they can be considered in local equilibrium, giving rise to a set of equilibrium restrictions that must be satisfied at all times. This assumption has the added advantage that phase changes do not appear explicitly and the number of equations is thereby reduced.

To define the amount of air dissolved in water, Henry's law is adopted. This law expresses a linear relationship between the concentration of air in dissolution and the partial pressure of air in the gaseous phase:

$$\theta_l^a = \omega_l^a \rho_l = \frac{P_a}{H} \frac{M_a}{M_w} \rho_l \quad [56]$$

where ω_l^a is the mass fraction of gas in the liquid phase and H Henry's constant (1000 MPa).

Finally, the vapour concentration in the gaseous phase is governed by the psychrometric law:

$$\theta_g^w = (\theta_g^w)^0 \exp\left(\frac{\psi M_w}{R(273.15 + T)\rho_l}\right) \quad [57]$$

where θ_g^w is the vapour concentration in the gas phase, $(\theta_g^w)^0$ is the vapour concentration in the gas phase in equilibrium with a liquid with a flat surface (at the same temperature), ψ is the total potential of the water (excluding gravity terms), M_w is the molecular mass of water (0.018 kg/mol) and R the gas constant (8.314 J/mol^oK).

6. Summary of formulation

A theoretical formulation that encompasses the main THM phenomena occurring in a porous medium has been described in some detail. The core of the formulation is constituted by the four balance conditions corresponding to water mass balance, air mass balance, internal energy balance and momentum balance, equations [25], [27], [29] and [20]. They must be solved together to account for the range of couplings between different phenomena. The formulation is completed by the set of constitutive laws and equilibrium restrictions. To summarize, a number of the most

important features and assumptions made in the development of the formulation are given here:

- State variables are: solid displacements, \mathbf{u} (three spatial directions); liquid pressure, P_l ; gas pressure, P_g ; and temperature, T .
- Balance of momentum for the medium as a whole is reduced to the equation of stress equilibrium together with a mechanical constitutive model to relate stresses with strains. Strains are defined in terms of displacements.
- Advective terms due to solid displacement can be neglected after the formulation is transformed in terms of material derivatives, if small strains and small strain rates are assumed for solid deformation. Then material derivatives are approximated as eulerian time derivatives and volumetric strains are properly considered.
- Thermal equilibrium between phases is assumed. This means that the three phases are at the same temperature
- Balance of momentum for dissolved species and for fluid phases are reduced to constitutive equations (Fick's law and Darcy's law).
- Dry air is considered a single species and, usually, it is the main component of the gaseous phase. Henry's law is used to express equilibrium of dissolved air.
- Vapour concentration is in equilibrium with the liquid phase, the psychrometric law expresses its concentration.
- Physical parameters in constitutive laws depend on pressure and temperature.

The formulation, once discretized and incorporated into a suitable numerical scheme, can be applied to the solution of THM engineering problems involving saturated and unsaturated porous media.

7. References

- BEAR, J. (1979). *Dynamics of Fluids in Porous Media*, 1979, American Elsevier.
- BEAR, J., BACHMAT, Y. (1986). Macroscopic modelling of transport phenomena in porous media. 2: Applications to mass, momentum and energy transport. *Transport in Porous Media*, 1, 213-240.
- BEAR, J., BENSABAT, J., NIR, A. (1991). Heat and mass transfer in unsaturated porous media at a hot boundary:1. One-dimensional analytical model, *Transport in Porous Media*, 6, 281-298.
- DE BOER, R. (1996). Highlights in the historical development of the porous media theory – toward a consistent macroscopic theory, *Appl. Mech. Rev.*, 49, 201-262.
- CHARLIER, R., RADU, J.-P., COLLIN, F. (2001): Numerical modelling of coupled transient phenomena, *Environmental Geomechanics*, Hermes Science Publications, Paris.
- COUSSY, O. (1995). *Mechanics of porous media*, J. Wiley and Sons, New York.
- COUSSY, O., EYMOND, R., LASSABATERE, T. (1998). Constitutive Modeling of unsaturated drying deforming materials, *J. Eng. Mechanics, ASCE*, 124, 658-667.

- EHLERS, W., VOLK, W. (1998) On theoretical and numerical methods in the theory of porous media based on polar and non-polar solid materials, *Int. J. Solids and Structures*, 35, 4597-4616.
- GENS, A., (1995). Constitutive laws, *Modern issues in non-saturated soils* (Gens, Jouanna, Schrefler, eds.), Springer Verlag, Wien, 129-158.
- HASSANIZADEH, S.M., GRAY, W.G. (1979a). General conservation equations for multiphase systems: 1. Averaging procedures, *Adv. Water Resour.*, 2, 131-144.
- HASSANIZADEH, S.M., GRAY, W.G. (1979b). General conservation equations for multiphase systems: 2. Mass, momenta, energy and entropy equations, *Adv. Water Resour.*, 2, 191-208.
- HASSANIZADEH, S.M., GRAY, W.G. (1980). General conservation equations for multiphase systems: 3. Constitutive theory for porous media, *Adv. Water Resour.*, 3, 5-40.
- HASSANIZADEH, S.M. (1986). Derivation of basic equations of mass transport in porous media, Part I. Macroscopic balance laws. *Adv. Water Resour.*, 9, 196-206.
- HASSANIZADEH, S.M., LEIJNSE, T. (1988). On the modelling of brine transport in porous media, *Water Resour. Res.*, 24, 321-330.
- LALOUI, L. (2001). Thermo-mechanical behaviour of soils, *Environmental Geomechanics*, Hermes Science Publications, Paris.
- LALOUI, L., GEISER, F., VULLIET, L. (2001). Constitutive modelling of unsaturated soils, *Environmental Geomechanics*, Hermes Science Publications, Paris.
- OLIVELLA, S., CARRERA, J., GENS, A., ALONSO, E.E. (1994). Non-isothermal multiphase flow of brine and gas through saline media, *Transport in Porous Media*, 15, 271-293.
- OLIVELLA, S., CARRERA, J., GENS, A., ALONSO, E.E. (1996). Porosity variations in saline media caused by temperature gradients coupled to multiphase flow and dissolution/precipitation, *Transport in Porous Media*, 25, 1-25.
- PANDAY, S., CORAPCIOGLU, M.Y. (1989). Reservoir transport equations by compositional approach, *Transport in Porous Media*, 4, 369-393.
- POLLOCK, D.W. (1986). Simulation of fluid flow and energy transport processes associated with high-level radioactive waste in unsaturated alluvium, *Water Resour. Res.*, 22, 765-775.
- REVIEW PANEL (1965). Engineering concepts of moisture equilibria and moisture changes in soils. *Moisture Equilibria and Moisture Changes in Soils Beneath Covered Areas*, Butterworth, Sidney, 7-21.
- ROMERO, E., VAUNAT, J. (2000). Retention curves of deformable clays, *Experimental Evidence and Theoretical Approaches in Unsaturated Soils* (Tarantino & Macuso, eds.), Balkema, Rotterdam, 91-106.
- THOMAS, H.R., CLEALL, P.J., (2001). Pollutant transport and chemical effects, *Environmental Geomechanics*, Hermes Science Publications, Paris.
- VAN GENUCHTEN, R. (1980). A closed-form equation for predicting the hydraulic conductivity of unsaturated soils, *Soil Sci. Soc. Am. J.*, 49, 892-898
- VAUNAT, J., ROMERO, E., JOMMI, C. (2000). An elastoplastic hydro-mechanical model for unsaturated soils, *Experimental Evidence and Theoretical Approaches in Unsaturated Soils* (Tarantino & Macuso, eds.), Balkema, Rotterdam, 121-138.
- VILLAR, M.V. (1998). *Ensayos para el proyecto FEBEX*, Report 70-IMA-l-5-51, 1998, CIEMAT, Madrid.
- VILLAR, M.V., (2000). *Caracterización termo-hidro-mecánica de una bentonita de Cabo de Gata*, Tesis Doctoral, 2000, Universidad Complutense de Madrid.
- VOLCKAERT, G.L., ORTIZ, L., DE CANNIERE, P., PUT, M., HORSEMAN, S.T., HARRINGTON, J.V., FIORAVANTE, V., IMPEY, M., (1994). Modelling and experiments in gas migration in repository host rocks, *MEGAS Project, Final Report, Phase 1*, 1994, European Commission, Brussels

Appendix F. Experimental evidences of high temperature effect, at lab scale (P. Delage)

EXPERIMENTAL EVIDENCES OF HIGH TEMPERATURE EFFECT, AT LAB SCALE

22 January 2020 • Pierre Delage, Ecole des Ponts ParisTech



The project leading to this application has received funding from the European Union's Horizon 2020 research and innovation programme under grant agreement n° 847593.

Date

Event

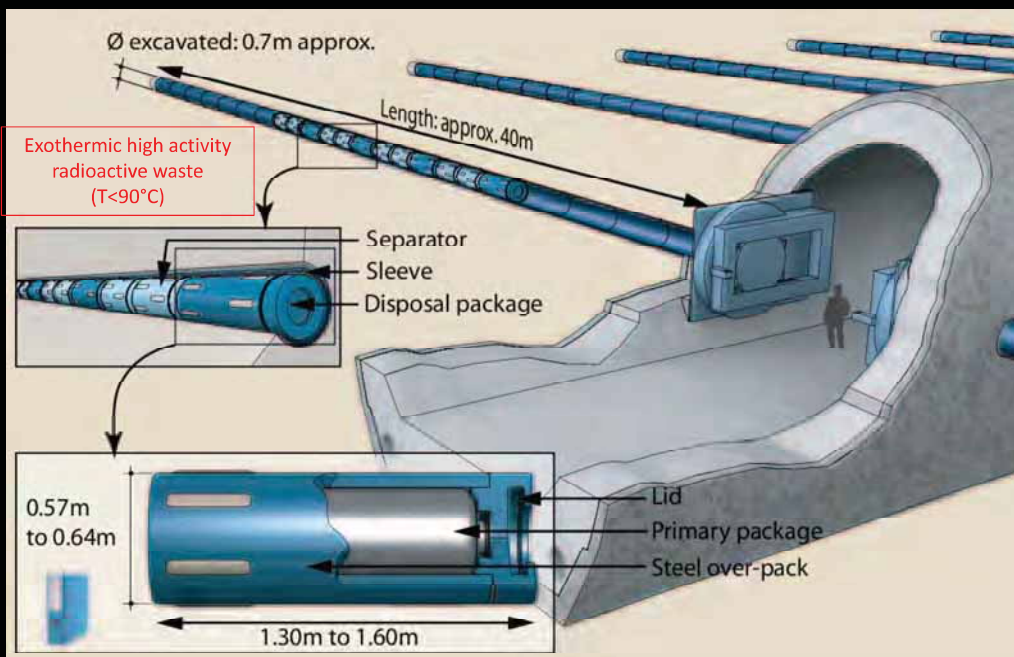
1

OUTLINE

- **Introduction**
- **Bentonites**
 - Water retention and transfer properties
 - Heat transfer properties
 - Effect of temperature on swelling
- **Clays and claystones**
 - Thermal pressurisation – Thermo-consolidation
 - Thermal volume changes
 - Effects of temperature on properties
- **Concluding remarks**



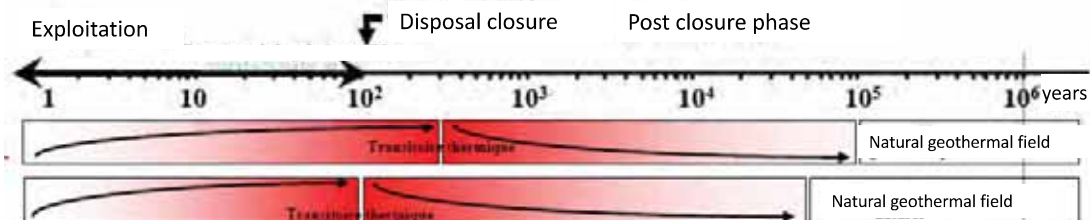
FRENCH CONCEPT, ANDRA: CLOSE CONTACT WITH HOST ROCK



eurad

3

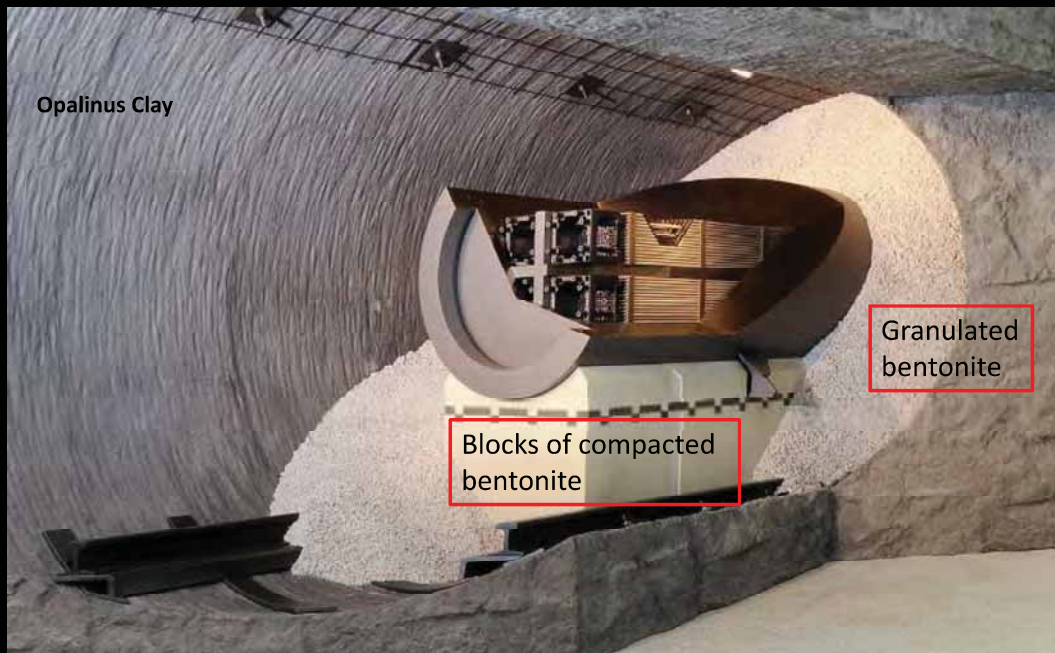
RADIOACTIVE WASTE DISPOSAL: THERMAL TRANSIENT PHASE (2)



eurad

4

SWISS CONCEPT, NAGRA: BENTONITE (THERMAL) BUFFER, GRANULATED BENTONITE



eurad

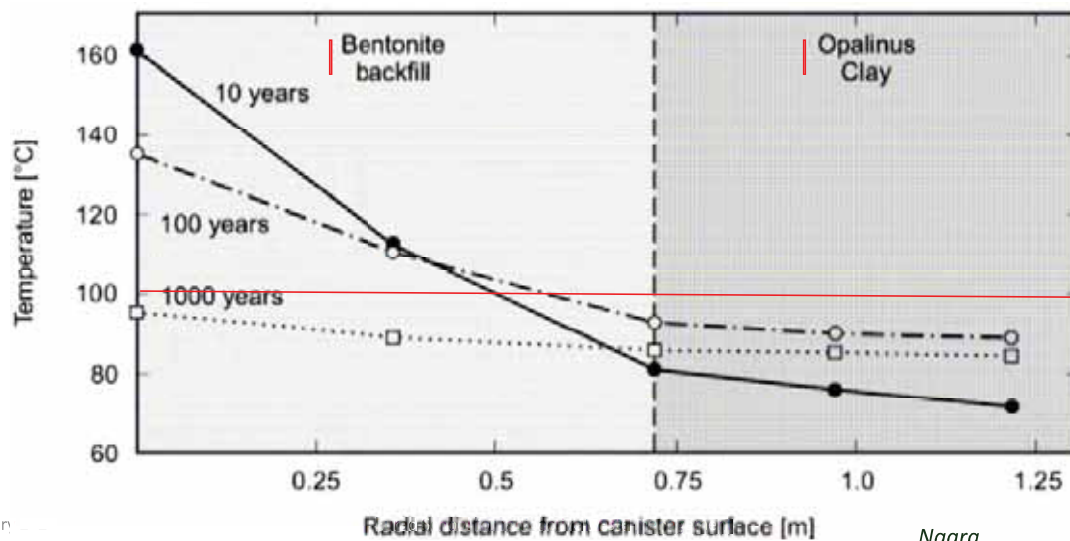
5

THERMAL TRANSIENT PHASE : SWISS CONCEPT



Temperatures > 100°C in compacted bentonite

Temperature < 100°C in host rock



eurad

6

FEBEX EXPERIMENT, COMPACTED BENTONITE BLOCKS (ENRESA)



1996

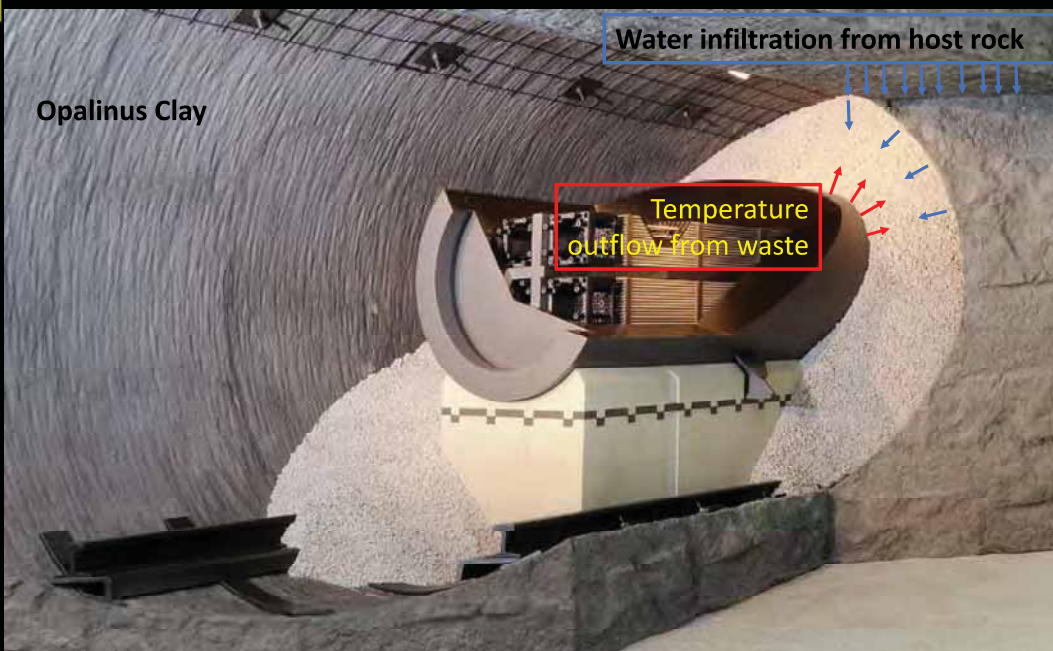


2014: 18 years T + H

eurad

7

COMBINED THM ACTIONS ON UNSATURATED SWELLING BUFFER



Opalinus Clay

Water infiltration from host rock

Temperature outflow from waste

Unsaturated state:
Water retention
Hydraulic conductivity

Unsaturated state:
Thermal conductivity

Liquid and vapour
transfers in a changing
porous medium, with
strong water/clay
interactions

eurad

8

BENTONITES

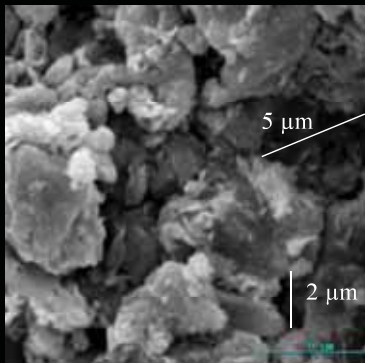
Water retention and transfer properties
Heat transfer properties
Effect of temperature on swelling

eurad

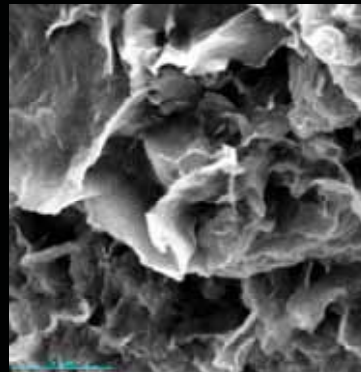
9

MICROSTRUCTURE OF ENGINEERED BARRIER SYSTEMS

Aggregate microstructure



Kunigel compacted clay,
dry density 1.8 Mg/m³



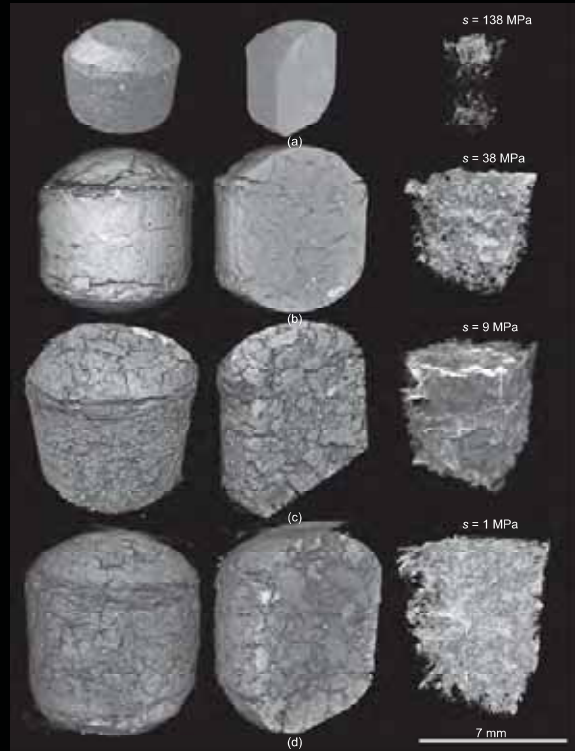
Free hydration

Cui, Loiseau and Delage (2002)

eurad

10

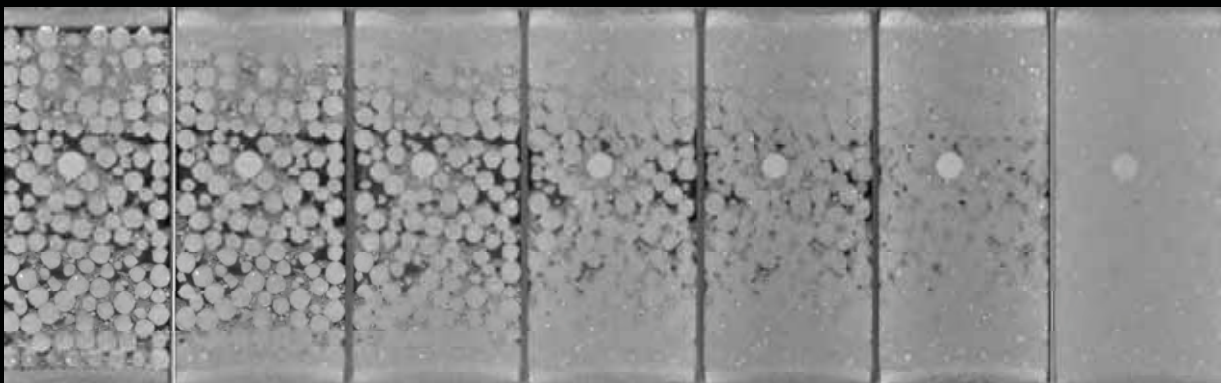
HYDRATION OF PELLETS



Molinero-Guerra, Delage, Cui et al. 2019

11

HYDRATION OF PELLETS



Event

Molinero-Guerra, Cui, Delage et al. 2018

12

CHARACTERISTICS OF SOME BENTONITES

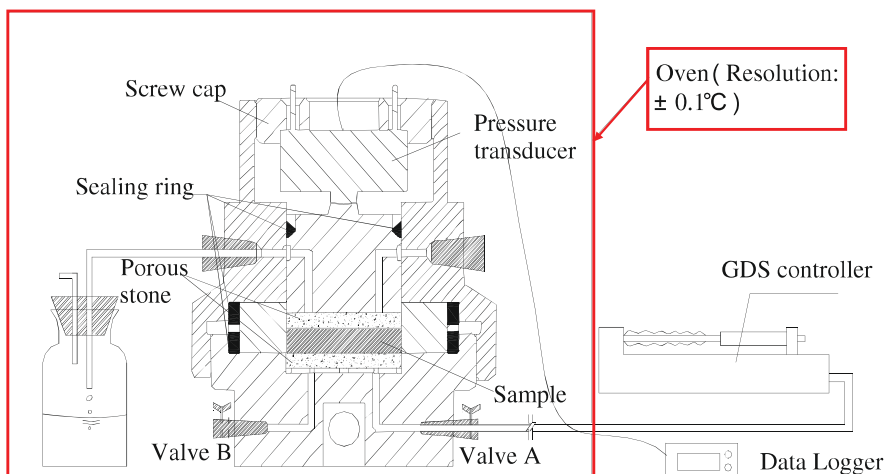
Parameter	Kunigel-V1 ^a	FoCa ^b	MX80 ^c	FEBEX ^d	GMZ ^e
Particle < 2 μm (%)	64.5	—	60	68	60
CEC (meq/100 g)	73.2	54	82.3	102 ^j	77.30
Base cations Exchange	Na-Ca	Ca	Na	Ca-Mg	Na-Ca
w_L (%)	474	112	519	102	313
w_P (%)	27	50	35	53	38
I_P	447	62	484	49	275
ρ_s (Mg/m ³)	2.79	2.67	2.76	2.70	2.66
S (m ² /g)	687	300	522	725	570

^aKomine (2004); ^bMarcial et al. (2002); ^cTang and Cui (2005); ^dENRESA (2000); ^eWen (2006).



EXPERIMENTAL TECHNIQUES

Constant volume swelling cell

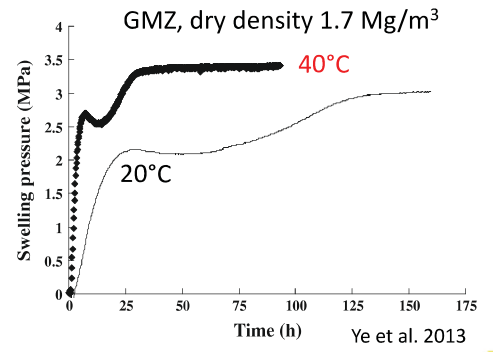
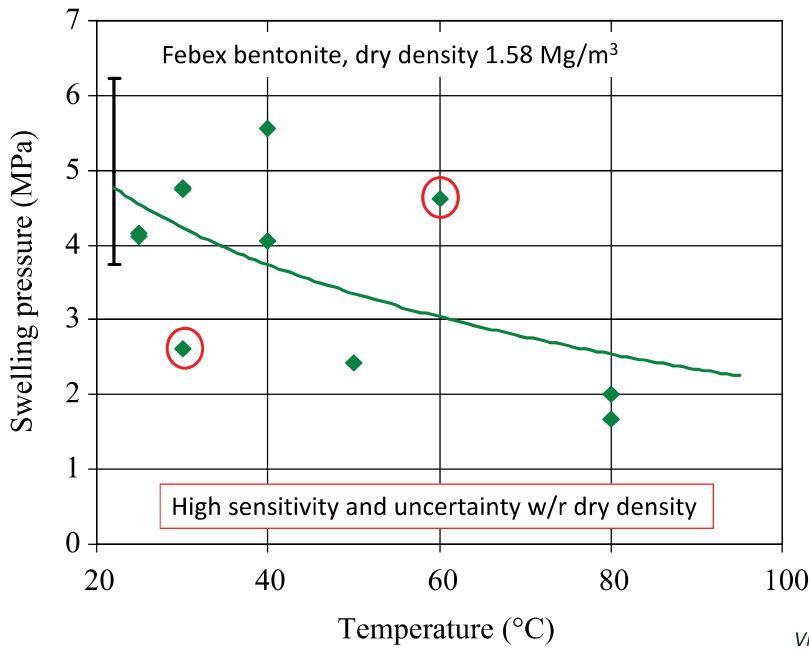


Temperature control techniques:

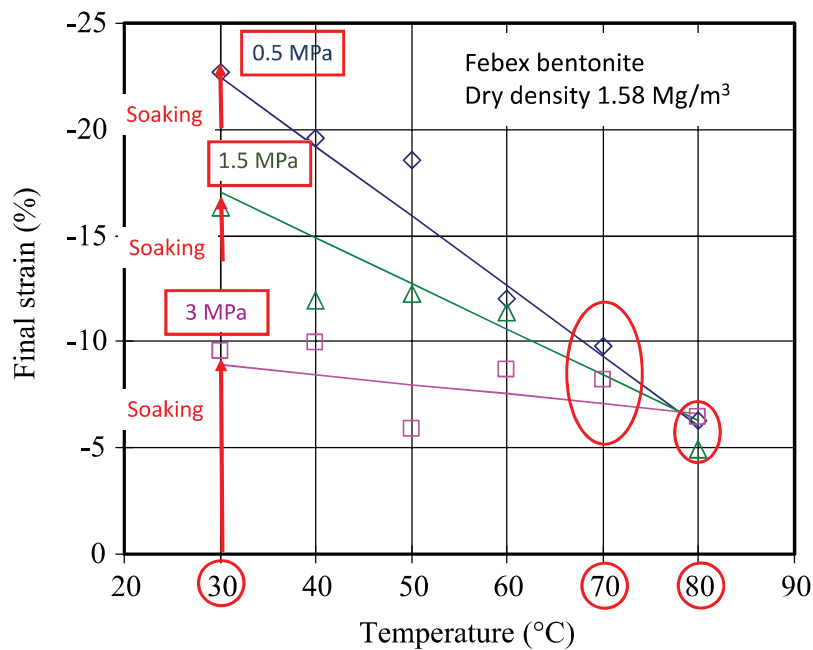
- Oven
- Temp. controlled bath
- Heating coil around cells



EFFECT OF TEMPERATURE ON SWELLING PRESSURE (CONSTANT VOLUME)

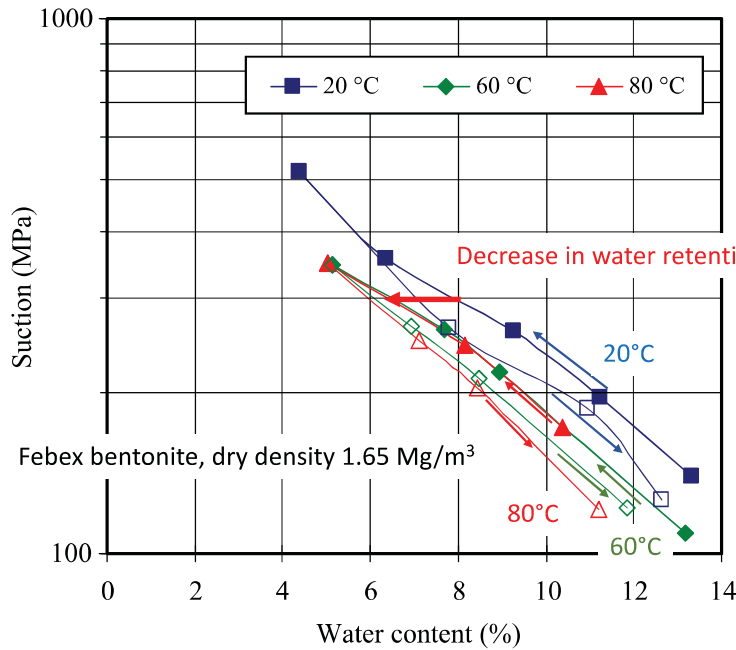


EFFECT OF TEMPERATURE ON SWELLING STRAIN





WATER RETENTION CURVES OF COMPACTED FEBEX BENTO AT VARIOUS TEMPERATURES (FREE SWELLING)

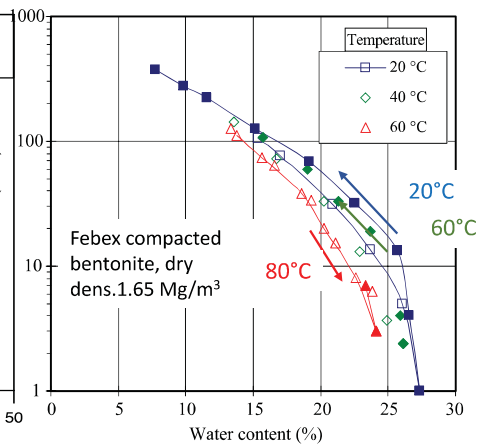
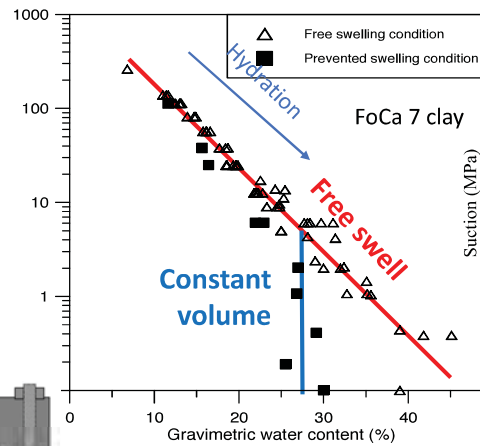


Vapour control of suction (imposed HR, Kelvin's law), high suctions (>100 MPa)

Villar & Lloret 2004

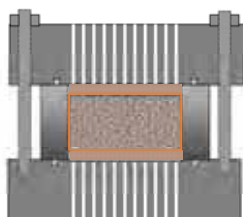


WATER RETENTION CURVES OF COMPACTED BENTONITE (CONSTANT VOLUME)



Villar & Lloret 2004, using the same procedure

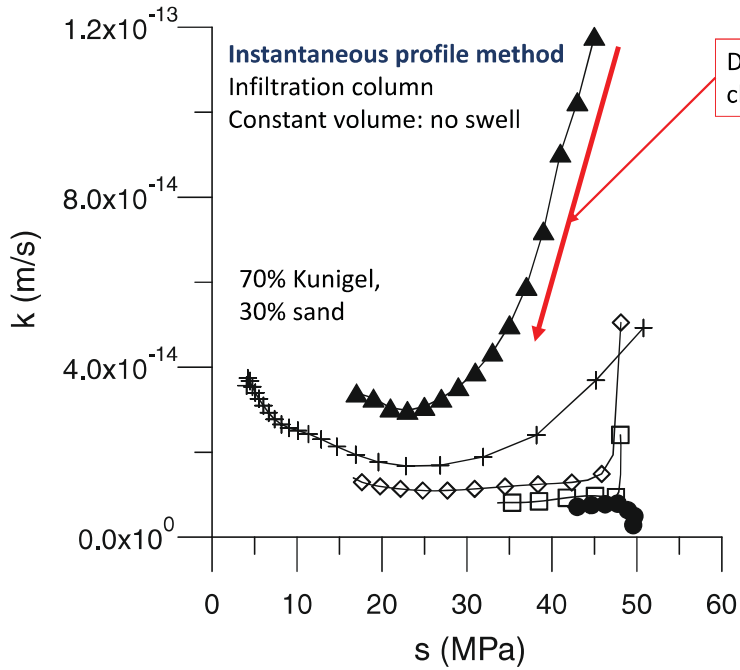
Constant volume cell for water retention, vapour control



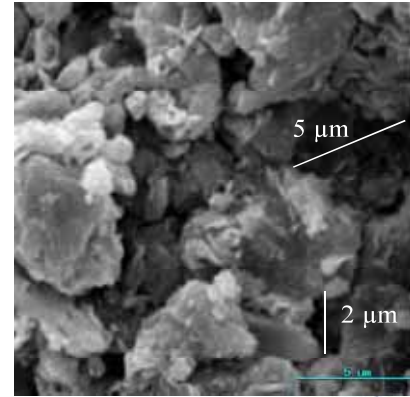
Yahia-Aissa, Delage and Cui 2001



UNSATURATED WATER PERMEABILITY IN COMPACTED BENTONITE

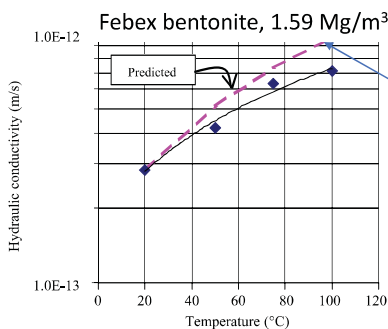


Decrease during saturation:
clogging of intra-aggregate pores

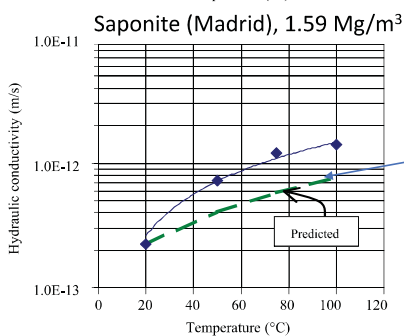


Cui et al. 2008

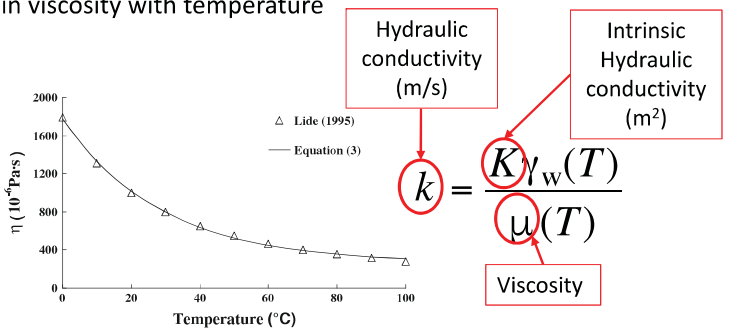
EFFECT OF TEMPERATURE ON SATURATED HYDRAULIC CONDUCTIVITY



Decrease in viscosity with temperature



Decrease in viscosity with temperature



Hydraulic conductivity (m/s)

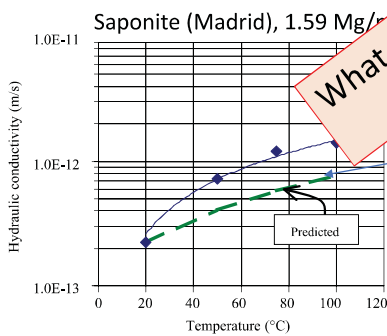
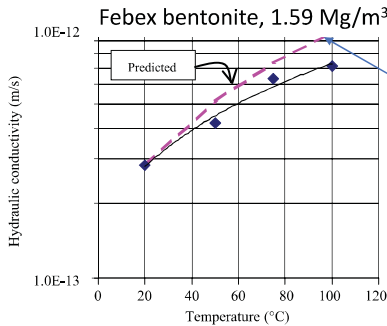
Intrinsic Hydraulic conductivity (m²)

$$k = \frac{K \gamma_w(T)}{\mu(T)}$$

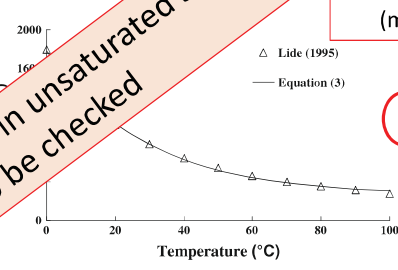
Viscosity

Rivas et al. 1991 in Villar & Lloret 2004

EFFECT OF TEMPERATURE ON SATURATED HYDRAULIC CONDUCTIVITY



What does occur in unsaturated states?
To be checked



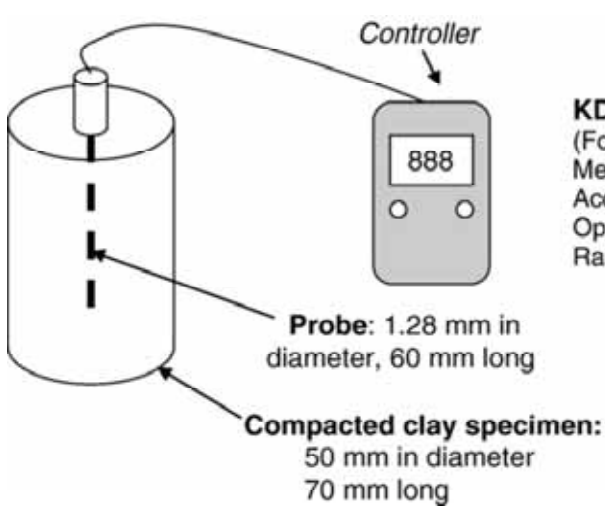
$$k = \frac{K \gamma_w(T)}{\mu(T)}$$

Hydraulic conductivity (m/s) \rightarrow k
 Intrinsic Hydraulic conductivity (m²) \rightarrow K
 Viscosity \rightarrow $\mu(T)$

Rivas et al. 1991 in Villar & Lloret 2004



TRANSIENT MEASUREMENT OF THERMAL CONDUCTIVITY



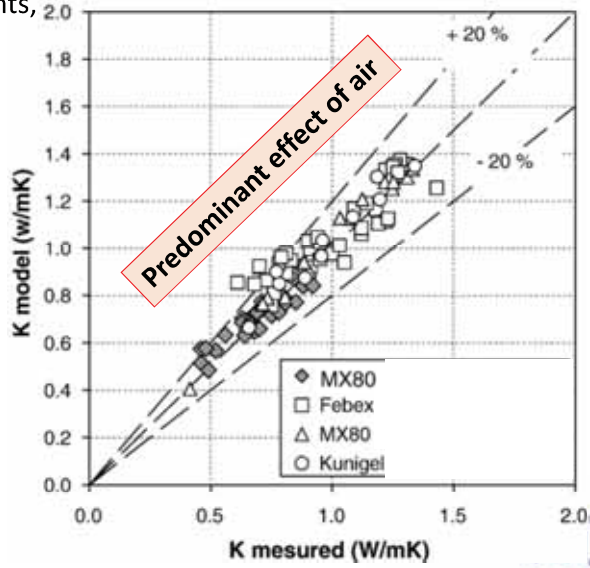
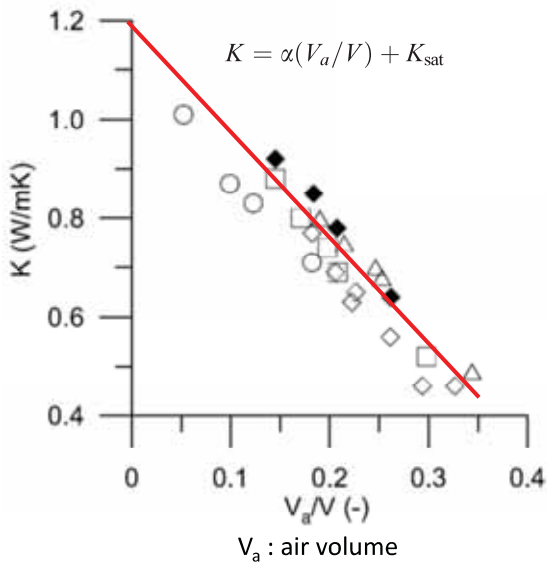
KD2 specifications:
 (For thermal conductivity measurement)
 Measurement speed: 2 minutes
 Accuracy: 5 %
 Operating environment: 5 to 40 °C
 Range of measurement: 0.02-2 W/mK

Tang et al. 2008a



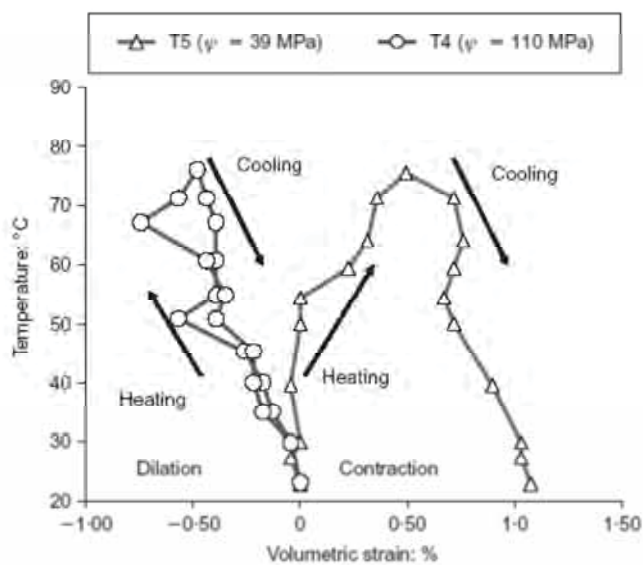
THERMAL CONDUCTIVITY OF COMPACTED BENTONITES

Averaging of thermal conductivity of all components, but!



Tang et al. 2008a

THERMAL VOLUME CHANGES OF COMPACTED MX80



Tang et al. 2008b

CLAY AND CLAYSTONES INVESTIGATED

	COX argillite	Opalinus clay	Boom clay
Dry density (g/cm ³)	2.21-2.33	2.22-2.33	1.61-1.78
Calcite content (%)	23 - 42	6 - 22	0 - 3
Porosity (%)	11-16	11-14	35-40
Water content (%)	<6.5	4 - 8	20-30
Interlayered illite-smectite (%)	50-65	55	40
Liquid limit (%)	21-25	25	
Plasticity index (%)	17	13-17	
Young's modulus (GPa)	3.6-6.5	4-10	0.2-0.4
UCS (MPa)	10-16	8-22	2-2.8
Permeability (m/s)	.7-5x10 ⁻¹³	.5-5x10 ⁻¹³	2-5x10 ⁻¹²
Geological stage	Callovo-Oxfordian	Aalenian	Rupelian
(millions of years)	156-164	171-176	28.4-33.9

Interlayered illite-smectite (%)

Clay rocks

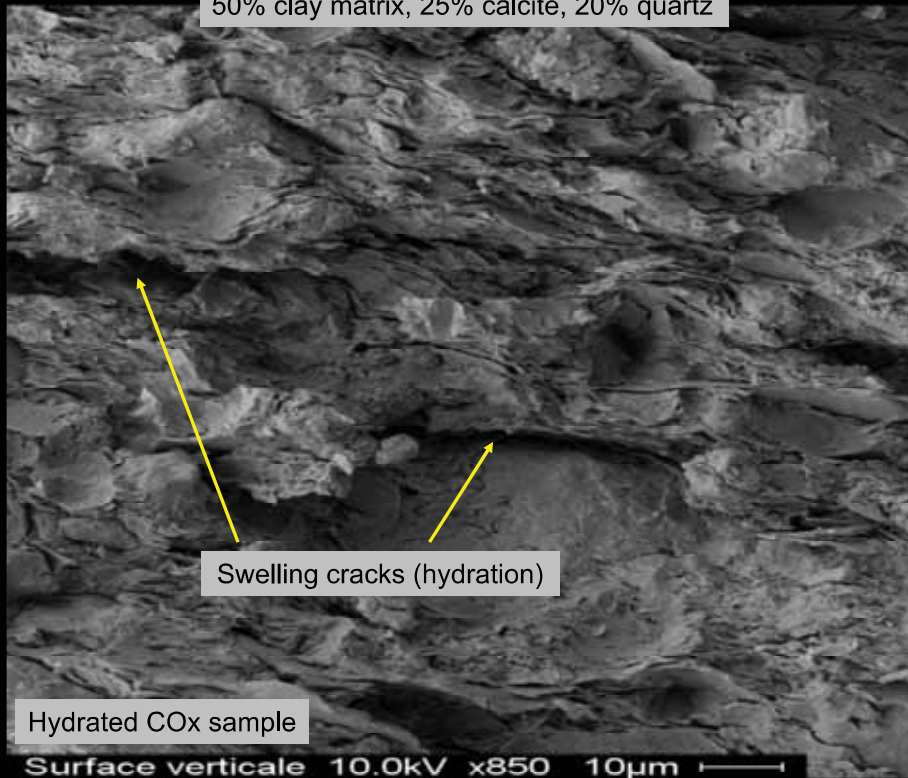
Stiff clay (soil)

Callovo Oxfordian claystone

- Stable geological context (155 My)
- Porosity: 14-19%
- Clay fraction 48-50% at 490m
- Very low permeability: 10⁻¹³ – 10⁻¹⁴ m/s
- Small deformability
- Good ability to retain radionuclides

Excavation Damaged Zone - EDZ

50% clay matrix, 25% calcite, 20% quartz



Delage & Tessier 2020

Hydrated COx sample

Surface verticale 10.0kV x850 10µm

THERMAL PRESSURISATION IN CLAYS AND CLAYSTONES

- The thermal expansion coefficient of water (α_w) is larger than that of the solid phase (α_s)

Mineral	Thermal expansion coefficient ($^{\circ}\text{C}^{-1}$)
Clay	$\alpha_s = 3.4 \times 10^{-5}$ (McTigue 1986) [12]
Quartz	$\alpha_s = 3.34 \times 10^{-5}$ (Palciauskas and Domenico, 1982) [13]
Calcite	$\alpha_s = 1.38 \times 10^{-5}$ (Fei 1995) [14]
Felspar	$\alpha_s = 1.11 \times 10^{-5}$ (Fei 1995) [14]
Water	$\alpha_w = 27 \times 10^{-5}$ (Spang 2002) [15]



THERMAL PRESSURISATION IN CLAYS AND CLAYSTONES

- The thermal expansion coefficient of water (α_w) is larger than that of the solid phase (α_s)
- Heat (thermal conductivity) moves faster than water (hydraulic conductivity)
 - Heating results in thermal pressurisation, followed by pore pressure dissipation

- Thermal pressurisation coefficient

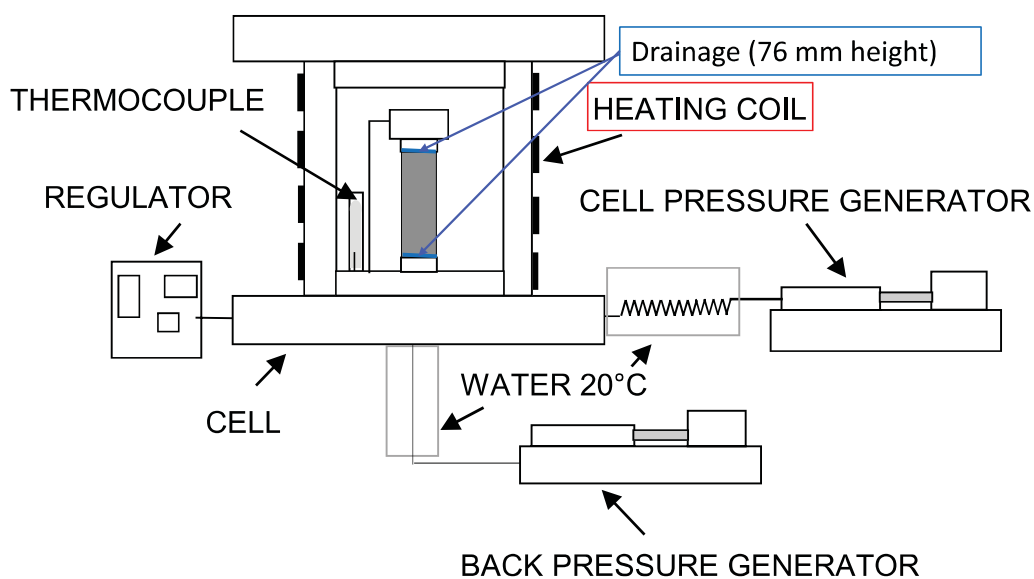
$$\Lambda = \Delta p / \Delta T (^{\circ}\text{C}/\text{MPa})$$

- Poro-elastic formulation

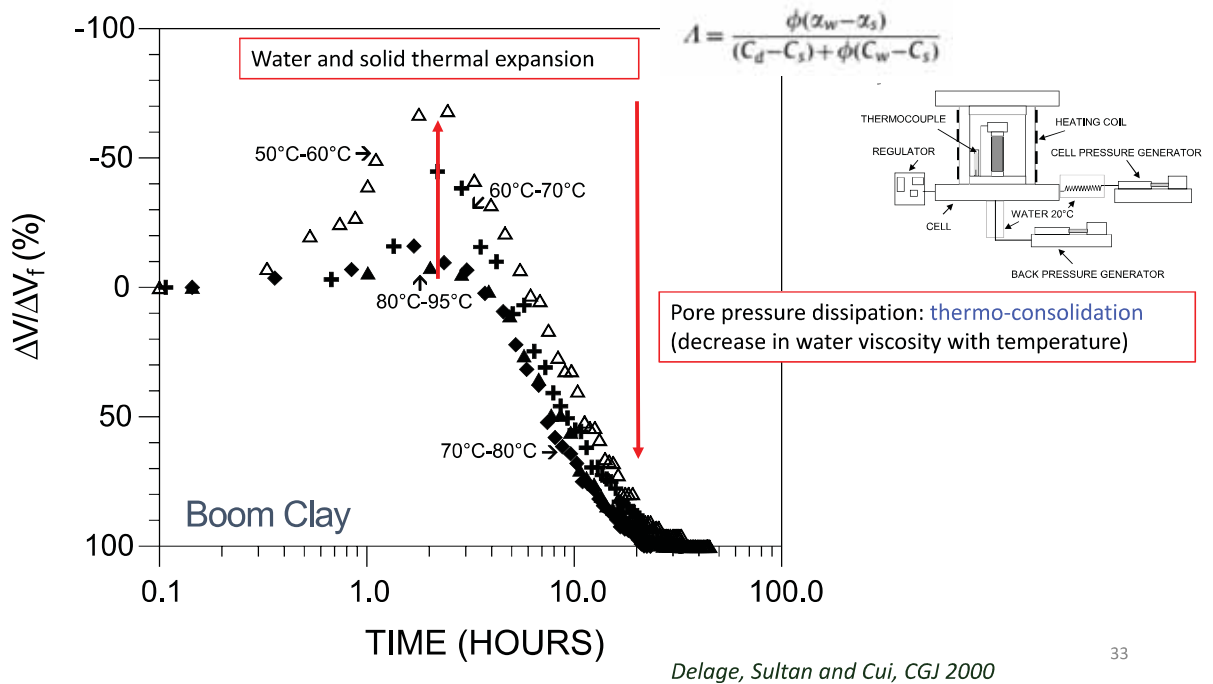
$$\Lambda = \frac{\text{Porosity} \cdot \text{Thermal expansion coefficients} \cdot \phi(\alpha_w - \alpha_s)}{\text{Compressibilities (drained, solids, water)} \cdot (C_d - C_s) + \phi(C_w - C_s)}$$



THERMAL CONSOLIDATION: ISOTROPIC THERMAL CELL

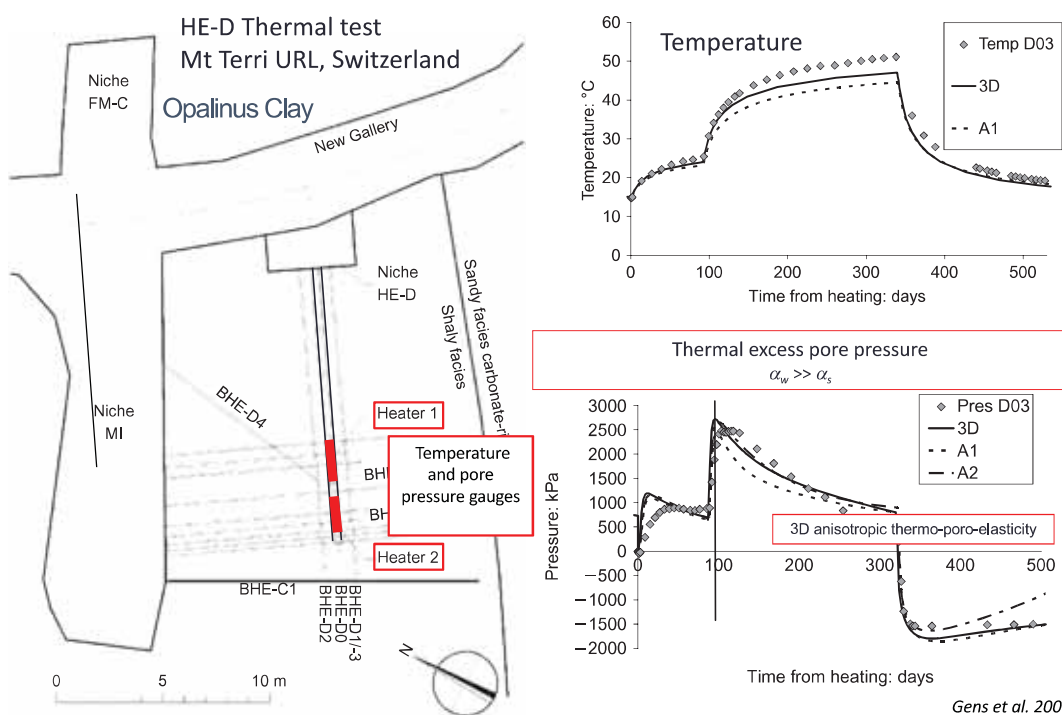


THERMAL CONSOLIDATION, BOOM CLAY, STEP HEATING



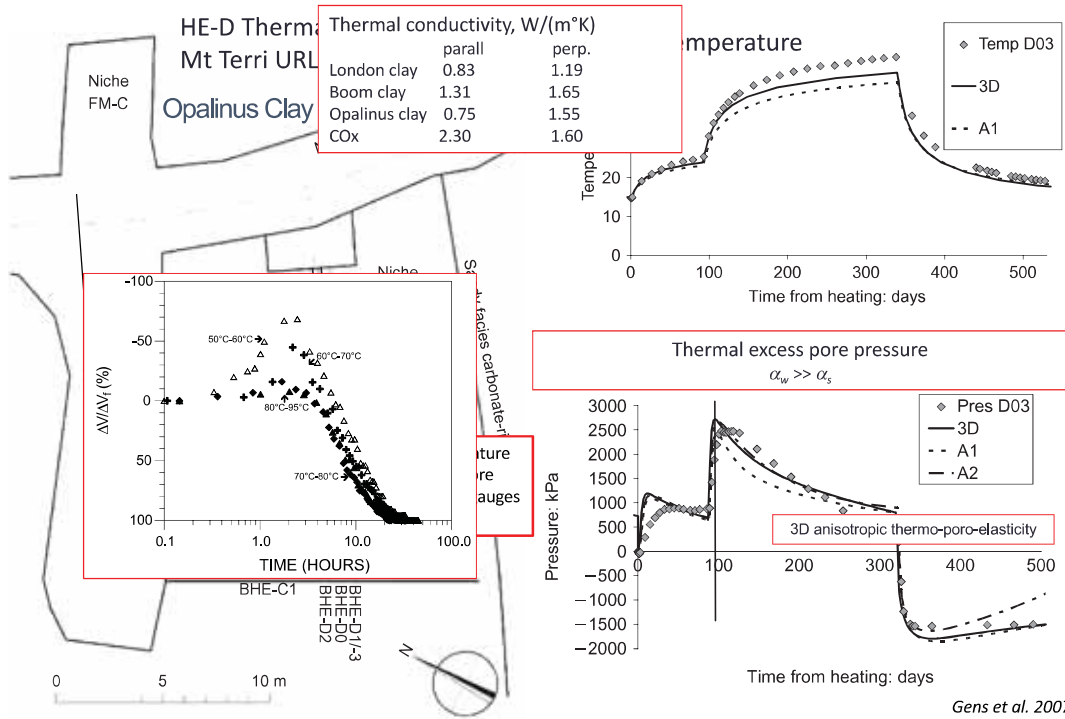
33

THERMAL PRESSURISATION, IN-SITU TEST



34

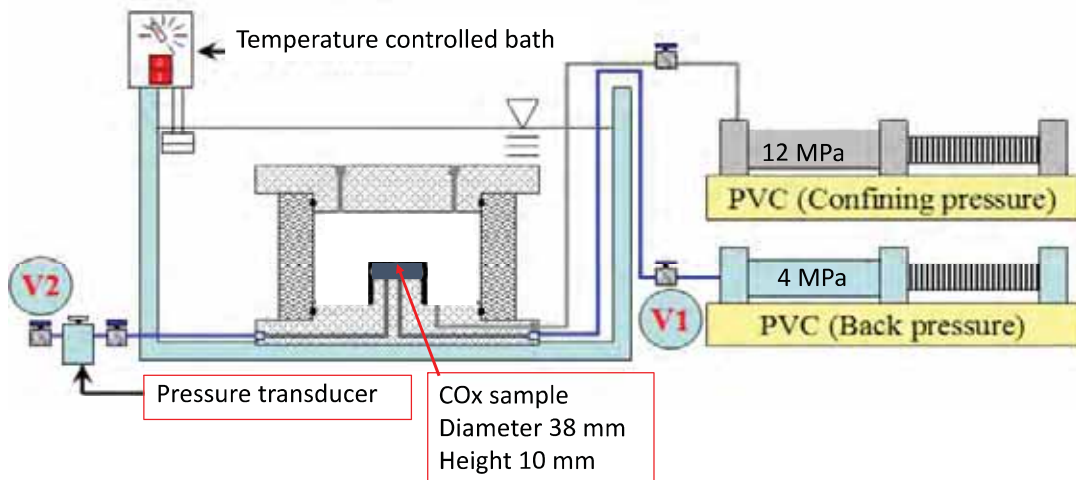
THERMAL PRESSURISATION, IN-SITU TEST



35

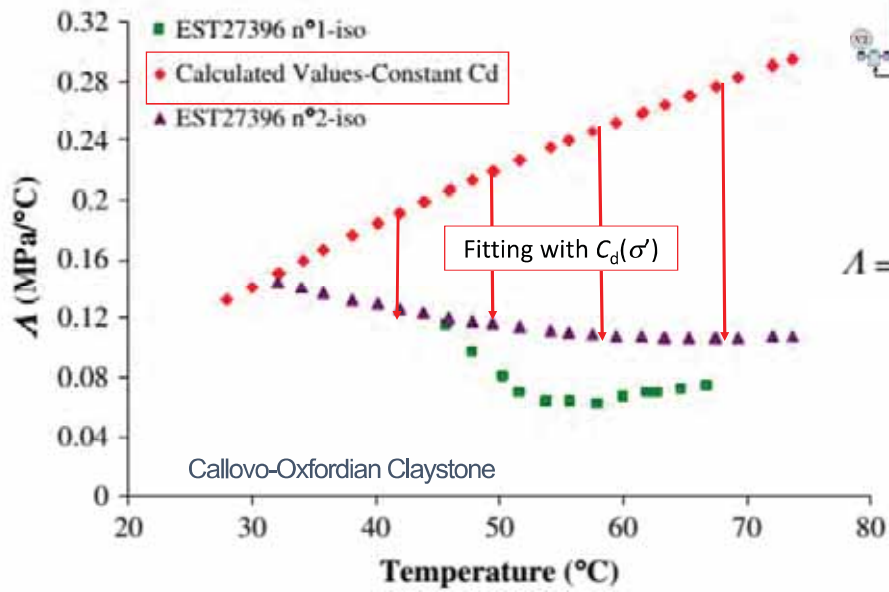
THERMAL PRESSURISATION: LABORATORY INVESTIGATION

Undrained heating under (isotropic) in-situ stress with pore pressure measurement



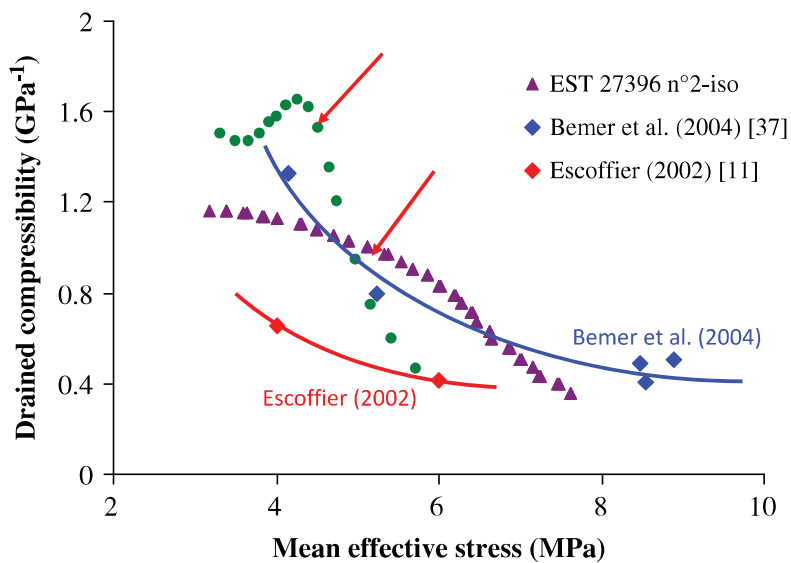
36

THERMAL PRESSURIZATION COEFFICIENT Λ



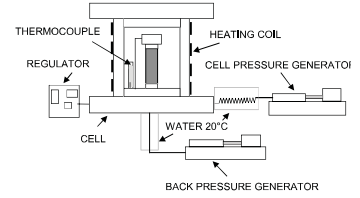
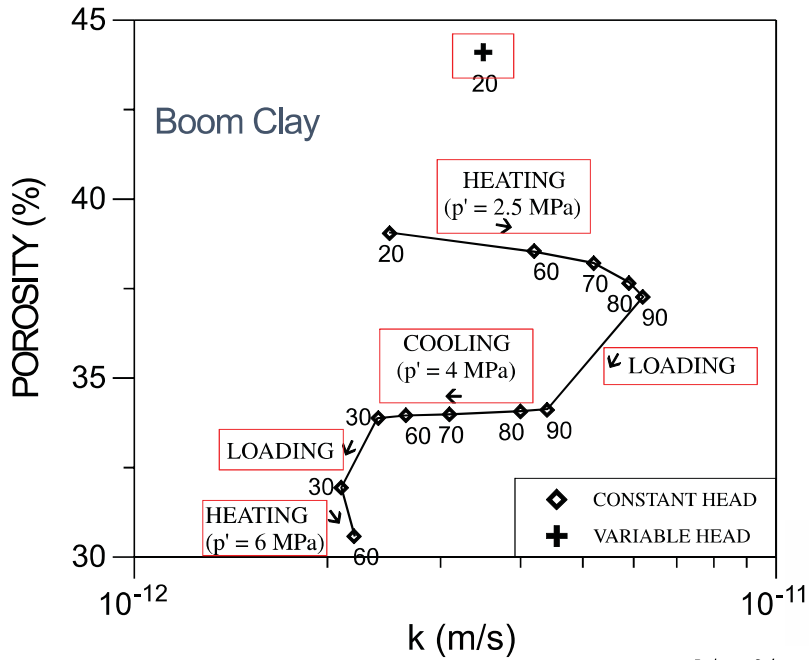
Mohajerani, Delage, Sulem, Monfared, Tang, Gatmiri IJRMMS 2012

FITTING OF C_D (VERSUS STRESS)



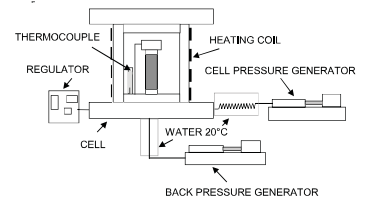
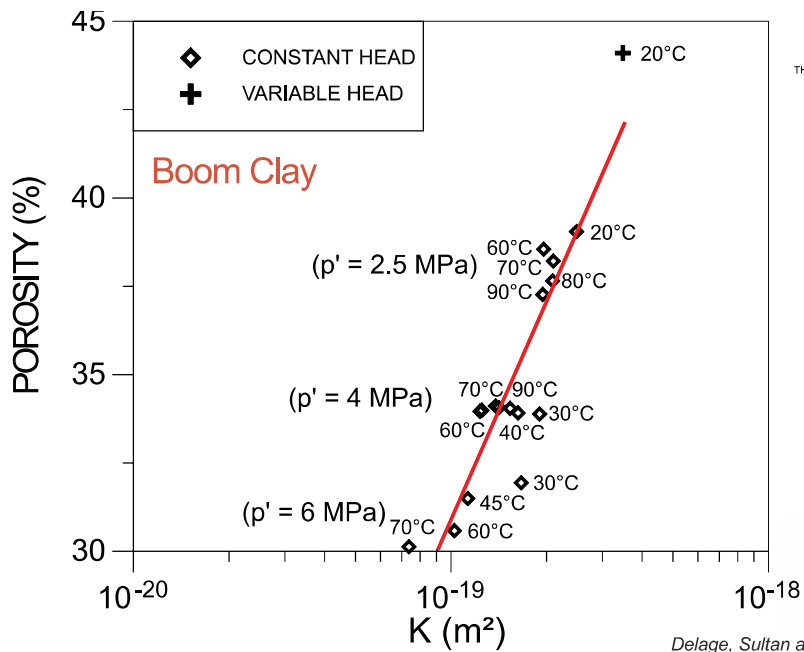
Mohajerani, Delage, Sulem, Monfared, Tang, Gatmiri IJRMMS 2012

EFFECT OF TEMPERATURE ON PERMEABILITY



Delage, Sultan and Cui, CGJ 2000

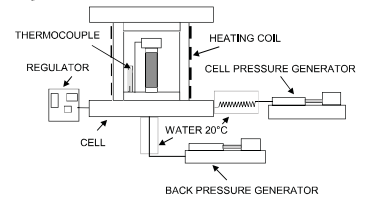
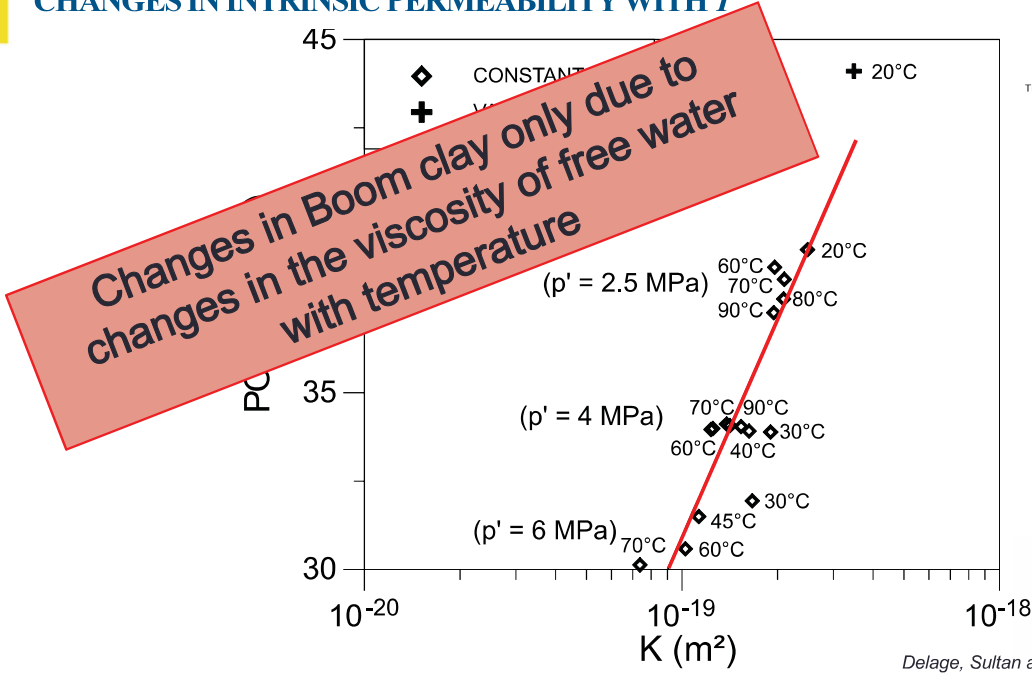
CHANGES IN INTRINSIC PERMEABILITY WITH T



Delage, Sultan and Cui, CGJ 2000

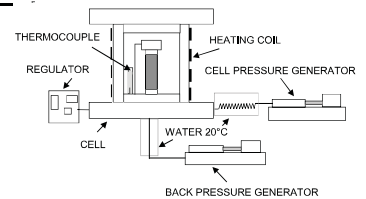
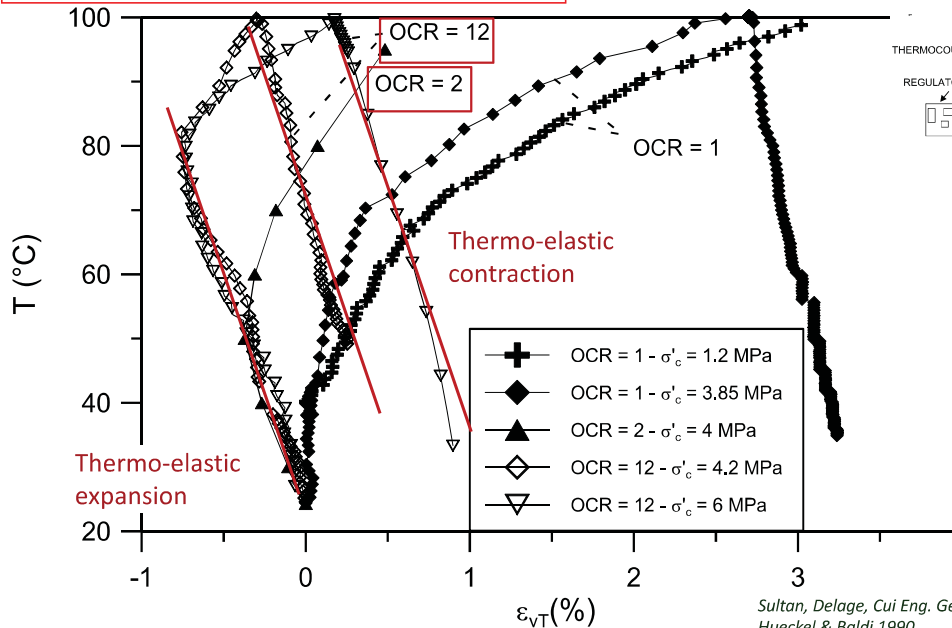


CHANGES IN INTRINSIC PERMEABILITY WITH T

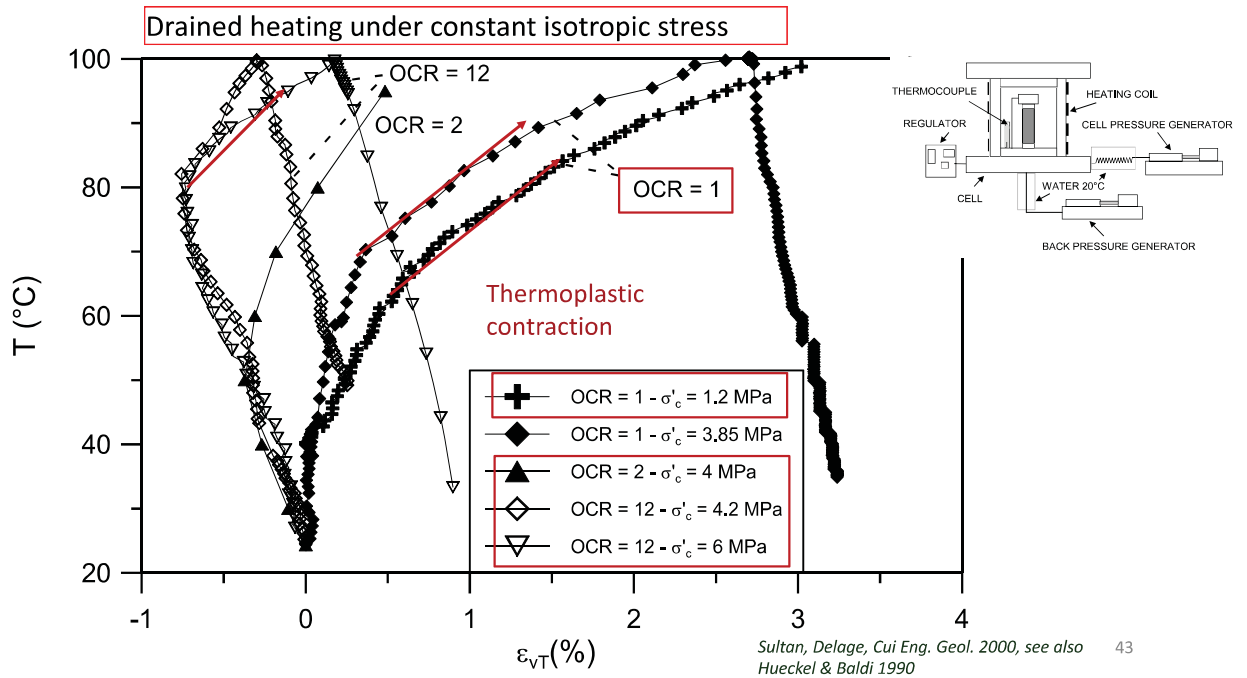


DRAINED THERMAL VOLUMETRIC CHANGES, BOOM CLAY

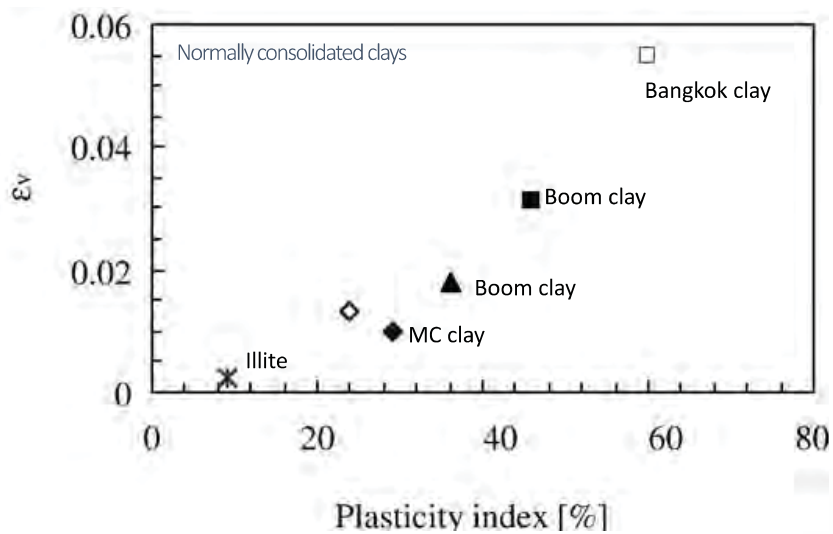
Drained heating, constant isotropic stress



DRAINED THERMAL VOLUMETRIC CHANGES, BOOM CLAY



EFFECT OF I_p ON THERMOPLASTIC CONTRACTION

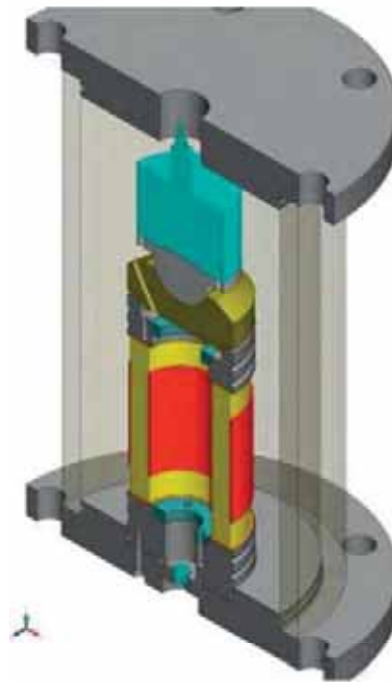


TIMODAZ* HOLLOW CYLINDER APPARATUS

External diameter 100 mm
 Internal diameter 60 mm
 Height 70 mm
 Internal and external pressures equal
 Top, bottom and lateral drainage

Drainage length $H = 10 \text{ mm}$
 (half the hollow cylinder thickness)

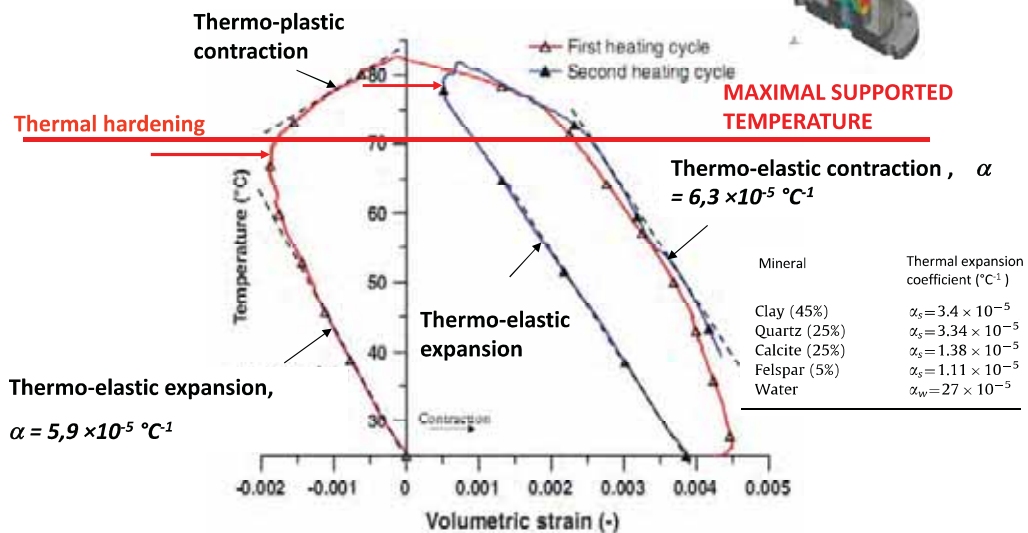
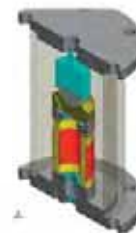
Using Soil mechanics concepts to test clay rocks



Monfared M., Delage P., Sulem J., Mohajerani M., Tang A.M., De Laune E. IJRMMS 2011

THERMAL HARDENING, OPALINUS CLAY

In situ stresses
 Drained heating, $1^\circ\text{C}/\text{h}$

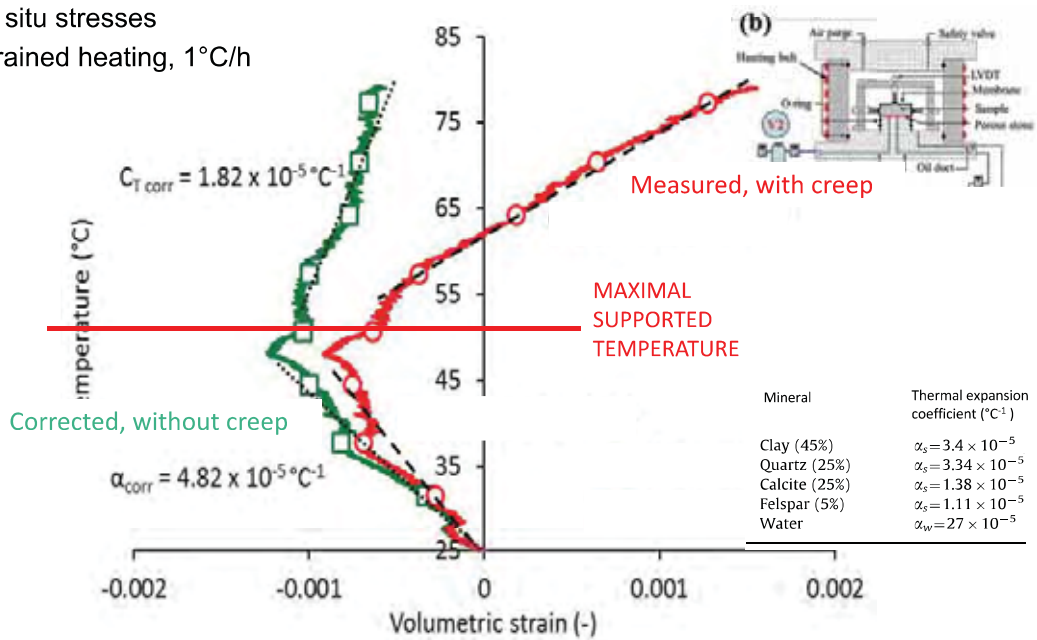


Monfared M., Sulem J., Delage P., Mohajerani M. RMRE 2011

THERMAL HARDENING, CALLOVO-OXFORDIAN CLAYSTONE

In situ stresses

Drained heating, 1°C/h



Belmokhtar M., Delage P., Ghabezloo S., Conil N. RMRE 2017

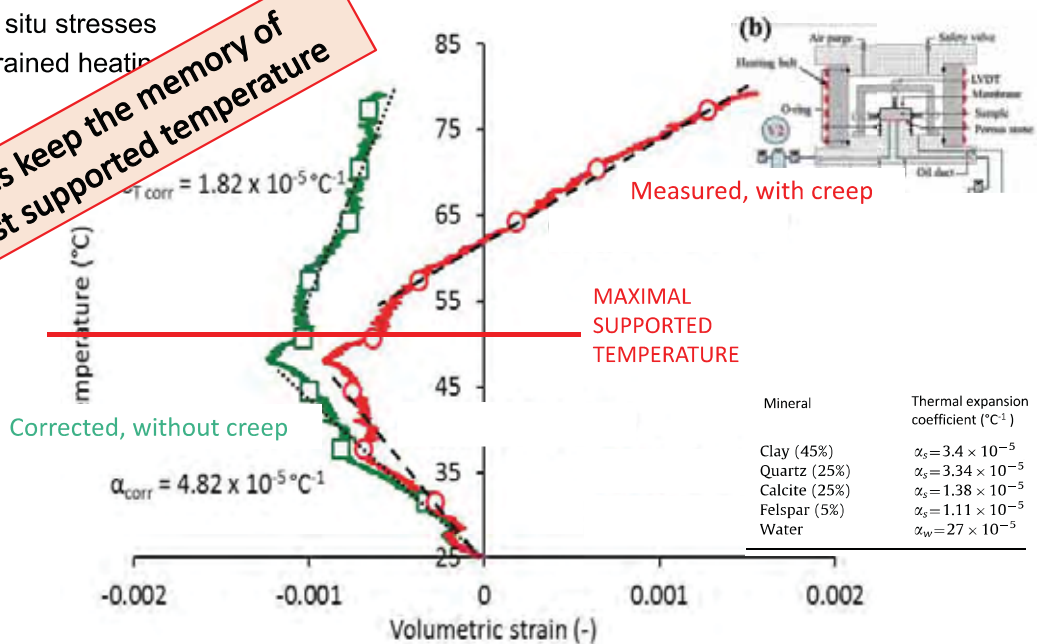
47

THERMAL HARDENING, CALLOVO-OXFORDIAN CLAYSTONE

In situ stresses

Drained heating

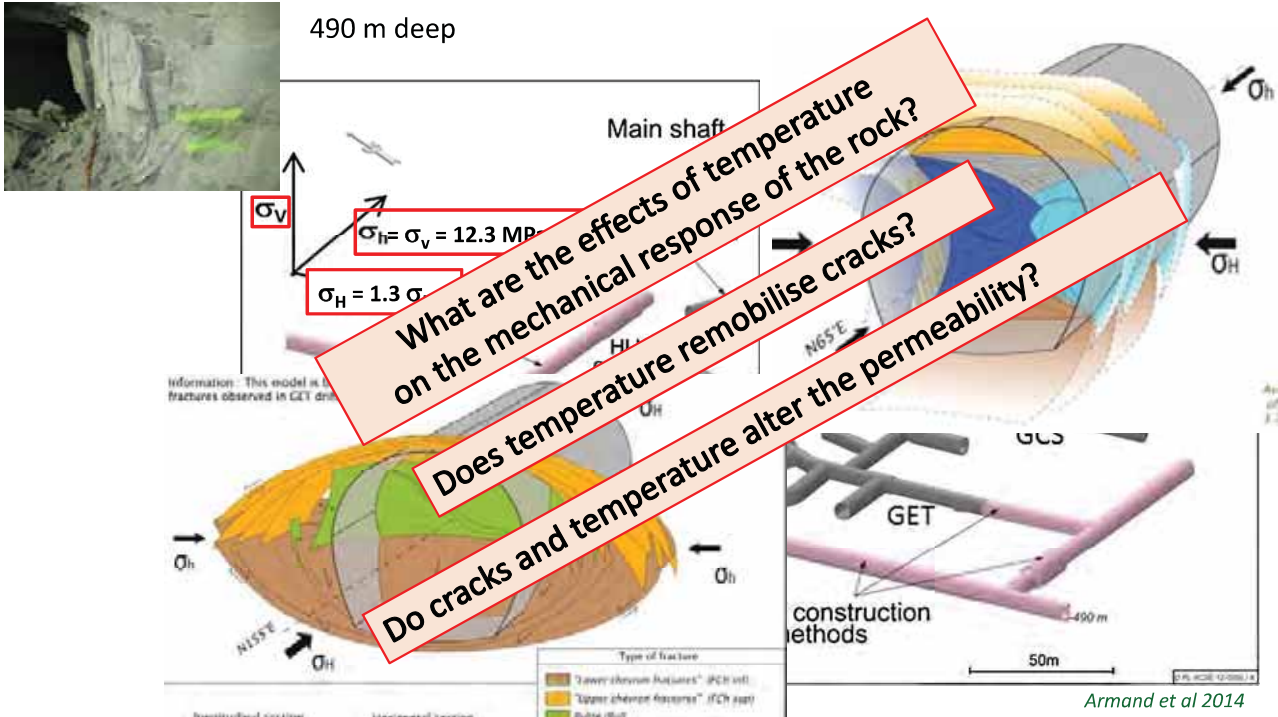
Claystones keep the memory of the highest supported temperature



Belmokhtar M., Delage P., Ghabezloo S., Conil N. RMRE 2017

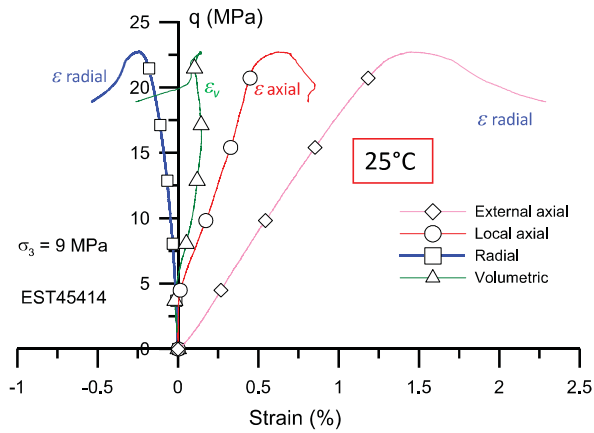
48

ANDRA'S UNDERGROUND RESEARCH LABORATORY AT BURE



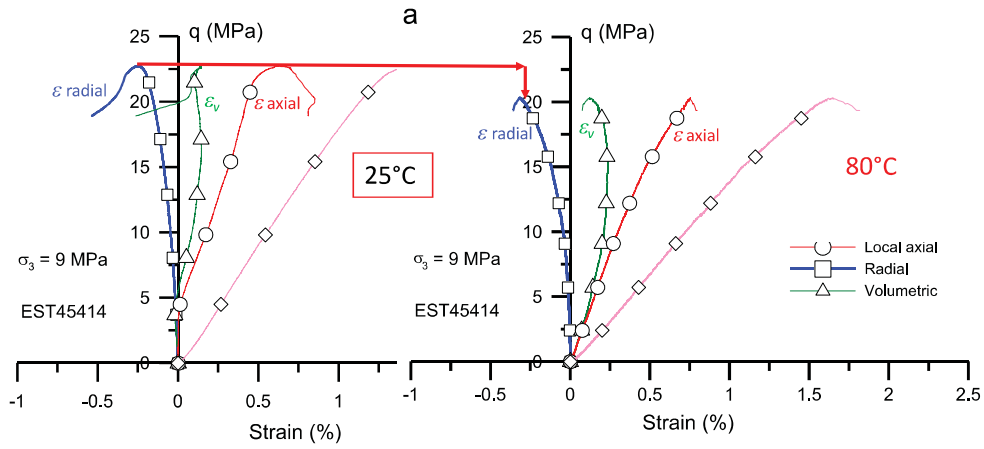
DRAINED TRIAXIAL TEST, COX

In-situ stress
(depth 490m)



DRAINED TRIAXIAL TEST, COX

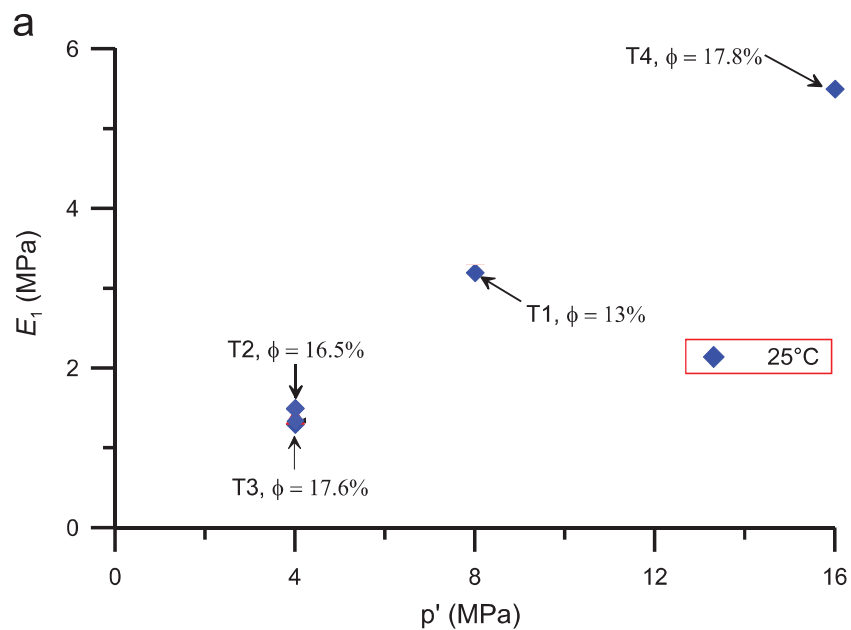
In-situ stress
(depth 490m)



Menaceur H., Delage P., Tang A.M., Conil N. RMRE 2015

51

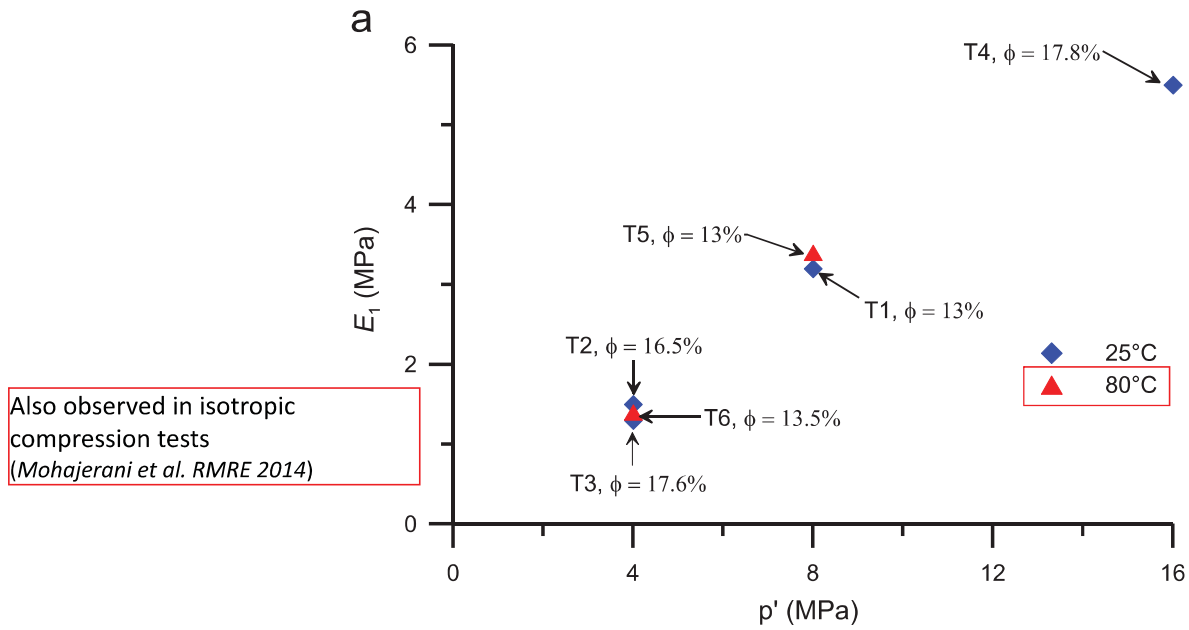
NO TEMPERATURE DEPENDENCE OF YOUNG MODULUS E_1



Menaceur H., Delage P., Tang A.M., Conil N. RMRE 2015

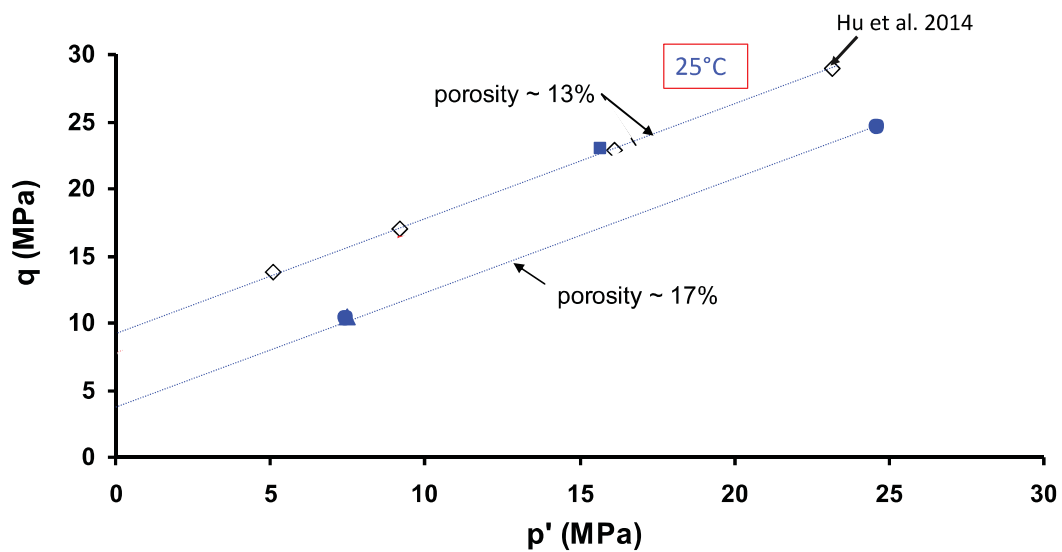
52

NO TEMPERATURE DEPENDENCE OF YOUNG MODULUS E_1



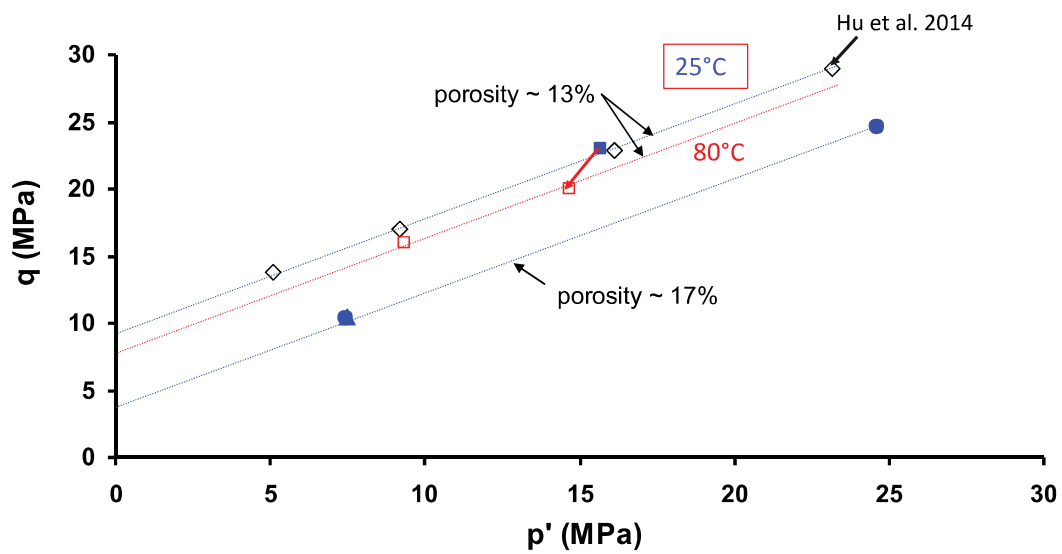
Menaceur H., Delage P., Tang A.M., Conil N. RMRE 2015

FAILURE CRITERION (TEMPERATURE), COX



Menaceur H., Delage P., Tang A.M., Conil N. RMRE 2015

FAILURE CRITERION (TEMPERATURE), COX

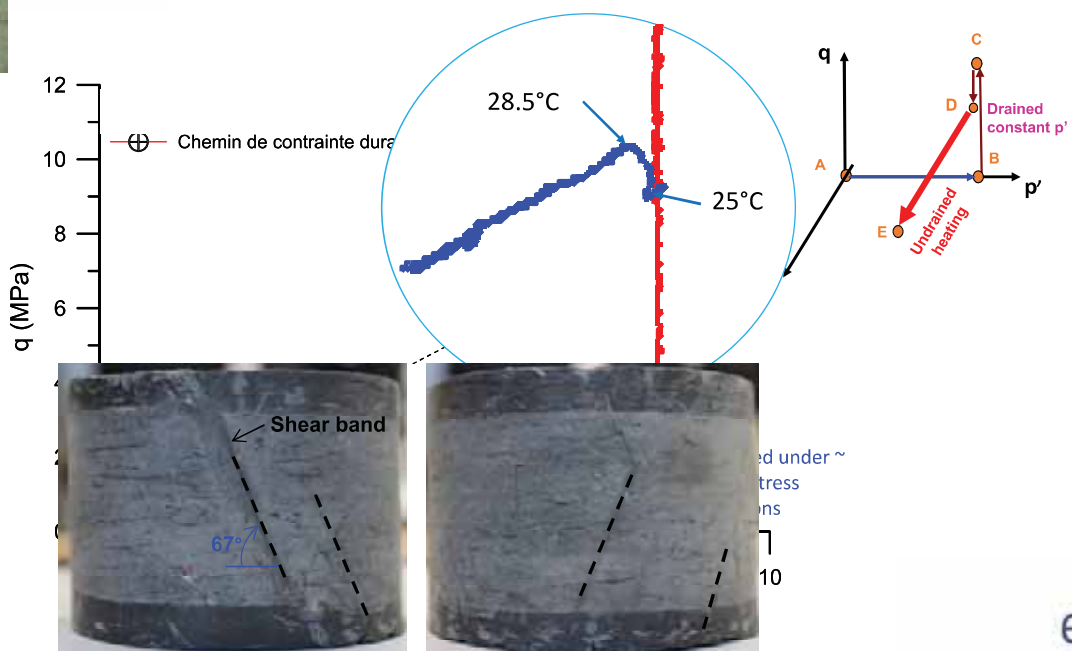


Menaceur H., Delage P., Tang A.M., Conil N. RMRE 2015

55



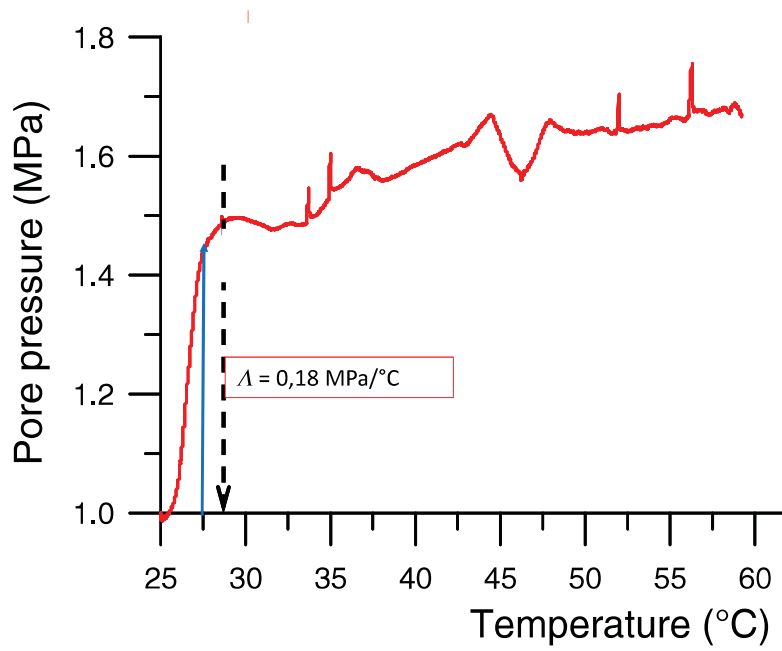
THERMAL REACTIVATION OF SHEAR PLANE



See also Monfared et al 2012 on Boom clay

Menaceur, Delage, Tang, Conil. RMRE 2016

TEST MONITORING

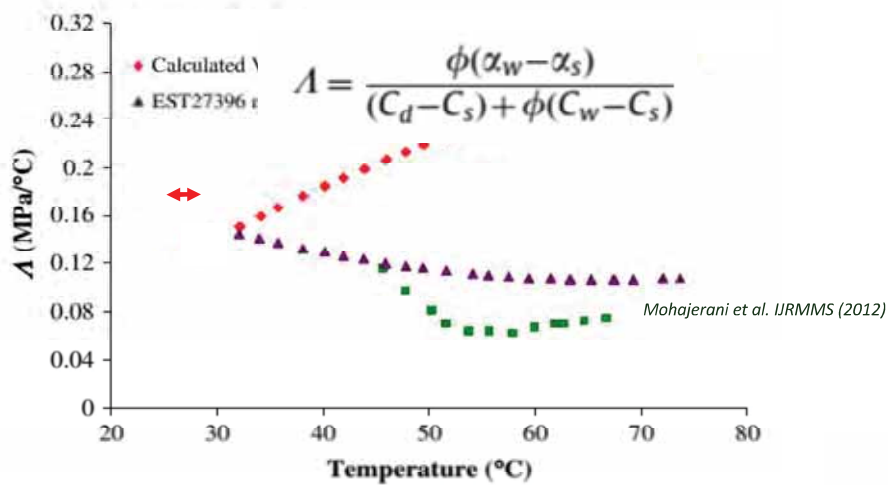


Menaceur, Delage, Tang and Conil. RMRE 2016

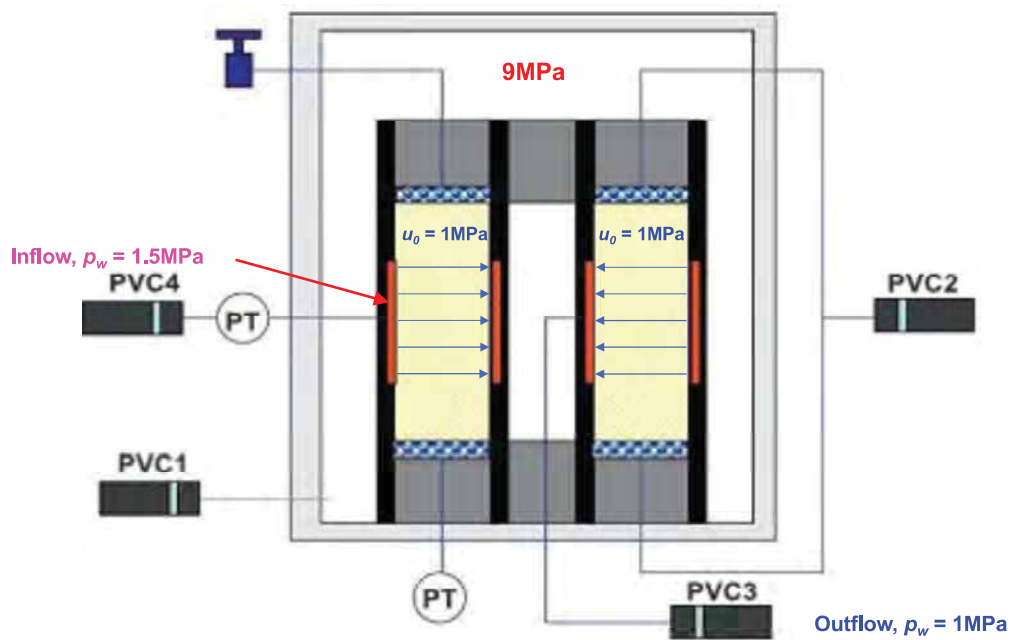
57



THERMAL PRESSURIZATION COEFFICIENT λ , CO CLAYSTONE

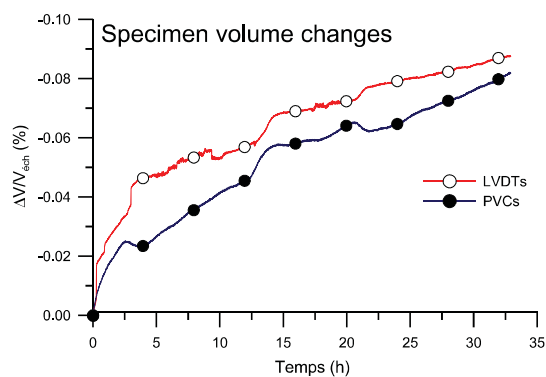
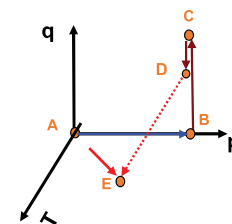
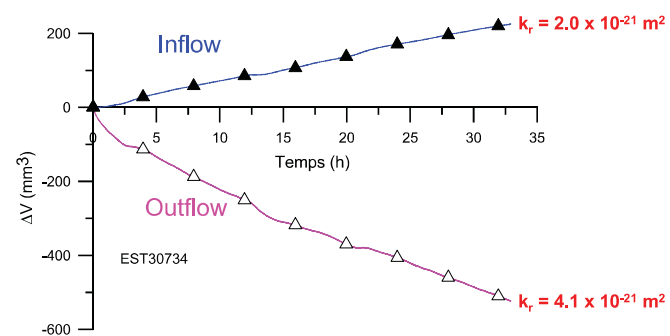


RADIAL PERMEABILITY TEST, COX CLAYSTONE (INTACT AND SHEARED)



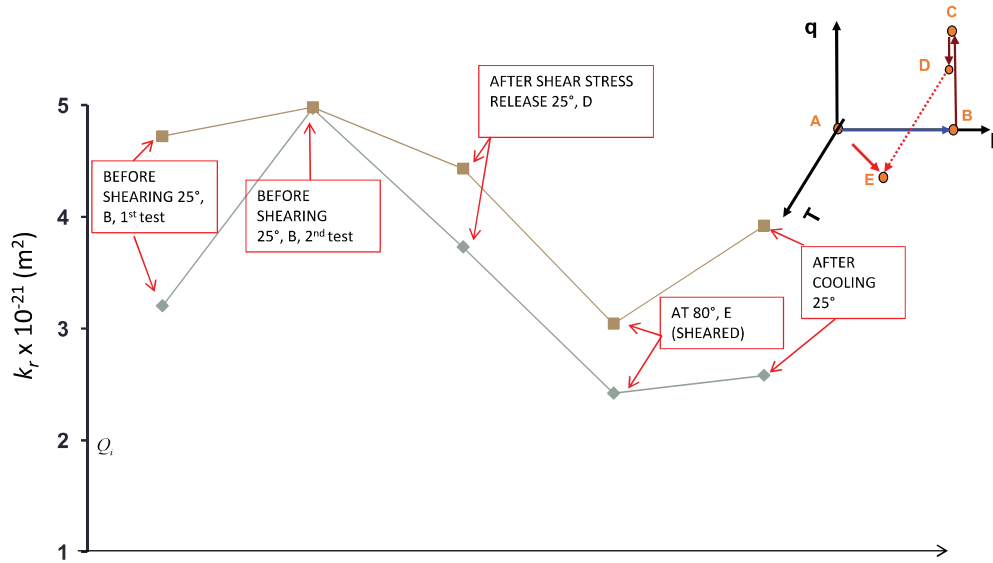
Menaceur, Delage, Tang and Conil. RMRE 2016

RADIAL PERMEABILITY TEST, SHEARED SPECIMEN

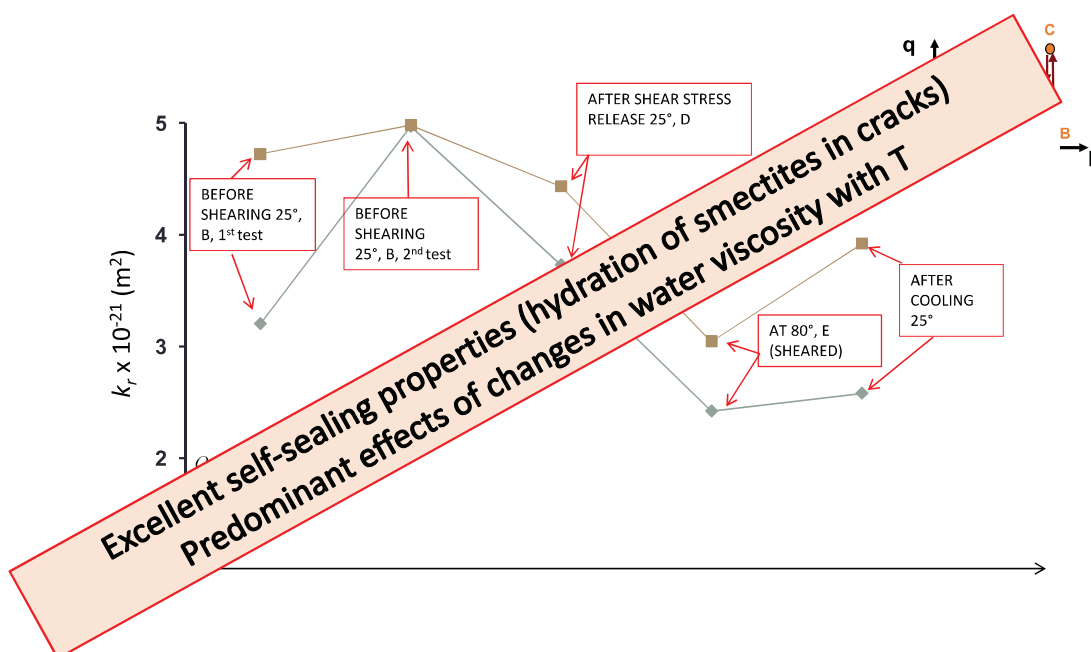


Menaceur, Delage, Tang and Conil. RMRE 2016

CHANGES IN PERMEABILITY, COX CLAYSTONE



CHANGES IN PERMEABILITY, COX CLAYSTONE





CONCLUDING REMARKS

- **Many sensitive THM issues in compacted bentonites, clays and claystones related to radioactive waste disposal**
- **Heat transfers**
 - satisfactorily calculated in saturated soils and rocks
 - more tricky in unsaturated compacted bentonite during infiltration: combined (liquid + vapour) water and heat transfers in a changing porous medium)
- **Effects of temperature**
 - Hydraulic transfers: strong effects of changes in water viscosity in saturated states (but not only); vapour transfers?
 - Tiny effect in swelling compacted bentonites (water retention, swelling pressure and strain), to be further investigated
 - Tiny effects on the mechanical response of saturated clays and claystones: reasonably well-known
 - No effect on elastic response
 - Slight weakening and decrease in strength
 - Thermal pressurisation in saturated clays and claystones: correct lab determination
 - Thermo-consolidation in stiff clay (changes in water viscosity)
 - Thermal volume changes:
 - *Elasto-plastic response: thermoelastic expansion – thermoplastic contraction*
 - *Thermal hardening in claystone*
 - Thermal remobilisation of shear planes (EDZ)
 - No effect of shear planes on permeability



SOME PERSPECTIVES INCLUDE:

- **Extension of investigations above 100°C, for EBS (and claystones?)**
- **Short term and (very) long-term behaviour**
- **Heat/water (vapour + liquid) transfers in EBS during infiltration: multi-phase physico-chemically active medium with changing microstructure**
- **Effects of changing mineralogy (MX80, FEBEX, KUNIGEL, CALCIGEL,...) and exchangeable cations (Na, Ca, Mg,...)**



REFERENCES

Thermal behaviour of bentonites

- Cui Y.J., Loiseau C. & Delage P. 2002. Microstructure changes of a confined swelling soil due to suction controlled hydration. Proceedings of the 3rd International Conference on Unsaturated Soils, UNSAT'2002, 593-598, Recife, Brazil, Balkema.
- Cui Y.J., A.M. Tang, C. Loiseau, P. Delage 2008. Determining the unsaturated hydraulic conductivity of a compacted sand-bentonite mixture under constant-volume and free-swell conditions. *Physics and Chemistry of the Earth* 33, S462-S47.
- Molinero Guerra A., Aïmedieu P., Bornert M., Cui Y.J., Tang A.M., Zhao S., Mokni N., Delage P., Bernier F. 2018. Analyses of the structural changes of a pellet/powder bentonite mixture upon wetting by X-ray computed microtomography. *Applied Clay Science* 165, 164 - 169
- Molinero Guerra A., Delage P., Cui Y.J., Mokni N., Tang A.M., Aïmedieu P., Bernier F. Bornert M., 2019. Water retention properties and microstructure changes of a bentonite pellet upon wetting/drying; application to radioactive waste disposal. *Géotechnique*, doi: 10.1680/jgeot.17.P.291.
- Tang A.M., Y.J. Cui, T.-T. Le 2008a. A study on the thermal conductivity of compacted bentonites. *Applied Clay Science* 41, 181-189.
- Tang, A.M., Cui, Y.J., Barnel, N., 2008b. Thermo-mechanical behaviour of compacted swelling clay. *Geotechnique* 58 (1), 45-54.
- Villar M.V., A. Lloret. 2004. Influence of temperature on the hydro-mechanical behaviour of a compacted bentonite, *Applied Clay Science* 26, 337-350.
- Wan M., W.M. Ye, Y.G. Chen, Y.J. Cui, J. Wang 2015. Influence of temperature on the water retention properties of compacted GMZ01 bentonite. *Environ Earth Sci* 73: 4053-4061.
- Yahia-Aïssa M., Delage P., & Cui Y.J. 2001. Suction-water relationship in swelling clays. *Clay science for engineering, IS-Shizuoka International Symposium on Suction, Swelling, Permeability and Structure of Clays*, 65-68, Adachi & Fukue eds, Balkema.
- Ye W.M., M. Wan, B. Chen, Y.G. Chen, Y. J. Cui, J. Wang 2012. Temperature effects on the swelling pressure and saturated hydraulic conductivity of the compacted GMZ01 bentonite. Temperature effects on the unsaturated permeability of the densely compacted GMZ01 bentonite under confined conditions. *Engineering Geology*, 126 1-7.
- Ye W.M., M. Wan, B. Chen, Y.G. Chen, Y.J. Cui, J. Wang 2012. Temperature effects on the nsaturated permeability of the densely compacted GMZ01 bentonite under confined conditions. *Engineering Geology*, 126 1-7.



REFERENCES

Thermal behaviour of clays and claystones

- Abuel-Naga H.M., Bergado D.T. & Bouazza A. 2007. Thermally induced volume changes and excess pore pressure of soft Bangkok clay. *Eng. Geol.* 89, 144 - 154.
- Belmokhtar M., Delage P., Ghabezloo S. and Conil N. 2017. Thermal volume changes and creep in the Callovo-Oxfordian claystone. *Rock Mechanics and Rock Engineering*, 50 (9), 2297-2309.
- Braun P., Ghabezloo S., Delage P., Sulem J. and Conil N. 2019. Determination of multiple thermo-hydro-mechanical rock properties in a single transient experiment: application to shales. *Rock Mechanics and Rock Engineering*, <https://doi.org/10.1007/s00603-018-1692-x>.
- Braun P., Delage P., Ghabezloo S., Sulem J., Conil N. 2019. Effect of transverse isotropy on the thermal volume changes of shales: insight from the Callovo-Oxfordian claystone. *Géotechnique Letters*, doi.org/10.1680/jgele.19.00045.
- Cui Y.J., Sultan N. & Delage P. 2000. A thermomechanical model for saturated clays. *Canadian Geotechnical Journal*, 37 (3) : 607-620.
- Delage P., Sultan N. & Cui Y.J. 2000. On the thermal consolidation of Boom clay. *Canadian Geotechnical Journal*, 37 (2): 343-354.
- Delage P., Tessier D. 2020. Macroscopic effects of nano and microscopic phenomena in clayey soils and clay rocks. *Geomechanics for Energy and the Environment*, doi:10.1016/j.gete.2019.100177.
- Gens A., Vaunat J., Garitte B. & Wileveau Y. 2007. In situ behaviour of a stiff layered clay subject to thermal loading: observations and interpretation. *Géotechnique* 57(2), 207-228.
- Gens A. 2011. On the hydromechanical behaviour of argillaceous hard soils-weak rocks. Proc. 15th ECSMGE, 71-11, Athens.
- Menaceur H, Delage P., Tang A.M. and Conil N. 2015. The thermo-mechanical behaviour of the Callovo-Oxfordian claystone. *International Journal of Rock Mechanics and Mining Sciences* 78, 290-303.
- Menaceur H., Delage P., Tang A.M. and Conil N. 2015. On the Thermo-Hydro-Mechanical behaviour of a sheared Callovo-Oxfordian claystone sample with respect to the EDZ behaviour. *Rock Mechanics and Rock Engineering*, 49(5), 1875-1888.



REFERENCES

- Mohajerani M., Delage P., Sulem J., Monfared M., Tang A.M., Gatmiri B. 2012. A laboratory investigation of thermally induced pore pressures in the Callovo-Oxfordian Claystone. *International Journal of Rock Mechanics and Mining Sciences*, vol. 52, 112-121.
- Mohajerani M., Delage P., Sulem J., Monfared M., Tang A.M., Gatmiri B. 2014. The thermal volume changes of the Callovo-Oxfordian claystone. *Rock Mechanics and Rock Engineering* 47: 131-142.
- Monfared M, Delage P, Sulem J, Mohajerani M, Tang AM, De Laure E 2011a. A new hollow cylinder triaxial cell to study the behaviour of geomaterials with low permeability, *IJRMMS* 48 (4); 637-649.
- Monfared M., Sulem J., Delage P., Mohajerani M. 2011b. A laboratory investigation on the thermal properties of the Opalinus claystone. *Rock Mechanics and Rock Engineering* 44, 735-747.
- Monfared M., Sulem J., Delage P., Mohajerani M. 2012. On the THM behaviour of a sheared Boom clay sample: application to the behaviour and sealing properties of the EDZ. *Engineering Geology* 124, 47-58.
- Monfared M., Sulem J., Delage P., Mohajerani M. 2014. Temperature and damage impact on the permeability of Opalinus clay. *Rock Mechanics and Rock Engineering* 47:101-110.
- Sultan N., Delage P. & Cui Y.J. 2002. Temperature effects on the volume change behaviour of Boom clay. *Engineering Geology*, Vol. 64, 2-3, 135-145.

Appendix G. Constitutive modelling for thermomechanical behavior of geomaterials (D. Masin)

Constitutive modelling for thermomechanical behaviour of geomaterials

David Mašín

Charles University, Prague



EURAD school for radioactive waste management
Liège, January 22, 2020

Navigation icons: back, forward, search, etc.

Outline

- 1 Introduction
- 2 THM modelling of single structure soils
 - Modelling of the mechanical behaviour
 - Modelling of the water retention behaviour
 - Hydro-mechanical coupling
 - Thermal effects
- 3 Double structure models
 - Double structure mechanical models
 - Double structure hydraulic models
 - Double structure hydro-mechanical coupling
 - Thermal effects
- 4 Triple structure models, local non-equilibrium

Navigation icons: back, forward, search, etc.

Introduction

- This lecture is giving overview of constitutive modelling of THM behaviour of geomaterials, with particular focus on expansive soils.
- I will cover features specific to the effects of *partial saturation* and *temperature*.
- Basic concepts of underlying models (*elasto-plasticity*, *hypoplasticity*) will not be covered. Though many features will often be demonstrated using hypoplasticity, concepts introduced can equally be applied to elasto-plastic and hypoplastic models in a hierarchical manner.

Introduction

- This lecture is giving overview of constitutive modelling of THM behaviour of geomaterials, with particular focus on expansive soils.
- I will cover features specific to the effects of *partial saturation* and *temperature*.
- Basic concepts of underlying models (*elasto-plasticity*, *hypoplasticity*) will not be covered. Though many features will often be demonstrated using hypoplasticity, concepts introduced can equally be applied to elasto-plastic and hypoplastic models in a hierarchical manner.

Introduction

- This lecture is giving overview of constitutive modelling of THM behaviour of geomaterials, with particular focus on expansive soils.
- I will cover features specific to the effects of *partial saturation* and *temperature*.
- Basic concepts of underlying models (*elasto-plasticity*, *hypoplasticity*) will not be covered. Though many features will often be demonstrated using hypoplasticity, concepts introduced can equally be applied to elasto-plastic and hypoplastic models in a hierarchical manner.

Outline

- 1 Introduction
- 2 THM modelling of single structure soils
 - Modelling of the mechanical behaviour
 - Modelling of the water retention behaviour
 - Hydro-mechanical coupling
 - Thermal effects
- 3 Double structure models
 - Double structure mechanical models
 - Double structure hydraulic models
 - Double structure hydro-mechanical coupling
 - Thermal effects
- 4 Triple structure models, local non-equilibrium

Effective stress?

Description of the unsaturated soil behaviour is much more debatable than modelling of saturated soils, starting from the definition of "effective" stress measure.

Recall the definition of the *effective stress* by Terzaghi.

Effective stress is the calculated stress that is effective in moving soil, i.e. causing displacements.

Effective stress?

Description of the unsaturated soil behaviour is much more debatable than modelling of saturated soils, starting from the definition of "effective" stress measure.

Recall the definition of the *effective stress* by Terzaghi.

Effective stress is the calculated stress that is effective in moving soil, i.e. causing displacements.

Stress description

The first attempt to define the *effective stress for unsaturated soils* was due to Bishop (1959).

$$\sigma' = \sigma_t - \mathbf{1} [\chi u_w + (1 - \chi) u_a]$$

where u_w and u_a represent pore water and air pressures respectively and σ_t is *total stress*.

There is a logics in this equation: average pore water pressure is calculated as a *weighted average* of the pore pressure of water and air. **But this does not work** within the sense of the effective stress definition.

Stress description

The first attempt to define the *effective stress for unsaturated soils* was due to Bishop (1959).

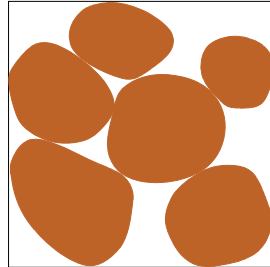
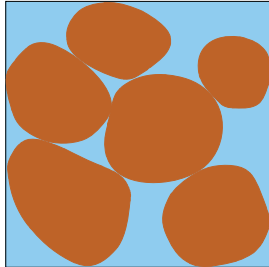
$$\sigma' = \sigma_t - \mathbf{1} [\chi u_w + (1 - \chi) u_a]$$

where u_w and u_a represent pore water and air pressures respectively and σ_t is *total stress*.

There is a logics in this equation: average pore water pressure is calculated as a *weighted average* of the pore pressure of water and air. **But this does not work** within the sense of the effective stress definition.

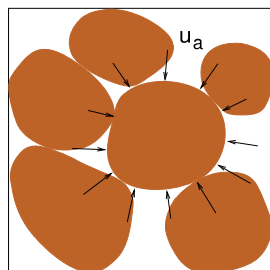
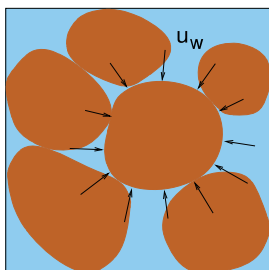
Stress description

Lets consider a soil where the pores are *fully saturated*. Either with water, or with air:



Stress description

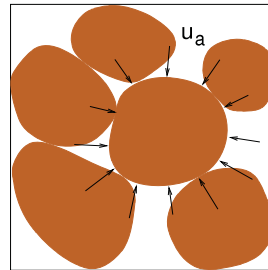
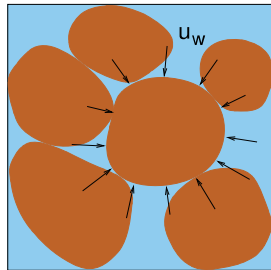
Lets consider a soil where the pores are *fully saturated*. Either with water, or with air:



Water and air imply isotropic (allround) stresses. If the total stress is not isotropic ($\tau \neq 0$), increase of pore pressure can increase probability of the contact shear failure (as $\tau' = \tau$ and $\sigma'_n = \sigma_n - u$).

Stress description

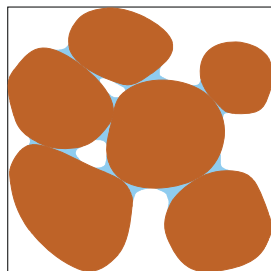
Lets consider a soil where the pores are *fully saturated*. Either with water, or with air:



Water and air imply isotropic (allround) stresses. If the total stress is not isotropic ($\tau \neq 0$), increase of pore pressure can increase probability of the contact shear failure (as $\tau' = \tau$ and $\sigma'_n = \sigma_n - u$).

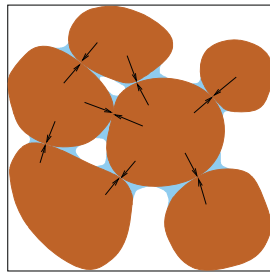
Stress description

Unlike in the saturated soil, in unsaturated soil *water menisci* form around the particle contacts



Stress description

Unlike in the saturated soil, in unsaturated soil *water menisci* form around the particle contacts



In addition to the allround stress, capillary menisci imply contact *normal forces*. They thus reduce shear load of the contacts and *strengthen* the soil skeleton.

Stress description

- Although this view is highly simplified, it demonstrates there are some additional mechanisms that play a role in unsaturated soils. Bishop equation cannot work as an effective stress *on its own*.
- It turns out that to describe the behaviour of unsaturated soils, we need *two* stress measures. One tensorial, describing the allround stress, and one scalar, describing the strengthening effect of the capillary menisci.

Stress description

- Although this view is highly simplified, it demonstrates there are some additional mechanisms that play a role in unsaturated soils. Bishop equation cannot work as an effective stress *on its own*.
- It turns out that to describe the behaviour of unsaturated soils, we need *two* stress measures. One tensorial, describing the allround stress, and one scalar, describing the strengthening effect of the capillary menisci.

Stress description

Even when we accept the need to have two stress variables in unsaturated soils, there are more options:

There is a number of possible combinations of σ_t , U_w and U_a , which lead to *one tensorial* and *one scalar* variable. Each of the combinations have its own merits and shortcomings for the constitutive model development, which means:

- 1 One combination can lead to a *complicated definition of the stress tensor*, which leads to more difficult evaluation of laboratory experiments. The effective stress cannot be controlled directly. The merit is in *simpler constitutive models*.
- 2 Different combination can lead to the other-way-round outcome.

In this lecture, we will see examples of both approaches.

Stress description

Even when we accept the need to have two stress variables in unsaturated soils, there are more options:

There is a number of possible combinations of σ_t , U_w and U_a , which lead to *one tensorial* and *one scalar* variable. Each of the combinations have its own merits and shortcomings for the constitutive model development, which means:

- 1 One combination can lead to a *complicated definition of the stress tensor*, which leads to more difficult evaluation of laboratory experiments. The effective stress cannot be controlled directly. The merit is in *simpler constitutive models*.
- 2 Different combination can lead to the other-way-round outcome.

In this lecture, we will see examples of both approaches.

Stress description

Even when we accept the need to have two stress variables in unsaturated soils, there are more options:

There is a number of possible combinations of σ_t , U_w and U_a , which lead to *one tensorial* and *one scalar* variable. Each of the combinations have its own merits and shortcomings for the constitutive model development, which means:

- 1 One combination can lead to a *complicated definition of the stress tensor*, which leads to more difficult evaluation of laboratory experiments. The effective stress cannot be controlled directly. The merit is in *simpler constitutive models*.
- 2 Different combination can lead to the other-way-round outcome.

In this lecture, we will see examples of both approaches.

Stress description

Even when we accept the need to have two stress variables in unsaturated soils, there are more options:

There is a number of possible combinations of σ_t , u_w and u_a , which lead to *one tensorial* and *one scalar* variable. Each of the combinations have its own merits and shortcomings for the constitutive model development, which means:

- 1 One combination can lead to a *complicated definition of the stress tensor*, which leads to more difficult evaluation of laboratory experiments. The effective stress cannot be controlled directly. The merit is in *simpler constitutive models*.
- 2 Different combination can lead to the other-way-round outcome.

In this lecture, we will see examples of both approaches.

Stress description

Even when we accept the need to have two stress variables in unsaturated soils, there are more options:

There is a number of possible combinations of σ_t , u_w and u_a , which lead to *one tensorial* and *one scalar* variable. Each of the combinations have its own merits and shortcomings for the constitutive model development, which means:

- 1 One combination can lead to a *complicated definition of the stress tensor*, which leads to more difficult evaluation of laboratory experiments. The effective stress cannot be controlled directly. The merit is in *simpler constitutive models*.
- 2 Different combination can lead to the other-way-round outcome.

In this lecture, we will see examples of both approaches.

Modelling of the mechanical behaviour

In this section, we summarise fundamentals of the unsaturated *mechanical behaviour*. For this purpose, we use the most simple combinations of σ_t , u_w and u_a (easy representation of laboratory tests, more complicated models):

- Tensorial variable is a *net stress* σ^{net} (σ_t denotes total stress)

$$\sigma^{net} = \sigma_t - \mathbf{1}u_a$$

- scalar variable is *matric suction* s

$$s = u_a - u_w$$

Modelling of the mechanical behaviour

In this section, we summarise fundamentals of the unsaturated *mechanical behaviour*. For this purpose, we use the most simple combinations of σ_t , u_w and u_a (easy representation of laboratory tests, more complicated models):

- Tensorial variable is a *net stress* σ^{net} (σ_t denotes total stress)

$$\sigma^{net} = \sigma_t - \mathbf{1}u_a$$

- scalar variable is *matric suction* s

$$s = u_a - u_w$$

Modelling of the mechanical behaviour

In this section, we summarise fundamentals of the unsaturated *mechanical behaviour*. For this purpose, we use the most simple combinations of σ_t , u_w and u_a (easy representation of laboratory tests, more complicated models):

- Tensorial variable is a *net stress* σ^{net} (σ_t denotes total stress)

$$\sigma^{net} = \sigma_t - \mathbf{1}u_a$$

- scalar variable is *matric suction* s

$$s = u_a - u_w$$

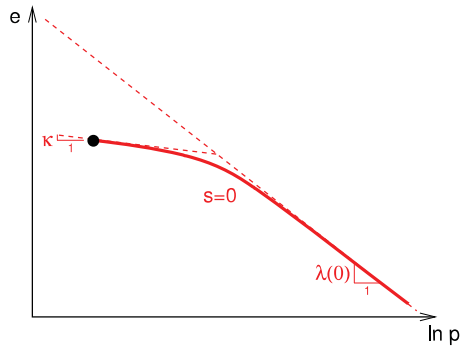
Modelling of the mechanical behaviour

The influence of *suction* on the soil compressibility (isotropic or oedometric loading) is as follows:



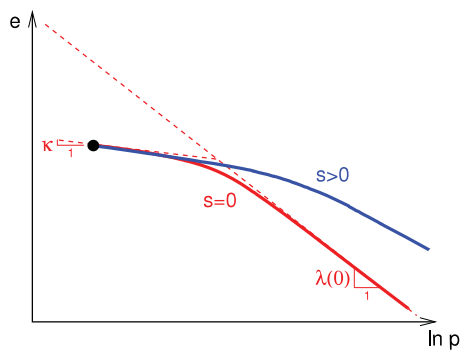
Modelling of the mechanical behaviour

The influence of *suction* on the soil compressibility (isotropic or oedometric loading) is as follows:



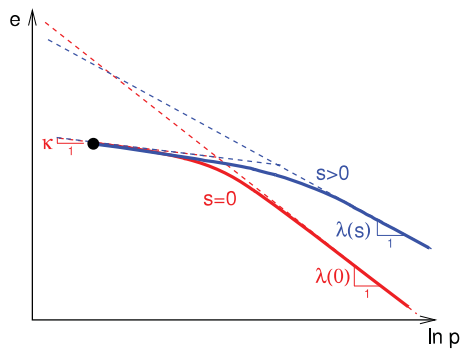
Modelling of the mechanical behaviour

The influence of *suction* on the soil compressibility (isotropic or oedometric loading) is as follows:



Modelling of the mechanical behaviour

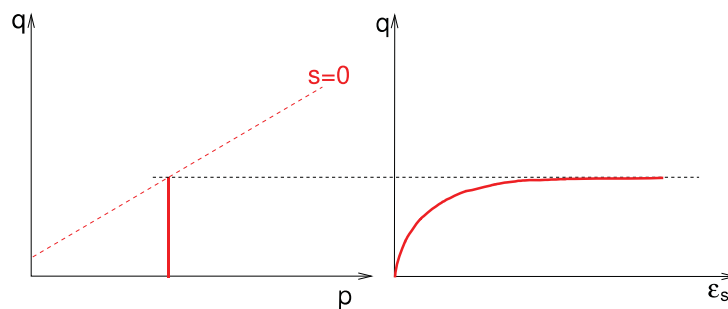
The influence of *suction* on the soil compressibility (isotropic or oedometric loading) is as follows:



Increase of suction is *increasing apparent preconsolidation pressure*.

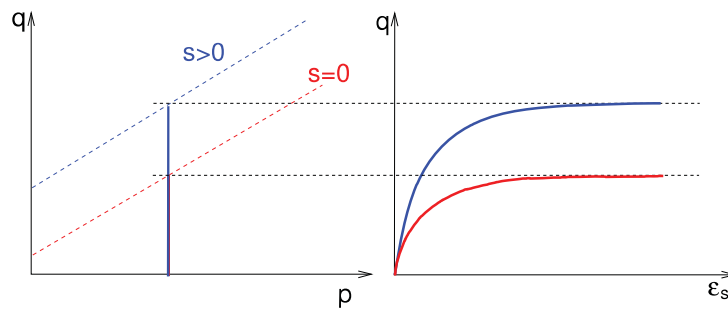
Modelling of the mechanical behaviour

Increase of *suction* is also increasing the soil shear strength, which can be interpreted as an increase of *cohesion* with constant *critical state friction angle*.



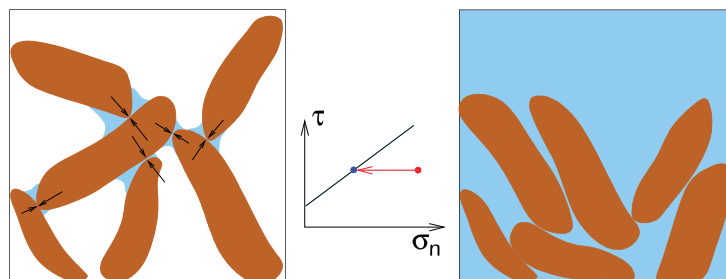
Modelling of the mechanical behaviour

Increase of *suction* is also increasing the soil shear strength, which can be interpreted as an increase of *cohesion* with constant *critical state friction angle*.



Modelling of the mechanical behaviour

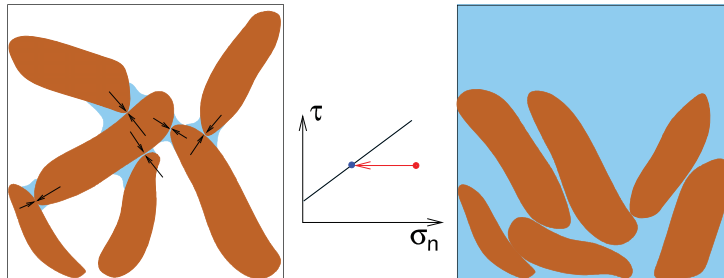
When the soil is loose (*open structure*), saturation (suction decrease) leads to a wetting-induced compaction ("collapse").



Reducing the capillary menisci and normal contact forces causes contact shear failure and compaction ("collapse of the structure").

Modelling of the mechanical behaviour

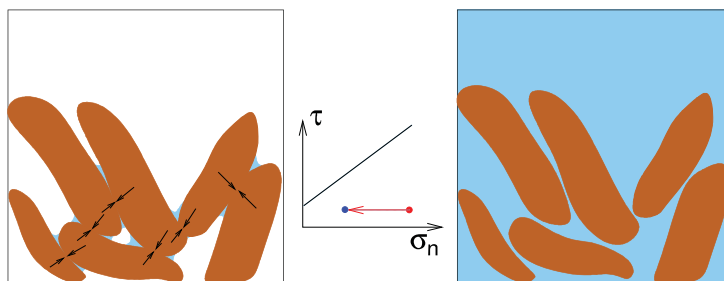
When the soil is loose (*open structure*), saturation (suction decrease) leads to a wetting-induced compaction ("collapse").



Reducing the capillary menisci and normal contact forces causes contact shear failure and compaction ("collapse of the structure").

Modelling of the mechanical behaviour

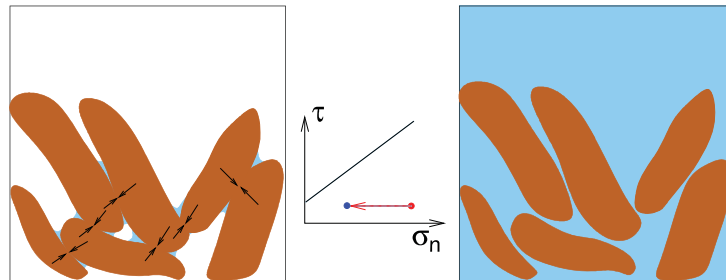
On the other hand, saturation of a *dense soil* causes wetting-induced swelling.



In this case, contacts are just unloaded (no shear failure).

Modelling of the mechanical behaviour

On the other hand, saturation of a *dense soil* causes wetting-induced swelling.



In this case, contacts are just unloaded (no shear failure).

Modelling of the mechanical behaviour

Barcelona basic model

- Interpretation of the above described unsaturated mechanical soil behaviour within constitutive modelling framework will be first described using the pioneering constitutive model for unsaturated soils: *Barcelona basic model - BBM* (Alonso *et al.*, 1990).
- Milestone model in representation of the unsaturated soil behavior.
- Stress state represented using the net stress σ^{net} and suction s . Suction is a state variable; for $s = 0$, the model reduces to the Modified Cam-clay model.

Modelling of the mechanical behaviour

Barcelona basic model

- Interpretation of the above described unsaturated mechanical soil behaviour within constitutive modelling framework will be first described using the pioneering constitutive model for unsaturated soils: *Barcelona basic model - BBM* (Alonso *et al.*, 1990).
- Milestone model in representation of the unsaturated soil behavior.
- Stress state represented using the net stress σ^{net} and suction s . Suction is a state variable; for $s = 0$, the model reduces to the Modified Cam-clay model.

Modelling of the mechanical behaviour

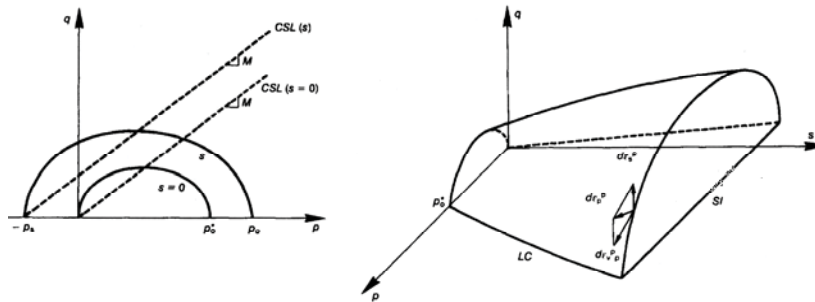
Barcelona basic model

- Interpretation of the above described unsaturated mechanical soil behaviour within constitutive modelling framework will be first described using the pioneering constitutive model for unsaturated soils: *Barcelona basic model - BBM* (Alonso *et al.*, 1990).
- Milestone model in representation of the unsaturated soil behavior.
- Stress state represented using the net stress σ^{net} and suction s . Suction is a state variable; for $s = 0$, the model reduces to the Modified Cam-clay model.

Modelling of the mechanical behaviour

Barcelona basic model

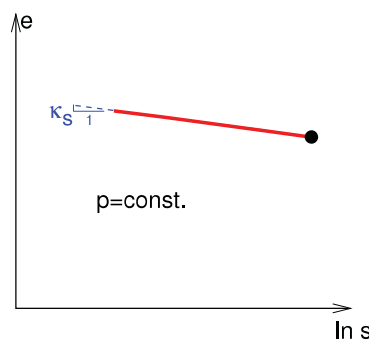
The yield surface of the *Modified Cam clay model* (which is a saturated counterpart of BBM) is made dependent on *suction*. This represents both the suction-induced increase of *critical state strength* (through apparent cohesion) and of *preconsolidation pressure*.



Modelling of the mechanical behaviour

Barcelona basic model

In an *overconsolidated state*, response to suction variation (wetting-induced swelling) is controlled by the parameter k_S^*



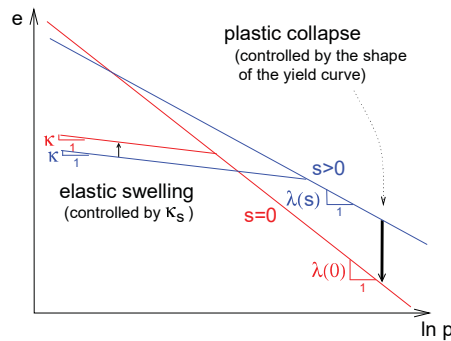
Note that k_S^* is needed in the model, as variation of suction does not involve any change of net stress.



Modelling of the mechanical behaviour

Barcelona basic model

In a *normally consolidated state*, response to suction variation is controlled by the adopted *hardening law* (dependency of λ on suction). This allows us to model *wetting induced collapse* as well as *swelling* of dense soil using a unified concept.



Navigation icons: back, forward, search, etc.

Modelling of the mechanical behaviour

Barcelona basic model

Barcelona basic model requires the following *nine parameters*

- M ... critical state stress ratio.
- $\lambda(0)$... slope of saturated normal compression line.
- κ ... slope of unloading line (p^{net} vs. e).
- k ... increase of apparent cohesion with suction.
- β, r ... variability of NCL slope with suction (also controls wetting-induced collapse).
- κ_s, λ_s ... Volumetric change due to variation in suction.
- G ... Elastic shear modulus.

The initial state is prescribed by preconsolidation pressure p_c .

Navigation icons: back, forward, search, etc.

Modelling of the mechanical behaviour

Effective stress in unsaturated soils

- As indicated earlier, many combinations of σ_t , u_w and u_a exist (simpler stress definition vs. simpler model formulation).
- We also indicated that no single *effective stress* may be found. We always need the additional "bonding" variable.
- In unsaturated soil mechanics, as an *effective stress* is denoted the stress which simplifies the model formulation such that:
 - The response in the *overconsolidated state* is governed solely by the effective stress (the same response due to suction variation and net stress variation) – Equivalent to the *effective stress* in saturated soil mechanics.
 - Within the same effective stress space, increase in suction does not cause any change of *critical state strength* (apparent cohesion due to suction variation is zero).

Modelling of the mechanical behaviour

Effective stress in unsaturated soils

- As indicated earlier, many combinations of σ_t , u_w and u_a exist (simpler stress definition vs. simpler model formulation).
- We also indicated that no single *effective stress* may be found. We always need the additional "bonding" variable.
- In unsaturated soil mechanics, as an *effective stress* is denoted the stress which simplifies the model formulation such that:
 - The response in the *overconsolidated state* is governed solely by the effective stress (the same response due to suction variation and net stress variation) – Equivalent to the *effective stress* in saturated soil mechanics.
 - Within the same effective stress space, increase in suction does not cause any change of *critical state strength* (apparent cohesion due to suction variation is zero).

Modelling of the mechanical behaviour

Effective stress in unsaturated soils

- As indicated earlier, many combinations of σ_t , u_w and u_a exist (simpler stress definition vs. simpler model formulation).
- We also indicated that no single *effective stress* may be found. We always need the additional "bonding" variable.
- In unsaturated soil mechanics, as an *effective stress* is denoted the stress which simplifies the model formulation such that:
 - The response in the *overconsolidated state* is governed solely by the effective stress (the same response due to suction variation and net stress variation) – Equivalent to the *effective stress* in saturated soil mechanics.
 - Within the same effective stress space, increase in suction does not cause any change of *critical state strength* (apparent cohesion due to suction variation is zero).

Modelling of the mechanical behaviour

Effective stress in unsaturated soils

- As indicated earlier, many combinations of σ_t , u_w and u_a exist (simpler stress definition vs. simpler model formulation).
- We also indicated that no single *effective stress* may be found. We always need the additional "bonding" variable.
- In unsaturated soil mechanics, as an *effective stress* is denoted the stress which simplifies the model formulation such that:
 - The response in the *overconsolidated state* is governed solely by the effective stress (the same response due to suction variation and net stress variation) – Equivalent to the *effective stress* in saturated soil mechanics.
 - Within the same effective stress space, increase in suction does not cause any change of *critical state strength* (apparent cohesion due to suction variation is zero).

Modelling of the mechanical behaviour

Effective stress in unsaturated soils

- As indicated earlier, many combinations of σ_t , u_w and u_a exist (simpler stress definition vs. simpler model formulation).
- We also indicated that no single *effective stress* may be found. We always need the additional "bonding" variable.
- In unsaturated soil mechanics, as an *effective stress* is denoted the stress which simplifies the model formulation such that:
 - The response in the *overconsolidated state* is governed solely by the effective stress (the same response due to suction variation and net stress variation) – Equivalent to the *effective stress* in saturated soil mechanics.
 - Within the same effective stress space, increase in suction does not cause any change of *critical state strength* (apparent cohesion due to suction variation is zero).

Modelling of the mechanical behaviour

Effective stress in unsaturated soils

- Two *empirical* relationships exist within the literature which were developed to have the above properties: Khalili and Khabbaz (1998) and Alonso et al. (2010).
- Principle of the investigation:
 - Define the *critical state strength envelope* using shear test on *saturated soils*.
 - Back-calculate the Bishop factor χ in $\sigma = \sigma_{net} + \chi s$ such that in the unsaturated state the critical strength envelope coincides with the one in a saturated state.
 - Evaluate the dependency of χ on common state variables (suction, degree of saturation, air entry value of suction...).
 - Check that the same value of χ represents properly also the volumetric response in overconsolidated state.

Modelling of the mechanical behaviour

Effective stress in unsaturated soils

- Two *empirical* relationships exist within the literature which were developed to have the above properties: Khalili and Khabbaz (1998) and Alonso et al. (2010).
- Principle of the investigation:
 - Define the *critical state strength envelope* using shear test on *saturated soils*.
 - Back-calculate the Bishop factor χ in $\sigma = \sigma_{net} + 1\chi s$ such that in the unsaturated state the critical strength envelope coincides with the one in a saturated state.
 - Evaluate the dependency of χ on common state variables (suction, degree of saturation, air entry value of suction...).
 - Check that the same value of χ represents properly also the volumetric response in overconsolidated state.

Modelling of the mechanical behaviour

Effective stress in unsaturated soils

- Two *empirical* relationships exist within the literature which were developed to have the above properties: Khalili and Khabbaz (1998) and Alonso et al. (2010).
- Principle of the investigation:
 - Define the *critical state strength envelope* using shear test on *saturated soils*.
 - Back-calculate the Bishop factor χ in $\sigma = \sigma_{net} + 1\chi s$ such that in the unsaturated state the critical strength envelope coincides with the one in a saturated state.
 - Evaluate the dependency of χ on common state variables (suction, degree of saturation, air entry value of suction...).
 - Check that the same value of χ represents properly also the volumetric response in overconsolidated state.

Modelling of the mechanical behaviour

Effective stress in unsaturated soils

- Two *empirical* relationships exist within the literature which were developed to have the above properties: Khalili and Khabbaz (1998) and Alonso et al. (2010).
- Principle of the investigation:
 - Define the *critical state strength envelope* using shear test on *saturated soils*.
 - Back-calculate the Bishop factor χ in $\sigma = \sigma_{net} + \mathbf{1}\chi s$ such that in the unsaturated state the critical strength envelope coincides with the one in a saturated state.
 - Evaluate the dependency of χ on common state variables (suction, degree of saturation, air entry value of suction...).
 - Check that the same value of χ represents properly also the volumetric response in overconsolidated state.

Modelling of the mechanical behaviour

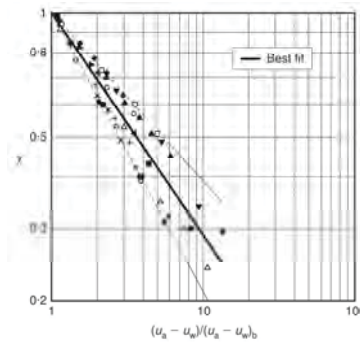
Effective stress in unsaturated soils

- Two *empirical* relationships exist within the literature which were developed to have the above properties: Khalili and Khabbaz (1998) and Alonso et al. (2010).
- Principle of the investigation:
 - Define the *critical state strength envelope* using shear test on *saturated soils*.
 - Back-calculate the Bishop factor χ in $\sigma = \sigma_{net} + \mathbf{1}\chi s$ such that in the unsaturated state the critical strength envelope coincides with the one in a saturated state.
 - Evaluate the dependency of χ on common state variables (suction, degree of saturation, air entry value of suction...).
 - Check that the same value of χ represents properly also the volumetric response in overconsolidated state.

Modelling of the mechanical behaviour

Effective stress in unsaturated soils

Khalili and Khabbaz (1998): back-calculated value of χ shows a clear dependency on the ratio of suction s and suction on air entry s_e , with a unique best-fit line for different soils.



Navigation icons: back, forward, search, etc.

Modelling of the mechanical behaviour

Effective stress in unsaturated soils

The best-fit line had an expression (with $\gamma = 0.55$)

$$\chi = \begin{cases} 1 & \text{for } s \leq s_e \\ \left(\frac{s_e}{s}\right)^\gamma & \text{for } s > s_e \end{cases}$$

Such a formulation predicts the following dependency of the critical state strength on suction:

Navigation icons: back, forward, search, etc.

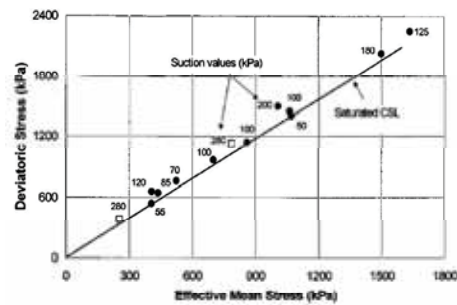
Modelling of the mechanical behaviour

Effective stress in unsaturated soils

The best-fit line had an expression (with $\gamma = 0.55$)

$$\chi = \begin{cases} 1 & \text{for } s \leq s_e \\ \left(\frac{s_e}{s}\right)^\gamma & \text{for } s > s_e \end{cases}$$

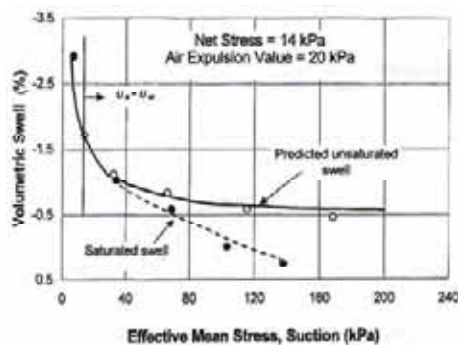
Such a formulation predicts the following dependency of the critical state strength on suction:



Modelling of the mechanical behaviour

Effective stress in unsaturated soils

The same expression then models properly the *volumetric response* due to variation of suction (at constant net stress) and variation of net stress (at constant suction)



Modelling of the mechanical behaviour

Effective stress in unsaturated soils

The same approach adopted by [Alonso et al. \(2010\)](#). They investigated a possibility to interpret χ using a hydraulic quantity S_r (note that $\chi = S_r$ is implied by some interpretations based on thermodynamic laws). [Alonso et al. \(2010\)](#) indicated that

- $\chi = S_r$ does not represent the soil behaviour properly when subject to the above effective stress definition.
- Many unsaturated soils have so-called *double structure*. [Alonso et al. \(2010\)](#) observed that

$$\chi = S_r^M$$

where S_r^M is the degree of saturation of macrostructure.

Modelling of the mechanical behaviour

Effective stress in unsaturated soils

The same approach adopted by [Alonso et al. \(2010\)](#). They investigated a possibility to interpret χ using a hydraulic quantity S_r (note that $\chi = S_r$ is implied by some interpretations based on thermodynamic laws). [Alonso et al. \(2010\)](#) indicated that

- $\chi = S_r$ does not represent the soil behaviour properly when subject to the above effective stress definition.
- Many unsaturated soils have so-called *double structure*. [Alonso et al. \(2010\)](#) observed that

$$\chi = S_r^M$$

where S_r^M is the degree of saturation of macrostructure.

Modelling of the mechanical behaviour

Effective stress in unsaturated soils

The same approach adopted by [Alonso et al. \(2010\)](#). They investigated a possibility to interpret χ using a hydraulic quantity S_r (note that $\chi = S_r$ is implied by some interpretations based on thermodynamic laws). [Alonso et al. \(2010\)](#) indicated that

- $\chi = S_r$ does not represent the soil behaviour properly when subject to the above effective stress definition.
- Many unsaturated soils have so-called *double structure*. Alonso et al. (2010) observed that

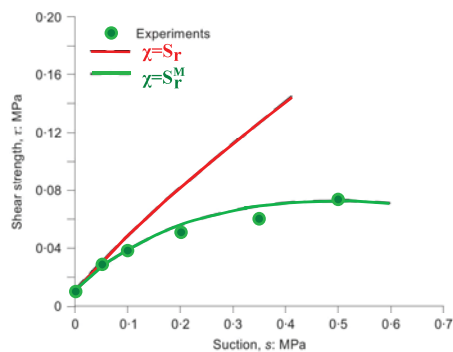
$$\chi = S_r^M$$

where S_r^M is the degree of saturation of macrostructure.

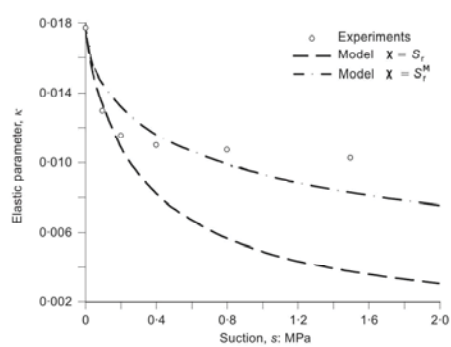
Modelling of the mechanical behaviour

Effective stress in unsaturated soils

Alonso et al. (2010):



shear strength data



volumetric response

Modelling of the mechanical behaviour

Effective stress-based mechanical modelling of unsaturated soils

- We already know *Barcelona basic model*, and we also know what can be gained by using *effective stress*.
- Lets try to guess merits and capabilities of *Barcelona basic model* defined using the effective stress instead of net stress.
- Given what we know, such a model should have the same capabilities *and shortcomings* as the net stress based model. However, we eliminate *two material parameters* - elastic parameter κ_s and suction-induced apparent cohesion controlling parameter k .
- Additional modelling capabilities can be gained by adopting saturated model predicting *non-linear behaviour* (hypoplasticity, bounding surface plasticity, generalised plasticity) instead of Cam clay.

Modelling of the mechanical behaviour

Effective stress-based mechanical modelling of unsaturated soils

- We already know *Barcelona basic model*, and we also know what can be gained by using *effective stress*.
- Lets try to guess merits and capabilities of *Barcelona basic model* defined using the effective stress instead of net stress.
- Given what we know, such a model should have the same capabilities *and shortcomings* as the net stress based model. However, we eliminate *two material parameters* - elastic parameter κ_s and suction-induced apparent cohesion controlling parameter k .
- Additional modelling capabilities can be gained by adopting saturated model predicting *non-linear behaviour* (hypoplasticity, bounding surface plasticity, generalised plasticity) instead of Cam clay.

Modelling of the mechanical behaviour

Effective stress-based mechanical modelling of unsaturated soils

- We already know *Barcelona basic model*, and we also know what can be gained by using *effective stress*.
- Lets try to guess merits and capabilities of *Barcelona basic model* defined using the effective stress instead of net stress.
- Given what we know, such a model should have the same capabilities *and shortcomings* as the net stress based model. However, we eliminate *two material parameters* - elastic parameter κ_s and suction-induced apparent cohesion controlling parameter k .
- Additional modelling capabilities can be gained by adopting saturated model predicting *non-linear behaviour* (hypoplasticity, bounding surface plasticity, generalised plasticity) instead of Cam clay.

Modelling of the mechanical behaviour

Effective stress-based mechanical modelling of unsaturated soils

- We already know *Barcelona basic model*, and we also know what can be gained by using *effective stress*.
- Lets try to guess merits and capabilities of *Barcelona basic model* defined using the effective stress instead of net stress.
- Given what we know, such a model should have the same capabilities *and shortcomings* as the net stress based model. However, we eliminate *two material parameters* - elastic parameter κ_s and suction-induced apparent cohesion controlling parameter k .
- Additional modelling capabilities can be gained by adopting saturated model predicting *non-linear behaviour* (hypoplasticity, bounding surface plasticity, generalised plasticity) instead of Cam clay.

Modelling of the mechanical behaviour

Effective stress-based mechanical modelling of unsaturated soils

- In the following, we demonstrate capabilities of such a *effective stress*-based *non-linear* modelling using the *hypoplastic model for unsaturated soils* (Mašín and Khalili, 2008).
- Clay hypoplasticity is the saturated driver. This model requires cam-clay parameters $\varphi_c, \lambda^*, \kappa^*, N, \nu$.
- Normal compression lines of unsaturated soils depend on suction. In an unsaturated model, two additional parameters n and l , controlling the dependency of N and λ^* on suction.

Modelling of the mechanical behaviour

Effective stress-based mechanical modelling of unsaturated soils

- In the following, we demonstrate capabilities of such a *effective stress*-based *non-linear* modelling using the *hypoplastic model for unsaturated soils* (Mašín and Khalili, 2008).
- Clay hypoplasticity is the saturated driver. This model requires cam-clay parameters $\varphi_c, \lambda^*, \kappa^*, N, \nu$.
- Normal compression lines of unsaturated soils depend on suction. In an unsaturated model, two additional parameters n and l , controlling the dependency of N and λ^* on suction.

Modelling of the mechanical behaviour

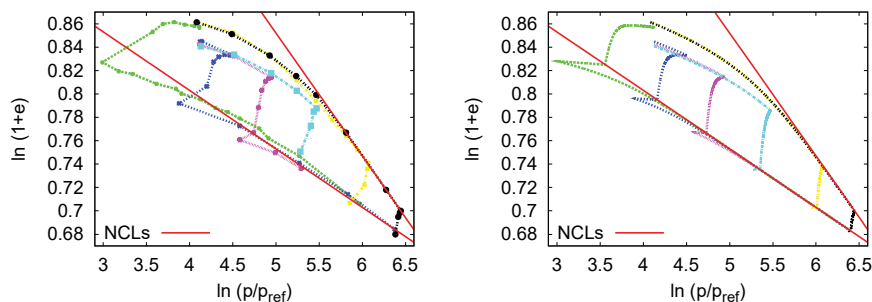
Effective stress-based mechanical modelling of unsaturated soils

- In the following, we demonstrate capabilities of such a *effective stress*-based *non-linear* modelling using the *hypoplastic model for unsaturated soils* (Mašín and Khalili, 2008).
- Clay hypoplasticity is the saturated driver. This model requires cam-clay parameters φ_c , λ^* , κ^* , N , ν .
- Normal compression lines of unsaturated soils depend on suction. In an unsaturated model, two additional parameters n and l , controlling the dependency of N and λ^* on suction.

Modelling of the mechanical behaviour

Effective stress-based mechanical modelling of unsaturated soils

Predictions of isotropic compression tests followed by wetting tests on soils with different apparent OCRs by *Sun et al. (2007)*.

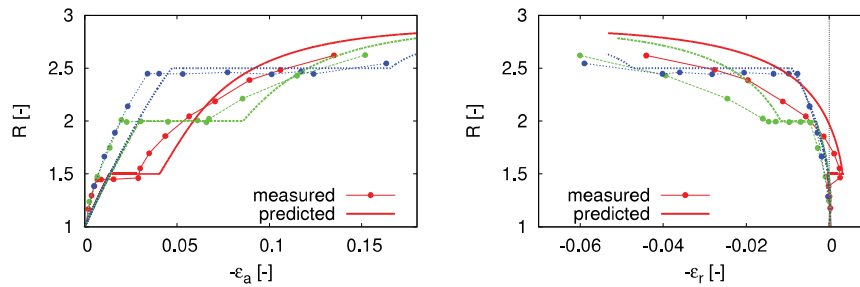


Mašín and Khalili (2008)

Modelling of the mechanical behaviour

Effective stress-based mechanical modelling of unsaturated soils

Predictions of constant suction and net mean stress tests wetted at different stress ratios R (data by *Sun et al., 2007*).



Mašín and Khalili (2008)

Outline

- 1 Introduction
- 2 THM modelling of single structure soils
 - Modelling of the mechanical behaviour
 - **Modelling of the water retention behaviour**
 - Hydro-mechanical coupling
 - Thermal effects
- 3 Double structure models
 - Double structure mechanical models
 - Double structure hydraulic models
 - Double structure hydro-mechanical coupling
 - Thermal effects
- 4 Triple structure models, local non-equilibrium

Modelling of the water retention behaviour

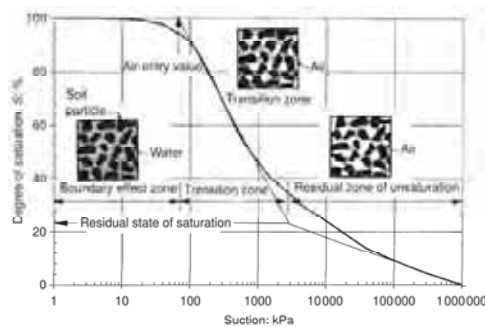
- To solve flow-deformation equations in partially saturated soils, the mechanical model must be accompanied by the model for the *water retention behaviour* (hydraulic model).

Water retention curve represents the amount of water that can be stored within the soil (measured by a degree of saturation $S_r = V_w/V_p$, water content $w_c = m_w/m_s$ etc.) on pore fluid pressures (measured typically by suction s)

Modelling of the water retention behaviour

- To solve flow-deformation equations in partially saturated soils, the mechanical model must be accompanied by the model for the *water retention behaviour* (hydraulic model).

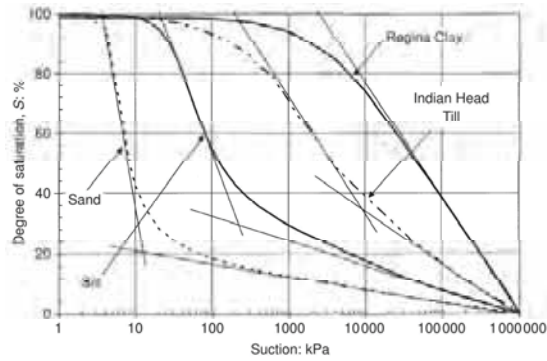
Water retention curve represents the amount of water that can be stored within the soil (measured by a degree of saturation $S_r = V_w/V_p$, water content $w_c = m_w/m_s$ etc.) on pore fluid pressures (measured typically by suction s)



(sketch from Vanapalli et al. 1999)

Modelling of the water retention behaviour

- Water retention curve shape and slope depends on soil type (in particular, notice variable **air entry value of suction**).

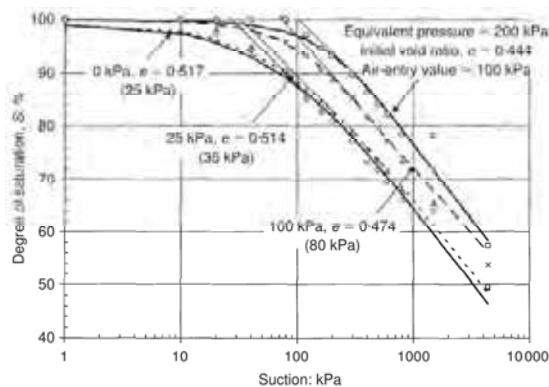


Vanapalli et al. (1999)

Navigation icons: back, forward, search, etc.

Modelling of the water retention behaviour

- Different soils in the previous slide differed by the **size of pores**. Size of pores (measured by **void ratio**) influences WRC also for one particular soil.

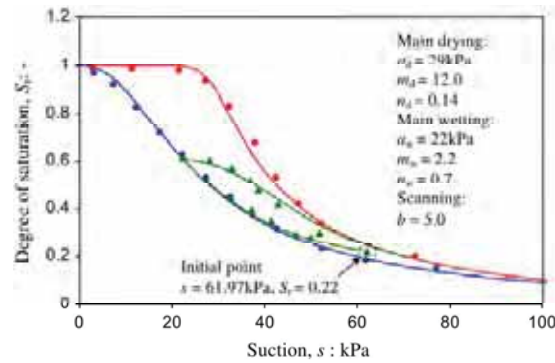


Vanapalli et al. (1999)

Navigation icons: back, forward, search, etc.

Modelling of the water retention behaviour

- The soil water retention curve is not *unique* in the S_r vs. s vs. e plane, but there are effects of *hydraulic hysteresis*.



data from Viaene et al. (1994), model Zhou et al. (2012)

Navigation icons: back, forward, search, etc.

Modelling of the water retention behaviour

- As we already know, *water retention curve* represents a dependency of the amount of water stored within the soil (measured by water content, *degree of saturation* etc.) on pore fluid pressures (measured often by *suction*).
- Water-retention model (*hydraulic model*) represents an additional constitutive equation needed to solve coupled flow-deformation problems in partially saturated soils.
- In general, the hydraulic model H may be written as

$$\dot{S}_r = H(\dot{s}, s, \dot{\epsilon})$$

Navigation icons: back, forward, search, etc.

Modelling of the water retention behaviour

- As we already know, *water retention curve* represents a dependency of the amount of water stored within the soil (measured by water content, *degree of saturation* etc.) on pore fluid pressures (measured often by *suction*).
- Water-retention model (*hydraulic model*) represents an additional constitutive equation needed to solve coupled flow-deformation problems in partially saturated soils.
- In general, the hydraulic model H may be written as

$$\dot{S}_r = H(\dot{s}, s, \dot{\epsilon})$$

Modelling of the water retention behaviour

- As we already know, *water retention curve* represents a dependency of the amount of water stored within the soil (measured by water content, *degree of saturation* etc.) on pore fluid pressures (measured often by *suction*).
- Water-retention model (*hydraulic model*) represents an additional constitutive equation needed to solve coupled flow-deformation problems in partially saturated soils.
- In general, the hydraulic model H may be written as

$$\dot{S}_r = H(\dot{s}, s, \dot{\epsilon})$$

Modelling of the water retention behaviour

Basic models

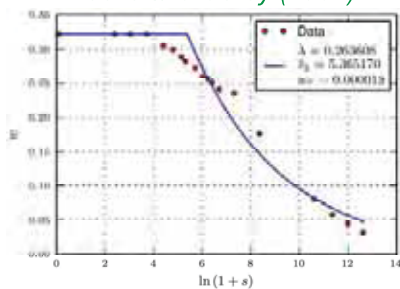
- The most simple hydraulic models do not consider hydraulic hysteresis and strain-dependency of S_r . They may then be written in a direct form $S_r = H(s)$

Modelling of the water retention behaviour

Basic models

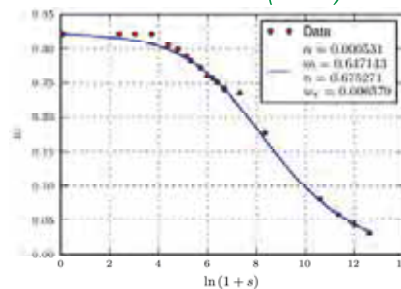
- The most simple hydraulic models do not consider hydraulic hysteresis and strain-dependency of S_r . They may then be written in a direct form $S_r = H(s)$

Brooks and Corey (1964)



calibration by Pedroso and Williams (2011)

van Genuchten (1980)

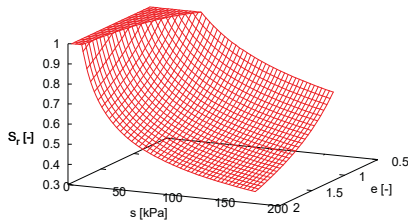


calibration by Pedroso and Williams (2011)

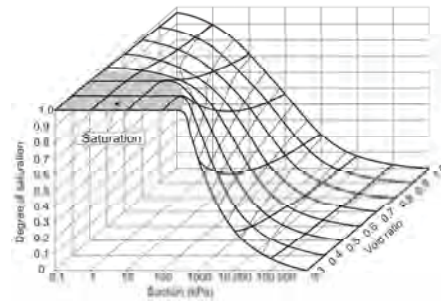
Modelling of the water retention behaviour

Models considering dependency of WRC on void ratio

- When void ratio dependency of WRC is considered without modelling the hydraulic hysteresis, the models can still be written in a total form $S_r = H(s, e)$. The models then represent a *surface* in the S_r vs. s vs. e space.



Mašín (2010)



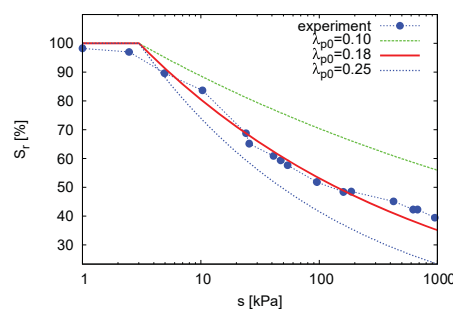
Salager et al. (2010)

Modelling of the water retention behaviour

Models considering dependency of WRC on void ratio

- Example model by Mašín (2010). The dependency of WRC on void ratio is automatically generated without any additional parameter.

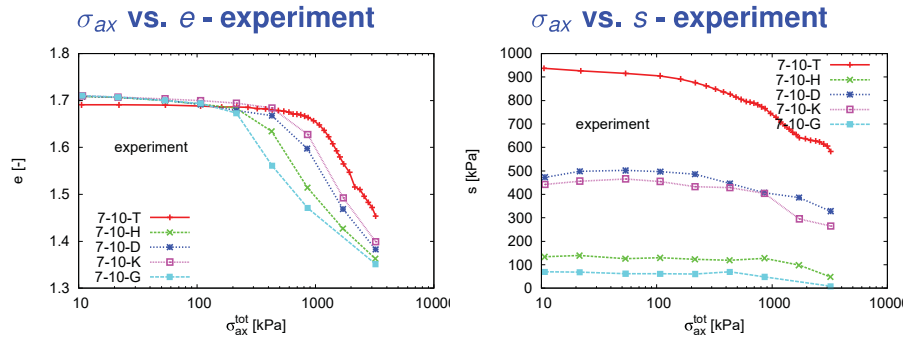
The experiments on *quartz silt* by *Jotisankasa et. al (2007)*. The authors provided measurements of WRC, allowing us to calibrate directly the model parameters λ_{p0} , s_{e0} and e_0



Modelling of the water retention behaviour

Models considering dependency of WRC on void ratio

Suction-monitored constant water content oedometric tests used for the model evaluation.

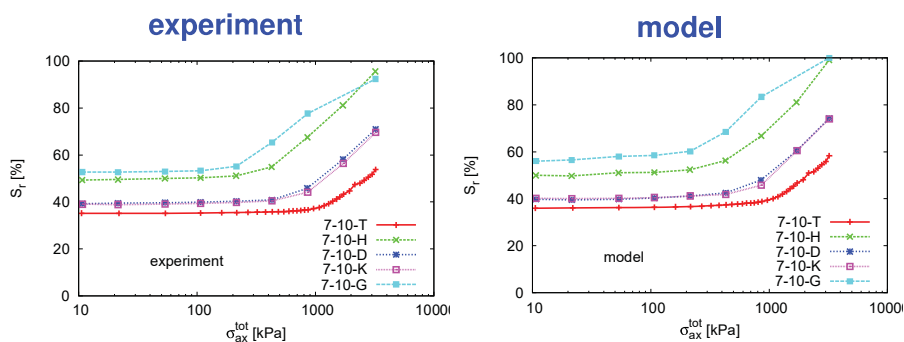


Navigation icons: back, forward, search, etc.

Modelling of the water retention behaviour

Models considering dependency of WRC on void ratio

Knowing the parameters for *single WRC* at the *void ratio* e_0 , variation of S_r was calculated using the described model.



Navigation icons: back, forward, search, etc.

Modelling of the water retention behaviour

Models considering hydraulic hysteresis

- Most advanced models consider both hydraulic hysteresis and the dependency of WRC on void ratio. These models must be defined in a *rate form*

$$\dot{S}_r = H(\dot{s}, s, \dot{\epsilon})$$

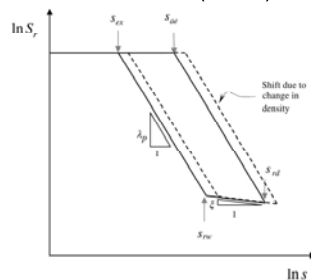
Modelling of the water retention behaviour

Models considering hydraulic hysteresis

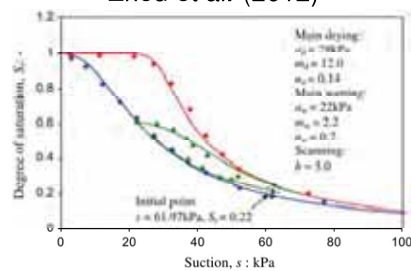
- Most advanced models consider both hydraulic hysteresis and the dependency of WRC on void ratio. These models must be defined in a *rate form*

$$\dot{S}_r = H(\dot{s}, s, \dot{\epsilon})$$

Brooks and Corey - based model by Khalili et al. (2008)



van Genuchten - based model by Zhou et al. (2012)



Outline

- 1 Introduction
- 2 THM modelling of single structure soils
 - Modelling of the mechanical behaviour
 - Modelling of the water retention behaviour
 - **Hydro-mechanical coupling**
 - Thermal effects
- 3 Double structure models
 - Double structure mechanical models
 - Double structure hydraulic models
 - Double structure hydro-mechanical coupling
 - Thermal effects
- 4 Triple structure models, local non-equilibrium

Hydro-mechanical coupling

- *Mechanical model* defined using *effective stress* σ .

$$\dot{\sigma} = \mathbf{G}(\sigma, \mathbf{q}, \dot{\epsilon}) \quad \text{with} \quad \sigma = \sigma^{net} - \mathbf{1}s\chi$$

where \mathbf{q} is a vector of state variables.

- *Hydraulic model* is defined using degree of saturation S_r .

$$\dot{S}_r = H(\dot{s}, s, \dot{\epsilon})$$

Hydro-mechanical coupling

- *Mechanical model* defined using *effective stress* σ .

$$\dot{\sigma} = \mathbf{G}(\sigma, \mathbf{q}, \dot{\epsilon}) \quad \text{with} \quad \sigma = \sigma^{net} - \mathbf{1}s\chi$$

where \mathbf{q} is a vector of state variables.

- *Hydraulic model* is defined using degree of saturation S_r .

$$\dot{S}_r = H(\dot{s}, s, \dot{\epsilon})$$

Hydro-mechanical coupling

- *Mechanical model* defined using *effective stress* σ .

$$\dot{\sigma} = \mathbf{G}(\sigma, \mathbf{q}, \dot{\epsilon}) \quad \text{with} \quad \sigma = \sigma^{net} - \mathbf{1}s\chi$$

where \mathbf{q} is a vector of state variables.

- *Hydraulic model* is defined using degree of saturation S_r .

$$\dot{S}_r = H(\dot{s}, s, \dot{\epsilon})$$

- *Hydro-mechanical coupling*: Hydraulic strain measure S_r depends on mechanical quantity $\dot{\epsilon}$. Mechanical response influenced by χ , which depends on a hydraulic quantity S_r or air-entry value of suction s_e .

Hydro-mechanical coupling

MUSE Benchmark

- Water retention and hydraulic models must in simulation of real problems always be considered together.
- Predictive capabilities of different coupled models evaluated by D'Onza et al. (2011). A benchmark exercise organised by the European network for unsaturated soil investigation *MUSE*.
- Different teams were free to select constitutive model according to their preferences. They were given experimental data which would be used for model calibration. Then, they were asked to present *blind predictions* - predictions of laboratory test which has been performed after the benchmark closure.

Hydro-mechanical coupling

MUSE Benchmark

- Water retention and hydraulic models must in simulation of real problems always be considered together.
- Predictive capabilities of different coupled models evaluated by D'Onza et al. (2011). A benchmark exercise organised by the European network for unsaturated soil investigation *MUSE*.
- Different teams were free to select constitutive model according to their preferences. They were given experimental data which would be used for model calibration. Then, they were asked to present *blind predictions* - predictions of laboratory test which has been performed after the benchmark closure.

Hydro-mechanical coupling

MUSE Benchmark

- Water retention and hydraulic models must in simulation of real problems always be considered together.
- Predictive capabilities of different coupled models evaluated by D'Onza et al. (2011). A benchmark exercise organised by the European network for unsaturated soil investigation *MUSE*.
- Different teams were free to select constitutive model according to their preferences. They were given experimental data which would be used for model calibration. Then, they were asked to present *blind predictions* - predictions of laboratory test which has been performed after the benchmark closure.

Hydro-mechanical coupling

MUSE Benchmark

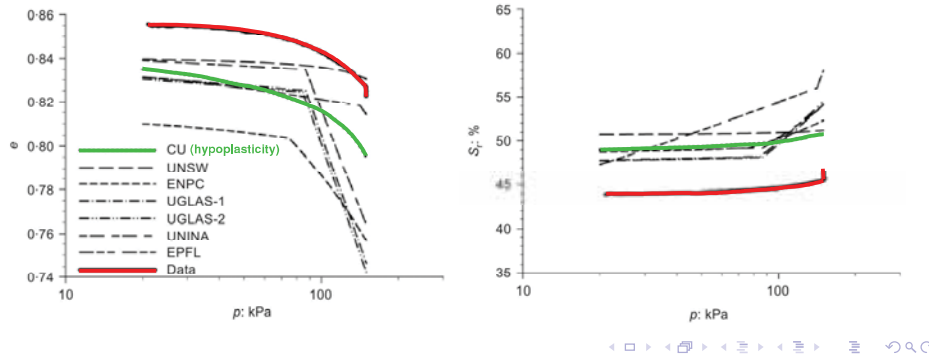
Blind test: *Constant suction* (100 kPa) isotropic loading, followed by *constant water content* shear.

Hydro-mechanical coupling

MUSE Benchmark

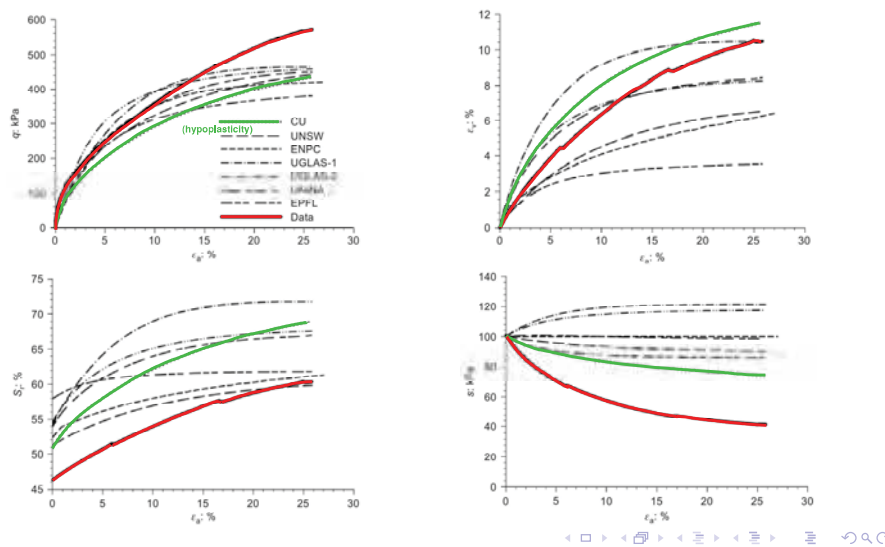
Blind test: Constant suction (100 kPa) isotropic loading, followed by constant water content shear.

Results of loading stage:



Hydro-mechanical coupling

MUSE Benchmark – results of constant water content shear stage

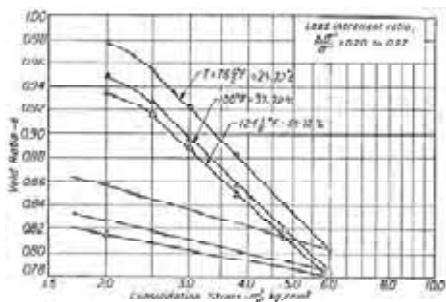


Outline

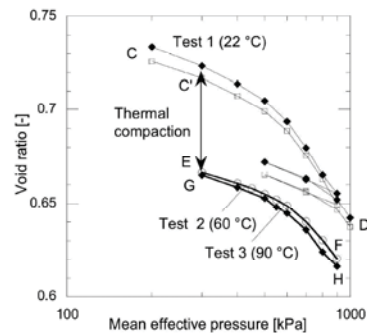
- 1 Introduction
- 2 THM modelling of single structure soils
 - Modelling of the mechanical behaviour
 - Modelling of the water retention behaviour
 - Hydro-mechanical coupling
 - **Thermal effects**
- 3 Double structure models
 - Double structure mechanical models
 - Double structure hydraulic models
 - Double structure hydro-mechanical coupling
 - Thermal effects
- 4 Triple structure models, local non-equilibrium

Compression behaviour under constant temperature

- Normal compression lines of soil at different temperatures are *shifted in the p vs. e plane* such that *heated soil has lower void ratio* than soil at lower temperature.



Campannella and Mitchell (1968)



Laloui and Cekerevac (2003)

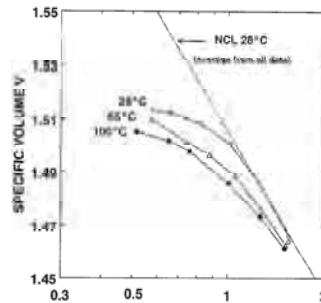
Compression behaviour under constant temperature

- Majority of results show that *normal compression lines may be considered as parallel*. In some cases, however, the slope of NCLs is different.
- With increasing temperature, slope of NCL is decreasing \Rightarrow the NCLs are *converging*.

Graham et al. (2001)

Compression behaviour under constant temperature

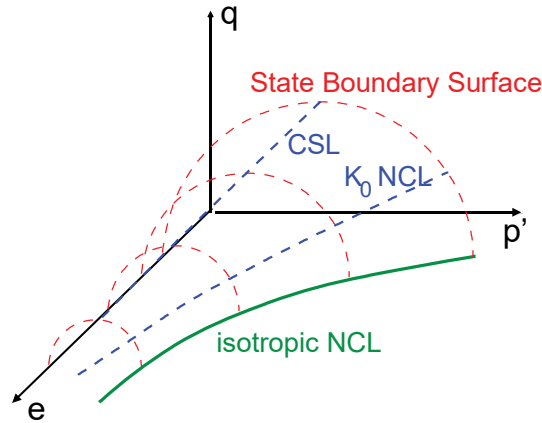
- Majority of results show that *normal compression lines may be considered as parallel*. In some cases, however, the slope of NCLs is different.
- With increasing temperature, slope of NCL is decreasing \Rightarrow the NCLs are *converging*.



Graham et al. (2001)

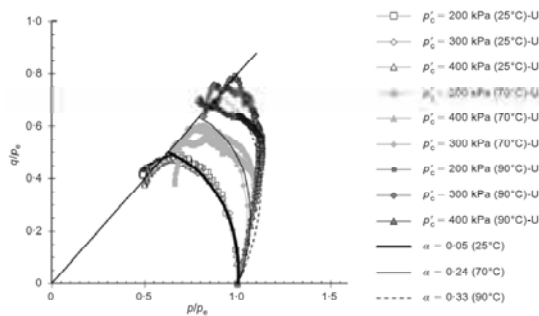
Behaviour in shear under constant temperature

Isotropic normal compression lines define the *size of the state boundary surface* (SBS). What about the influence of temperature on the *shape* of the SBS?

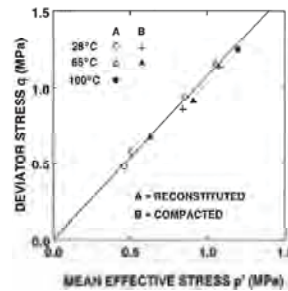


Behaviour in shear under constant temperature

- Experimental results on the thermal - dependency of *peak friction angle* are contradictory. However, most results agree that the *critical state friction angle* is *independent of temperature*.



Abuel-Naga et al. (2009)



Graham et al. (2001)



Behaviour in shear under constant temperature

- Results on the dependency of *peak friction angle* on temperature contradictory.
- Some authors report *decrease of the peak strength* with temperature – consistent with the dependency of *apparent OCR* on temperature.

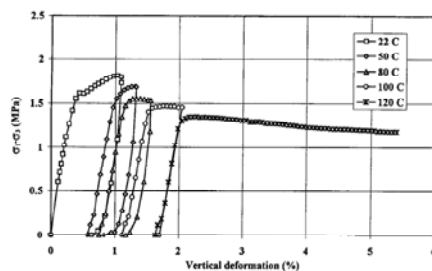
- All these results may still be explained with *constant shape and different size* of the SBS with T .

Hueckel et al. (1998)



Behaviour in shear under constant temperature

- Results on the dependency of *peak friction angle* on temperature contradictory.
- Some authors report *decrease of the peak strength* with temperature – consistent with the dependency of *apparent OCR* on temperature.



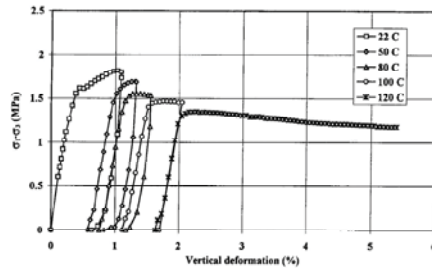
Hueckel et al. (1998)

- All these results may still be explained with *constant shape and different size* of the SBS with T .



Behaviour in shear under constant temperature

- Results on the dependency of *peak friction angle* on temperature contradictory.
- Some authors report *decrease of the peak strength* with temperature – consistent with the dependency of *apparent OCR* on temperature.

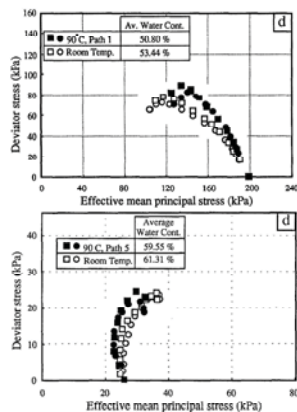


Hueckel et al. (1998)

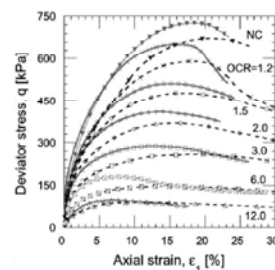
- All these results may still be explained with *constant shape and different size* of the SBS with T .

Behaviour in shear under constant temperature

- However, some authors report *increase of peak strength AND decrease of apparent preconsolidation pressure* with temperature.



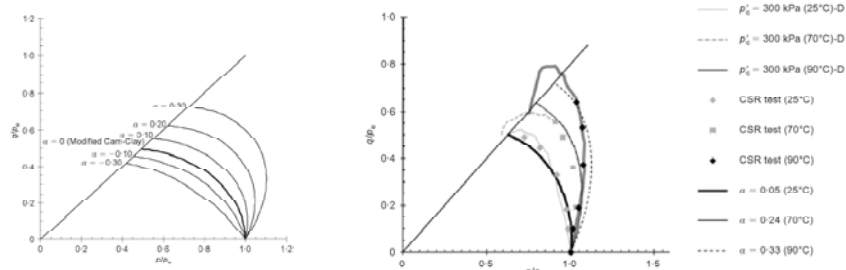
Kuntiwattanukul (1995)



Cekerevac and Laloui (2004)

Behaviour in shear under constant temperature

- Such a variability of *peak strength* with temperature may be explained by *variable shape of the SBS with T* only.



Abuel-Naga et al. (2009)

Behaviour due to temperature variation

- To explain the soil behaviour due to variation in temperature, different cases need to be considered:
 - Behaviour due to temperature *decrease*
 - Behaviour due to temperature *increase* at high OCR
 - Behaviour due to temperature *increase* at low OCR
- Behaviour due to temperature *decrease* is independent of OCR. At high OCR, behaviour due to temperature changes is essentially *reversible*.
- In these cases, *no rearrangement of the soil skeleton takes place*. Thermal behaviour of soil is then controlled *solely by thermal expansion/cooling contraction* of the solid grains.

Behaviour due to temperature variation

- To explain the soil behaviour due to variation in temperature, different cases need to be considered:
 - Behaviour due to temperature *decrease*
 - Behaviour due to temperature *increase* at high OCR
 - Behaviour due to temperature *increase* at low OCR
- Behaviour due to temperature *decrease* is independent of OCR. At high OCR, behaviour due to temperature changes is essentially *reversible*.
- In these cases, *no rearrangement of the soil skeleton takes place*. Thermal behaviour of soil is then controlled *solely by thermal expansion/cooling contraction* of the solid grains.

Behaviour due to temperature variation

- To explain the soil behaviour due to variation in temperature, different cases need to be considered:
 - Behaviour due to temperature *decrease*
 - Behaviour due to temperature *increase* at high OCR
 - Behaviour due to temperature *increase* at low OCR
- Behaviour due to temperature *decrease* is independent of OCR. At high OCR, behaviour due to temperature changes is essentially *reversible*.
- In these cases, *no rearrangement of the soil skeleton takes place*. Thermal behaviour of soil is then controlled *solely by thermal expansion/cooling contraction* of the solid grains.

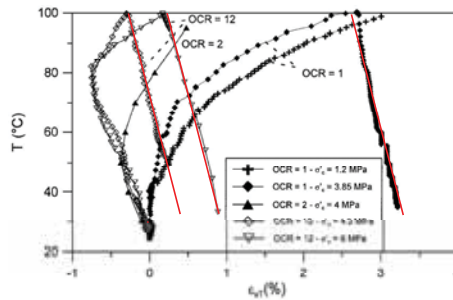
Behaviour due to temperature variation

Cooling and heating at high OCR

- Thermal expansion coefficient of the solid grains α_s , defined as

$$\dot{\epsilon}_V = \alpha_s \dot{T}$$

can be considered as *independent of confining stress and temperature*:



Sultan et al. (2002)

Behaviour due to temperature variation

Cooling and heating at high OCR

- An interesting consequence of the fact that during cooling and heating at high OCR *no rearrangement of the soil skeleton takes place* has been pointed out by Khalili et al. (2010):
 - α_s of the skeleton is the same as the one of the grains. It is thus also *independent of porosity*
 - Moreover, thermal expansion and cooling contraction *impose no change in void ratio*.
- Rate of void ratio thus cannot be calculated from $\dot{e} = (1 + e) \text{tr} \dot{\epsilon}$, as in soil under constant temperature, but from the *stretching corrected for thermal expansion*:

$$\dot{e} = (1 + e) \text{tr}(\dot{\epsilon} - \dot{\epsilon}^{TE}) \quad \text{where} \quad \dot{\epsilon} = \frac{1}{3} \alpha_s \dot{T}$$

Behaviour due to temperature variation

Cooling and heating at high OCR

- An interesting consequence of the fact that during cooling and heating at high OCR *no rearrangement of the soil skeleton takes place* has been pointed out by Khalili et al. (2010):
 - α_s of the skeleton is the same as the one of the grains. It is thus also *independent of porosity*
 - Moreover, thermal expansion and cooling contraction *impose no change in void ratio*.
- Rate of void ratio thus cannot be calculated from $\dot{e} = (1 + e) \text{tr} \dot{\epsilon}$, as in soil under constant temperature, but from the *stretching corrected for thermal expansion*:

$$\dot{e} = (1 + e) \text{tr}(\dot{\epsilon} - \dot{\epsilon}^{TE}) \quad \text{where} \quad \dot{\epsilon} = \frac{1}{3} \alpha_s \dot{T}$$

Behaviour due to temperature variation

Cooling and heating at high OCR

- An interesting consequence of the fact that during cooling and heating at high OCR *no rearrangement of the soil skeleton takes place* has been pointed out by Khalili et al. (2010):
 - α_s of the skeleton is the same as the one of the grains. It is thus also *independent of porosity*
 - Moreover, thermal expansion and cooling contraction *impose no change in void ratio*.
- Rate of void ratio thus cannot be calculated from $\dot{e} = (1 + e) \text{tr} \dot{\epsilon}$, as in soil under constant temperature, but from the *stretching corrected for thermal expansion*:

$$\dot{e} = (1 + e) \text{tr}(\dot{\epsilon} - \dot{\epsilon}^{TE}) \quad \text{where} \quad \dot{\epsilon} = \frac{1}{3} \alpha_s \dot{T}$$

Behaviour due to temperature variation

Cooling and heating at high OCR

- An interesting consequence of the fact that during cooling and heating at high OCR *no rearrangement of the soil skeleton takes place* has been pointed out by Khalili et al. (2010):
 - α_s of the skeleton is the same as the one of the grains. It is thus also *independent of porosity*
 - Moreover, thermal expansion and cooling contraction *impose no change in void ratio*.
- Rate of void ratio thus cannot be calculated from $\dot{e} = (1 + e) \text{tr} \dot{\epsilon}$, as in soil under constant temperature, but from the *stretching corrected for thermal expansion*:

$$\dot{e} = (1 + e) \text{tr}(\dot{\epsilon} - \dot{\epsilon}^{TE}) \quad \text{where} \quad \dot{\epsilon} = \frac{1}{3} \alpha_s \dot{T}$$

Behaviour due to temperature variation

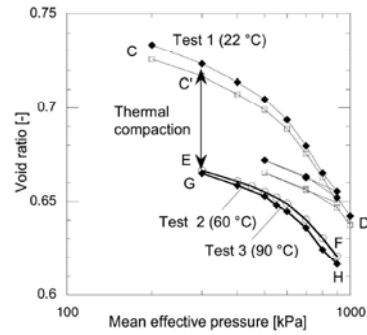
Heating at low OCR – thermal compaction

- Soil at low OCR has *open structure*. As pointed out when speaking about compression behaviour under constant temperature, *heated soil has at given p lower void ratio at NCL than cooler soil*.
- Soil state cannot be outside SBS \Rightarrow **thermal compaction**. Concept first introduced by Hueckel (1992).

Behaviour due to temperature variation

Heating at low OCR – thermal compaction

- Soil at low OCR has *open structure*. As pointed out when speaking about compression behaviour under constant temperature, *heated soil has at given p lower void ratio at NCL than cooler soil.*



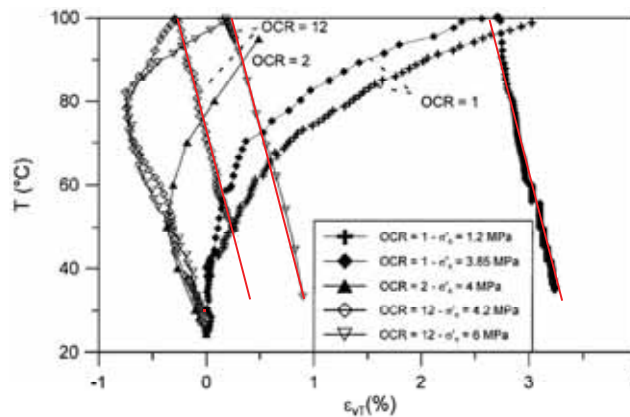
- Soil state cannot be outside SBS \Rightarrow **thermal compaction**. Concept first introduced by Hueckel (1992).

Laloui and Cekerevac (2003)

Behaviour due to temperature variation

Heating at low OCR – thermal compaction

- The amount of thermal compaction depends on OCR



Sultan et al. (2002)

Example predictions - thermal hypoplastic model

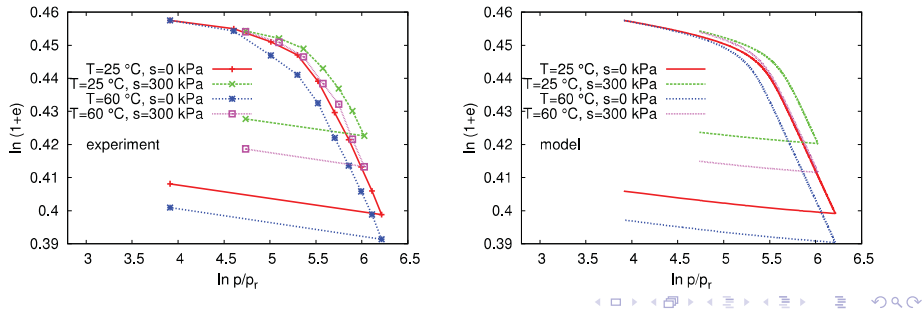
- The model has been combined with existing *hypoplastic model for unsaturated soils* by (Mašín and Khalili, 2010).
- Evaluated with respect to a comprehensive set of experimental data on unsaturated soils at *different temperatures and suctions* by Uchaipchat and Khalili (2009).
- Isotropic compression at different temperatures and suctions:

Example predictions - thermal hypoplastic model

- The model has been combined with existing *hypoplastic model for unsaturated soils* by (Mašín and Khalili, 2010).
- Evaluated with respect to a comprehensive set of experimental data on unsaturated soils at *different temperatures and suctions* by Uchaipchat and Khalili (2009).
- Isotropic compression at different temperatures and suctions:

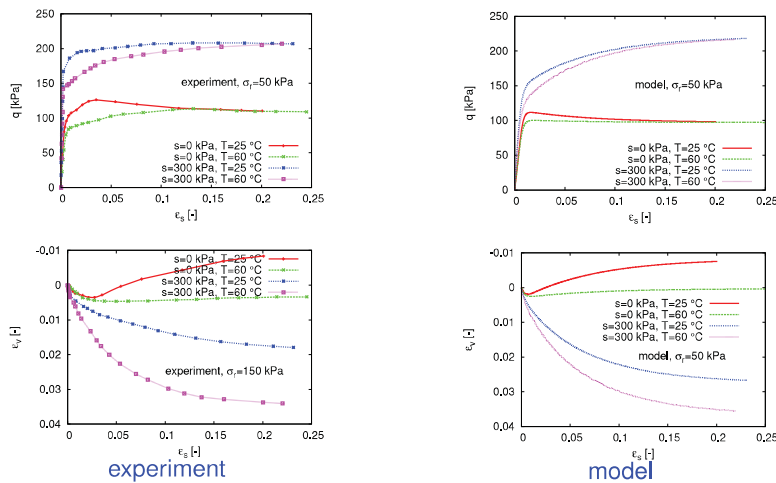
Example predictions - thermal hypoplastic model

- The model has been combined with existing *hypoplastic model for unsaturated soils* by (Mašín and Khalili, 2010).
- Evaluated with respect to a comprehensive set of experimental data on unsaturated soils at *different temperatures and suctions* by Uchaipchat and Khalili (2009).
- Isotropic compression at different temperatures and suctions:



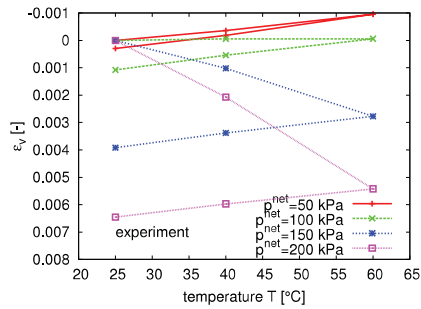
Example predictions - thermal hypoplastic model

- Drained triaxial tests at different suctions and temperatures

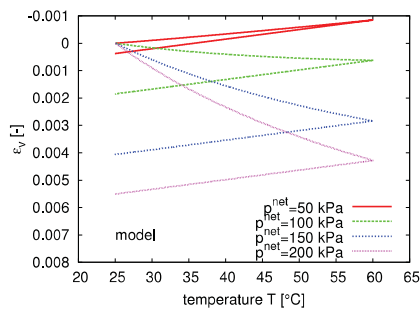


Example predictions - thermal hypoplastic model

- Volumetric response due to **heating-cooling cycles** at different stress levels (*different OCRs*)



experiment



model

Navigation icons: back, forward, search, etc.

Outline

- 1 Introduction
- 2 THM modelling of single structure soils
 - Modelling of the mechanical behaviour
 - Modelling of the water retention behaviour
 - Hydro-mechanical coupling
 - Thermal effects
- 3 **Double structure models**
 - Double structure mechanical models
 - Double structure hydraulic models
 - Double structure hydro-mechanical coupling
 - Thermal effects
- 4 Triple structure models, local non-equilibrium

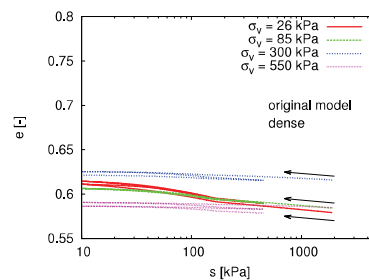
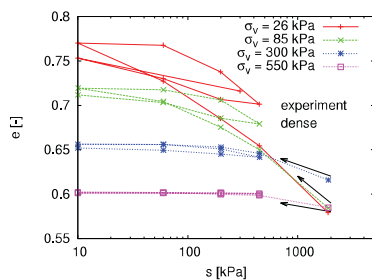
Navigation icons: back, forward, search, etc.

Limitation of single-structure models to predict expansive soils

- Single structure models work well for soils with low to medium plasticity. However, they *significantly underpredict swelling* of more expansive clays, such as bentonite.
- Oedometric wetting tests on Boom clay (data from Romero, 1999):

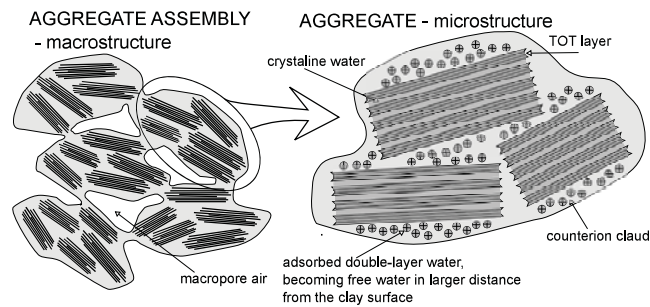
Limitation of single-structure models to predict expansive soils

- Single structure models work well for soils with low to medium plasticity. However, they *significantly underpredict swelling* of more expansive clays, such as bentonite.
- Oedometric wetting tests on Boom clay (data from Romero, 1999):



Double structure models

- Double structure models have been proposed first by Gens and Alonso (1992) and Alonso et al. (1999) (*mechanical model*) and Romero et al. (2011) (*water retention model*),
- These models explicitly consider *two structural levels* of bentonite:



Outline

- 1 Introduction
- 2 THM modelling of single structure soils
 - Modelling of the mechanical behaviour
 - Modelling of the water retention behaviour
 - Hydro-mechanical coupling
 - Thermal effects
- 3 **Double structure models**
 - **Double structure mechanical models**
 - Double structure hydraulic models
 - Double structure hydro-mechanical coupling
 - Thermal effects
- 4 Triple structure models, local non-equilibrium



Double structure mechanical models

Global strain rate is composed of the strain rates of *macrostructure* (typically predicted by the "single-structure" models) and *microstructure* (described by a separate, often elastic, model):

$$\dot{\epsilon} = \dot{\epsilon}^M + f_m \dot{\epsilon}^m$$

where $0 \leq f_m \leq 1$ specifies occlusion of macropores by aggregates.

- $\Rightarrow f_m = 0$... aggregates can freely swell into macrovoids without imposing global deformation - typical behaviour of *open structure*.
- $\Rightarrow f_m = 1$... aggregates cannot occupy the macrovoids, global strain is equal to aggregate strain - typical behaviour of *dense structure*.



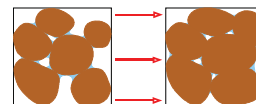
Double structure mechanical models

Global strain rate is composed of the strain rates of *macrostructure* (typically predicted by the "single-structure" models) and *microstructure* (described by a separate, often elastic, model):

$$\dot{\epsilon} = \dot{\epsilon}^M + f_m \dot{\epsilon}^m$$

where $0 \leq f_m \leq 1$ specifies occlusion of macropores by aggregates.

- $\Rightarrow f_m = 0$... aggregates can freely swell into macrovoids without imposing global deformation - typical behaviour of *open structure*.
- $\Rightarrow f_m = 1$... aggregates cannot occupy the macrovoids, global strain is equal to aggregate strain - typical behaviour of *dense structure*.



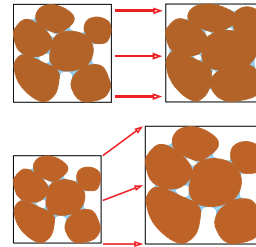
Double structure mechanical models

Global strain rate is composed of the strain rates of *macrostructure* (typically predicted by the "single-structure" models) and *microstructure* (described by a separate, often elastic, model):

$$\dot{\epsilon} = \dot{\epsilon}^M + f_m \dot{\epsilon}^m$$

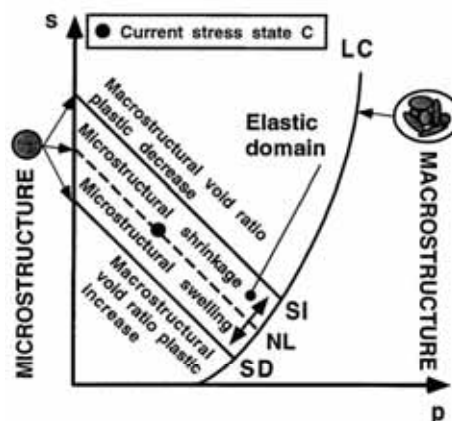
where $0 \leq f_m \leq 1$ specifies occlusion of macropores by aggregates.

- ⇒ $f_m = 0$... aggregates can freely swell into macrovoids without imposing global deformation - typical behaviour of *open structure*.
- ⇒ $f_m = 1$... aggregates cannot occupy the macrovoids, global strain is equal to aggregate strain - typical behaviour of *dense structure*.



Double structure mechanical models

- Double structure representation within *elasto-plasticity*: "barcelona expansive model" (BExM) by Alonso et al. (1999), based on Gens and Alonso (1992).

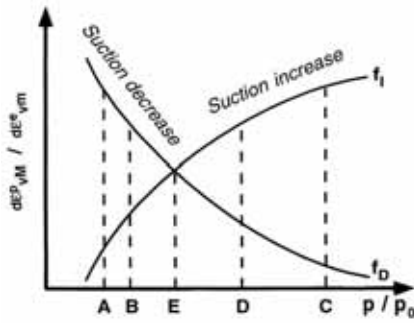


Alonso et al. (1999)



Double structure mechanical models

- When SD or SI yield surfaces are activated, *macrostructural plastic strains* are calculated from *microstructural strains* using *coupling functions* f_D and f_I .



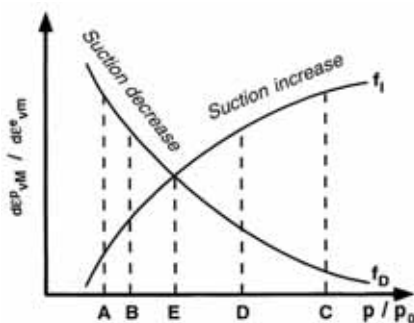
Alonso et al. (1999)

- Local hydraulic and mechanical equilibrium is assumed between the two levels of structure!

◀ ▶ ⏪ ⏩ ⏴ ⏵ ⏶ ⏷ ⏸ ⏹ ⏺ ⏻ ⏼ ⏽ ⏾ ⏿ 🔍 ↻

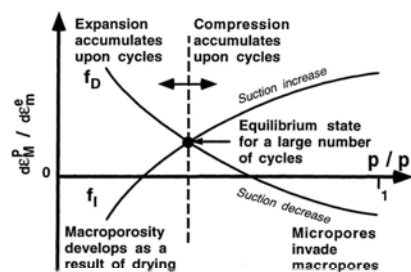
Double structure mechanical models

- When SD or SI yield surfaces are activated, *macrostructural plastic strains* are calculated from *microstructural strains* using *coupling functions* f_D and f_I .



Alonso et al. (1999)

- Local hydraulic and mechanical equilibrium is assumed between the two levels of structure!



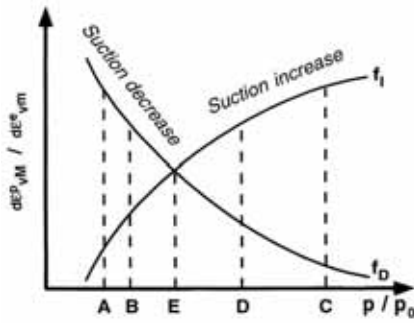
Alonso et al. (1999)

- Local hydraulic and mechanical equilibrium is assumed between the two levels of structure!

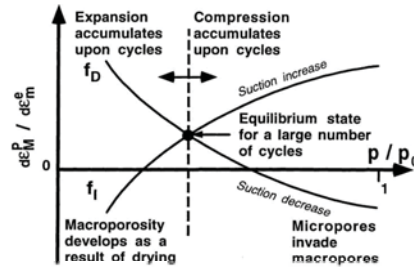
◀ ▶ ⏪ ⏩ ⏴ ⏵ ⏶ ⏷ ⏸ ⏹ ⏺ ⏻ ⏼ ⏽ ⏾ ⏿ 🔍 ↻

Double structure mechanical models

- When SD or SI yield surfaces are activated, *macrostructural plastic strains* are calculated from *microstructural strains* using *coupling functions* f_D and f_I .



Alonso et al. (1999)



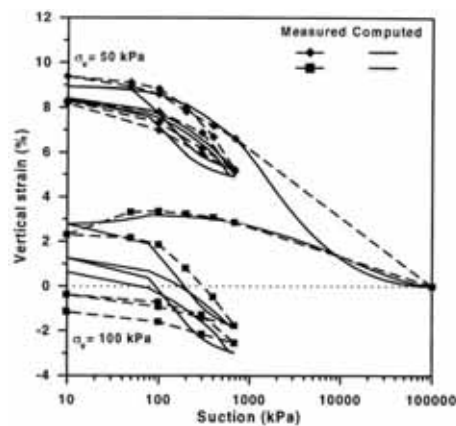
Alonso et al. (1999)

- Local hydraulic and mechanical equilibrium is assumed between the two levels of structure!

Navigation icons: back, forward, search, etc.

Double structure mechanical models

- BExM predicted response of boom clay subjected to suction cycles under oedometric conditions at two different vertical loads.



Alonso et al. (1999)

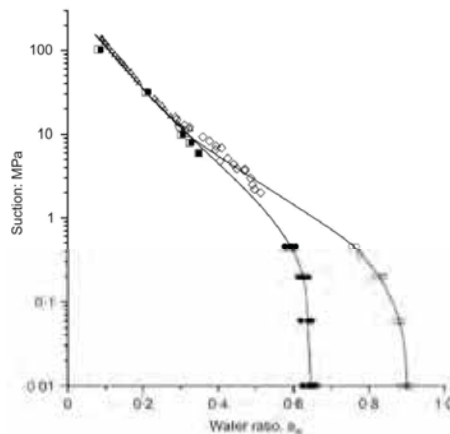
Navigation icons: back, forward, search, etc.

Outline

- 1 Introduction
- 2 THM modelling of single structure soils
 - Modelling of the mechanical behaviour
 - Modelling of the water retention behaviour
 - Hydro-mechanical coupling
 - Thermal effects
- 3 Double structure models
 - Double structure mechanical models
 - **Double structure hydraulic models**
 - Double structure hydro-mechanical coupling
 - Thermal effects
- 4 Triple structure models, local non-equilibrium

Double structure hydraulic models

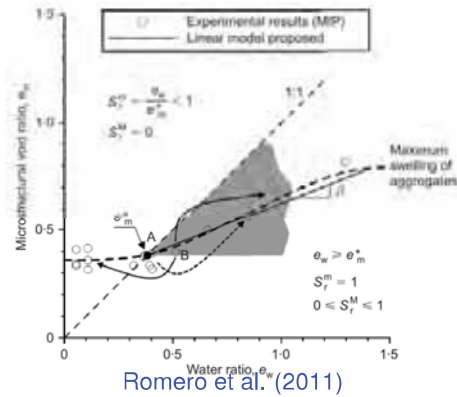
- Double structure affects also water retention behaviour, as proposed by Romero et al. (2011) - here, $e_w = S_r e = V_w / V_s$



Romero et al. (2011)

Double structure hydraulic models

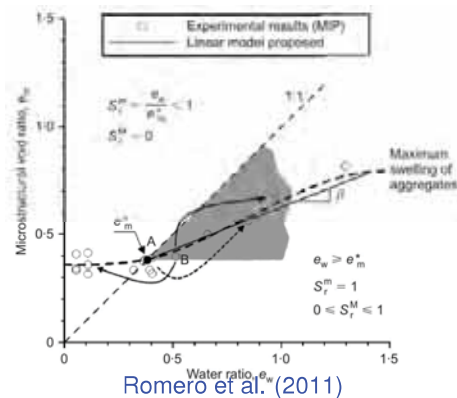
- For high water ratios, aggregates are fully saturated and e_w is composed of two contributions: S_r^M and aggregate swelling



- For low water ratios, macrostructure is dry ($S_r^M = 0$) and aggregates may not be fully saturated ($S_r^m < 1$)

Double structure hydraulic models

- For high water ratios, aggregates are fully saturated and e_w is composed of two contributions: S_r^M and aggregate swelling



- For low water ratios, macrostructure is dry ($S_r^M = 0$) and aggregates may not be fully saturated ($S_r^m < 1$)

Outline

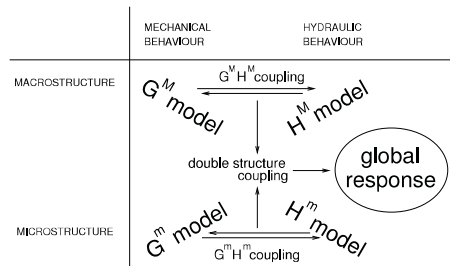
- 1 Introduction
- 2 THM modelling of single structure soils
 - Modelling of the mechanical behaviour
 - Modelling of the water retention behaviour
 - Hydro-mechanical coupling
 - Thermal effects
- 3 **Double structure models**
 - Double structure mechanical models
 - Double structure hydraulic models
 - **Double structure hydro-mechanical coupling**
 - Thermal effects
- 4 Triple structure models, local non-equilibrium

Double structure hydro-mechanical coupling

- In principle, *fully coupled hydro-mechanical (HM) unsaturated model* can be specified for *each of the two structural levels*.
- Double structure coupling functions linking the two *HM* models to obtain the response in terms of the global quantities:

Double structure hydro-mechanical coupling

- In principle, *fully coupled hydro-mechanical (HM) unsaturated model* can be specified for *each of the two structural levels*.
- Double structure coupling functions linking the two *HM* models to obtain the response in terms of the global quantities:



Double structure hydro-mechanical coupling

- *Mechanical models* defined using *effective stresses* σ^M and σ^m .

$$\dot{\sigma}^M = \mathbf{G}^M(\sigma^M, \mathbf{q}^M, \dot{\epsilon}^M) \quad \text{with} \quad \sigma^M = \sigma^{net} - \mathbf{1}s\chi^M$$

$$\dot{\sigma}^m = \mathbf{G}^m(\sigma^m, \mathbf{q}^m, \dot{\epsilon}^m) \quad \text{with} \quad \sigma^m = \sigma^{net} - \mathbf{1}s\chi^m$$

- *Hydraulic models* using micro- and macrostructural S_r .

$$\dot{S}_r^M = H^M(\dot{s}, s, \dot{\epsilon}^M)$$

$$\dot{S}_r^m = H^m(\dot{s}, s, \dot{\epsilon}^m)$$

Double structure hydro-mechanical coupling

- *Mechanical models* defined using *effective stresses* σ^M and σ^m .

$$\dot{\sigma}^M = \mathbf{G}^M(\sigma^M, \mathbf{q}^M, \dot{\epsilon}^M) \quad \text{with} \quad \sigma^M = \sigma^{net} - \mathbf{1}s\chi^M$$

$$\dot{\sigma}^m = \mathbf{G}^m(\sigma^m, \mathbf{q}^m, \dot{\epsilon}^m) \quad \text{with} \quad \sigma^m = \sigma^{net} - \mathbf{1}s\chi^m$$

- *Hydraulic models* using micro- and macrostructural S_r .

$$\dot{S}_r^M = H^M(\dot{s}, s, \dot{\epsilon}^M)$$

$$\dot{S}_r^m = H^m(\dot{s}, s, \dot{\epsilon}^m)$$

Double structure hydro-mechanical coupling

- *Mechanical models* defined using *effective stresses* σ^M and σ^m .

$$\dot{\sigma}^M = \mathbf{G}^M(\sigma^M, \mathbf{q}^M, \dot{\epsilon}^M) \quad \text{with} \quad \sigma^M = \sigma^{net} - \mathbf{1}s\chi^M$$

$$\dot{\sigma}^m = \mathbf{G}^m(\sigma^m, \mathbf{q}^m, \dot{\epsilon}^m) \quad \text{with} \quad \sigma^m = \sigma^{net} - \mathbf{1}s\chi^m$$

- *Hydraulic models* using micro- and macrostructural S_r .

$$\dot{S}_r^M = H^M(\dot{s}, s, \dot{\epsilon}^M)$$

$$\dot{S}_r^m = H^m(\dot{s}, s, \dot{\epsilon}^m)$$

- *Hydro-mechanical coupling*: Hydraulic strain measure S_r^M depends on mechanical quantity $\dot{\epsilon}^M$. Mechanical response influenced by χ^M , which may depend on a hydraulic quantity S_r^M .

Example coupled model - THM hypoplasticity

- Mechanical model for *macrostructure*: *Hypoplastic model for unsaturated soils* by Mašín and Khalili (2008).
 - Water retention model for *microstructure*: $S_r^m = 1$.
 - Effective stress for microstructure: $\chi^m = S_r^m = 1$ (Terzaghi stress).
 - Mechanical model for *microstructure*: elastic volumetric.
-
- Water retention model for macrostructure: void ratio-dependent Brooks and Corey - type hysteretic model

Example coupled model - THM hypoplasticity

- Mechanical model for *macrostructure*: *Hypoplastic model for unsaturated soils* by Mašín and Khalili (2008).
 - Water retention model for *microstructure*: $S_r^m = 1$.
 - Effective stress for microstructure: $\chi^m = S_r^m = 1$ (Terzaghi stress).
 - Mechanical model for *microstructure*: elastic volumetric.
-
- Water retention model for macrostructure: void ratio-dependent Brooks and Corey - type hysteretic model

Example coupled model - THM hypoplasticity

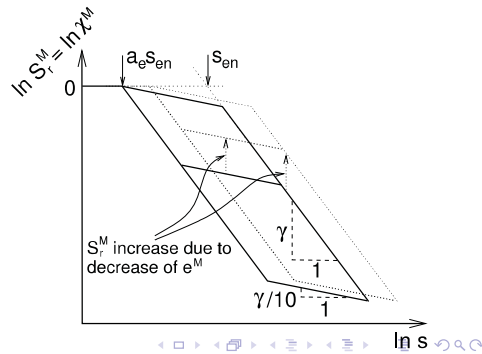
- Mechanical model for *macrostructure*: *Hypoplastic model for unsaturated soils* by Mašín and Khalili (2008).
 - Water retention model for *microstructure*: $S_r^m = 1$.
 - Effective stress for microstructure: $\chi^m = S_r^m = 1$ (Terzaghi stress).
 - Mechanical model for *microstructure*: elastic volumetric.
-
- Water retention model for macrostructure: void ratio-dependent Brooks and Corey - type hysteretic model

Example coupled model - THM hypoplasticity

- Mechanical model for *macrostructure*: *Hypoplastic model for unsaturated soils* by Mašín and Khalili (2008).
 - Water retention model for *microstructure*: $S_r^m = 1$.
 - Effective stress for microstructure: $\chi^m = S_r^m = 1$ (Terzaghi stress).
 - Mechanical model for *microstructure*: elastic volumetric.
-
- Water retention model for macrostructure: void ratio-dependent Brooks and Corey - type hysteretic model

Example coupled model - THM hypoplasticity

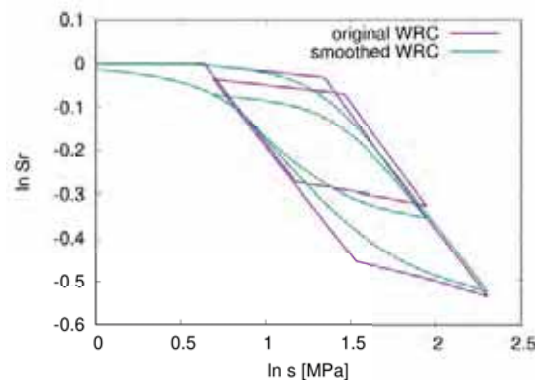
- Mechanical model for *macrostructure*: *Hypoplastic model for unsaturated soils* by Mašín and Khalili (2008).
- Water retention model for *microstructure*: $S_r^m = 1$.
- Effective stress for microstructure: $\chi^m = S_r^m = 1$ (Terzaghi stress).
- Mechanical model for *microstructure*: elastic volumetric.



- Water retention model for macrostructure: void ratio-dependent Brooks and Corey - type hysteretic model

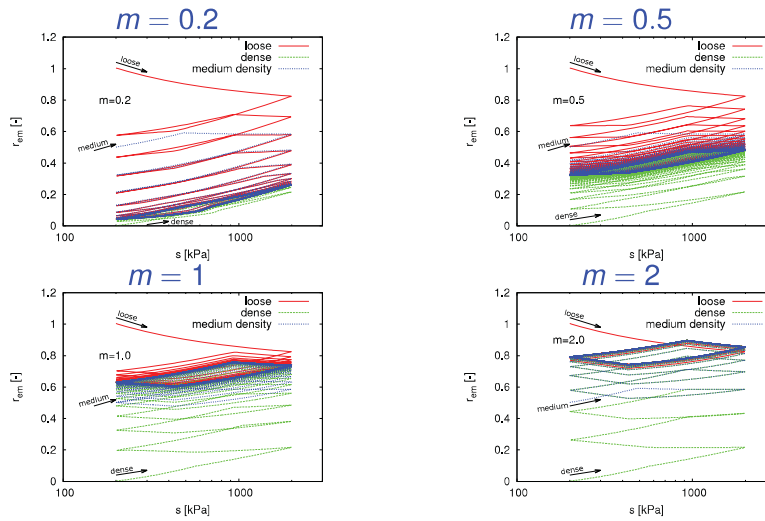
Example coupled model - THM hypoplasticity

- More recent model version of the model, rounded WRC formulation is used to better fit experimental data and *increase numerical robustness* (Mašín and Scaringi, BEACON, 2020)



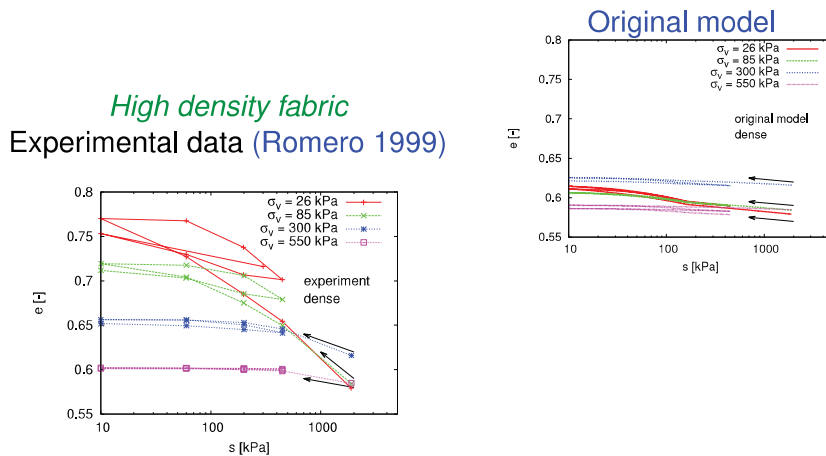
Example coupled model - THM hypoplasticity

Cyclic wetting-drying isotropic free-swelling test



Example coupled model - THM hypoplasticity

Oedometric free-swelling test

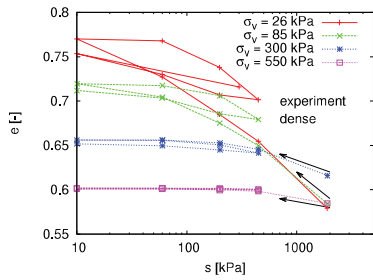


Example coupled model - THM hypoplasticity

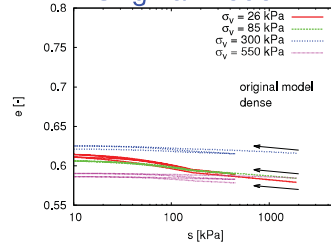
Oedometric free-swell test

High density fabric

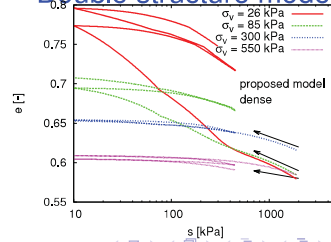
Experimental data (Romero 1999)



Original model



Double structure model

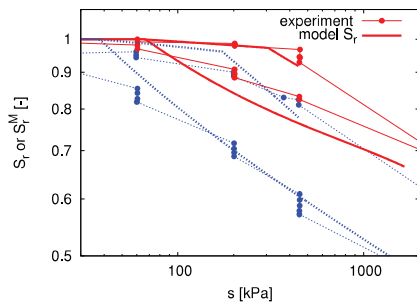


Example coupled model - THM hypoplasticity

Water retention behaviour (confined swelling test)

$$e = e^M + e^m + e^M e^m$$

$$S_r = S_r^M + \frac{e^m}{e} (S_r^m - S_r^M)$$



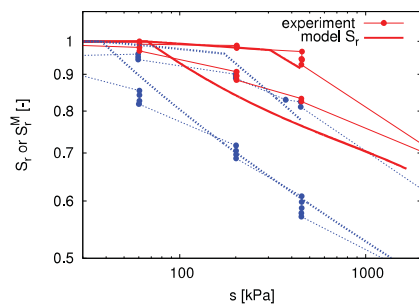
exp. data by Romero et al. (2011)

Example coupled model - THM hypoplasticity

Water retention behaviour (confined swelling test)

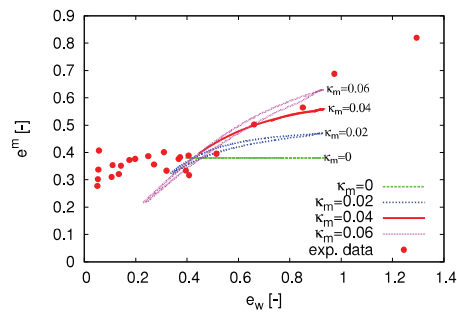
$$e = e^M + e^m + e^M e^m$$

$$S_r = S_r^M + \frac{e^m}{e} (S_r^m - S_r^M)$$



exp. data by Romero et al. (2011)

Interpretation in terms of water ratio e_w :



Navigation icons: back, forward, search, etc.

Outline

- 1 Introduction
- 2 THM modelling of single structure soils
 - Modelling of the mechanical behaviour
 - Modelling of the water retention behaviour
 - Hydro-mechanical coupling
 - Thermal effects
- 3 Double structure models
 - Double structure mechanical models
 - Double structure hydraulic models
 - Double structure hydro-mechanical coupling
 - **Thermal effects**
- 4 Triple structure models, local non-equilibrium

Navigation icons: back, forward, search, etc.

Double structure thermo-hydro-mechanical model

Effect of temperature on microstructure deformation

- Temperature affects microstructural strains through influencing both *basal spacing* and *diffuse double-layer thickness*.
- Morodome and Kawamura (2009) observed that in Na-montmorillonites, for the given hydration state, *basal spacing is not affected by temperature significantly*. However, with increasing temperature the clay stacks tend to stay longer in the lower hydration state during wetting, which means that *increasing temperature decreases stack volume*. Contrarily, a more gradual decrease in basal spacing with temperature was observed in Ca-montmorillonites.

Double structure thermo-hydro-mechanical model

Effect of temperature on microstructure deformation

- Temperature affects microstructural strains through influencing both *basal spacing* and *diffuse double-layer thickness*.
- Morodome and Kawamura (2009) observed that in Na-montmorillonites, for the given hydration state, *basal spacing is not affected by temperature significantly*. However, with increasing temperature the clay stacks tend to stay longer in the lower hydration state during wetting, which means that *increasing temperature decreases stack volume*. Contrarily, a more gradual decrease in basal spacing with temperature was observed in Ca-montmorillonites.

Double structure thermo-hydro-mechanical model

Effect of temperature on microstructure deformation

- A different effect of temperature from that on basal spacing is observed on the diffuse double-layer thickness. The diffuse double-layer theory predicts *an increase in double-layer thickness with temperature*. At the same time, however, *increasing temperature causes a decrease in dielectric constant*, which in turn implies a decrease in double-layer thickness with temperature.
- At the end, temperature can cause *both microstructural swelling and shrinkage*, depending on bentonite mineralogical composition.

Double structure thermo-hydro-mechanical model

Effect of temperature on microstructure deformation

- A different effect of temperature from that on basal spacing is observed on the diffuse double-layer thickness. The diffuse double-layer theory predicts *an increase in double-layer thickness with temperature*. At the same time, however, *increasing temperature causes a decrease in dielectric constant*, which in turn implies a decrease in double-layer thickness with temperature.
- At the end, temperature can cause *both microstructural swelling and shrinkage*, depending on bentonite mineralogical composition.

Double structure thermo-hydro-mechanical model

Effect of temperature on microstructure deformation

- In some clays, *contraction and decreasing swelling pressures were reported with temperature* (FEBEX, Romero et al. 2005; Villar and Lloret 2004). In other clays, *expansion and increasing swelling pressures were reported with temperature* (MX80, Tang et al. 2008). These contradictory effects can in some cases *cancel out*, leading to swelling pressures more or less independent of temperature (Zhang et al., 1993).
- Constitutive model should allow for both microstructural swelling and shrinkage:

$$\dot{\epsilon}^m = \frac{1}{3} \left(\alpha_s \dot{T} - \frac{\kappa_m}{p^m} \dot{p}^m \right)$$

Double structure thermo-hydro-mechanical model

Effect of temperature on microstructure deformation

- In some clays, *contraction and decreasing swelling pressures were reported with temperature* (FEBEX, Romero et al. 2005; Villar and Lloret 2004). In other clays, *expansion and increasing swelling pressures were reported with temperature* (MX80, Tang et al. 2008). These contradictory effects can in some cases *cancel out*, leading to swelling pressures more or less independent of temperature (Zhang et al., 1993).
- Constitutive model should allow for both microstructural swelling and shrinkage:

$$\dot{\epsilon}^m = \frac{1}{3} \left(\alpha_s \dot{T} - \frac{\kappa_m}{p^m} \dot{p}^m \right)$$

Double structure thermo-hydro-mechanical model

Effect of temperature on retention properties

- Temperature affects *retention properties*. This is predominantly caused by the effect of temperature on *surface tension*, but experimental studies indicate more significant decrease of retention capacity (Romero et al. 2001; Villar and Lloret 2004; Jacinto et al. 2009). This effect can be included by modifying the *air-entry value of suction*

$$s_{en} = s_{e0} \left(\frac{a + bT}{a + bT_r} \right)$$

Double structure thermo-hydro-mechanical model

Effect of temperature on retention properties

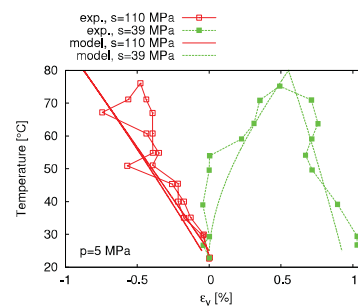
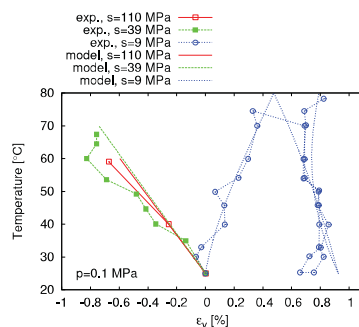
- However, temperature also causes *microstructural swelling or shrinkage*, as described above. As S_r^m is high (often considered as 1 in the models), this causes *increase or decrease* of global retention capacity
- Global retention capacity is caused by *interplay* between the two effects above, but most experimental studies (Villar and Lloret 2004; Yong et al. 1963; Jacinto et al. 2009) indicate a *slight decrease in global water retention capacity with temperature*.

Double structure thermo-hydro-mechanical model

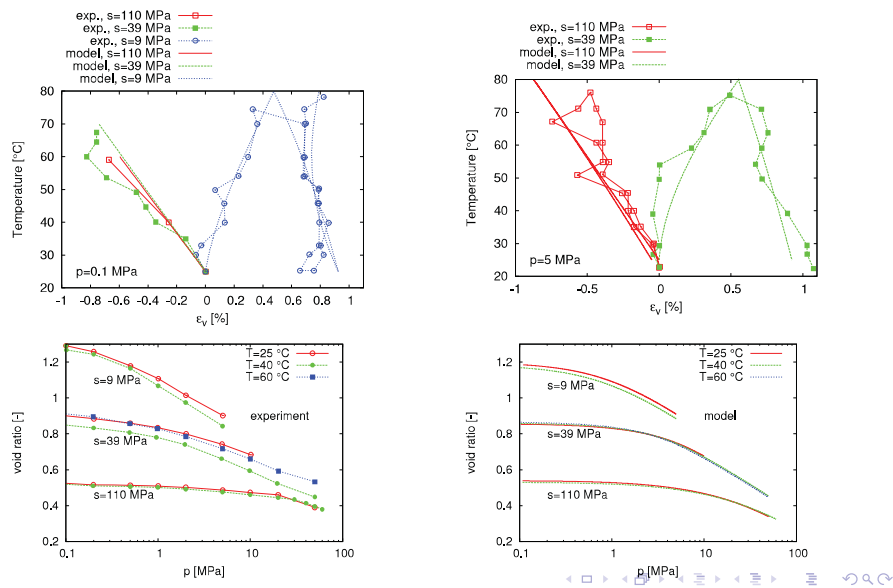
Effect of temperature on retention properties

- However, temperature also causes *microstructural swelling or shrinkage*, as described above. As S_r^m is high (often considered as 1 in the models), this causes *increase or decrease* of global retention capacity
- Global retention capacity is caused by *interplay* between the two effects above, but most experimental studies (Villar and Lloret 2004; Yong et al. 1963; Jacinto et al. 2009) indicate a *slight decrease in global water retention capacity with temperature*.

Double structure thermo-hydro-mechanical model



Double structure thermo-hydro-mechanical model



Outline

- 1 Introduction
- 2 THM modelling of single structure soils
 - Modelling of the mechanical behaviour
 - Modelling of the water retention behaviour
 - Hydro-mechanical coupling
 - Thermal effects
- 3 Double structure models
 - Double structure mechanical models
 - Double structure hydraulic models
 - Double structure hydro-mechanical coupling
 - Thermal effects
- 4 Triple structure models, local non-equilibrium

Triple structure models, local non-equilibrium

- The above models work reasonably well for compacted bentonite blocks. However, their predictive capability is lower when bentonite is used in the form of *pellets*.
 - Pellets - highly compacted bentonite granules of mm to cm in size.
 - Water flow is (initially) governed by *macro-void-driven permeability*, while *swelling pressure evolution is much slower*, as it is controlled by pellet saturation.
 - The assumption of *local equilibrium* (the same water pressures in microstructure and macrostructure) is no-more relevant.

Triple structure models, local non-equilibrium

- The above models work reasonably well for compacted bentonite blocks. However, their predictive capability is lower when bentonite is used in the form of *pellets*.



Talandier et al. (2018)

- Pellets - highly compacted bentonite granules of mm to cm in size.
- Water flow is (initially) governed by *macro-void-driven permeability*, while *swelling pressure evolution is much slower*, as it is controlled by pellet saturation.
- The assumption of *local equilibrium* (the same water pressures in microstructure and macrostructure) is no-more relevant.

Triple structure models, local non-equilibrium

- The above models work reasonably well for compacted bentonite blocks. However, their predictive capability is lower when bentonite is used in the form of *pellets*.



Talandier et al. (2018)

- Pellets - highly compacted bentonite granules of mm to cm in size.
- Water flow is (initially) governed by *macro-void-driven permeability*, while *swelling pressure evolution is much slower*, as it is controlled by pellet saturation.
- The assumption of *local equilibrium* (the same water pressures in microstructure and macrostructure) is no-more relevant.



Triple structure models, local non-equilibrium

- The above models work reasonably well for compacted bentonite blocks. However, their predictive capability is lower when bentonite is used in the form of *pellets*.



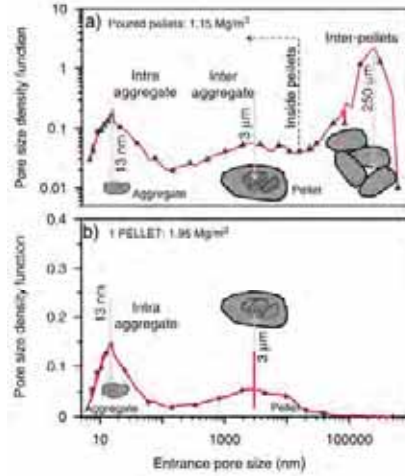
Talandier et al. (2018)

- Pellets - highly compacted bentonite granules of mm to cm in size.
- Water flow is (initially) governed by *macro-void-driven permeability*, while *swelling pressure evolution is much slower*, as it is controlled by pellet saturation.
- The assumption of *local equilibrium* (the same water pressures in microstructure and macrostructure) is no-more relevant.



Triple structure models, local non-equilibrium

- "*Tripple structure*" of pellet material.

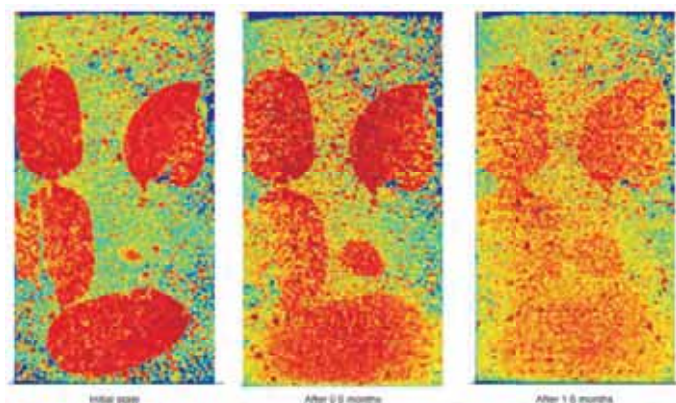


Hoffmann et al. (2007)



Triple structure models, local non-equilibrium

- Distribution of dry densities of pellet bentonite during hydration as measured by CT-scanning

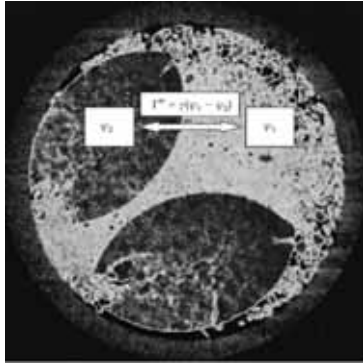


Van Geet et al. (2005) in Gens et al. (2011)



Triple structure models, local non-equilibrium

- In pellet material, it is no-more sufficient to assume the same suctions in microstructure and macrostructure



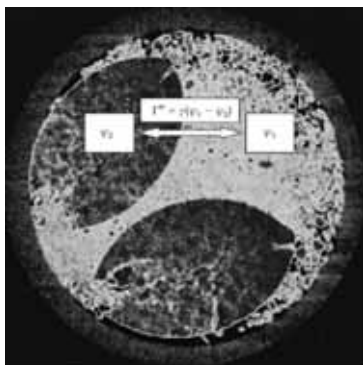
Gens et al. (2011)

- Water exchange term needs to be added to describe balance of water between pellet and inter-pellet pores. *Gens et al. (2011)* proposed to use double structure approach, where "*macrostructure*" is now formed by pellets, not by bentonite aggregates:

$$\Gamma^w = \gamma(\psi_M - \psi_m)$$

Triple structure models, local non-equilibrium

- In pellet material, it is no-more sufficient to assume the same suctions in microstructure and macrostructure



Gens et al. (2011)

- Water exchange term needs to be added to describe balance of water between pellet and inter-pellet pores. *Gens et al. (2011)* proposed to use double structure approach, where "*macrostructure*" is now formed by pellets, not by bentonite aggregates:

$$\Gamma^w = \gamma(\psi_M - \psi_m)$$

Triple structure models, local non-equilibrium

- The water mass balance equation for these two overlapping flow media reads:

$$\frac{\partial}{\partial t} (\rho_w S_{wj} \phi_j) + \nabla \cdot (\mathbf{j}_{wj}) \pm \Gamma^w = f_j^w; j = M, m$$

This is combined with hydraulic constitutive equations (Darcy's laws) at both structural levels, allowing to separately model permeability of pellet and macrostructure. \mathbf{j}_{wj} total mass fluxes of water in liquid phase, f_j^w external source.

- Mechanical equilibrium is still assumed, that is, total stresses act the same in microstructure and macrostructure

$$\nabla \cdot \boldsymbol{\sigma} + \mathbf{b} = \mathbf{0}$$

- Modelling can go further, Navarro et al. (2020) proposed triple-structure model considering all three structural levels.



Triple structure models, local non-equilibrium

- The water mass balance equation for these two overlapping flow media reads:

$$\frac{\partial}{\partial t} (\rho_w S_{wj} \phi_j) + \nabla \cdot (\mathbf{j}_{wj}) \pm \Gamma^w = f_j^w; j = M, m$$

This is combined with hydraulic constitutive equations (Darcy's laws) at both structural levels, allowing to separately model permeability of pellet and macrostructure. \mathbf{j}_{wj} total mass fluxes of water in liquid phase, f_j^w external source.

- Mechanical equilibrium is still assumed, that is, total stresses act the same in microstructure and macrostructure

$$\nabla \cdot \boldsymbol{\sigma} + \mathbf{b} = \mathbf{0}$$

- Modelling can go further, Navarro et al. (2020) proposed triple-structure model considering all three structural levels.



Triple structure models, local non-equilibrium

- The water mass balance equation for these two overlapping flow media reads:

$$\frac{\partial}{\partial t} (\rho_w S_{wj} \phi_j) + \nabla \cdot (\mathbf{j}_{wj}) \pm \Gamma^w = f_j^w; j = M, m$$

This is combined with hydraulic constitutive equations (Darcy's laws) at both structural levels, allowing to separately model permeability of pellet and macrostructure. \mathbf{j}_{wj} total mass fluxes of water in liquid phase, f_j^w external source.

- Mechanical equilibrium is still assumed, that is, total stresses act the same in microstructure and macrostructure

$$\nabla \cdot \boldsymbol{\sigma} + \mathbf{b} = \mathbf{0}$$

- Modelling can go further, Navarro et al. (2020) proposed triple-structure model considering all three structural levels.

Thank you for your attention

Appendix H. FE numerical modelling of THM couplings in geomaterials (F. Collin)



MULTIPHYSICAL COUPLINGS IN GEOMECHANICS, A FOCUS ON THERMAL EFFECT AND GAS TRANSFER IMPACT ON THE BEHAVIOUR OF GEOMATERIALS

FE numerical modelling of THM couplings in geomaterials

23/01/2020 • COLLIN Frédéric – CORMAN Gilles



The project leading to this application has received funding from the European Union's Horizon 2020 research and innovation programme under grant agreement n° 847593.

23/01/2020

EURAD School for Radioactive Waste Management / GAS & HITEC



MULTIPHYSICAL COUPLINGS IN GEOMATERIALS

Long-term management of radioactive wastes



Intermediate (long-lived) & high activity wastes



Deep geological disposal
Repository in deep geological media with good confining properties
(Low permeability $K < 10^{-12}$ m/s)

Underground structures
= network of galleries



Disposal facility of Cigéo project in France (Labalette et al., 2013)

23/01/2020

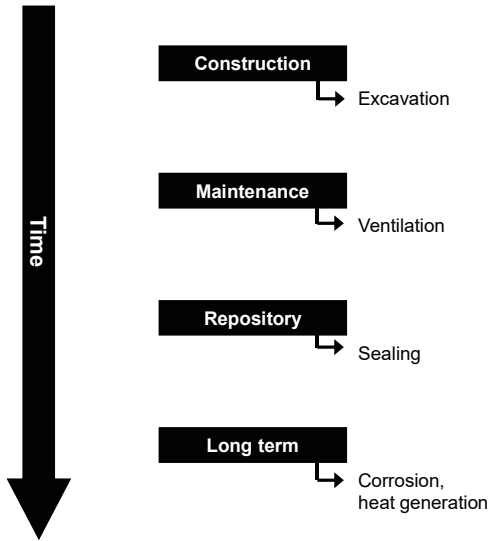
EURAD School for Radioactive Waste Management / GAS & HITEC





MULTIPHYSICAL COUPLINGS IN GEOMATERIALS

Repository phases

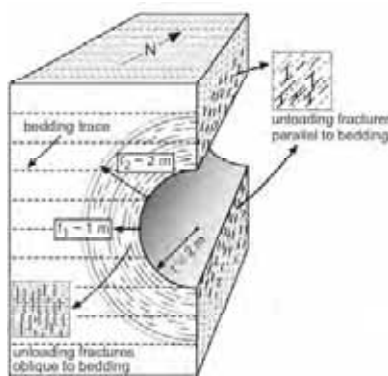
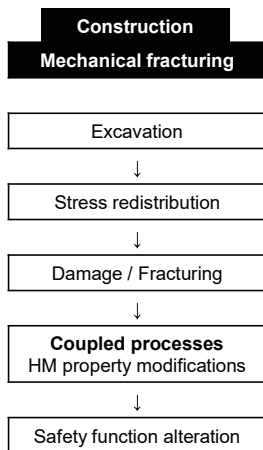


Type C wastes (Andra, 2005)



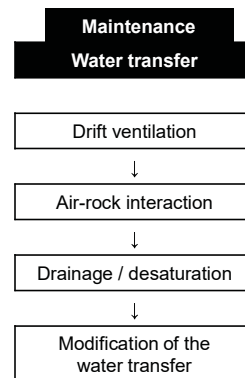
MULTIPHYSICAL COUPLINGS IN GEOMATERIALS

Excavation Damaged Zone (EDZ)

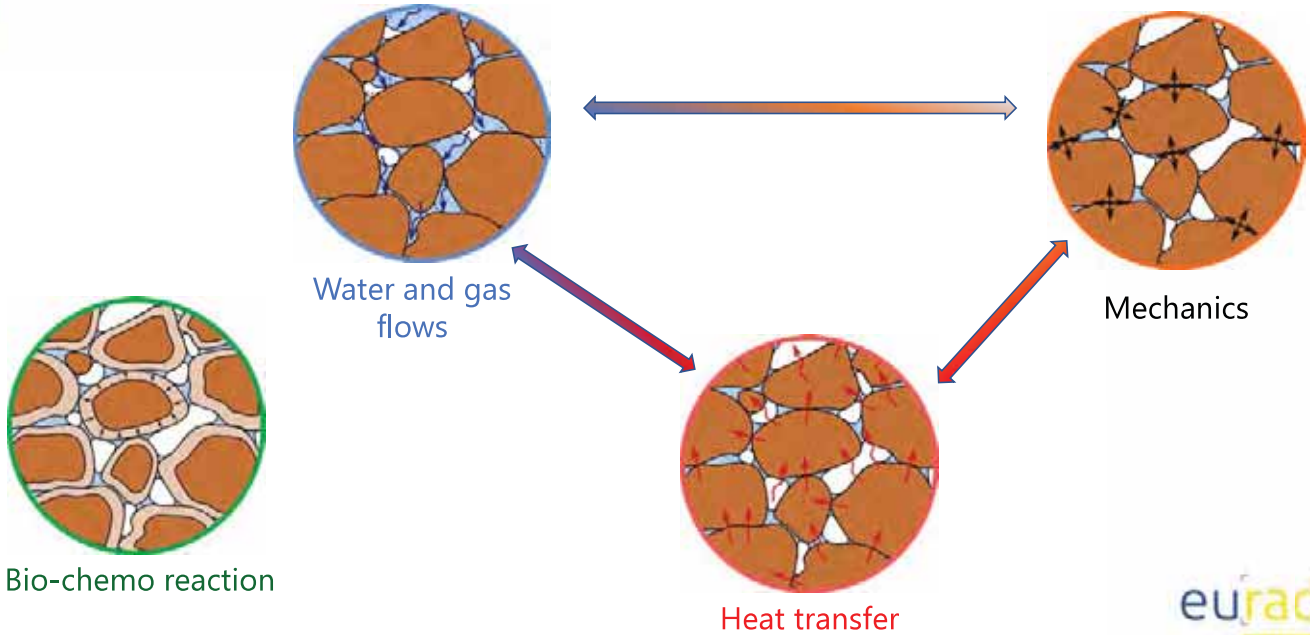


Fracturing & permeability increase (several orders of magnitude)

Opalinus clay in Switzerland (Bossart et al., 2002)



MULTIPHYSICAL COUPLINGS IN GEOMATERIALS



23/01/2020

EURAD School for Radioactive Waste Management / GAS & HITEC

eurad

5

CONTENT

- Introduction
- Formulation of the flow problem
- Hydro-mechanical problem
- Hydro-mechanical problem in unsaturated conditions
- Thermo-hydro-mechanical problem

23/01/2020

EURAD School for Radioactive Waste Management / GAS & HITEC

eurad

6



MULTIPHYSICAL COUPLINGS IN GEOMATERIALS

In multi-physics problems, several physical processes occur simultaneously and interact each other. In the sequel, we will limit the presentation to (quasi-) static problems.

As for any engineering problem, we will use the following balance equations:

- **Momentum balance equation:** it corresponds to the equilibrium equations (translation and rotation) of the considered body.
- **Mass balance equation:** the mass of the system remains constant (open or closed system)
- **Energy balance equation:** we will express that the enthalpy of the system remains constant (open or closed system)
- **Second thermodynamics law**

Depending on the studied problem, we will use some of these latter balance equations. The remaining equations will be assumed more or less consciously.

In addition to these equations, we will need some state relationships (constitutive laws, thermodynamics relations ...) that will be defined in order to close the system.



MULTIPHYSICAL COUPLINGS IN GEOMATERIALS

Non linearities in our problem come mainly from the **constitutive behaviour** of the geomaterials, the **time-dependent** physical processes (flows, heat transfer, chemical reaction) and the **interactions** between all the phenomena.

Focus on the coupling terms at the level of the finite element (monolithical approach)

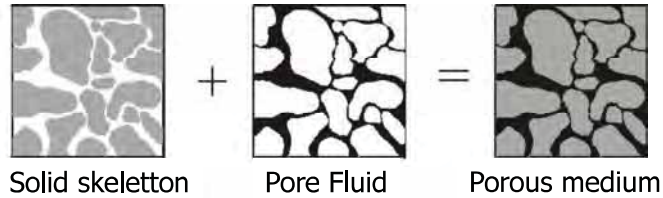
Depending on the problem, a coupling effect might be more or less important and the numerical modelling is thus different.

The following developments correspond to the Finite Element Code Lagamine, but other codes are available for THM problem like Code Bright, ASTER ...



FORMULATION OF THE FLOW PROBLEM

Saturated porous medium



The porous medium is considered as the **superimposition of two continua**, made of two chemical species (solid grain and water) and two phases (solid and fluid).

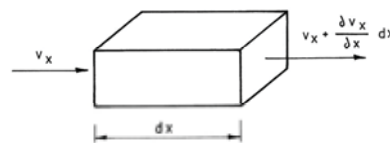
For the flow problem, the mass balance equation is written for **the pore fluid**.



FORMULATION OF THE FLOW PROBLEM

In an open system: the fluid mass balance equation expresses that the mass remains constant.

$$\frac{\partial M_f}{\partial t} = 0$$



After the Reynolds theorem, the total derivative of M_f with respect to time writes for an Eulerian referential:

$$\int \frac{\partial(\rho_f \cdot \varphi)}{\partial t} + \frac{\partial \rho_f \cdot v_i}{\partial x_i} d\Omega = 0$$

v_i being **the apparent flow rate of the fluid with respect to the fixed referential**, ρ_f is the fluid density and φ is the porosity.

$$\frac{\partial S}{\partial t} + \frac{\partial \rho_f \cdot v_i}{\partial x_i} = Q$$

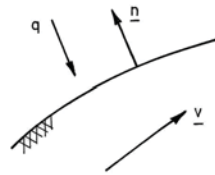


FORMULATION OF THE FLOW PROBLEM

The expression of the boundary condition is:

$$n_i \cdot \rho_f \cdot v_i + q = 0$$

The convention sign assumes in the following that the quantities Q and q are positive for incoming fluid flows in the system.



FORMULATION OF THE FLOW PROBLEM

The previous equation is the **strong form** of the fluid mass balance equation. Assuming this equation is met at every point of a medium, it is possible to find an analytical solution for any flow problem.

$$\frac{\partial(\rho_f \cdot \varphi)}{\partial t} + \frac{\partial \rho_f \cdot v_i}{\partial x_i} = Q$$

Using numerical models, there exists several approaches in the literature. In the sequel, we will use the **Virtual Power principle** to solve numerically the flow problem:

Be δp a small virtual perturbation of the pressure field. Under the virtual pressure field, the external loading (volume flux Q and boundary flows q) will develop an external virtual power :

$$\delta W_E = \int_{\Omega} Q \delta p d\Omega + \int_{\Gamma} q \delta p d\Gamma$$

FORMULATION OF THE FLOW PROBLEM

Using the boundary condition equation and the mass balance equation, it is possible to express the external virtual power as a function of internal quantities:

$$\int_{\Omega} \left(\frac{\partial S}{\partial t} \delta p + \operatorname{div} \rho_f \underline{v} \delta p - \operatorname{div} (\rho_f \underline{v} \delta p) \right) d\Omega = W_e$$

Using Leibniz formula, the previous equation can be rewritten as:

$$\int_{\Omega} \left(\frac{\partial S}{\partial t} \delta p - \rho_f \underline{v} \cdot \underline{\operatorname{grad}} \delta p \right) d\Omega = W_e$$

This latter equation corresponds to the internal virtual power.

The equality of the internal and external virtual powers for any virtual pressure field leads to compliance with the local mass balance equations at all points in the domain, therefore the overall balance. The equality checked for a limited number of disturbances leads to the respect on average of the global and local balance.

CONSTITUTIVE EQUATIONS

1. Darcy's law

- Fluid Linear momentum balance equation (strong form)

$$\frac{\partial p}{\partial X_i} + F_i^{S/W} + \rho_w g_i = 0$$

$$\text{Viscous drag force : } F_i^{S/W} = \frac{\rho_w \cdot \phi \cdot g}{K} v_i^{W/S}$$

$$v_i = -\frac{K}{\rho_w \cdot g} \left(\frac{\partial p}{\partial X_i} + \rho_w \cdot g_i \right) = -\frac{k}{\mu} \left(\frac{\partial p}{\partial X_i} + \rho_w \cdot g_i \right)$$

Where K is the hydraulic conductivity (m/s) and k the intrinsic permeability (m²)



CONSTITUTIVE EQUATION

2. Storage term

In transient state, the quantity of water is evolving, depending on:

- variation of the porosity (not accessible in flow problem)
- compressibility of water

This term is usually express as a function of a storage coefficient:

$$\dot{S} = c_p \cdot \dot{p}$$



FORMULATION OF THE FLOW PROBLEM

Formulation of the finite element

The equation to be solved is provided to us by the virtual power principle, which allows local balance to be respected on average. The latter is expressed as follows:

$$\int_{\Omega} Q \delta p d\Omega + \int_{\Gamma} q \delta p d\Gamma = \int_{\Omega} \left(\frac{\partial S}{\partial t} \delta p - \rho_f \underline{\nu} \cdot \underline{\text{grad}} \delta p \right) d\Omega$$

In order to solve this problem, we propose to use the finite element technique. The discretized variable is the pressure field. We use here iso-parametric elements; the geometry and the pressure field are discretized using the same interpolation functions:

$$\underline{x} = \sum_{L=1}^{N_{\text{nodes}}} N_L \underline{x}_L \qquad p = \sum_{L=1}^{N_{\text{nodes}}} N_L p_L$$

where N_L are the interpolation functions and p_L are the nodal unknowns.

FORMULATION OF THE FLOW PROBLEM

Using the same discretization for the virtual pressure field, the power of the internal forces is rewritten as follows:

$$\begin{aligned}\delta W_f^{\text{élément}} &= \int_{\Omega} \left(\frac{\partial S}{\partial t} N_L \delta p_L - \rho_f \underline{v} \cdot \underline{\text{grad}} N_L \delta p_L \right) d\Omega \\ \delta W_f^{\text{élément}} &= \int_{\Omega} \left(\frac{\partial S}{\partial t} N_L - \rho_f \underline{v} \cdot \underline{\text{grad}} N_L \right) d\Omega \delta p_L = F_L \delta p_L \\ F_L &= \int_{\Omega} \left(\frac{\partial S}{\partial t} N_L - \rho_f \underline{v} \cdot \underline{\text{grad}} N_L \right) d\Omega\end{aligned}$$

In reality these quantities can be evaluated element by element. We can therefore express the preceding quantities as a sum over all the finite elements

$$F_L = \sum_{\text{élément}} \int_{\Omega_{\text{élément}}} \left(\frac{\partial S}{\partial t} N_L - \rho_f \underline{v} \cdot \underline{\text{grad}} N_L \right) d\Omega_{\text{élément}}$$

External forces related to boundary conditions must be computed.

FORMULATION OF THE FLOW PROBLEM

The problem to be solved therefore consists in verifying the equality of internal and external forces:

$$\sum_{n \text{ éléments}} F_L^{\text{extérieur}} = \sum_{n \text{ éléments}} F_L^{\text{intérieur}} \text{ pour tout } L.$$

In this case, the global balance is assured and thanks to the principle of virtual powers, the local balance is also met on average.



FORMULATION OF THE FLOW PROBLEM

Time discretization

A time step is defined by time t^A (beginning of the step) and time t^B (end of the step).

Pressure will be assumed to vary **linearly** on the time step.

Using an isoparametric formalism, it comes that :

$$\begin{aligned}t &= N^A t^A + N^B t^B \\ p &= N^A p^A + N^B p^B \\ N^A &= 1 - \xi \\ N^B &= \xi \\ \xi &\in [0, 1]\end{aligned}$$



FORMULATION OF THE FLOW PROBLEM

Equilibrium equation

It is obvious that we can not ensure the equilibrium at any time. It must therefore be respected on average over the time step. To do this, we can use the method of weighted residuals, with a weighting function W varying over time. The temporally and spatially discretized balance equation is then written:

$$\int_{t^A}^{t^B} W(t) F_L^{\text{extérieur}} dt = \int_{t^A}^{t^B} W(t) F_L^{\text{intérieur}} dt$$

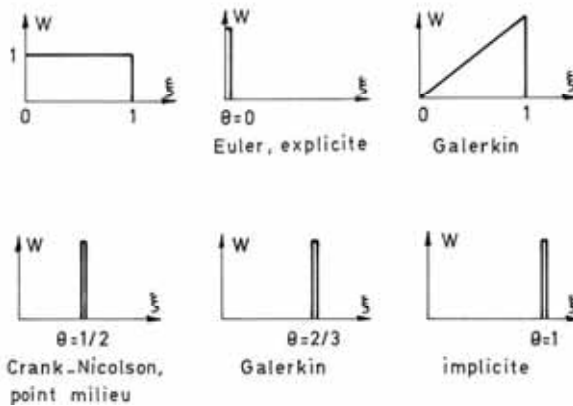


FORMULATION OF THE FLOW PROBLEM

Equilibrium equation

Usually, the weighting function is reduced to a collocation. We express balance in a single instant:

$$\sum F_L^{\text{extérieur}}(\theta) = \sum F_L^{\text{intérieur}}(\theta)$$



23/01/2020



FORMULATION OF THE FLOW PROBLEM: ITERATION PROCEDURE

If the balance is not met, a new better solution must be sought. The objective is to reduce the out-of-balance forces out of equilibrium by modifying the pressure field. If the problem is nonlinear, there exists a nonlinear relation between the nodal flows and pressures. It is impossible to solve this problem without linearizing it. To do this, we carry out a Taylor series development, limited to the first order, of out-of-balance nodal flows, around the last known approximation of the pressures (the one which is not in equilibrium):

$$F_L^{HE} = F_L^{HE}(p^0) + \frac{\partial F_L^{HE}}{\partial p_k} dp_k + O^2$$

The objective is to find $F_L = 0$ in the next iteration. $F_L^{HE}(p^0)$ is the out-of-balance force at the current iteration. The previous equation can thus be rewritten as :

$$\frac{\partial F_L^{HE}}{\partial p_k} dp_k = -F_L^{HE}(p^0) \quad \sum_{\text{élément}} \frac{\partial F_L^{HE}}{\partial p_k} dp_k = \sum_{\text{élément}} F_L^{\text{ext}}(p^0) - F_L^{\text{int}}(p^0)$$

For finite pore pressure increments :

$$\underline{K} \cdot \underline{dp} = \underline{F}^{\text{ext}} - \underline{F}^{\text{int}} \quad \underline{K} = \sum_{\text{élément}} \frac{\partial \underline{F}^{HE}}{\partial \underline{p}}$$

23/01/2020



FORMULATION OF THE FLOW PROBLEM: ELEMENT STIFFNESS MATRIX

Considering that only the internal force depends on the nodal unknowns, we can rewrite the internal nodal forces:

$$F_L = \int_{\Omega} \left(\frac{\partial S^g}{\partial t} N_L - \rho_r v^g \cdot \underline{\text{grad}} N_L \right) d\Omega$$

The derivative with respect to the nodal pressure at the end of the step p_B gives:

$$K_{Lj} = \frac{\partial F_L}{\partial p_j^B} = \frac{\partial}{\partial p_j^B} \int_{\Omega} \left(\frac{\partial S^g}{\partial t} N_L - \rho_r v^g \cdot \underline{\text{grad}} N_L \right) d\Omega$$

The general expression of the iteration matrix is thus :

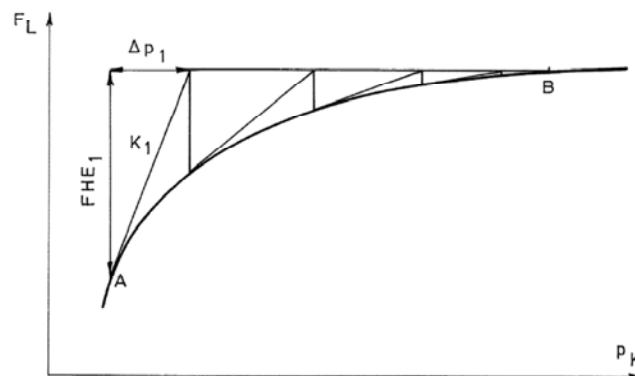
$$K_{Lj} = \int_{\Omega} \left(\frac{\partial}{\partial p_j^B} \left(\frac{\partial S^g}{\partial t} \right) N_L - \frac{\partial \rho_r v^g}{\partial p_j^B} \cdot \underline{\text{grad}} N_L \right) d\Omega$$

$$p^g = (1-g)p^A + g.p^B$$

$$p^B = \sum_{j=1}^{Noeuds} N_j \cdot p_j^B$$

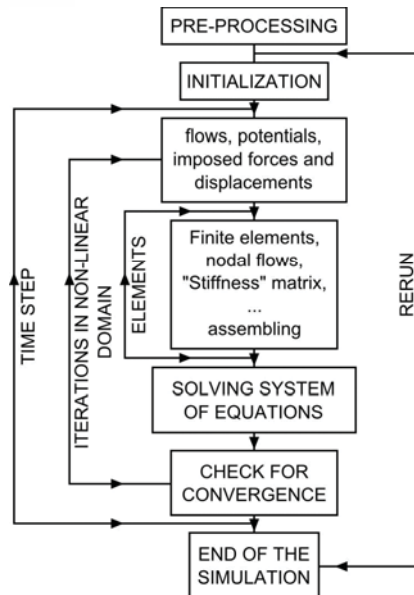
FORMULATION OF THE FLOW PROBLEM

In the non-linear domain, the iteration matrix is represented by the tangent to the (non-linear) curve linking flow and pressure. It changes depending on the pressure. A single resolution of the system of equations does not give an exact solution, but reduces the residual out-of-equilibrium flows. It is necessary to repeat several times the operation (computation of the tangent matrix, inversion, resolution) so that the flows out of equilibrium become sufficiently low.



FORMULATION OF THE FLOW PROBLEM

General Algorithm



23/01/2020

EURAD School for Radioactive Waste Management / GAS & HITEC

FORMULATION OF THE FLOW PROBLEM

Temporal stability

Temporal discretization schemes may introduce problems of precision, stability and oscillations. The study of stability and precision is difficult, if not impossible, on a system with a large number of degrees of freedom, as well as on a nonlinear system.

Let us therefore consider a linear problem with no external solicitations but with out-of-balance forces. The mass balance equation reads:

$$\int_{\Omega} \left(\frac{\partial S}{\partial t} N_L \delta p_L - \rho_f \underline{\underline{grad}} N_L \delta p_L \right) d\Omega = 0$$

This latter equation can be rewritten in a general form as:

$$\underline{\underline{C}}^T \underline{\underline{K}} p + \dot{p} = 0$$

23/01/2020

EURAD School for Radioactive Waste Management / GAS & HITEC



FORMULATION OF THE FLOW PROBLEM

Temporal stability

Let us study a system with only one degree of freedom. The problem becomes much simpler. Consider further the case where no external nodal flow is imposed (unsolicited problem).

The previous equation becomes:

$$\dot{p} + \alpha^2 p = 0$$

The problem is that of the damping or the relaxation of an initial state of pressure characterized by a non-zero initial value. The whole study of precision and stability is carried out on this equation.

The exact solution is : $p(t) = p(0) e^{-\alpha^2 t}$

The discretized solution can be found assuming: $p = (1-\theta) p_n + \theta p_{n+1}$
 $\dot{p} = \frac{p_{n+1} - p_n}{\Delta t}$

The equation becomes then: $\frac{p_{n+1} - p_n}{\Delta t} + \alpha^2 [(1-\theta) p_n + \theta p_{n+1}] = 0$

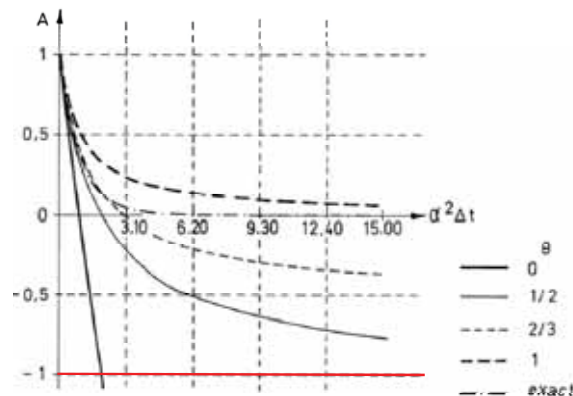


FORMULATION OF THE FLOW PROBLEM

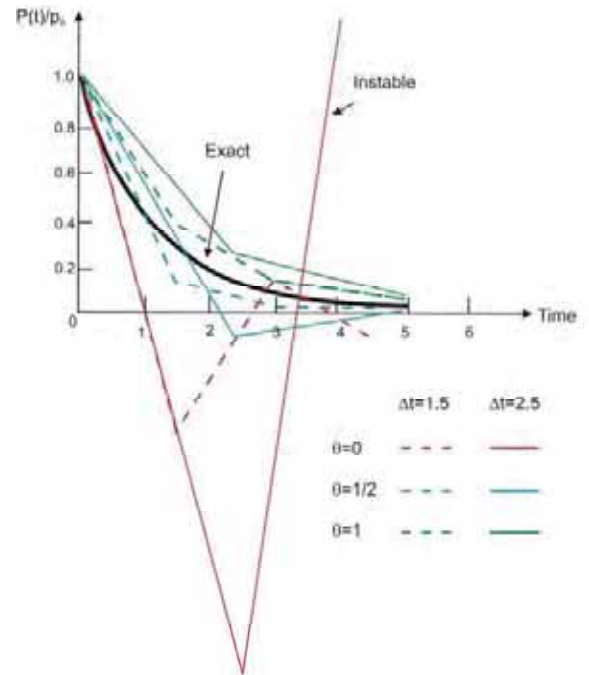
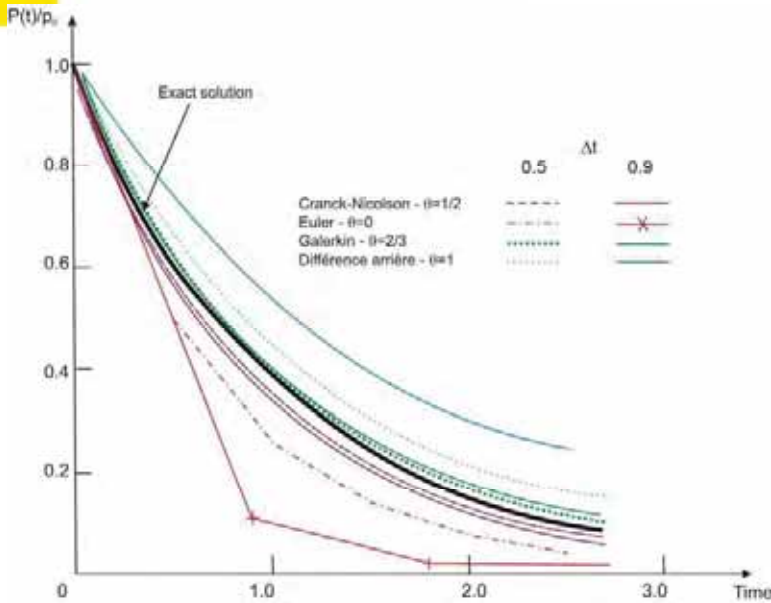
Temporal stability

Temporal discretization allows to compute a numerical estimate of the pressure at step $n + 1$ as a function of its value at step n . Their ratio is hereinafter called amplification factor A :

$$p_{n+1} = A p_n \quad A_{\text{numérique}} = \frac{1 - (1-\theta)\alpha^2 \Delta t}{1 + \theta\alpha^2 \Delta t} \quad A_{\text{exact}} = e^{-\alpha^2 \Delta t}$$



FORMULATION OF THE FLOW PROBLEM



23/01/2020

EURAD School for Radioactive Waste Management / GAS & HITEC

29

FORMULATION OF THE FLOW PROBLEM

Spatial oscillations

When applying rapid pressure variation to the boundary of a porous medium, spatial oscillations of the response may appear. Let us consider for example a semi-infinite uniaxial case, and apply to its border a brutal variation of the pressure. At time t , the pressure profile can be evaluated analytically:

$$p = \bar{p} + (p_0 - \bar{p})G\left(\frac{x}{2\sqrt{\frac{K}{\gamma c_p}t}}\right)$$

In this expression, G is the Gauss error integral function, which varies from 0 to 1. Consider the abscissa at which this function is equal to 0.9: at this point, there remains only 10% of the solicitation at the boundary.

This place is located in: $a = 2,30\sqrt{\frac{K}{\gamma c_p}t}$

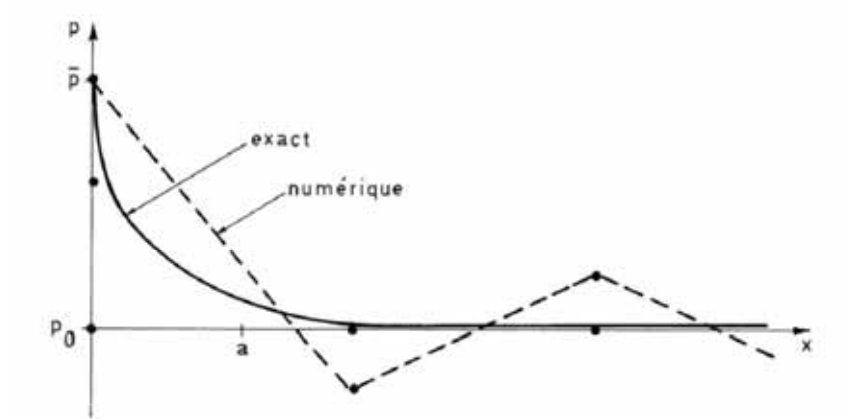
23/01/2020

EURAD School for Radioactive Waste Management / GAS & HITEC



FORMULATION OF THE FLOW PROBLEM

Spatial oscillation



23/01/2020

EURAD School for Radioactive Waste Management / GAS & HITEC



CONTENT

- Introduction
- Formulation of the flow problem
- Hydro-mechanical problem
- Hydro-mechanical problem in unsaturated conditions
- Thermo-hydro-mechanical problem

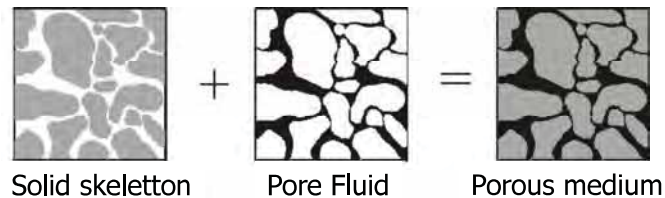
23/01/2020

EURAD School for Radioactive Waste Management / GAS & HITEC



FORMULATION OF THE HM PROBLEM

Saturated porous medium



The porous medium is considered as the **superimposition of two continua**, made of two chemical species (solid grain and water) and two phases (solid and fluid).

The balance equations can be alternatively written for **each species** or the **mixture and one of the species**.

23/01/2020

EURAD School for Radioactive Waste Management / GAS & HITEC



FORMULATION OF THE HM PROBLEM

Mechanical problem

Soils and rocks have a non linear behaviour and may undergo very large deformations. Lagamine code has been developed in the context of large strain, large displacement problems.

In this case, the initial configuration is different from the actual one. One may write the balance equations in the initial configuration or in the current one.

This latter choice is made in Lagamine code: we use the actualised deformed configuration as reference one (**Up-dated Lagrangian formulation**).

The flow problem is also written in this actualised deformed configuration and the modification of water storage due to solid displacement is therefore implicitly taken into account.

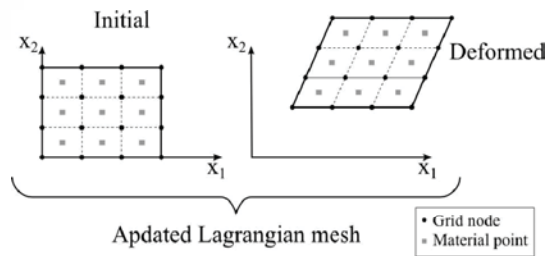
23/01/2020

EURAD School for Radioactive Waste Management / GAS & HITEC





FORMULATION OF THE HM PROBLEM



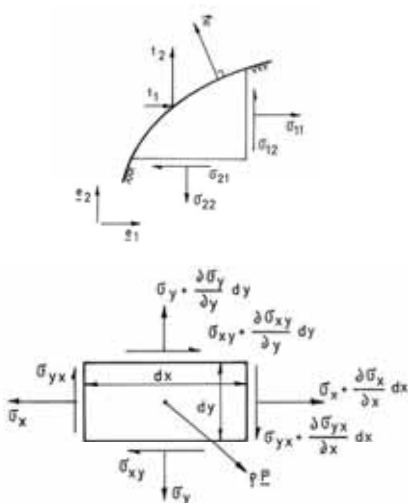
Among the different types of stress formulation (and the deformations associated with them), we will use the Cauchy stress tensor and the Cauchy strain rate defined as:

$$\dot{\epsilon}_{ij} = \frac{1}{2} \left(\frac{\partial \dot{u}_i}{\partial x_j} + \frac{\partial \dot{u}_j}{\partial x_i} \right)$$



FORMULATION OF THE HM PROBLEM

Local equilibrium equation



Boundary condition: $t_j = n_i \sigma_{ij}$

Linear momentum: $\partial_i \sigma_{ij} + F_j = 0$

Moment of momentum: $\sigma_{ij} = \sigma_{ji}$



FORMULATION OF THE HM PROBLEM

Global equilibrium equation

From the strong form of balance equations, it is possible to obtain their weak form using the principle of virtual work:

$$\delta W_\varepsilon = \int_{\Omega} \underline{F}^T \cdot \delta \underline{\dot{u}} \cdot d\Omega + \int_{\Gamma} \underline{t}^T \cdot \delta \underline{\dot{u}} \cdot d\Gamma$$

$$\delta W_I = \int_{\Omega} \sigma_{ij} \cdot \delta \dot{\varepsilon}_{ij} \cdot d\Omega \quad (\text{taking into account the symmetry of the stress tensor})$$

The equality of the internal and external virtual powers, for any kinematically admissible perturbation of the displacement rate implies respect for the local balance at all points of the solid and vice versa.



FORMULATION OF THE HM PROBLEM

- Fluid Linear momentum balance equation (strong form)

$$\frac{\partial p}{\partial x_i} + F_i^{S/W} + \rho_w g_i = 0$$

$$\text{Viscous drag force : } F_i^{S/W} = \frac{\rho_w \cdot \phi \cdot g}{K} V_i^{W/S}$$

- Solid mass balance equation (strong form)

$$\frac{\partial(\rho_s(1-\phi)\Omega)}{\partial t} = 0$$

FORMULATION OF THE HM PROBLEM

- Linear momentum balance equation for the mixture (weak form)

$$\int_{\Omega} \sigma_{ij} \varepsilon_{ij}^* d\Omega = \int_{\Omega} \rho_{mix} g_i u_i^* d\Omega + \int_{\Gamma} \bar{t}_i u_i^* d\Gamma$$

Terzaghi's postulate $\sigma_{ij} = \sigma'_{ij} - \rho \delta_{ij}$

Boundary condition $\sigma_{ij} n_j = \bar{t}_i$

Mixture density $\rho_{mix} = \rho_s \cdot (1 - \phi) + \phi \cdot \rho_w$

FORMULATION OF THE HM PROBLEM

- Fluid mass balance equation (weak form)

$$\int_{\Omega} \dot{M} p^* - m_i \frac{\partial p^*}{\partial x_i} d\Omega = \int_{\Omega} Q p^* d\Omega + \int_{\Gamma} \bar{q} p^* d\Gamma$$

Boundary condition $\bar{q} = m_i n_i$

Darcy's law $m_i = -\rho_w \frac{\kappa}{\mu} \left(\frac{\partial p}{\partial x_i} + \rho_w g_i \right)$

Storage law $\dot{M} = \rho_w \frac{\dot{p}}{k^w} \phi + \rho_w \frac{\dot{\Omega}}{\Omega}$

FORMULATION OF THE HM PROBLEM (SATURATED CONDITIONS)

- Terzaghi postulate: $\sigma_{ij}^t = \sigma_{ij}^n - p^t \delta_{ij}$
- Viscous drag forces $F_i^{S/W,t} = \frac{\rho^{w,t} \phi^t g}{K} V_i^{W/S,t}$
- Relative velocity of the fluid: $m_i^t = -\frac{K}{g} \left(\frac{\partial p^t}{\partial x_i^t} + \rho^{w,t} g_i \right) = -\rho^{w,t} \frac{K}{\mu} \left(\frac{\partial p^t}{\partial x_i^t} + \rho^{w,t} g_i \right)$
- Rate of fluid mass: $\dot{M}^t = \rho^{w,t} \left[\frac{\dot{p}^t}{k^w} \phi^t + \frac{\dot{\Omega}^t}{\Omega^t} \right]$
- Boundary conditions: total stresses $\sigma_{ij} n_j = \bar{t}_i$
- Boundary conditions: fluxes $\bar{q}^t = m_i^t n_i^t$

23/01/2020

EURAD School for Radioactive Waste Management / GAS & HITEC



FORMULATION OF THE HM PROBLEM (SATURATED CONDITIONS)

- System of equations to be solved:

$$\int_{\Omega} \sigma_{ij} \varepsilon_{ij}^* d\Omega = \int_{\Omega} \rho_{mix} g_i u_i^* d\Omega + \int_{\Gamma} \bar{t}_i u_i^* d\Gamma$$

$$\int_{\Omega} \dot{M} p^* - m_i \frac{\partial p^*}{\partial x_i} d\Omega = \int_{\Omega} Q p^* d\Omega + \int_{\Gamma} \bar{q} p^* d\Gamma$$

For the description of the HM FE in the Lagamine code see:

Influence of evaporation and seepage on the convergence of a ventilated cavity. P Gerard, R Charlier, R Chambon, F Collin - Water resources research, 2008

23/01/2020

EURAD School for Radioactive Waste Management / GAS & HITEC



FORMULATION OF THE HM PROBLEM (SATURATED CONDITIONS)

The out-of-balance forces are usually different from zero and an iterative procedure is necessary to find a new configuration in equilibrium (where the out-of-balance forces vanish). Let's consider a first configuration τ_1 which is not in equilibrium:

$$\begin{aligned} \int_{\Omega^{\tau_1}} \sigma_{ij}^{\tau_1} \frac{\partial u_i^*}{\partial x_j^{\tau_1}} d\Omega^{\tau_1} - \int_{\Omega^{\tau_1}} (\varrho^{s,\tau_1}(1-\phi^{\tau_1}) + \varrho^{w,\tau_1}\phi^{\tau_1}) g_i u_i^* d\Omega^{\tau_1} - \int_{\Gamma_s^{\tau_1}} \bar{t}_i^{\tau_1} u_i^* d\Gamma^{\tau_1} \\ = \int_{\Omega^{\tau_1}} F_i^{\text{HE}} u_i^* d\Omega^{\tau_1} \\ \int_{\Omega^{\tau_1}} (M^{\tau_1} p^* - m_i^{\tau_1} \frac{\partial p^*}{\partial x_i^{\tau_1}}) d\Omega^{\tau_1} - \int_{\Omega^{\tau_1}} Q^{\tau_1} p^* d\Omega^{\tau_1} + \int_{\Gamma_p^{\tau_1}} \bar{q}^{\tau_1} p^* d\Gamma^{\tau_1} \\ = \int_{\Omega^{\tau_1}} F_p^{\text{HE}} p^* d\Omega^{\tau_1} \end{aligned}$$

Our goal is to find a new configuration τ_2 for which the out-of-balance forces vanish:

$$\begin{aligned} \int_{\Omega^{\tau_2}} \sigma_{ij}^{\tau_2} \frac{\partial u_i^*}{\partial x_j^{\tau_2}} d\Omega^{\tau_2} - \int_{\Omega^{\tau_2}} (\varrho^{s,\tau_2}(1-\phi^{\tau_2}) + \varrho^{w,\tau_2}\phi^{\tau_2}) g_i u_i^* d\Omega^{\tau_2} - \int_{\Gamma_s^{\tau_2}} \bar{t}_i^{\tau_2} u_i^* d\Gamma^{\tau_2} = 0 \\ \int_{\Omega^{\tau_2}} (M^{\tau_2} p^* - m_i^{\tau_2} \frac{\partial p^*}{\partial x_i^{\tau_2}}) d\Omega^{\tau_2} - \int_{\Omega^{\tau_2}} Q^{\tau_2} p^* d\Omega^{\tau_2} + \int_{\Gamma_p^{\tau_2}} \bar{q}^{\tau_2} p^* d\Gamma^{\tau_2} = 0 \end{aligned}$$

23/01/2020

eu[rad]

43

FORMULATION OF THE HM PROBLEM (SATURATED CONDITIONS)

In order to find this better approximation τ_2 , we rewrite these latter equations in the configuration τ_1 and the resulting equations are subtracted from the initial equations. This yields first for the momentum balance equation:

$$\int_{\Omega^{\tau_1}} \frac{\partial u_i^*}{\partial x_k^{\tau_1}} (\sigma_{ij}^{\tau_2} \frac{\partial x_k^{\tau_1}}{\partial x_j^{\tau_2}} \det F - \sigma_{ik}^{\tau_1}) d\Omega^{\tau_1} = \int_{\Omega^{\tau_1}} F_i^{\text{HE}} u_i^* d\Omega^{\tau_1}$$

In a first step, let's assume that the pore pressure is identical in the two configurations. We define δu_i as the differences between the configurations τ_1 and τ_2 .

$$x_i^{\tau_2} = x_i^{\tau_1} + \delta u_i$$

Evaluation of the left-hand term of the equation yields:

$$\begin{aligned} \sigma_{ij}^{\tau_2} (\delta_{jk} - \frac{\partial \delta u_k}{\partial x_j^{\tau_2}}) \det F - \sigma_{ik}^{\tau_1} \\ = \sigma_{ik}^{\tau_2} \det F - \sigma_{ij}^{\tau_2} \frac{\partial \delta u_k}{\partial x_j^{\tau_2}} \det F - \sigma_{ik}^{\tau_1} \\ = (\sigma_{ik}^{\tau_2} - \sigma_{ik}^{\tau_1}) - \sigma_{ij}^{\tau_2} \frac{\partial \delta u_k}{\partial x_j^{\tau_2}} \det F + \sigma_{ik}^{\tau_2} (\det F - 1) \quad \text{HITC} \end{aligned}$$

23/01/2020

eu[rad]

44



FORMULATION OF THE HM PROBLEM (SATURATED CONDITIONS)

Assuming that the two configurations are close, we may assume that δu_i tends to du_i , and the det F can be rewritten as:

$$\det F = 1 + \frac{\partial du_i}{\partial x_i^t}$$

Using a Taylor expansion of the equation and discarding terms of degree greater than one yields after some algebra :

$$d\sigma_{ik}^t - \sigma_{ij}^t \frac{\partial du_k}{\partial x_j^t} + \sigma_{ik}^t \frac{\partial du_j}{\partial x_j^t}$$

The increment of total stress can be expressed as follow:

$$d\sigma_{ik}^t = C_{iklj} \frac{\partial du_l}{\partial x_j^t} - dp \delta_{ik}$$

The following expression of the stiffness matrix holds:

$$\int_{\Omega^t} \frac{\partial u_i^*}{\partial x_k^t} \left(C_{ijkl} \frac{\partial du_l}{\partial x_j^t} - \sigma_{ij}^t \frac{\partial du_k}{\partial x_j^t} + \sigma_{ik}^t \frac{\partial du_j}{\partial x_j^t} \right) d\Omega^t + \int_{\Omega^t} \frac{\partial u_i^*}{\partial x_k^t} (-dp^t \delta_{ik}) d\Omega^t = \int_{\Omega^t} F_i^{HE} u_i^* d\Omega^t$$

← Small strain term
→ HM coupling term
→ Large strain term: stress matrix

23/01/2020



FORMULATION OF THE HM PROBLEM (SATURATED CONDITIONS)

Let's consider now the fluid mass balance equation and follow the same procedure.

Assuming the same configuration in $\tau 1$ and $\tau 2$ but different pore pressure $p^{\tau 2} = p^{\tau 1} + \delta p$ we obtain the classical flow stiffness matrix:

$$\int_{\Omega^t} p^* \left(\rho^{w,t} \frac{dp}{k^w} \frac{\phi^t}{k^w} \dot{p}^t + \rho^{w,t} \frac{\phi^t}{k^w} \frac{dp}{k^w} \frac{d\Omega^t}{dt} + \rho^{w,t} \frac{dp}{k^w} \frac{\dot{\Omega}^t}{\Omega^t} \right) d\Omega^t - \int_{\Omega^t} \frac{\partial p^*}{\partial x_k^t} \left(-\rho^{w,t} \frac{dp}{k^w} \frac{\kappa}{\mu} \left(\frac{\partial p^t}{\partial x_k^t} + \rho^{w,t} \cdot g_k \right) - \rho^{w,t} \frac{\kappa}{\mu} \left(\frac{\partial dp}{\partial x_k^t} + \rho^{w,t} \frac{dp}{k^w} \cdot g_k \right) \right) d\Omega^t = \int_{\Omega^t} F_p^{HE} p^* d\Omega^t$$

Considering now the influence of the configuration provides us the HM coupling terms:

$$\int_{\Omega^t} p^* \left(\rho^{w,t} \frac{1-\phi^t}{k^w} \dot{p}^t \frac{1}{\Omega^t} \frac{\partial du_i}{\partial x_i^t} + \rho^{w,t} \left(\frac{1}{\Omega^t \cdot dt} - \frac{\dot{\Omega}^t}{\Omega^2} \frac{1}{\Omega^t} \right) \frac{\partial du_i}{\partial x_i^t} + \dot{M} \frac{\partial du_i}{\partial x_i^t} \right) d\Omega^t - \int_{\Omega^t} \frac{\partial p^*}{\partial x_k^t} \left(\rho^{w,t} \frac{\kappa}{\mu} \frac{\partial p^t}{\partial x_k^t} \frac{\partial du_i}{\partial x_k^t} + m_i \frac{\partial du_k}{\partial x_i^t} + m_k \frac{\partial du_i}{\partial x_k^t} \right) d\Omega^t = \int_{\Omega^t} F_p^{HE} p^* d\Omega^t$$

→ HM coupling term
→ Large strain term: « stress matrix »

23/01/2020



FORMULATION OF THE HM PROBLEM (SATURATED CONDITIONS)

We have now the expression of the iteration matrix, necessary to find the corrections of the displacement fields du_i and the corrections of the pressure dp to be added to their respective current values to obtain a new current configuration, and a new pore pressure field closer to a well-balanced configuration:

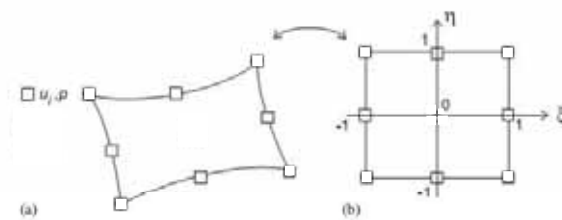
$$\begin{bmatrix} F_x^{HE} \\ F_y^{HE} \\ F_p^{HE} \end{bmatrix} = \underline{\underline{K}} \begin{bmatrix} du_x \\ du_y \\ dp \end{bmatrix} \quad \underline{\underline{K}} = \begin{bmatrix} K_{MM}(2 \times 2) & K_{WM}(2 \times 1) \\ K_{MW}(1 \times 2) & K_{WW}(1 \times 1) \end{bmatrix}$$

The classical matrices are located on the diagonal. The K_{MM} submatrix takes into account for the material and geometrical non linearities. The two other submatrices contain the effect of the Hydro-mechanical couplings.

FORMULATION OF THE HM PROBLEM (SATURATED CONDITIONS)

The field equations are spatially discretized using 2D plane strain isoparametric finite elements with eight nodes for u_i and dp . The usual quadratic serendipity shape function are used.

$$\begin{aligned} X_i &= \phi_L X_{iL} \\ x_i &= \phi_L x_{iL} \\ p &= \phi_L p_L \end{aligned}$$



(a) Quadrilateral element

(b) parent element

FORMULATION OF THE HM PROBLEM (SATURATED CONDITIONS)

In the element, the internal virtual work equations are computed:

$$\partial W_I^{Meca} = \int_{\Omega} \sigma_{ij} \varepsilon_{ij}^* d\Omega = \int_{\Omega} \sigma_{ij} \frac{1}{2} \left(\frac{\partial \dot{u}_i^*}{\partial x_j} + \frac{\partial \dot{u}_j^*}{\partial x_i} \right) d\Omega$$

$$\partial W_I^{Fluid} = \int_{\Omega} \dot{M} \cdot p^* - m_i \frac{\partial p^*}{\partial x_i} d\Omega$$

Where the virtual quantities (displacement rate and pore pressure variation) are expressed as a function of nodal values:

$$\dot{u}^* = \phi_L \cdot \dot{u}_L^* \quad p^* = \phi_L \cdot p_L^*$$

In 2D plane strain state, we obtain the expression of the nodal forces and flux:

$$F_{1L} = \sum_{PI} \left(\sigma_{11} \frac{\partial \phi_L}{\partial x_1} + \sigma_{12} \frac{\partial \phi_L}{\partial x_2} \right) t |J| W_{PI}$$

$$F_{2L} = \sum_{PI} \left(\sigma_{21} \frac{\partial \phi_L}{\partial x_1} + \sigma_{22} \frac{\partial \phi_L}{\partial x_2} \right) t |J| W_{PI}$$

$$F_{pL} = \sum_{PI} \left(\dot{M} \cdot \phi_L - m_i \frac{\partial \phi_L}{\partial x_i} \right) t |J| W_{PI}$$

23/01/2020

MENTE SAS & HITEC



49

FORMULATION OF THE HM PROBLEM (SATURATED CONDITIONS)

1. General principal

When equilibrium is not met, a new configuration should be found for which the out of balance forces vanish. Based on the mathematical formulation of the auxiliary linear problem and introducing the isoparametric function, we can define the stiffness matrix:

$$\int_{\Omega^t} \frac{\partial \phi_L}{\partial x_k^t} \dot{u}_{i,L}^* \left(C_{ijkl} \frac{\partial \phi_J}{\partial x_j^t} du_{i,J} - \sigma_{ij}^t \frac{\partial \phi_J}{\partial x_j^t} du_{k,J} + \sigma_{ik}^t \frac{\partial \phi_J}{\partial x_i^t} du_{l,J} \right) d\Omega^t + \int_{\Omega^t} \frac{\partial \phi_L}{\partial x_k^t} \dot{u}_i^* \left(-\phi_J dp_J \delta_{ik} \right) d\Omega^t = \int_{\Omega^t} F_i^{HE} \phi_L \dot{u}_{i,L}^* d\Omega^t$$

$$\int_{\Omega^t} \phi_L p_L^* \left(\rho^{w,t} \frac{\phi_J dp_J}{k^w} \frac{\phi^t}{k^w} \dot{p}^t + \rho^{w,t} \frac{\phi^t}{k^w} \frac{\phi_J dp_J}{dt} + \rho^{w,t} \frac{\phi_J dp_J}{k^w} \frac{\dot{\Omega}^t}{\Omega^t} \right) d\Omega^t +$$

$$\int_{\Omega^t} \phi_L p_L^* \left(\rho^{w,t} \frac{1-\phi^t}{k^w} \dot{p}^t \frac{1}{\Omega^t} \frac{\partial \phi_J}{\partial x_i^t} du_{i,J} + \rho^{w,t} \left(\frac{1}{\Omega^t \cdot dt} - \frac{\dot{\Omega}^t}{\Omega^t} \frac{1}{\Omega^t} \right) \frac{\partial \phi_J}{\partial x_i^t} du_{i,J} + \dot{M} \frac{\partial \phi_J}{\partial x_i^t} du_{i,J} \right) d\Omega^t$$

$$- \int_{\Omega^t} \frac{\partial \phi_L}{\partial x_k^t} p_L^* \left(-\rho^{w,t} \frac{\phi_J dp_J}{k^w} \frac{\kappa}{\mu} \left(\frac{\partial p^t}{\partial x_k^t} + \rho^{w,t} \cdot g_k \right) - \rho^{w,t} \frac{\kappa}{\mu} \left(\frac{\partial \phi_J}{\partial x_k^t} dp_J + \rho^{w,t} \frac{\phi_J dp_J}{k^w} \cdot g_k \right) \right) d\Omega^t$$

$$- \int_{\Omega^t} \frac{\partial \phi_L}{\partial x_k^t} p_L^* \left(\rho^{w,t} \frac{\kappa}{\mu} \frac{\partial p^t}{\partial x_k^t} \frac{\partial \phi_J}{\partial x_k^t} du_{i,J} + m_i \frac{\partial \phi_J}{\partial x_i^t} du_{k,J} + m_k \frac{\partial \phi_J}{\partial x_k^t} du_{i,J} \right) d\Omega^t = \int_{\Omega^t} F_p^{HE} \phi_L \cdot p_L^* d\Omega^t$$

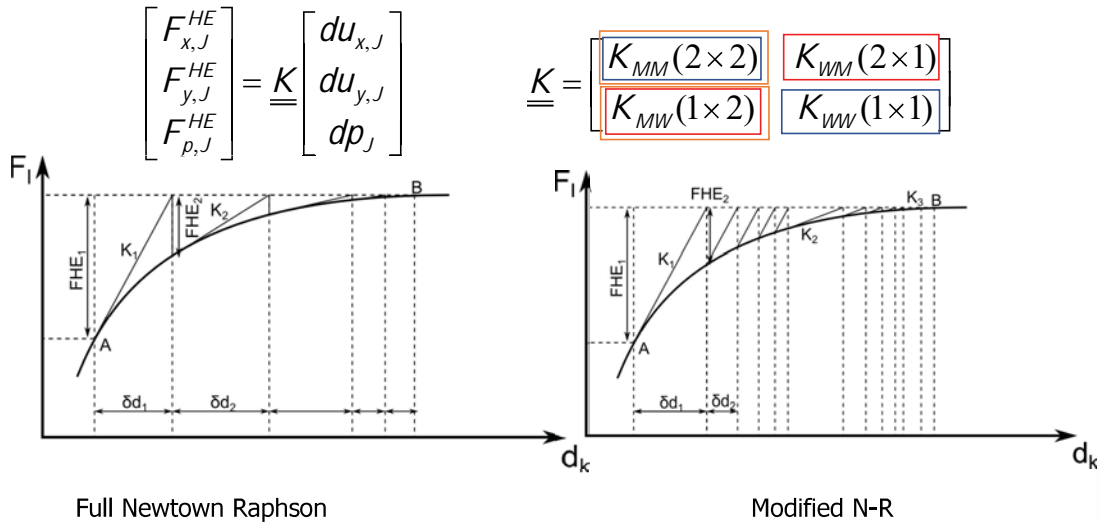
23/01/2020

EURAD School for Radioactive Waste Management / SAS & HITEC



50

FORMULATION OF THE HM PROBLEM (SATURATED CONDITIONS)



23/01/2020

EURAD School for Radioactive Waste Management / GAS & HITEC



FORMULATION OF THE HM PROBLEM (SATURATED CONDITIONS)

3. Convergence norm

By default the norm of the out of balance forces is evaluated through the following relationship:

$$\|F^{HE}\| = \frac{\sqrt{\sum (F^{HE})^2}}{N_{equation}} \sqrt{\frac{\sum (F^{imp})^2}{N_{Force}} + \frac{\sum (F^{react})^2}{N_{React}}}$$

Knowing that the order of magnitude of the out of balance forces for the mechanical problem and the flow problem respectively are really different. It is therefore necessary to sum the norm of each problem computed separately:

$$\|F^{HE}\| = \|F^{HE}\|^{Meca} + \|F^{HE}\|^{hydro}$$

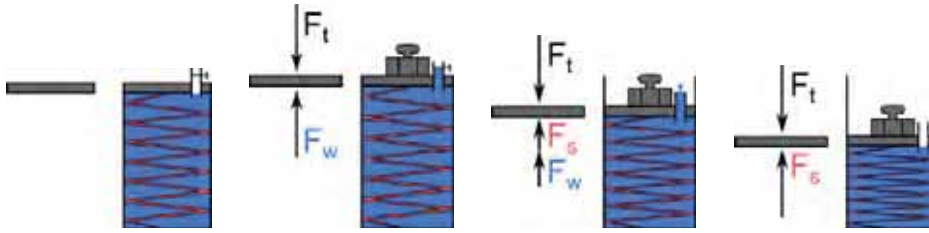
23/01/2020

EURAD School for Radioactive Waste Management / GAS & HITEC





APPLICATION OF HM PROBLEM: CONSOLIDATION PROCESS



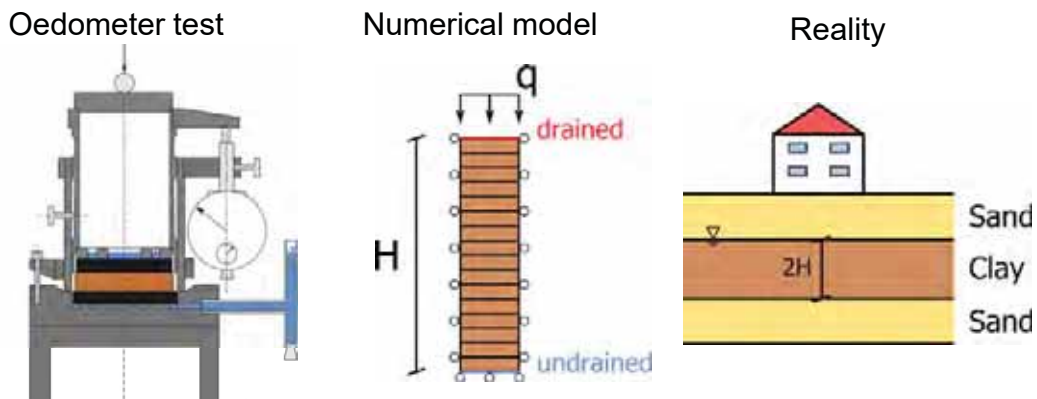
STEP	Load	Drainage	Stress (soil)	Overpressure (water)
1	No	No	No	No
2	Yes	No	No	Maximum
3	Yes	Yes	Increasing	Decreasing
4	Yes	Yes	Maximum	No

23/01/2020

EURAD School for Radioactive Waste Management / GAS & HITEC



APPLICATION OF HM PROBLEM: CONSOLIDATION PROCESS



Characteristics :

- Soil height : $2H$
- Vertical displacement only
- Drained bases
- Constant load

23/01/2020

EURAD School for Radioactive Waste Management / GAS & HITEC



APPLICATION OF HM PROBLEM: CONSOLIDATION PROCESS

Analytical Solution (two drained bases)

Maximum settlement :

$$s_{\max}^e = \frac{H}{m_v \cdot q}$$

Adimensional time :

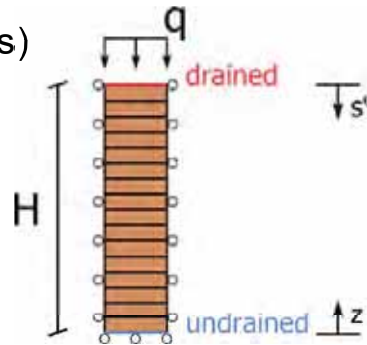
$$T_v = \frac{c_v \cdot t}{H^2}$$

Adimensional settlement :

$$\frac{s(T_v)}{s_{\max}^e} = 1 - \sum_{n=1,2}^N \frac{8}{n^2 \cdot \pi^2} \cdot \exp\left(-\frac{n^2 \cdot \pi^2}{4} \cdot T_v\right)$$

Adimensional pore pressure distribution :

$$\frac{u^e(z, T_v)}{q} = \sum_{n=1}^N \frac{-2}{n \cdot \pi} \cdot (-1)^n \cdot \exp\left(-\frac{n^2 \cdot \pi^2}{4} \cdot T_v\right) \cdot \sin\left(\frac{\pi \cdot n}{2 \cdot H} \cdot z\right)$$



Soil parameters

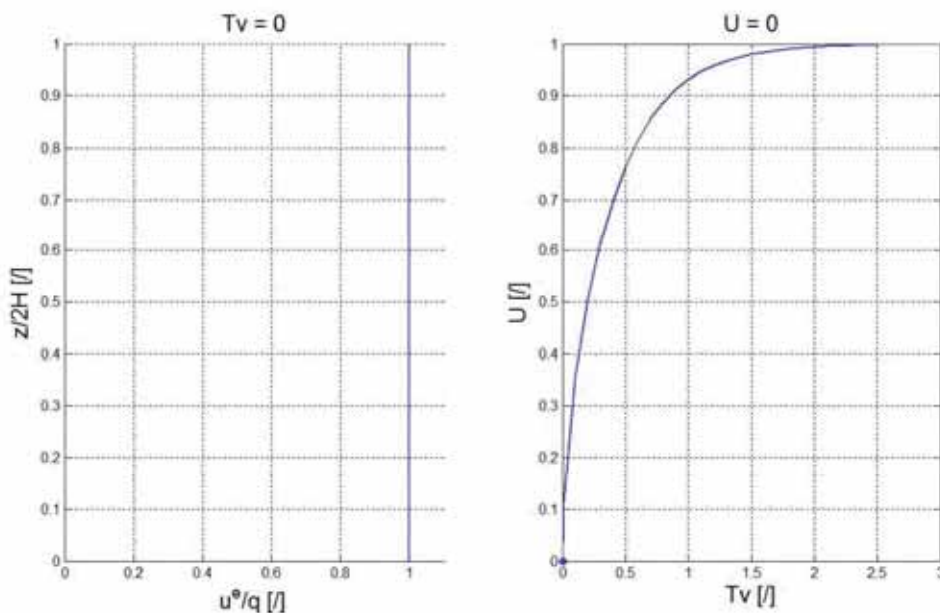
$$m_v = \frac{1}{E} \cdot \left(1 - \frac{2 \cdot \nu^2}{1 - \nu}\right)$$

$$c_v = \frac{K_0}{\gamma_w \cdot m_v}$$

23/01/2020

EURAD School for Radioactive Waste Management / GAS & HITEC

APPLICATION OF HM PROBLEM: CONSOLIDATION PROCESS



23/01/2020

EURAD School for Radioactive Waste Management / GAS & HITEC

APPLICATION OF HM PROBLEM: CONSOLIDATION PROCESS

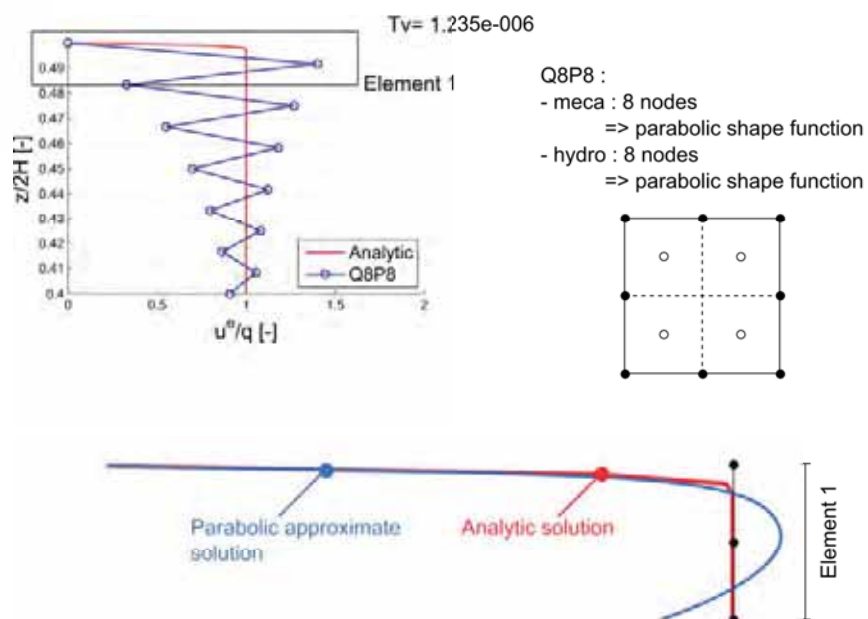
Comparison : Analytic solution & LAGAMINE

E [Pa]	ν [-]	k [m ²]	H [m]
10 ⁷	0.2	10 ⁻¹⁸	0.03

Geometry : 30 elements CSOL2

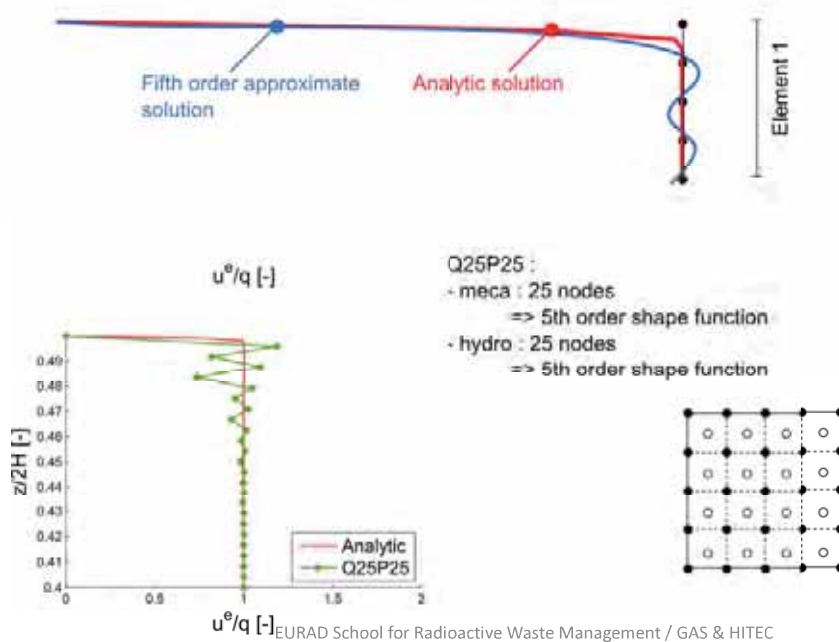
	Q8P8	Q8P4	Q25P25
DoF's	300	241	1563

APPLICATION OF HM PROBLEM: CONSOLIDATION PROCESS



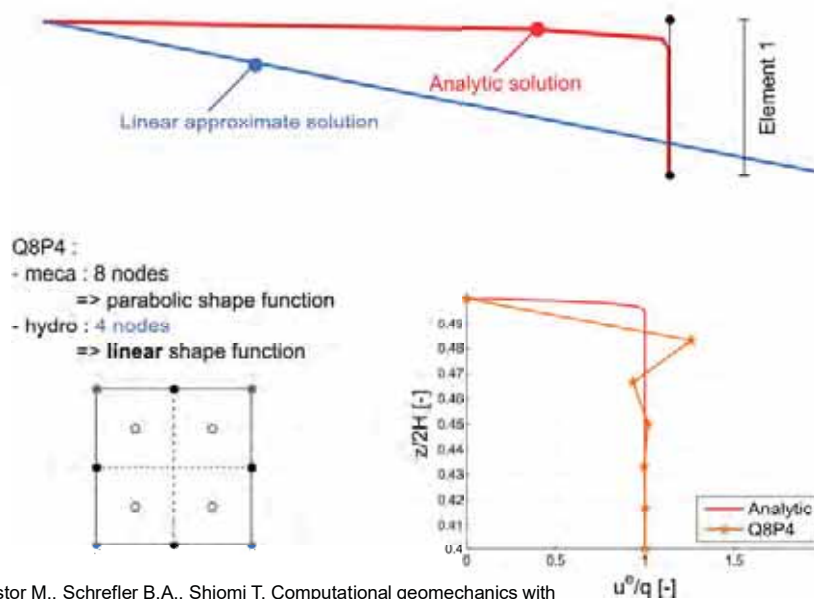
APPLICATION OF HM PROBLEM: CONSOLIDATION PROCESS

$Tv = 1.235e-006$



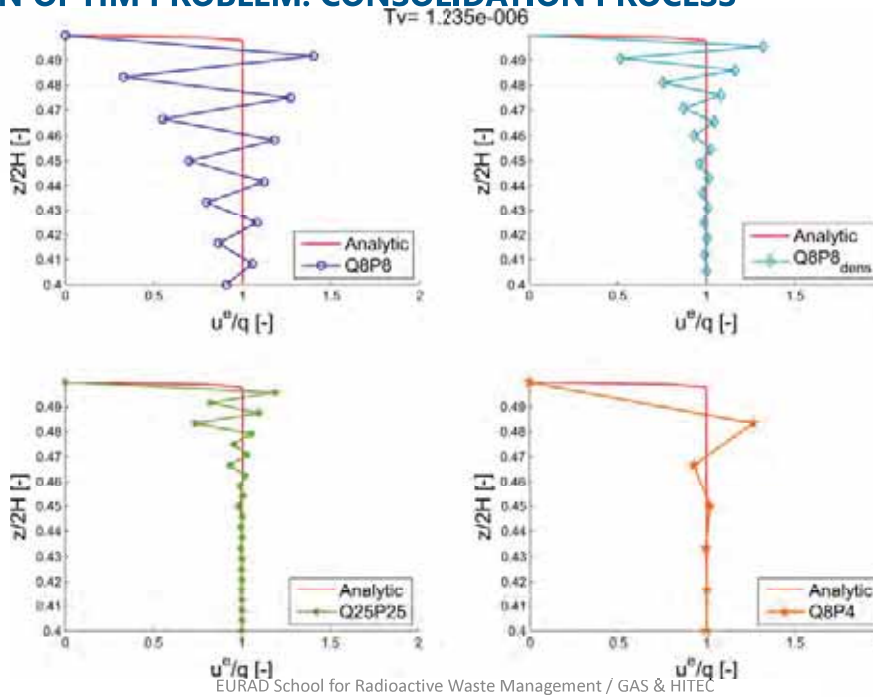
APPLICATION OF HM PROBLEM: CONSOLIDATION PROCESS

$Tv = 1.235e-006$



* Zienkiewicz O.C., Chan A.H.C., Pastor M., Schrefler B.A., Shiomi T. Computational geomechanics with special reference to earthquake engineering, Wiley, Chichester, 1999.

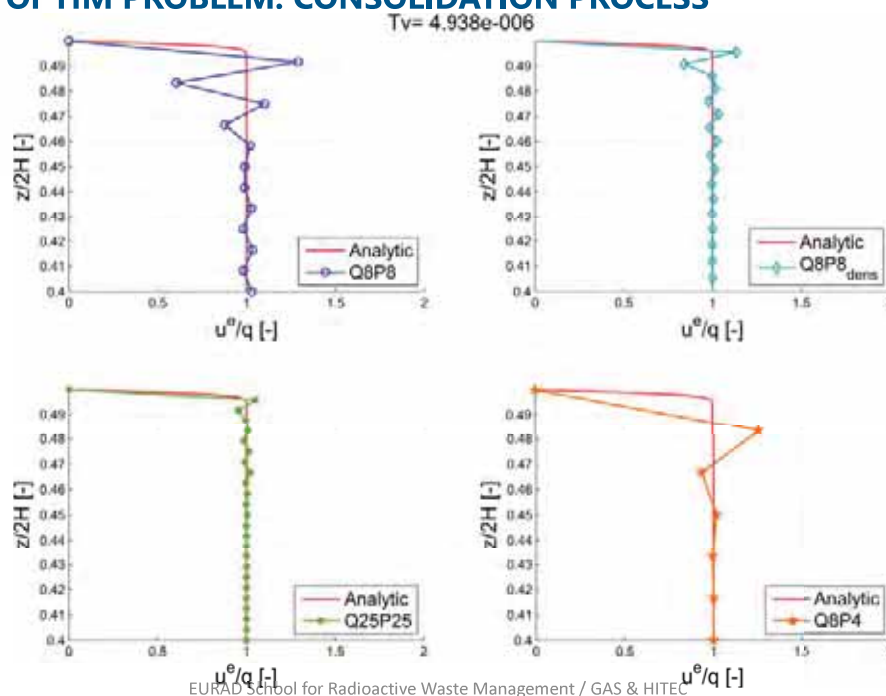
APPLICATION OF HM PROBLEM: CONSOLIDATION PROCESS



23/01/2020

EURAD School for Radioactive Waste Management / GAS & HITEC

APPLICATION OF HM PROBLEM: CONSOLIDATION PROCESS

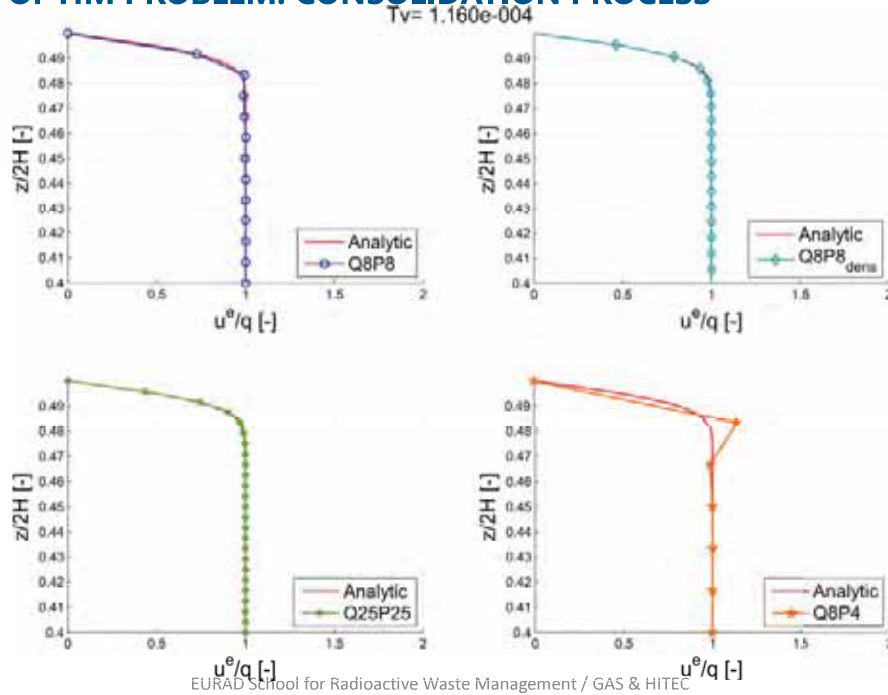


23/01/2020

EURAD School for Radioactive Waste Management / GAS & HITEC



APPLICATION OF HM PROBLEM: CONSOLIDATION PROCESS

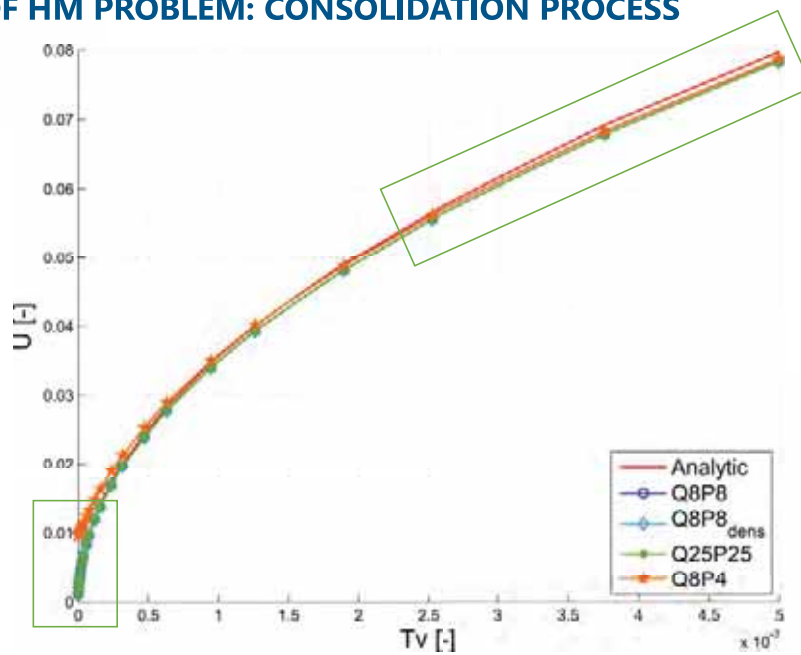


23/01/2020

EURAD School for Radioactive Waste Management / GAS & HITEC



APPLICATION OF HM PROBLEM: CONSOLIDATION PROCESS



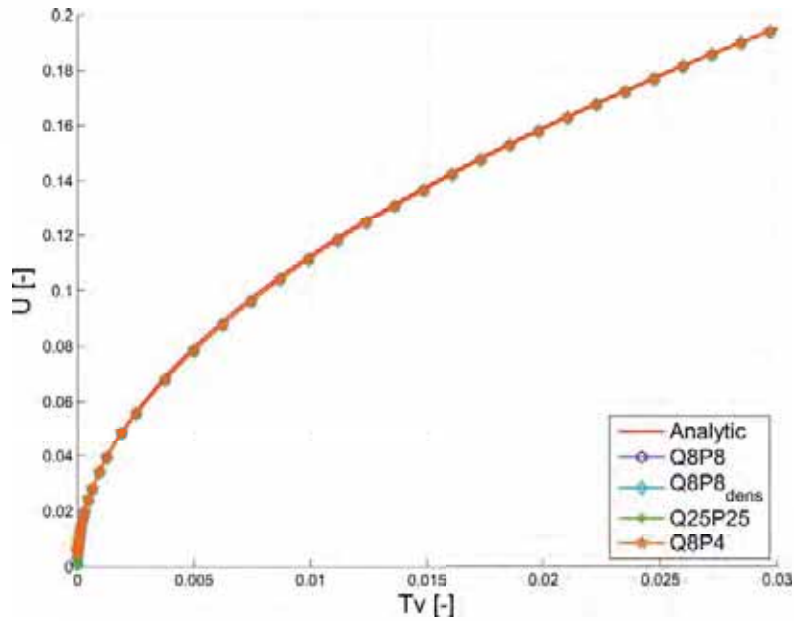
23/01/2020

EURAD School for Radioactive Waste Management / GAS & HITEC





APPLICATION OF HM PROBLEM: CONSOLIDATION PROCESS



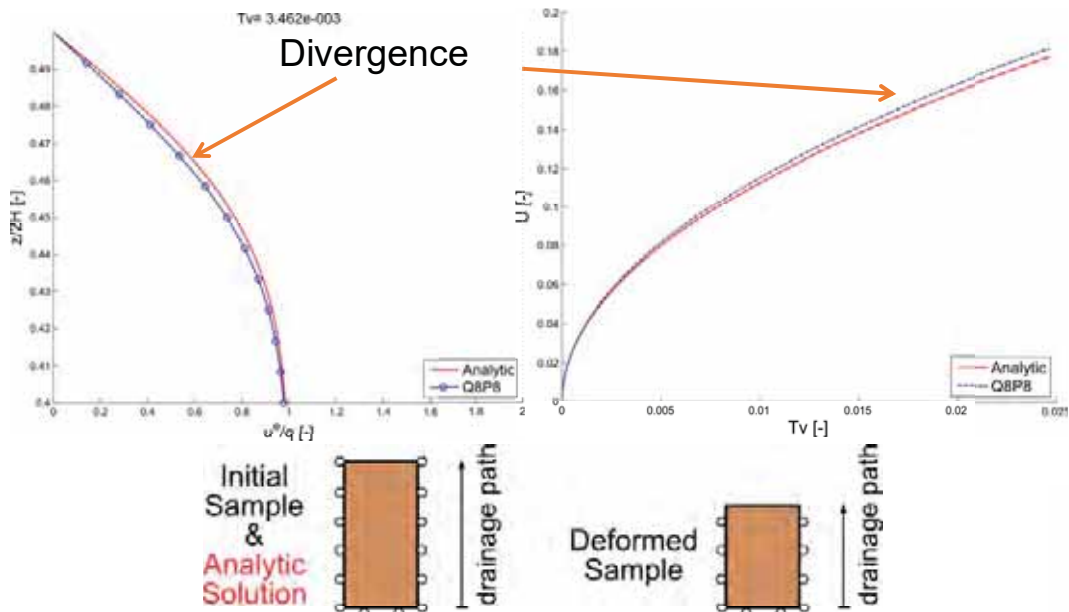
23/01/2020

EURAD School for Radioactive Waste Management / GAS & HITEC



APPLICATION OF HM PROBLEM: CONSOLIDATION PROCESS

Comparison for $E=10^6$ Pa



23/01/2020

EURAD School for Radioactive Waste Management / GAS & HITEC





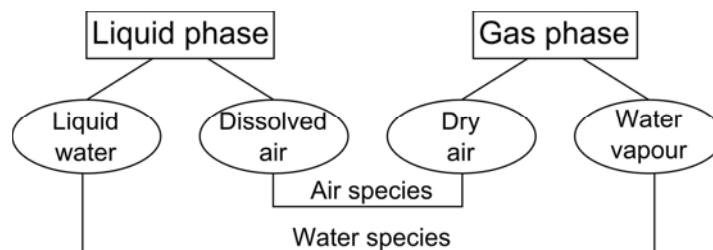
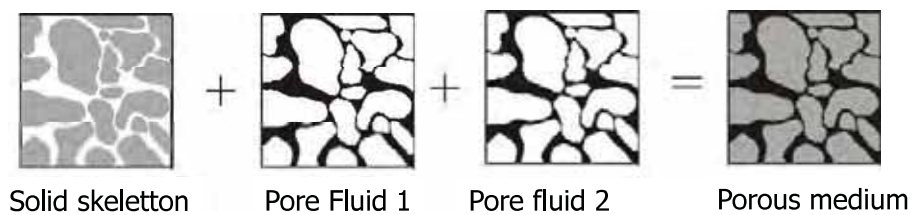
CONTENT

- Introduction
- Formulation of the flow problem
- Hydro-mechanical problem
- Hydro-mechanical problem in unsaturated conditions
- Thermo-hydro-mechanical problem



UNSATURATED HM PROBLEM AT CONSTANT TEMPERATURE

Unsaturated porous medium



UNSATURATED HM PROBLEM AT CONSTANT TEMPERATURE

$$\text{Liquid water: } \dot{S}_{(H_2O)_l} + \text{div}(f_{(H_2O)_l}) + \dot{E}_{H_2O}^{l \rightarrow g} = Q_{(H_2O)_l}$$

$$\text{Water vapour: } \dot{S}_{(H_2O)_g} + \text{div}(f_{(H_2O)_g}) - \dot{E}_{H_2O}^{l \rightarrow g} = Q_{(H_2O)_g}$$

$\dot{S}_{(H_2O)_l} / \dot{S}_{(H_2O)_g}$: Storage term liquid water / water vapour

$f_{(H_2O)_l} / f_{(H_2O)_g}$: mass flow of liquid water / water vapour

$\dot{E}_{H_2O}^{l \rightarrow g}$: Evaporation mass rate

$Q_{(H_2O)_l} / Q_{(H_2O)_g}$: Production – consumption of liquid water / water vapour

$$f_{(H_2O)_l} = \rho_w \cdot \underline{q}_l$$

\underline{q}_l et \underline{q}_g : liquid and gas phase flow

$$f_{(H_2O)_g} = \rho_{H_2O}^g \cdot \underline{q}_g + \dot{i}_{(H_2O)_g}$$

$\dot{i}_{(H_2O)_g}$: diffusive water vapour flow

$$\rightarrow \frac{\partial}{\partial t} (\rho_w \cdot \varphi \cdot S_{r,w} + \rho_{H_2O}^g \cdot \varphi \cdot S_{r,g}) + \text{div}(\rho_w \cdot \underline{q}_l) + \text{div}(\rho_{H_2O}^g \cdot \underline{q}_g + \dot{i}_{(H_2O)_g}) - Q_{H_2O} = 0$$

Q_{H_2O} : Production – consumption of water

23/01/2020

EURAD School for Radioactive Waste Management / GAS & HITEC



UNSATURATED HM PROBLEM AT CONSTANT TEMPERATURE

$$\text{Gaseous air: } \dot{S}_{(Air)_g} + \text{div}(f_{(Air)_g}) + \dot{E}_{Air}^{g \rightarrow d} = Q_{(Air)_g}$$

$$\text{Dissolved air: } \dot{S}_{(Air)_d} + \text{div}(f_{(Air)_d}) - \dot{E}_{Air}^{g \rightarrow d} = Q_{(Air)_d}$$

$\dot{S}_{(Air)_g} / \dot{S}_{(Air)_d}$: Storage term dry air / dissolved air

$f_{(Air)_g} / f_{(Air)_d}$: mass flow of dry air / dissolved air

$\dot{E}_{Air}^{g \rightarrow d}$: Dissolution mass rate

$Q_{(Air)_g} / Q_{(Air)_d}$: Production – consumption of dry air / dissolved air

$$f_{(Air)_g} = \rho_{Air}^g \cdot \underline{q}_g + \dot{i}_{(Air)_g}$$

\underline{q}_l et \underline{q}_g : liquid and gas phase flow

$$f_{(Air)_d} = \rho_{Air}^g \cdot H_{Air} \cdot \underline{q}_l + \dot{i}_{(Air)_d}$$

$\dot{i}_{(Air)_g} / \dot{i}_{(Air)_d}$: diffusive dry air and dissolved air flow

$$\rightarrow \frac{\partial}{\partial t} (\rho_{Air}^g \cdot \varphi \cdot S_{r,g} + \rho_{Air}^g \cdot H_{Air} \cdot \varphi \cdot S_{r,w}) + \text{div}(\rho_{Air}^g \cdot \underline{q}_g + \dot{i}_{(Air)_g}) + \text{div}(\rho_{Air}^g \cdot H_{Air} \cdot \underline{q}_l + \dot{i}_{(Air)_d}) - Q_{(Air)} = 0$$

$Q_{(Air)}$: Production – consumption of air

23/01/2020

EURAD School for Radioactive Waste Management / GAS & HITEC



UNSATURATED HM PROBLEM AT CONSTANT TEMPERATURE

Liquid phase: *Liquid water + Dissolved air*

➤ Liquid phase advection (unsaturated Darcy's flow) $\underline{q}_l = -\frac{kk_r^w(S_{r,w})}{\mu_w}(\nabla p_w + \rho_w g \nabla z)$

➤ Dissolved air diffusion (Fick's law) $\underline{i}_{(Ar)_d} = -\rho_w S_{r,w} D_{Ar}^{H_2O} \nabla \left(\frac{\rho_{Ar}^w}{\rho_w} \right)$

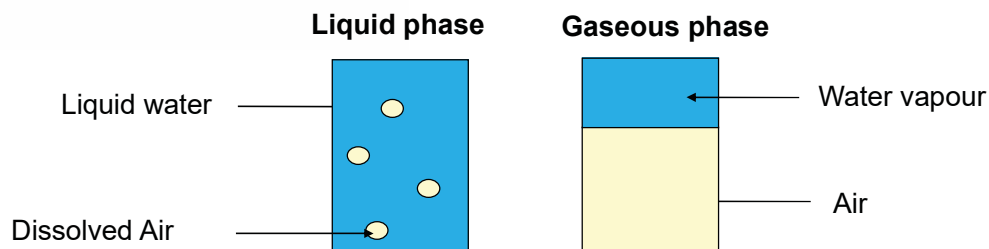
$$\text{Henry's law} \quad \rho_{Ar}^w = H_{Ar}(T) \cdot \rho_{Ar}^g$$

Gaseous phase: *Water vapour + dry air*

➤ Gaseous phase advection $\underline{q}_g = -\frac{kk_r^g(S_{r,g})}{\mu_g}(\nabla p_g + \rho_g g \nabla z)$

➤ Dry air – water vapour diffusion $\underline{i}_{(Ar)_g} = -\rho_g S_{r,g} D_{Ar}^{vapeur} \nabla \left(\frac{\rho_{Ar}^g}{\rho_g} \right) = -\underline{i}_{(H_2O)_g}$

UNSATURATED HM PROBLEM AT CONSTANT TEMPERATURE



Water mass balance $\text{div}(\underline{f}_{-w}) + \text{div}(\underline{f}_{-v}) + \dot{S}_w + \dot{S}_v - Q_{H_2O} = 0$

Air mass balance $\text{div}(\underline{f}_{-a}) + \text{div}(\underline{f}_{-a-d}) + \dot{S}_a + \dot{S}_{a-d} - Q_a = 0$

Momentum balance $\text{div}(\underline{\sigma}_{ij}) + \rho g_i = 0$

For the description of the H²M FE in the Lagamine code see:
Thermo-hydro-mechanical coupling in clay barriers. F Collin, XL Li, JP Radu, R Charlier - Engineering Geology, 2002

UNSATURATED HM PROBLEM AT CONSTANT TEMPERATURE

As an extension of the hydro-mechanical problem, the stiffness matrix of the MWAT2 element has the following expression:

$$\begin{bmatrix} F_x^{HE} \\ F_y^{HE} \\ F_{p_w}^{HE} \\ F_{p_g}^{HE} \end{bmatrix} = \underline{\underline{K}} \begin{bmatrix} du_x \\ du_y \\ dp_w \\ dp_g \end{bmatrix} = \underline{\underline{K}} = \begin{bmatrix} K_{MM}(2 \times 2) & K_{WM}(2 \times 1) & K_{GM}(2 \times 1) \\ K_{MW}(1 \times 2) & K_{WW}(1 \times 1) & K_{GW}(1 \times 1) \\ K_{MG}(1 \times 2) & K_{WG}(1 \times 1) & K_{GG}(1 \times 1) \end{bmatrix}$$

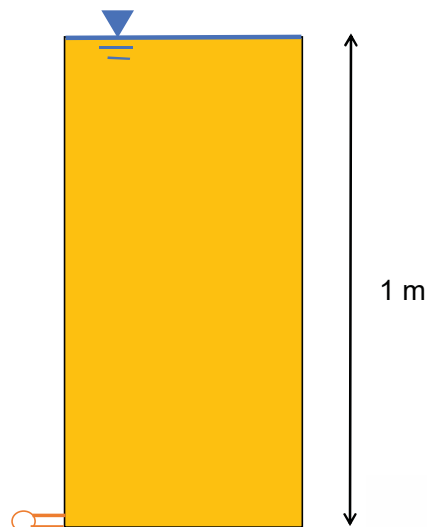
Knowing that the order of magnitude of the out of balance forces for the mechanical problem, and the flow problems are really different, it is therefore necessary to sum the norm of each problem computed separately:

$$\|F^{HE}\| = \|F^{HE}\|^{Meca} + \|F^{HE}\|^{hydro+air}$$

APPLICATION OF UNSATURATED HM PROBLEM (CONSTANT TEMP.)

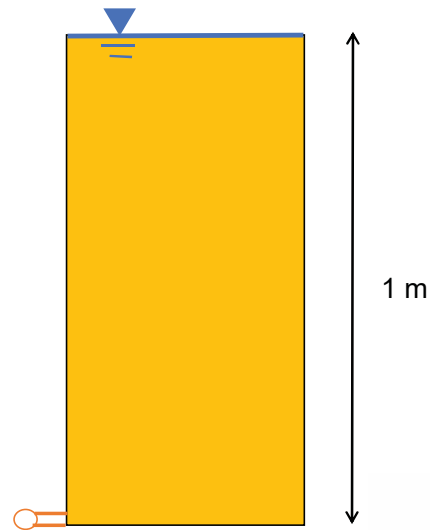
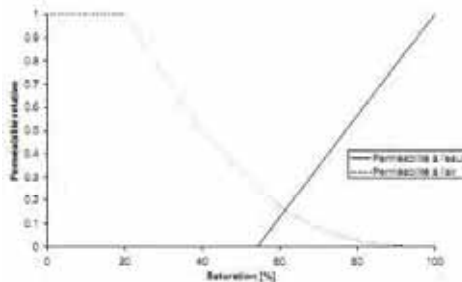
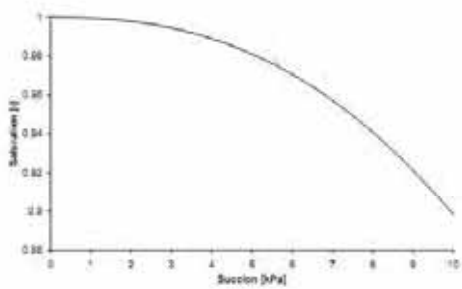
Liakopoulos (1965) experiment on a column of del Monte sand

Benchmark exercise*



- JOMMI C., VAUNAT J., GENS A., GAWIN D. & SCHREFLER B. – Multiphase flow in porous media : a numerical benchmark – Proceedings NAFEMS World Congress Stuttgart, 1997.
- VAUNAT J., GENS A. & JOMMI C. – A Strategy for Numerical Analysis of the Transition between Saturated and Unsaturated Flow Conditions – Numerical Models in Geomechanics, pp. 297-302, 1997.

APPLICATION OF UNSATURATED HM PROBLEM (CONSTANT TEMP.)



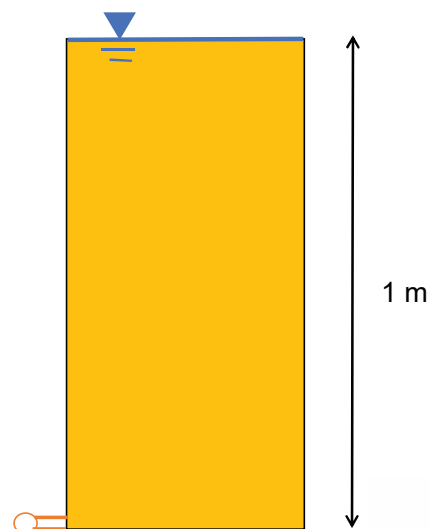
23/01/2020

EURAD School for Radioactive Waste Management / GAS & HITEC

APPLICATION OF UNSATURATED HM PROBLEM (CONSTANT TEMP.)

Non linearities induced by the retention curve.

Time derivation of the storage term induces excessive mass balance error if direct chain rule is used -> **use of numerical discretization of the time derivative.**



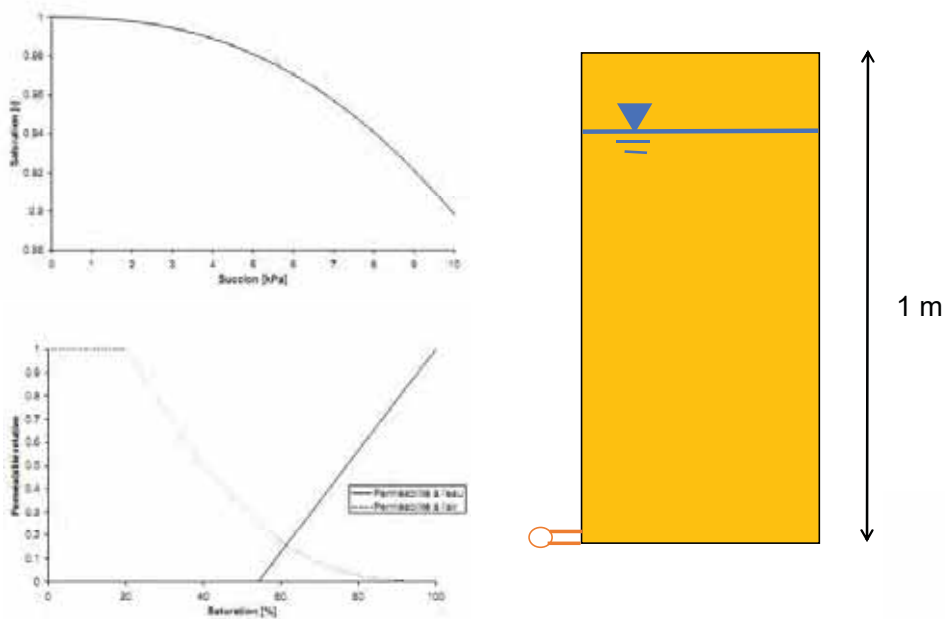
- Sanavia L., Pesavento F., Schrefler B.A. Finite element analysis of non-isothermal multiphase geomaterials with application to strain localization simulation, Computational Mechanics, 37(4), 331-348 (2006)
- Celia M.A., Bouloutas E.T., Zarba R.L., A general Mass-conservative Numerical Solution for the Unsaturated flow Equation, Water Resources Research, Vol 26(7), pp. 1483-1496 (1990)

23/01/2020

EURAD School for Radioactive Waste Management / GAS & HITEC



APPLICATION OF UNSATURATED HM PROBLEM (CONSTANT TEMP.)

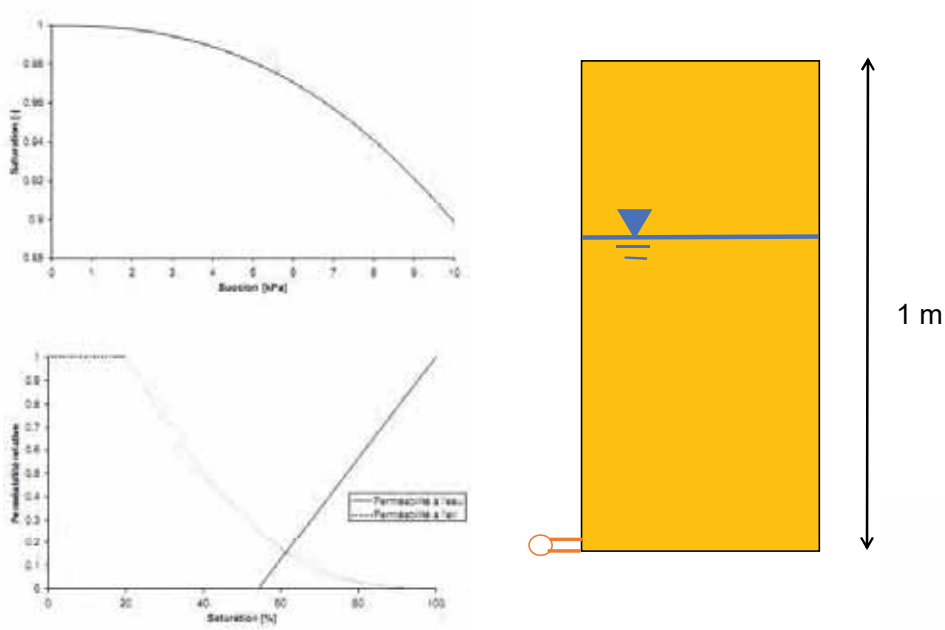


23/01/2020

EURAD School for Radioactive Waste Management / GAS & HITEC



APPLICATION OF UNSATURATED HM PROBLEM (CONSTANT TEMP.)



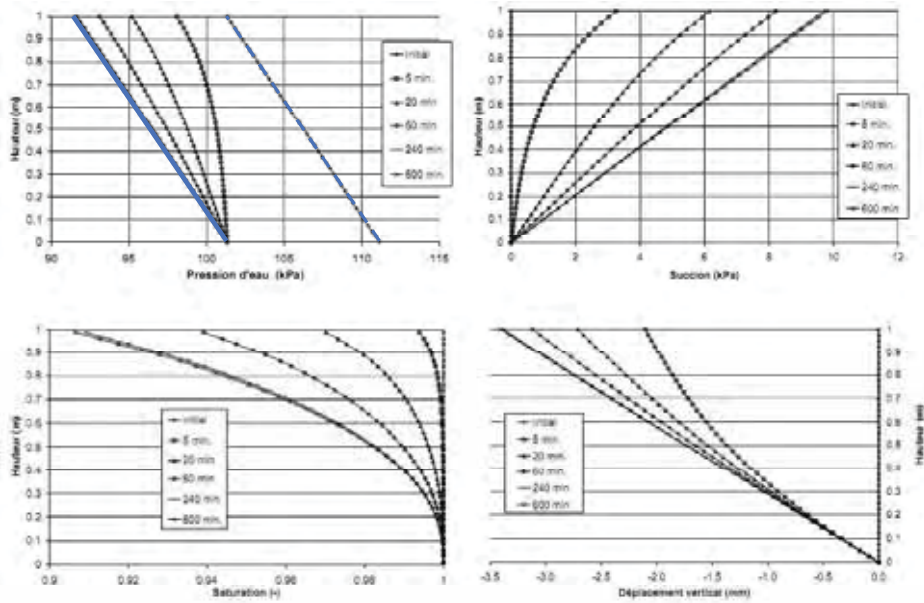
23/01/2020

EURAD School for Radioactive Waste Management / GAS & HITEC



APPLICATION OF UNSATURATED HM PROBLEM (CONSTANT TEMP.)

Modelling with fixed gas pressure

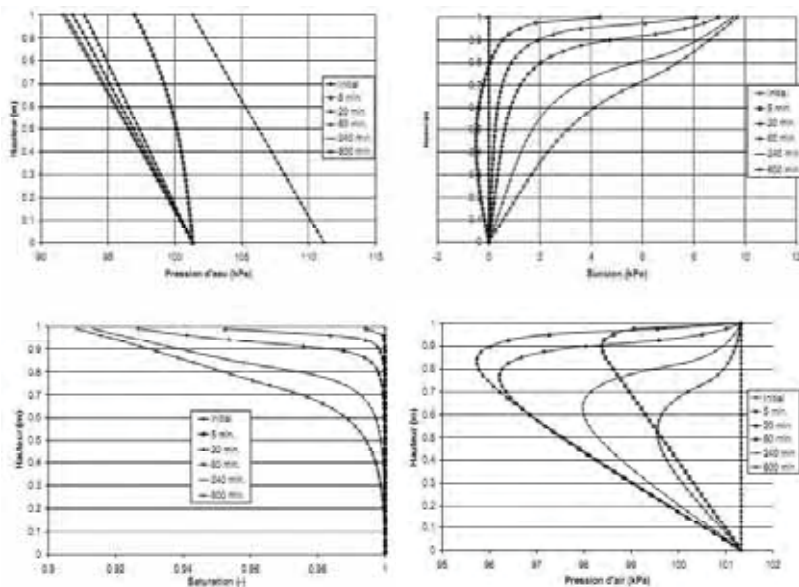


23/01/2020



APPLICATION OF UNSATURATED HM PROBLEM (CONSTANT TEMP.)

Modelling with variable gas pressure ($k_{r,min} < 0$ – without dissolved gas)



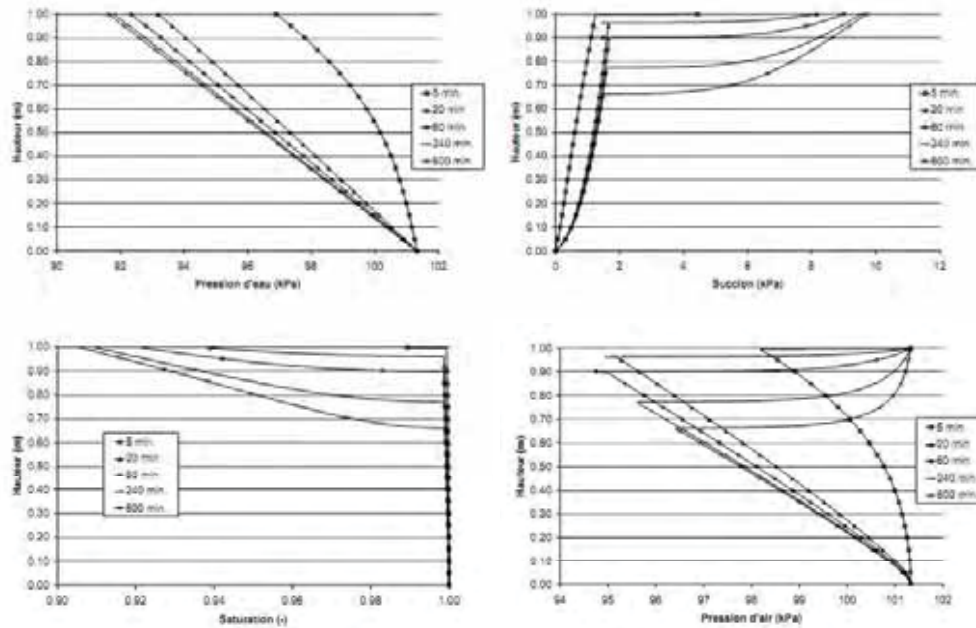
23/01/2020





APPLICATION OF UNSATURATED HM PROBLEM (CONSTANT TEMP.)

Modelling with variable gas pressure (+dissolved gas)



23/01/202



CONTENT

- Introduction
- Formulation of the flow problem
- Hydro-mechanical problem
- Hydro-mechanical problem in unsaturated conditions
- Thermo-hydro-mechanical problem

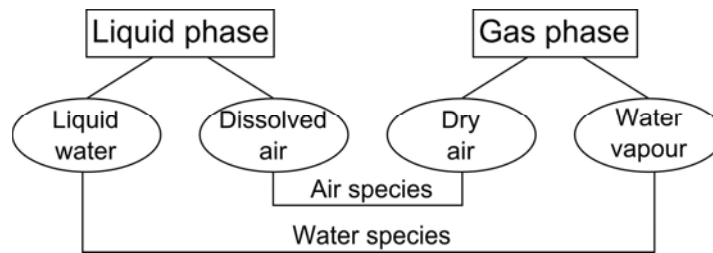
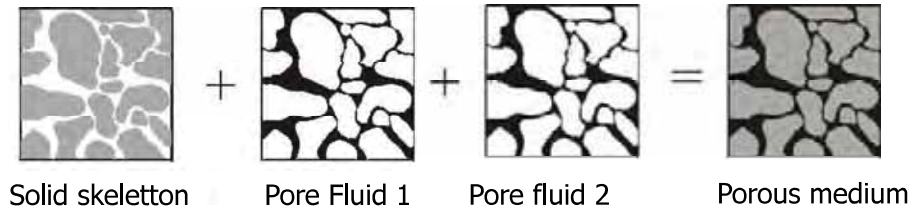
23/01/2020





UNSATURATED THM PROBLEM

THM porous medium



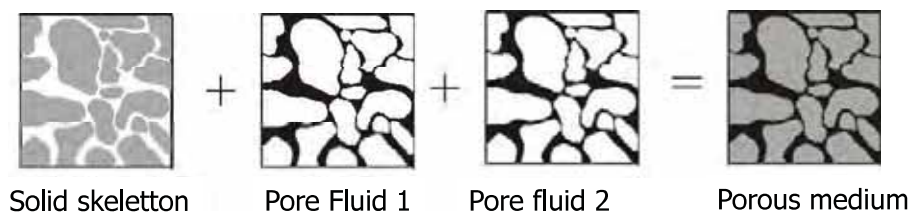
23/01/2020

EURAD School for Radioactive Waste Management / GAS & HITEC



UNSATURATED THM PROBLEM

THM porous medium



Assumptions:

A unique temperature T for the different species

Thermodynamic equilibrium between water vapour and liquid water

Thermodynamic equilibrium between dissolved air and dry air

23/01/2020

EURAD School for Radioactive Waste Management / GAS & HITEC



UNSATURATED THM PROBLEM

$$\text{Heat transfer: } \dot{S}_T + \dot{E}_{H_2O}^{W \rightarrow V} \cdot L + \text{div}(\underline{f}_T) - Q_T = 0$$

\dot{S}_T : Storage term of heat

\underline{f}_T : Heat flow

$\dot{E}_{Air}^{g \rightarrow d}$: Evaporation mass rate

Q_T : Production – consumption of heat

L : Evaporation Latent Heat

$$\underline{f}_T = \dot{i}_{cond} + \sum_i H_i \cdot \underline{f}_{-i}^{eff}$$

H_i : Enthalpy of species i

$$\dot{i}_{cond} = -\Gamma_m \cdot \underline{grad}(T)$$

\dot{i}_{cond} : Conductive heat flow

$$\text{Water vapour: } \dot{S}_{(H_2O)_g} + \text{div}(\underline{f}_{(H_2O)_g}) - \dot{E}_{H_2O}^{l \rightarrow g} = Q_{(H_2O)_g}$$

23/01/2020

EURAD School for Radioactive Waste Management / GAS & HITEC



UNSATURATED THM PROBLEM

$$\text{Heat transfer: } \dot{S}_T + \dot{E}_{H_2O}^{W \rightarrow V} \cdot L + \text{div}(\underline{f}_T) - Q_T = 0$$

\dot{S}_T : Storage term of heat

\underline{f}_T : Heat flow

$\dot{E}_{Air}^{g \rightarrow d}$: Evaporation mass rate

Q_T : Production – consumption of heat

L : Evaporation Latent Heat

$$\underline{f}_T = \dot{i}_{cond} + \sum_i H_i \cdot \underline{f}_{-i}^{eff}$$

H_i : Enthalpy of species i

$$\dot{i}_{cond} = -\Gamma_m \cdot \underline{grad}(T)$$

\dot{i}_{cond} : Conductive heat flow

$$\Rightarrow \dot{S}_T + \dot{S}_v \cdot L + \text{div}(\underline{V}_v) \cdot L + \text{div}(\dot{i}_{cond}) + \sum_i H_i \cdot \underline{V}_{-i}^{eff} - Q_T = 0$$

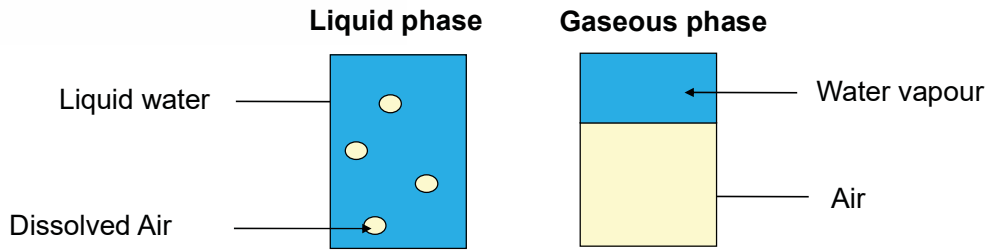
$Q_{(Air)}$: Production – consumption of heat

23/01/2020

EURAD School for Radioactive Waste Management / GAS & HITEC



UNSATURATED THM PROBLEM



Water mass balance $div(\underline{f}_{-w}) + div(\underline{f}_{-v}) + \dot{S}_w + \dot{S}_v - Q_{H_2O} = 0$

Air mass balance $div(\underline{f}_{-a}) + div(\underline{f}_{-a-d}) + \dot{S}_a + \dot{S}_{a-d} - Q_a = 0$

Momentum balance $div(\sigma_{ij}) + \rho g_i = 0$

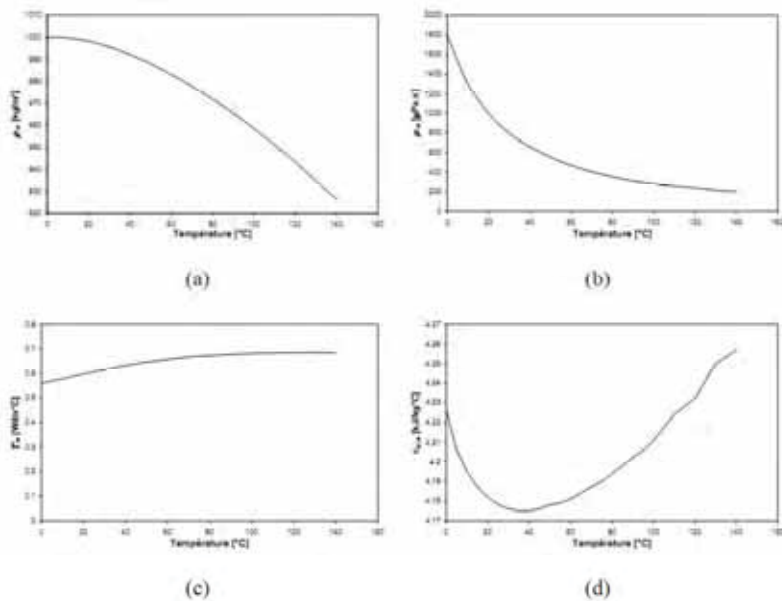
Energy balance $\dot{S}_T + \dot{E}_{H_2O}^{W \rightarrow V} \cdot L + div(\underline{f}_{-T}) - Q_T = 0$

23/01/2020

EURAD School for Radioactive Waste Management / GAS & HITEC

UNSATURATED THM PROBLEM

Liquid water properties



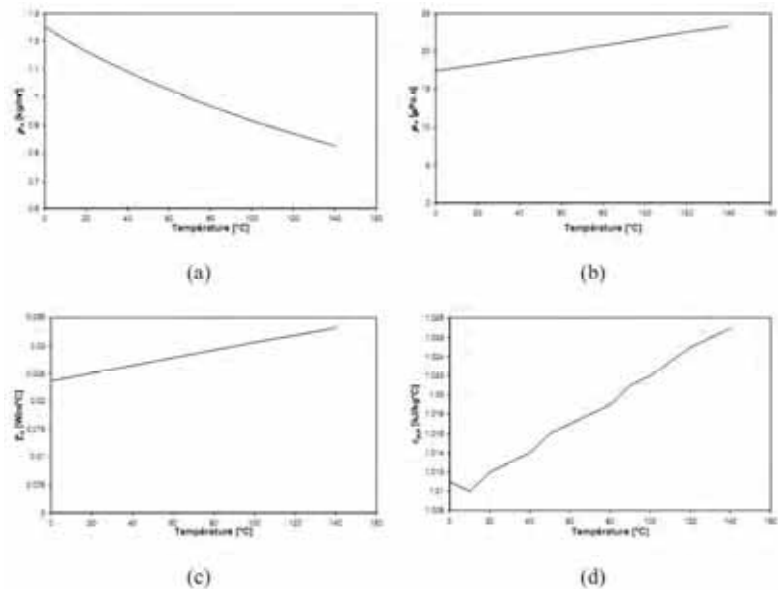
23/01/2020

EURAD School for Radioactive Waste Management / GAS & HITEC



UNSATURATED THM PROBLEM

Dry air properties



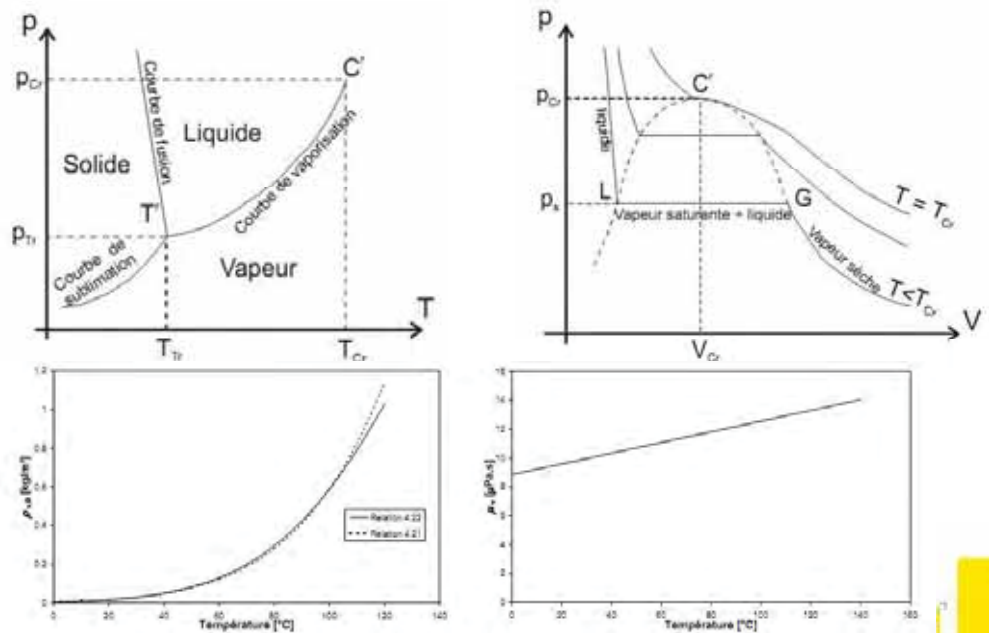
23/01/2020

EURAD School for Radioactive Waste Management / GAS & HITEC



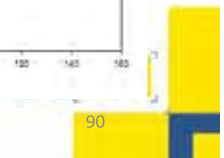
UNSATURATED THM PROBLEM

Water vapour properties



23/01/2020

EURAD School for Radioactive Waste Management / GAS & HITEC



UNSATURATED THM PROBLEM

As an extension of the hydro-mechanical problem, the stiffness matrix of the MWAT2 element has the following expression:

$$\begin{bmatrix} F_x^{HE} \\ F_y^{HE} \\ F_{p_w}^{HE} \\ F_{p_g}^{HE} \\ F_T^{HE} \end{bmatrix} = \underline{\underline{K}} \begin{bmatrix} du_x \\ du_y \\ dp_w \\ dp_g \\ dT \end{bmatrix} \quad \underline{\underline{K}} = \begin{bmatrix} K_{MM}(2 \times 2) & K_{WM}(2 \times 1) & K_{GM}(2 \times 1) & K_{TM}(2 \times 1) \\ K_{MW}(1 \times 2) & K_{WW}(1 \times 1) & K_{GW}(1 \times 1) & K_{TW}(1 \times 1) \\ K_{MG}(1 \times 2) & K_{WG}(1 \times 1) & K_{GG}(1 \times 1) & K_{TG}(1 \times 1) \\ K_{MT}(1 \times 2) & K_{WT}(1 \times 1) & K_{GT}(1 \times 1) & K_{TT}(1 \times 1) \end{bmatrix}$$

Knowing that the order of magnitude of the out of balance forces for the mechanical problem, the flow and the heat problem are really different, it is therefore necessary to sum the norm of each problem computed separately:

$$\|F^{HE}\| = \|F^{HE}\|^{Meca} + \|F^{HE}\|^{hydro+air} + \|F^{HE}\|^{Thermal}$$

APPLICATION OF A SATURATED THM PROBLEM

General framework of ATLAS experiment at Mol URL

ATLAS (Admissible Thermal Loading for Argillaceous Storage)

- ATLAS I & II

Part of the EC INTERCLAY-II project (1990-1994)
An experiment for modellers (blind predictions)

- ATLAS III (April 2007 → April 2008) – EC TIMODAZ project

Investigate the characterisation of the effect of thermal loading on thermo-hydro-mechanical properties of Boom Clay (thermal conductivity, THM coupling in clay...)

Heating
borehole



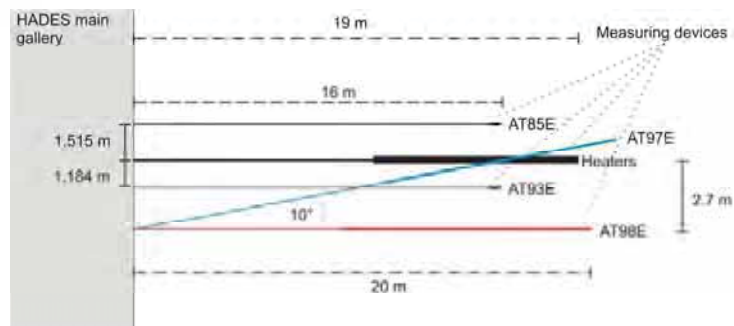
Installation of
instrumentation in
observation borehole



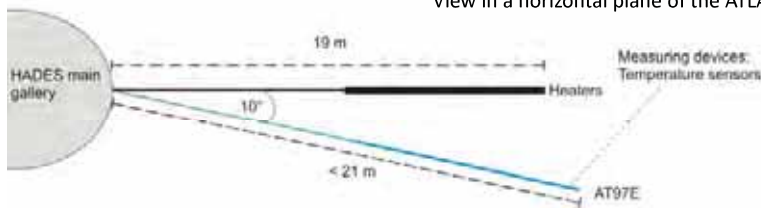
APPLICATION OF A SATURATED THM PROBLEM

ATLAS III

- 2 new boreholes
 - AT98E (P_w , T)
 - AT97E (T)



View in a horizontal plane of the ATLAS experiment



View in a vertical plane of the ATLAS experiment

23/01/2020

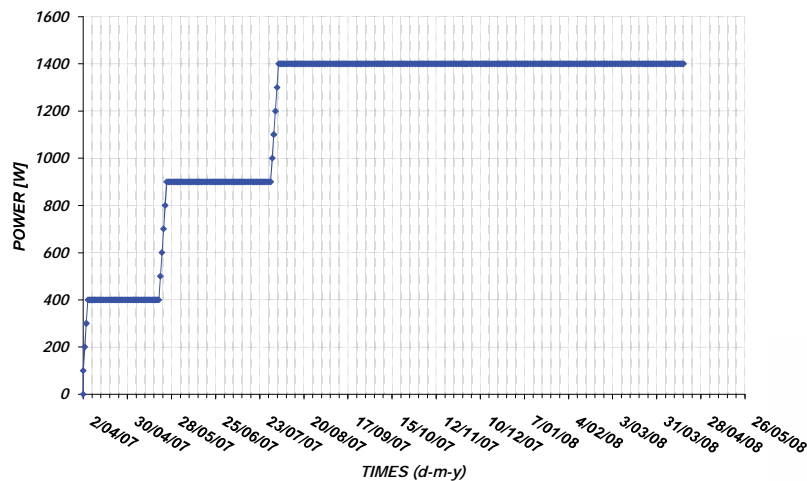
EURAD School for Radioactive Waste Management / GAS & HITEC



APPLICATION OF A SATURATED THM PROBLEM

Power evolution during **ATLAS III**

Heating phase in 3 steps: 7 weeks, 10 weeks, 43 weeks



23/01/2020

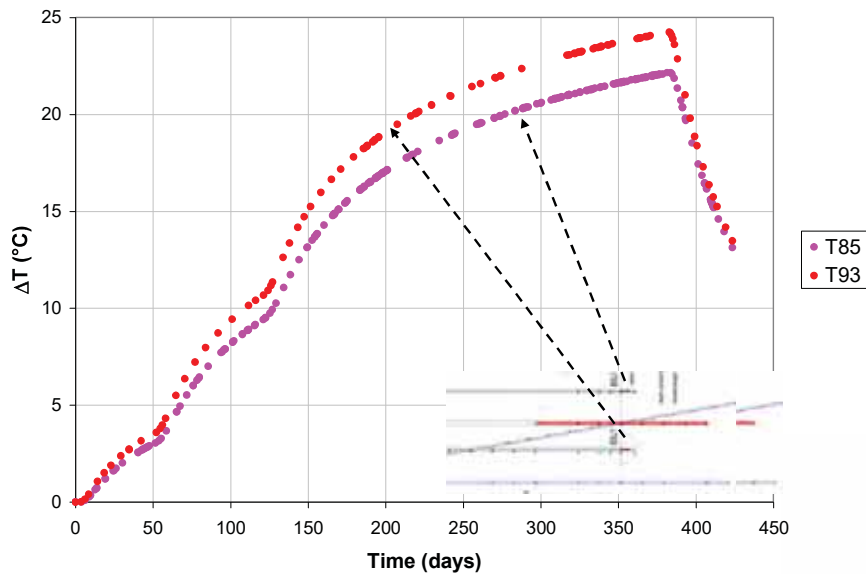
EURAD School for Radioactive Waste Management / GAS & HITEC





APPLICATION OF A SATURATED THM PROBLEM

Results *ATLAS III*: evolution of the temperature with time



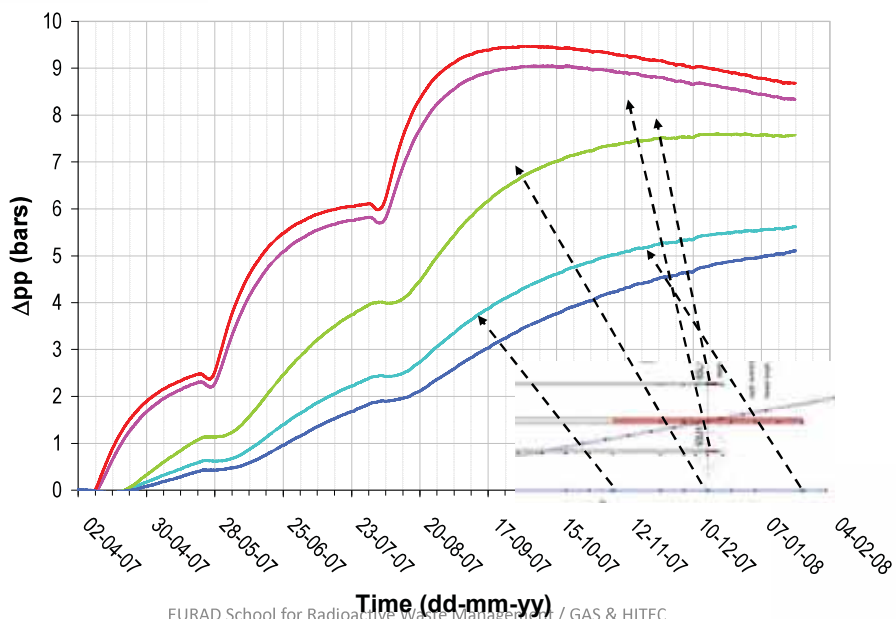
23/01/2020

EURAD School for Radioactive Waste Management / GAS & HITEC



APPLICATION OF A SATURATED THM PROBLEM

Results *ATLAS III*: evolution of pore pressure with time



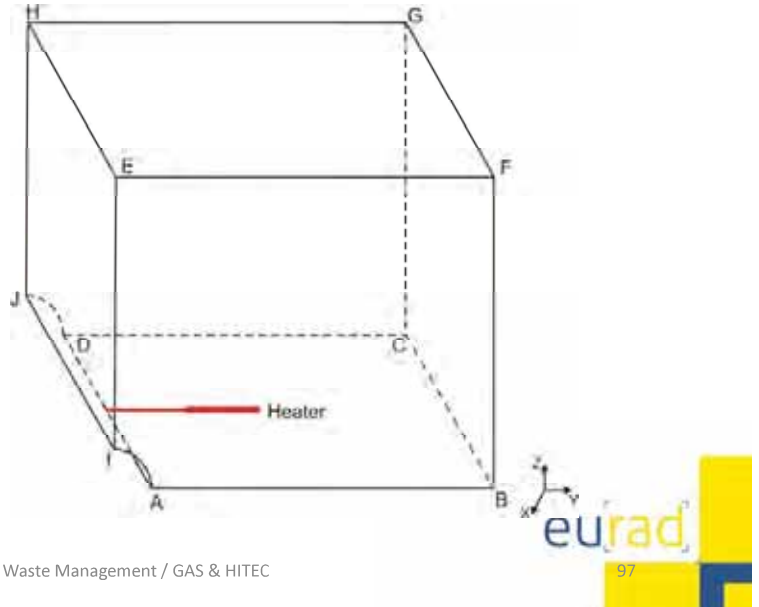
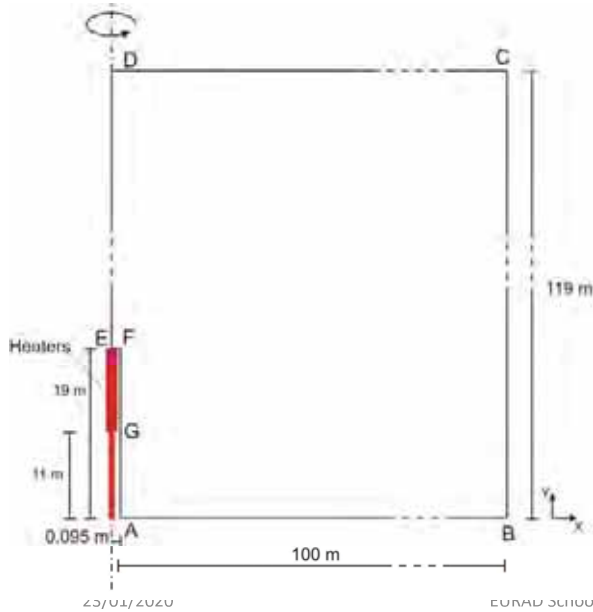
23/01/2020

EURAD School for Radioactive Waste Management / GAS & HITEC



APPLICATION OF A SATURATED THM PROBLEM

Prediction *ATLAS III: choice of the FE model (2D vs 3D)*

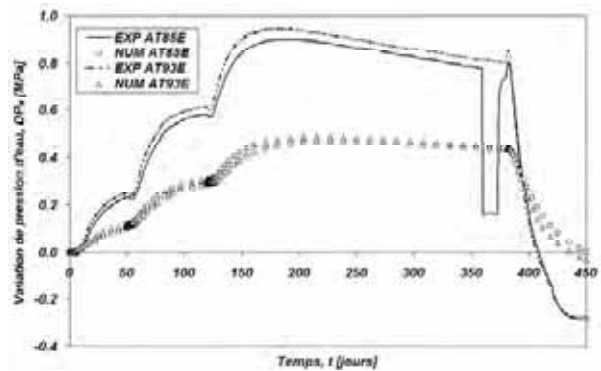
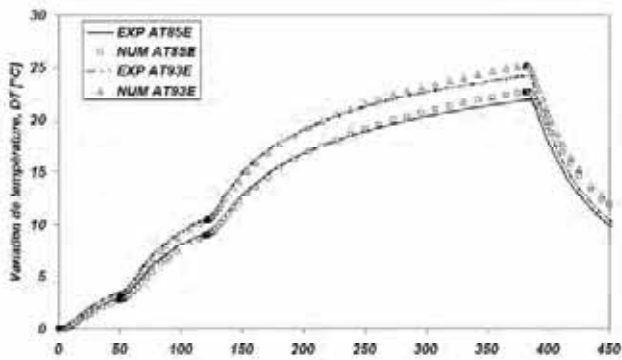


EURAD School for Radioactive Waste Management / GAS & HITEC

97

APPLICATION OF A SATURATED THM PROBLEM

Prediction *ATLAS III: 2D axisymmetric model*



- ATLAS III in situ heating test in boom clay: Field data, observation and interpretation. GJ Chen, X Sillen, J Verstricht, XL Li - Computers and Geotechnics, 2011
- DIZIER A. – CARACTÉRISATION DES EFFETS DE TEMPÉRATURE DANS LA ZONE ENDOMMAGÉE AUTOUR DE TUNNELS DE STOCKAGE DE DÉCHETS NUCLÉAIRES DANS DES ROCHES ARGILEUSES – PhD thesis, 2011.

23/01/2020

EURAD School for Radioactive Waste Management / GAS & HITEC

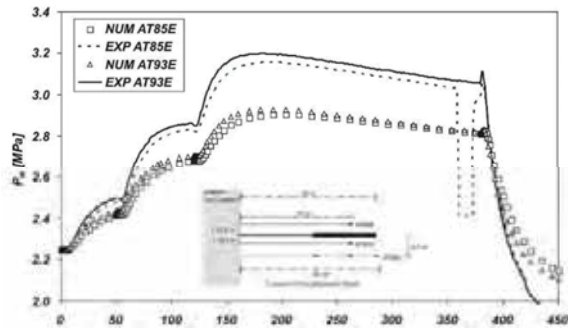
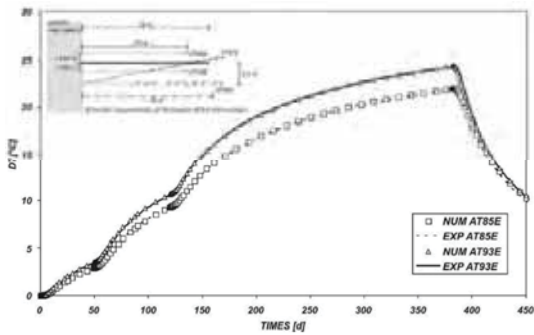
eurad

98



APPLICATION OF A SATURATED THM PROBLEM

Prediction *ATLAS III: 3D with anisotropic constitutive model*



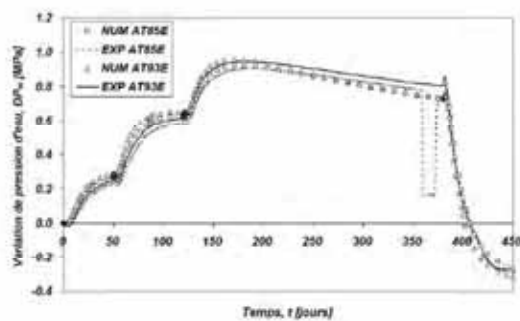
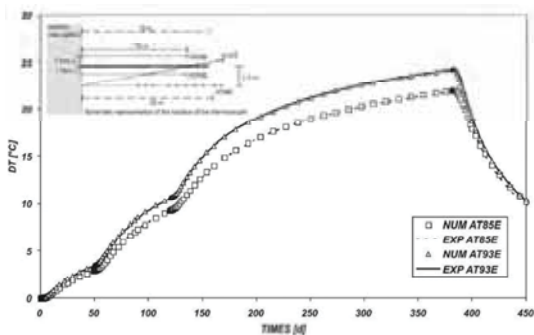
23/01/2020

EURAD School for Radioactive Waste Management / GAS & HITEC



APPLICATION OF A SATURATED THM PROBLEM

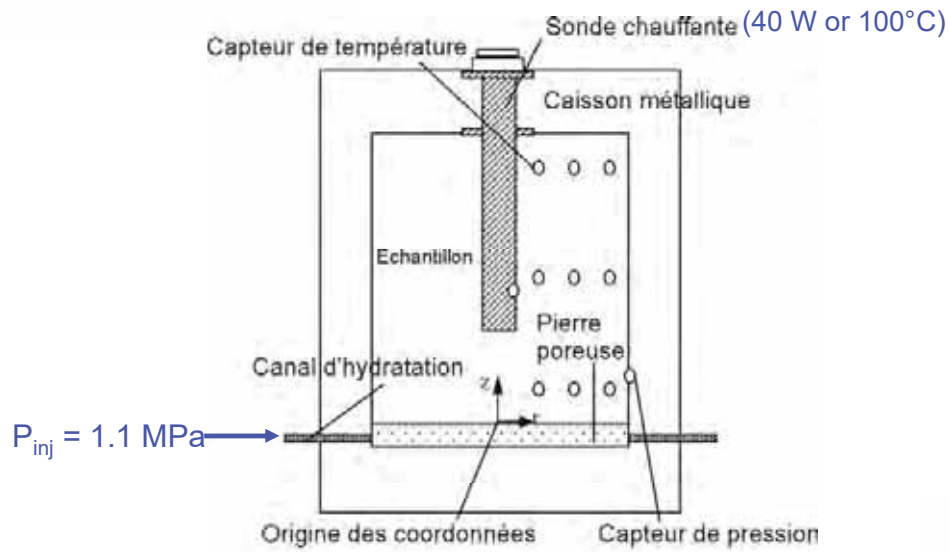
Prediction *ATLAS III: 3D with anisotropic constitutive model and small strain stiffness*



23/01/2020

EURAD School for Radioactive Waste Management / GAS & HITEC

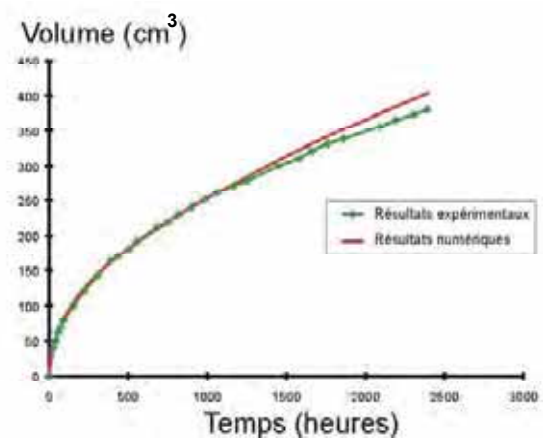
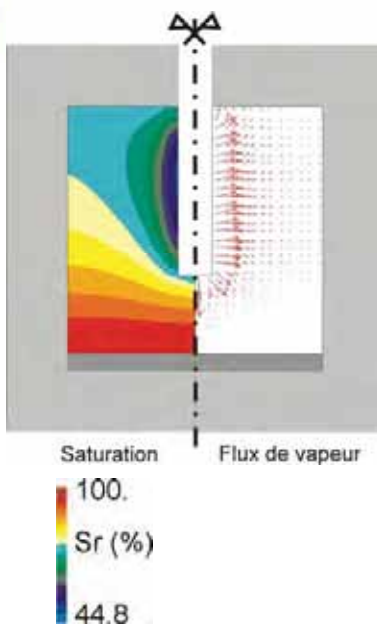
APPLICATION OF AN UNSATURATED THM PROBLEM



23/01/2020

EURAD School for Radioactive Waste Management / GAS & HITEC

APPLICATION OF AN UNSATURATED THM PROBLEM

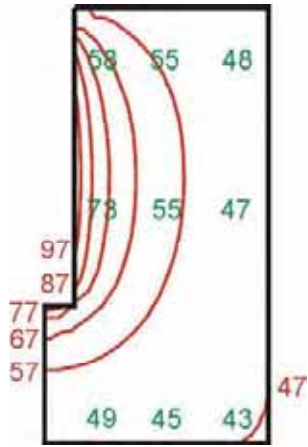


23/01/2020

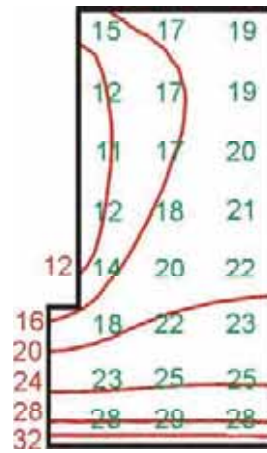
EURAD School for Radioactive Waste Management / GAS & HITEC



APPLICATION OF AN UNSATURATED THM PROBLEM



Temperature [°C]



Water content [%]

Appendix I. Numerical modelling of coupled transient phenomena (F. Collin)

Numerical modelling of coupled transient phenomena

Robert Charlier, Jean-Pol Radu and Frédéric Collin

Université de Liège, Institut de Génie Civil et de Mécanique, Chemin des Chevreuils 1, 4000 Liège - Sart Tilman, Belgique – E-mail: Robert.Charlier@ulg.ac.be

ABSTRACT. The basic phenomena involved in thermo-hydro-mechanical processes in geomaterials have been described in the 1st chapter. The equations describing these phenomena are non-linear differential equations. Their solution can generally only be approximated thanks to numerical methods. This is the main subject of the present chapter. First the type of problems and the set of equations to be solved will be shortly recalled. Emphasis will be given on the non-linear contributions. In a second section, the mostly developed numerical method, i.e. the finite difference and the finite element methods will be discussed under the light of the problems to be treated. The iterative techniques allowing the solution of non linear equations will be described. A third section will be dedicated to the coupling terms and to their modelling. The question that rises then is How to model efficiently problems, which may differ highly from, the point of view of the time and length scales?

KEY WORDS: Finite element method, iterative methods, non-linear phenomena, coupled phenomena.

1. Introduction – problems to be treated

We are here interested in a number of different physical phenomena (Gens, 2001), including:

- The non-linear solid mechanics, and especially the soil, rock or concrete mechanics: We consider the relations between displacements, strains, stresses and forces within solids. The material behaviour is described by a constitutive model, which can take into account elastoplasticity or elasto-visco-plasticity. On the other hand, large transformations and large strains may lead to geometrical non-linearities.
- The fluid flow within porous media: Fluid can be a single phase of various natures (water, air, gas, oil, ...) or it can be an association of two fluids, leading to unsaturated media (water and air, oil and gas, oil and water,...). In the second case, partial saturation is leading to permeability and storage terms depending on the saturation degree or on the suction level, involving non-linear aspects.
- The thermal transfers within porous media. Conduction is the leading process in solid (in the geomaterial matrix), but convection can also occur in the porous volume, as a consequence of the fluid flow. Radiation transfer could also occur inside the pores, but it will be neglected here. Conduction coefficients and latent heat may depend on the temperature.
- The pollutant transport or any spatial transfer of substance thanks to the fluid flow. The pollutant concentration may be high enough to modify the densities, involving non-linear effects.

All these problems are non-linear ones, and can be formulated with sets of partial differential equations. Moreover only three types of differential equations have to be considered, concerning respectively i) solid mechanics, ii) diffusion and iii) advection-diffusion problems.

1.1. Solid mechanics

On the one hand, solid mechanics can be modelled on the following basis. The equilibrium equation is:

$$\partial_i \sigma_{ij} + P_j = 0 \quad [1]$$

where \underline{P} is the vector of volume forces, $\underline{\sigma}$ is the Cauchy's stress tensor and ∂ represents the spatial partial derivative operator:

$$\partial_i \equiv \frac{\partial}{\partial x_i} \quad [2]$$

The stress tensor is obtained thanks to the time integration of a (elastic, elastoplastic or elasto-visco-plastic) constitutive equation (Laloui, 2001 ; Coussy, 2001):

$$\dot{\sigma}_{ij} = fct(\sigma, D, k) \quad [3]$$

where $\check{\underline{\sigma}}$ is the stress rate, \underline{D} is the strain rate and k is a set of history parameters (state variables, like e.g. the preconsolidation stress). In the most classical case of elastoplasticity, this equation reduces to :

$$\check{\underline{\sigma}}_{ij} = C_{ijkl} D_{kl} \quad [4]$$

Most constitutive equations for geomaterials are non-linear ones.

When modelling a solid mechanics problem with the finite element method, the most used formulation is based on displacements \underline{u} or on actualised coordinates \underline{x} . If one considers only small strains and small displacements, the strain rate reduces to the well-known Cauchy's strain rate :

$$D_{ij} = \dot{\epsilon}_{ij} = \frac{1}{2} (\partial_i \dot{u}_j + \partial_j \dot{u}_i) \quad [5]$$

However, if large strains are to be considered, the preceding equations have to be reconsidered. The stress – strain rate couple has to be more precisely defined, with respect to the configuration evolution. Among multiple other choices (cf. Piola-Kirchoff stress – Green strain), we will only consider here the Cauchy's stress and the Cauchy's strain rate. These tensors are defined in global axis in the current configuration, which is continuously deforming. If we note \underline{X} the coordinates in a reference state¹, and \underline{x} the coordinates in the current configuration (figure 1), we can define the Jacobian tensor of the transformation :

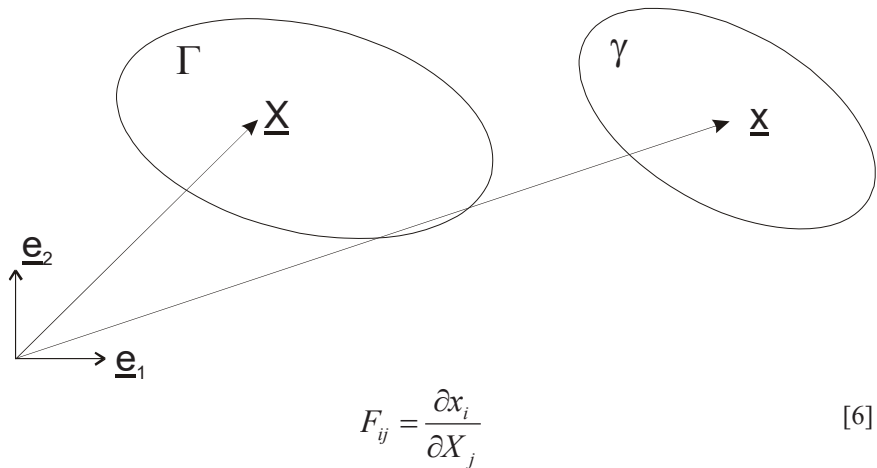


Figure 1 : initial and current configurations

The velocity gradient is defined as :

¹ An initial one. However initial state in geomechanics is always arbitrary.

$$\underline{L} = \frac{\partial \underline{u}}{\partial \underline{X}} = \dot{\underline{F}} \underline{F}^{-1} \quad [7]$$

The symmetric part of the velocity gradient is the strain rate associated to the Cauchy's stress :

$$\underline{D} = \text{sym}(\underline{L}) = \frac{1}{2}(\underline{L} + \underline{L}^T) \quad [8]$$

The material stress evolution must then be described as a function of the strain rate, thanks to a constitutive equation [3]. This subject is described in other chapters of this book. However, as the Cauchy's stress tensor is defined in global axis, the solid rotations will modify the tensor Cartesian components. This evolution is not linked to strains and so is not described by the constitutive equation. Among other possibilities, the Jaumann's objective derivative of the stress is a good component update :

$$\dot{\underline{\sigma}} = \frac{D\underline{\sigma}}{dt} = \check{\underline{\sigma}} + \underline{\omega} \underline{\sigma} + \underline{\sigma} \underline{\omega}^T \quad [9]$$

$$\underline{\omega} = \text{skw}(\underline{L}) = \frac{1}{2}(\underline{L} - \underline{L}^T) \quad [10]$$

Such large strain model [6-10] is non-linear.

Time dimension is not to be addressed for solid mechanics problems, unless when viscous term are considered in the constitutive model. Generally, the time that appears in the time derivatives in [3,4,5,7-10] is only a formal one.

1.2. Diffusion

Fluid flow in porous media and thermal conduction exchanges in solids are modelled thanks to similar diffusion equations.

The balance equation writes :

$$\partial_i f_i + Q = \dot{S} \quad [11]$$

where f represents a flux of fluid or heat, Q represents a sink term and S represents the storage of fluid or of heat. When modelling a diffusion problem with the finite element method, the most used formulation is based on fluid pore pressure p or on temperature T .

Then the Darcy's law for fluid flow in porous media gives the fluid flux :

$$f_i = -\frac{k}{\mu} (\partial_i p + \partial_i \rho g z) \quad [12]$$

with the intrinsic permeability k (possibly depending on the saturation degree), the dynamic viscosity μ , the density ρ , and the gravity acceleration g . The fluid storage term depends on the saturation degree S_r and on the fluid pressure :

$$\dot{S} = fct(p, S_r) \quad [13]$$

For thermal conduction one obtains the Fourier's law :

$$f_i = -\lambda \partial_i T \quad [14]$$

with the conductivity coefficient λ . The heat storage (enthalpy) term depends on the temperature :

$$\dot{S} = fct(T) \quad [15]$$

The diffusion problem is non linear when :

- the permeability depends (directly or indirectly) on the fluid pore pressure,
- the fluid storage is a non-linear function of the pore pressure,
- partial saturation occurs,
- the conductivity coefficient depends on the temperature,
- the enthalpy is a non-linear function of the temperature.

When the storage term is considered, time dimension of the problem has to be addressed.

1.3. Advection – diffusion

Transport of pollutant or of heat in porous media is governed by a combination of advection and diffusion (Thomas, 2001). Advection phenomenon is related to the transport (noted as a flow f_{adv}) of any substance by a fluid flow, described by its velocity f_{diff}^{fluid} :

$$f_{adv} = C f_{diff}^{fluid} \quad [16]$$

The substance concentration C is generally supposed to be small enough not to influence the fluid flow. In porous media, due to the pores network tortuosity and to the friction, advection is always associated to a diffusion characterised by diffusion – dispersion tensor \underline{D} . Therefore, the total flux of substance is :

$$f_{i,adv} = C f_{diff}^{fluid} - \lambda \underline{D} \partial_i C \quad [17]$$

Balance equation and storage equations may be written in a similar way to the one for diffusion problems [11,13,15].

Compared to diffusion constitutive law [12,14], it appears here an advection term which doesn't depend on the concentration gradient, but directly on the concentration. This is modifying completely the nature of the equations to be solved. Problems dominated by advection are very difficult to solve numerically (Charlier and Radu, 2001). In order to evaluate the relative advection effect, it is useful to evaluate the Peclet's number, which is a ratio between diffusive and advective effects :

$$Pe = \frac{f_{diff}^{fluid} h}{2D} \quad [18]$$

where h is an element dimension.

1.4. Boundary conditions

In the preceding section, differential equations were given for three types of problems. Solving these equations needs to define boundary and initial conditions. Classical boundary conditions may be considered : imposed displacements or forces for solid mechanics problems, imposed fluid pressures / temperatures / concentrations or imposed fluxes for diffusion and advection – diffusion problems.

However, it may be useful to consider much complex boundary conditions. For example, in solid mechanics, unilateral contact with friction or interface behaviour is often to be considered.

When coupling phenomena, the question of boundary conditions rises in complexity and has to be discussed.

On the other hand, initial conditions are often difficult to determine in geomechanics. Consider for example the problem of initial stress state. A long discussion may be proposed with respect for example to the long-term tectonic effect (Barnichon, 1998).

2. Numerical tools : the finite element method

2.1. Introduction

An approximated solution of most problems described by a set of partial differential equations may be obtained thanks to numerical method like the finite element method (FEM), the discrete element method (DEM), the finite difference method (FDM), the finite volume method (FVM), or the boundary element method (BEM). For the problems concerned here, the most used methods are the finite element one and the finite difference one.

Non-linear solid mechanics is better solved thanks to the finite element method. Boundary element methods have strong limitation in the non-linear field. Finite difference methods are not easy to apply to tensorial equations (with the exception of the FLAC code, developed by Itasca).

Diffusion and advection – diffusion problems are often solved by finite difference or finite element method. Some finite difference codes are very popular for fluid flow, like e.g. *MODFLOW* for aquifer modelling or *ECLIPSE* (Eclipse, 2000) for oil reservoir modelling. These codes have been developed for a number of years and possess a number of specific features allowing taking numerous effects into account. However, they suffer from some drawbacks, which limit their potentialities for modelling coupled phenomena. Therefore we will only give little information about finite differences.

2.2. Finite element method

The basic idea of the finite element method is to divide the field to be analysed into sub-domains, the so-called *finite elements*, of simple shape : e.g. triangles, quadrilaterals with linear, parabolic, cubic sides for two-dimensional analysis. In each finite element, an analytical simple equation is postulated for the variable to be determined, i.e. the coordinate or displacement for solid mechanics, and the fluid pressure, temperature, concentration for diffusion problems. In order to obtain C_0 continuity, the unknown variable field has to be continuous at the limit between finite elements. This requirement is obtained thanks to common values of the field at specific points, the so-called *nodes*, which are *linking* the finite elements together. The field values at nodal points are the discretised problem unknowns.

For most solid mechanics and diffusion problems, isoparametric finite elements seem to be optimal (Zienkiewicz et al, 1989). The unknown field \underline{x} may then be written, for solid mechanics cases² :

$$\underline{x} = N_L(\xi, \eta) \underline{x}_L \quad L = 1, nnode \quad [19]$$

It depends on the nodal unknowns \underline{x}_L and on shape functions N_L , themselves depending on isoparametric coordinates ξ, η defined on a reference normalised space. Then the strain rate and the spin may be derived thanks to equations [8] and [10], the stress rate is obtained by [3], [4] and [9] and is time integrated. Eventually, equilibrium [1] has to be checked (§2.4).

For scalar diffusion or advection – diffusion problems, the unknown field p (we will use hereafter the pore pressure notation, however temperature T or concentration C could be also considered changing the notation) may then be written :

$$p = N_L(\xi, \eta) p_L \quad L = 1, nnode \quad [20]$$

It depends on the nodal unknowns p_L and on shape functions N_L . Then the fluid Darcy's velocity and the storage evolution may be derived thanks to equations [12] and [13] (respectively [14-15] or [16-17]). No time integration is required here. Eventually, balance equation [11] has to be checked (§2.4).

The finite element method allows an accurate modelling of the boundary condition, thanks to easily adapted finite element shape. Internal boundaries of any shape between different geological layers or different solids can be modelled. Specific finite elements for interfaces behaviour or for unilateral boundaries may have also been developed (e.g. Charlier et al, 1990). Variations of the finite element size and density over the mesh are also easy to manage thanks to present mesh generators.

2.3. Finite difference method

² For the sake of simplicity, we limit ourselves here to two-dimensional cases.

The finite difference method doesn't postulate explicitly any specific shape of the unknown field. As we are concerned with partial differential equations, exact derivative are replaced by an approximation based on neighbour values of the unknown :

$$\left(\frac{\partial p}{\partial x}\right)_i = \frac{p_{i+1} - p_{i-1}}{2h} \quad [21]$$

where the subscript i denotes the cell number and h denotes the cell size. For an orthogonal mesh, such derivatives are easily generalised to variable cell dimensions. However non-orthogonal meshes are asking question highly difficult to solve and are generally not used. Boundary conditions have then to be modelled by the juxtaposition of orthogonal cells, giving a kind of stairs for oblique or curved boundaries. Similarly, local refinement of the mesh induces irreducible global refinement. These aspects are the most prominent drawbacks of the finite difference method compared to the finite element one. On the other hand computing time is generally much lower with finite differences than with finite elements.

2.4. Solving the non-linear problem – the Newton Raphson method

Let us now concentrate on the finite element method. The fundamental equation to be solved is the equilibrium equation [1] (respectively the balance equation [11] for diffusion phenomena). As the numerical methods are giving an approximated solution, the equilibrium / balance equation has to be solved with the best compromise. This is obtained thanks to a global weak form of the local equation. Using weighted residuals, for solid mechanics, one obtains :

$$\int_V [\sigma_{ij} \delta \varepsilon_{ij}] dV = \int_V P_i \delta u_i dV + \int_A \bar{p} \delta u_i dA \quad [22]$$

And for diffusion phenomena :

$$\int_V [\dot{S} \delta p - f_i \partial_i (\delta p)] dV = \int_V Q \delta p dV + \int_A q \delta p dA \quad [23]$$

where \bar{p} and q are surface terms of imposed loads / fluxes. The weighting functions are denoted δu and δp . And $\delta \varepsilon$ represents a derivative of the weighting function based on the Cauchy's strain derivate operator. An equivalent equation could be obtained based on the virtual power principle. The δu and δp would then be interpreted as virtual arbitrary displacements and pressures. Within the finite element method, these global equilibrium / balance equation will be verified for a number of fundamental cases equivalent to the degrees of freedom (dof) of the problem, i.e. the number of nodes times the number of freedom degrees per node, minus to imposed values. The corresponding weighting functions will have simple forms based on the element shape functions³.

³ This concerns Galerkin's approximation. For advection dominated problems, other weighting function have to be used.

Giving a field of stress or of flux, using the weighting functions, one will obtain a value for each dof, which is equivalent to a nodal expression of the equilibrium / balance equation.

More precisely, for solid mechanics problems, one will obtain internal forces equivalent to stresses :

$$F_{Li}^{int} = \int_V \sigma_{ij} B_{Lj} dV \quad [24]$$

where B is a matrix of derivatives of the shape functions N . If equilibrium is respected from the discretised point of view, these internal forces are equal to external forces (if external forces are distributed, a weighting is necessary) :

$$F_{Li}^{int} = F_{Li}^{ext} \quad [25]$$

Similarly, for diffusion phenomena the nodal internal fluxes are equivalent to the local fluxes:

$$F_L^{int} = \int_V [\dot{S}N_L - f_i \partial_i N_L] dV \quad [26]$$

If the balance equation is respected from the discretised point of view, these internal fluxes are equal to external ones :

$$F_L^{int} = F_L^{ext} \quad [27]$$

However, as we are considering non linear-problems, equilibrium / balance cannot be obtained immediately, but needs to iterate. This means that the equations [25,27] are not fulfilled until the last iteration of each step.

Non-linear problems are solved for some decades, and different methods have been used. From our point of view, the Newton – Raphson is the reference method and probably the best one for a large number of problems. Let us describe the method. In the equation [25] the internal forces F^{int} are depending on the basic unknown of the problem, i.e. the displacement field. Similarly in equation [27] the internal fluxes are depending on the pressure (temperature, concentration, ...) field.

If they don't equilibrate the external forces / fluxes, the question to be treated can be formulated under the following form :

How should we modify the displacement field (the pressure field) in order to improve the equilibrium (the balance) as stated by equation [25,27] ?

Following the Newton – Raphson method, one develops the internal force as a first order Taylor's series around the last approximation of the displacement field :

$$F_{Li}^{int} = F_{Li}^{int}(u_{(i)}) + \frac{\partial F_{Li}^{int}}{\partial u_{Kj}} du_{Kj} + O^2 = F_{Li}^{ext} \quad [28]$$

This is a linearisation of the non-linear equilibrium equation. It allows obtaining a correction of the displacement field :

$$\Delta u_{Kj} = \left(\frac{\partial F_{Li}^{int}}{\partial u_{Kj}} \right)^{-1} (F_{Li}^{int}(u^{(i)}) - F_{Li}^{ext}) = K_{Li,Kj} (F_{Li}^{int}(u^{(i)}) - F_{Li}^{ext}) \quad [29]$$

The matrix noted $K_{Li,Kj}$ is the so-called stiffness matrix. With the corrected displacement field, one may evaluate new strain rates, new stress rates, and new improved internal forces. Equilibrium should then be improved.

The same meaning may be developed for diffusion problems : Taylor's development of the internal fluxes with respect to the pressures / temperatures / concentrations nodal unknowns.

The iterative process may be summarised as shown on figure 2 for one-dof solid mechanics problem. Starting from a first approximation of the displacement field $u_{(1)}$ one compute the internal forces $F_{(1)}^{int}$ (point $A^{(1)}$) that are lower then the imposed external forces F^{ext} . Equilibrium is then not fulfilled and a new approximation of the displacement field is searched. The tangent stiffness matrix is evaluated and an improved displacement is obtained $u_{(2)}$ (point $B^{(1)}$) [29]. One computes again the internal forces $F_{(2)}^{int}$ (point $A^{(2)}$) that are again lower then the external forces F^{ext} . As equilibrium is not yet fulfilled, a new approximation of the displacement field is searched $u_{(3)}$ (point $B^{(2)}$). The procedure has to be repeated until the equilibrium / balance equation is fulfilled with a given accuracy (numerical convergence norm). The process has a quadratic convergence, which is generally considered as the optimum numerical solution.

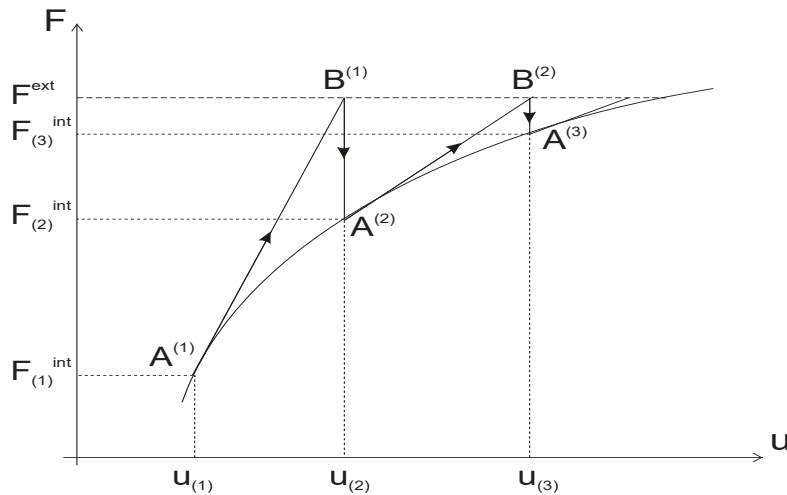


Figure 2 : illustration of the Newton – Raphson process

However the Newton – Raphson method has an important drawback : it needs important work to be developed as well as to be run on a computer. Especially the

stiffness matrix K is time consuming for the analytical development and for the numerical inversion. Therefore other methods have been proposed :

- Approximate stiffness matrix, in which some non-linear terms are neglected.
- Successive use of the same stiffness matrix avoiding new computation and inversion at each iteration

It should be noted that each alternative is reducing the numerical convergence rate. For some highly non-linear problems, the convergence may be loosed, and then no numerical solution may be obtained.

Some other authors, considering the properties and the efficiency of explicit time schemes in rapid dynamic (like for shocks modelling) add an artificial mass to the problem in order to solve it as a quick dynamic one. It should be clear that such technique might degrade the accuracy of the solution, as artificial inertial effects are added and the static equilibrium equation [1] is not checked.

2.5. The stiffness matrix

From equation [29], it appears that the stiffness matrix is a derivative of the internal forces :

$$K_{Li,Kj} = \frac{\partial F_{Li}^{int}}{\partial u_{Kj}} = \frac{\partial}{\partial u_{Kj}} \left(\int_V \sigma_{ij} B_{Lj} dV \right) \quad [30]$$

Two contributions will be obtained. On the one hand, one has to derive the stress state with respect with the strain field, itself depending on the displacement field. On the other hand, the integral is performed on the volume and the B matrix depends on the geometry. If we are concerned with large strains and if we are using the Cauchy's stresses, geometry is defined in the current configuration, which is changing from step to step, and even from one iteration to the other. These two contributions, the material one, issued from the constitutive model, and the geometric one have to be accurately computed in order to guaranty the quadratic convergence rate.

A similar discussion may be given for diffusive problems. However, the geometry is not modified for pure diffuse problems, so only the material term is to be considered.

2.6. Transient effects : the time dimension

Time dimension appears in first order time derivative in the constitutive mechanical model [3,9] and in the diffusion problems though the storage term. We will here discuss the time integration procedure and the accuracy and stability problems that are involved.

2.6.1 Time integration – diffusion problems

The period to be considered is divided in time steps. Linear evolution of the basic variable with respect to the time is generally considered within a time step :

$$p = \frac{t-t_A}{t_B-t_A} p_B + \frac{t_B-t}{t_B-t_A} p_A \quad [31]$$

where the subscripts $_{A,B}$ denote respectively the beginning and the end of a time step. Then the pressure rate is :

$$\dot{p} = \frac{dp}{dt} = \frac{p_B - p_A}{t_B - t_A} = \frac{\Delta p}{\Delta t} \quad [32]$$

This time discretisation is equivalent to a finite difference scheme. It allows evaluating any variable at any time within a time step.

The balance equation should ideally be fulfilled at any time during any time step. Of course this is not possible for a discretised problem. Only a mean assessment of the balance equation can be obtained. Weighted residual formulations have been proposed in a similar way as for finite elements (Zienkiewicz et al. 1989). However the implementation complexity is too high with respect with the accuracy. Then the easiest solution is to assess only the balance equation at a given time noted θ inside the time step :

$$\theta = \frac{t\theta - t_A}{t_B - t_A} \quad [33]$$

All variables have then to be evaluated at the reference time θ . Different classical schemes have been discussed for some decades :

- Fully explicit scheme - $\theta = 0$: all variables and the balance are expressed at the time step beginning, where everything is known (solution of the preceding time step). The solution is therefore apparently very easy to be obtained.
- Crank-Nicholson scheme or mid-point scheme - $\theta = 1/2$
- Galerkin's scheme - $\theta = 2/3$
- Fully implicit scheme - $\theta = 1$

The last three schemes are function of the pore pressure / temperature / concentration at the end of the time step, and may need to iterate if non-linear problems are considered.

For some problems, phase changes or similar large variations of properties may occur abruptly. For example, icing or vaporising of water is associated to latent heat consumption and abrupt change of specific heat and thermal conductivity. Such rapid change is not easy to model. The change in specific heat may be smoothed using an enthalpy formulation, because enthalpy H is an integral of the specific heat c . Then finite difference of the enthalpy evaluated over the whole time step gives a mean value \bar{c} and so allows accurate balance equation :

$$H = \int_T c dT \quad [34]$$

$$\bar{c} = \frac{H_B - H_A}{t_B - t_A} \quad [35]$$

2.6.2 Time integration – solid mechanics

For solid mechanics problems, the constitutive law form [3,4] is an incremental one at the difference with the ones for diffusion problems [12]. The knowledge of the stress tensor at any time implies to have time integrated the constitutive law. The stress tensor is a state variable that is stored and transmitted from step to step based on its final / initial value, and this value plays a key role in the numerical algorithm.

Then, in quite all finite element code devoted to modelling, equilibrium is expressed at the end of the time steps, following then a fully implicit scheme - $\theta = 1$, and using the end of step stress tensor value.

However, integrating the stress history with enough accuracy is crucial for the numerical process stability and global accuracy. Integrating the first order differential equation:

$$\underline{\sigma}^B = \underline{\sigma}^A + \int_{t^A}^{t^B} \underline{\underline{C}}^{ep} \underline{\dot{\varepsilon}} dt \quad [36]$$

can be based on similar concepts as the one described in the preceding paragraph. Various time schemes based on different θ values may be used. Stability and accuracy discussion (§2.6.3) are similar.

When performing large time steps, obtaining enough accuracy may require to use sub-stepping: within each global time step (as regulated by the global numerical convergence and accuracy problem), the stress integration is performed at each finite element integration point after division of the step in a number a sub-steps allowing high accuracy and stability.

2.6.3 Scheme accuracy

The theoretical analysis of a time integration scheme accuracy and stability is generally based on a simplified problem (Zienkiewicz et al, 1989). Let consider diffusion phenomena restricted to linear case. Introducing the discretised field [20] into the constitutive equations gives for the Darcy law (neglecting here the gravity term for the sake of simplicity) :

$$f_i = -\frac{k}{\mu} \partial_i p = -\frac{k}{\mu} (\partial_i N_L) p_L \quad [37]$$

Similarly the storage law (linear case) gives :

$$\dot{S} = c \dot{p} = c N_L \dot{p}_L \quad [38]$$

where c is a storage parameter. Neglecting source terms, the weak form of the balance equation [23] writes then :

$$\int_V [\dot{S} \delta p - f_i \partial_i (\delta p)] dV = \int_V c N_L \dot{p}_L N_K \delta p_K dV - \int_V -\frac{k}{\mu} \partial_i N_L p_L \partial_i N_K \delta p_K dV = 0 \quad [39]$$

Considering that nodal values are not concerned by the integration, it comes :

$$\left(\int_V c N_L N_K dV \right) \dot{p}_L \delta p_K + \left(\int_V \frac{k}{\mu} \partial_i N_L \partial_i N_K dV \right) p_L \delta p_K = 0 \quad [40]$$

$$C_{KL} \dot{p}_L \delta p_K + K_{KL} p_L \delta p_K = 0$$

which is valid for any arbitrary perturbation δp . Then :

$$C_{KL} \dot{p}_L + K_{KL} p_L = 0 \quad [41]$$

which is a simple system of linear equations with a time derivative, a storage matrix \underline{C} and a permeability matrix \underline{K} . One can extract eigenvalues of this system and so arrive to a series of scalar independent equations of similar form :

$$\dot{p}_L + \alpha_L^2 p_L = 0 \quad (\text{no summation}) \quad [42]$$

where L represents now the number of the eigenmode with the eigenvalue α_L and will not be noted in the following. The exact solution for equation [42] is a decreasing exponential :

$$p(t) = p(t_0) e^{-\alpha^2 t} \quad [43]$$

This problem represents then the damping of a perturbation for a given eigenmode. Numerically, the modelling is approximated and numerical errors always appear. If the equation [43] is well modelled, any numerical error will be rapidly damped, if the error source is not maintained. Following this analysis, the whole accuracy and stability discussion may be given on these last scalar equations [42,43].

Introducing the time discretisation [32,33] in [42] gives :

$$\frac{p_B - p_A}{\Delta t} + \alpha^2 [(1-\theta) p_A + \theta p_B] = 0 \quad [44]$$

which allows to evaluate the end of step pressure as a function of the beginning of step one :

$$p_B = A p_A \quad [45]$$

with the amplification factor :

$$A = \frac{1 - (1-\theta)\alpha^2 \Delta t}{1 + \theta\alpha^2 \Delta t} \quad [46]$$

To ensure the damping process of the numerical algorithm, which is the *stability condition*, it is strictly necessary that the amplification factor remains lower than unity :

$$-1 < A < 1 \quad [47]$$

This condition is always verified if $\theta \geq 1/2$, and conditionally satisfied otherwise :

$$\Delta t \leq \frac{2}{(1-2\theta)\alpha^2} \text{ if } \theta < 1/2 \quad [48]$$

This last equation is not easy to verify, as it depends on the eigenvalues, which are generally not computed. Therefore, for classical diffusion process considered in geomaterials, the condition $\theta \geq 1/2$ is generally used.

It should be noted that the amplification factor becomes negative for large time steps, unless for the fully implicit scheme. Then the pertubated pressure decreases monotonically in amplitude but with changes of sign. This may be questionable for some coupled phenomena, as it could induce oscillation of the coupled problem.

Let us now consider the accuracy of the numerical schemes. Developing in Taylor's series the exact and numerical solution allows to compare them :

$$\begin{aligned} A_{exact} &= 1 - x + \frac{1}{2}x^2 - \frac{1}{6}x^3 + \dots \\ A_{numérique} &= 1 - x + \theta x^2 - \theta^2 x^3 + \dots \\ x &= \alpha^2 \Delta t \end{aligned} \quad [49]$$

It appears that the only Crank-Nicholson scheme $\theta = 1/2$ has second order accuracy properties. However this conclusion is limited to infinitesimal time steps. For larger time steps, as in most numerical models, the Galerkin's scheme $\theta = 2/3$ gives the optimal compromise and should be generally used.

The whole discussion related to the stability and accuracy of the proposed time numerical schemes was based on eigenmodes of a linear problem. Can we extrapolate them to general problems ? The eigenvalue passage is only a mathematical tool to be able to consider scalar problems, and has no influence on our conclusions. Oppositely, the non-linear aspects could modify sometimes our conclusions. However, it is impossible to develop the analysis for a general non-linear problem, and the preceding conclusions should be adopted as guidelines, as they appear to be fruitful in most cases.

2.7. Advection diffusion processes

Let us first consider a purely advective process. Then the transport is governed by the advection equation [16] and by the balance equation [11]. Associating these two equations, one obtains:

$$(\nabla^T C) \cdot \underline{f}_{diff}^{fluid} + \dot{C} = 0 \quad [50]$$

which is a hyperbolic differential equation. It cannot be solved by the finite element or finite difference problem, but by characteristic methods. The idea is to follow the

movement of a pollutant particle by simply integrating step by step the fluid velocity field. This integration has to be accurate enough, as errors are cumulated from one step to the next.

On the other hand, if advection is very small compared to diffusion, then the finite element and finite difference methods are really efficient.

For most practical cases, an intermediate situation holds. It can be checked by the Peclet's number [18], which is high for mainly advective processes and low for mainly diffusive one. As diffusion has to be taken into account, the numerical solution must be based on the finite element method (the finite difference one may also be used but will not be discussed here). However, numerical experiments show that the classical Galerkin's formulation gives very poor results with high spatial oscillations and artificial dispersion. Then new solutions have been proposed (Zienkiewicz and Taylor, 1989, Charlier and Radu, 2001). A first solution is based on the use in the weighted residual method of weighting function that differs from the shape one by an upwind term, i.e. a term depending in amplitude and direction on the fluid velocity field. The main advantage of this method is to maintain the finite element code formalism. However, it is never possible to obtain a highly accurate procedure. Numerical dispersion will always occur.

Other solutions are based on the association of the characteristic method for the advection part of the process and of the finite element method for the diffusive part (Li et al 1997). The characteristic method may be embedded in the finite element code, what has a strong influence on the finite element code structure. It is also possible to manage the two methods in separated codes, as in a staggered procedure (cf. section 3.3.).

3. Coupling various problems

3.1. Finite element modelling: monolithical approach

Modelling the coupling between different phenomena should imply to model each of them and, simultaneously, all the interactions between them. A first approach consists in developing new finite elements and constitutive laws especially dedicated to the physical coupled problem to be modelled. This approach allows taking accurately all the coupling terms into account. However there are some drawbacks that will be discussed in a later section.

Constitutive equations for coupled phenomena will be shortly discussed in the following sections.

The number of basic unknowns and following the number of degrees of freedom – dof per node are increased. This has a direct effect on the computer time used for

solving the equation system (up to the third power of the total dof number). Coupled problems are highly time consuming.

Isoparametric finite element will often be considered. However some specific difficulties may be encountered for specific problems. Nodal forces or fluxes are computed in the same way as for decoupled problems (see § 2.4). However stiffness matrix evaluation is much more complex, as interactions between the different phenomena are to be taken into account. Remember that the stiffness or iteration matrix [29] is the derivative of internal nodal forces / fluxes with respect to the nodal unknowns (displacements / pressures / ...). The complexity is illustrated by the following scheme of the stiffness matrix, restricted to the coupling between two problems:

Derivative of problem 1 nodal forces with respect to problem 1 nodal unknowns	Derivative of problem 1 nodal forces with respect to problem 2 nodal unknowns
Derivative of problem 2 nodal forces with respect to problem 1 nodal unknowns	Derivative of problem 2 nodal forces with respect to problem 2 nodal unknowns

The part of the stiffness matrix in cells 1-1 and 2-2 are similar or simpler to the ones involved in uncoupled problems. The two other cells 1-2 and 2-1 are new and may be of certain complexity. Remember also that the derivative consider internal nodal forces / fluxes as obtained numerically, i.e. taking into account all numerical integration / derivation procedures. On the other hand, large difference of orders of magnitude between different terms may cause troubles in solving the problem and so need to be checked.

Numerical convergence of the Newton – Raphson process has to be evaluated carefully. It is generally based on some norms of the out-of-balance forces / fluxes. However, coupling implies often mixing of different kinds of dof, which may not be compared without precaution. Convergence has to be obtained for each basic problem modelled, not only for one, which would then predominate in the computed indicator.

3.2. Physical aspects: various terms of coupling

A large number of different phenomena may be coupled. It is impossible to discuss here all potential terms of coupling, and we will restrict ourselves to some basic cases often implied in environmental geomaterial mechanics. In the following paragraphs, some fundamental aspects of potential coupling are briefly described. More information can be obtained in dedicated chapters of this journal or specialised books.

3.2.1 Hydromechanical coupling

Number of dof per node : 3 (2 displacements + 1 pore pressure) for 2D analysis and 4 (3 displacements + 1 pore pressure) for 3D analysis.

Coupling mechanical deformation of soils or rock mass and water flow in pores is a frequent problem in geomechanics. The first coupling terms are related to the influence of pore pressure on mechanical equilibrium through the Terzaghi's postulate

$$\underline{\sigma} = \underline{\sigma}' + p\underline{I} \quad [51]$$

with the effective stress tensor $\underline{\sigma}'$ related to the strain rate tensor thanks to the constitutive equation [3], and the unity tensor \underline{I} .

The second type of coupling concerns the influence of the solid mechanics behaviour on the flow process, which comes first through the storage term. Storage of water in saturated media is mainly due to pores strains, i.e. to volumetric changes in soil / rock matrix :

$$\dot{S} = \dot{\epsilon}_v \quad [51]$$

A other effect, which may be considered, is the permeability change related to the pore volume change, which may for example be modelled by the Kozeny – Carman law as a function of the porosity $k = k(n)$.

Biot proposed an alternative formulation for rocks where contacts between grains are much more important than in soils. Following Biot, the coupling between flow and solid mechanics are much more important (Detournay, 1991, Thimus – proc. Biot Conf.).

The time dimension may cause some problems. First implicit scheme are used for the solid mechanics equilibrium and various solutions are possible for the pore pressure diffusion process. Consistency would imply to use fully explicit schemes for the two problems. Moreover, it has been shown (§2.6.2) that time oscillations of the pore pressure may occur for other time schemes. Associated to the Terzaghi's postulate, oscillations could appear also on the stress tensor, what can degrade the numerical convergence rate for elastoplastic or elastoviscoplastic constitutive laws.

Large strains and large displacements have been analysed for solid mechanics. When solid mechanics is coupled with pore pressure diffusion, the Darcy's fluid velocity and the balance equations have to be computed in the geometry of the current configuration, which is changing from one iteration to the other. Therefore a geometric coupling term appears in the iteration matrix when derivating the nodal water fluxes with respect to the nodal displacements. On the other hand, the solid and fluid specific weights have to be actualised taking into account the large strain process (Barnichon 1998).

When using isoparametric finite elements, the shape function for geometry and for pore pressure are identical. Let us consider for example a second order finite element. As the displacement field is of second order, the strain rate field is linear. For an elastic material, the effective stress tensor rate is then also linear. However the pore pressure field is quadratic. Then the Terzaghi's postulate mixes linear and quadratic field, which is not highly consistent. Some authors have then proposed to mix in one element quadratic shape functions for the geometry and linear shape functions for pore pressure. But then problems arrive with the large strain geometry evolution and with the choice of spatial integration points (1 or 4 Gauss points ?).

Numerical locking problems may also appear for isoparametric finite element when the two phases material (water + soil) is quite incompressible, i.e. for very short time steps with respect with the fluid diffusion time scale. Specific elements have to be developed for such problems .

3.2.2. Two fluids flow in rigid porous media coupling

Flow in partly saturated rigid media is here considered. For unsaturated soils, the fluids are water and air. Often, the air phase is considered to be at constant pressure, what is generally a relevant approximation as air doesn't affect highly the water flow. Then only one dof per node is sufficient, and the classical diffusion equations (section 1.2) are relevant, with parameters depending on the suction or saturation level.

Flow in oil or gas reservoirs two or three fluids among oil, gas, condensates and water. Partial solving or mixture between different fluid are sometimes possible. Then two or more dof per node are to be considered. The permeability and storage equation of each phase are depending on the suction or saturation level, and so the problem may be highly non-linear. However, coupling is not difficult to numerically be developed, as the formulation are similar for each phase.

3.2.3. Diffusion and transport coupling

Heat and one fluid flow in a rigid porous media or salted water flow in coastal aquifers are concerned here. The fluid specific weight and viscosity is depending on the temperature or salt concentration, and the heat or salt transport by advection – diffusion process is depending on the fluid flow. Then a diffusion process and an advection – diffusion process have to be solved simultaneously.

Number of dof per node: 2 (fluid pore pressure and salt concentration of temperature).

3.2.4. Thermo-hydro-mechanical coupling

The phenomena considered here (as for example for problems related to underground storage of nuclear waste disposals – (Gens 2001)) are much more complex as they associates multiphase fluid flow (cf. section 3.2.2), hydromechanical coupling (cf. section 3.2.1) and temperature effects. All the features described in the preceding section are to be considered here, associated to some new points.

Heat diffusion has to be modelled. Temperature variation affects fluid flow, by a modification of the fluid specific weight or viscosity. Moreover, if the two fluids concerned are a liquid and a gas (e.g. water and air), then equilibrium between the phases has to be modelled: dry air – vapour equilibrium.

Heat transfer is governed not only by conduction but also by advection by the liquid and gas movements. Similarly transfers of vapour and dry air in the gas phase are governed by diffusion and gradient of species density, but also but advection by the global gas movements. If the concerned geomaterials has a very low permeability (like clay for engineered barriers), then the diffusion effects will predominate and advection doesn't necessitate specific formulation (cf. section 2.7) (Collin et all, 1999)

Finally the total number of dof per node is 5 for a 2D problem : 2 displacements, 2 fluid pore pressures and the temperature.

3.3. Finite element modelling: staggered approach

Monolithical approach of coupled phenomena implies identical space and time meshes for each phenomenon. This is not always possible, for various reasons. The coupled problems may have different numerical convergence properties, generally associated to different physical scales or non-linearities. For example, a coupled hydromechanical problem may need large time steps for the fluid diffusion problem, in order to allow in each step fluid diffusion along distance of the order of magnitude of the finite elements. In the same time, strong non-linearities may occur in solid mechanics behaviour (strong elastoplasticity changes, interface behaviour, strain localisation...) and then the numerical convergence needs short time – loading steps, which should be adapted automatically to the rate of convergence. Then it is quite impossible to obtain numerical convergence for identical time and space meshes.

Research teams of different physical and numerical culture have progressively developed different problems modelling. As an example, fluid flow has been largely developed using the finite difference method for hydrogeology problems including pollutant transport, and for oil reservoir engineering (see section 2.1 and 2.3) taking multiphase fluid flow (oil, gas, condensate, water,...) into account. Coupling such fluid flow with geomechanics in a monolithical approach would imply to implement all the physical features already developed respectively in finite elements and finite differences codes. The global human effort would be very important.

Coupled problems are generally presenting a higher non-linearity level than uncoupled ones. Then inaccuracy in parameters or in the problem idealisation may cause degradations of the convergence performance.

How can we solve such problems and obtain a convincing solution? First of all, a good strategy would be to start with the uncoupled modelling of the leading process, and to try to obtain a first not too bad solution. Then one can add a first level of coupling and complexity, followed by a second one... until the full solution is obtained.

However such trick is not always sufficient. Staggered approaches may then give an interesting solution. In a staggered scheme, the different problems to be coupled are solved separately, with (depending on the cases) different space or time mesh, or different numerical codes. However, the coupling is ensured thanks to transfer of information between the separated models at regular meeting points. This concept is summarised on the figure 3. It allows theoretically coupling any models together.

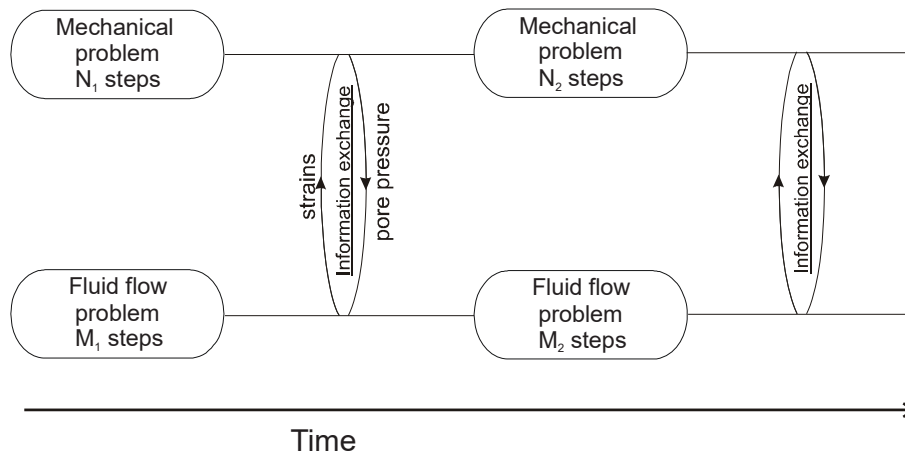


Figure 3 : *Scheme of a staggered coupling*

When using different spatial meshes, or when coupling finite elements and finite differences codes, the transfer of information needs often an interpolation procedure, as the information to be exchanged are not defined at the points in the different meshes.

The accuracy of the coupling scheme will mainly depend on the information exchanges frequency (which is limited by the lower time step that can be used) and by the type of information exchanged. The stability and accuracy of the process has been checked by different authors (Turska et al 1993, Zienkiewicz et al, 1988). It

has been shown that a good choice of the information exchange may improve highly the procedure efficiency.

4. References

- [BAR 98] BARNICHON J.D., « Finite element modelling in structural and petroleum geology », thèse de doctorat, Faculté des Sciences Appliquées, Université de Liège, 1998
- [CHA 01] CHARLIER R. RADU JP. « Rétention et transfert des polluants chimiques solubles : mécanismes fondamentaux et modélisation numérique », Traite de Mécanique et Ingénierie des Matériaux – MIM, Géomécanique environnementale, Editions Hermes, 2001
- [CHA 90] R. CHARLIER et A-M. HABRAKEN. « Numerical Modelisation of Contact with friction phenomena by the finite element method », Computer and Geomechanics, Vol. 9, N° 1 and 2, 1990.
- [COL 99] F. COLLIN, X.L. LI, J-P. RADU, R. CHARLIER, « Clay barriers assessment : a coupled mechanical and moisture transfer model », Proc. ECCM'99, European Conference on Computational Mechanics, Munich (Sept. 1999).
- [COU 01] COUSSY O., ULM FJ., « Basic concepts of durability mechanics of concrete structures », RFGC, 2001.
- [DET 91] DETOURNAY E., CHENG A.H.D., « Fundamental of poroelasticity », in Comprehensive Rock Engineering, Practice and Projects, Vol. 2, J.A. Hudson ed., Pergamon Press, 1991.
- [ECL 00] ECLIPSE Technical Description, Schlumberger, 2000.
- [GEN 01a] GENS A., « Fundamentals of THM phenomena in saturated and unsaturated materials. General formulation. Thermal and hydraulic constitutive laws », RFGC, 2001.
- [GEN 01b] GENS A., « Clay barriers in radioactive waste disposal », RFGC, 2001.
- [LAL 01] LALOUI L. « Thermo-mechanical behaviour of soils », RFGC, 2001
- [LI 97] LI Xikui, RADU J.P, CHARLIER. R. « Numerical Modeling of Miscible Pollutant Transport by Ground Water in Unsaturated Zones », Computer Methods and Advances in Geomechanics, Yuan Ed., 1997, pp. 1255-1260.
- [RAD 94] J.P. RADU, R. CHARLIER. Modelling of the Hydromechanical Coupling for Non Linear Problems: Fully Coupled and Staggered Approaches. Proc. of the 8th Int. Conf. of the Int. Ass. for Computer Methods and Advances in Geomechanics, West Virginia, USA, May 1994
- [TUR 93] TURSKA E., SCHREFLER B.A., « On convergence conditions of partitioned solution procedures for consolidation problems », Comp. Meth. InAppl. Mech. And Eng., 106 : 51-63, 1993.
- [ZIE 89] ZIENKIEWICZ O.C., TAYLOR R.L., *The Finite Element Method*, Mac Graw-Hill Book Company, vol. 2, ch. 12, 4° ed., 1989.
- [ZIE 88] ZIENCKIEWICZ O.C., PAUL D.K., CHAN A.H.C., “Unconditionally stable staggered solution procedure for soil-pore fluid interaction problems”, Int. J. for Num. Meth. In Engineering, Vol 26,: 1039-1055, 1988.

Acknowledgements

Authors are grateful to FNRS, La Communauté Française de Belgique and the European Commission for the financial help to their research projects.

Appendix J. THM behaviour of engineered and natural clay barriers (F. Collin)

THM behaviour of engineered and natural clay barriers

Frédéric Collin *** – Robert Charlier*

* Université de Liège
Institut de Génie Civil et de Mécanique
Chemin des Chevreuils 1, 4000 Liège
Sart Tilman, Belgique

Robert.Charlier@ulg.ac.be

**Chargé de Recherches, Fonds National Belge de la Recherche Scientifique

RÉSUMÉ. Cet article traite de deux problèmes en relation avec l'enfouissement de déchets nucléaires dans des couches géologiques profondes. D'une part, une expérience d'hydratation et de chauffage sur une argile gonflante a été conduite à petite échelle au laboratoire. Sa modélisation thermo-hydro-mécanique est proposée et discutée. D'autre part, l'extension de la zone endommagée lors du creusement d'une galerie est discutée sur base d'une modélisation hydromécanique avec une mise en évidence de la localisation des déformations en bandes de cisaillement, amorce de fractures.

ABSTRACT. This paper is concerned with two problems related to deep underground storage of nuclear waste. On one hand, a small-scale laboratory experiment has allowed to heat and wet a confined swelling clay. A thermo-hydro-mechanical modelling is proposed and discussed. On the other hand, the extent of the damaged zone produced during tunnelling in clay is discussed based on an hydromechanical modelling showing evidences of strain localisation, i.e. a fracture initiation.

MOTS-CLÉS : barrière argileuse, localisation des déformations, couplages multi-physiques, THM, hydromécanique, enfouissement de déchets.

KEYWORDS: clay barriers, strain localisation, multi-physics coupling, THM, hydromechanics, underground storage.

1. Introduction

One solution nowadays proposed for long term nuclear waste is the realization of waste repositories in deep geological low permeability layers: the Boom Clay formation in Belgium, clay-stone formation in France and granite and claystone formations in Switzerland for example. In order to develop and to assess this approach, Underground Research Laboratories (URL) have been constructed in several countries in Europe (France, Switzerland, Belgium, ...). Different experiments can be achieved: on one hand, at the gallery scale, *in-situ* measurements are made in thermo-hydro-mechanical (THM) conditions close to those that will be created when the nuclear waste will be deposited. On the other hand, it is also interesting to achieve small-scale experiment in order to test (at lower cost) different set-up of engineered barriers. These kind of tests on the filling material (usually clay material) reproduce the conditions in the gallery: resaturation by the host formation, heat production due to waste activity and confinement of engineered barrier.

Modelling such kind of experiment requires complex constitutive laws (See [LAL05] and [GEN05] in the same book) in order to tackle the different coupled phenomena and needs also advanced experimentations in order to determine the parameters of the constitutive models. In the second section, a small-scale heating and hydration test is presented and a THM modelling is proposed.

Another aspect of this problem is the necessity to ensure that gallery excavation does not damage the host formation. Indeed if some fracturation processes appear, they will constitute preferential paths for pollutant migration like radionuclide. The tunnelling method should then minimize the damaged zone (EDZ) around the excavation. In the existing URL, the mechanical behaviour of the host formation is usually brittle and the constitutive laws usually used to reproduce their behaviour are damaged models or strain-softening models. Such kind of models allows to reproduce the progressive decrease of material strength during testing; consequently, they predict also strain localisation, which is observed *in-situ* ([MER 04]). In the third section, it is proposed to model the excavation process with a very simple strain-softening constitutive law in order to exhibit the main phenomena appearing during tunnelling.

2. Modelling of the THM behaviour of unsaturated clay

In the following, a small-scale heating and hydration test is first presented and a modelling is proposed. This latter one was a part of a benchmark exercise in the framework of CATSIUS CLAY European project ([ALO 99]): experimental results of an heating and hydration test on a clay material were known ([VIL 94], [VOL 96]). The different partners were asked to model the experiment, being free to chose the mechanical constitutive law. Series of tests on the material ([VIL 94], [PIN 97]) allow to determine the parameters.

2.1. Experiment set-up

The clay material used for the experiment is the S2 bentonite, which is a montmorillonite coming from Almeria in Spain. This clay was axially compacted at a dry density of 1.66 g/cm^3 ($S_{rw} = 49\%$ and $W = 11.8\%$) and was inserted in a cell, which dimension (in cm) are given in the Figure 1.

The total duration of the experiment is 2401.6 hours; clay sample is saturated and heated. Different temperature and water content measurement are available during the test.

- The heater is a vertical cylinder inserted in the upper part of the cell (Figure 1). It is a resistance electronically regulated by an ON/OFF temperature controller with a thermocouple sensor. A power of 40 W is supplied up to a temperature of 100°C and turned off still the temperature decreases below 97°C . The cell containing the sample is in direct contact with ambient laboratory atmosphere, which is assumed to be at 25°C .
- Hydration of the bottom of the sample is realized through a porous stone and the injection pressure equals 1.1 MPa.

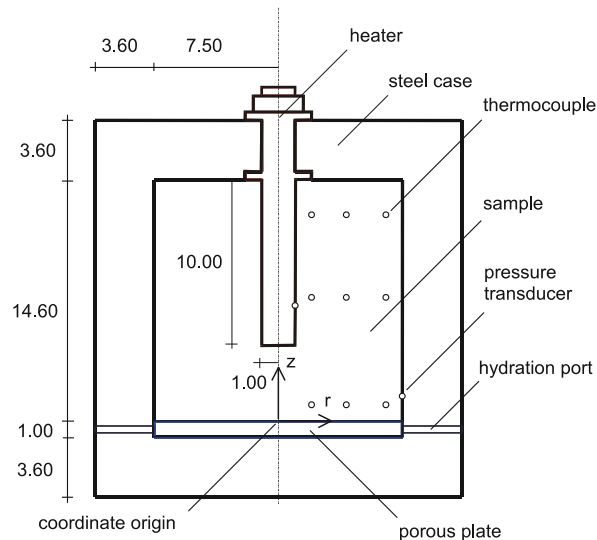


Figure 1. Experiment set-up

- During experiment, water volume intake is monitored as well as the total pressure at the bottom of the sample. Moreover, several thermocouples allow to know the temperature evolution within the

sample all along the test. After 2401.6 hours, the clay sample is extracted from the cell and cut into slices, which allow to know the final water content distribution.

The aim of the modelling is to be able to reproduce the measurements realized during the experiment. It should be noticed that the information on the mechanical behaviour comes only from one pressure transducer. Thus sound conclusions on the mechanical aspects will not be drawn here. *A contrario* measurements of temperature and water content allow to have a better comprehension of hydric exchanges during experiment.

2.3. Modelling predictions

The constitutive law used for the mechanical behaviour of the S2-Bentonite is the BBM model ([ALO 90]), which is written in terms of net stress and suction. A multiphasic model is used to reproduce the water, air and thermal flows that appear in an unsaturated media. Water vapour flows are also taken into account (following Phillip and De Vries expression [PHI 57]) and are very important in such low permeability medium.

The determination of the model's parameters is a crucial task to get a proper modelling of the problem. Many advanced experiments are needed for the complex constitutive models we used but it remains always some parameters that the engineers have to estimate. A detailed description of the parameters determination and the numerical implementation could be found in [LI 00] and [COL 02].

In the following computations, the fully coupled finite elements have five degrees of freedom: geometrical coordinates, water pressure, gas pressure and temperature. They are used to mesh the steel case, the porous stone and the sample. Some additional boundary finite elements are needed to model the action of the heater and the thermal exchanges between the steel case and the ambient air.

2.3.1. Initial and boundary conditions

The sample is initially at ambient temperature ($T_0 = 25$ °C) in the steel case. Knowing the saturation of the sample at the beginning of the experiment ($S_{rw} = 49\%$) and assuming an atmospheric gas pressure, the initial water pressure is given by the corresponding suction and equals -78,53 MPa. The clay material is inserted in the cell without compaction and is thus initially stress free.

Injection of water is realized through the porous stone at a pressure of 1.1 MPa. For the modelling gas pressure will be assumed constant and equal to 100 kPa. This supposes that air can flow out the cell without strong overpressure. For TH modelling, the influence of air pressure variation was studied [COL 02] and it was shown that this implies a lower water saturation degree near the heater. For the thermal problem, a 40 W heat flow is applied at the sample surface in contact with

the heater and this flow is controlled in order to reach a maximum temperature of 100°C. Moreover, thermal exchanges appear between the external face of the cell and the ambient air, due to convective fluxes. The exchange coefficient was chosen to a value of 6.5 W/m² thanks to a back analysis of the temperature field.

The steel case and the porous stone are assumed to be rigid and a perfect sliding contact condition is considered between the sample and the confinement (the cell, the porous stone and the heater).

2.3.3. Numerical Results

In the modelling presented here, all the physical phenomena are coupled. Therefore it is interesting to study the different problems separately to understand what happens during the experiment. Considering first the thermal problem only, the exchange coefficient is calibrated by comparison with experiment measurements. Further (coupled) computations showed that temperature field is only slightly influenced by water flow and strains. Indeed, the thermal problem is essentially conductive. Figure 2-a presents a comparison between experiments and numerical responses (for coupled T-H-M modelling), at the bottom, the middle and the top of the sample. Predictions are very closed to the measurements except at the middle near the heater where the model overestimates the temperature. Of course, these results show that temperature is higher near the heater (about 75°C in 1 cm from the heater). Material is colder far from the hot spot: temperature is then directly related by the ambient air temperature. It is also important to notice that temperature field does not vary much between 25.6 hours and the end of experiment. Indeed, thermal steady state is reached after 13 hours [VIL 94].

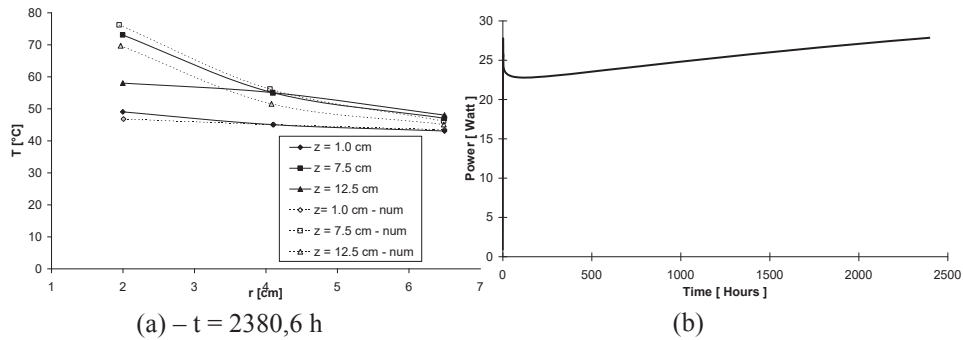


Figure 2. Temperature field in the sample

The supplied heat power is sufficient enough to reach 100°C at the heater. In the beginning of the experiment, the power actually supplied is equal to 27 W. Then, it decreases to 23 W and finally increases during the remaining experiment time due to the progressive sample resaturation (Figure 2-b).

During the experiment, water injection is realized at the bottom of the sample. Figure 3-a shows that the model reproduces very well the water intake curve. The curve depends mainly on the bentonite permeability. However, it is not much influenced by the thermal field. Experiment shows clearly a resaturation of the sample, from its bottom and a desiccation of the clay near the heater due to the increase of temperature and the water vapour transfer (Figure 3-b). Thus, in order to reproduce the desaturation, it is necessary to include in the model water vapour flow; if it is not the case, desaturation will not be very important. Related to this effect, the parameter controlling the intensity of vapour fluxes is the tortuosity. The value chosen (tortuosity = 0.15) was calibrated by back analysis in order to reproduce the water content near the heater. At the end of the experiment, despite the water injection at the bottom, water content near the heater has decreased due to water evaporation. Near the bottom of the sample, clay is fully saturated and the water content is about 35%.

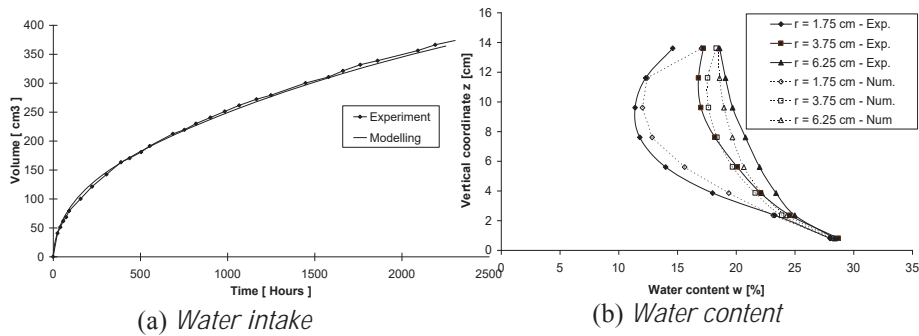


Figure 3. Hydric transfer in the sample

Due to the confinement of the sample, clay material cannot sustain large strains; thus a swelling pressure is created, and the porosity changes, what has a strong influence on the water content (figure 3-b). Indirectly, it appears that the model mechanical response is qualitatively good.

2.4. Conclusions

The developed model was able to predict the bentonite behaviour under thermo-hydro-mechanical loading. Modelled temperatures are quite equivalent to measured ones. The hot zone ($T = 100\text{ °C}$) is located near the heater while the temperature near the casing is controlled by the convection condition with ambient air.

Water content modelled and measured are similar; a saturated zone is produced near the porous stone. In the upper part of the sample, the bentonite cannot fully saturate, because the water is vaporised near the heater and the material is dried.

Water transfers in vapour phase are therefore crucial to be modelled in such kind of problem.

Eventually, it should be noticed that such a modelling was possible thanks to a very large experimental program on bentonite material. This allowed to determine its mechanical, hydraulic and thermal properties. The models ask for many parameters, which is consequence of the modelling complexity of highly coupled phenomena.

3. Tunnelling in clay/claystone for nuclear waste disposal

In the following, it is proposed to model the excavation process with a very simple strain-softening constitutive law in order to exhibit the main phenomena appearing during tunnelling : the progressive decrease of material strength during testing and the strain localisation. This coupled modelling is a benchmark exercise proposed by the GDR-Momas and organized by EDF-CEA ([CHA 05]).

3.1. Description of the problem

The proposed constitutive law is an elasto-plastic strain-softening model. The yield criterion is a Drucker-Prager model given by the following equation:

$$F \equiv \sqrt{\frac{3}{2}} II_{\sigma^*} + m \left(I_{\sigma} - \frac{3c}{\tan \phi} \right) = 0 \quad [1]$$

where II_{σ^*} is the second deviatoric stress invariant, I_{σ} is the first stress invariant, ϕ is the friction angle, parameter m is a function of ϕ : $m = 2 \sin(\phi)/(3-\sin(\phi))$, the cohesion $c = \omega f(\gamma^p)$ is the softening variable, ω is the initial cohesion and γ^p is the equivalent deviatoric plastic deformation.

A cylindrical unsupported cavity of 3 m diameter is located in an homogeneous low permeability formation. The initial state of stress and pore pressure is the following:

$$\begin{aligned} \sigma'_{xx} &= \sigma'_{zz} = -7.74 \text{ MPa} \\ \sigma'_{yy} &= -11.64 \text{ MPa} \\ p_w &= 4.7 \text{ MPa} \end{aligned}$$

The excavation process is modelled by decreasing both radial total stress and the pore pressure at the cavity nodes:

$$\text{at } r=3\text{m} \left\{ \begin{array}{l} 0 \leq t \leq T \\ \sigma_{xx} = \sigma'_{xx} - bp_w = -11.5 \left(1 - \frac{t}{T}\right) \text{MPa} \\ \sigma_{yy} = \sigma'_{yy} - bp_w = -15.4 \left(1 - \frac{t}{T}\right) \text{MPa} \\ p_w = 4.7 \left(1 - \frac{t}{T}\right) \text{MPa} \\ t > T \\ \sigma_{xx} = \sigma_{yy} = p_w = 0 \end{array} \right. \text{ and at } r=\infty \left\{ \begin{array}{l} \sigma_{xx} = -11.5 \text{MPa} \\ \sigma_{yy} = -15.4 \text{MPa} \\ p_w = 4.7 \text{MPa} \end{array} \right.$$

The excavation duration T is equal to 1.5 Ms (about 17 days) and the final modelling time is 300 Ms (about 9.5 years).

3.2. Model predictions

During the excavation, the behaviour of the material becomes plastic near the tunnel and permanent strains are created. The yield criterion is first met in the direction where the orthoradial stress is the major principal stress. Dilatancy effects are evidenced on Figure 4-a, where the pore pressure becomes negative at the end of the tunnelling. Then, during the remaining modelling time, the pore pressure increases progressively. Figure 4-b shows the radial displacement curve: during the tunnelling phase, cavity convergence remains around 1,5 cm. Most of the convergence appears later and reaches 22,6 cm. Indeed, negative pore pressure allows a additional cohesive strength; this effect is maximum after 1,5 Ms and decreases progressively still 300 Ms.

Shear band localization is also influenced by the hydro-mechanical coupling. Indeed, at the end of excavation, there is no clear localization patterning even if the Rice's criterion is verified. After that phase, pore pressure increases progressively and a patterning is gradually created. Figure 5-a presents a map of equivalent strains, where the different shear bands appears clearly. The Vilotte's indicator is shown in Figure 5-b; this indicator evidences the strain activity of the shear band. One can see here that only the external shear band is active at the end of the simulation and that a chip is finally created. It is clear however that these results are mesh dependent and enhanced models are necessary for an objective post-localization modelling (See [ZER 01] for an example of excavation and [ZHA 04], [CHA 04] for coupled enhanced models).

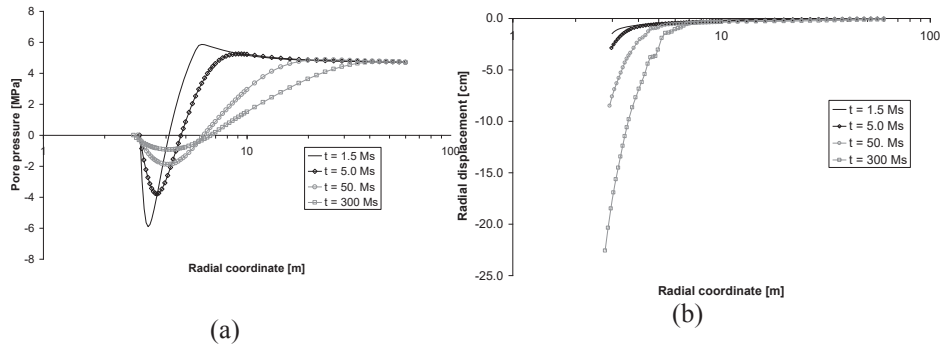


Figure 4. Pore pressure and displacement curve during coupled excavation

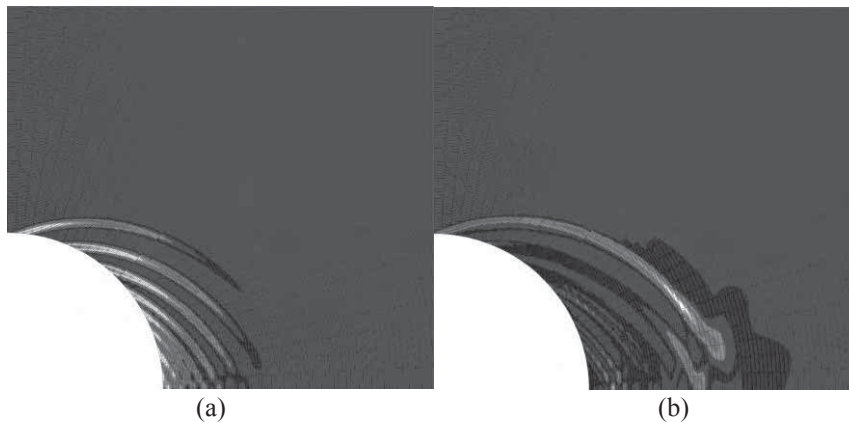


Figure 5. Equivalent strain and Vilotte's indicator for active shear band ($t = 300$ Ms)

3.3. Influence of hydric boundary condition

In the previous section, the boundary condition for the flow problem is the following: a decrease of the pore pressure from its initial value till the atmospheric pressure (Defined as Case A). Due to the hydro-mechanical coupling (dilatancy effect), this implies an injection of water into the formation (See Figure 4-a). A more realistic condition is a dripping boundary condition: a water flow can be

created only if the pore pressure in the formation is greater than the atmospheric pressure (Unilateral flow condition). This case will be referred as case B in the following. For long-term predictions, one can assumed an equilibrium between the pore pressure at the tunnel and the relative humidity of the cavity atmosphere. Indeed, this relative humidity can be controlled in waste disposal. A third case (Case C) is then considered, where a negative pressure of -5 MPa is imposed as boundary condition.

Figure 6 shows the resulting pore pressure distribution for the two latter cases. In Case B, the pore pressure becomes negative near the cavity at the end of the excavation. Then pore pressure increases progressively. In case C, the results is similar at the end of the excavation. However, after this first phase, the pore pressure remains negative as it is imposed by the boundary condition and the suction diffuses in the formation.

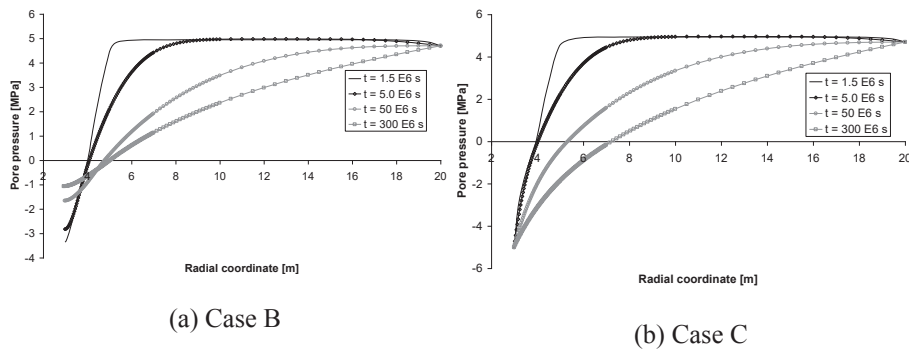


Figure 6. Pore pressure distribution in case B and case C

These pore pressure distributions have a direct influence on the convergence predicted. Table 1 presents the results for the three cases. At the end of the excavation, the convergences are more or less the same. But for the long-term response, the predicted displacements are rather different. Indeed in case C, the remaining suction near the tunnel ensures an additional strength and limits the material deformations. Moreover, the boundary condition inhibits totally the creation of shear bands pattern. The case C condition is then conservative in comparison with the two other ones.

	Case A	Case B	Case C
t = 1,5 Ms	1,5 cm	1,26 cm	1,42 cm
t = 300 Ms	22,6 cm	12,8 cm	1,44 cm

Table 1: *Cavity convergence for Cases A, B and C.*

3.4. Conclusions

Tunnelling in clay formations may induce strain localisation and fracture, as recently observed in Mol URL. An hydromechanical modelling with a strain softening constitutive model allows to reproduce such phenomena. The results are strongly dependent on the hydraulic boundary condition at the tunnel face, which has to be better analysed.

4. Conclusions

Deep underground storage of (high level and long life) nuclear waste induces severe conditions on the host rock (especially of clay/claystone) and on the engineered barrier, which is generally made of swelling clay. The long-term integrity of the permeability barriers has to be proved. The good understanding of such disposal needs high-level numerical models, including different aspects: thermal and partial saturation hydraulics effects, suction–mechanics interaction, strain localisation and fracture prediction. Highly coupled non-linear finite element codes are today necessary to tackle such challenge.

Acknowledgments

The authors are grateful to FNRS and UE (under RTN-DIGA project) for the help and grant they received.

5. References

- [ALO 90] Alonso E. E., Gens A., Josa A., A constitutive model for partially saturated soils, *Géotechnique* 40(3), pp 405-430, 1990.

- [ALO 99] Alonso E., Alcoverro J., CATSIUS CLAY PROJECT, Calculation and Testing of Behaviour of Unsaturated Clay as Barrier in Radioactive Waste Repositories, Stage 2 : Validation exercises at laboratory scale, Publication Tecnica Num. 11/99, 1999, ENRESA.
- [CHA 04] Chambon R., Collin F., Hydro mechanical numerical modelling of geotechnical problems using local second gradient models, *Modelling of Cohesive Frictional Materials* Vermeer Ehlers Hermann Ramm eds. AA Balkema, 2004, pp. 209-221
- [CHA 05] Chavant C., Fernandes R., *Evaluating the reliability of hydro-mechanical simulation : a benchmark of numerical techniques carried out by Research Group of MoMas*, 2nd International Meeting Clays in Natural & Engineered Barriers for Radioactive Waste Confinement, Tours, 14-18 March 2005, pp 249-250.
- [COL 02] Collin F., Li X.L., Radu J.P., Charlier R., Thermo-hydro-mechanical coupling in clay barriers, *Engineering Geology*, 64, 2002, pp. 179-193.
- [GEN 05] Gens A., Guimarães L., Olivella S., THMC coupling in partially saturated geomaterials. *Revue Européenne de Génie Civil*, 2005.
- [LAL 05] Laloui L., Cekerevac C., François B. Constitutive modelling of the thermo-plastic behaviour of soils. *Revue Européenne de Génie Civil*, 2005.
- [LI 00] Li X.L., Comportement hydromécanique des sols fins : de l'état saturé à l'état non-saturé, PhD Thesis, University of Liège, 2000.
- [MER 04] Mertens J., Bastiaens W., Dehandschutter B., Characterisation of induced discontinuities in the Boom Clay around the underground excavations (URF, Mol, Belgium), *Applied Clay Science* 26, pp 413– 428, 2004.
- [PHI 57] Philip J.R., De Vries D.A., Moisture movement in porous materials under temperature gradients, *EOS Trans. AGU*, 38(2), pp 222-232, 1957.
- [PIN 97] Pintado X., Lloret A. & al., TMH Laboratory tests in FEBEX phase 3, UPC Report 70-UPC-L-3-01, Barcelona, 37 pp, 1997.
- [VIL 94] Villar M.V. & al., Modelling and validation of the thermal-hydraulic-mechanical and geochemical behaviour of the clay barrier, Final report 1991-1994 CEC Contract FI2W-CT91-0102 (DOEO), 1994, CIEMAT Madrid.
- [VOL 96] Volckaert G., Bernier F., Alonso E., Gens A., Samper J., Villar M., Martin-Martin P.L., Cuevas J., Campos R., Thomas H., Imbert C., Zingarelli V., Thermal-hydraulic-mechanical and geochemical behaviour of the clay barrier in radioactive waste repositories (Model development and validation), Final report Contract Nos FI2W/CT90/0033 and FI2W/CT91/0102, 1996, European Commission, Nuclear science and technology.
- [ZER 01] Zervos A., Papanastasiou P., Vardoulakis I., Modelling of localisation and scale-effect in thick-walled cylinders with gradient elastoplasticity, *Int. J. Solids and Struct.* 38, 2001, pp. 5081-5095.
- [ZHA 04] Zhang C, Schrefler B.A., Particular aspects of internal length scales in strain localization analysis of multiphase porous materials. *Computer Methods in Applied Mechanics and Engineering*, 193, 2004, pp. 2867–2884.

Appendix K. Microstructure of bentonites: characterisation and evolution under mechanical and environmental loads (A-C. Dieudonné)

STRUCTURE OF BENTONITES

Characterisation and evolution under mechanical and hydraulic loads

23 January 2020 • Anne-Catherine Dieudonné (TU Delft)



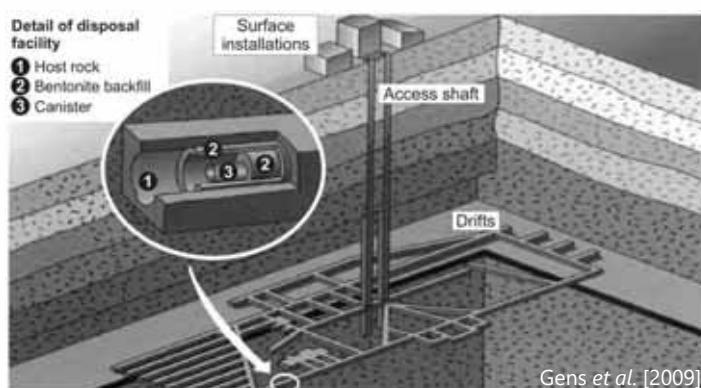
The project leading to this application has received funding from the European Union's Horizon 2020 research and innovation programme under grant agreement n° 847593.

23 January 2020

EURAD School for Radioactive Waste Management

1

MULTI-BARRIER SYSTEM



Isolation is provided by a **combination of natural and engineered barriers**

- **Natural barrier**
 - Host rock
- **Engineered barrier system**
 - Canister
 - Concrete
 - Bentonite-based materials
 - ...

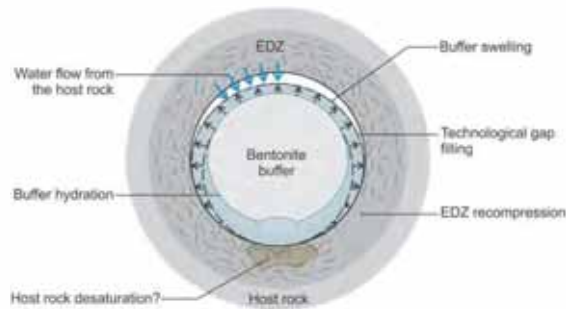
23 January 2020

EURAD School for Radioactive Waste Management

2

BENTONITE

- **Bentonite = clay material that primarily consists of montmorillonite** → tight contact with the surrounding geological formation, thereby delaying the release of radionuclides to the biosphere
 - 1) Significant swelling upon hydration = *swelling capacity*
 - 2) Very low *permeability* ($\sim 10^{-20} - 10^{-21} m^2$ in saturated conditions)
 - 3) Important radionuclides retardation capacities



23 January 2020

EURAD School for Radioactive Waste Management

eurad

3

3

BENTONITE

- **Bentonite = clay material that primarily consists of montmorillonite**
 - 1) Significant swelling upon hydration = *swelling capacity*
 - 2) Very low *permeability* ($\sim 10^{-20} - 10^{-21} m^2$ in saturated conditions)
 - 3) Important radionuclides retardation capacities
- **Different bentonites:** B75, FoCa7, Febex, GMZ, Kunigel, MX-80...
- **Different forms:** powder, compacted blocks, pellets



Febex Experiment
[Alonso et al. 2005]



REM Experiment
[Andra]

23 January 2020

EURAD School for Radioactive Waste Management

eurad

4

4

BENTONITE

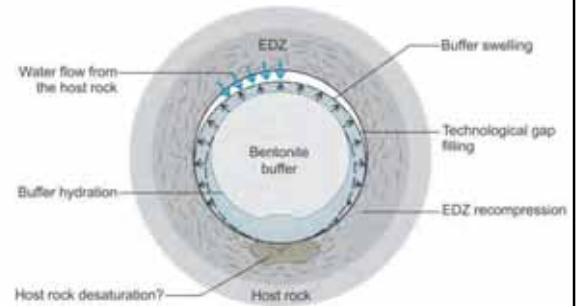
Complex behaviour under repository conditions

- Mechanical behaviour
- Water retention properties
- Permeability evolution

The sensitivity of the bentonite-based materials to mechanical and environmental loads arises from

- The **mineralogical composition** of bentonite
- The **(micro)structure** of the material

This lecture aims to provide insights into the role of the **mineralogical composition** and **(micro)structure** of bentonites on the macroscopic behaviour of the material



OUTLINE

- I. Structure of clay minerals
- II. Structure of compacted bentonites
- III. Impact of structure changes on the water retention behaviour of bentonites

OUTLINE

- I. Structure of clay minerals
- II. Structure of compacted bentonites
- III. Impact of structure changes on the water retention behaviour of bentonites

23 January 2020

EURAD School for Radioactive Waste Management

eurad

7

7

MINERALOGICAL COMPOSITION

Bentonite	Origin	Phyllosilicate	SiO ₂	K-feldspar	Plagioclase
B75 ^a	Czech Republic	75.5% montmorillonite 3.9% illite 3.1% kaolinite	9.5%		
Febex ^b	Spain	92% interstratified montmorillonite-illite (10-15% illite)	2%	traces	2%
FoCa7 ^c	France	80-85% interstratified smectite-kaolinite (50% Ca-beidellite, 50% kaolinite) 4-6% kaolinite	1.4-6%		
GMZ ^d	China	75.4% montmorillonite 0.8% kaolinite	20%	4.3%	
Kunigel V1 ^e	Japan	46-49% montmorillonite	29-38%	2.7-5.5%	4%
MX-80 ^f	USA	75-90% montmorillonite	2.8-15.2%	2-8%	9.2%

Bentonite primarily consists of **montmorillonite**, a clay mineral of the **smectite** group

^aGondoli & Večerník [2014]^bWen [2006]^cFernandez [2004], Lioret & Villar [2007]^dJNC [2000], Nakashima [2004]^eProust et al. [1990], Bruno [1993], Lajudie et al. [1994]^fLajudie et al. [1994], Madsen [1998], Montes-H [2002]

23 January 2020

EURAD School for Radioactive Waste Management

eurad

8

8

STRUCTURE OF CLAY MINERALS

Clay minerals belong to the **phyllosilicate group** (> φύλλον = leaf)

Tetrahedral and octahedral sheet

○ ○ Oxygen ● ○ Silicon

○ ○ Hydroxyl ● Aluminum, Magnesium, etc.

TOT layer
9.6 Å

TO layer
7.2 Å

Stacked in various ways

water + ions
Smectite

...

...

The type of layers and the nature of the interlayer determine the properties of the clay minerals

23 January 2020

EURAD School for Radioactive Waste Management

9

STRUCTURE OF CLAY MINERALS

Tetrahedral sheet
 Octahedral sheet

TO layer

Stacked in various ways

Kaolinite

Halloysite

Pyrophyllite

TOT layer

Stacked in various ways

Smectite

Vermiculite

Illite

Chlorite

Interstratified

23 January 2020

EURAD School for Radioactive Waste Management

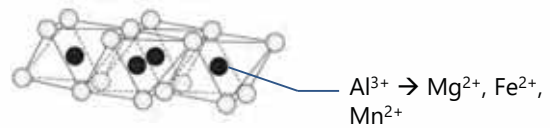
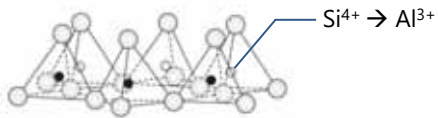
10

PHYSICOCHEMICAL PROPERTIES OF CLAY MINERALS

The surface of phyllosilicate is **not electrically neutral** !

	Kaolinite	Illite	Montmorillonite
Surface charges (meq/100 g)	5-15	20-40	80-100

- **Isomorphous substitutions**



- **Local charges**

23 January 2020

EURAD School for Radioactive Waste Management

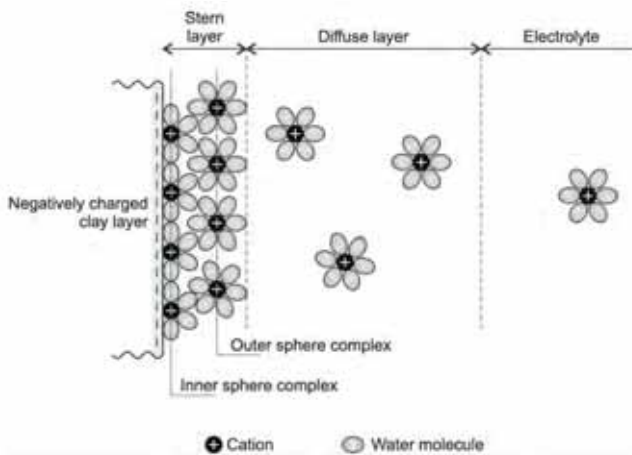
eurad

11

11

PHYSICOCHEMICAL PROPERTIES OF CLAY MINERALS

The natural tendency is to ensure **electroneutrality**



- **Cation Exchange Capacity** (meq/100g)

= number of exchangeable positive charges / 100g of dry clay mineral

- **Specific Surface area** (m^2/g)

= (interlayer surface area + clay particle external surface area) / g of clay mineral

23 January 2020

EURAD School for Radioactive Waste Management

eurad

12

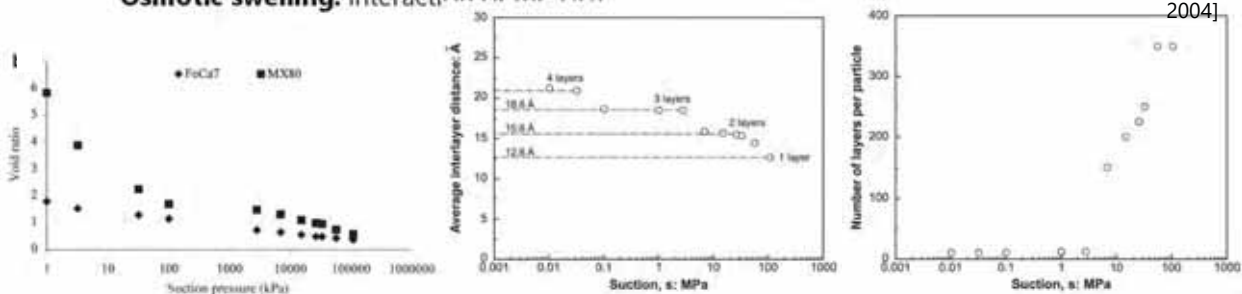
12

HYDRATION AND SWELLING MECHANISMS

Starting from dry conditions:

- **Crystalline swelling:** progressive intercalation of discrete layers of water in the interlayer space
- **Osmotic swelling:** interaction of the DDI

Compacted MX-80 bentonite [Saiyouri *et al.*, 2004]



23 January 2020

EURAD School for Radioactive Waste Management

eurad

13

13

OUTLINE

- I. Structure of clay minerals
- II. Structure of compacted bentonites
- III. Impact of structure changes on the water retention behaviour of bentonites

23 January 2020

EURAD School for Radioactive Waste Management

eurad

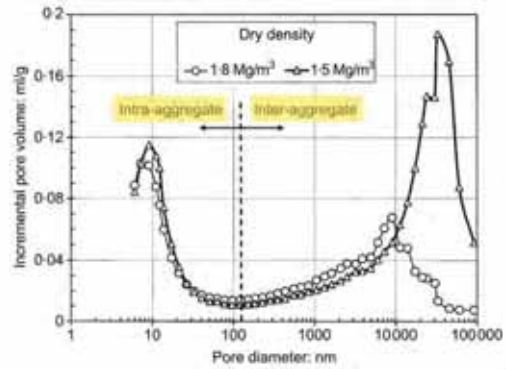
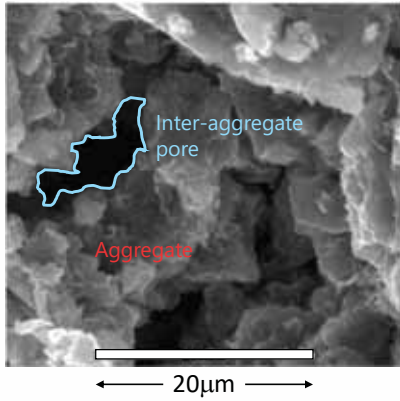
14

14

STRUCTURE OF COMPACTED BENTONITES

Compaction of bentonite on the dry side of optimum confers to the material an **aggregated fabric** with an (apparent) **bimodal pore size distribution**

Compacted Febex bentonite
Lloret *et al.* [2003]



23 January 2020

EURAD School for Radioactive Waste Management

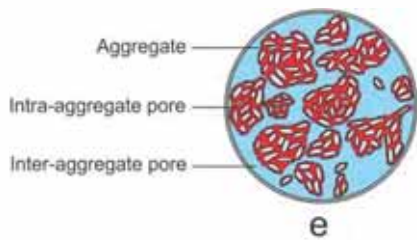
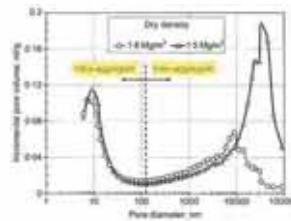
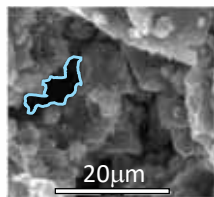
eurad

15

15

STRUCTURE OF COMPACTED BENTONITES

Compacted Febex bentonite
Lloret *et al.* [2003]



23 January 2020

EURAD School for Radioactive Waste Management

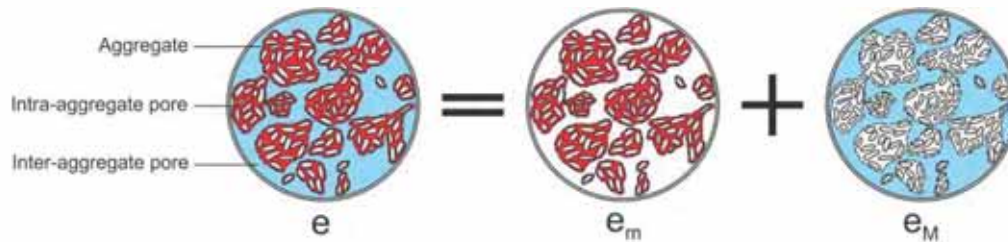
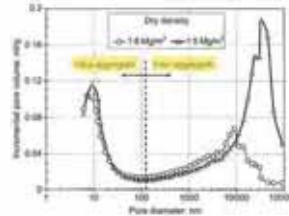
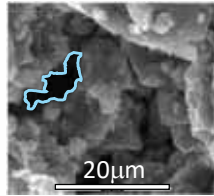
eurad

16

16

STRUCTURE OF COMPACTED BENTONITES

Compacted Febex bentonite
Lloret *et al.* [2003]



23 January 2020

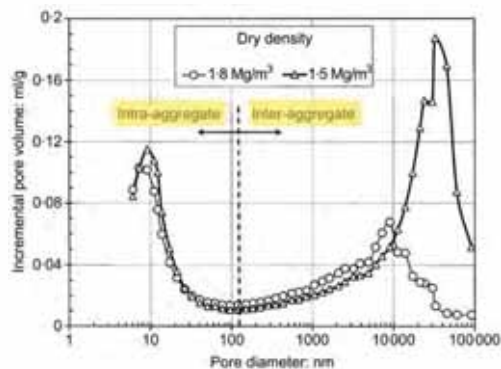
EURAD School for Radioactive Waste Management

eurad

17

17

EFFECT OF MECHANICAL LOADS



Compacted Febex bentonite
Lloret *et al.* [2003]

23 January 2020

EURAD School for Radioactive Waste Management

eurad

18

18

- Pore volume:** increasing the compaction effort at constant water content decreases the volume of macropores, while the volume of micropores is hardly affected
- Pore size:** compaction shifts the size of dominant macropores towards smaller pore radii (#AEV)

STRUCTURE OF COMPACTED BENTONITES

BUT... This is not the end of the story !

23 January 2020

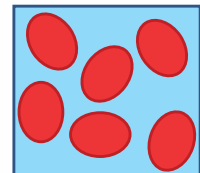
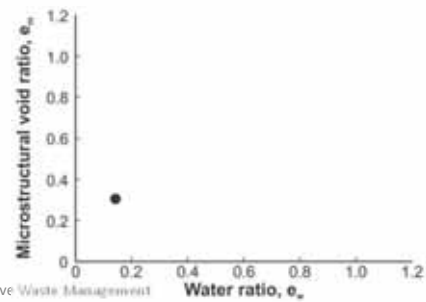
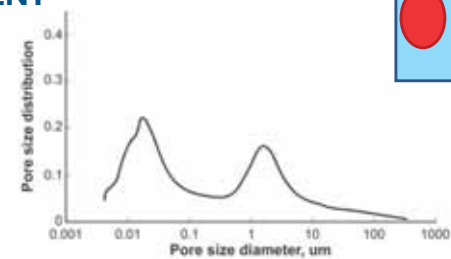
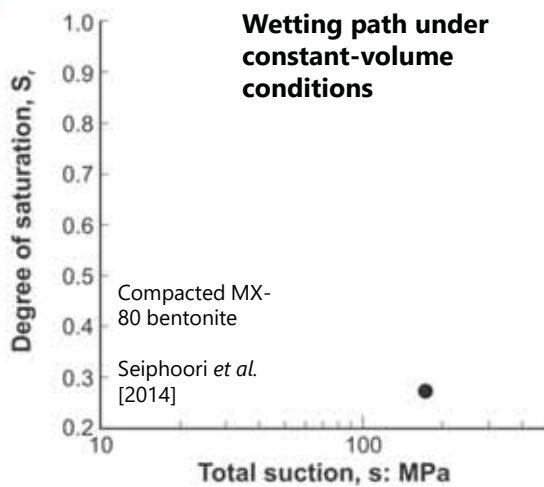
EURAD School for Radioactive Waste Management

eurad

19

19

EFFECT OF CHANGES IN WATER CONTENT



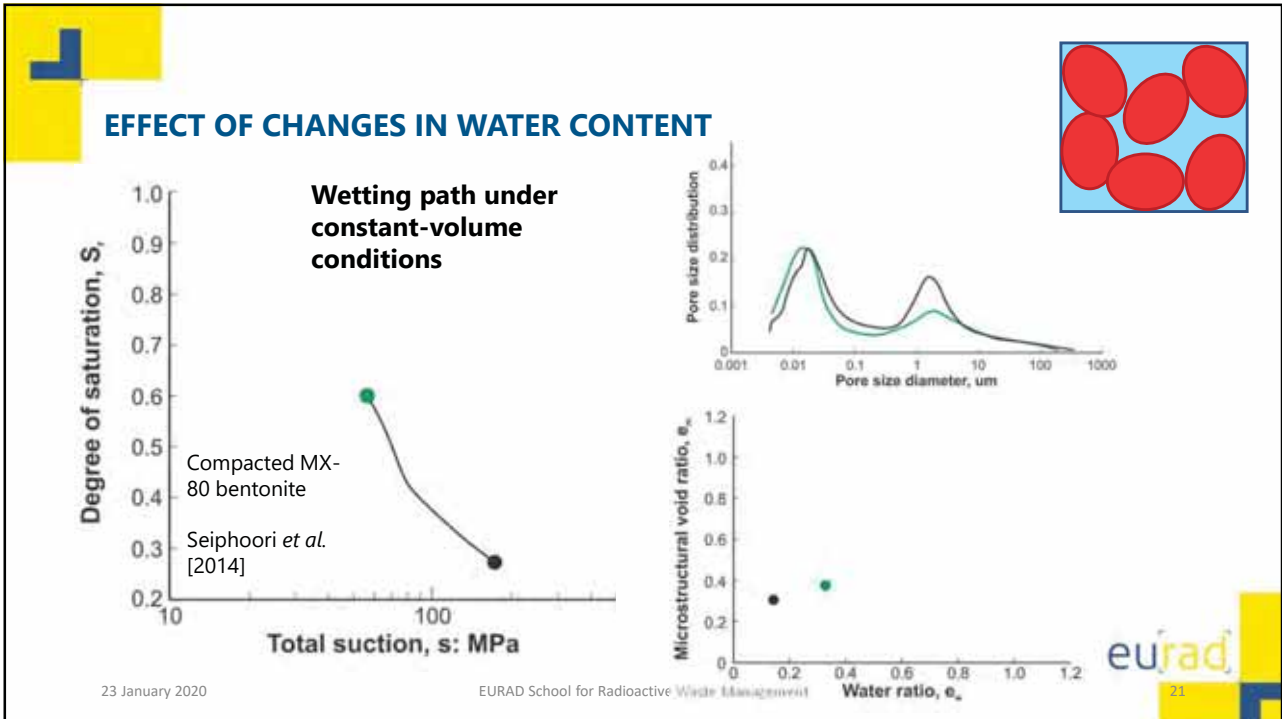
23 January 2020

EURAD School for Radioactive Waste Management

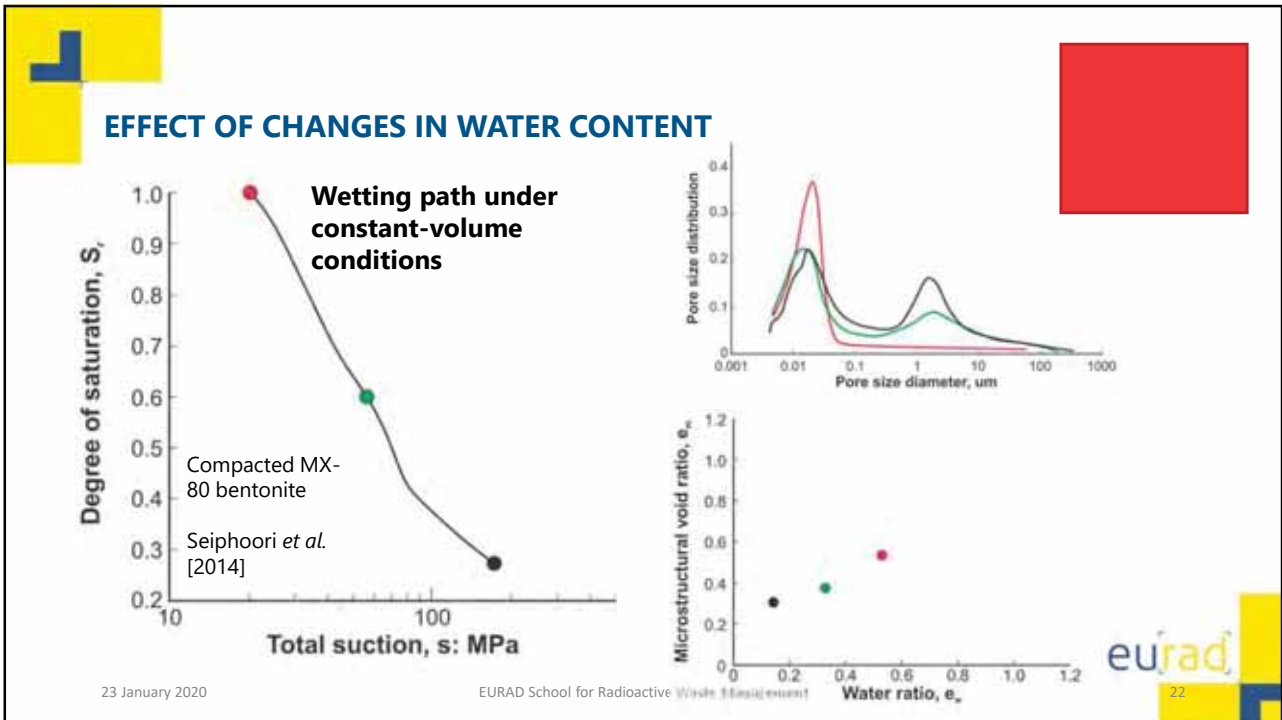
eurad

20

20



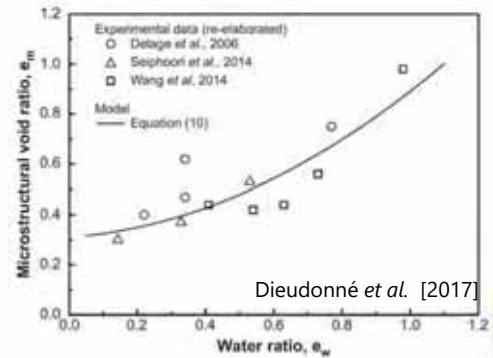
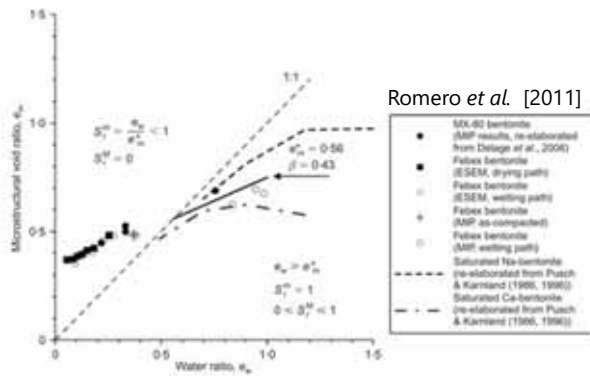
21



22

MICROSTRUCTURE EVOLUTION

- Mechanical loads do not affect the volume of micropores
- Wetting leads to an increase of the micropore volume



23 January 2020

EURAD School for Radioactive Waste Management

23

23

OUTLINE

- I. Structure of clay minerals
- II. Structure of compacted bentonites
- III. Impact of structure changes on the water retention behaviour of bentonites

23 January 2020

EURAD School for Radioactive Waste Management

eurad

24

24

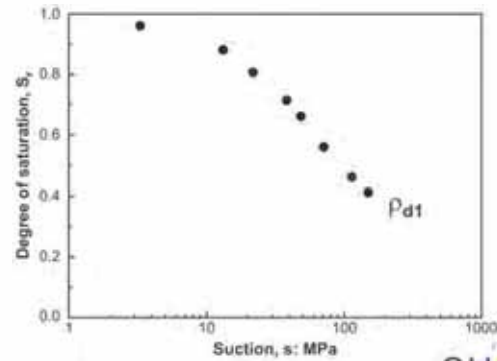
LIMITATIONS OF TRADITIONAL WATER RETENTION MODEL

Water retention curve: **amount of water stored = $f(\text{suction...})$**

(generally a unique relationship !)

Classical approaches for modelling the water retention behaviour:

parameters to be fit using experimental data



23 January 2020

EURAD School for Radioactive Waste Management

25

25

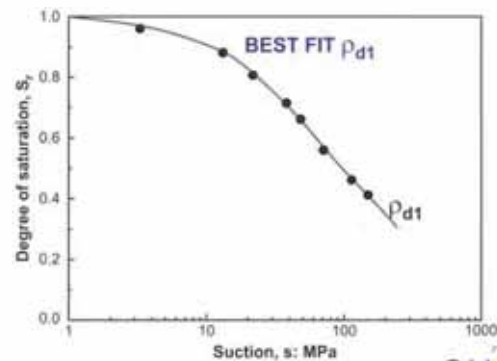
LIMITATIONS OF TRADITIONAL WATER RETENTION MODEL

Water retention curve: **amount of water stored = $f(\text{suction...})$**

(generally a unique relationship !)

Classical approaches for modelling the water retention behaviour:

parameters to be fit using experimental data



23 January 2020

EURAD School for Radioactive Waste Management

26

26

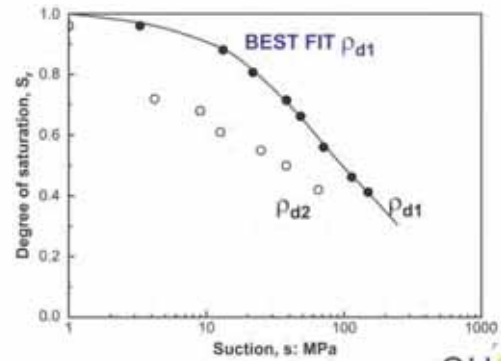
LIMITATIONS OF TRADITIONAL WATER RETENTION MODEL

Water retention curve: amount of water stored = $f(\text{suction...})$

(generally a unique relationship !)

Classical approaches for modelling the water retention behaviour:

parameters to be fit using experimental data



23 January 2020

EURAD School for Radioactive Waste Management

eurad

27

27

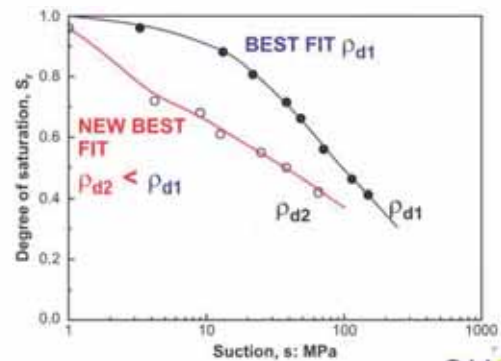
LIMITATIONS OF TRADITIONAL WATER RETENTION MODEL

Water retention curve: amount of water stored = $f(\text{suction...})$

(generally a unique relationship !)

Classical approaches for modelling the water retention behaviour:

parameters to be fit using experimental data



23 January 2020

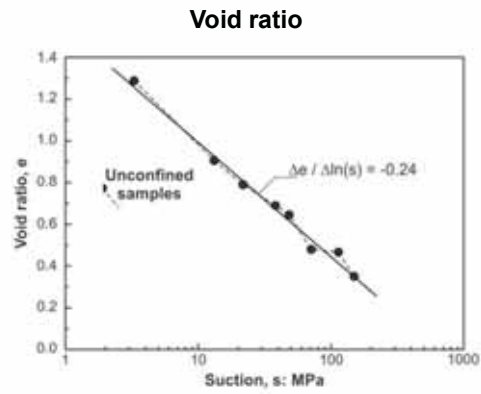
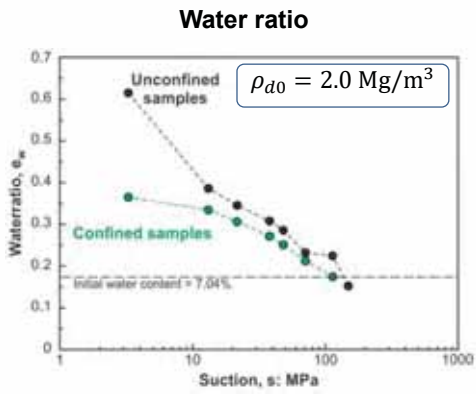
EURAD School for Radioactive Waste Management

eurad

28

28

WATER RETENTION BEHAVIOUR



Compacted MX-80 bentonite/sand mixture
Gatabin *et al.* [2016]

23 January 2020

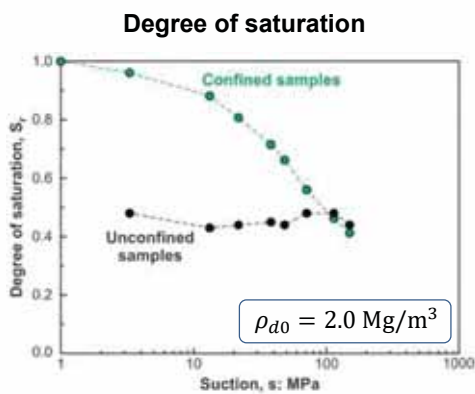
EURAD School for Radioactive Waste Management



29

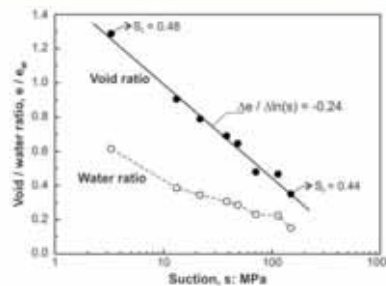
29

WATER RETENTION BEHAVIOUR



→ Strong **competing effects** of

- Water uptake (Δe_w)
- Swelling (Δe)



Compacted MX-80 bentonite/sand mixture
Gatabin *et al.* [2016]

23 January 2020

EURAD School for Radioactive Waste Management



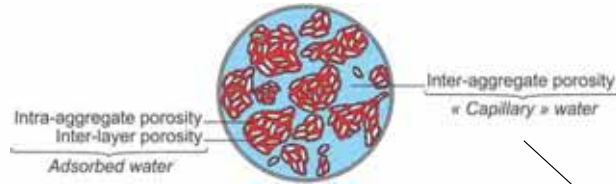
30

30

WATER RETENTION MODEL

$$e_w = S_r \cdot e = e_{wm} + e_{wM}$$

Dieudonné et al. [2017]



Dubinin model

$$e_{wm}(s, e_m) = e_m \exp[-(C_{ads}s)^{n_{ads}}]$$

« Van-Genuchten » model

$$e_{wM}(s, e, e_m) = (e - e_m) \left[1 + \left(\frac{s}{a} \right)^n \right]^{-m}$$

With $a = \frac{A}{e - e_m}$

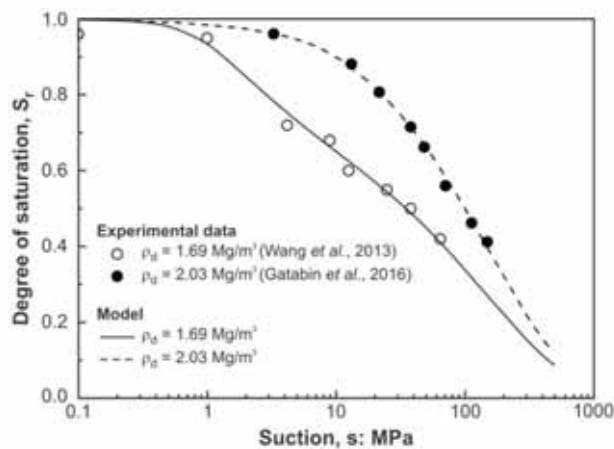


31

31

VALIDATION OF THE WATER RETENTION MODEL

Calibration of the model along constant volume wetting paths

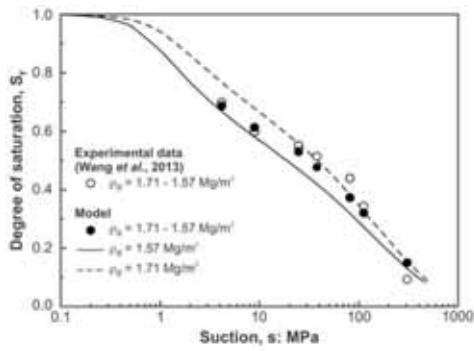


32

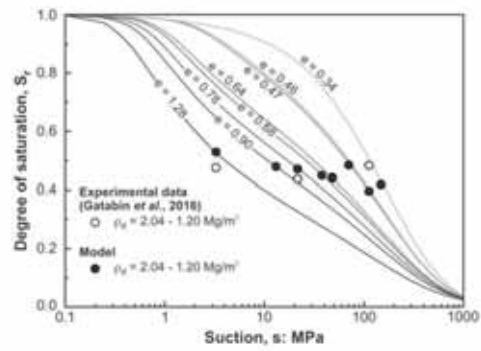
32

VALIDATION OF THE WATER RETENTION MODEL

Validation of the model along free swelling wetting paths

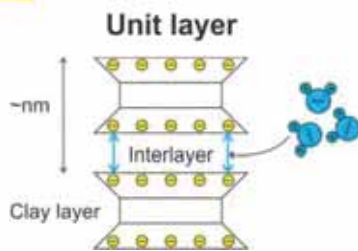


$$\rho_{d0} = 1.67 \text{ Mg/m}^3$$

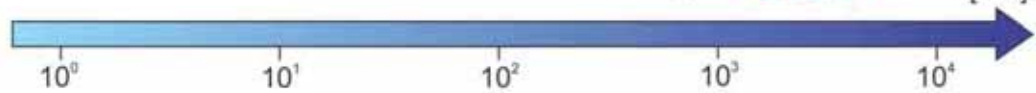


$$\rho_{d0} = 2.0 \text{ Mg/m}^3$$

SUMMARY



- Montmorillonite layers are electronegative
- The natural tendency is to ensure electroneutrality
- Hydrated cations and water molecules are attracted in the interlayer



SUMMARY

- Aggregated structure created upon compaction
- Structure evolves with mechanical and hydraulic loads, among others

23 January 2020 EURAD School for Radioactive Waste Management

35

CHALLENGES

- **Defining quantitative descriptors of the microstructure**
 - So far, the microstructure has essentially been described by pore volumes
- **Incorporating information from the microstructure in constitutive/numerical models**
- **Keep in mind the limitations of imaging and microstructure investigation techniques (and of the interpretation of their results)**
- **Other aspects have not been addressed in this presentation:**
 - Time-dependency and ageing (cf. non-equilibrium conditions)
 - Effects of temperature, water chemistry...
 - Pellet mixtures (bring another level of complexity)

23 January 2020 EURAD School for Radioactive Waste Management

36



STRUCTURE OF BENTONITES

Characterisation and evolution under mechanical and hydraulic loads

23 January 2020 • Anne-Catherine Dieudonné (TU Delft)



The project leading to this application has received funding from the European Union's Horizon 2020 research and innovation programme under grant agreement n° 847593.

23 January 2020

EURAD School for Radioactive Waste Management

Appendix L. Microstructure of bentonites : characterisation and evolution under mechanical and environmental loads (A-C. Dieudonné) - Paper

Microstructure of bentonites: characterisation and evolution under mechanical and environmental loads

Anne-Catherine Dieudonné

Delft University of Technology, the Netherlands

1 Introduction

The role of engineered barriers in geological disposal of radioactive waste is to form a tight contact with the host rock, and thereby limit the release of radionuclides to the biosphere. The low permeability and important swelling capacity of bentonites are therefore essential properties. In order to characterize the swelling capacity of compacted bentonites, two macroscopic physical quantities can be measured: the swelling potential and the swelling pressure. These quantities are determined after saturation of a bentonite sample under different confining conditions. The swelling potential $\Delta H/H_i$ corresponds to the ratio between the change in sample height ΔH upon saturation under oedometer conditions, and its initial height H_i . On the contrary, the swelling pressure S_P is defined as the pressure required to prevent volume changes upon wetting. Figure 1 presents the evolution of the swelling pressure of five reference bentonites with dry density. While important differences are observed between the different bentonites, they all show an increase of their swelling pressure with dry density. Furthermore, the swelling pressures reached upon saturation (typically of the order of few MPa to around 15 MPa for dry densities ranging between 1.5 and 1.7 Mg/m^3) are significantly higher than for non-swelling clays (few hundreds kPa).

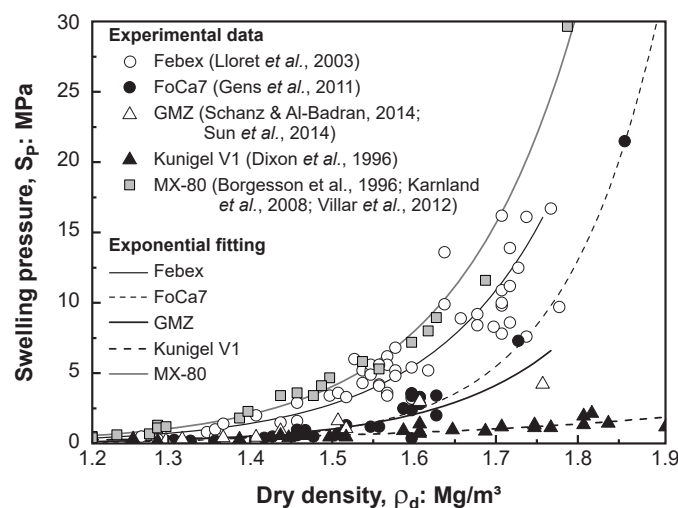


Figure 1: Evolution of the swelling pressure of five reference bentonites with dry density.

While the swelling capacity of compacted bentonite is firstly observed at the macroscopic scale, this property essentially results from physicochemical phenomena taking place at a microscopic scale. Therefore, a good comprehension of the material microstructure is of paramount importance for a better understanding of the hydromechanical behaviour of compacted bentonites and for the development of physically-based constitutive models.

These lecture notes are organized as follows. The mineralogical composition of bentonites is first presented. The structure and coupled processes taking place in compacted bentonites are then described

starting from the smallest scale of interest, namely the scale of the clay minerals. Accordingly, the structure and physicochemical properties of clay minerals are presented. Attention is then focused on the hydration and swelling mechanisms in smectites, the main constituents of bentonites. Increasing the scale of observation, the structure of compacted bentonites is addressed. The water storage and hydration mechanisms are analysed. The different factors, both mechanical and environmental, affecting the material structure are presented. Finally, modelling challenges and prospects are addressed.

2 Definition and mineralogical composition of bentonites

The name bentonite dates back to the late 19th century when Knight [1898] used the term to describe highly plastic and swelling clays from the Cretaceous Fort Benton group in Wyoming, USA. The first definitions of bentonite [Hewitt, 1917; Wherry, 1917; Ross & Shannon, 1926] suggested a genetic origin of the material, generally from the alteration of tuff or volcanic ash. Nowadays, the term bentonite has lost its mineralogical definition and refers to any smectite-rich material regardless of its geological origin [Grim, 1968]. More specifically, in the context of nuclear waste disposal, bentonite primarily consists of montmorillonite, a clay mineral of the smectite group which exhibits significant swelling upon hydration [Apted, 1995].

Table 1 presents the mineralogical composition of five reference bentonites which are studied as potential barriers for the isolation of high-level and intermediate-level radioactive waste. Besides montmorillonite, these bentonites contain variable quantities of other clay minerals (generally kaolinite and illite, which are non-swelling clay minerals), quartz¹, feldspars, plagioclase, gypsum, pyrite and calcite. They can also hold small amounts of organic matter (usually less than 0.5%). Although present in limited quantities, some of these accessory minerals may influence the properties of bentonites, especially their chemical reactivity [Sellin & Leupin, 2013].

Bentonite	Origin	Phyllosilicate	SiO ₂	K-feldspar	Plagioclase
Febex ^a	Spain	92% interstratified montmorillonite–illite (10–15% illite)	2%	traces	2%
FoCa7 ^b	France	80–85% interstratified smectite–kaolinite (50% Ca-beidellite, 50% kaolinite) 4–6% kaolinite	1.4–6%		
GMZ ^c	China	75.4% montmorillonite 0.8% kaolinite	20%	4.3%	
Kunigel V1 ^d	Japan	46–49% montmorillonite	29–38%	2.7–5.5%	4%
MX-80 ^e	USA	75–90% montmorillonite	2.8–15.2%	2–8%	9.2%

^aFernandez [2004], Lloret & Villar [2007]

^bProust *et al.* [1990], Bruno [1993], Lajudie *et al.* [1994]

^cWen [2006]

^dJNC [2000], Nakashima [2004]

^eLajudie *et al.* [1994], Madsen [1998], Montes-H [2002]

Table 1: Mineralogical composition (main minerals) of five reference bentonites.

¹In Table 1, the content in SiO₂ corresponds to the total content in quartz, cristobalite and tridymite.

3 Structure of clay minerals

3.1 Structure and mineralogy

Clay minerals belong to the phyllosilicate group. The term phyllosilicate derives from the Greek *phylon*, leaf, emphasizing the layered structure of clay minerals. This structure is based on the combination of two basic crystal structural units, namely the tetrahedral sheet and the octahedral sheet.

The tetrahedral sheet is also called silica sheet. As shown in Figure 2(a), it is made up of silica tetrahedra (SiO_4)⁴⁻, which are linked together by sharing three of their four oxygen ions. All tetrahedra of the silica sheet are oriented in the same direction and define hexagonal cavities. Similarly, Figure 2(b) shows the structure of the octahedral sheet, also termed alumina sheet. The octahedral sheet is composed of aluminium or magnesium octahedra in which the cation bonds with six oxygen atoms or hydroxyl groups. Octahedra are all laid on a triangular face and linked together by sharing their six oxygens or hydroxyls.

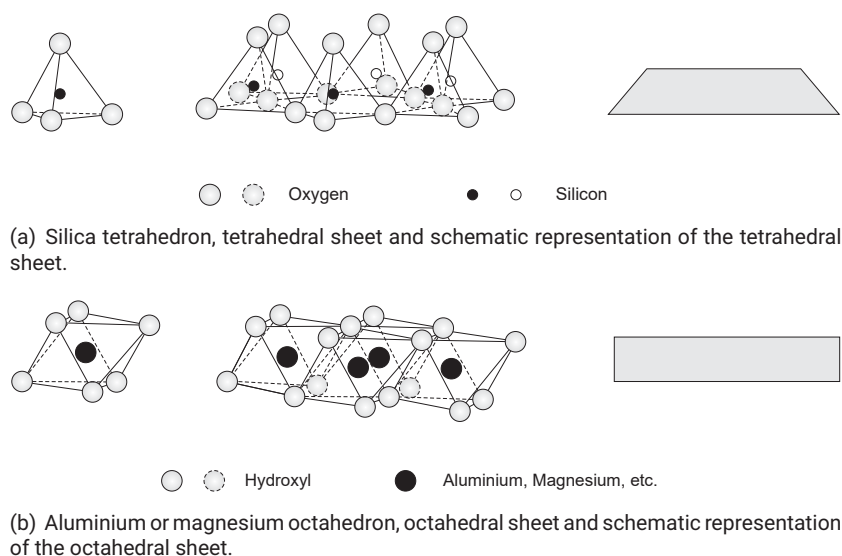


Figure 2: Basic crystal structural units of phyllosilicates [Mitchell & Soga, 2005].

Tetrahedral and octahedral sheets bond together to form layers. Two types of layers are defined, namely the TO layer and the TOT layer. The TO layer, also called 1:1 layer, is made up of one tetrahedral sheet and one octahedral sheet, and has a thickness of 7.2 Å. On the other hand, the TOT layer, or 2:1 layer, consists of an octahedral sheet sandwiched between two tetrahedral sheets. Its thickness in the absence of any polar molecule is 9.6 Å. In both cases, strong primary bonds exist between the sheets of a same layer [Stępkowska, 1990].

Conversely, the bonds between two successive layers are generally weaker. The type of layers and the nature of the interlayer determine the properties of the different clay minerals and, in particular, their behaviour in presence of water. On this basis, clay minerals are classified into different groups, as depicted in Figure 3. The main clay minerals composing bentonites, namely smectite, kaolinite and illite, are to be found in this classification.

The structure of kaolinite is based on the TO layer, whereas the structures of smectite and illite are built on the TOT layer. In kaolinite, hydroxyl groups and oxygen ions of two consecutive layers are bonded through hydrogen bonds which maintain the interlayer closed and prevent swelling. Only the external surfaces can adsorb water, allowing limited swelling. In smectites, water molecules and ions are able to penetrate the interlayer space, causing the expansion of the mineral upon wetting. Conversely, the interlayer space of illite is occupied by potassium ions whose molecular size is close to the one of the hexagonal cavities of the tetrahedral sheet, and which therefore strongly lock the layers together through ionic bonds, thereby preventing swelling. When layers of different types are stacked together, the mineral is referred to as a mixed-layer or interstratified mineral, and its behaviour depends on the nature of the different layers and interlayers.

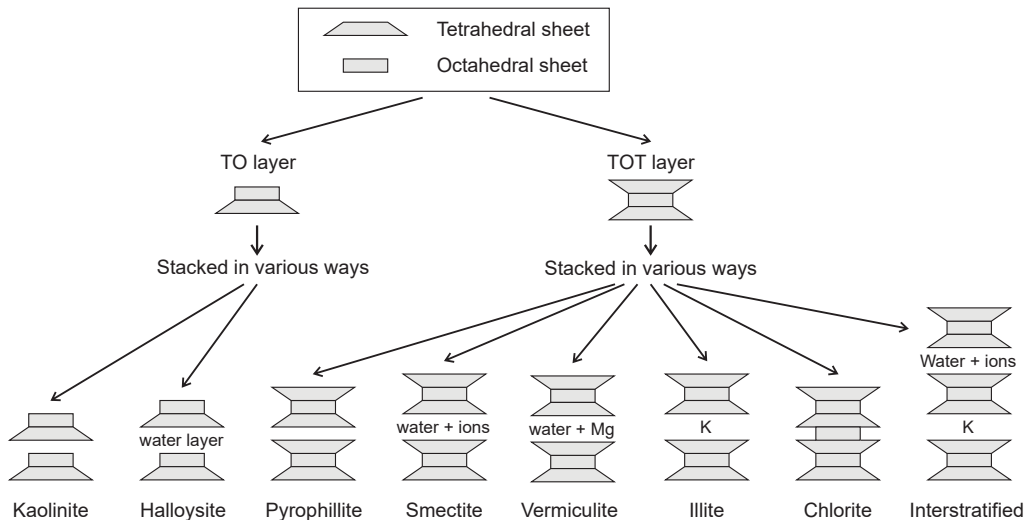


Figure 3: Classification of clay minerals [Mitchell & Soga, 2005].

Finally, clay layers stack together to form particles. Depending on the nature of the interlayer and the water content, the number of layers in a particle may vary from a few to several hundreds [Saiyouri *et al.*, 2004]. The behaviour of the different clay minerals in presence of water is further discussed in the next two sections, with a special attention given to smectites.

3.2 Physicochemical properties

A fundamental characteristic of clay minerals is their electronegativity. The surface of phyllosilicates is indeed not electrically neutral and surface charges exist (Table 2). These charges have two different origins:

- **Isomorphous substitutions**, which refer the replacements of ions in the tetrahedral or octahedral sheets for other ions, without significant change in the layer structure. When a cation in a tetrahedral or octahedral sheet is replaced by a lower valency ion, the substitution leads to an excess of negative charge at the surface of the layer. The most common isomorphous substitutions in clay minerals are Al^{3+} for Si^{4+} in the tetrahedral sheet and Mg^{2+} , Fe^{2+} and Mn^{2+} for Al^{3+} in the octahedral sheet.

Isomorphous substitutions are common in smectites, which explains their important surface charges compared to other phyllosilicates (Table 2). Depending on the position of the charges, smectites are classified into montmorillonites, whose charges are predominantly in octahedral position, and beidellite, whose charges are predominantly located in tetrahedral position. Bentonites are mainly composed of montmorillonite.

- **Local charges**, which are due to broken bonds and an incomplete neutralization of charges on the edges of the layers. The value of these local charges depends on the pH of the solution [Grunberger, 1995]. In acid environments, charges are positive due to the fixation of H^+ protons on the O^{2-} anions; they are negative if the solution is basic.

According to Mitchell & Soga [2005], local charges are thought to contribute up to 20% towards the total charge deficit.

	Kaolinite	Illite	Montmorillonite
Surface charges (meq/100 g)	5–15	20–40	80–100

Table 2: Range of surface charges in kaolinite, illite and montmorillonite [Yong *et al.*, 2009].

The natural tendency is to ensure electroneutrality of the clay particle and therefore, the layer will tend to adsorb cations present in the environment. These cations that form the interlayer are called exchangeable cations as they can be exchanged with other cations of the solution [Van Olphen, 1963]. According to Sposito *et al.* [1984], exchangeable cations are adsorbed at the surface of the layer by at least three different mechanisms:

- **Inner-sphere complexation**, by which cations bind to the clay surface (through primary bonds) without any interposed water molecule.
- **Outer-sphere complexation**, by which solvated cations are attracted and bonded to the clay surface through hydrogen bonds and electrostatic forces.

Inner-sphere and outer-sphere complexes form the Stern layer [Stern, 1924] (Figure 4). These complexes may be insufficient to balance the negative charges at the clay surface, so that a third mechanism allows to neutralize the residual charges.

- **Electrostatic attraction** of solution cations, resulting from the presence of unbalanced charges at the surface of the clay layer. The attracted cations from the solution form the diffuse double layer (Figure 4).

As mentioned by Sposito *et al.* [1984], outer-sphere complexes differ from cations adsorbed in the diffuse layer in their residence time, i.e. the amount of time that a cation remains adsorbed at a given position. The residence time of cations from the diffuse layer is of the order of 10 ps, which is significantly shorter than the 100 ps residence time of outer-sphere complexes and over 10 ns of inner-sphere complexes (the strongest the bonding, the longest the residence time).

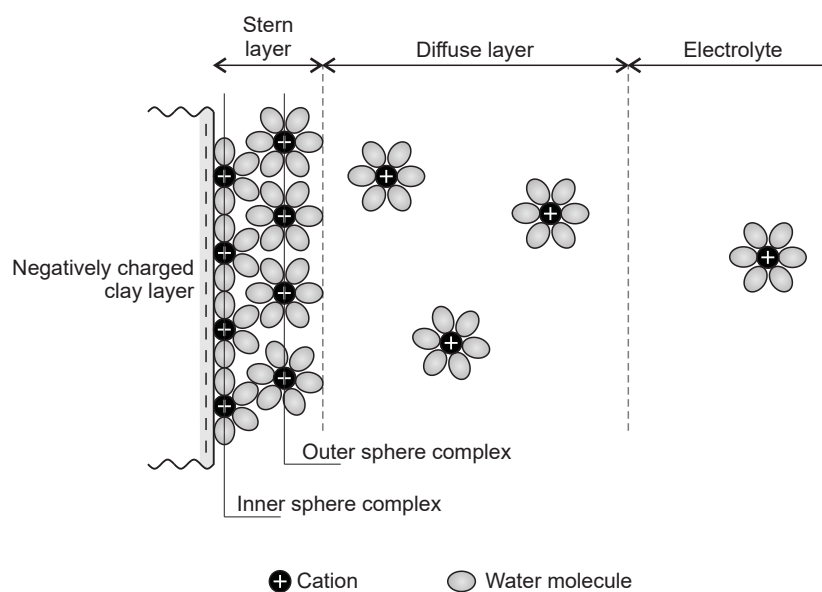


Figure 4: Mechanisms of cation adsorption at the surface of a clay layer [after Meunier, 2005; Yong *et al.*, 2009].

The cation exchange capacity (CEC) measures the ability of smectites to adsorb cations from the solution. The CEC is defined as the number of exchangeable positive charges per 100 g of dry clay mineral. It is expressed in milliequivalents per 100 g of dry clay (meq/100 g). In general, the interlayer comprises a mixture of different cation species, essentially Na^+ , Ca^{2+} and Mg^{2+} in bentonites. Table 3 presents the CEC and main exchangeable cations of five reference bentonites. Based on the nature of the dominating exchangeable cations, bentonites are referred to as sodium bentonite or calcium bentonite: Febex and Foca7 are calcium bentonites, GMZ and Kunigel V1 are sodium-calcium bentonites, while MX-80 is a sodium bentonite. As explained in the next section, the nature of the exchangeable cation influences the swelling capacity of the bentonite, with a higher capacity in sodium bentonites.

Finally, another important physicochemical parameter of clay minerals is their specific surface area S_S , expressed in m^2/g . The total specific surface area comprises both the interlayer surface area and the

Bentonite	CEC (meq/100 g)	Exchangeable cations			Specific surface (m ² /g)
		Na ⁺ (meq/100 g)	Ca ²⁺ (meq/100 g)	Mg ²⁺ (meq/100 g)	
Febex ^a	111	25	47	36	725
FoCa7 ^b	69	3	63		454
GMZ ^c	77.3	43	29	12	570–597
Kunigel V1 ^d	73	41	29	3	389–687
MX-80 ^e	76–88	61–67	8–10	3–5	512–800

^aLloret & Villar [2007]

^bSaiyouri *et al.* [2004]

^cWen [2006], Ye *et al.* [2009]

^dKomine & Ogata [1996], JNC [2000], Marcial *et al.* [2002], Komine [2004]

^ePusch [1982], Madsen [1998], Bradbury & Baeyens [2003], Villar [2007]

Table 3: Cation exchange capacity and specific surface of five reference bentonites.

clay particle external surface area. Table 3 presents the values of specific surface area for five reference bentonites. Obviously, a strong correlation of the CEC with the specific surface is observed, the CEC being all the more important that the specific surface is large.

3.3 Hydration and swelling mechanisms in smectites

The swelling capacity of clay minerals refers to their ability to expand upon hydration and shrink upon drying. Accordingly, a good understanding of the hydration mechanisms is required to puzzle out the swelling mechanisms. Starting from dry conditions, two regimes of swelling are generally identified [Norrish, 1954]:

- **Crystalline swelling**, which is predominant at low water contents and corresponds to the progressive intercalation of discrete layers of water in the interlayer space (development of the Stern layer). In the case of smectites, one, two, three or four layers of water molecules are sequentially intercalated, leading the interlayer to increase sequentially from 9.6 Å with no water to 12.6 Å, 15.6 Å, 18.6 Å and 21.6 Å respectively. Figure 5(a) presents the evolution of the interlayer thickness during hydration of compacted MX-80 bentonite.

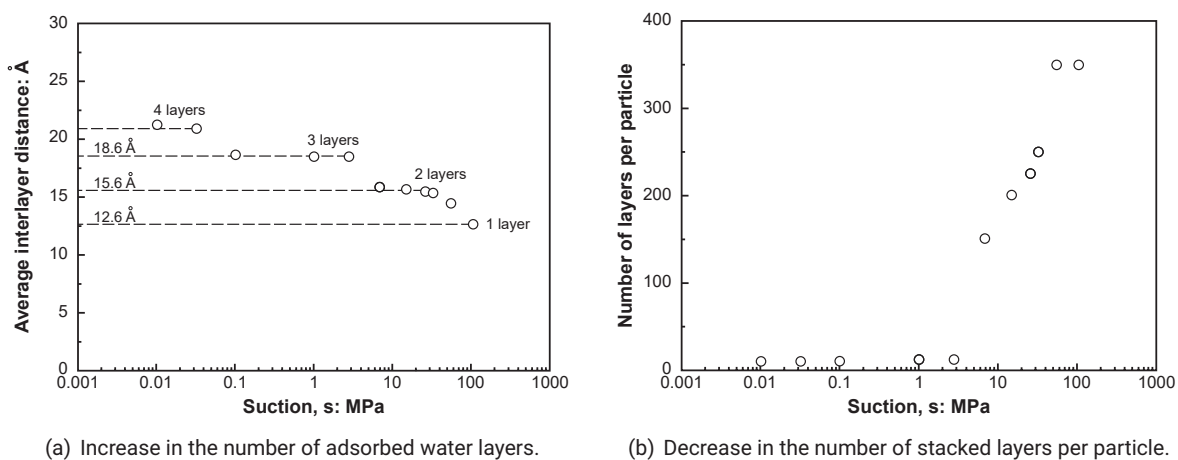


Figure 5: Effect of hydration (suction decrease) on particles of MX-80 bentonite [Saiyouri *et al.*, 2004].

As shown in Figure 5(b), the insertion of layers of water molecules in the interlayer space leads to a reorganisation of the solid matrix [Tessier, 1978]. During hydration, clay particles initially made

of 350 layers divide into smaller structures of around 10 layers. These smaller particles are able to fix high amount of water and form water layers up to 100 Å thick [Saiyouri *et al.*, 2000].

- **Osmotic swelling**, which is associated with interactions of the diffuse double layer. Under high water content, the interlayer is a highly concentrated medium as compared with the bulk solution. As a consequence of the difference in cation concentrations, the cations near the clay surface tend to diffuse away. However, the negative electric field at the clay surface prevents the cation to freely diffuse. Contrary to crystalline swelling, swelling is a continuous phenomenon in the osmotic domain. Furthermore, it occurs both between clay layers and between clay particles [Cases *et al.*, 1990; Mitchell & Soga, 2005].

Neglecting the existence of the Stern layer, the clay – water system has traditionally been described using the diffuse double layer (DDL) theory early developed by Gouy [1910] and Chapman [1913]. In the DDL theory, a unique particle surrounded by an ionic solution is considered. The clay layer is supposed uniformly charged over its surface and ions are considered as point charges without interaction. The electrical potential Ψ around the clay layer (Figure 6(a)) is then given by

$$\Psi = \Psi_0 \exp(-\kappa x_c) \quad (1)$$

where Ψ_0 is the electrical potential at the clay layer surface and x_c is the distance from the clay layer surface. κ^{-1} is the Debye-Hückel length given by

$$\kappa^{-1} = \left(\frac{\varepsilon_r \varepsilon_0 k T}{2 n_0 e^2 z^2} \right)^{1/2} \quad (2)$$

where ε_r is the dielectric constant of the electrolyte, ε_0 is the dielectric permittivity of the vacuum ($= 8.8542 \times 10^{-12} \text{ C}^2/\text{J}\cdot\text{m}$), k is the Boltzmann constant ($= 1.38 \times 10^{-23} \text{ J/K}$), T is the absolute temperature, n_0 is the ion concentration in the electrolyte, e is the electric elementary charge ($= 1.602 \times 10^{-19} \text{ C}$) and z the valency of the ion in the electrolyte.

The diffuse double layer theory can be used to describe the behaviour of colloidal solutions in which clay minerals are dispersed in a continuous liquid phase [Van Olphen, 1963]. However, in compacted bentonites, the density is such that clay minerals interact through their diffuse double layer and a repulsion force takes place, similarly to two magnets that are brought close to each other. This repulsion force may be assimilated to a swelling pressure (Figure 6(b)). Bolt [1956] used the diffuse double layer theory to predict the swelling pressure developed between two parallel clay layers. Although one can show that this hypothesis is not satisfied in compacted bentonites [see Segad *et al.*, 2010, for a discussion], the theory provides interesting qualitative results. In particular, the repulsive swelling pressure σ_R is expressed as

$$\sigma_R = 2 n_0 k T (\cosh u - 1) \quad (3)$$

where u is a non-dimensional potential at the mid-plane between the two clay layers². This non-dimensional potential u will be all the more important given that the electrical potential Ψ around a single clay layer is large.

Despite the restrictive assumptions behind the double diffuse layer theory, some interesting and qualitative conclusions may be drawn concerning the factors affecting the swelling pressure of bentonite-based materials:

- the higher the dry density, the higher the swelling pressure (Figure 1). Under the assumption of homogeneous and parallel particle distribution, an increase in the dry density yields a decrease in the distance between clay minerals, hence an increase in the mid-plane potential u (Figure 6(b)).
- the higher the CEC, the higher the swelling pressure. A high CEC corresponds to an important surface charge density, hence an important electric potential Ψ_0 and an important mid-plane potential u .
- the lower the valency z of the exchangeable cation, the higher the mid-plane potential u and the higher the swelling pressure. Accordingly, the swelling properties are enhanced for sodium bentonites compared to calcium bentonites.

²Details concerning the precise determination of u can be found in Van Olphen [1977] and Tripathy *et al.* [2004].

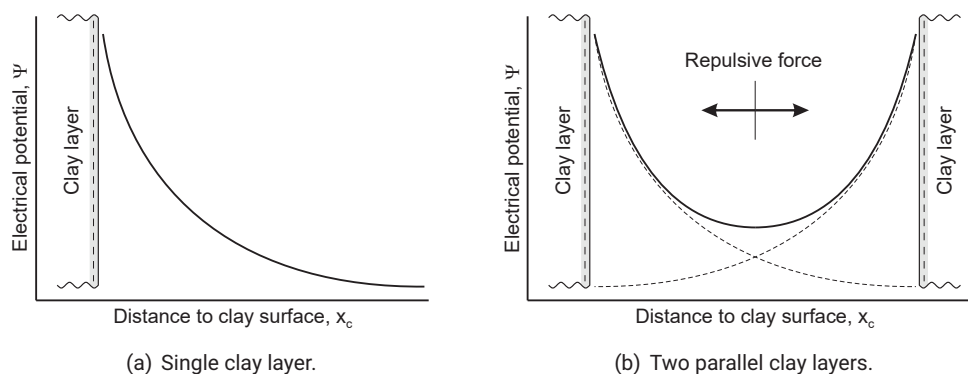


Figure 6: Representation of the double diffuse layer, according to Gouy-Chapman theory. Evolution of the electrical potential as a function of the distance from the clay layer surface.

Analysing in details the mineralogical composition (Table 1), cation exchange capacity and specific surface (Table 3) of the five reference bentonites, the obvious difference in swelling pressure developed by the different materials may be partly explained by the diffuse double layer theory. For instance, one can observe that the low montmorillonite content of Kunigel V1 bentonite is associated with low swelling pressures. Conversely, the important montmorillonite content and Na^+ dominant exchangeable cation of MX-80 bentonite lead to the development of very high swelling pressures upon hydration under constant volume conditions.

4 Structure of compacted bentonites

4.1 Experimental techniques

The microstructure of compacted bentonites³ can be investigated by using different experimental techniques depending on the type of information required and the scale under consideration. The information that may be obtained from microstructural experimental study includes the pore types, distribution and connectivity, the arrangement and distribution of clay particles and aggregates, the aggregate size and morphology, and the inter-particle contact orientations and contact force directions [Romero & Simms, 2008]. The scale that can be investigated ranges from the nm to the mm. Figure 7 presents the range of applications of five experimental techniques that are commonly used to study the structure of compacted bentonites:

- **Adsorption techniques** are used to determine the specific surface area of clay minerals. Different gases, including nitrogen and carbon dioxide, as well as methylene blue, can be used as sorbates. A description of the different adsorption techniques can be found in Adamson [1990] and Santamarina *et al.* [2002].
- **X-ray diffraction (XRD)** allows the characterization of the mineral phases present in samples. Qualitative and semi-quantitative descriptions of the nature of the clay minerals are possible. The technique may also be used to investigate the effects of the hydration process at the scale of the clay layers [see Cases *et al.*, 1997; Devineau *et al.*, 2006; Likos & Lu, 2006; Villar *et al.*, 2012, among others]. A complete presentation and guide for the interpretation of XRD results are found in Moore & Reynolds [1997].
- **Mercury intrusion porosimetry (MIP)** is a qualitative and quantitative technique used to investigate the pore size distribution (PSD) of a porous sample. The principle is based on the injection of mercury into a sample previously dried. A review of the applications of MIP for the investigation of unsaturated soils microstructure is presented by Romero & Simms [2008].
- **Electron microscopy** provides essentially qualitative information on the pore structure via micrographs of the material, although some quantitative information may be obtained by using digital

³In these notes, the term microstructure is used to refer to the structure of materials as observed at a small scale, called microscopic scale, typically ranging from 1 nm to 1 mm.

image analysis. Different techniques exist, such as Scanning Electron Microscopy (SEM), Environmental Scanning Electron Microscopy (ESEM), Transmission Electron Microscopy (TEM). A review of the applications of ESEM for the investigation of unsaturated soils microstructure is presented by Romero & Simms [2008].

- **Computed tomography (CT)**, including microfocus tomography (μ CT), is a high-resolution non-destructive 3D observation technique based on the combination of a high number of X-ray images. This class of experimental techniques provides similar information to electron microscopy but in three dimensions.

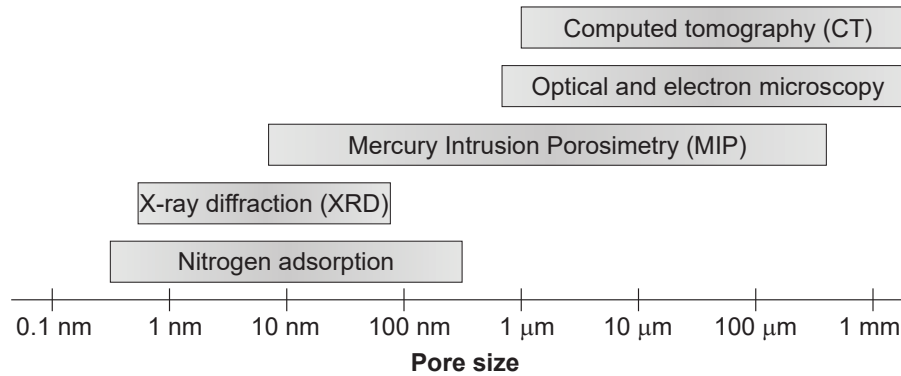
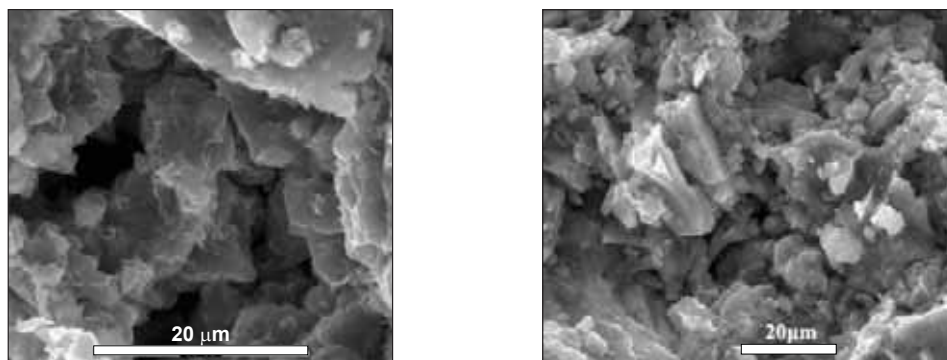


Figure 7: Range of applications of various experimental techniques used to investigate the microstructure of porous materials.

4.2 Experimental observations and representation

Figures 8(a) and 8(b) present ESEM micrographs of compacted Febex and GMZ bentonites respectively. In these micrographs, aggregates with sizes of the order of $20 \mu\text{m}$ are clearly observed. These aggregates are clusters of clay particles and are formed upon compaction of bentonite dry of optimum. Besides the clay layer and the clay particle, the aggregate represents a third level of organisation in compacted bentonites. Accordingly, the space between aggregates defines a new pore family, called inter-aggregate porosity, or macroporosity.



(a) Compacted Febex bentonite with dry density $\rho_d = 1.72 \text{ Mg/m}^3$ and water content $w = 13.7\%$ [Lloret *et al.*, 2003].

(b) Compacted GMZ bentonite with dry density $\rho_d = 1.75 \text{ Mg/m}^3$ and water content $w = 11.1\%$ [Ye *et al.*, 2009].

Figure 8: Micrographs of two compacted bentonites obtained using an environmental scanning electron microscope.

Mercury intrusion porosimetry provides further insight into the structure of the compacted bentonites and the pore size distribution. Figure 9 presents the pore size distributions obtained by Lloret *et al.* [2003] on Febex bentonite compacted to dry densities of 1.5 Mg/m^3 and 1.8 Mg/m^3 . In this figure, a bimodal distribution is clearly observed, the two peaks being in the range of pore sizes of 10 nm and $10 \mu\text{m}$ for

the highest dry density, and 10 nm and 40 μm for the lowest dry density. The size of the larger pores is consistent with the inter-aggregate pores observed in Figure 8(a).

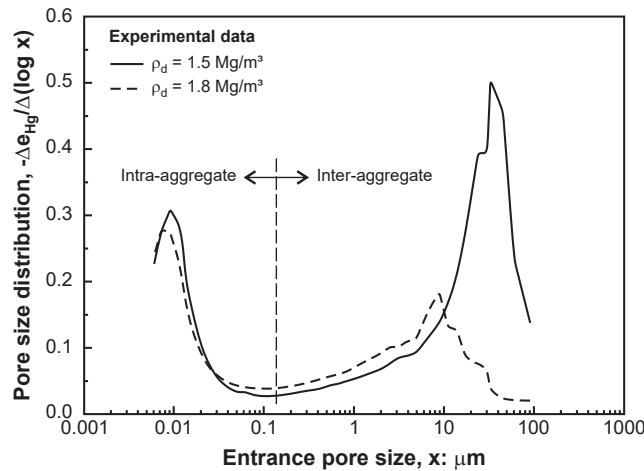


Figure 9: Pore size distribution of Febex bentonite compacted at different dry densities, $\rho_d = 1.5 \text{ Mg/m}^3$ and $\rho_d = 1.8 \text{ Mg/m}^3$ [Lloret et al., 2003].

In Figure 9, the pore family with the peak around 10 nm corresponds to the intra-aggregate porosity, and more specifically the inter-particle porosity. Note that pores smaller than around 6 nm (corresponding essentially to intra-particle pores) cannot be investigated by using mercury intrusion porosimetry. The intra-aggregate porosity is therefore not homogeneous and includes pores between particles (inter-particle porosity) and inside a particle (inter-layer porosity). In the following, the term microporosity is used to refer to the total intra-aggregate porosity.

4.3 Water storage and hydration mechanisms

Water in compacted bentonite is present under different forms: structural water, adsorbed water and capillary or free water [Kezdi, 1974; Stępkowska, 1990]. Structural water or hydroxyl is part of the minerals structure and does not leave the solid phase below 350°C. It is therefore excluded from water content measurements which are obtained after drying the sample at a temperature slightly over 100°C. Adsorbed water corresponds to the water which is adsorbed on both internal and external surfaces of the clay minerals, i.e. which is stored in the intra-aggregate pores (micropores). Finally, capillary or free water is stored in the macropores. Figure 10 presents a conceptual representation of the structure of compacted bentonites and the different types of water.

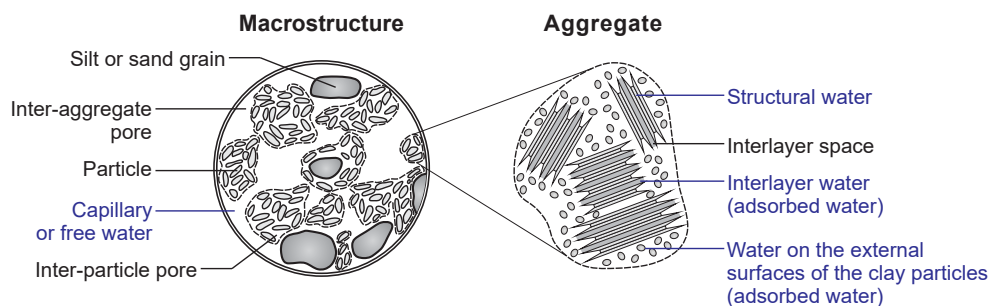


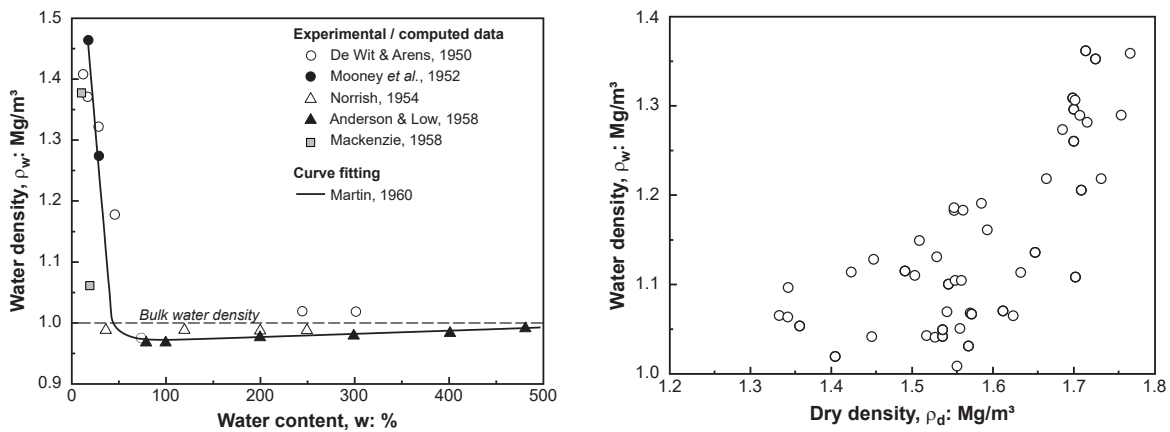
Figure 10: Conceptual representation of the structure of compacted bentonite (in black) and the different water storage mechanisms (in blue) [modified after Gens & Alonso, 1992; Jacinto et al., 2012].

The physical state of water in the vicinity of the charged clay layers differs from the one of bulk water, and both values of viscosity and density are affected [Langmuir, 1917; Baver & Winterkorn, 1935; Winterkorn, 1943]. Low [1979] and Bourg *et al.* [2003] showed that the viscosity of the adsorbed water is higher than the one of bulk water. Moreover, due to the strong physicochemical interactions between water and the clay particles, the density of adsorbed water is significantly higher than that of bulk water [Hawkins & Egelstaff, 1980; Derjaguin *et al.*, 1986; Swenson *et al.*, 2000; Jacinto *et al.*, 2012], and may reach values higher than 1.4 Mg/m³ (Figure 11(a)).

From a practical point of view, the water density has a strong influence on the computed degree of saturation. The degree of saturation S_r is indeed obtained from the gravimetric water content w according to

$$S_r = \frac{\rho_s w}{\rho_w e} \tag{4}$$

where ρ_s is the density of the solids, ρ_w is the water density and e is the void ratio (defined as the ratio between the volume of voids and the volume of solids). When the degree of saturation is calculated with the density of bulk water ($\rho_w = 1 \text{ Mg/m}^3$), values higher than 1 are systematically obtained close to saturation [Villar, 2002; Marcial, 2003; Jacinto *et al.*, 2012]. Knowing the water content and void ratio of presumably saturated samples, Villar [2000] computed the equivalent water density in compacted Febex bentonite. Figure 11(b) shows that the mean water density is higher for denser samples, although water densities higher than 1 are found for looser samples.



(a) Water density in sodium montmorillonite as a function of water content [Martin, 1960].

(b) Water density in Febex bentonite as a function of dry density [Villar, 2000].

Figure 11: Water density in compacted bentonites.

In practice, the different types of water cannot be easily separated. Thermogravimetric analysis is generally used to this end, although the interpretation of the results is not straightforward [Cases *et al.*, 1997, 1995; Salles *et al.*, 2009]. At relative humidities lower than 90%, water is mainly found in the interlayer and adsorbed on the external surface of the particles. When the relative humidity increases, some capillary condensation is believed to take place in the macropores. However, as discussed in the next section, important porosity redistribution occurs upon wetting and leads a reduction of the macroporosity under confined conditions, hence limiting the amount of free water. The amount of free water in compacted bentonites is therefore usually estimated to be only a few percent of the total water, under saturated conditions [Pusch *et al.*, 1990; Bradbury & Baeyens, 2003; Fernandez *et al.*, 2004].

4.4 Factors affecting the structure

The mechanisms affecting the structure of soils may be classified into internal and external factors. Internal factors (also called intrinsic) include the mineralogy, clay particles size and morphology, and water chemistry. External factors are the compaction method and its energy, and the water content. In this section, the structure evolution is only considered from the point of view of the pore size distribution, as little information is available about the morphology of the pores and aggregates structure.

4.4.1 Mechanical loading

Figure 9 presents the pore size distributions of Febex bentonite compacted at two different dry densities, namely 1.5 Mg/m^3 and 1.8 Mg/m^3 , but the same water content. In both cases, a bimodal pore size distribution is observed, even at high dry density. The compaction process has two main effects. Firstly, regarding the porous volume, increasing the compaction effort at constant water content decreases the volume of macropores, while the volume of micropores is hardly affected. Secondly, compaction shifts the size of dominant macropores towards smaller pore radii.

4.4.2 Water content changes

As a result of the sensitivity of clay minerals to water, the structure of compacted bentonites is significantly affected by changes in water content. An increase in the water content leads indeed to the swelling of clay layers and particles, hence aggregates. Figure 12 shows the evolution of the pore size distribution of MX-80 bentonite compacted to a dry density of 1.79 Mg/m^3 and hydrated under constant volume conditions. The experimental data show an increase of volume of the smaller pores and a progressive decrease of the inter-aggregate pore volume. Consequently, the structure of the material evolves from a bimodal pore size distribution (as-compacted material) towards a mono-modal distribution under fully saturated conditions. According to Romero [2013], the evolution of the macropores volume upon changes in water content is the consequence of both multi-scale and multi-physical processes. During wetting, the expanding clay particles invade indeed the macropores, hence decreasing the macropores volumes. On the other hand, wetting is likely to lead to collapse of the macrostructure. At the macroscopic scale, collapse is indeed often detected during saturation of compacted bentonites and is generally interpreted as an instability of the material structure.

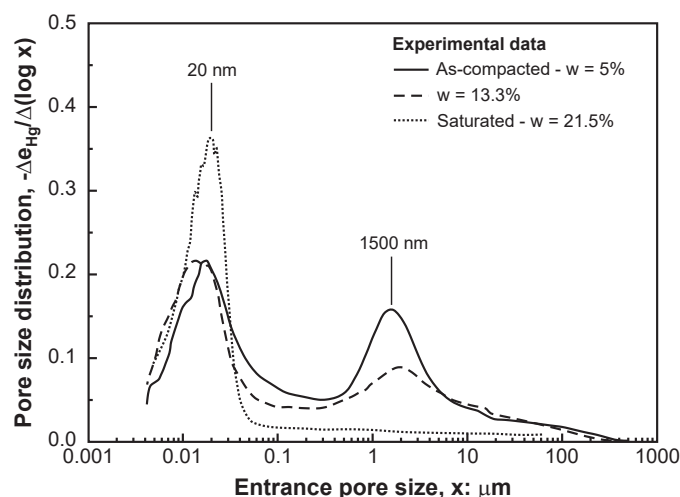


Figure 12: Influence of the water content on the pore size distribution of MX-80 bentonite compacted to a dry density $\rho_d = 1.79 \text{ Mg/m}^3$ and hydrated under constant volume conditions [Seiphoori *et al.*, 2014]

Figure 13 presents an interesting picture, obtained by cryo-Focused Ion Beam nanotomography [see Keller *et al.*, 2014, for details on this technique], of partially saturated MX-80 bentonite compacted to a dry density of 1.46 Mg/m^3 with a water content of 22.6%. The picture shows that the inter-aggregate pores are filled with a loose material comparable to a gel or colloidal solution. This material is characterized by a special structures referred to as honeycomb [Keller *et al.*, 2014]. For higher dry densities (1.67 Mg/m^3), Keller *et al.* [2014] did not observe such a structure, presumably because of the lack of large inter-aggregate pores (Figure 12).

Wang *et al.* [2013a] observed a different behaviour of the microstructure of a MX-80 bentonite/sand mixture hydrated under confined conditions, and noticed the development of two-dimensional fissure-like pores. These pores were detected with both mercury intrusion porosimetry (pore group with a mean diameter of $50 \mu\text{m}$ and $1 \mu\text{m}$ in Figure 14(a)) and scanning environmental microscope (Figure 14(b)). Wang *et al.* [2013a] suggested that these pores may result from the division of clay particles within the aggregates due to swelling. However, further investigations are required since the release of the swelling pressure before freeze-drying of the sample could also influence the observations.

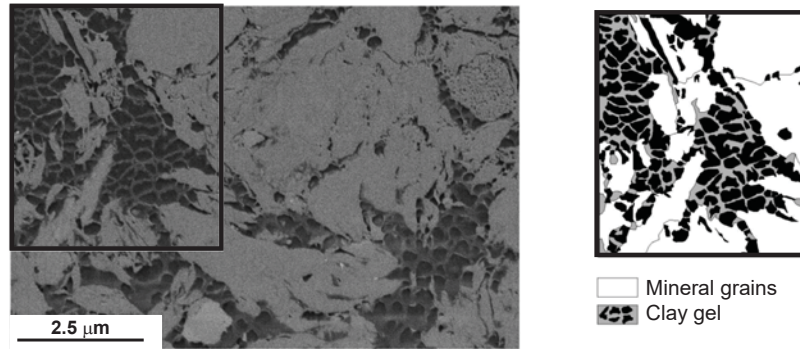
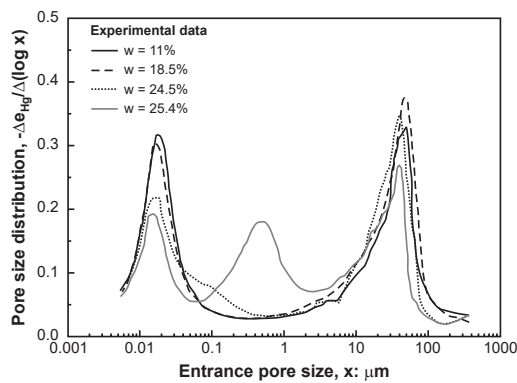
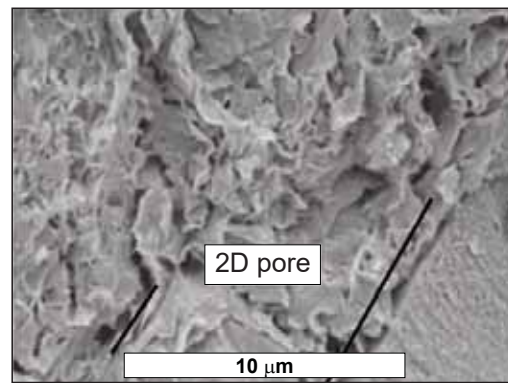


Figure 13: Microstructure of compacted MX-80 bentonite with dry density $\rho_d = 1.46 \text{ Mg/m}^3$ and water content $w = 22.6\%$ obtained by cryo-Focused Ion Beam nanotomography [Keller *et al.*, 2014].



(a) Evolution of the pore size distribution.



(b) Micrograph for saturated conditions ($w = 25.5\%$).

Figure 14: Development of two-dimensional fissure like pores during hydration of a MX-80 bentonite/sand mixture under constant volume conditions [Wang *et al.*, 2013a]

Finally, few experimental data are available concerning the reversibility of the microstructure behaviour upon wetting and drying cycles. According to Romero [2013], the aggregates of as-compacted bentonites swell and shrink almost reversibly upon wetting and drying. Therefore Romero [2013] qualifies the aggregates of compacted clayey soils as a permanent feature of the microstructure. However, Seiphoori *et al.* [2014] observed significant and permanent modifications of the structure of granular MX-80 bentonite saturated under constant volume conditions. Indeed, no significant structural changes were observed upon drying. Seiphoori *et al.* [2014] interpreted this irreversibility of the structure behaviour as a consequence of the irreversible subdivision of smectite particles (see Section 3.3).

4.4.3 Ageing

Ageing effects refer to time-dependent phenomena. These effects were studied by Delage *et al.* [2006] on MX-80 bentonite (Figure 15). The study showed that significant changes in the material structure were observed when bentonite samples were maintained under constant volume and constant water content for different periods of time ranging from 1 day to 90 days. In particular, a decrease in the inter-aggregate porosity and an increase in the non-intruded porosity (interpreted as inter-layer porosity) were observed. These observations were interpreted in terms of progressive placement of interlayer water molecules within the particles and subdivision of clay particles.

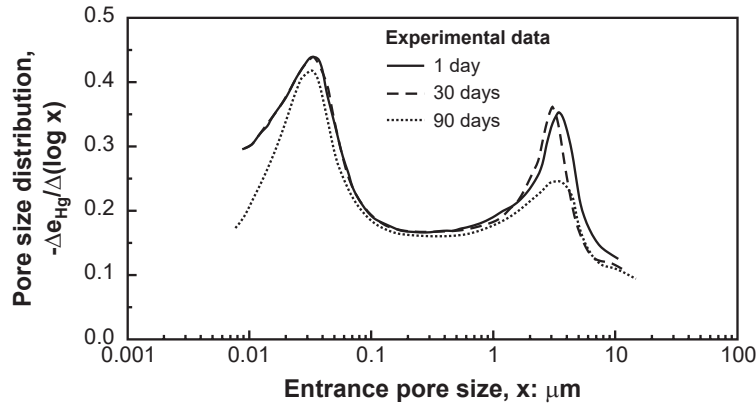


Figure 15: Changes in pore size distribution with time of compacted MX-80 bentonite with dry density $\rho_d = 1.61 \text{ Mg/m}^3$ and water content $w = 8.2\%$ [Delage *et al.*, 2006].

4.5 Model for the microstructure evolution

In the previous section, the effects of hydraulic and mechanical loading on the microstructure of compacted bentonites were underlined. In particular, the experimental observations showed that the microstructure of compacted bentonites created upon compaction was not fixed, but evolving along hydromechanical stress paths. In this section, attention is focused on quantifying the evolution of the microstructure.

The experimental technique the most often used to gather quantitative information on the structure of porous media is mercury intrusion porosimetry. While the technique provides only partial information on the material microstructure, the results can be used to obtain a scalar measure of the interconnected pore sizes and volumes. Accounting for this limitation, mercury intrusion porosimetry data are often used and analysed in order to highlight tendencies in the evolution of the pore size distribution of compacted bentonites along hydromechanical stress paths [Romero *et al.*, 2011; Della Vecchia *et al.*, 2015]. In particular, the following quantities are defined:

- the **microporosity** ϕ_m is the ratio between the micropores volume Ω_m and the total volume Ω

$$\phi_m = \frac{\Omega_m}{\Omega}. \quad (5)$$

The microporosity coincides with the total intra-aggregate porosity and includes both inter- and intra-particles pores.

- the **microstructural void ratio** e_m is the ratio between the micropores volume Ω_m and the solid volume Ω_s

$$e_m = \frac{\Omega_m}{\Omega_s} = \frac{\phi_m}{\phi} e \quad (6)$$

where ϕ and e are respectively the (total) porosity and void ratio.

- the **macroporosity** ϕ_M is the ratio between the macropores volume Ω_M and the total volume Ω

$$\phi_M = \frac{\Omega_M}{\Omega}. \quad (7)$$

The macroporosity coincides with the inter-aggregate porosity.

- the **macrostructural void ratio** e_M is the ratio between the macropores volume Ω_M and the solid volume Ω_s

$$e_M = \frac{\Omega_M}{\Omega_s} = \frac{\phi_M}{\phi} e \quad (8)$$

with the total porosity $\phi = \phi_m + \phi_M$ and total void ratio $e = e_m + e_M$.

From a practical point of view, these quantities can be estimated based on experimental pore size distributions. Therefore a criterion should be defined to distinguish micropores from macropores. Three main approaches are identified and briefly summarized:

- **Approach 1:** an entrance pore size is selected based on the pore size distribution of the as-compacted material and is used to separate intra-aggregate and inter-aggregate pores.
- **Approach 2:** data from a mercury intrusion and extrusion cycles are used. The difference between the intruded and extruded mercury volume is assumed to correspond to the inter-aggregate porosity [Delage & Lefebvre, 1984; Delage *et al.*, 1996].
- **Approach 3:** the entrance pore size coinciding with the dominant peak of the pore size distribution of the material saturated under constant volume conditions is detected. It is used to separate intra-aggregate and inter-aggregate pores [Della Vecchia, 2009; Romero *et al.*, 2011].

The different criteria are further described and discussed in Romero *et al.* [2011]. In addition, a fourth approach, based on the discrimination of water retention domains, was proposed by Romero *et al.* [1999]. Yet, if the approaches are conceptually different, they generally provide similar quantitative results in terms of porosities evolution.

Based on the experimental observations presented in the previous section, two main conclusions can be drawn. Firstly, mechanical loading does not affect the volume of micropores. This is at least true for the range of loads and dry densities commonly investigated. Secondly, hydraulic loading strongly affects the micropores volume. In particular, wetting yields an increase of the micropores volume. Accordingly, Romero *et al.* [2011] suggested to plot the microstructural void ratio e_m obtained from the analysis of pore size distributions as a function of the water ratio e_w (defined as the ratio between the volume of water and the volume of solids). By doing so, Romero *et al.* [2011] and Della Vecchia *et al.* [2013] observed that, below a given water ratio $e_w = e_m^*$, the microstructural void ratio of moderately active clays was almost constant and not affected by the water ratio. On the contrary, for higher water ratios, the microstructural void ratio increases almost linearly with the water ratio. Therefore, Romero *et al.* [2011] and Della Vecchia *et al.* [2013] proposed the following law for the evolution of the microstructural void ratio with the water ratio

$$e_m = e_m^* + \beta \langle e_w - e_m^* \rangle \quad (9)$$

where $\langle \rangle$ designates the Macaulay brackets (ramp function), e_m^* is the water ratio corresponding to fully saturated micropores and β quantifies the swelling tendency of the aggregates.

Dieudonné *et al.* [2013], Della Vecchia *et al.* [2015] and Dieudonné *et al.* [2017] analysed a large number of mercury intrusion porosimetry results on different bentonites. The materials include Febex bentonite [Lloret *et al.*, 2003; Lloret & Villar, 2007; Romero *et al.*, 2011], Kunigel V1 bentonite [Romero, 2012, and present work], MX-80 bentonite [Delage *et al.*, 2006; Wang, 2012; Seiphoori *et al.*, 2014] and a mixture of MX-80 bentonite and sand [Wang *et al.*, 2013b; Saba *et al.*, 2014]. The analysis of the experimental results and their representation in the $(e_w - e_m)$ plane does not allow identifying any threshold water content below which the microstructural water ratio remains constant. On the contrary, the micropores volume appears to be continuously evolving with the water ratio (Figure 16). This observation is in accordance with results presented by Romero *et al.* [2011] on Febex and MX-80 bentonites.

Accordingly, Dieudonné *et al.* [2013] proposed to describe the evolution of microstructural void ratio with the water ratio

$$e_m = e_{m0} + \beta_0 e_w + \beta_1 e_w^2 \quad (10)$$

where e_{m0} is the microstructural void ratio for the dry material ($e_w = 0$) and β_0 and β_1 are parameters that quantify the swelling potential of the aggregates. Table 4 presents the model parameters calibrated for four bentonite-based materials, namely Febex, Kunigel V1 and MX-80 bentonites, and a mixture of MX-80 bentonite and sand. In particular, Figure 16 provides an example of the calibration for MX-80 bentonite, using experimental data from Delage *et al.* [2006], Seiphoori *et al.* [2014] and Wang *et al.* [2014].

Three remarks are formulated concerning the proposed model. First of all, it should be noted that for high values of dry density and water content, Equation (10) may lead to values of e_m higher than the total void ratio e . In this case, it is assumed that the microstructure is completely developed and $e_m = e$. This remark is directly related to the fact that Equation (10) does not provide any limiting value of e_m with e_w , although such a limit probably exists. However, the proposed relation is meant to describe the microstructure of compacted bentonites for which the range of water ratios is limited to $0.15 \leq e_w \leq 0.95$. Finally, in a reasonable range of water ratios, Equation (10) provides predictions similar to those of the

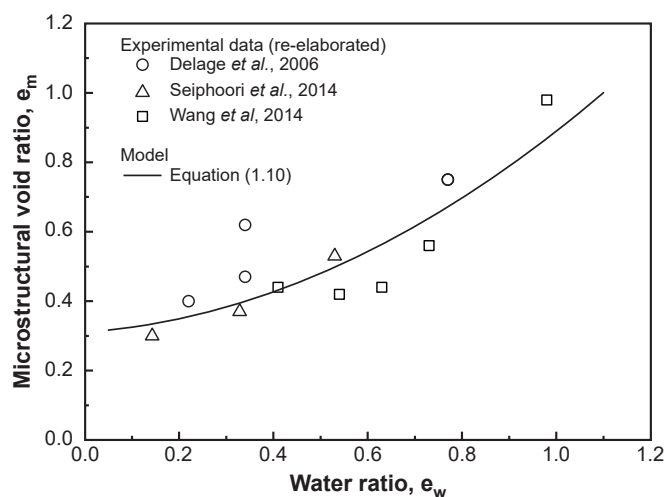


Figure 16: Evolution of the microstructural void ratio e_m with the water ratio e_w from MIP results on compacted MX-80 bentonite.

Material	e_{m0}	β_0	β_1
Febex	0.35	0.25	0.15
Kunigel V1	0.4	0.03	0.21
MX-80	0.31	0.1	0.48
MX-80/sand mixture (70/30)	0.29	0.1	0.18

Table 4: Parameters of the microstructure evolution law for four bentonite-based materials.

bilinear expression proposed by Romero *et al.* [2011], whilst providing a continuous evolution of e_m with the water ratio.

5 Summary

Bentonites exhibit a complex behaviour under repository conditions, owing to the high sensitivity of the material to mechanical and environmental (thermal, hydraulic and pneumatic) loads. This sensitivity of bentonites to external factors arises from both the mineralogical composition and the multi-scale structure of the material, which can be investigated by using modern experimental techniques.

In these lecture notes, attention was first focused on the physicochemical properties of smectites and the hydration and swelling mechanisms of these minerals. At the scale of the clay particle, hydration leads to an increase of the average interlayer distance and a division of the clay particles into smaller structures, both contributing to the particle swelling. A precise description of the processes is complex. Yet, the diffuse double layer theory provides interesting qualitative results on the factors affecting swelling. In particular, the theory allows a first explanation of the considerably different swelling pressures reached by different bentonites upon saturation.

The hydration and swelling mechanisms were then addressed at the scale of the compacted material microstructure. The experimental data show that hydration of compacted bentonite under confined conditions is associated with a progressive increase of the micropores volume and a decrease of the inter-aggregate porosity. On the contrary, under unconfined conditions, swelling taking place at the clay layer yields important swelling strains observed at the macroscopic scale. Based on the interpretation of a large number of pore size distributions on compacted bentonites, a model for the microstructure evolution is proposed.

References

- Adamson, A. W. (1990). *Physical chemistry of surfaces*. John Wiley & Sons.
- Anderson, D. M. & Low, P. F. (1958). The density of water adsorbed by Li-, Na-, and K-bentonite. *Soil Science Society of America Proceedings* **22**, 99–103.
- Apted, M. (1995). The scientific and regulatory basis for the geological disposal of radioactive waste. In *Repository and barrier concepts* (Savage, D., Ed.), Wiley.
- Baver, L. D. & Winterkorn, H. W. (1935). Sorption of liquids by soil colloids: II. Surface behaviour in the hydration of clays. *Soil Science* **40**, No. 5, 403–418.
- Bolt, G. H. (1956). Physico-chemical analysis of the compressibility of pure clays. *Géotechnique* **6**, No. 2, 86–93.
- Bourg, I. C., Bourg, A. C. M. & Sposito, G. (2003). Modeling diffusion and adsorption in compacted bentonite: a critical review. *Journal of Contaminant Hydrology* **61**, No. 1–4, 293–302.
- Bradbury, M. H. & Baeyens, B. (2003). Porewater chemistry in compacted re-saturated MX-80 bentonite. *Journal of Contaminant Hydrology* **61**, No. 1–4, 329–338.
- Bruno, G. (1993). *Etude expérimentale des mécanismes de réduction et d'oxydation du Fer d'une argile naturelle – Evolution de ses propriétés physiques et chimiques*. Ph.D. thesis, Université de Poitiers.
- Börgesson, L., Karnland, O. & Johannesson, L. E. (1996). Modelling of the physical behaviour of clay barriers close to water saturation. *Engineering Geology* **41**, No. 1–4, 127–144.
- Cases, J. M., Berend, I., Besson, G., Francois, M., Uriot, J. P., Thomas, F. & Poirier, J. E. (1995). Mechanism of adsorption and desorption of water vapor by homoionic montmorillonites: 2. The Li⁺, Na⁺, K⁺, Rb⁺ and Cs⁺- exchanged forms. *Clays and Clay Minerals* **43**, No. 3, 324–336.
- Cases, J. M., Berend, I., Delon, J. F., François, M., Grillet, Y., Michot, I., Poirier, J. E. & Yvon, J. (1990). Quelques aspects de l'étude des propriétés texturales des argiles. In *Matériaux argileux: structure, propriétés et applications*, Société Française de Minéralogie, Groupe français des argiles (Decarreau, A., Ed.), pp. 309–342.
- Cases, J. M., Berend, I., Francois, M., Uriot, J. P., Michot, L. J. & Thomas, F. (1997). Mechanism of adsorption and desorption of water vapor by homoionic montmorillonite. 3. The Mg²⁺, Ca²⁺, and Ba²⁺ exchanged forms. *Clays and Clay Minerals* **45**, No. 1, 8–22.
- Chapman, D. L. (1913). A contribution to the theory of electro-capillarity. *Physiological Magazine* **25**, No. 6, 475–481.
- De Wit, C. T. & Arens, P. L. (1950). Moisture content and density of some clay minerals and some remarks on the hydration pattern of clay. In *Proceeding of the Fourth International Congress of Soil Sciences*, pp. 59–62.
- Delage, P., Audiguier, M., Cui, Y. & Howat, M. (1996). Microstructure of a compacted silt. *Canadian Geotechnical Journal* **33**, No. 1, 150–158.
- Delage, P. & Lefebvre, G. (1984). Study of the structure of a sensitive Champlain clay and of its evolution during consolidation. *Canadian Geotechnical Journal* **21**, No. 1, 21–35.
- Delage, P., Marcial, D., Cui, Y. J. & Ruiz, X. (2006). Ageing effects in a compacted bentonite: a microstructure approach. *Géotechnique* **56**, No. 5, 291–304.
- Della Vecchia, G. (2009). *Coupled hydro-mechanical behaviour of compacted clayey soils*. Ph.D. thesis, Politecnico di Milano.
- Della Vecchia, G., Dieudonne, A. C., Jommi, C. & Charlier, R. (2015). Accounting for evolving pore size distribution in water retention models for compacted clays. *International Journal for Numerical and Analytical Methods in Geomechanics* **39**, No. 7, 702–723.



- Della Vecchia, G., Jommi, C. & Romero, E. (2013). A fully coupled elastic–plastic hydromechanical model for compacted soils accounting for clay activity. *International Journal for Numerical and Analytical Methods in Geomechanics* **37**, No. 5, 503–535.
- Derjaguin, B. V., Karasev, V. V. & Khromova, E. N. (1986). Thermal expansion of water in fine pores. *Journal of Colloid and Interface Science* **109**, No. 2, 586–587.
- Devineau, K., Bihannic, I., Michot, L., Villiéras, F., Masrouri, F., Cuisinier, O., Fragneto, G. & Michau, N. (2006). In situ neutron diffraction analysis of the influence of geometric confinement on crystalline swelling of montmorillonite. *Applied Clay Science* **31**, No. 1–2, 76–84.
- Dieudonné, A. C., Della Vecchia, G. & Charlier, R. (2017). Water retention model for compacted bentonites. *Canadian Geotechnical Journal* **54**, 915–925.
- Dieudonné, A. C., Levasseur, S., Charlier, R., Della Vecchia, G. & Jommi, C. (2013). A water retention model for compacted clayey soils. In *Computational Geomechanics*, Cracow, Poland, pp. 23–31.
- Dixon, D. A., Gray, M. N. & Graham, J. (1996). Swelling and hydraulic properties of bentonites from Japan, Canada and the USA. *Environmental Geotechnics* **1**, 43–48.
- Fernandez, A. M. (2004). *Caracterización y modelización del agua intersticial en materiales arcillosos: estudio de la bentonita de Cortijo de Archidona*. Ph.D. thesis, CIEMAT.
- Fernandez, A. M., Baeyens, B., M., B. & Rivas, P. (2004). Analysis of the pore water chemical composition of a spanish compacted bentonite used in an engineered barrier. *Physics and Chemistry of the Earth* **29**, No. 1, 105–118.
- Gens, A. & Alonso, E. E. (1992). A framework for the behaviour of unsaturated expansive clays. *Canadian Geotechnical Journal* **29**, No. 6, 1013–1032.
- Gens, A., Vallejan, B., Sánchez, M., Imbert, C., Villar, M. V. & Van Geet, M. (2011). Hydromechanical behaviour of a heterogeneous compacted soil: experimental observations and modelling. *Géotechnique* **61**, No. 5, 367–386.
- Gouy, M. (1910). Sur la constitution de la charge électrique à la surface d'un électrolyte. *Journal de Physique Théorique et Appliquée* **9**, No. 1, 457–468.
- Grim, R. E. (1968). *Clay mineralogy*. New-York, USA: McGraw-Hill.
- Grunberger, D. (1995). *Etude expérimentale de l'évolution des microstructures et des propriétés physiques et mécaniques des argiles au cours de la compaction*. Ph.D. thesis, Université de Montpellier II.
- Hawkins, R. K. & Egelstaff, P. A. (1980). Interfacial water structure in montmorillonite from neutron diffraction experiments. *Clays and Clay Minerals* **28**, No. 1, 19–28.
- Hewitt, D. F. (1917). The origin of bentonites. *Washington Academy of Sciences Journal* **7**, 196–198.
- Jacinto, A. C., Villar, M. V. & Ledesma, A. (2012). Influence of water density on the water-retention curve of expansive clays. *Géotechnique* **62**, No. 8, 657–667.
- JNC (2000). H12 project to establish technical basis for HLW disposal in Japan. Supporting report 3: safety assessment of the geological disposal system. *Technical report*, Japan Nuclear Cycle Development Institute.
- Karnland, O., Nilsson, U., Weber, H. & Wersin, P. (2008). Sealing ability of Wyoming bentonite pellets foreseen as buffer material – Laboratory results. *Physics and Chemistry of the Earth* **33**, 472–475.
- Keller, L. M., Seiphoori, A., Gasser, P., Lucas, F., Holzer, L. & Ferrari, A. (2014). The pore structure of compacted and partly saturated MX-80 bentonite at different dry densities. *Clays and Clay Minerals* **62**, No. 3, 174–187.
- Kezdi, A. (1974). *Handbook of soil mechanics. Soil physics*. Elsevier Scientific.
- Knight, W. C. (1898). Bentonite. *Engineering and Mining Journal* **66**, 491.

- Komine, H. (2004). Simplified evaluation on hydraulic conductivities of sand–bentonite mixture backfill. *Applied Clay Science* **26**, No. 1–4, 13–19.
- Komine, H. & Ogata, N. (1996). Prediction for swelling characteristics of compacted bentonite. *Canadian Geotechnical Journal* **33**, No. 1, 11–22.
- Lajudie, A., Raynal, J., Petit, J. C. & Toulhoat, P. (1994). Clay-based materials for engineered barriers: a review. *Materials Research Society Symposium Proceedings* **353**, 221–229.
- Langmuir, I. (1917). The constitution and fundamental properties of solids and liquids. *Journal of the American Chemical Society* **39**, 1848–1906.
- Likos, W. J. & Lu, N. (2006). Pore-scale analysis of bulk volume change from crystalline interlayer swelling in Na⁺- and Ca²⁺-smectite. *Clays and Clay Minerals* **54**, No. 4, 515–528.
- Lloret, A. & Villar, M. V. (2007). Advances on the knowledge of the thermo-hydro-mechanical behaviour of heavily compacted FEBEX bentonite. *Physics and Chemistry of the Earth* **32**, No. 8–14, 701–715.
- Lloret, A., Villar, M. V., Sánchez, M., Gens, A., Pintado, X. & Alonso, E. E. (2003). Mechanical behaviour of heavily compacted bentonite under high suction changes. *Géotechnique* **53**, No. 1, 27–40.
- Low, P. F. (1979). Nature and properties of water in montmorillonite-water systems. *Soil Science Society of America Journal* **43**, No. 4, 651–658.
- Mackenzie, R. C. (1958). Density of water sorbed on montmorillonite. *Nature* **181**, 334.
- Madsen, F. T. (1998). Clay mineralogical investigations related to nuclear waste disposal. *Clay Minerals* **33**, No. 1, 109–129.
- Marcial, D. (2003). *Comportement hydromécanique et microstructural des matériaux de barrière ouvragée*. Ph.D. thesis, Ecole Nationale des Ponts et Chaussées.
- Marcial, D., Delage, P. & Cui, Y. J. (2002). On the high stress compression of bentonites. *Canadian Geotechnical Journal* **39**, No. 4, 812–820.
- Martin, T. R. (1960). Adsorbed water on clay: a review. *Clays and Clay Minerals* **9**, No. 1, 28–70.
- Meunier, A. (2005). *Clays*. Springer.
- Mitchell, J. K. & Soga, K. (2005). *Fundamentals of soil behaviour*. Wiley.
- Montes-H, G. (2002). *Etude expérimentale de la sorption d'eau et du gonflement des argiles par microscopie électronique à balayage environnementale (ESEM)*. Ph.D. thesis, Université Louis Pasteur.
- Mooney, R. W., Keenan, A. G. & Wood, L. A. (1952). Adsorption of water vapor by montmorillonite. II. Effect of exchangeable ions and lattice swelling as measured by X-ray diffraction. *Journal of the American Chemical Society* **74**, No. 6, 1371–1374.
- Moore, D. M. & Reynolds, R. C. (1997). *X-ray diffraction and the identification and analysis of clay minerals*. Oxford University Press.
- Nakashima, Y. (2004). Nuclear magnetic resonance properties of water-rich gels of Kunigel-V1 bentonite. *Journal of Nuclear Science and Technology* **41**, No. 10, 981–992.
- Norrish, K. (1954). The swelling of montmorillonite. *Discussions of the Faraday Society* **18**, 120–134.
- Proust, D., Lechelle, J., Lajudie, A. & Meunier, A. (1990). Hydrothermal reactivity of mixed-layer kaolinite/smectite: experimental transformation of high-charge to low-charge smectite **38**, No. 4, 415–425.
- Pusch, R. (1982). Mineral-water interactions and their influence on the physical behavior of highly compacted Na bentonite. *Canadian Geotechnical Journal* **19**, No. 3, 381–387.
- Pusch, R., Karnland, O. & Hokmark, H. (1990). GMM - a general microstructural model for qualitative and quantitative studies of smectite clays. *Technical report*, SKB.
- Romero, E. (2012). Complementary triaxial compression and direct shear tests under high matric suctions on low-density Kunigel V1. *Technical report*, Universitat Politècnica de Catalunya.

- Romero, E. (2013). A microstructural insight into compacted clayey soils and their hydraulic properties. *Engineering Geology* **165**, 3–19.
- Romero, E., Della Vecchia, G. & Jommi, C. (2011). An insight into the water retention properties of compacted clayey soils. *Géotechnique* **61**, No. 4, 313–328.
- Romero, E., Gens, A. & Lloret, A. (1999). Water permeability, water retention and microstructure of unsaturated compacted Boom clay. *Engineering Geology* **54**, No. 1–2, 117–127.
- Romero, E. & Simms, P. H. (2008). Microstructure investigation in unsaturated soils: a review with special attention to contribution of mercury intrusion porosimetry and environmental scanning electron microscopy. *Geotechnical and Geological Engineering* **26**, No. 6, 705–727.
- Ross, C. S. & Shannon, E. V. (1926). The minerals of bentonite and related clays and their physical properties. *Journal of the American Ceramic Society* **9**, No. 2, 77–96.
- Saba, S., Delage, P., Lenoir, N., Cui, Y. J., Tang, A. M. & Barnichon, J. D. (2014). Further insight into the microstructure of compacted bentonite-sand mixture. *Engineering Geology* **168**, 141–148.
- Saiyouri, N., Hicher, P. Y. & Tessier, D. (2000). Microstructural approach and transfer water modelling in highly compacted unsaturated swelling clays. *Mechanics of Cohesive-Frictional Materials* **5**, 41–60.
- Saiyouri, N., Tessier, D. & Hicher, P. Y. (2004). Experimental study of swelling in unsaturated compacted clays. *Clay Minerals* **39**, 469–479.
- Salles, F., Douillard, J. M., Denoyel, R., Bildstein, O., Jullien, M., Beurroies, I. & Van Damme, H. (2009). Hydration sequence of swelling clays: evolutions of specific surface area and hydration energy. *Journal of Colloid and Interface Science* **333**, No. 2, 510–522.
- Santamarina, J. C., Klein, W. Y. H., K. A. & Prencke, E. (2002). Specific surface: determination and relevance. *Canadian Geotechnical Journal* **39**, No. 1, 233–241.
- Schanz, T. & Al-Badran, Y. (2014). Swelling pressure characteristics of compacted Chinese Gaomiaozhi bentonite GMZ01. *Soils and Foundations* **54**, No. 4, 748–759.
- Segad, M., Jönsson, B., Akesson, T. & Cabane, B. (2010). Ca/Na montmorillonite: structure, forces and swelling properties. *Langmuir* **26**, No. 8, 5782–5790.
- Seiphoori, A., Ferrari, A. & Laloui, L. (2014). Water retention behaviour and microstructural evolution of MX-80 bentonite during wetting and drying cycles. *Géotechnique* **64**, No. 9, 721–734.
- Sellin, P. & Leupin, O. X. (2013). The use of clay as an engineered barrier in radioactive-waste management – a review. *Clays and Clay Minerals* **61**, No. 6, 477–498.
- Sposito, G., Skipper, N. T., Sutton, R., Park, S. H., Soper, A. K. & Greathouse, J. A. (1984). Surface geochemistry of the clay minerals. *Proceedings of the National Academy of Sciences* **96**, No. 7, 3358–3364.
- Stern, O. (1924). Zur Theorie der elektrolytischen Doppelschicht (The theory of the electrolytic double-layer). *Zeitschrift für Elektrochemie und Angewandte Physikalische Chemie* **30**, 508–516.
- Stępkowska, E. T. (1990). Aspects of the clay/electrolyte/water system with special reference to the geotechnical properties of clays. *Engineering Geology* **28**, No. 3–4, 249–267.
- Sun, W. J., Liu, S. Q., Sun, D. A. & Fang, L. (2014). Swelling characteristics and permeability of bentonite. In *Proceedings of the Sixth International Conference on Unsaturated Soils, UNSAT 2014* (Khalili, N., Russell, A. & Khoshghalb, A., Eds.), Sydney, Australia, pp. 1211–1217.
- Swenson, J., Bergman, R. & Howells, W. S. (2000). Quasielastic neutron scattering of two-dimensional water in vermiculite clay. *Journal of Chemical Physics* **113**, No. 7, 2873–2879.
- Tessier, D. (1978). Etude de l'organisation des argiles calciques. Evolution au cours de la dessiccation. *Annales d'Agronomie* **29**, No. 4, 319–355.
- Tripathy, S., Sridharan, A. & Schanz, T. (2004). Swelling pressures of compacted bentonites from diffuse double layer theory. *Canadian Geotechnical Journal* **41**, No. 3, 437–450.



- Van Olphen, H. (1963). *An introduction to clay colloid chemistry*. John Wiley & Sons.
- Van Olphen, H. (1977). *An introduction to clay colloid chemistry: for clay technologists, geologists and soil scientists*. Wiley-Interscience.
- Villar, M. V. (2000). *Caracterizacion thermo-hidro-mecanica de una bentonita de Cabo de Gata*. Ph.D. thesis, Universidad Complutense de Madrid.
- Villar, M. V. (2002). Thermo-hydro-mechanical characterisation of a bentonite from Cabo de Gata. *Technical report*, CIEMAT.
- Villar, M. V. (2007). Water retention of two natural compacted bentonites. *Clays and Clay Minerals* **55**, No. 3, 311–322.
- Villar, M. V., Gómez-Espina, R. & Guitiérrez-Nebot, L. (2012). Basal spacings of smectite in compacted bentonite. *Applied Clay Science* **65–66**, 95–105.
- Wang, Q. (2012). *Hydro-mechanical behaviour of bentonite-based materials used for high-level radioactive waste disposal*. Ph.D. thesis, Université Paris-Est.
- Wang, Q., Cui, Y. J., Tang, A. M., Barnichon, J. D., Saba, S. & Ye, W. M. (2013a). Hydraulic conductivity and microstructure changes of compacted bentonite/sand mixture during hydration. *Engineering Geology* **164**, 67–76.
- Wang, Q., Cui, Y. J., Tang, A. M., Li, X. L. & Ye, W. M. (2014). Time- and density-dependent microstructure features of compacted bentonite. *Soils and Foundations* **54**, No. 4, 657–666.
- Wang, Q., Tang, A. M., Cui, Y. J., Delage, P., Barnichon, J. D. & Ye, W. M. (2013b). The effects of technological voids on the hydro-mechanical behaviour of compacted bentonite–sand mixture. *Soils and Foundations* **53**, No. 2, 232–245.
- Wen, Z. J. (2006). Physical property of China's buffer material for high-level radioactive waste repositories. *Chinese Journal of Rock Mechanics and Engineering* **25**, 794–800.
- Wherry, E. T. (1917). Clay derived from volcanic dust in the Pierre of South Dakota. *Washington Academy of Sciences Journal* **7**, 576–583.
- Winterkorn, H. F. (1943). The condition of water in porous systems. *Soil Science* **56**, 109–115.
- Ye, W. M., Cui, Y. J., Qian, L. X. & Chen, B. (2009). An experimental study of the water transfer through confined compacted GMZ bentonite. *Engineering Geology* **108**, No. 3–4, 169–176.
- Yong, R. N., Pusch, R. & Nakano, M. (2009). *Containment of high-level radioactive and hazardous solid wastes with clay barriers*. CRC Press.

Appendix M. Experimental evidences of advective gas transfers at lab scale (E. Romero & L. Gonzalez Blanco)

UNIVERSITAT POLITÈCNICA DE CATALUNYA
BARCELONATECH

Department of Civil and Environmental
Engineering
Geotechnical Engineering and Geosciences


European Joint Programme
on Radioactive Waste Management

EXPERIMENTAL EVIDENCES OF ADVECTIVE GAS TRANSFER AT LAB SCALE

A DETAILED RESEARCH METHODOLOGY ON BOOM CLAY

Laura Gonzalez-Blanco & Enrique Romero


CIMNE / UPC




The project leading to this application has received funding from the European Union's Horizon 2020 research and innovation programme under grant agreement n° 847593.

23 January 2020

School for Radioactive Waste Management 2020




1





OUTLINE OF THE LECTURE

1. Motivation and content
2. Insight into gas transfer (gas generation, gas transport mechanisms, multi-scale aspects)
3. Some observations regarding gas testing (experimental protocols)
4. A detailed research methodology on Boom Clay:
 - Material characterization
 - Stress paths followed
 - Gas test protocols
 - Test results at different scales (macroscopic results and microstructural features)
5. Final comments. Future challenges



<https://www.dropbox.com/sh/wkqnzldepguxxm/AAB8G3Si9B83dBSbbbv22NWua?dl=0>

2

WHAT IS THE MOTIVATION OF THIS LECTURE? SOME COMMENTS

To present an '**updated perspective**' on the use of **laboratory techniques** (multi-physics testing) to understand macroscopic (phenomenological) features of **advective gas transport in saturated clayey materials**. Laboratory tests are necessary to improve the **understanding of the basics** and to **provide data for the development of predictive tools**.

Discontinuities, fractures and heterogeneity play an important role in this understanding. **Microstructural tests** are mandatory to study the changes (before and after gas injection) in the **pore size distribution**, reconstruct fissure/pathway patterns (estimate the **total volume of pathways** and their **connectivity**), and provide information on the **heterogeneous distribution of porosity** ('low-density' pathways).



3

WHAT IS THE MOTIVATION OF THIS LECTURE? SOME COMMENTS

Experimental techniques used to study coupled multi-physics process **do not always present the complete picture of understanding** (information on local behavior usually remains unknown). Often, theoretical and/or **numerical models must accompany the interpretation of the physical tests to better exploit the information provided by measurements** and to offer additional confidence on the experimental results (validation of the experimental techniques).

Advective gas tests are associated with so-called '**critical phenomena**' that are at the **verge of predictability** (particularly at specimen scale), and **microstructural features set on compaction / stress paths** affecting pore size distribution and connectivity issues (multiple gas pathways, dominant single cluster, ...) are admitted to **play an important role in the scatter**.

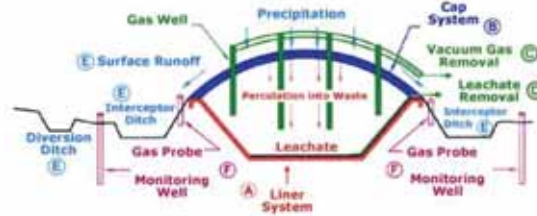


4

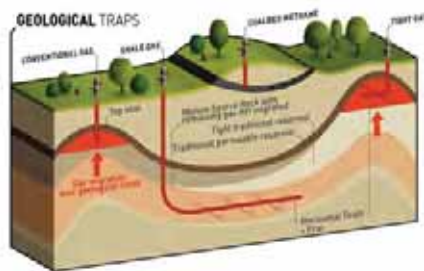
WHY GAS TRANSPORT ISSUES ARE OF INTEREST?

Understanding gas transport process is an important issue in the assessment of radioactive waste repository performance and other energy / environmental geotechnics related fields (shale gas, CO₂ capture, landfill design, ...)

Landfill design (methane, ...)



Conventional/unconventional gas reserves



Safely storing CO₂



Peterhead CCS Project (UK)

eu^{rad}

5

5

GEOLOGICAL DISPOSAL FACILITIES

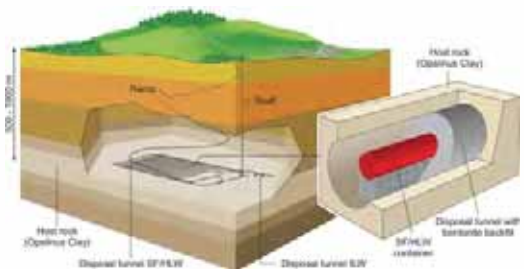
Based on the multi-barrier system concept for long-term isolation

• **Artificial barriers:**

- Waste canister
- Metallic overpack
- **Sealing and buffer materials EBS** to prevent / delay the release of radionuclides, gases and other contaminants

• **Natural barriers:**

- Geosphere: **geological formation** and groundwater (host rock)



Swiss concept (NAGRA)



1. Glass matrix, containing radioactive material
2. Metal container
3. Backfill with bentonite
4. Host rock

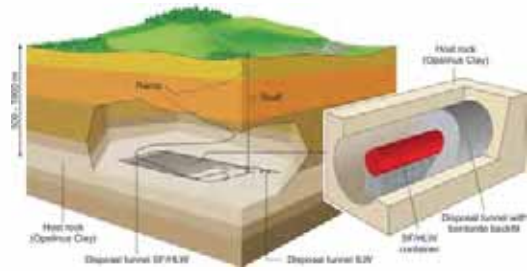
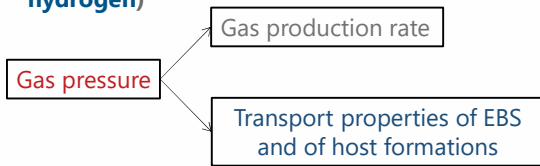
eu^{rad}

6

6

GAS GENERATION SOURCES

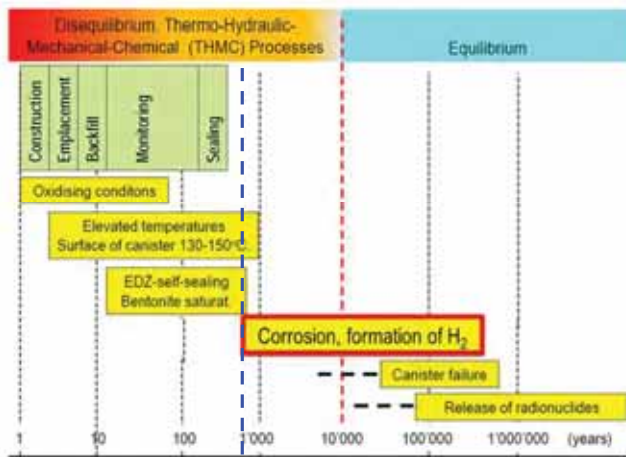
- Degradation of organic matter: methane and carbon dioxide
- Radiolysis: hydrogen, oxygen, carbon dioxide, methane, etc
- Alpha decay process: helium
- **Anaerobic corrosion of ferrous materials in metallic overpacks** (largest source and production of hydrogen)



- Swiss disposal concept for High Level Waste**
- Total volume of produced gas: 20 Mio m³ (STP)
 - Total pore volume of backfilled underground structures: 0.105 Mio m³
 - **Upper limit of gas pressure: 20 MPa**

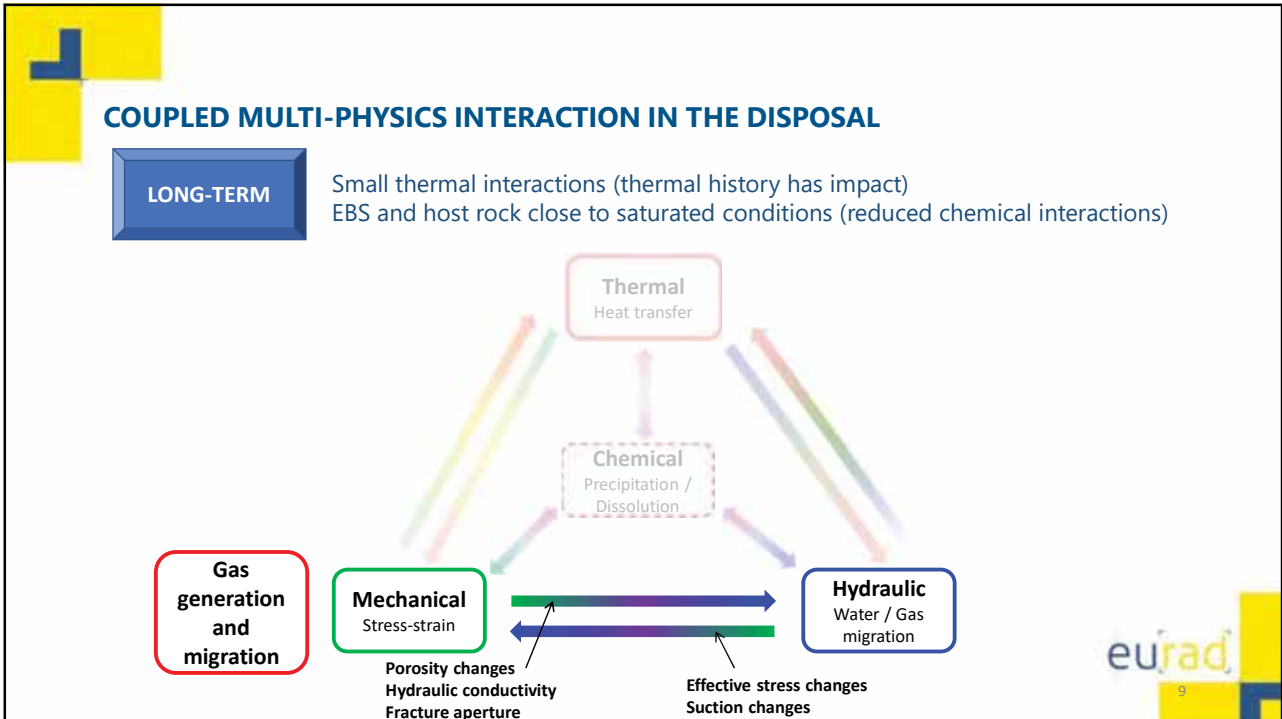
Gas pressure build-up may cause the failure of the EBS and the possible release of radionuclides into environment

MULTI-BARRIER PERFORMANCE



NAGRA (www.mont-terri.ch)

- **Large number of past THM-C processes** and phenomena that interact
- **No overlapping with bentonite saturation and EDZ self-sealing**
- Predictions required for **long periods of time**



9

GAS MIGRATION IN SATURATED POROUS MEDIA: GAS TRANSPORT MECHANISMS

(a) Phenomenological description

(b) Transport mechanisms

(c) Geomechanical regime

(d) Barrier function of host rock

Marschall et al. (2005)

Gas dissolved in water migrates through diffusion (low gas generation rates)

- Gas pressure builds up due to the **slow diffusive transport in low permeable media** (high gas generation rates)

Gas flow through the matrix partially displacing water (two-phase flow)

- Flow affected by **mechanical effects** (intrinsic permeability affected by porosity changes)

Gas flow through pressure-dependent pathways/fractures (existing/induced) (microscopic fissuring, macroscopic fracture)

- Flow properties affected by **mechanical effects and fracture aperture**

eu rad

10

GAS TRANSPORT PATHWAYS AT THE MACRO-SCALE

Plastic host rock: gas migration along bedding planes or discontinuities in the EDZ

Extension of EDZ in Connecting Gallery (Boom Clay, HADES URL, Belgium)

- Dissolution & diffusion
- Gas flow through existing porosity (2-ψ flow)
- Gas flow through μ-cracks, fractures (pathway dilation, creation)

ONDRAF/NIRAS (2016)

eurad

11

Salehnia et al. (2015)

11

RANGES OF PORE SIZES (TOMOGRAPHIC TECHNIQUES, BOOM CLAY)

MIP: Mercury intrusion porosimetry (450 μm and 7 nm)

100 μm 10 μm 1 μm 100 nm

100 μm CT μ-CT BIB-SEM FIB-SEM

3D μ-CT 3D BIB-SEM 3D FIB-SEM

2 μm

BIB-SEM: broad ion beam scanning electron microscopy
FIB-SEM: dual-beam system (focused ion beam scanning electron microscopy)

Hemes et al. (2015)

Multi-scale characterisation of porosity in Boom Clay (HADES-level, Mol, Belgium)

Digital image analyses using tomography (X-ray μ-CT, BIB-SEM / FIB-SEM tomography) (rendering graphics software ImageJ, Avizo, ...)

3D volume reconstruction from slice-and-view images, and stacking multiple planar images with a known separation

Resolution depending on system and sample size (typically between 0.01 to 100 μm) (1000-2000x the object cross-section diameter)

eurad

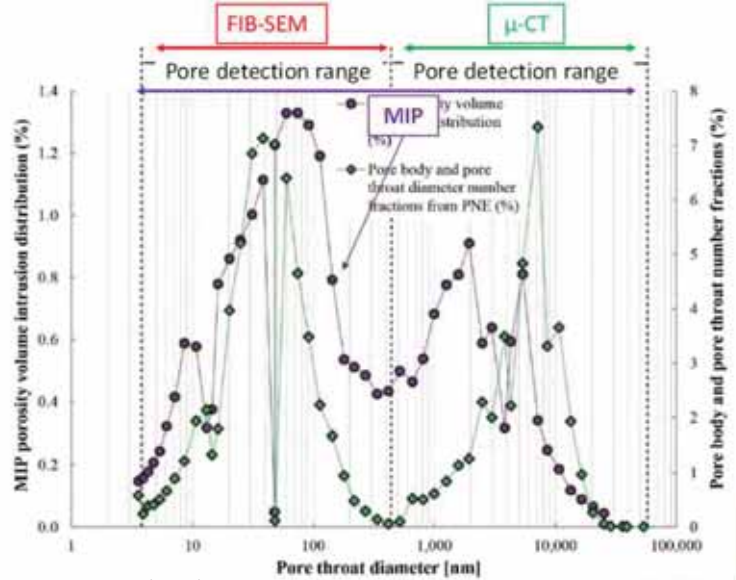
12

12

RANGES OF PORE SIZES (TOMOGRAPHIC TECHNIQUES, BOOM CLAY)

Multi-scale characterisation of porosity in Boom Clay (HADES-level, Mol, Belgium)

Image analyses (**pore size distribution**, pore bodies / pore throats, fissure / pore volume through filtering process, **connectivity** and morphology of the pore space, **random porosity distribution**, ...



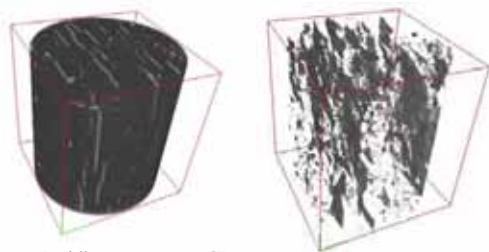
Hemes et al. (2015)

13

GAS TRANSPORT PATHWAYS AT THE MICRO-SCALE

Plastic host rock: gas migration affected by bedding planes (natural discontinuities)

Boom Clay, Belgium (depth 223 m)



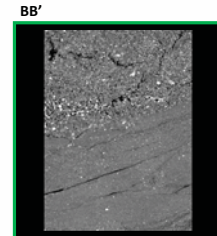
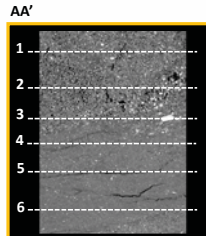
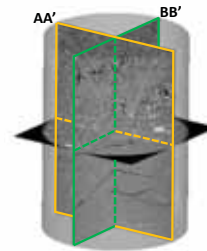
Bedding patterns μ -CT
 $V_{\text{sample}} = 1900 \text{ mm}^3$

Bedding planes initially 'closed' that are **activated during gas injection** (pressure-dependent fissures)

Gonzalez-Blanco et al. (2017)



$\phi = 12 \text{ mm}$
 $h = 16 \text{ mm}$



Ypresian clays, Belgium (depth 283 m)

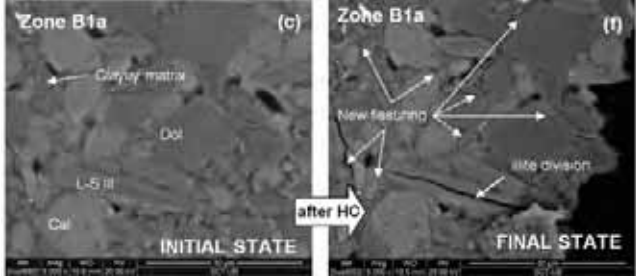
Sau et al. (in prep.)



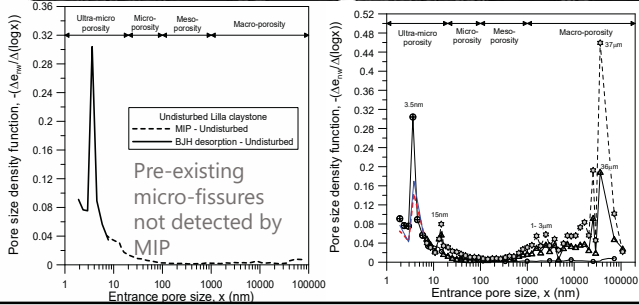
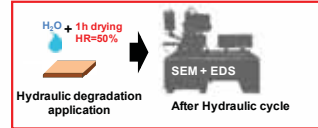
14

14

DEGRADATION / FISSURING ISSUES ON INDURATES CLAY ROCK BEFORE GAS PERMEABILITY TESTS



Tertiary (Eocene) Lilla claystone (Spain).
Rock matrix (clayey fraction + large size minerals)



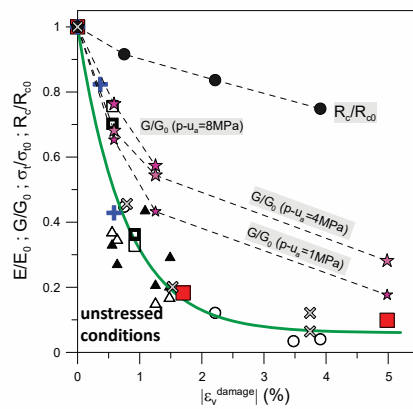
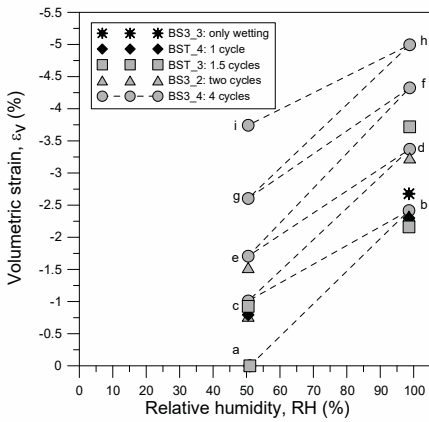
Micro-fissuring developed mainly at the interfaces between the clayey matrix and the large-size minerals (rigid inclusions)

Pineda, Alonso & Romero (2014)



DEGRADATION / FISSURING ISSUES ON INDURATES CLAY ROCK BEFORE GAS PERMEABILITY TESTS

RH cycles (ventilation)



D law for both rock stiffness (Young and shear moduli) and tensile strength

$$(1 - D) = [(1 - D_0)] \exp^{-\alpha |\epsilon_v^{damage}|}$$

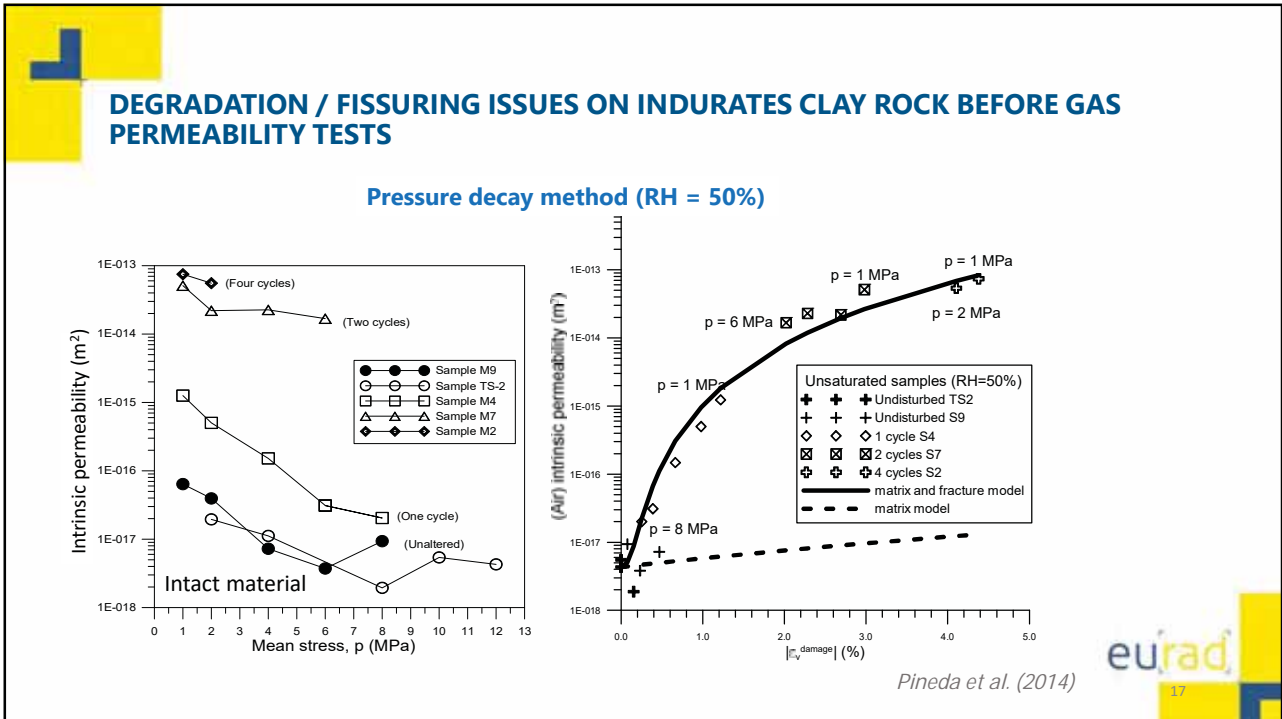
$$(E - E_r) / E_0 = (1 - D)$$

$$(G - G_r) / G_0 = (1 - D)$$

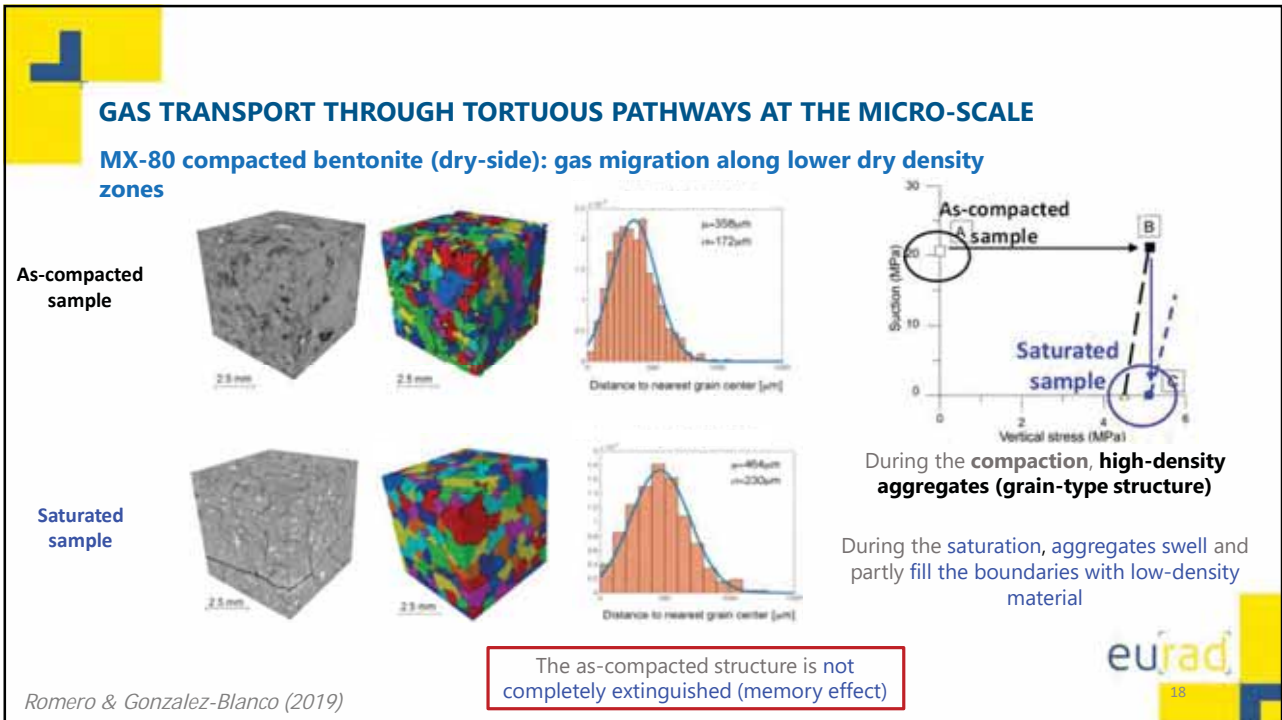
$$(\sigma_t - \sigma_{tr}) / \sigma_{t0} = (1 - D)$$

Pineda, Alonso & Romero (2014)





17



18

HETEROGENEITY EFFECTS AT THE MICRO-SCALE (DRY-SIDE COMPACTED MX-80)

As-compacted sample

Grey value [-]

Saturated sample

Density ρ [g/ccm]

Density (porosity) calibration to take into account local heterogeneity

The covariance range of the structure reaches **correlation lengths of at least 3 mm**

Sample	As-compacted	Saturated
Degree of saturation	$S_r \sim 0.7$	$S_r = 1$
L_{RVE} (μm)	2849	1156
ρ_{mean} (Mg/m^3)	1.53	1.53
Density range (Mg/m^3)	1.46-1.62	1.52-1.56
$\Delta\rho$ (Mg/m^3)	0.16	0.04
Standard deviation σ	0.031	0.010
Coefficient of variation	0.020	0.005

*eu*rad

Romero & Gonzalez-Blanco (2019)

19

HETEROGENEITY EFFECTS AT THE MICRO-SCALE (DRY-SIDE COMPACTED MX-80)

Density (porosity) calibration to take into account local heterogeneity

Random porosity field in coupled FEM simulation:

Distribution according to μ -CT with no correlation length (diameter 50 mm)

*eu*rad

Romero & Gonzalez-Blanco (2019)

20

ADVECTIVE GAS EXPERIMENTS AT LAB SCALE: SOME ISSUES OF CONCERN

- Effects of the **stress state** and **stress history** (mechanical, saturation, thermal) on gas migration
- **Volume change behaviour** during the stress history and along gas injection / dissipation (changes in gas and liquid pressures and their impact on gas permeability). **Stress changes** during gas injection under soil constant volume conditions
- Role played by natural **discontinuities and their orientation** (anisotropy) and **low-density pathways** (material heterogeneity)
- **Changes in the pore / fissure network and their connectivity** due to gas injection / dissipation (opening of bedding planes / fissures / pathways)
- **Gas migration after resaturation** (reopening of fissures)
- **Liquid displacements (desaturation of pathways)** during gas injection / dissipation
- Influence of the **gas injection rate and gas type**
- **Mobilisation of bentonite material along the gas percolation path** (internal erosion)

Simple concepts but **no so simple tests to perform and interpret**. Need for **coupled modelling to complement the information** not provided by measurements ('boundary value tests')

eurad

21

21

HOW TO PERFORM ADVECTIVE GAS INJECTION/DISSIPATION TESTS?

Importance of:

- **Hydro-mechanical characterization** of tested material (uncertainty / variability assessment)
- **Restoring in situ stress state** (effective stress) (natural samples)
- **Reproducible sample preparation methods** (artificially prepared samples)
- **Defining the stress paths to follow prior to gas injection** (saturation path)
- **Measuring volume changes** in stress-controlled tests / **stress state** under isochoric conditions
- ...

eurad

22

22

HOW TO PERFORM ADVECTIVE GAS INJECTION/DISSIPATION TESTS?

Gas injection protocol:

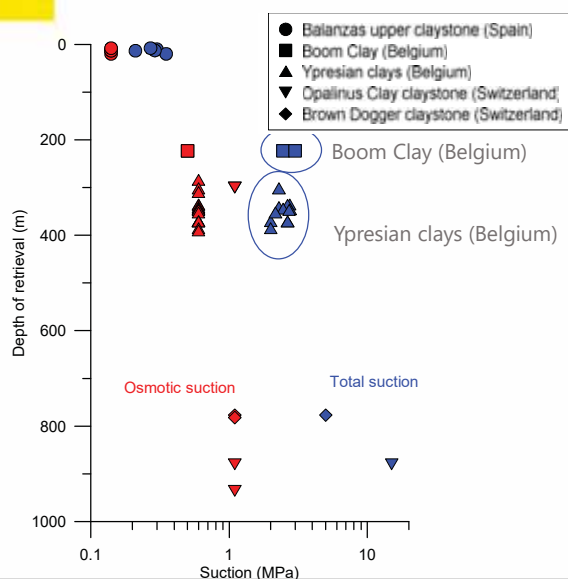
- Stress controlled (dilatant pathways) or **controlled volume conditions** (isochoric test)
- Type of fluid at the boundaries (gas – gas) / (gas – liquid). **Gas type** (air / nitrogen N₂ / helium He ...)
- Flow direction with respect to **bedding orientation** (anisotropy features)
- Surface to apply **gas injection** (gas on entire sample surface, point injection)
- **Gas injection method** (pressure ramp / controlled volume or mass rate injection)
- **Gas injection rate** (slow – fast) (dynamic effects on water retention curve)
- **Type of test** ('soft breakthrough' with maximum pressure close to AEV / 'hard breakthrough' until gas outflow)
- **Information on system volumes** (inflow/outflow volumes, dead volume up to valves, gaps, ...)
- ...

eurad

23

23

IMPORTANCE OF RESTORING IN SITU STRESS STATE (EFFECTIVE STRESS)



Occurrence of (matric) suction despite the nearly saturated state:

- Release of total stresses under water undrained conditions upon retrieval
- Some drying undergone during sampling, transportation, storage and preparation

$$p_i = p'_i - u_{wi} \text{ with } p'_i = \frac{1}{3}(1 + 2K_0)\sigma'_{vi}$$

$$p_f = 0$$

$$\Delta p = -p_i = -p'_i - u_{wi}$$

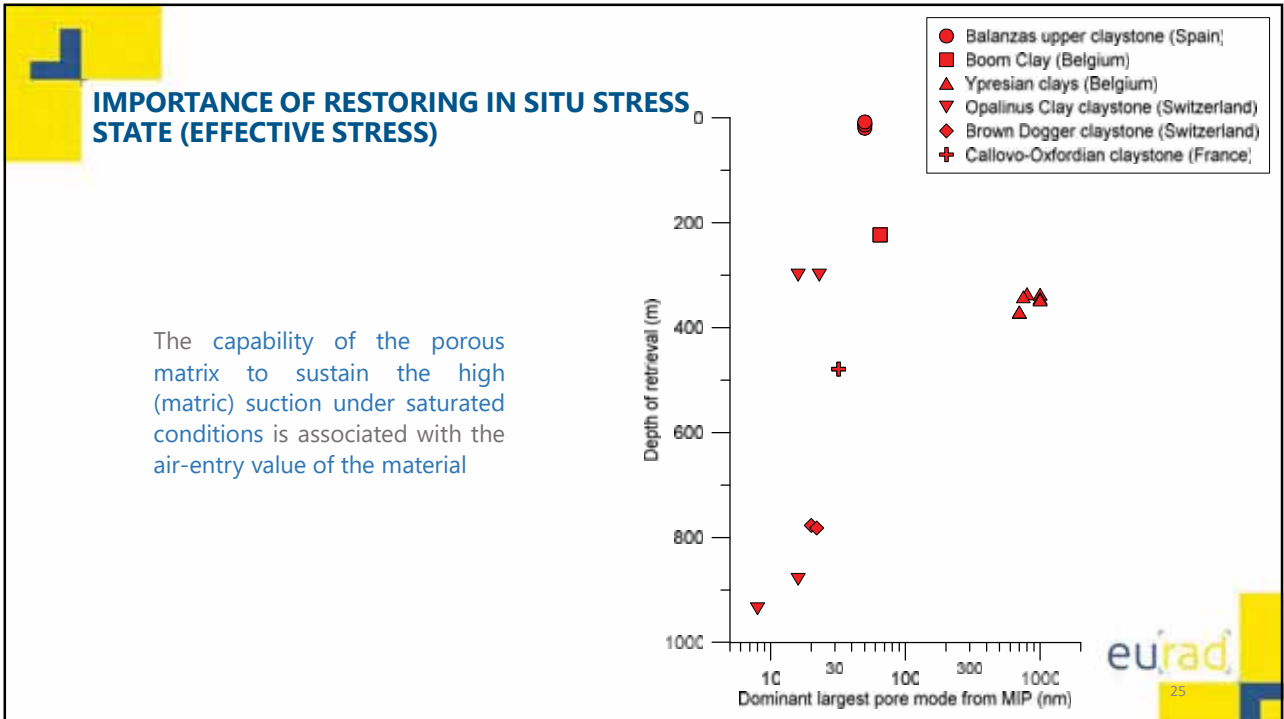
$$\Delta u_w = \Delta p \text{ (constant effective stress)}$$

$$u_{wf} = u_{wi} + \Delta u_w$$

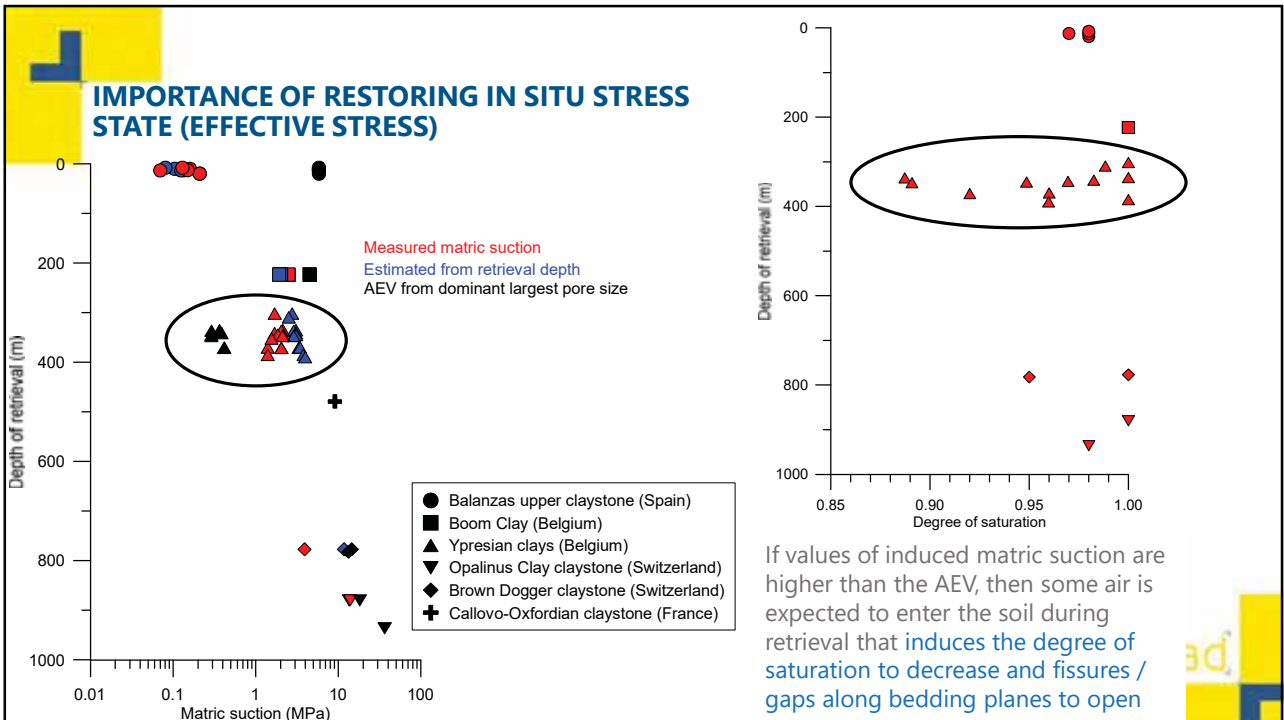
eurad

24

24

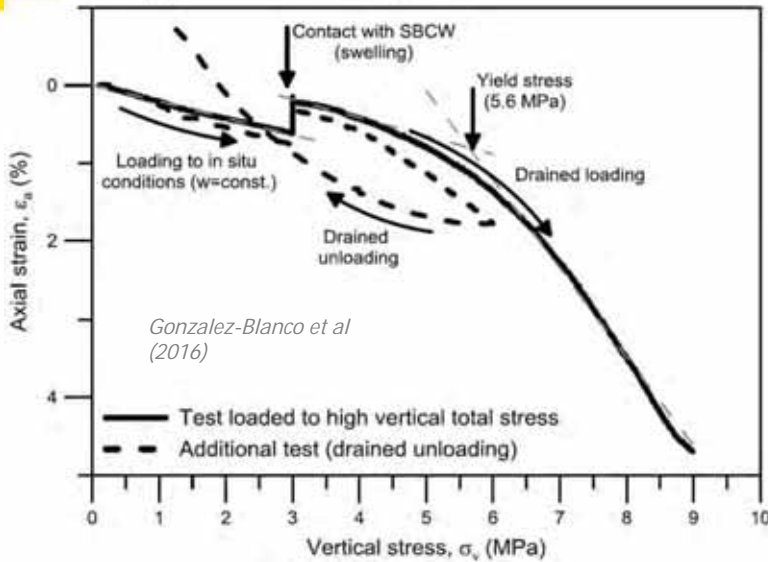


25



26

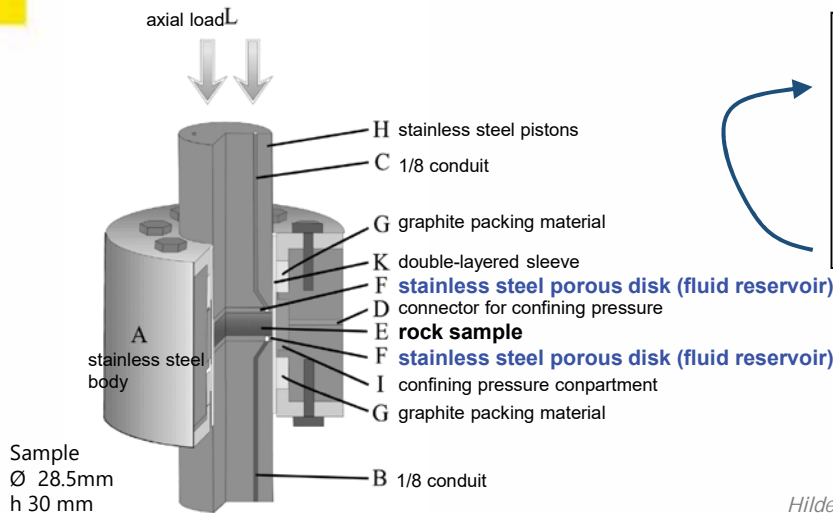
IMPORTANCE OF RESTORING IN SITU STRESS STATE (EFFECTIVE STRESS)



- Boom Clay loaded under water undrained conditions to in situ vertical stress (3 MPa)
- Placed in contact with synthetic water SBCW at atmospheric pressure (despite being saturated there is still some remaining matric suction around 0.15 MPa)
- Afterwards vertical stress and water pressure can be translated (constant vertical effective stress) for water back-pressure application

27

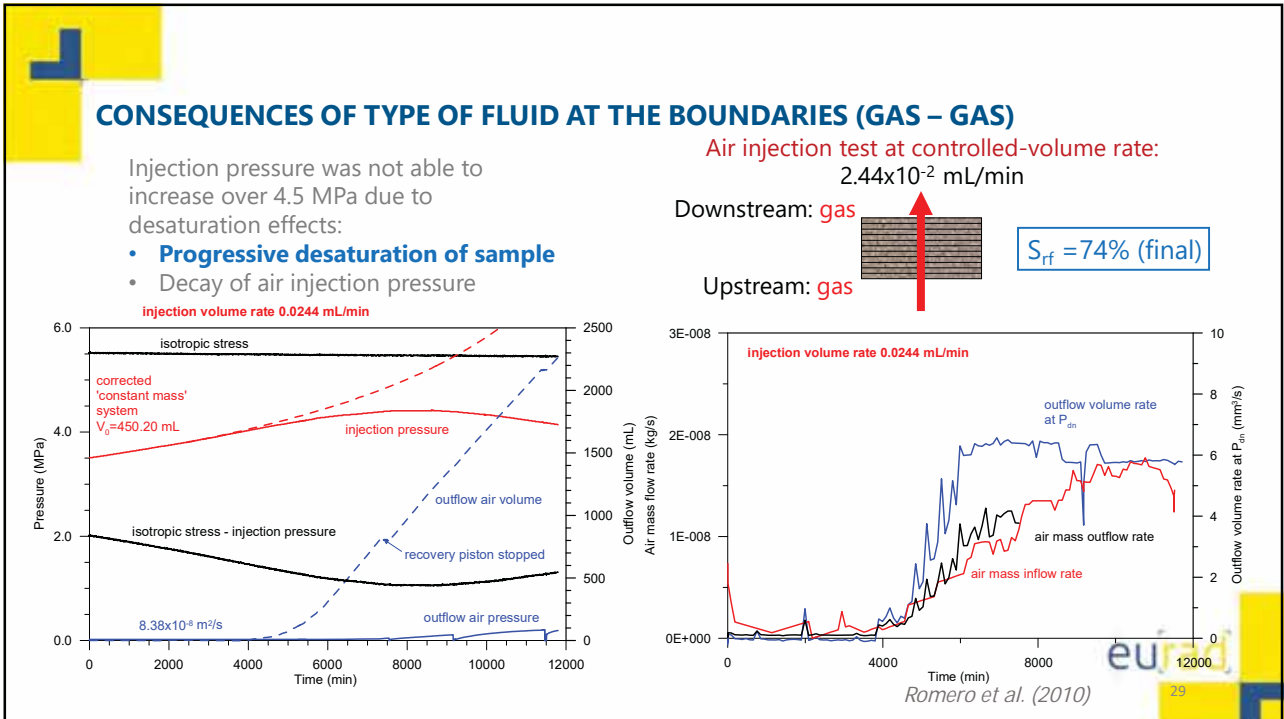
TYPICAL LABORATORY TEST STAGES BEFORE GAS INJECTION



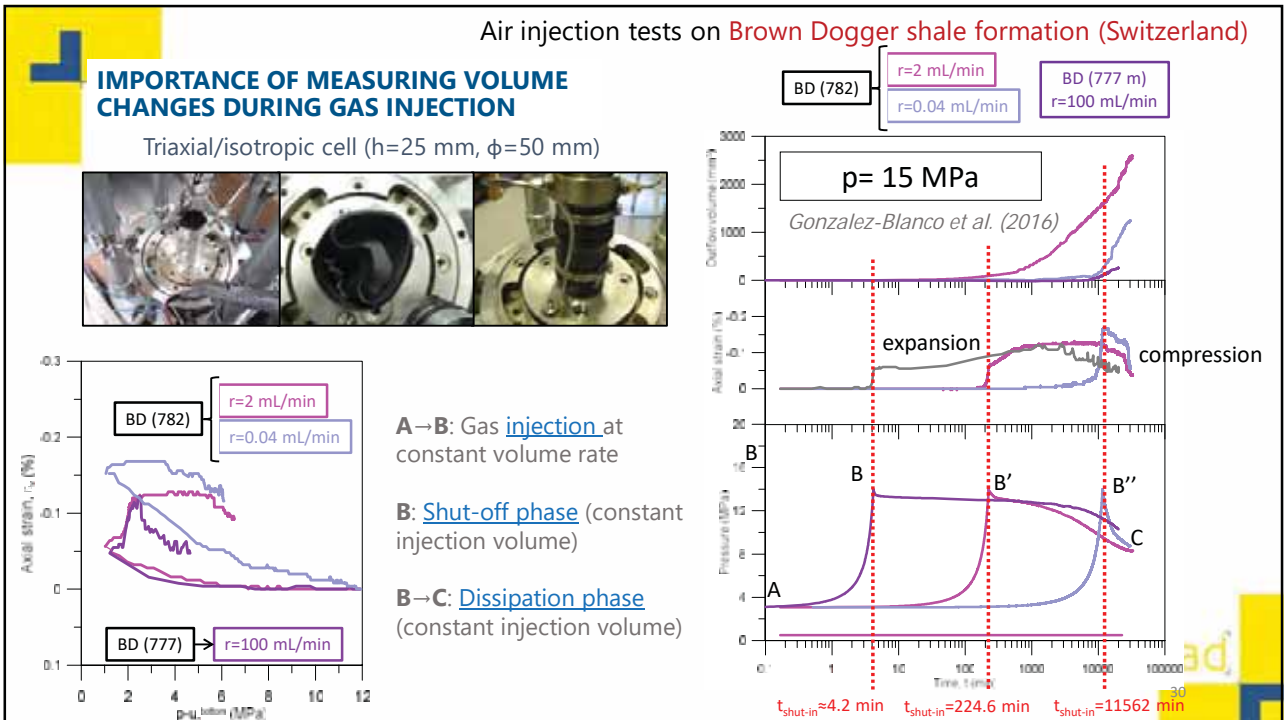
- Test stages:**
- Saturation
 - Water permeability
 - Removal of water from porous disks
 - Gas injection test

Hildebrand et al. (2002)

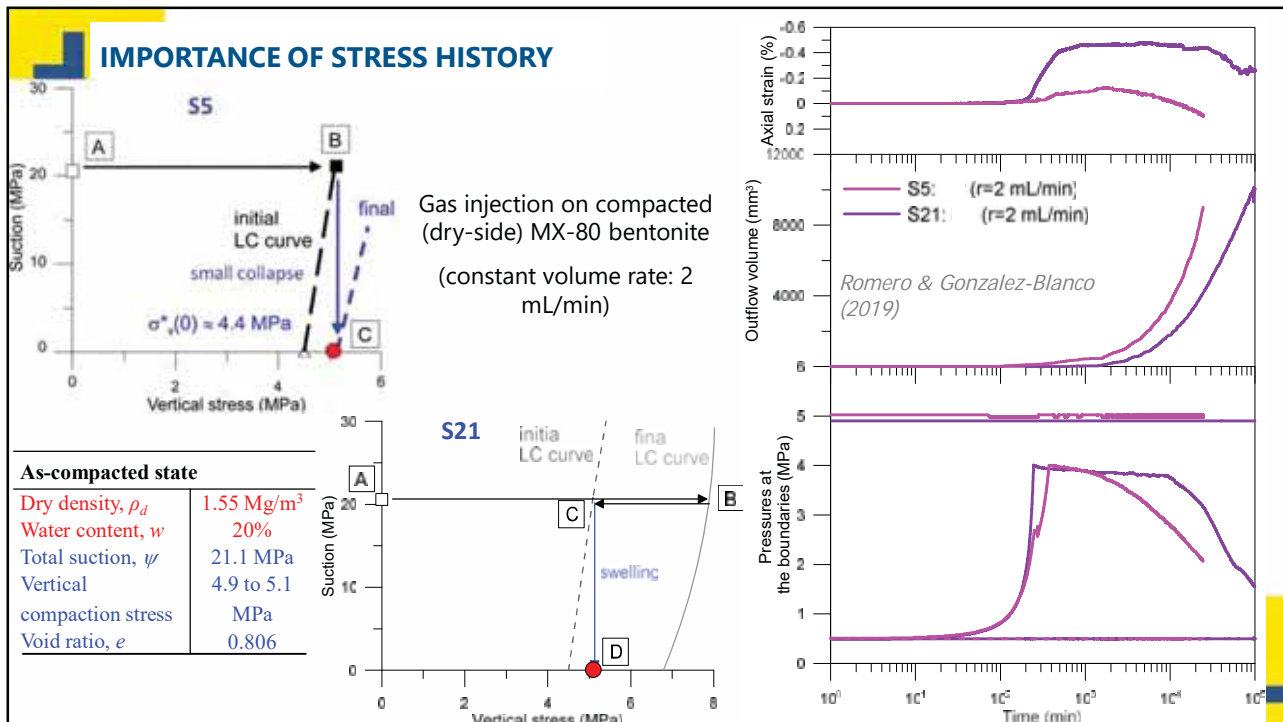
28



29



30



31

OUTLINE OF THE LECTURE

1. Motivation and content
2. Insight into gas transfer (gas generation, gas transport mechanisms, multi-scale aspects)
3. Some observations regarding gas testing (experimental protocols)
4. **A detailed research methodology on Boom Clay:**
 - Material characterization
 - Stress paths followed
 - Gas test protocols
 - Test results at different scales (macroscopic results and microstructural features)
5. Final comments. Future challenges

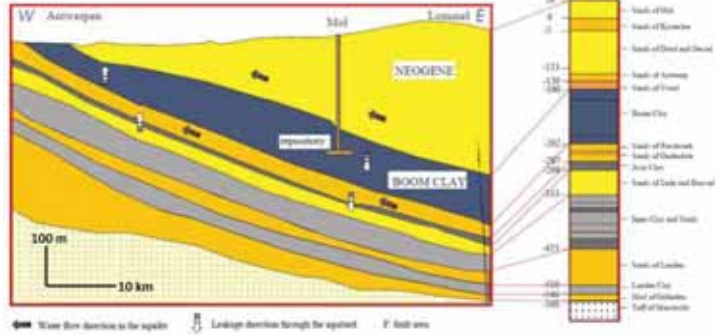
eu^{rad}

32

BOOM CLAY



Marine sediment of the Cenozoic (Rupelian age, 30 My)



Sillen & Marivoet (2007)

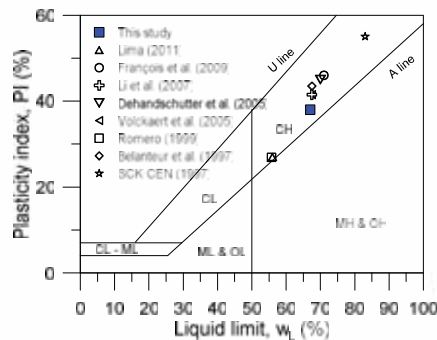
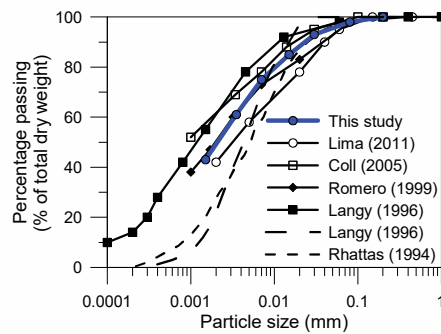
Samples retrieved at **HADES URL** level (223 m depth) in boreholes horizontally drilled



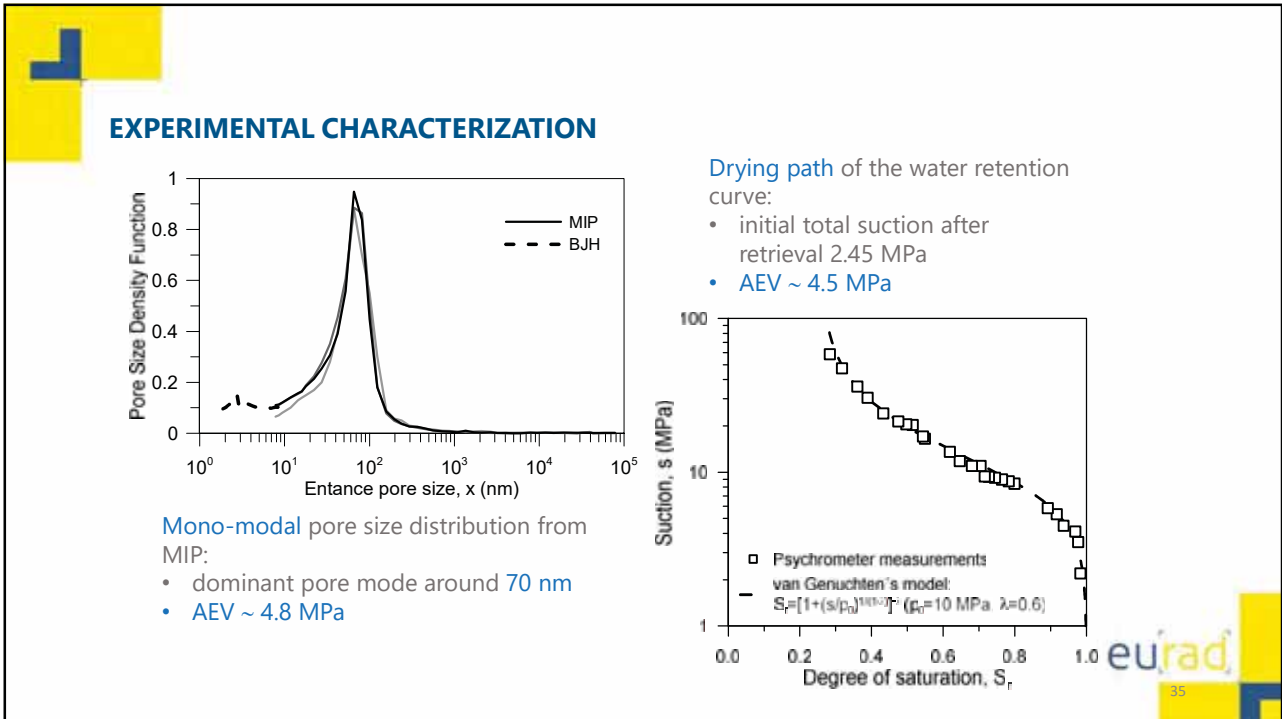
33

EXPERIMENTAL CHARACTERIZATION

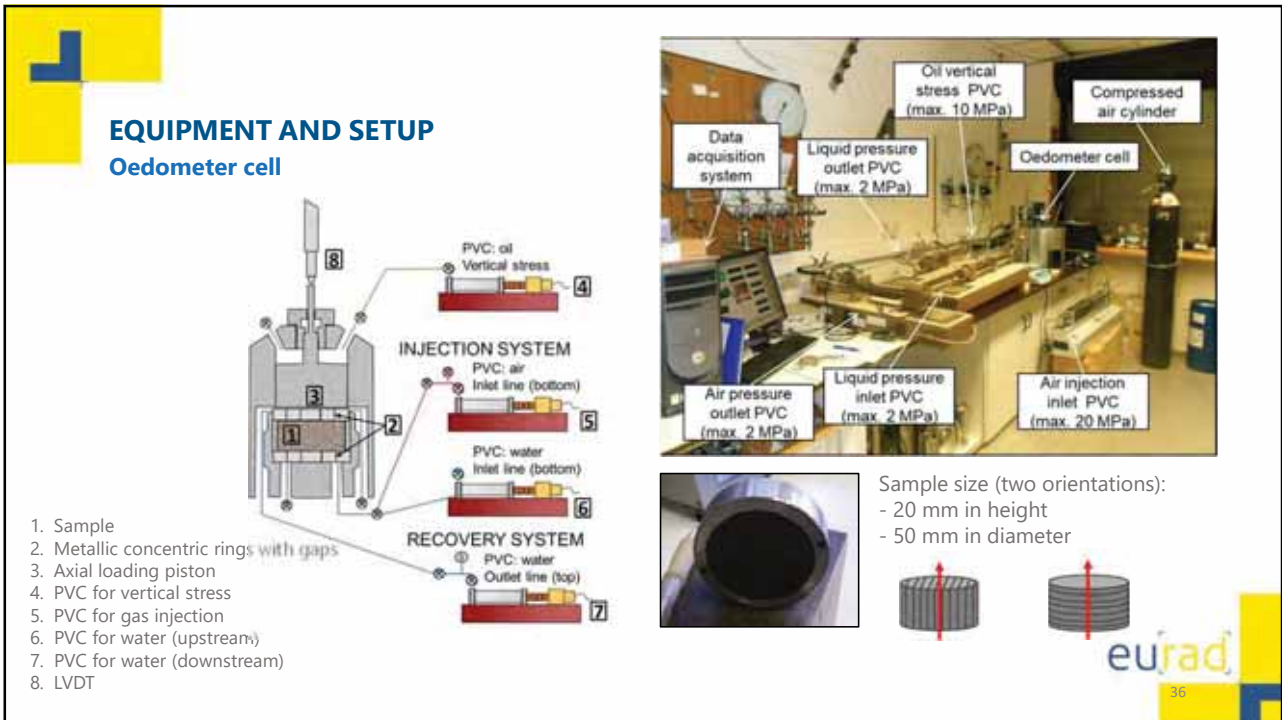
Parameter	Value
Geotechnical properties	
Density of soils, ρ_s (Mg/m^3)	2.67
Liquid limit w_L (%)	67
Plasticity index, I_p (%)	38
Initial conditions	
Density, ρ (Mg/m^3)	2.02-2.06
Dry density, ρ_d (Mg/m^3)	1.63-1.69
Porosity, n	0.37-0.39
Void ratio, e	0.58-0.63
Water content, w (%)	22.6-24.0
Degree of saturation	close to 1
Total suction after retrieval, Ψ (MPa)	2.45
Air-entry value from MIP (MPa)	4.8
Dominant pore mode from MIP (nm)	65



34



35



36

PRE-CONDITIONING STAGE

Objectives:

- to apply similar stress state than *in situ*
- to reduce initial suction
- to avoid expansion and degradation of the sample induced by suction reduction at low stress levels

At 223 m depth (*in situ* conditions)

$$\begin{cases} \sigma_{1v} = 4.50 \text{ MPa} \\ u_{wi} = 2.25 \text{ MPa} \\ \sigma'_{1i} = 2.25 \text{ MPa} \\ \sigma_1^{rmax} = 5.2 \text{ MPa} \end{cases}$$

After retrieval (undrained unloading)

$$\begin{cases} \Delta\sigma_1; \Delta\sigma_3 \rightarrow \Delta u_w = B \left[\Delta\sigma_3 + \frac{1}{3}A(\Delta\sigma_1 - \Delta\sigma_3) \right] \\ B = 1; A = 1/3 \\ \Delta u_w = \frac{\Delta\sigma_1 + 2\Delta\sigma_3}{3} = \Delta p = -4.5 \text{ MPa} \\ u_{wf} = u_{wi} + \Delta u_w = -2.25 \text{ MPa} \end{cases}$$

Post-storage

$$\begin{cases} \Psi = 2.45 \text{ MPa} & \text{High initial suction} \\ S_r \sim \text{close to } 1 & \text{due to stress relief} \end{cases}$$

Large deformation when soaking at 0.02 MPa

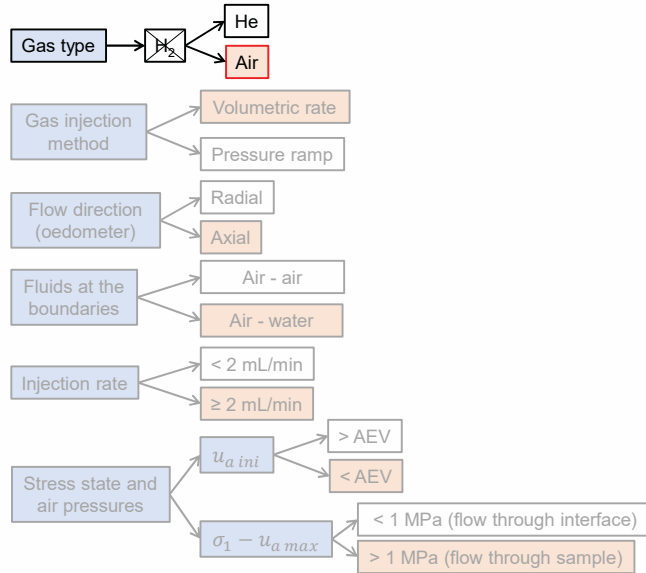
Soaking at 3 MPa

Della Vecchia et al (2011)

HOW TO PERFORM THE GAS INJECTION STAGE?

- Gas type → He, Air
- Gas injection method → Volumetric rate, Pressure ramp
- Flow direction (oedometer) → Radial, Axial
- Fluids at the boundaries → Air - air, Air - water
- Injection rate → < 2 mL/min, ≥ 2 mL/min
- Stress state and air pressures →
 - $u_{a \text{ ini}}$ → > AEV, < AEV
 - $\sigma_1 - u_{a \text{ max}}$ → < 1 MPa (flow through interface), > 1 MPa (flow through sample)

HOW TO PERFORM THE GAS INJECTION STAGE?

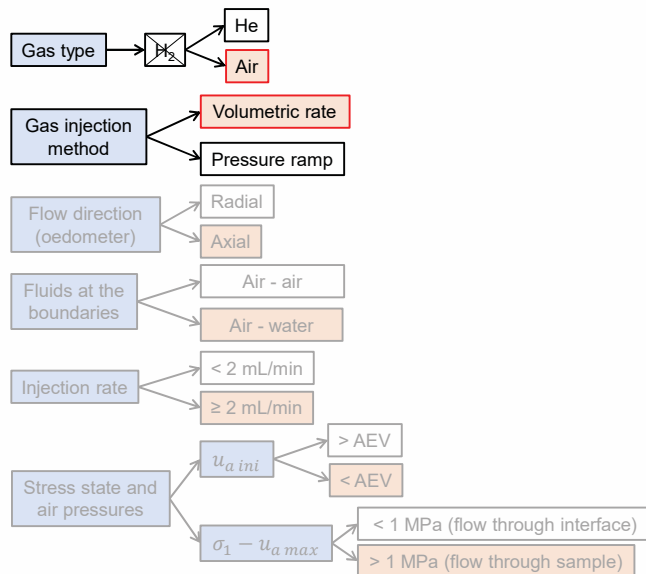


eurad

39

39

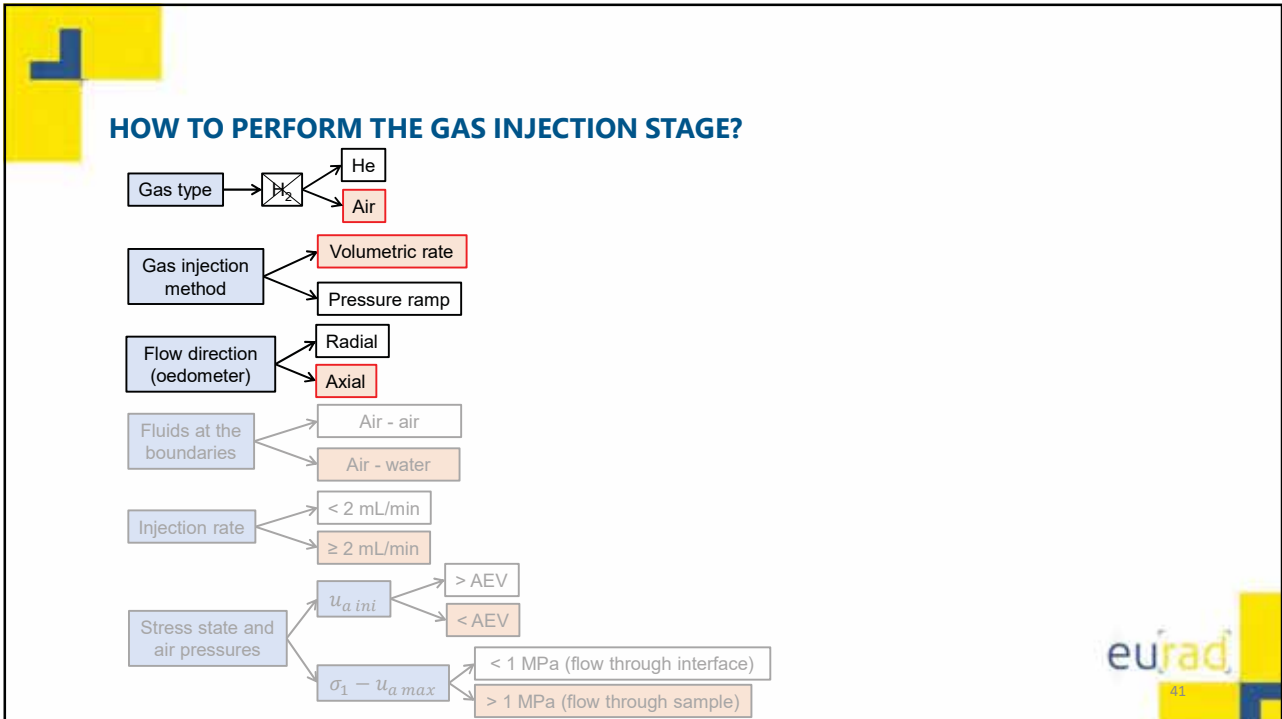
HOW TO PERFORM THE GAS INJECTION STAGE?



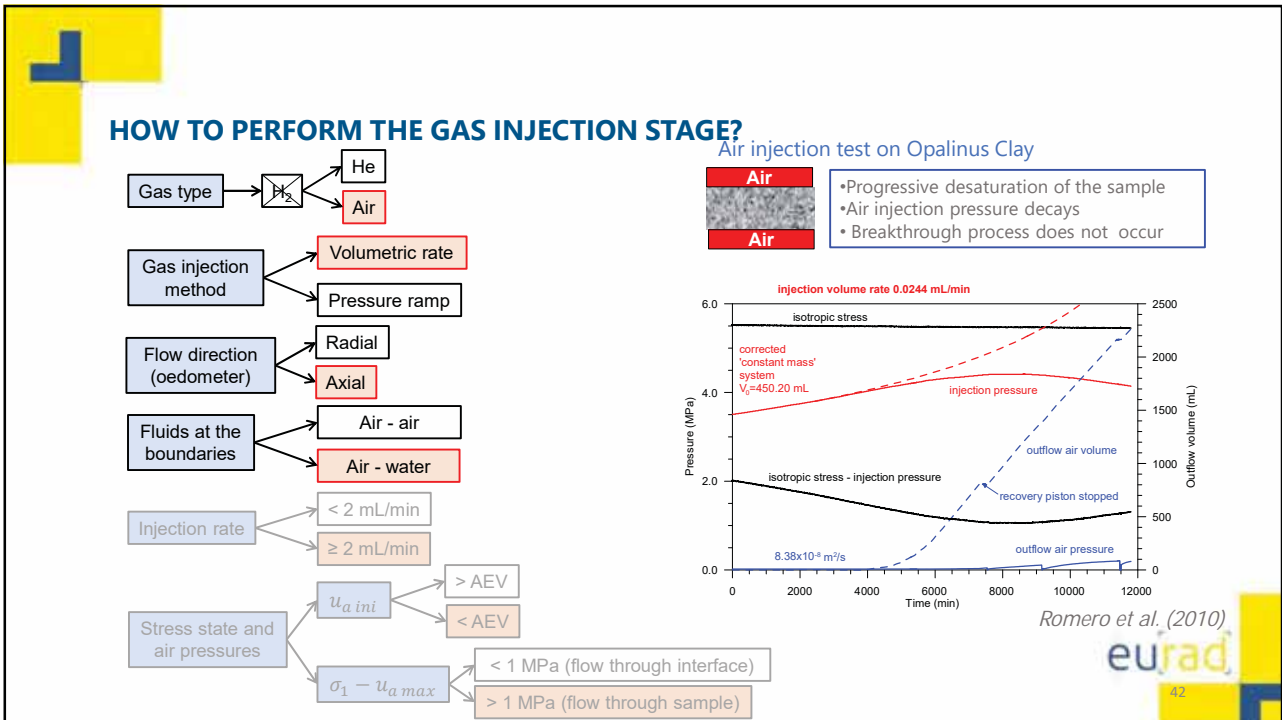
eurad

40

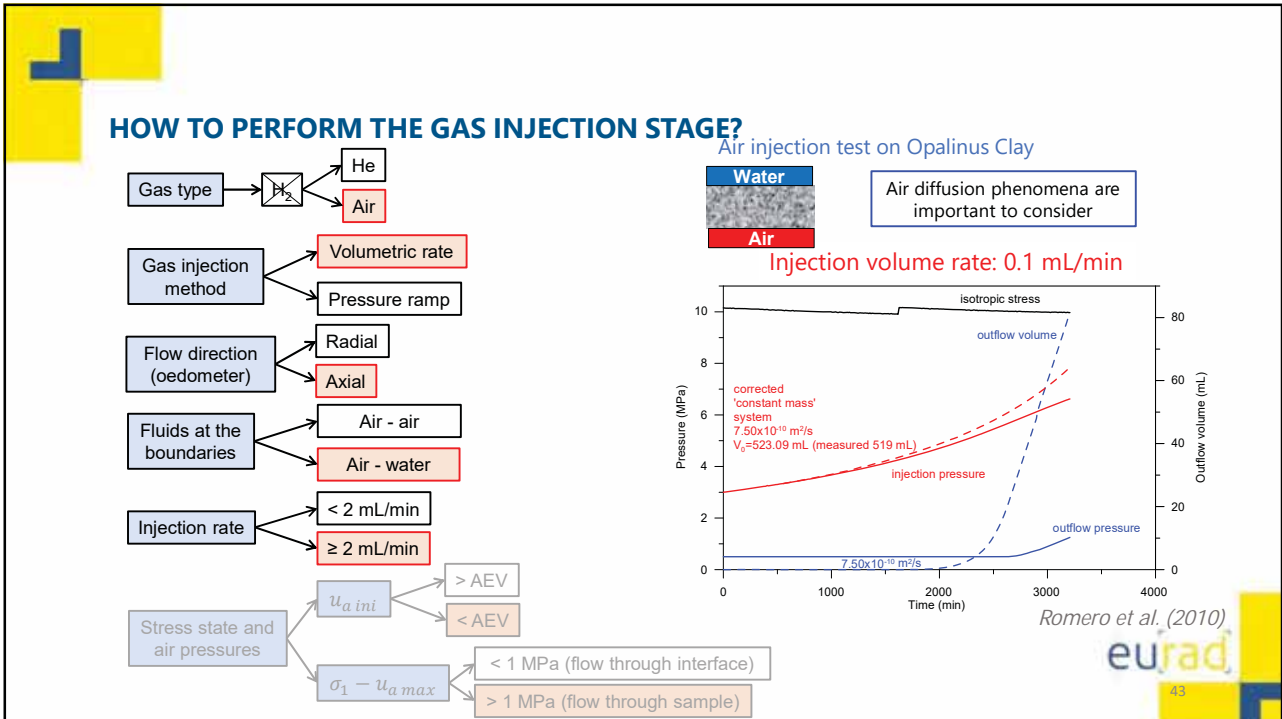
40



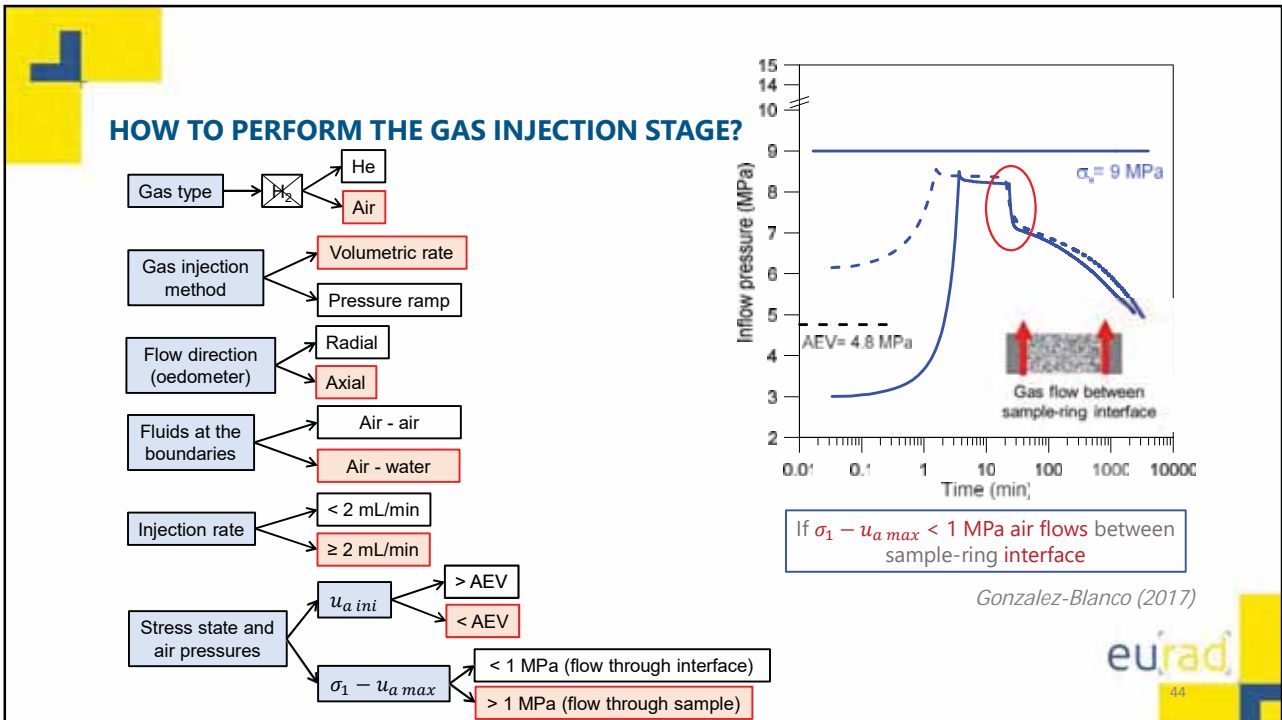
41



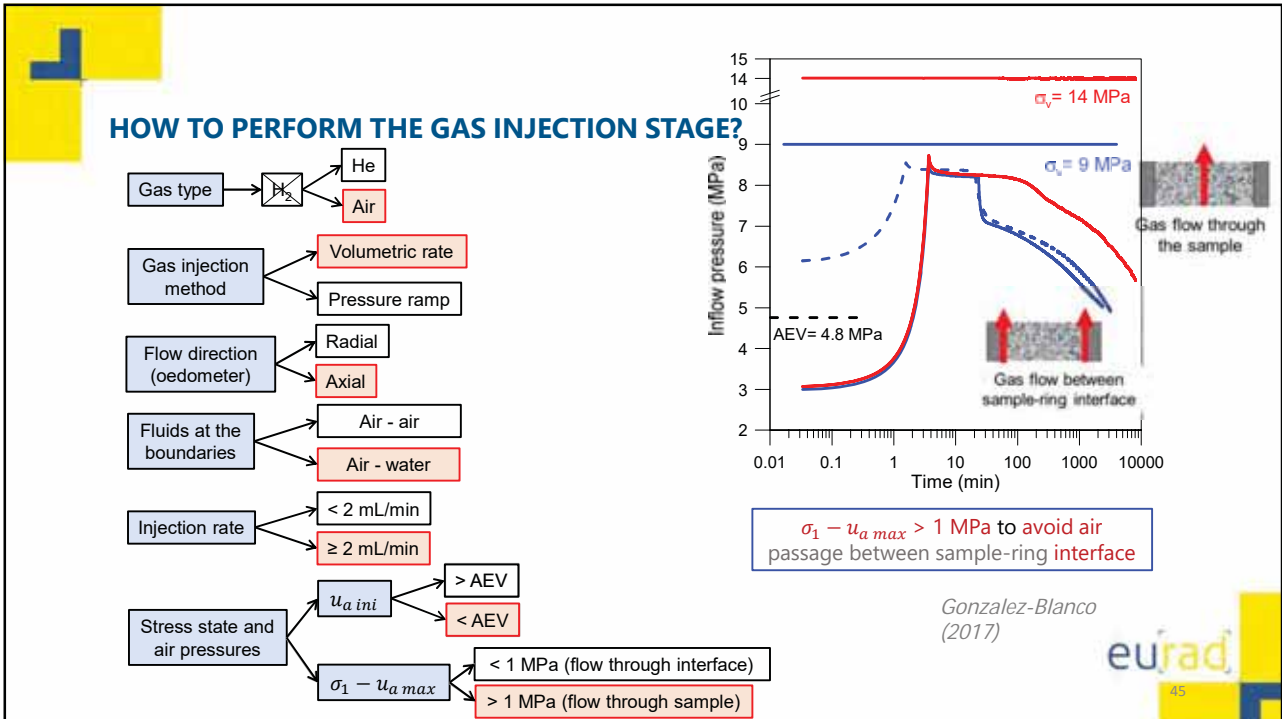
42



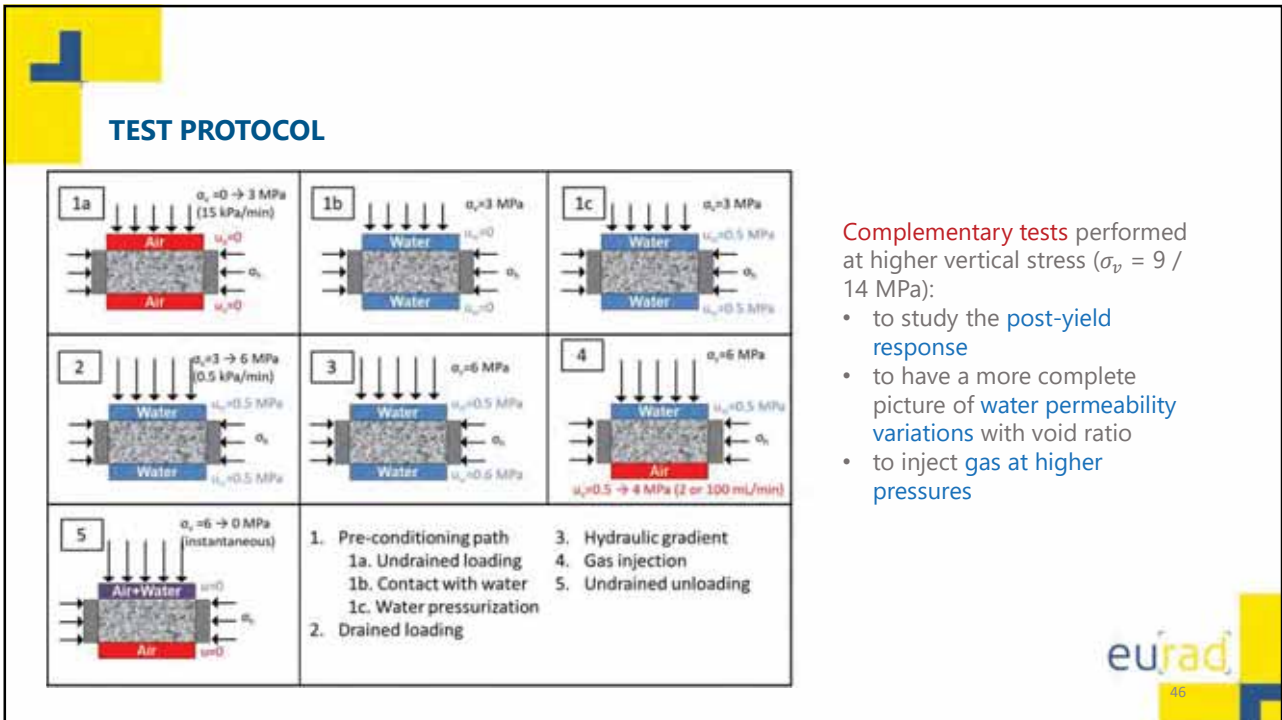
43



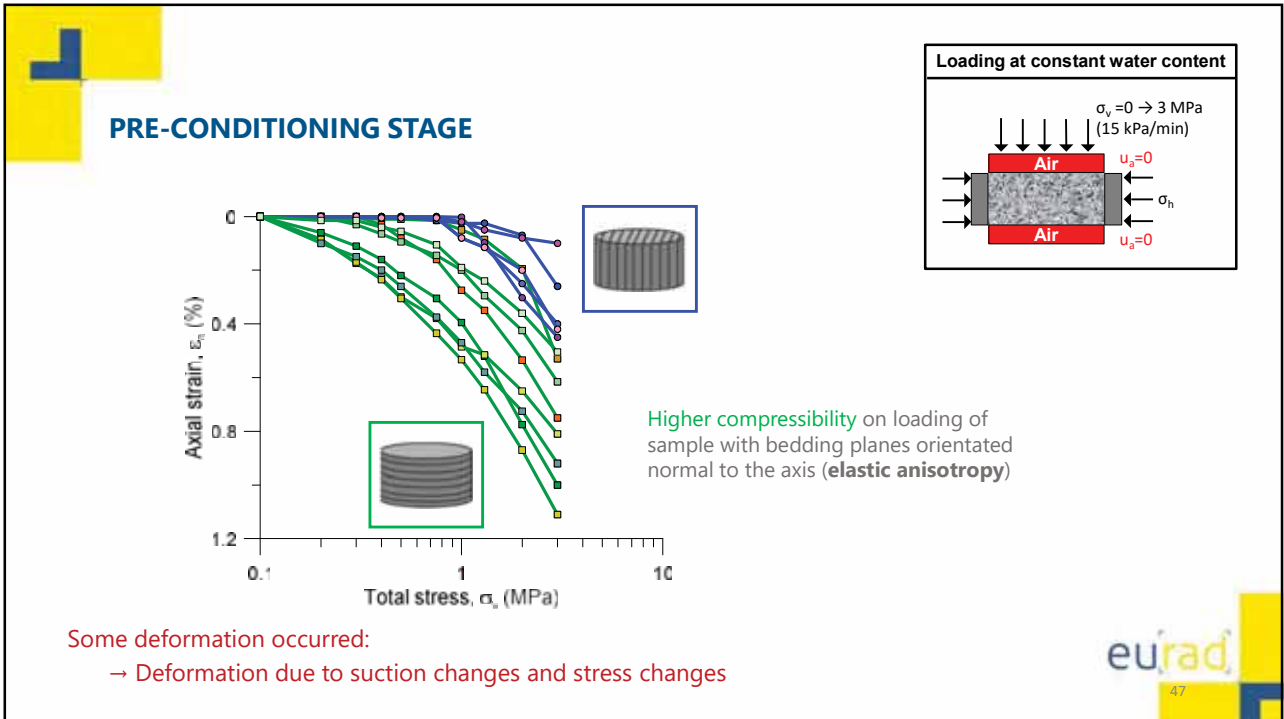
44



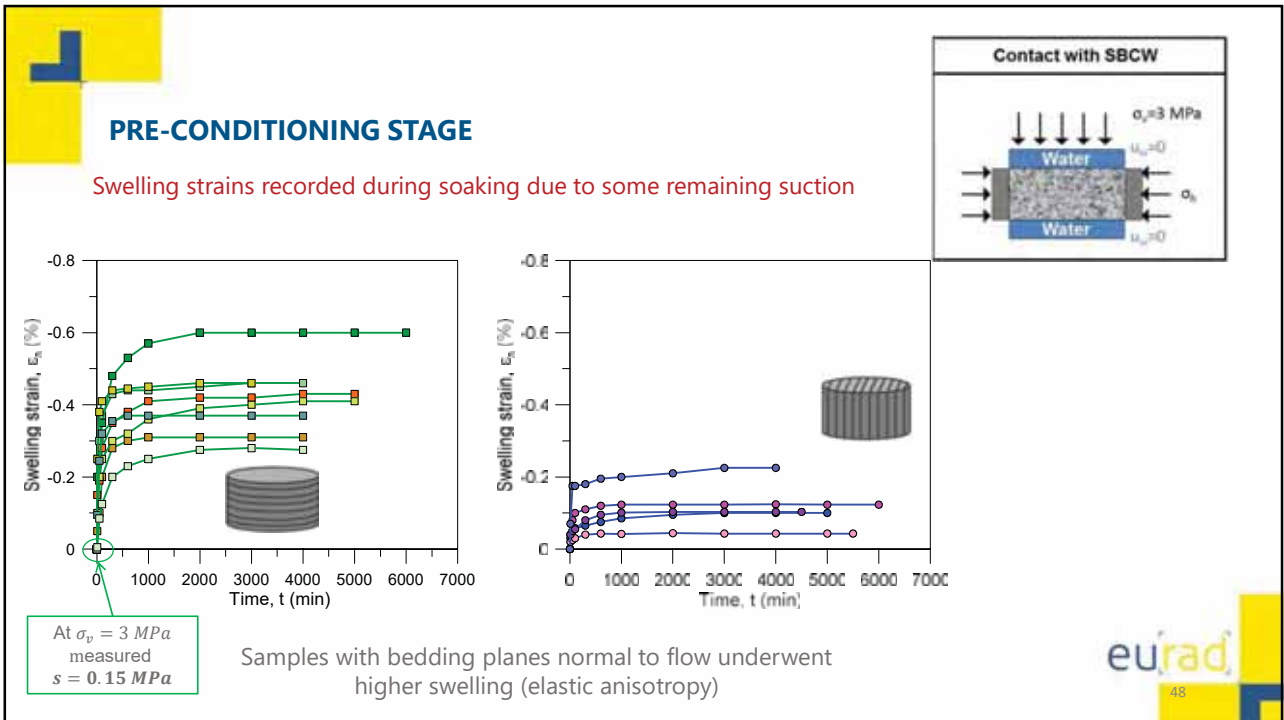
45



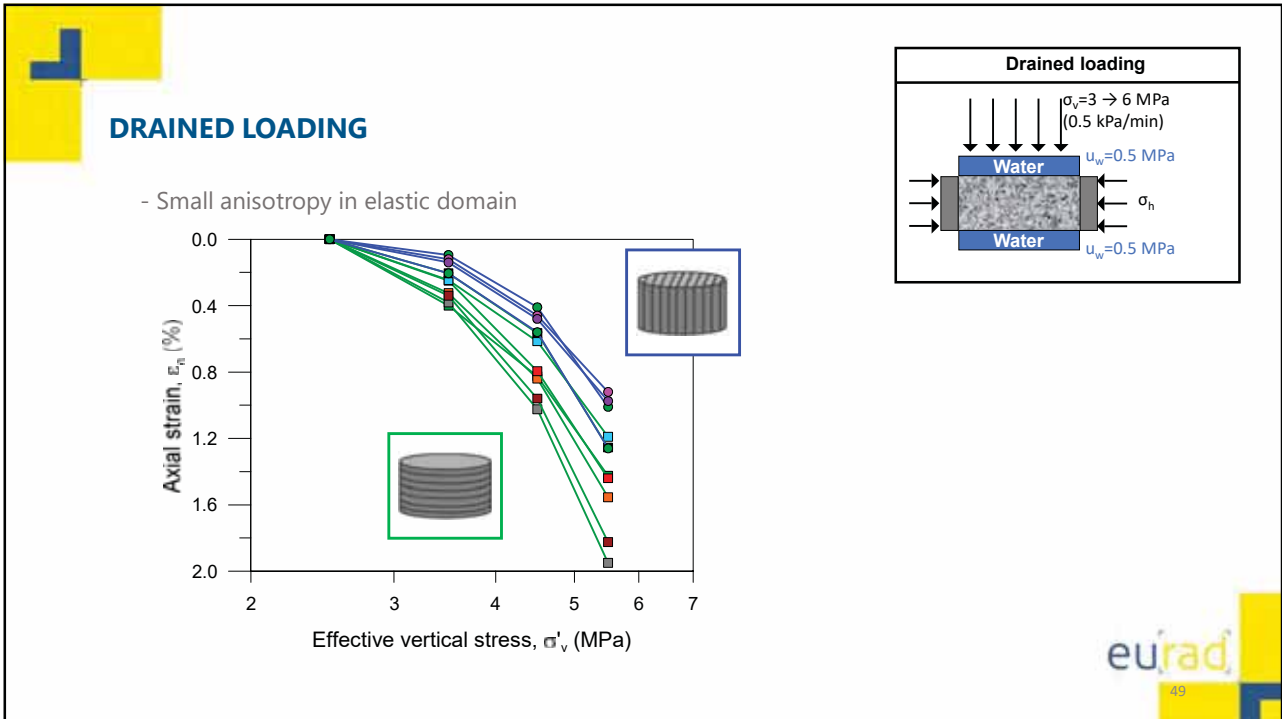
46



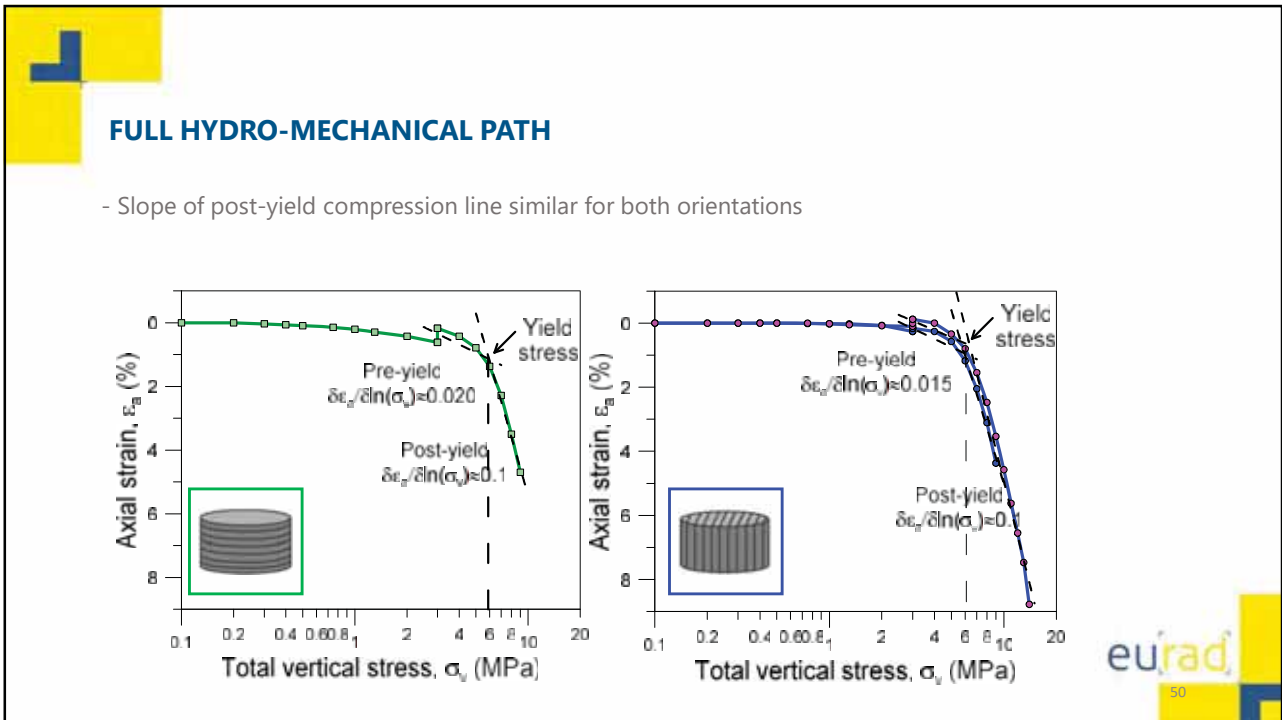
47



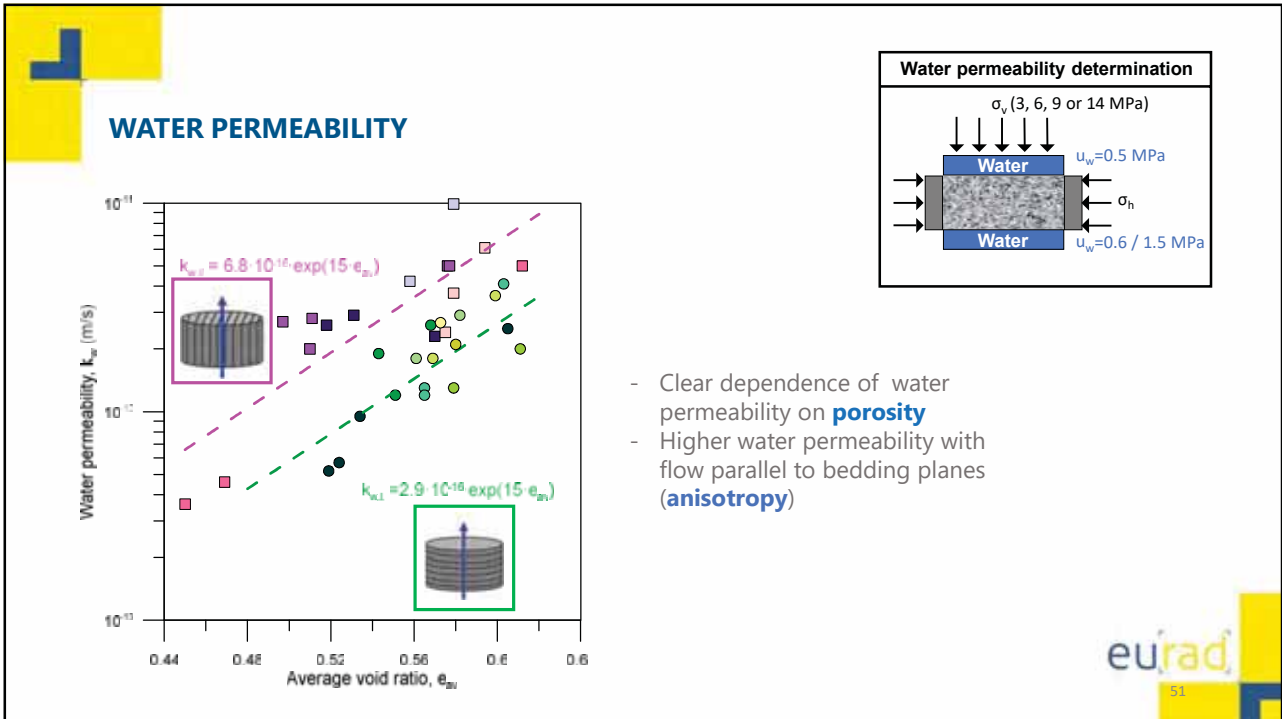
48



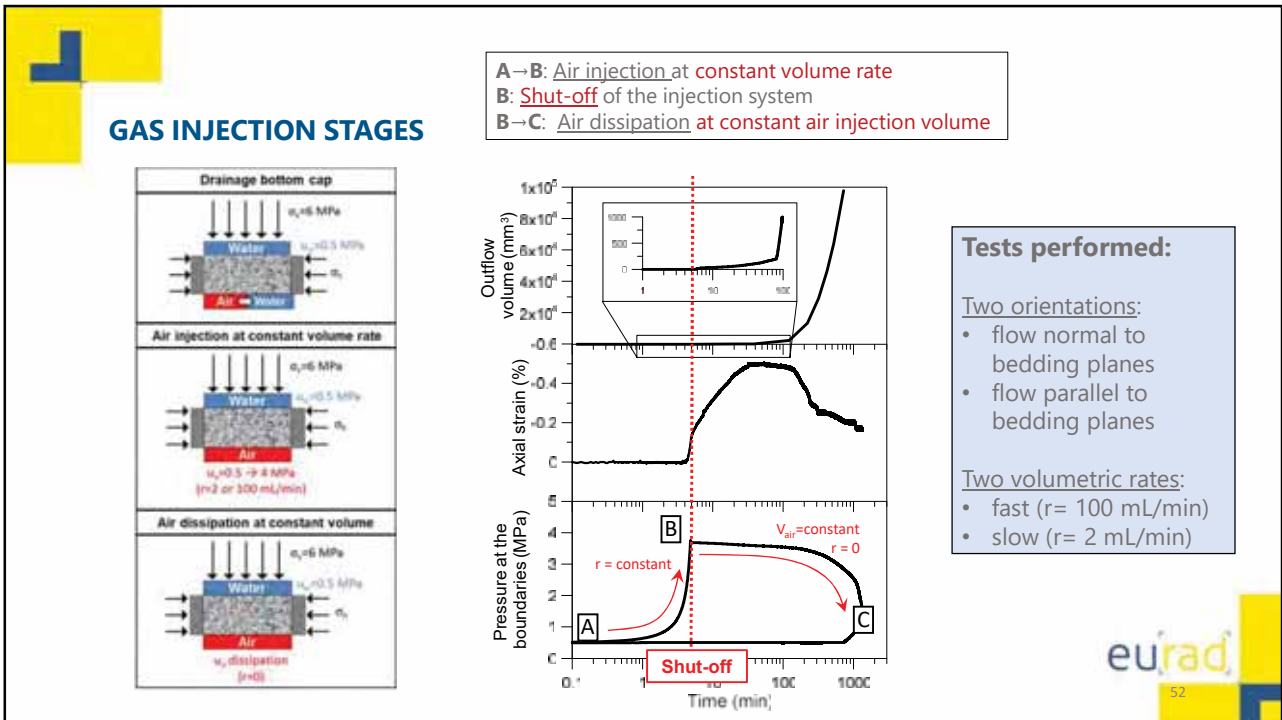
49



50



51



52

TEST RESULTS

A→B: Fast air injection at constant volume rate 100 mL/min up to 4 MPa

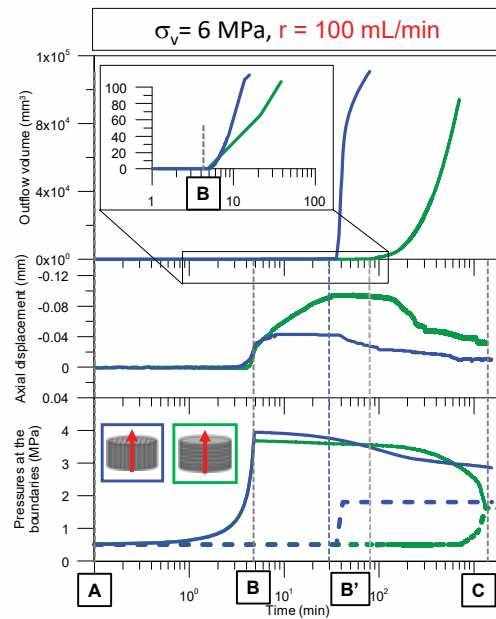
- No important expansion detected
- No outflow detected

B→B': Shut-off and dissipation phase at constant injection volume

- Expansion while air pressure front propagates (constitutive stress decreases)

B'→C: Dissipation phase at constant injection volume

- When outflow volume rate increases, air pressure decreases and samples undergo compression (constitutive stress increases)



eurad

53

53

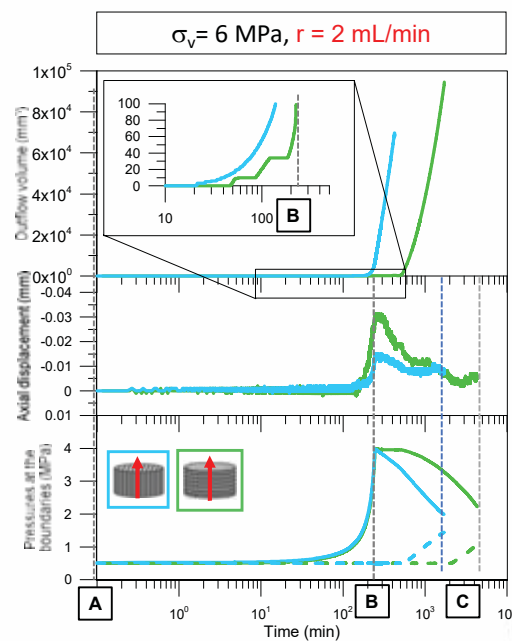
TEST RESULTS

A→B: Slow air injection at constant volume rate 2 mL/min up to 4 MPa

- Expansion while air pressure front propagates (constitutive stress decreases)
- First outflow detected during the injection

B→C: Shut-off and dissipation phase at constant injection volume

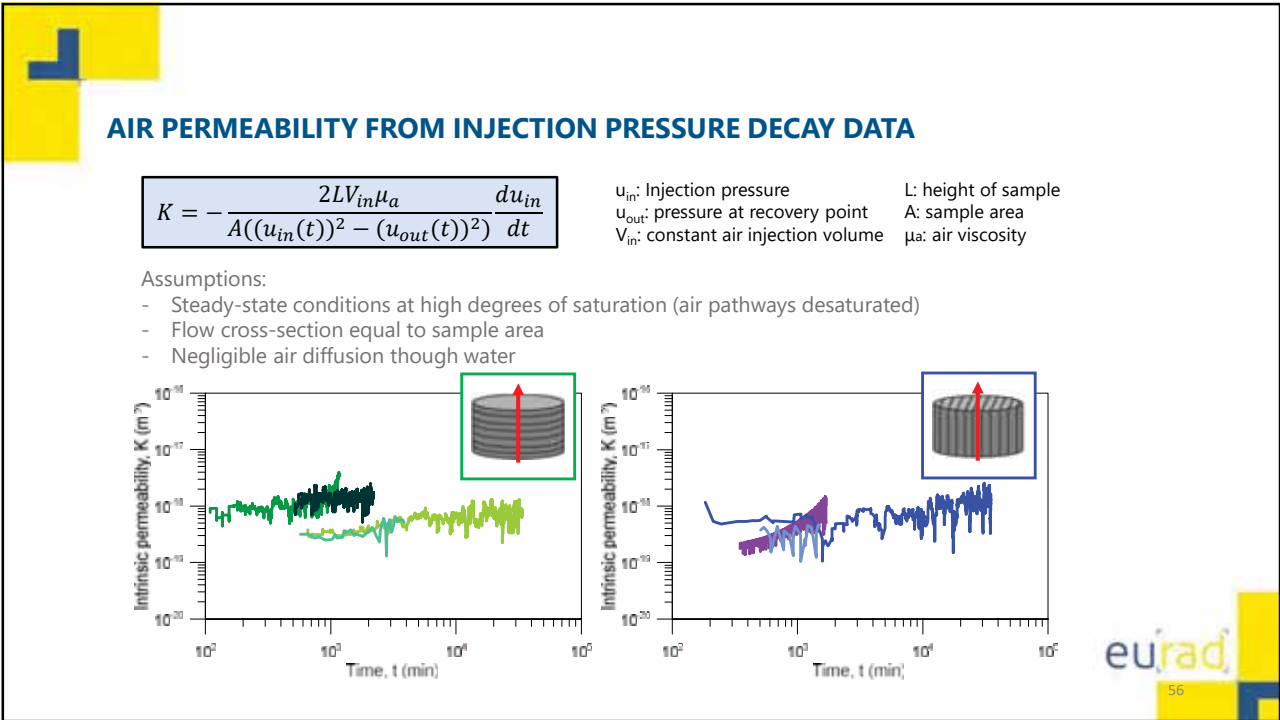
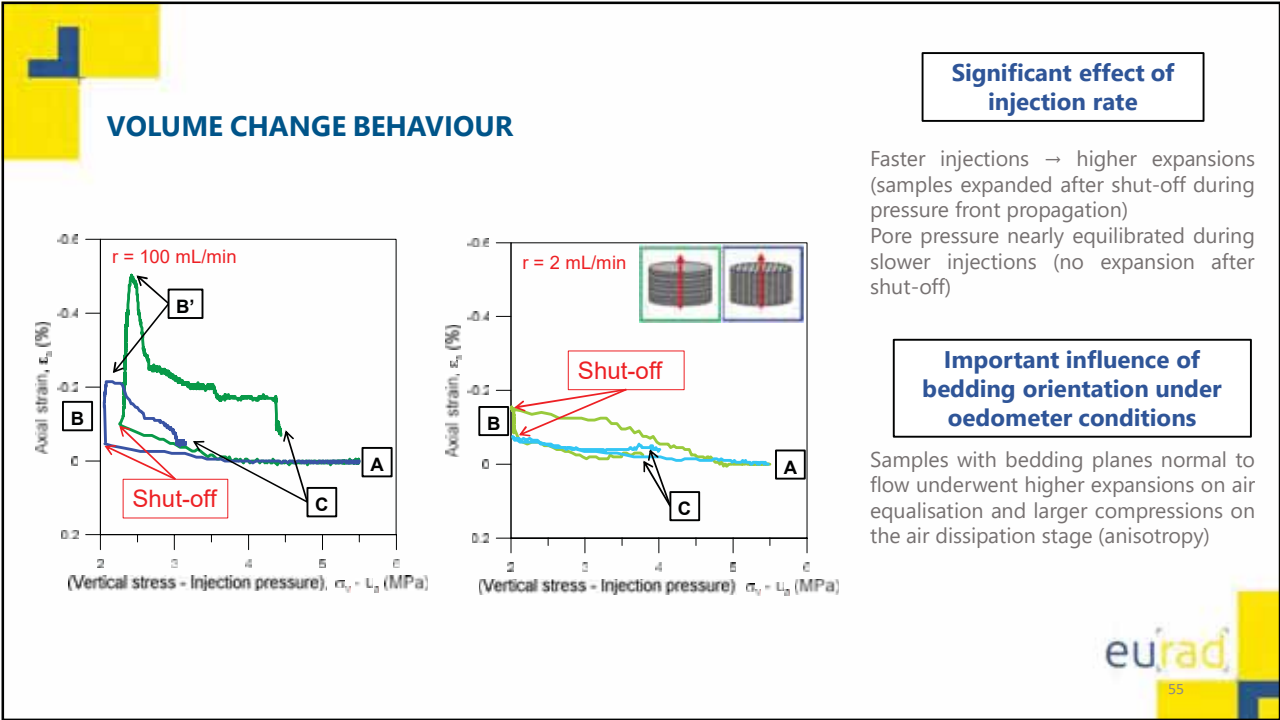
- Immediately after shut-in, the outflow volume rate increases, the air pressure decreases and samples undergo compression (constitutive stress increases)

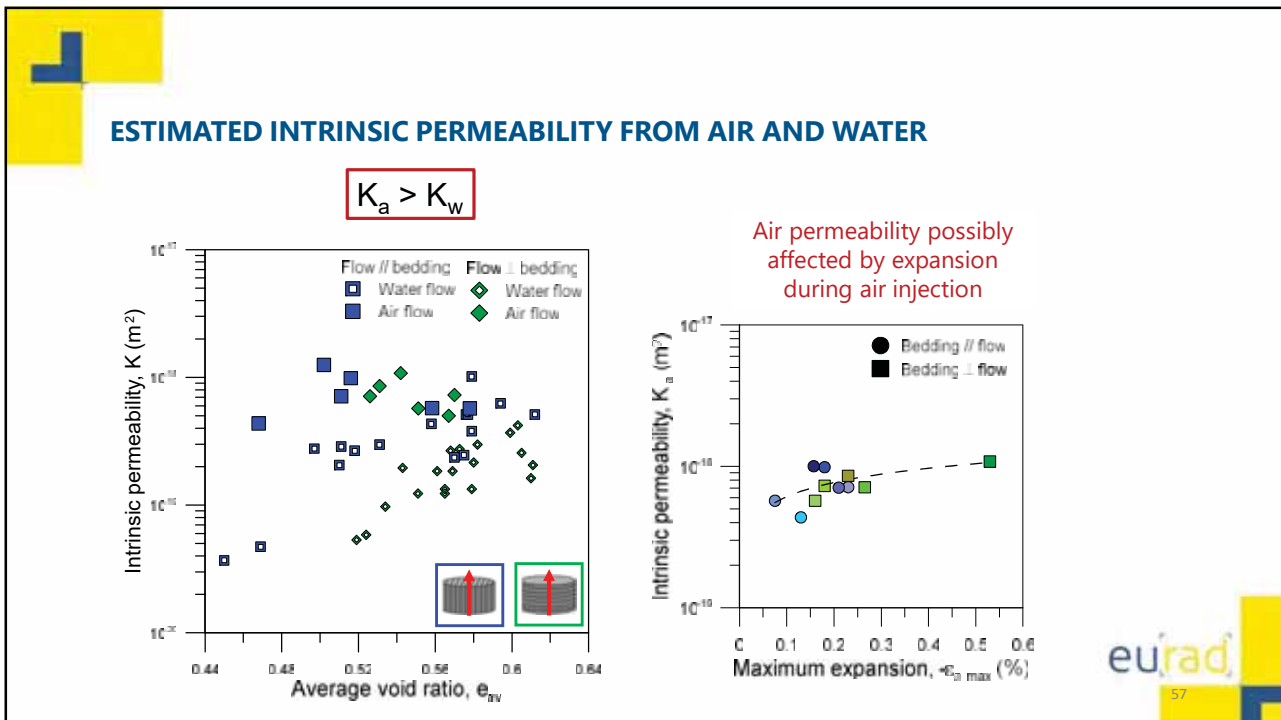


eurad

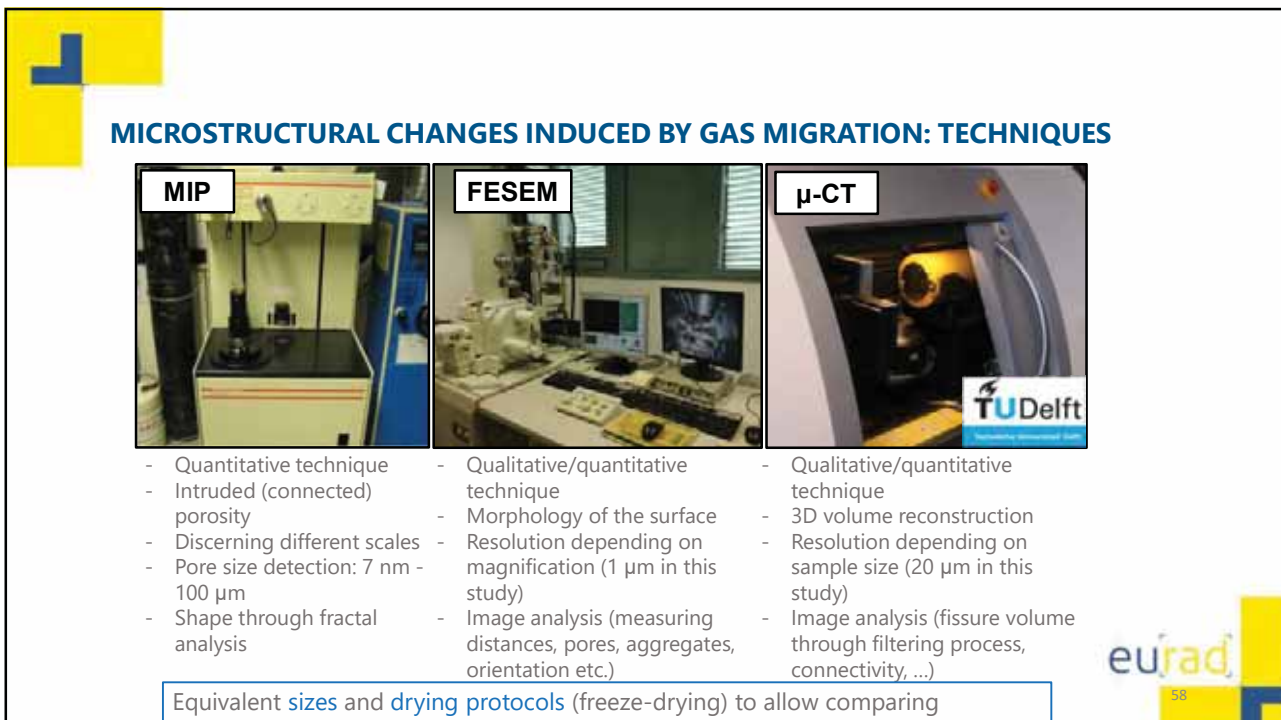
54

54





57

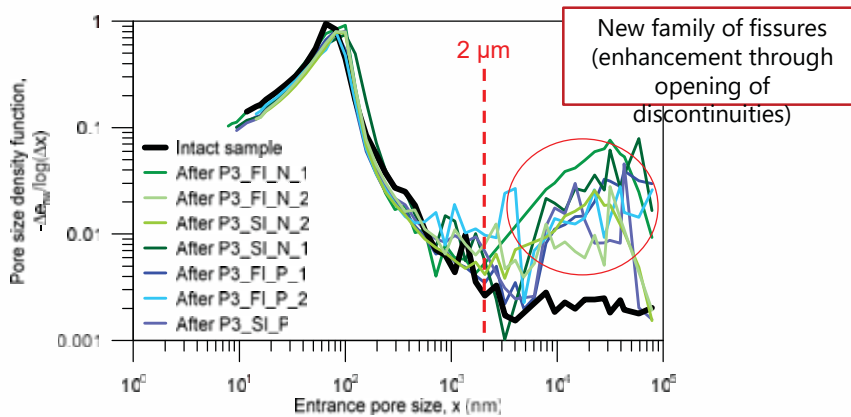


58

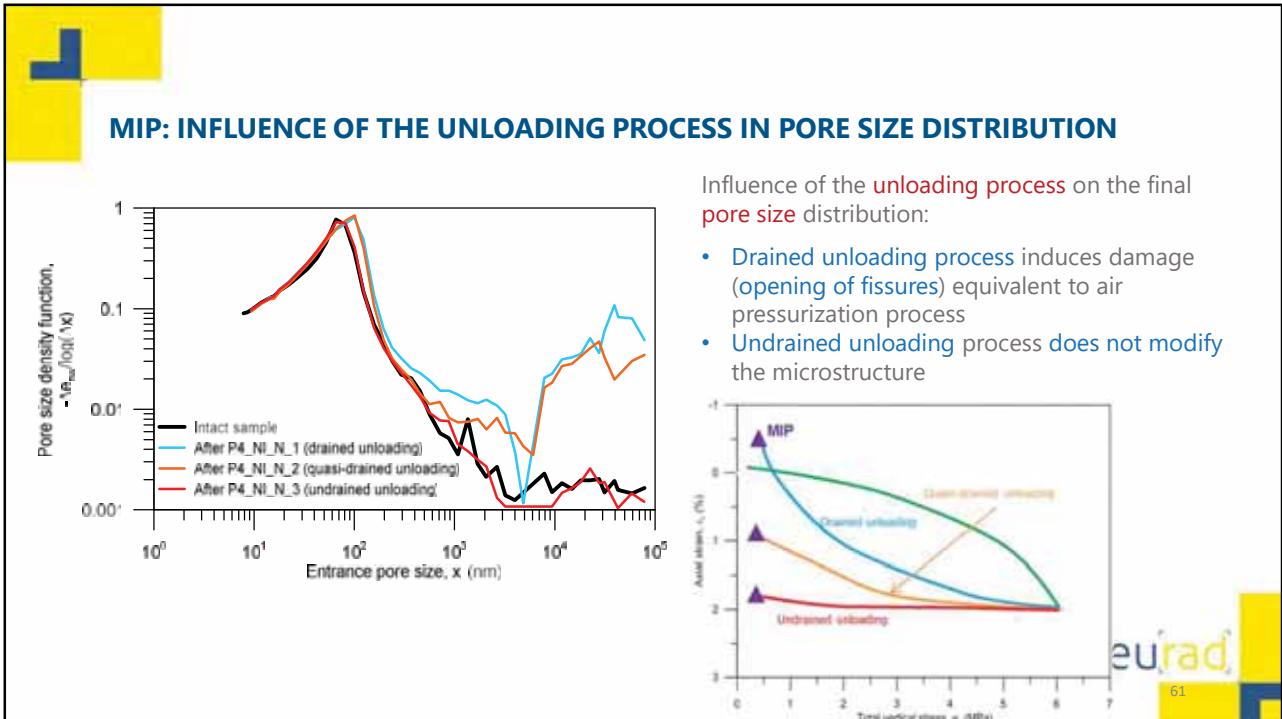
MICROSTRUCTURAL CHANGES INDUCED BY GAS MIGRATION: TECHNIQUES



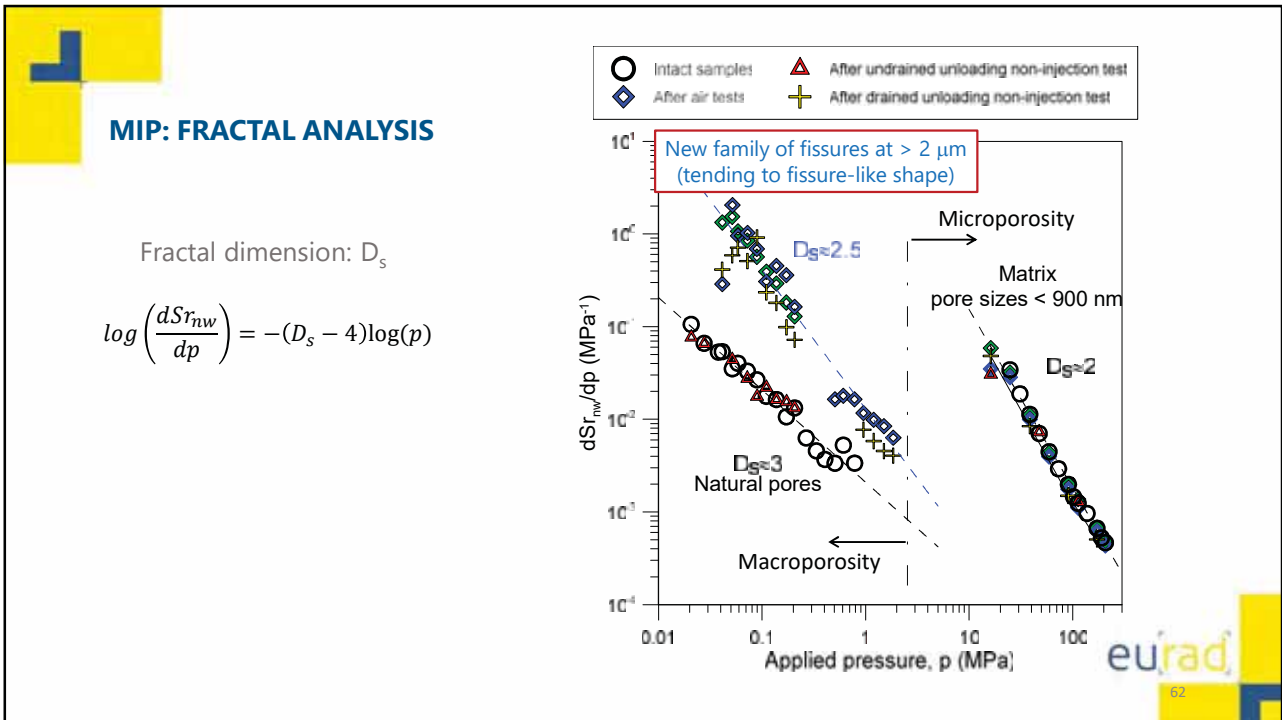
MIP: PORE SIZE DISTRIBUTION



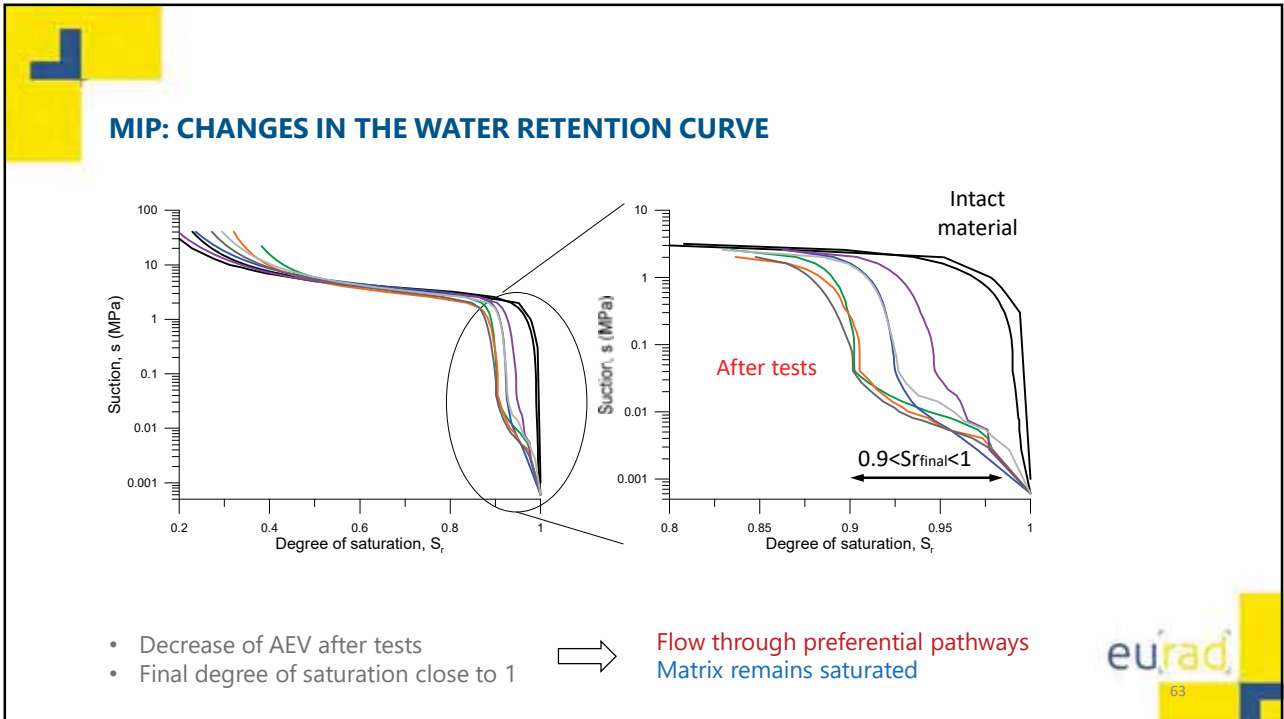
Bi-modal pore size distribution after air tests:
 natural pores (matrix) and fissures (damage/degradation)



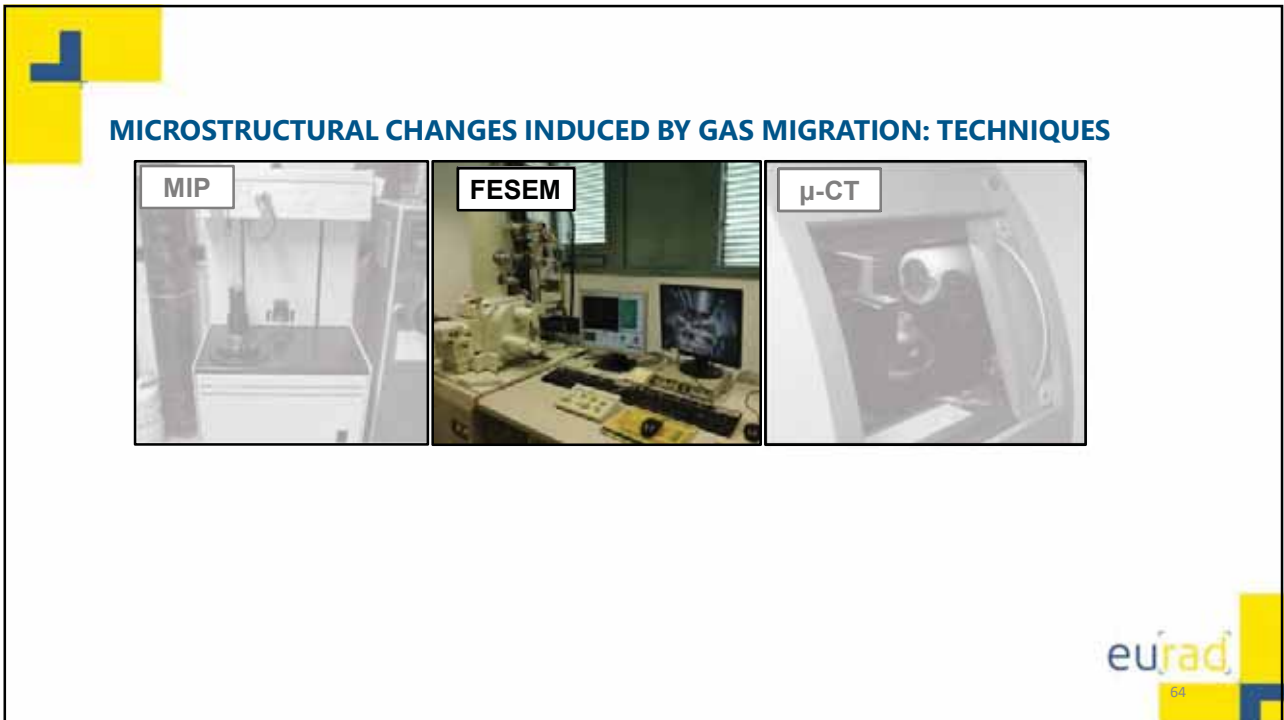
61



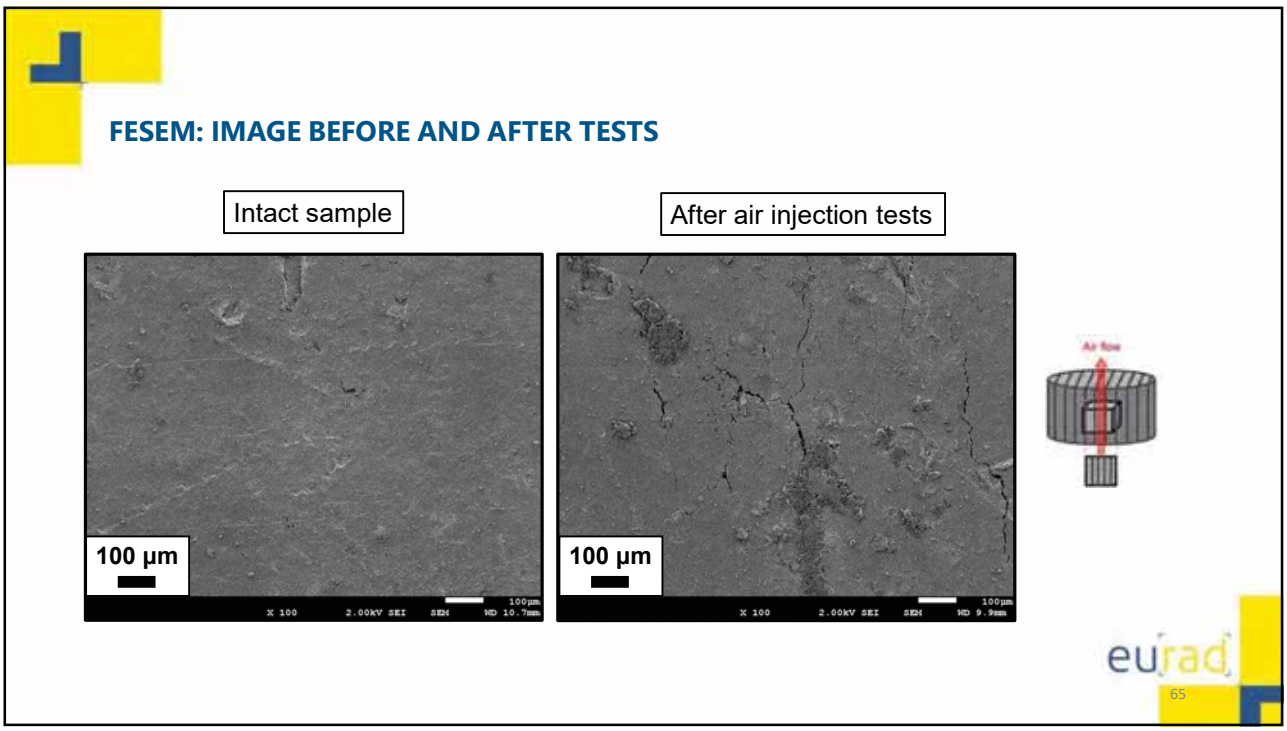
62



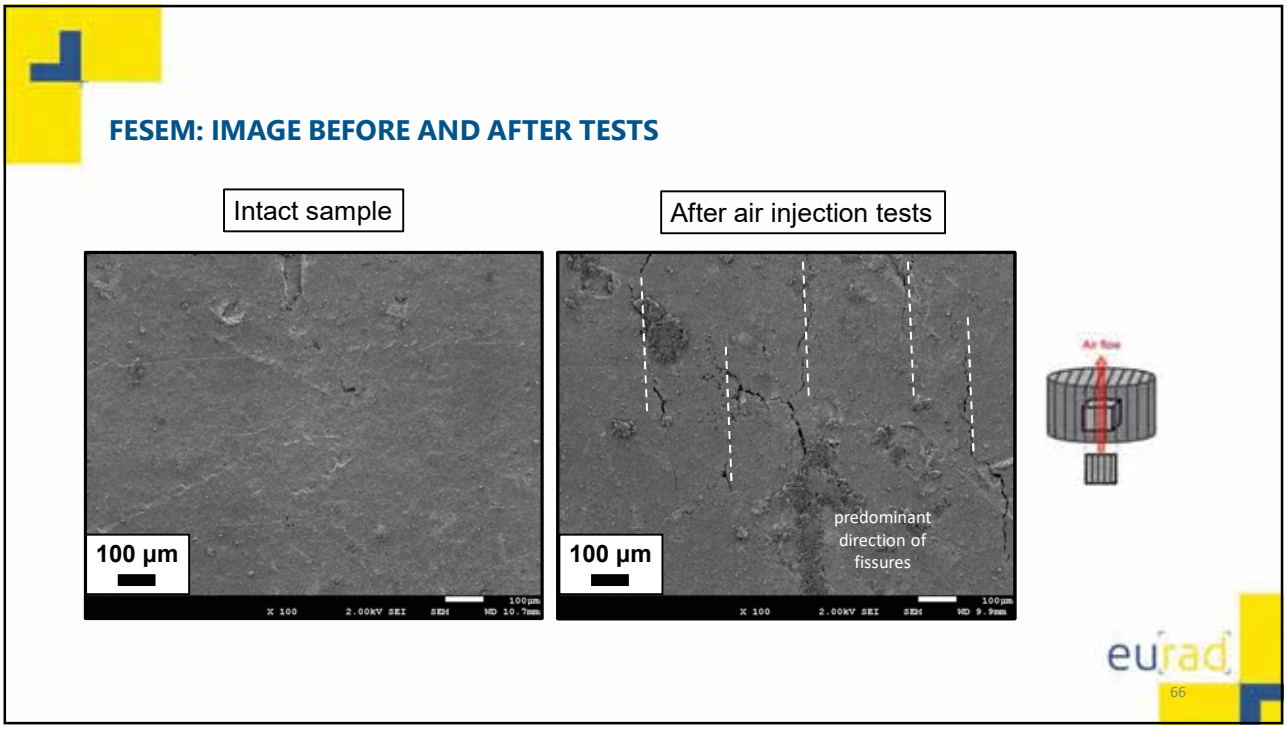
63



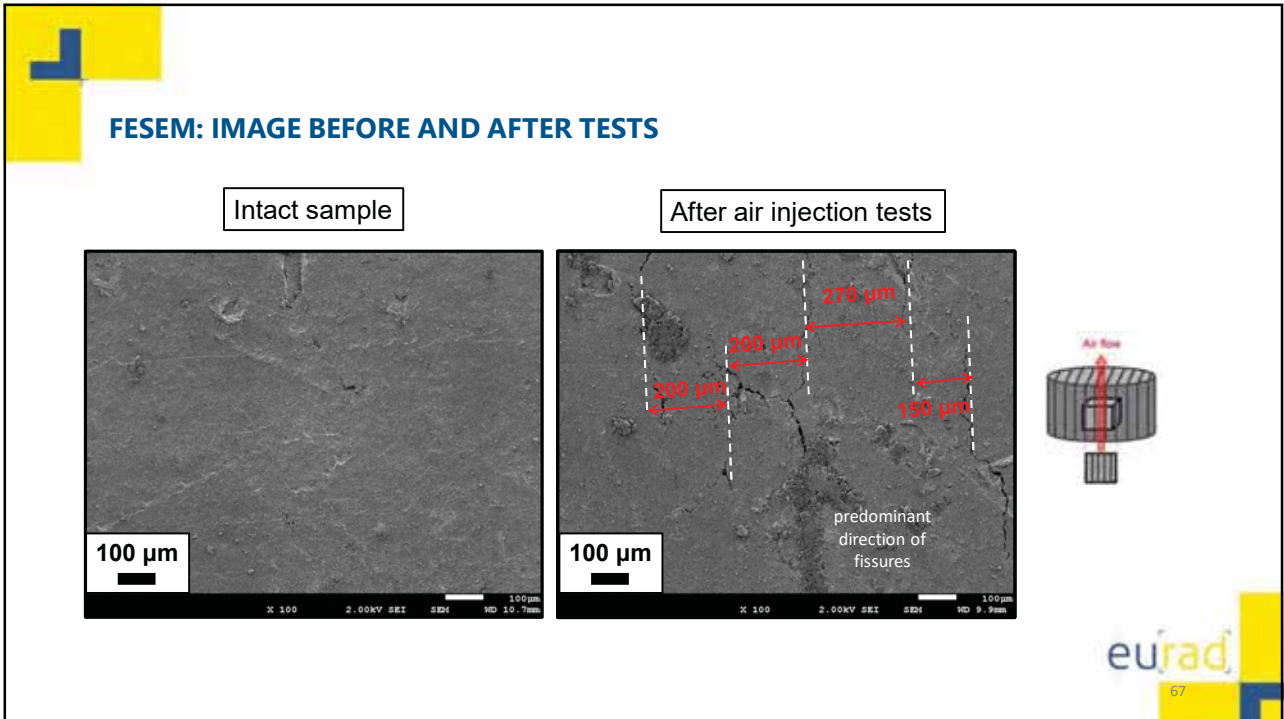
64



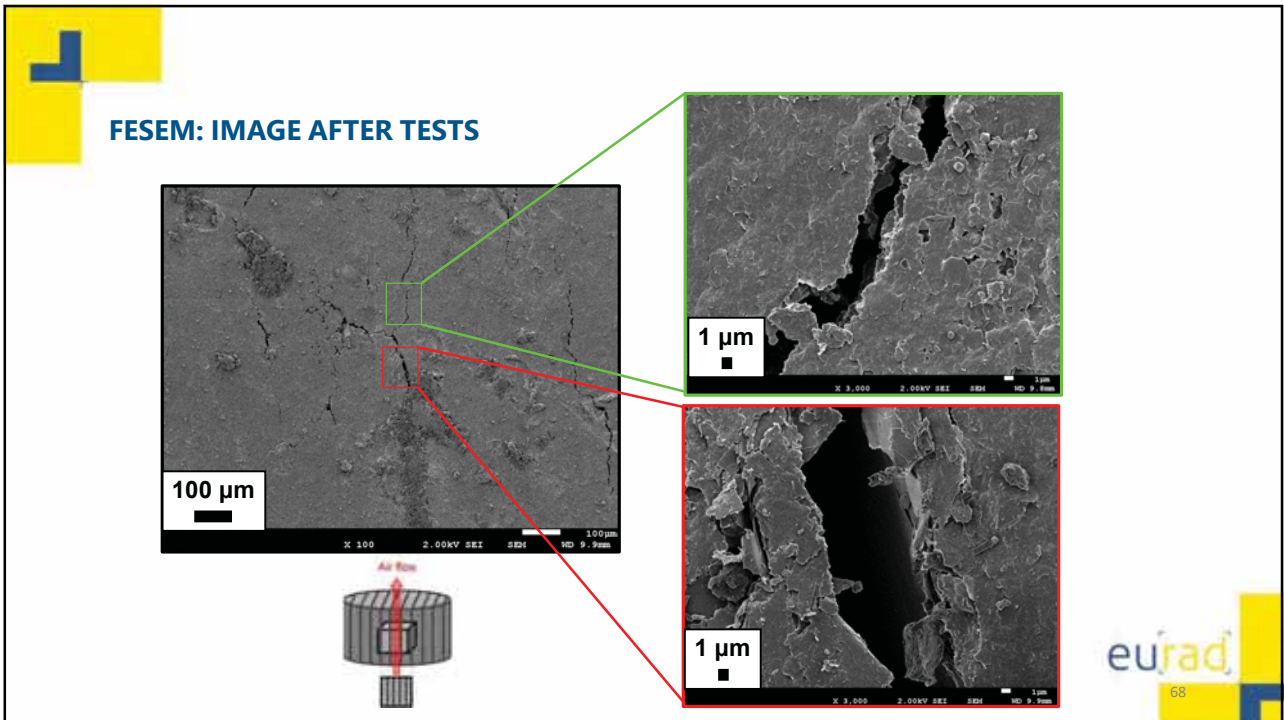
65



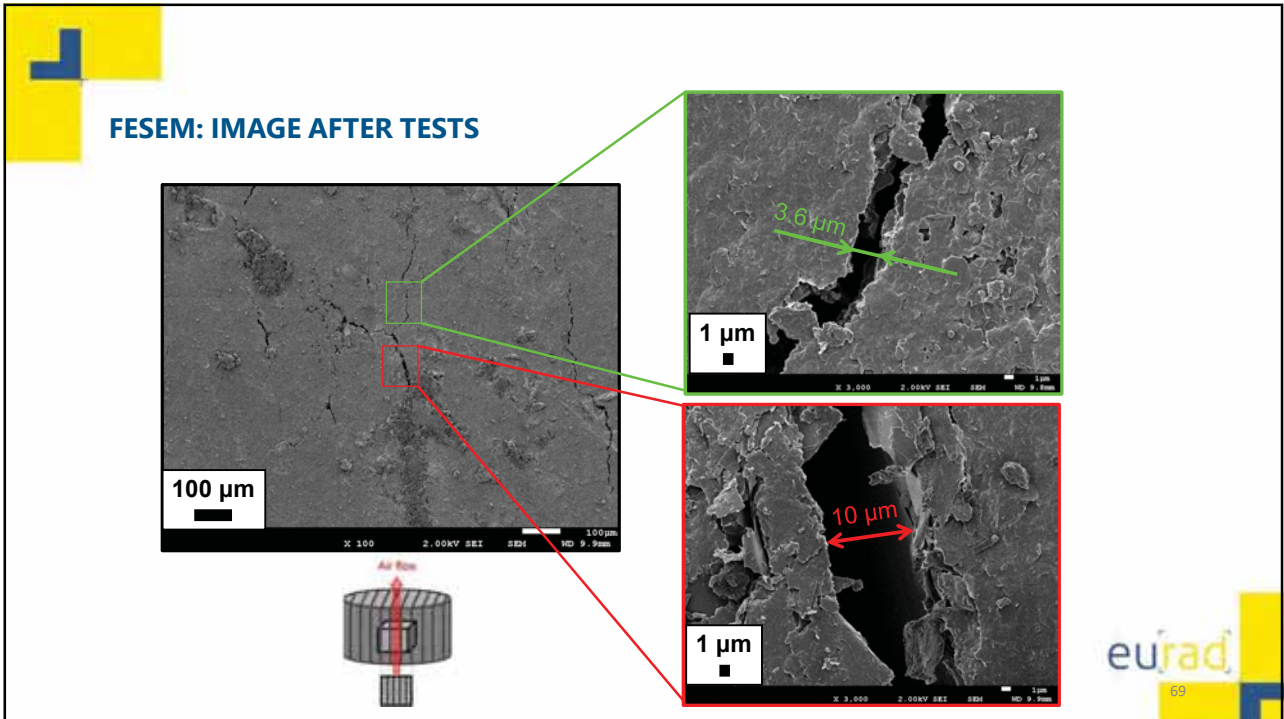
66



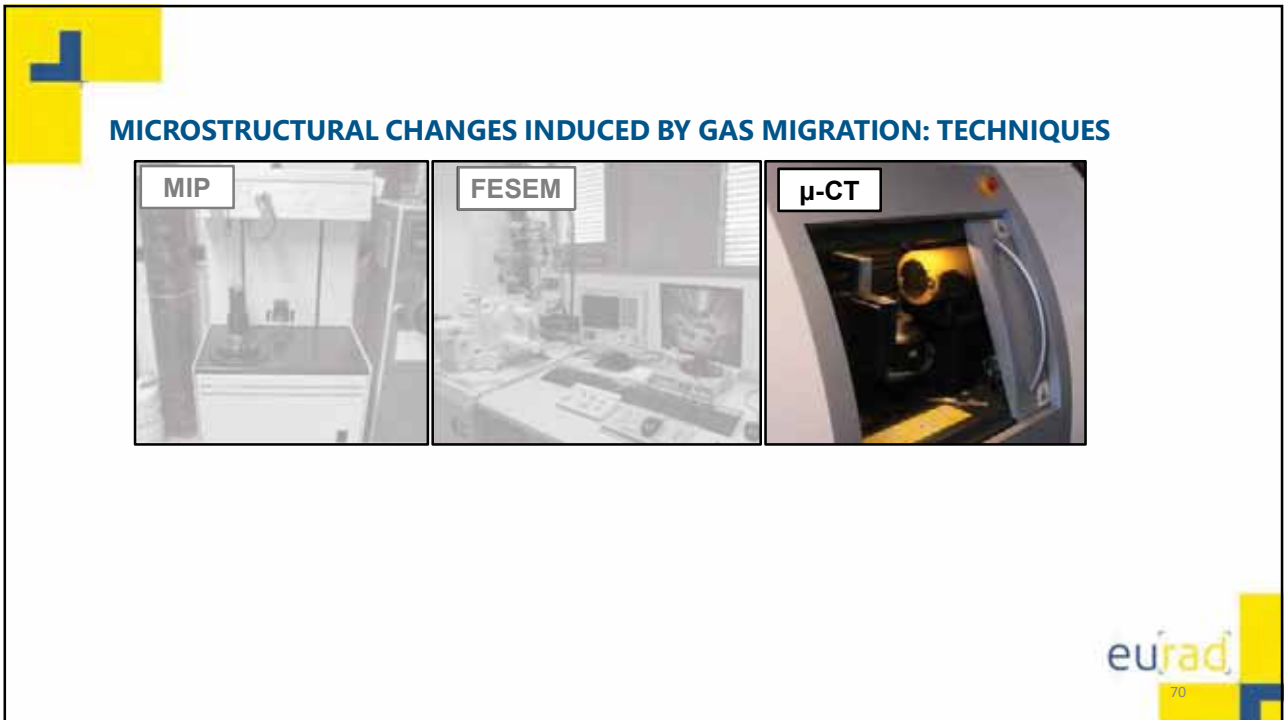
67



68



69



70

MICRO-CT: IMAGE TREATMENT

Procedure for μ -CT image analysis:

- Define Region of Interest (ROI)
- Identify features
- Volume reconstruction
- Filtering process (if required)
- Connectivity filter (if required)

3D volume reconstruction (rendering) of intact sample

Bedding direction not visible

Software ImageJ
(Schneider et al, 2012)

71

71

MICRO-CT: FEATURES IDENTIFICATION

a) Intact sample

b) After air injection: bedding // flow

c) After air injection: bedding \perp flow

Calcium carbonate concretions pyrite

Fissures

1 mm

72

72

MICRO-CT: FISSURE FILTERING

Isolation of fissure pattern by using: Multiscale Hessian fracture filtering (*Voorn et al., 2013*)

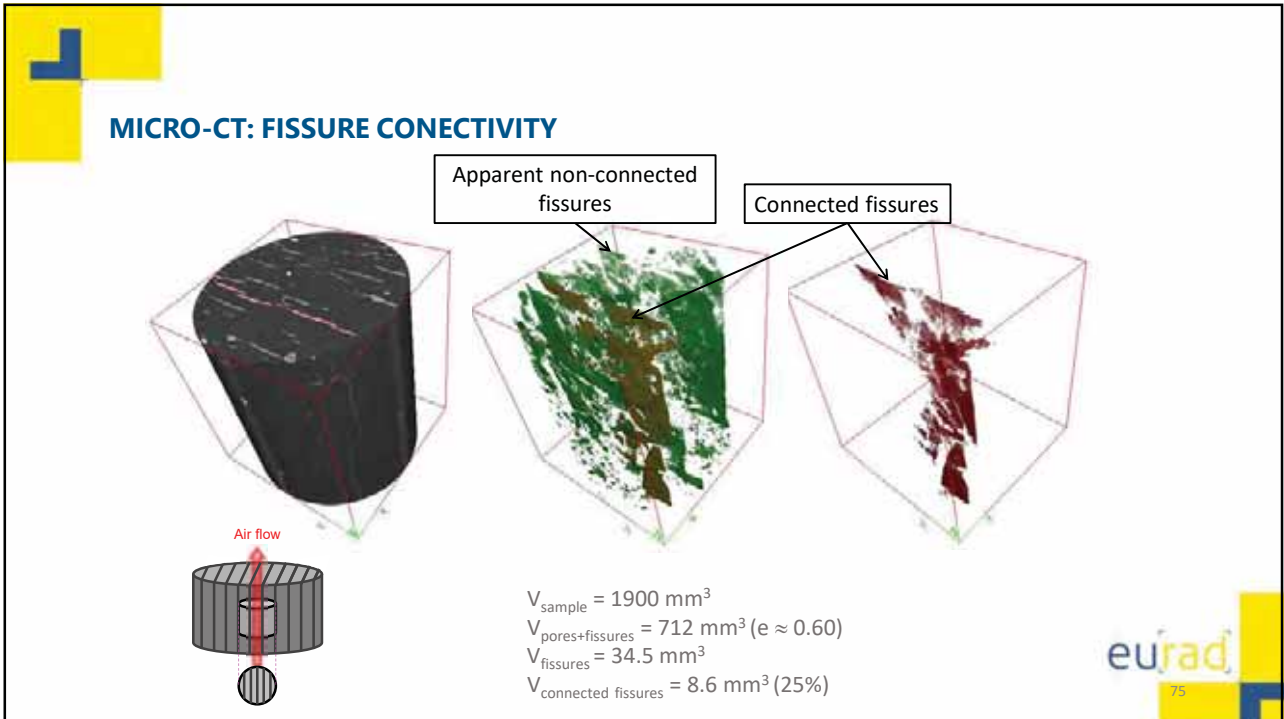
73

MICRO-CT: ISOLATION OF FISSURE NETWORK

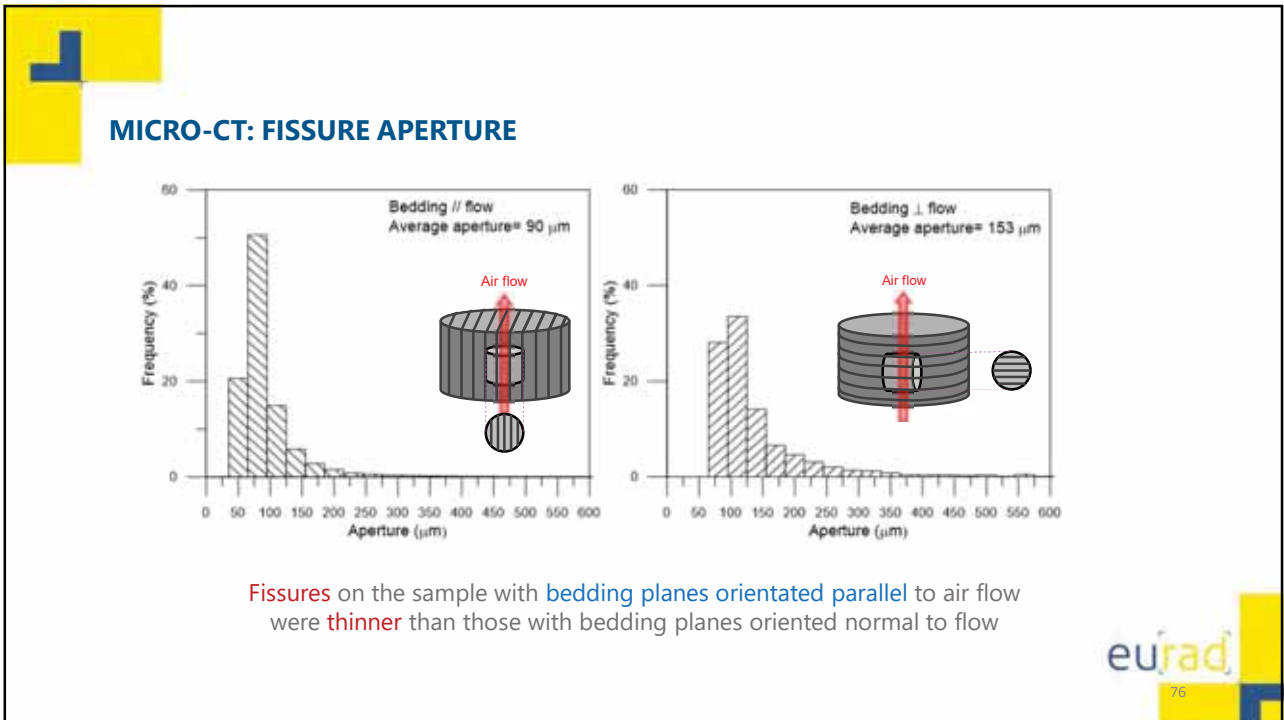
$V_{\text{sample}} = 1900 \text{ mm}^3$
 $V_{\text{pores+fiissures}} = 712 \text{ mm}^3$ ($e \approx 0.60$)
 $V_{\text{fiissures}} = 34.5 \text{ mm}^3$

$V_{\text{sample}} = 1600 \text{ mm}^3$
 $V_{\text{pores+fiissures}} = 960 \text{ mm}^3$ ($e \approx 0.60$)
 $V_{\text{fiissures}} = 23.9 \text{ mm}^3$

74

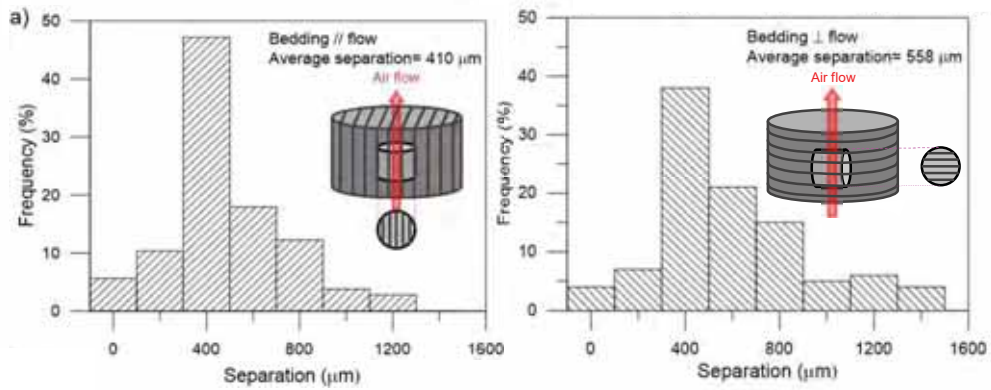


75



76

MICRO-CT: FISSURE SEPARATION



Fissures on the sample with bedding planes orientated parallel to air flow were slightly closer than those with bedding planes oriented normal to flow

eurad

77

77

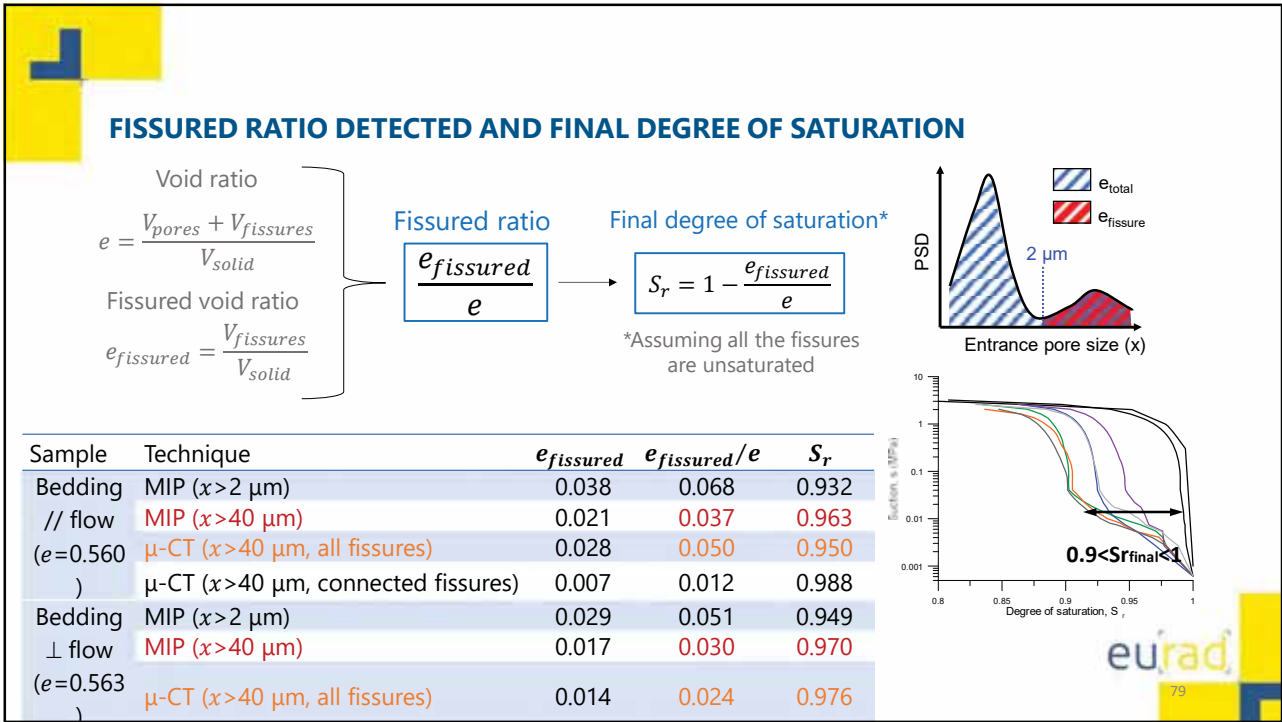
MICROSTRUCTURAL CHANGES INDUCED BY GAS MIGRATION: TECHNIQUES



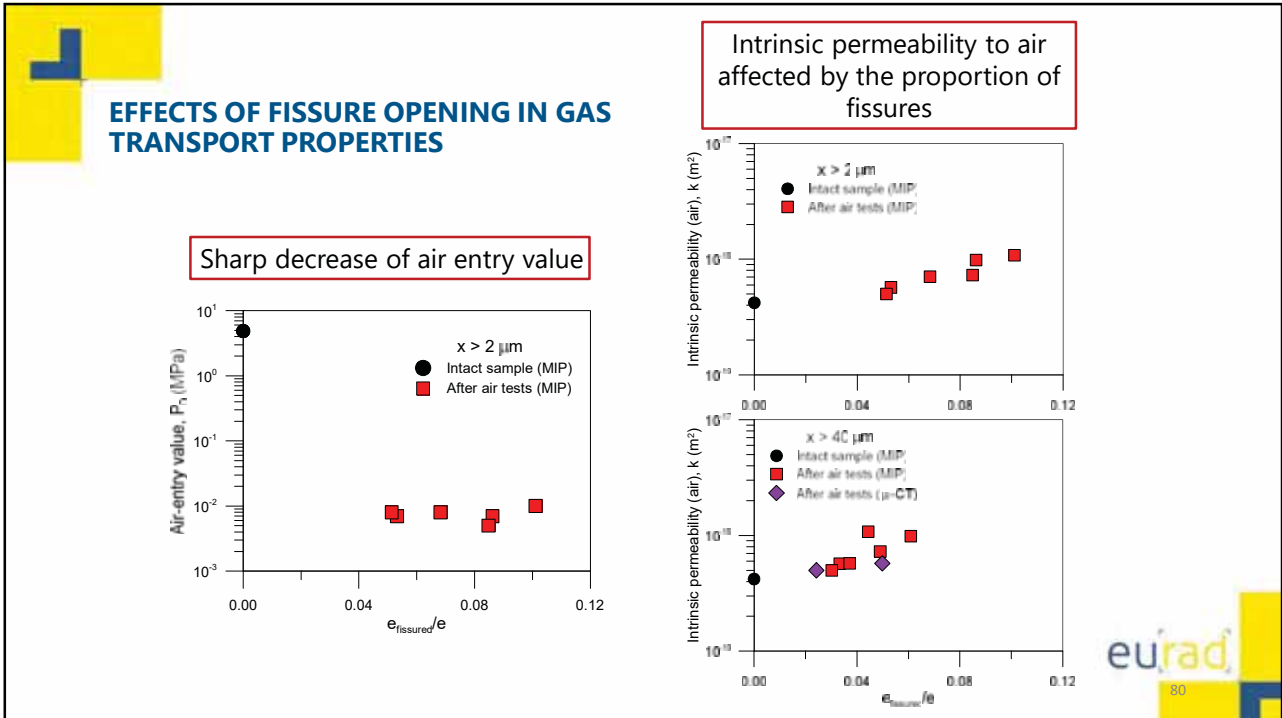
eurad

78

78



79



80

DAMAGE VARIABLE FOR ACCOUNTING THE EFFECTS INDUCED BY GAS MIGRATION

Damage variable definition $D = \frac{\frac{e_{fissured}}{e}}{\frac{e_{fissured\ max}}{e}} = \frac{e_{fissured}}{e_{fissured\ max}}$

Similar to the proposed by Fall et al. (2014)

$D = 0 \rightarrow$ Undamaged state
 $D = 1 \rightarrow$ Fully damaged state

Damage laws :

$$P_0 = P_{0UD} \{ (1 - P_{0min}) \exp(\chi D) + P_{0min} \}$$

$$k = k_{UD} + k_D = k_{UD} + \left\{ \left[1 - \left(1 + D^{1/\xi} \right)^{-\xi} \right] (k_{max} - k_{UD}) \right\}$$

P_{0UD}, k_{UD} values of the undamaged state
 χ, ξ parameters that control the rate of degradation
 P_{0min} residual value at high degrees of degradation
 k_{max} maximum value for high values of damage

81

81

EVOLUTION OF PORE SIZE DISTRIBUTION

82

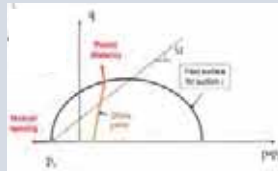
82

GAS TRANSPORT MECHANISM IN BOOM CLAY

Intrinsic permeability and air entry value governed by the opening of fissures



'Dilatational pathways'
Zones in which fractures are developed if certain conditions are attained (opening due to tensile strains, plastic dilatancy, unloading path, material degradation due to irreversible straining, ...)



eurad

83

83

EXPERIMENTAL DATA AT MULTI-SCALE LEVEL NECESSARY FOR THE DEVELOPMENT AND VALIDATION OF CONSTITUTIVE MODELS

Embedded fracture permeability model
(Olivella & Alonso, 2008)

$$\text{Fracture aperture } b = \begin{cases} b_0 + \Delta b & b < b_{max} \\ b = b_{max} & b \geq b_{max} \end{cases} \quad \Delta b = a \Delta \varepsilon$$

$$\text{Equivalent permeability } k = k_{matrix} + \frac{b^3}{12a}$$

$$\text{Air entry capillary pressure changes } P = \frac{2\sigma}{b} = P_0 \sqrt{\frac{k_0}{k}}$$

Publication	Material	b_0 (μm)	b_{max} (μm)	a (μm)
Olivella & Alonso 2008	Opalinus Clay	0.1	-	600
Arnedo et al. 2008	Sand/bentonite	0.1		
Arnedo et al. 2013a	Tertiary Mudstone Norwegian Shelf	0.001	0.3 - 0.5	5000
Romero et al. 2016	Ypresian clay	0.7		95

eurad

84

84

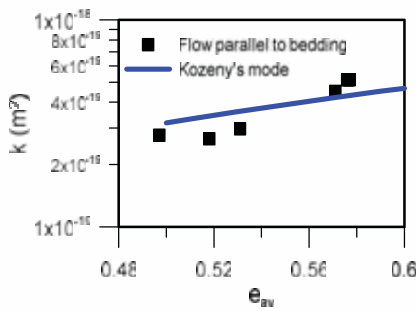
EXPERIMENTAL DATA AT MULTI-SCALE LEVEL NECESSARY FOR THE DEVELOPMENT AND VALIDATION OF CONSTITUTIVE MODELS

Embedded fracture permeability model
(Olivella & Alonso, 2008)

Fracture aperture $b = \begin{cases} b_0 + \Delta b & b < b_{max} \\ b = b_{max} & b \geq b_{max} \end{cases} \quad \Delta b = a\Delta\varepsilon$

Equivalent permeability $k = k_{matrix} + \frac{b^3}{12a}$

Air entry capillary pressure changes $P = \frac{2\sigma}{b} = P_0 \sqrt[3]{\frac{k_0}{k}}$



Intrinsic permeability of the matrix changes with porosity: Kozeny's model

$$k_{matrix}(\phi) = k_0 \frac{\phi^3}{(1-\phi)^2} \frac{(1-\phi_0)^2}{\phi_0^3}$$



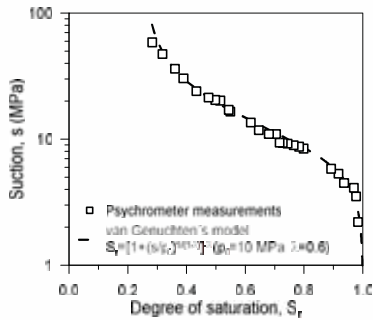
EXPERIMENTAL DATA AT MULTI-SCALE LEVEL NECESSARY FOR THE DEVELOPMENT AND VALIDATION OF CONSTITUTIVE MODELS

Embedded fracture permeability model
(Olivella & Alonso, 2008)

Fracture aperture $b = \begin{cases} b_0 + \Delta b & b < b_{max} \\ b = b_{max} & b \geq b_{max} \end{cases} \quad \Delta b = a\Delta\varepsilon$

Equivalent permeability $k = k_{matrix} + \frac{b^3}{12a}$

Air entry capillary pressure changes $P = \frac{2\sigma}{b} = P_0 \sqrt[3]{\frac{k_0}{k}}$



AEV of the matrix is considered constant and derived from van Genuchten's model

$$S_r = [1 + (s/P_0)^{(1/(1-\lambda))}]^{-\lambda}$$



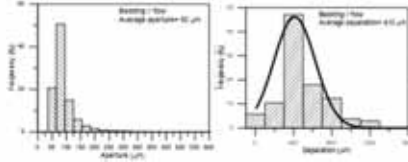
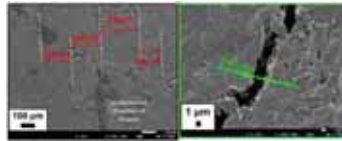
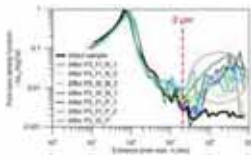
EXPERIMENTAL DATA AT MULTI-SCALE LEVEL NECESSARY FOR THE DEVELOPMENT AND VALIDATION OF CONSTITUTIVE MODELS

Embedded fracture permeability model
(Olivella & Alonso, 2008)

Fracture aperture $b = \begin{cases} b_0 + \Delta b & b < b_{max} \\ b = b_{max} & b \geq b_{max} \end{cases} \quad \Delta b = a\Delta\varepsilon$

Equivalent permeability $k = k_{matrix} + \frac{b^3}{12a}$

Air entry capillary pressure changes $P = \frac{2\sigma}{b} = P_0 \sqrt[3]{\frac{k_0}{k}}$



	MIP	FESEM	μ-CT
Aperture: b (μm)	> 2	3 - 10	90'' - 150 \pm
Separation: a (μm)	-	150 - 270	410'' - 560 \pm

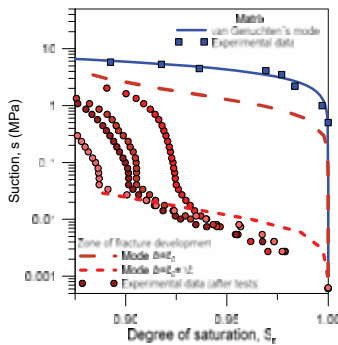
EXPERIMENTAL DATA AT MULTI-SCALE LEVEL NECESSARY FOR THE DEVELOPMENT AND VALIDATION OF CONSTITUTIVE MODELS

Embedded fracture permeability model
(Olivella & Alonso, 2008)

Fracture aperture $b = \begin{cases} b_0 + \Delta b & b < b_{max} \\ b = b_{max} & b \geq b_{max} \end{cases} \quad \Delta b = a\Delta\varepsilon$

Equivalent permeability $k = k_{matrix} + \frac{b^3}{12a}$

Air entry capillary pressure changes $P = \frac{2\sigma}{b} = P_0 \sqrt[3]{\frac{k_0}{k}}$



Air entry capillary pressure changes fitted using WRC data from MIP after gas tests

$$S_r = [1 + (s/P_0)^{1/(1-\lambda)}]^{-\lambda}$$

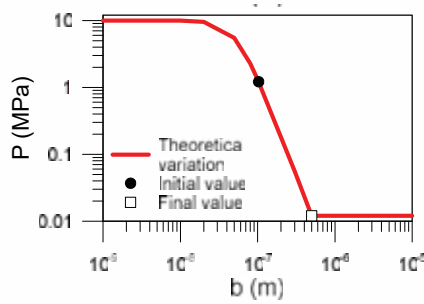
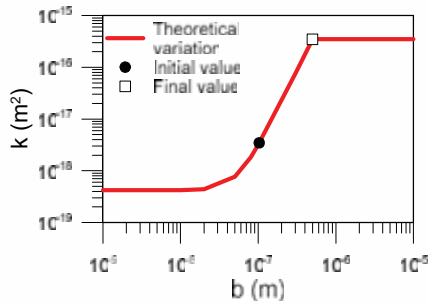
EXPERIMENTAL DATA AT MULTI-SCALE LEVEL NECESSARY FOR THE DEVELOPMENT AND VALIDATION OF CONSTITUTIVE MODELS

Embedded fracture permeability model
(Olivella & Alonso, 2008)

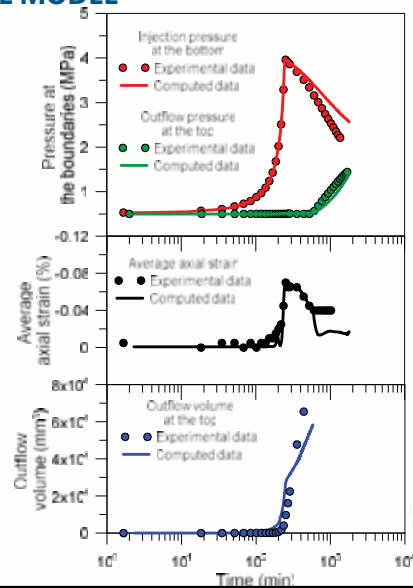
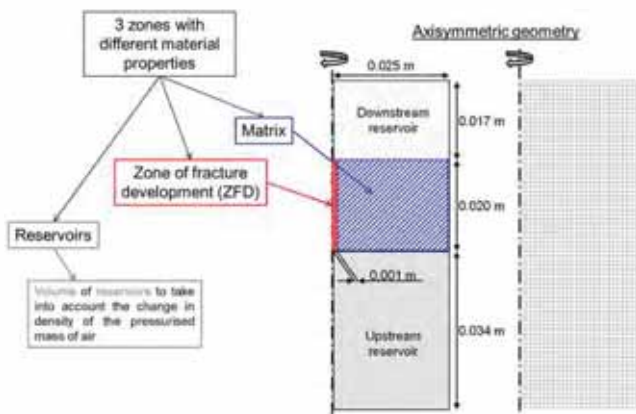
$$\text{Fracture aperture } b = \begin{cases} b_0 + \Delta b & b < b_{max} \\ b = b_{max} & b \geq b_{max} \end{cases} \quad \Delta b = a\Delta\varepsilon$$

$$\text{Equivalent permeability } k = k_{matrix} + \frac{b^3}{12a}$$

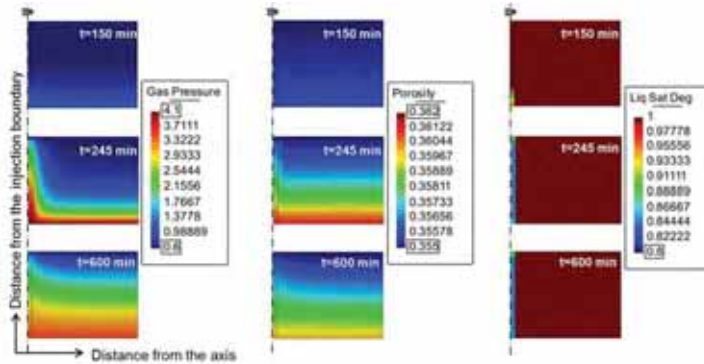
$$\text{Air entry capillary pressure changes } P = \frac{2\sigma}{b} = P_0 \sqrt[3]{\frac{k_0}{k}}$$



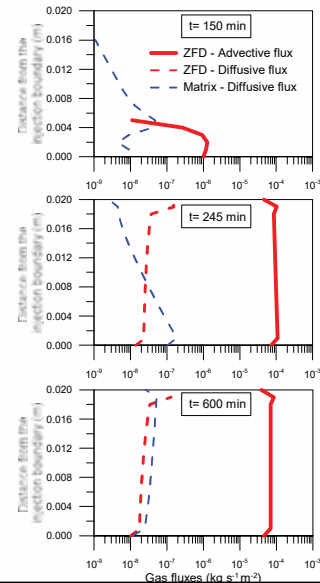
APPLICATION OF THE EMBEDDED FRACTURE MODEL



SIMULATION OF EXPERIMENTAL RESULTS ALLOWED BETTER EXPLOITING THE INFORMATION PROVIDED BY MEASUREMENTS



t= 150 min → During gas injection
 t= 245 min → At shut-off (end of the injection)
 t= 600 min → During gas dissipation



eu rad

91

91

REFERENCES OF THIS WORK

- Gonzalez-Blanco, L., Romero, E., Jommi, C., Li, X. & Sillen, X. (2016). Gas migration in a cenozoic clay: Experimental results and numerical modelling. *Geomechanics for Energy and the Environment*, 6, pp.81–100.
- Gonzalez-Blanco, L., Romero, E., Li, X., Sillen, X., Marschall, P. & Jommi, C. (2016) Air injection tests in two argillaceous rock formations: experimental results and modelling. *1st International Conference on Energy Geotechnics ICETG, Kiel, Germany, Wuttke, Bauer & Sánchez (Eds.)*.
- Gonzalez-Blanco, L., Romero, E., Jommi, C. Li, X. & Sillen, X. (2017). Exploring fissure opening and its connectivity in a Cenozoic clay during gas injection. Chapter in Springer Series in Geomechanics and Geoengineering, January, 2017 In book: *Advances in Laboratory Testing and Modelling of Soils and Shales (ATMSS)*, 288-295.
- Gonzalez-Blanco, L., (2017). Gas migration in deep argillaceous formations: Boom Clay and indurated clays. *PhD Thesis, Universitat Politècnica de Catalunya, Barcelona, Spain*.
- Gonzalez-Blanco, L. & Romero, E. (submitted) A multi-scale insight into gas migration in a deep Cenozoic clay. *Géotechnique*.

eu rad

92

92

OUTLINE OF THE LECTURE

1. Motivation and content
2. Insight into gas transfer (gas generation, gas transport mechanisms, multi-scale aspects)
3. Some observations regarding gas testing (experimental protocols)
4. A detailed research methodology on Boom Clay:
 - Material characterization
 - Stress paths followed
 - Gas test protocols
 - Test results at different scales (macroscopic results and microstructural features)
5. Final comments. Future challenges

eurad

93

93

FUTURE CHALLENGES

WORK PACKAGE 6 – GAS - Mechanistic understanding of gas transport in clay materials

TASK 2: Transport mechanisms

- To determine gas diffusion parameters on different clayey materials at different degrees of water saturation using pore network modelling to support experimental data interpretation
- To study if gas sorption could be a relevant retardation mechanism for diffusive transport under repository conditions, in clays that are partially or fully saturated with pore water
- To study gas advection flow (displacement vs. dilation) providing data under a broad range of conditions investigating how petro-physical parameters (mineralogy, density, etc.) or stress state influence free gas transport

TASK 3: Barrier integrity

- To investigate the evolution of damage in clay-rich geomaterials when subjected to excessive water / gas pressures: fracture opening and fracture sliding mechanisms in host rocks and pathway dilation and particle mobilization on buffer materials
- To study the self-sealing capacity of the tested geomaterials: after gas injection experiments, the samples will be subjected to re-saturation. Then, final water permeability testing will be conducted to qualify the loss of hydraulic barrier function
- To use model-based interpretation for complementing experimental data

eurad
European Joint Programme
on Radioactive Waste Management

eurad

94

94





THANK YOU FOR YOUR ATTENTION!!

Financial support of ONDRAF/NIRAS (Belgium) and NAGRA (Switzerland) with CIMNE/UPC (Spain) through several research projects is greatly acknowledged





95

95



REFERENCES

- Arnedo, D., Alonso, E.E. & Olivella, S. (2013) Gas flow in anisotropic claystone: modelling triaxial experiments. *International Journal for Numerical and Analytical Methods in Geomechanics* **37**, pp. 2239-2256.
- Arnedo, D., Alonso, E.E., Olivella, S., & Romero, E. (2008) Gas injection tests on sand/bentonite mixtures in the laboratory. Experimental results and numerical modelling. *Physics and Chemistry of the Earth*, **33**, pp. 237-247.
- Della Vecchia, G., Jommi, C., Lima, A., & Romero, E. (2011) Some remarks on the hydro-mechanical constitutive modelling of natural and compacted Boom clay. *International Conference of Unsaturated Soils, Barcelona, Spain, Taylor & Francis Group, London*.
- Fall, M., Nasir, O. & Nguyen, T.S. (2014) A coupled hydro-mechanical model for simulation of gas migration in host sedimentary rocks for nuclear waste repositories. *Engineering Geology*, **176**, pp. 24-44.
- Harrington, J.F. & Horseman, S.T. (2003) Gas Migration in KBS-3 Buffer Bentonite: Sensitivity of Test Parameters to Experimental Boundary Conditions. *SKB Technical Report No. TR-03-02*.
- Hemes, S., Desbois, G., Urai, J.L., Schröppel, B. & Schwarz, J.O. (2015) Multi-scale characterization of porosity in Boom Clay (HADES-level, Mol, Belgium) using a combination of X-ray μ -CT, 2D BIB-SEM and FIB-SEM tomography. *Microporous and Mesoporous Materials*, **208**, pp. 1-20.
- Hildenbrand, A., Schlömer, S., & Krooss, B.M. (2002) Gas breakthrough experiments on fine-grained sedimentary rocks. *Geofluids*, **2**, pp. 3-23.
- Marschall, P., Horseman, S., & Gimmi, T. (2005) Characterisation of Gas Transport Properties of the Opalinus Clay, a Potential Host Rock Formation for Radioactive Waste Disposal. *Oil & Gas Science and Technology*, **60(1)**, pp. 121-139.



96

96

REFERENCES

- Olivella, S. & Alonso, E.E. (2008). Gas flow through clay barriers. *Géotechnique*, 58(3), pp. 157–176.
- ONDRAR/NIRAS (2016) Conceptualisations of gas related issues. *Workshop on: Gas related issues in clay based repository programmes*
- Pineda, J., Alonso, E.E. & Romero, E. (2014) Environmental degradation of claystones. *Géotechnique*, 64(1), pp.64–82.
- Pineda, J., Romero, E., Alonso, E. Pérez, T. (2014) A New High-Pressure Triaxial Apparatus for Inducing and Tracking Hydro-Mechanical Degradation of Clayey Rocks. *Geotechnical Testing Journal*, 37 (6), pp. 1-15.
- Romero, E. & Gonzalez-Blanco, L. (2015) Complementary water and air permeability tests on core samples from Schlattingen SLA-1 borehole. *Nagra Technical Report NAB 15-06*.
- Romero, E. & Gonzalez-Blanco, L. (2019) Hydro-mechanical processes associated with gas transport in MX-80 Bentonite in the context of Nagra's RD&D programme. *Nagra Technical Report NAB 19-06*
- Romero, E., Arnedo, D., Alonso, E.E., & Marschall, P. (2010) Gas Injection Laboratory Experiments on Opalinus Clay. In: *Clays in Natural & Engineered Barriers for Radioactive Waste Confinement, 4th International Meeting, March 2010, Nantes, France*, pp. 113–114.
- Romero, E., Sau, N., Lima, A., Van Baelen, H., Sillen, X., & Li, X. (2016) Studying the thermal conductivity of a deep Eocene clay formation: Direct measurements vs back-analysis results. *Geomechanics for Energy and the Environment*, 8, pp. 1–14.
- Romero, E., Senger, R., Marschall, P. & Gómez, R. (2012). Air tests on low-permeability claystone formations. Experimental results and simulations. *Theme lecture. Int. Workshop AMTSS - Advances in Multiphysical Testing of Soils and Shales, EPFL Lausanne (Switzerland), 3 - 5 September, 2012.*

REFERENCES

- Salehnia, F., Collin, F., Li, X., Dizier, A., Sillen, X. & Charlier, R. (2015) Coupled modeling of Excavation Damaged Zone in Boom clay: Strain localization in rock and distribution of contact pressure on the gallery's lining. *Computers and Geotechnics*, 69, pp. 396-410.
- Schneider, C.A., Rasband, W.S., & Eliceiri, K.W. (2012) NIH Image to ImageJ: 25 years of image analysis. *Nature Methods*, 9 (7), pp. 671–675.
- Senger, R., Romero, E. and Marschall, P. (2017). Modelling of gas migration through low-permeability clay rock using information on pressure and deformation from fast air injection tests. *Transport in Porous Media*, 123 (3), pp. 563-579.
- Senger, R., Romero, E., Ferrari, A. and Marschall, P. (2014). Characterization of gas flow through low-permeability claystone: laboratory experiments and two-phase flow analyses. *Geological Society London, Special Publications*, 400, pp. 1-13.
- Sillen, X. & Marivoet, J. (2007) Thermal impact of a HLW repository in clay. *External Report SCK-CEN-ER-38*.
- Voorn, M., Exner, U. & Rath, A. (2013) Multiscale Hessian fracture filtering for the enhancement and segmentation of narrow fractures in 3D image data. *Computers & Geosciences* 57, pp. 44-53.

Appendix N. Modelling for gas transfers in geomaterials (S. Olivella)

MODELLING GAS FLOW IN POROUS MEDIA

Applications using CODE_BRIGHT

January 2020 • Sebastià Olivella



The project leading to this application has received funding from the European Union's Horizon 2020 research and innovation programme under grant agreement n° 847593.

Date

Event

1

CONTENTS

1. Fundamentals
2. Gas mixtures
3. Multiphase flow
4. Coupled deformation
5. Energy balance
6. Applications
7. Summary

IDEAL GAS LAW

- We remember from our early courses of physics: $pV = nRT_a$
 - Where: p is pressure, V is volume, n is number of moles, T_a is absolute temperature and R is the universal gas constant ($R = 8.31 \frac{\text{J}}{\text{mol K}}$)
- How can this be used in porous media flow?
 - Density and molar mass are defined as:

$$\rho = \frac{m}{v} \text{ and } M = \frac{m}{n}$$

$$\text{So: } v = \frac{m}{\rho} \text{ and } n = \frac{m}{M}$$
 - The equation for **ideal gas** is used to calculate gas density: $\rho = \frac{pM}{RT_a}$



NON IDEAL OR REAL GAS LAW

- Van der Waals:

$$\left(p + \frac{a}{v_m^2}\right)(v_m - b) = RT_a \quad p = \frac{RT_a}{v_m - b} - \frac{a}{v_m^2} \quad \left(v_m = \frac{v}{n}\right)$$

- Redlich-Kwong:

$$v_m^3 - \frac{RT_a}{p} v_m^2 - \left(\frac{RT_a b}{p} - \frac{a}{p\sqrt{T_a}} + b^2\right) v_m - \frac{ab}{p\sqrt{T_a}} = 0$$

Definitions: $v_m = \frac{v}{n}$ and $\rho = \frac{m}{v} = \frac{Mn}{v_m n} = \frac{M}{v_m}$

VAN DER WAALS EQUATION FOR REAL GASES

$$\underbrace{\left(p + \frac{a}{v_m^2}\right)}_{\text{measured (real) } P_{\text{IDEAL}}} \times \underbrace{\left(v_m - b\right)}_{\text{correct for attractive forces } V_{\text{IDEAL}}} = nRT$$

(P + a/v²) × (V - nb) = nRT
 measured (real) P_{IDEAL} correct for attractive forces correct for container (real) V of particles = nRT

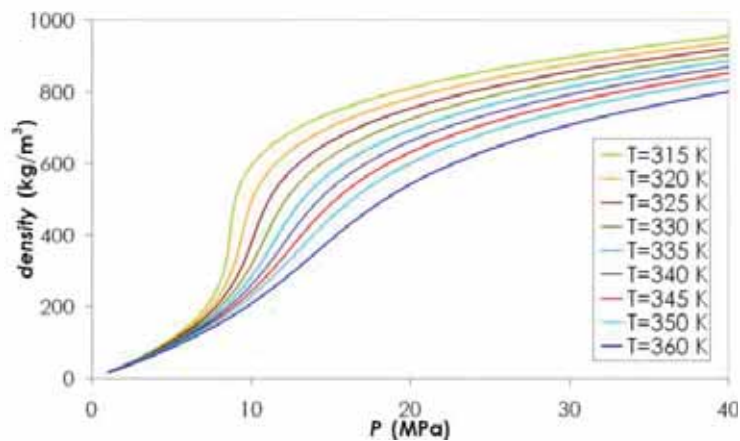
$$p = \frac{RT_a}{v_m - b} - \frac{a}{v_m(v_m + b)\sqrt{T_a}}$$

Redlich-Kwong equation of state is an empirical, algebraic **equation** that relates temperature, pressure, and volume of gases. It is generally more accurate than the van der Waals **equation** and the ideal gas **equation** at temperatures above the critical temperature.

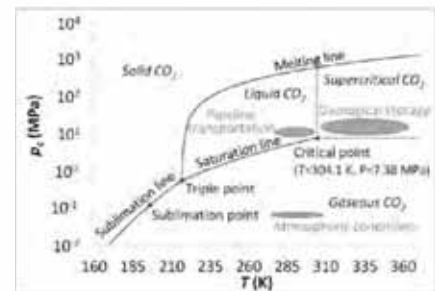


NON IDEAL OR REAL GAS LAW

- Example for CO₂



Redlich-Kwong EOS with Spycher et al. (2003) parameters

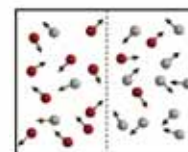
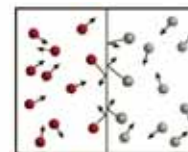


eurad

GAS DIFFUSIVITY

- Diffusion of a **gas in a liquid**
 - Dissolution of gas in a liquid by Henry's law
 - Diffusion in porous media by Fick's law: $\mathbf{i}_i^l = -\phi \rho_l S_i \tau D_i^l \nabla \omega_i^l$, based on theory for solutes in liquids.
 - D_i^l is different for each gas. Dispersion can be added
- Diffusion of a **gas in a gas mixture**
 - Theories of gas mixtures (kinetic theory of gases)
 - Binary mixtures
 - Diffusion by Fick's law or Dusty gas model

(See next section for gas mixtures)

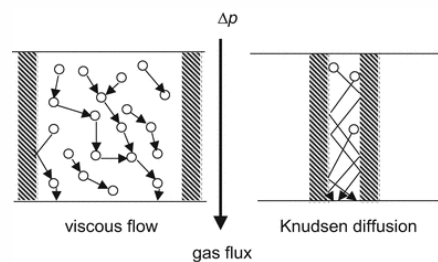


eurad

GAS VISCOSITY

- Gas viscosity has an important role in Darcy equation for gas flow
- Gas viscosity can be calculated using: $\mu_g = \frac{A\sqrt{T_a}}{\left(1+\frac{B}{T_a}\right)}$
- For Knudsen diffusion or Klinkenberg effect, viscosity can be corrected as: $\mu_g = \frac{A\sqrt{T_a}}{\left(1+\frac{B}{T_a}\right)} \left(\frac{1}{1+\frac{b_k}{p}}\right)$ where $b_k = C - Dk \geq 0$ and k is intrinsic permeability

(See next section for gas mixtures)



eurad

GAS FLOW IN DRY POROUS MEDIA

- The mass conservation of a gas in a porous medium is:

$$\frac{\partial(\rho_g \phi)}{\partial t} + \nabla \cdot (\rho_g \mathbf{q}_g) = 0$$

- Where: ρ_g is gas density, ϕ is porosity and \mathbf{q}_g is the flux of gas.

- This equation can be transformed, for isothermal conditions, into:

$$\phi \frac{\partial p_g}{\partial t} + \nabla \cdot (p_g \mathbf{q}_g) = 0$$

- Neglecting gravity, this is a non-linear diffusion equation:

$$\phi \frac{\partial p_g}{\partial t} = \frac{k}{\mu_g} \nabla \cdot (p_g \nabla p_g)$$

- Gas experiments in dry porous materials can be modelled with this simple equation (analytically or numerically)

eurad

GAS FLOW IN DRY POROUS MEDIA

- For a small drill hole minipermeameter probe, in situ permeability measurement (Dinwiddie, Molz, Castle, 2003) can be done using:

$$k_g = \frac{2q_1\mu_g p_1}{aG(p_1^2 - p_0^2)}$$

k_g is gas permeability

q_1 is flow rate

p_1 is injection pressure

p_0 is atmospheric pressure

μ_g is gas viscosity

a is internal radius of tip seal

G is a dimensionless geometric factor

The geometrical factor, when calculated numerically for a given sample and probe geometry, accounts for the complex multidimensional flow pattern throughout the porous medium, capturing the edge effects associated with the geometry of the sample and probe, and thus boundary conditions that are simply not accounted for by an empirical calibration using core plugs.

Dinwiddie, C. L., Molz, F. J., and Castle, J. W. (2003), A new small drill hole minipermeameter probe for in situ permeability measurement: Fluid mechanics and geometrical factors, *Water Resour. Res.*, 39, 1178, doi:[10.1029/2001WR001179](https://doi.org/10.1029/2001WR001179), 7.



CONTENTS

1. Fundamentals
2. Gas mixtures
3. Multiphase flow
4. Coupled deformation
5. Energy balance
6. Applications
7. Summary



MIXTURES OF GASES

- The Dusty Gas Model (DGM) is a generalized theory to calculate the component fluxes in a mixture of gases. It is based on the Stefan-Maxwell equations but it also incorporates the Knudsen diffusion effects. An advective flux, calculated through Darcy's law can also be added to the DGM model.
- **Mason EA, Malinauskas AP (1983)** Gas transport in porous media: the dusty-gas model, Chemical engineering monographs 17. Elsevier, Amsterdam [Google Scholar](#)
- **Maxwell JC (1962)** Illustration of the dynamical theory of gases. Part II. On the process of diffusion of two or more kinds of moving particles among one another. Philos Mag 20(1860):21 (Reprinted in "Scientific Papers", vol 1, pp 392–409, New York) [Google Scholar](#)



DUSTI GAS MODEL

- According to Abu-El-Sha'r and Abriola (1997) the Dusty Gas Model equations, after incorporation of the advective flux term (gravity neglected) are:

$$\frac{\chi^i \mathbf{N}^j - \chi^j \mathbf{N}^i}{D_{ij}} + \frac{\chi^i \mathbf{N}^k - \chi^k \mathbf{N}^i}{D_{ik}} - \frac{\mathbf{N}^i}{D_i^k} = \frac{p_g \nabla \chi^i}{RT_a} + \left(1 + \frac{k p_g}{D_i^k \mu_g}\right) \frac{\chi^i \nabla p_g}{RT_a}$$

For $i, j, k = 1, 2, 3$ and $2, 3, 1$ and $3, 1, 2$

- This theory can be simplified

$$\mathbf{N}_g^i = -D_{12} \frac{p_g}{RT_a} \nabla \chi^i - \left(D^k + \frac{k p_g}{\mu_g}\right) \frac{\chi^i \nabla p_g}{RT_a}, i = 1, 2$$

- Which contains molecular diffusion (D_{12}), advective flow (k/μ_g) and Knudsen diffusion (D^k).

- Mole fractions are used in these equations

Wa'il Abu-El-Sha'r and Abriola, L. M.: 1997, Experimental assessment of gas transport mechanisms in natural porous media. Parameter estimation, *Water Resour. Res.* **33**(4), 505–516.



BINARY MIXTURES

- In porous media we use:

$$\rho_g = \sum_i \rho_g^i \quad \text{and} \quad p_g = \sum_i p_g^i$$

For mas density (kg), the equations imply that an equivalent molar mass should be defined as:

$$M_g = \frac{\sum_i M^i p_g^i}{\sum_i p_g^i} = \frac{\sum_i M^i p_g^i}{p_g}$$

Mass density (kg): $\frac{p_g^i M^i}{RT_a}$ versus molar density: $\frac{p_g^i}{RT_a}$

Mass fraction (kg): $\omega_g^i = \frac{p_g^i M^i}{p_g M_g}$ versus molar fraction: $\chi_g^i = \frac{p_g^i}{p_g}$



BINARY MIXTURES

- In porous media we use:

$$\mathbf{j}_g^i = -S_g \phi \rho_g \tau D \nabla \omega_g^i - \omega_g^i \rho_g \frac{\mathbf{k} k_{rg}}{\mu_g} (\nabla p_g + \rho_g \nabla z)$$

This is the total flux of a gas component (i) in the gas phase (for a rigid porous media). The Knudsen diffusion can

be incorporated in the viscosity as: $\mu_g = \frac{\mu_g(T)}{(1 + \frac{b_k}{p})}$

The fact that mass fraction is used implies the assumption that Darcy is a mass averaged velocity (provided that binary diffusion coefficient is the same for the 2 components of the mixture).



CONTENTS

1. Fundamentals
2. Gas mixtures
3. Multiphase flow
4. Coupled deformation
5. Energy balance
6. Applications
7. Summary

eurad

MASS CONSERVATION

- Mass conservation of a multiphasic system (for each component):

$$\frac{\partial(\rho_l^i S_l \phi + \rho_g^i S_g \phi)}{\partial t} + \nabla \cdot (\mathbf{i}_l^i + \mathbf{i}_g^i + \rho_l^i \mathbf{q}_l + \rho_g^i \mathbf{q}_g + (\rho_l^i S_l + \rho_g^i S_g) \phi \frac{\partial \mathbf{u}}{\partial t}) = 0$$

$$\rho_l^i = \omega_l^i \rho_l \text{ and } \rho_g^i = \omega_g^i \rho_g$$

- Where, for instance: $i = H_2, w, a$
- Mass conservation of an i -component can be combined with solid conservation to convert porosity variations into deformations.

eurad

MASS CONSERVATION

- Solid mass conservation using material derivative:

$$\frac{D\phi}{Dt} = \frac{(1-\phi)D\rho_s}{\rho_s Dt} + (1-\phi)\nabla \cdot \frac{d\mathbf{u}}{dt}$$

- Mass conservation of i -component using material derivative and with solid mass conservation substituted:

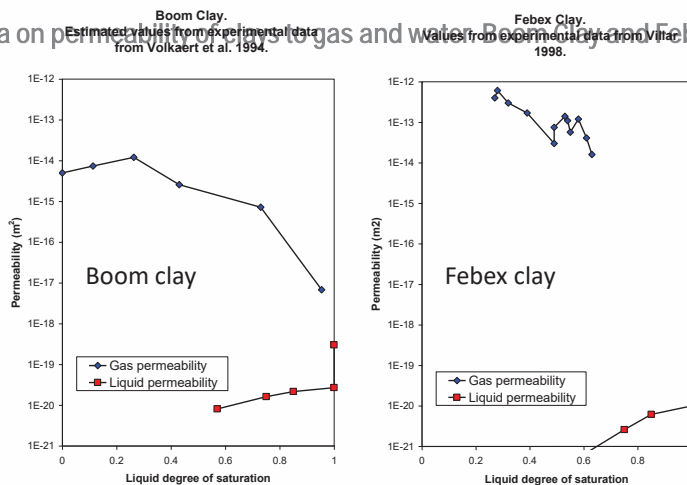
$$\phi \frac{D(\rho_l^i S_l + \rho_g^i S_g)}{Dt} + \nabla \cdot (\mathbf{i}_l^i + \mathbf{i}_g^i + \rho_l^i \mathbf{q}_l + \rho_g^i \mathbf{q}_g) + (\rho_l^i S_l + \rho_g^i S_g) \nabla \cdot \frac{\partial \mathbf{u}}{\partial t} = 0$$

- Where $\nabla \cdot \frac{\partial \mathbf{u}}{\partial t}$ is the volumetric strain rate
- And $\mathbf{i}_g^i + \rho_g^i \mathbf{q}_g = -\tau S_g \phi D\rho_g \nabla \omega_g^i - \omega_g^i \rho_g \frac{k k_{rg}}{\mu_g} (\nabla p_g + \rho_g g \nabla z)$
(Fick and Darcy)

eurad

INTRINSIC PERMEABILITY FOR CLAYS

- Is "intrinsic permeability" a good concept for clays? No. Clay materials display an intrinsic permeability that depends on the water content. This is due to changes in material structure.
- Compiled data on permeability for Boom Clay and Febex Clay (Olivella and Gens, 2000).



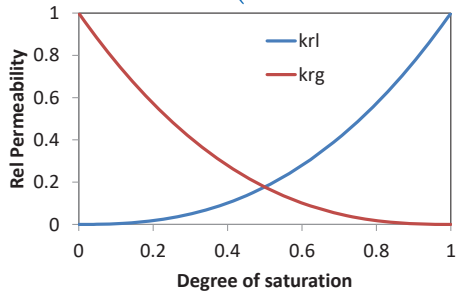
S. OLIVELLA and A. GENS, Vapour Transport in Low Permeability Unsaturated Soils with Capillary Effects *Transport in Porous Media* 40: 219–241, 2000.

eurad

RELATIVE PERMEABILITY

- Van Genuchten – Mualem liquid and gas relative permeabilities

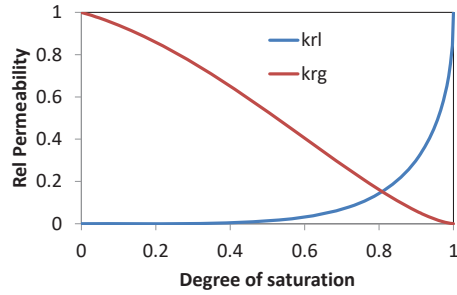
$$k_{rl} = (S_{el})^\gamma \left(1 - \left(1 - S_{el}^{(1/\lambda)} \right)^\lambda \right)^2$$



$\lambda \rightarrow 1$

Granular soils

$$k_{rg} = (1 - S_{el})^\gamma \left(1 - S_{el}^{(1/\lambda)} \right)^{2\lambda}$$



$\lambda \leq 0.5$

Silty Clayey soils



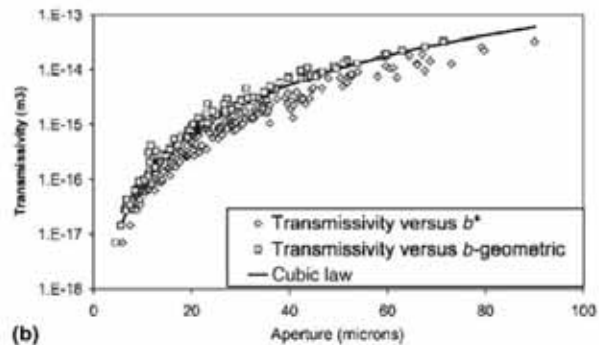
INTRINSIC PERMEABILITY FOR FRACTURES

- Fractures are preferential paths for flow
- Aperture can be used to calculate the transmissivity of a fracture using cubic law ($b^* = (3b_{max} + b_{min})/4$). Ramaajo et al 2002

Intrinsic transmissivity

$$T_{int} = kb = \frac{b^3}{12}$$

b for mechanical and hydraulic processes is not the same



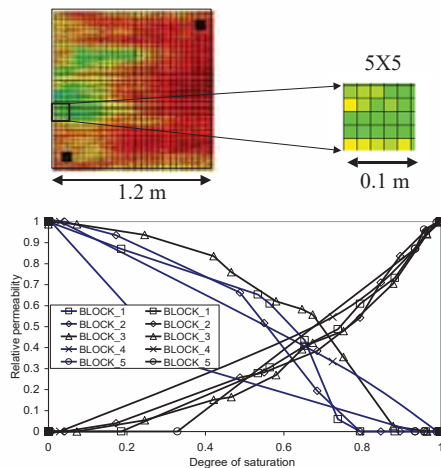
(b) H. RAMAJO, S. OLIVELLA, J. CARRERA and X. SANCHEZ-VILA, Simulation of Gas Dipole Tests in Fractures at the Intermediate Scale Using a New Upscaling Method, Transport in Porous Media 46: 269–284, 2002



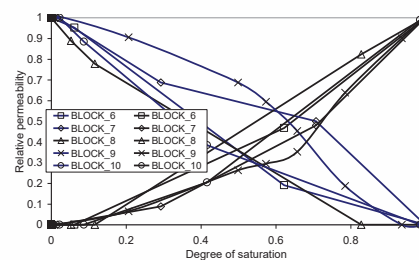
Section 3: Multiphase flow

RELATIVE PERMEABILITY

- Relative permeability calculated numerically for a fracture with heterogeneity (Ramajo et al 2002). Normally, curvature of liquid and gas relative permeability are different.



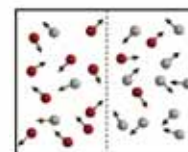
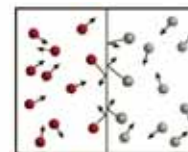
H. RAMAJO, S. OLIVELLA, J. CARRERA and X. SANCHEZ-VILA, Simulation of Gas Dipole Tests in Fractures at the Intermediate Scale Using a New Upscaling Method, Transport in Porous Media 46: 269–284, 2002



eurad

GAS DISPERSION

- Diffusion/dispersion of a **gas in a liquid**
 - Dissolution of gas in a liquid by Henry's law
 - Fick's law: $\mathbf{i}_l^i = -(\mathbf{D}_l^{mech} + \mathbf{D}_l^i) \nabla \omega_l^i$
 - D_l^i is different for each gas. Dispersion can be added
 - \mathbf{D}_l^{mech} is to be calculated using liquid phase flux
- Diffusion/dispersion of a **gas in a gas mixture**
 - Theories of gas mixtures (kinetic theory of gases)
 - Fick's law: $\mathbf{i}_g^i = -(\mathbf{D}_g^{mech} + \mathbf{D}_g^i) \nabla \omega_g^i$
 - \mathbf{D}_g^{mech} is to be calculated using gas phase flux



eurad



CONTENTS

1. Fundamentals
2. Gas mixtures
3. Multiphase flow
4. Coupled deformation
5. Energy balance
6. Applications
7. Summary



eurad



NET AND EFFECTIVE STRESSES

- Net and effective stress

$$\sigma' = \sigma - \max(p_g, p_l)$$

- Net and effective stress variations are responsible for deformations:

$$\Delta \varepsilon \propto \Delta \sigma'$$

- Changes in deformations lead to changes in permeability:

$$\Delta k \propto \Delta \varepsilon$$

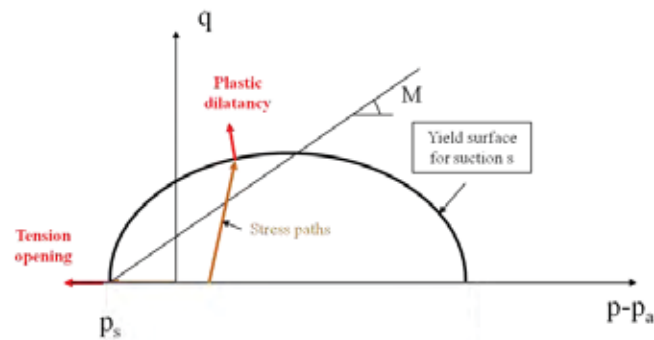


eurad



DEFORMATIONS AND PERMEABILITY VARIATIONS

- Elastoplastic deformations that may cause permeability increase:
 - Expansion induced by unloading
 - Dilatancy induced by shear deformation
 - Extension induced by tensile stress



eurad

CONTENTS

1. Fundamentals
2. Gas mixtures
3. Multiphase flow
4. Coupled deformation
5. Energy balance
6. Applications
7. Summary

eurad

INTERNAL ENERGY AND ENTHALPY

- First thermodynamics principle can be expressed in two different ways (heat is transformed into internal energy and work or mechanical energy):

$$dq = de + pdv = de - \frac{p}{\rho^2} d\rho$$

Where $v = 1/\rho$

- If enthalpy is introduced here ($h = e + pv$), the corresponding equation is:

$$dq = dh - vdp = dh - \frac{1}{\rho} dp$$



INTERNAL ENERGY AND ENTHALPY

- Balance of energy including mechanical work, can be written as:

$$\frac{\partial(e_g \rho_s (1 - \phi) + e_g \rho_g S_g \phi + e_l \rho_l S_l \phi)}{\partial t} - \frac{\phi S_g p_g}{\rho_g} \frac{\partial \rho_g}{\partial t} + \nabla \cdot (\mathbf{i}_c + \mathbf{j}_{es} + \mathbf{j}_{eg} + \mathbf{j}_{el}) = f^Q$$

- Or in terms of enthalpy:

$$\frac{\partial(h_s \rho_s (1 - \phi) + h_g \rho_g S_g \phi + h_l \rho_l S_l \phi)}{\partial t} - \phi S_g \frac{\partial p_g}{\partial t} + \nabla \cdot (\mathbf{i}_c + \mathbf{j}_{hs} + \mathbf{j}_{hg} + \mathbf{j}_{hl}) = f^Q$$

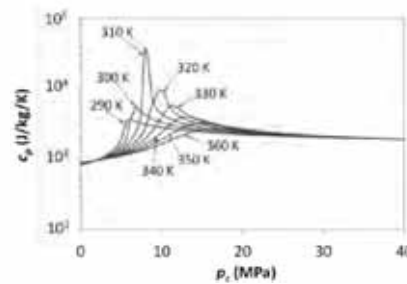
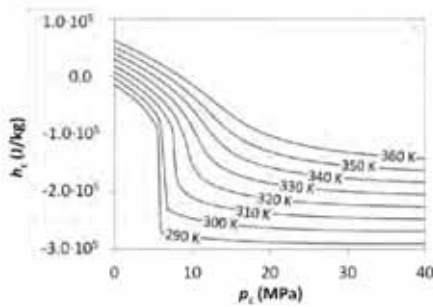


INTERNAL ENERGY AND ENTHALPY

- Example for CO₂

$$h_c(p_c, T) - h_c^*(p_0, T) = \left(p_c V - RT - \frac{1.5a - a_1 T}{\sqrt{T}b} \ln \left(1 + \frac{b}{V} \right) \right) / M_{CO_2}$$

$$c_p = \frac{\partial h^*(p_0, T)}{\partial T} + \left(p_c \frac{\partial V}{\partial T} - R + \frac{0.75a}{b\sqrt{T^3}} \ln \left(1 + \frac{b}{V} \right) + \frac{1.5a - a_1 T}{\sqrt{T}(V+b)V} \frac{\partial V}{\partial T} \right) / M_{CO_2}$$



Redlich-Kwong EOS (1949)

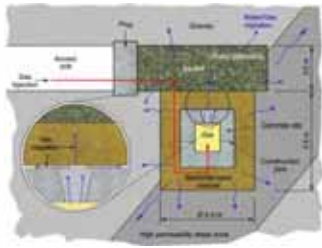
eurad

CONTENTS

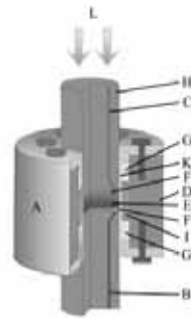
1. Fundamentals
2. Gas mixtures
3. Multiphase flow
4. Coupled deformation
5. Energy balance
6. Applications
7. Summary

eurad

APPLICATIONS



GMT: 2009



ARGILLITE: 2012



BENTONITE: 2019

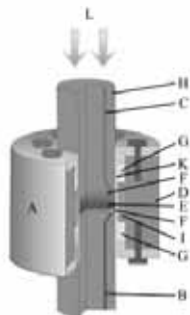
Date

Event

eurad

31

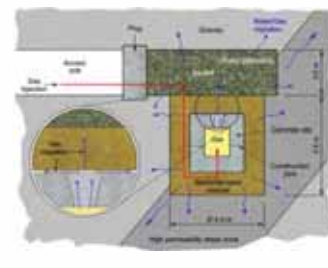
APPLICATIONS



ARGILLITE: 2012



BENTONITE: 2019



GMT: 2009

Date

Event

eurad

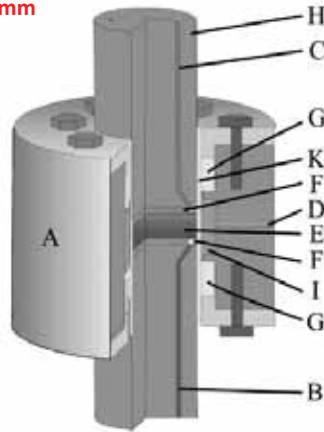
32

BREAKTHROUGH TESTS

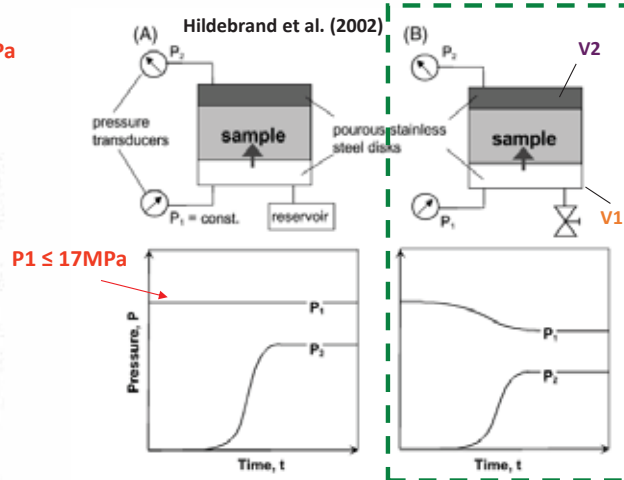
• Experimental Set-up

Isotropic confining pressure = 30MPa

Sample
 \varnothing 28.5mm
 h_{MAX} 30mm



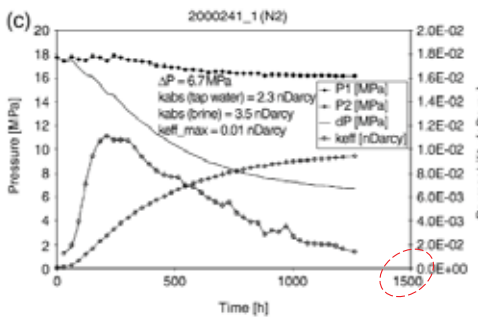
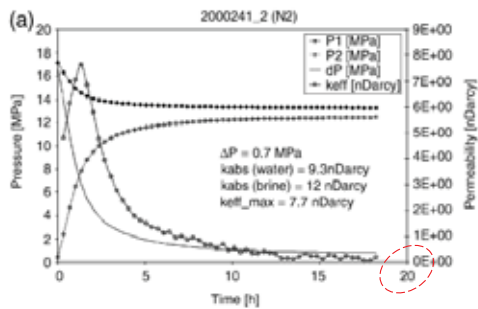
Arnedo D., E. E. Alonso and S. Olivella, Gas flow in anisotropic claystone: modelling triaxial experiments, Int. J. Numer. Anal. Meth. Geomech. (2012), 2013; 37:2239–2256, DOI: 10.1002/nag.2132



Scheme of the two experimental modes used in this study. (A) constant pressure at upstream side; (B) introduction of gas into a fixed upstream volume; downstream volume fixed in both instances.



BREAKTHROUGH TESTS

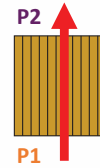


Hildebrand et al. (2002)

1 nDarcy = $10^{-21}m^2$

Flow parallel to bedding planes

TEST1

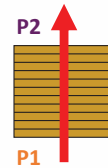


Tertiary Mudstone (Norwegian Shelf)

$$k_{eff} = - \frac{V_2 \cdot \eta \cdot 2 \Delta x \cdot dP_2}{A(P_2^2 - P_1^2) dt}$$

TEST2

Flow perpendicular to bedding planes

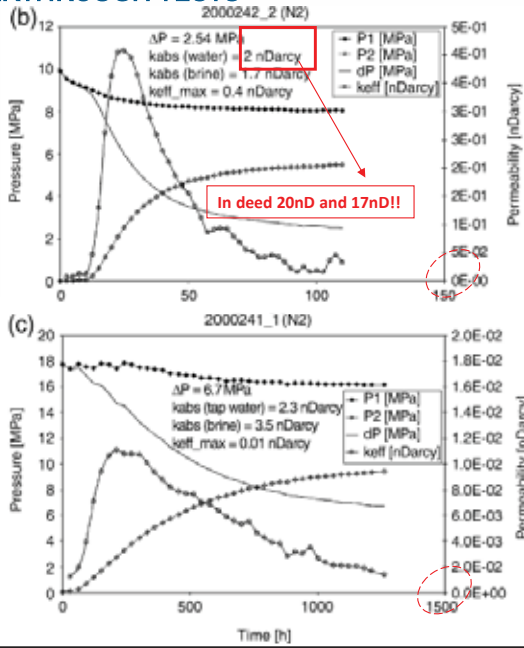


Date

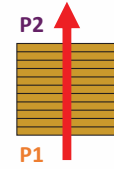
ent



BREAKTHROUGH TESTS



Flow **perpendicular** to bedding planes
← TEST3



Tertiary Mudstone (Norwegian Shelf)

Hildebrand et al. (2002)

$$k_{eff} = - \frac{V_2 \cdot \eta \cdot 2 \Delta x \cdot dP_2}{A(P_2^2 - P_1^2) dt}$$

← TEST2
Flow perpendicular to bedding planes

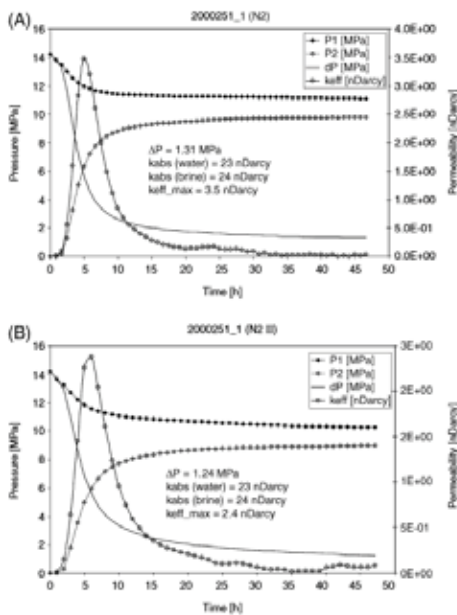


1 nDarcy = 10⁻²¹m²

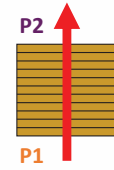


Date

BREAKTHROUGH TESTS



Flow **perpendicular** to bedding planes
←

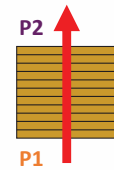


Boom Clay

Hildebrand et al. (2002)

$$k_{eff} = - \frac{V_2 \cdot \eta \cdot 2 \Delta x \cdot dP_2}{A(P_2^2 - P_1^2) dt}$$

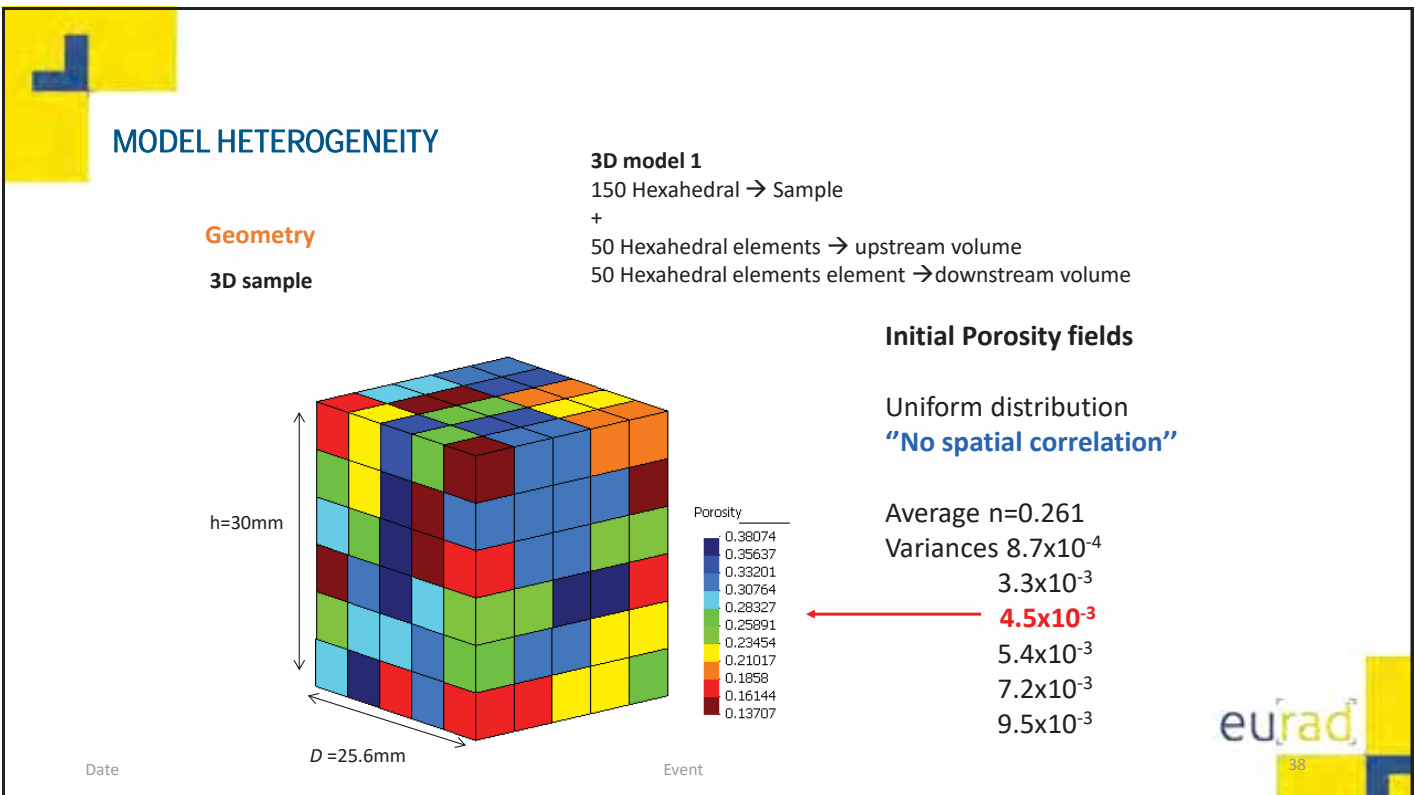
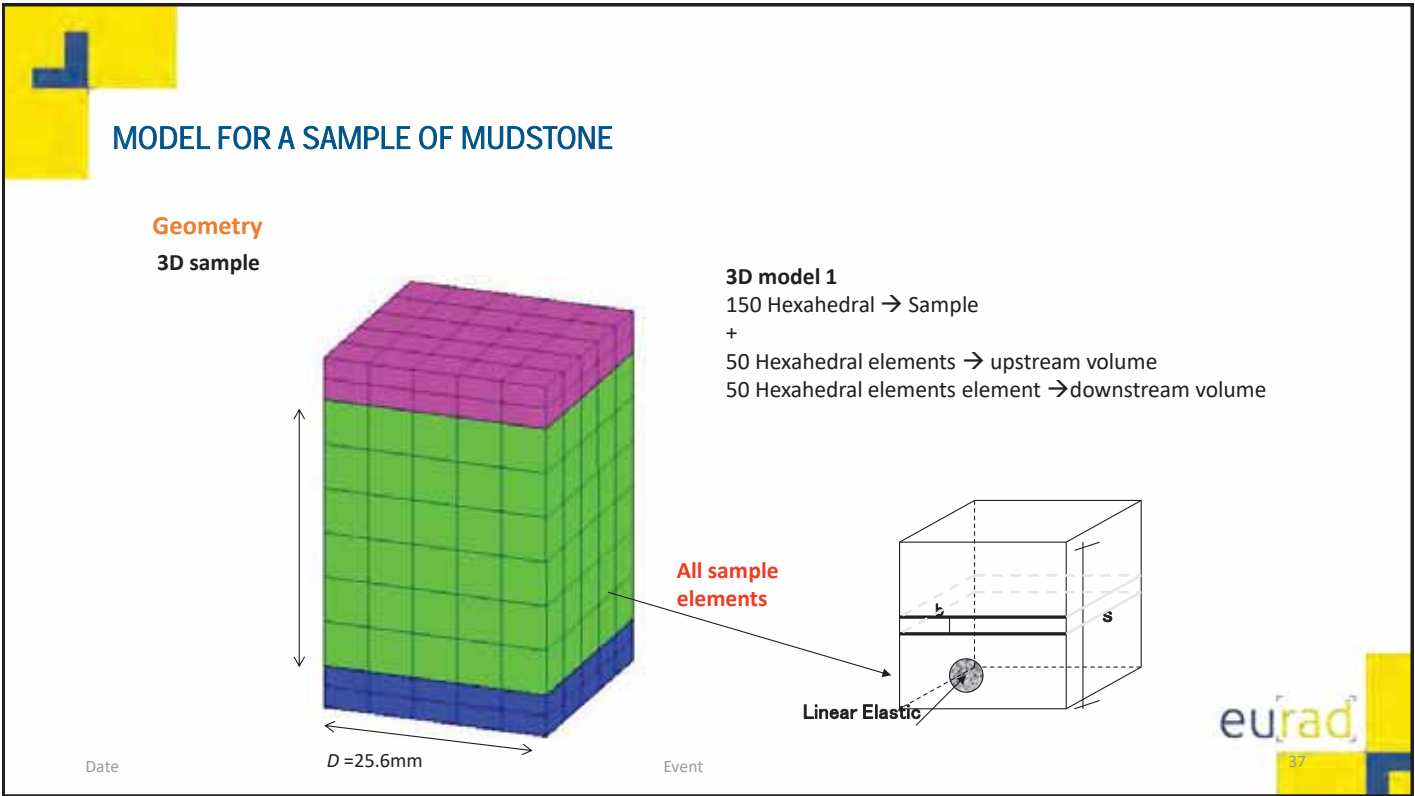
←
Flow perpendicular to bedding planes



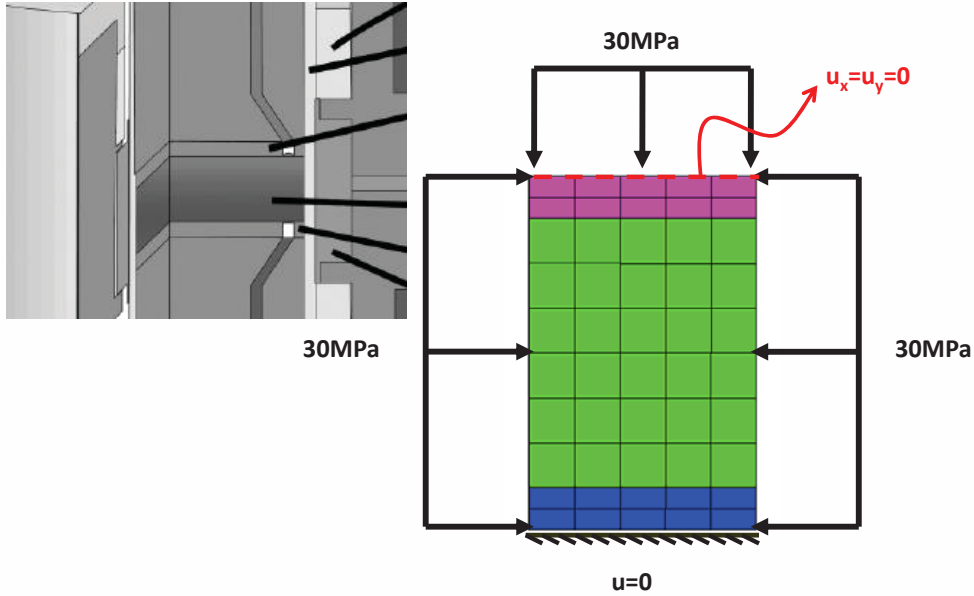
1 nDarcy = 10⁻²¹m²



Date



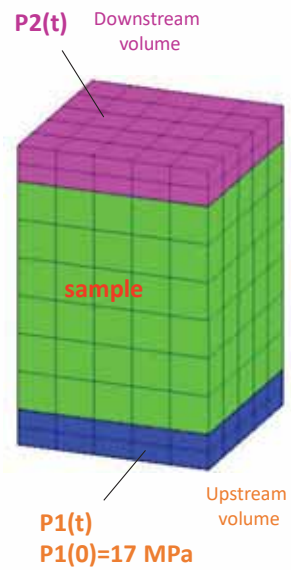
MODEL BOUNDARY CONDITIONS



eurad

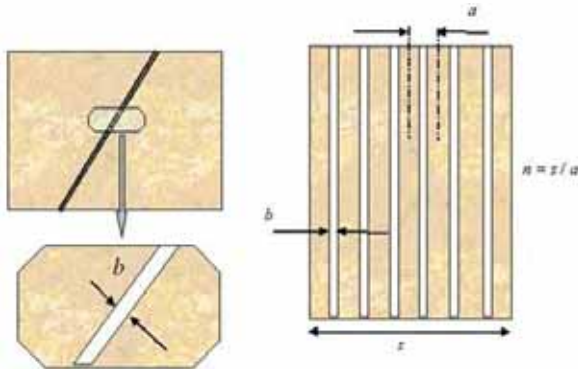
MODEL PROTOCOL

Time (days)	Stage
-1 to 0	Initial Stress Equilibrium Under 30MPa Confining Stress
0 to 0.0006	Pressure Ramp at Upstream Compartment $P_{initial} \rightarrow P1$
0.0006 to 0.0009	Constant Upstream Pressure P1
0.0009 to 200	Deactivation of Upstream Boundary Condition (P1 decay)



eurad

EMBED



Multiple fractures in an element

s = element size
a = fracture spacing
n = number of fractures/element

Normal strain*
Volumetric strain

$$k = k_{matrix} \left(\frac{s - nb}{s} \right) + \sum_{i=1}^n \left(k_{fracture} \frac{b \cdot a}{a \cdot s} \right) = k_{matrix} \left(\frac{s - nb}{s} \right) + \sum_{i=1}^n \left(k_{fracture} \frac{b \cdot 1}{a \cdot n} \right) \cong k_{matrix} + \frac{b^3}{12a}$$

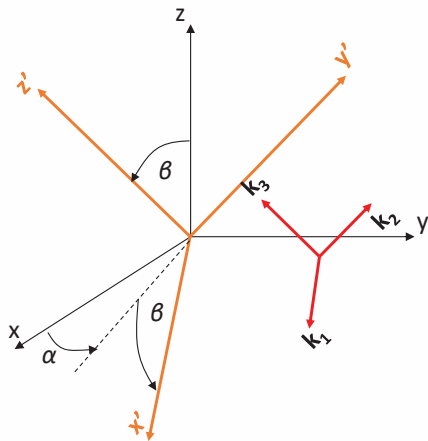
$$b = b_0 + \Delta b$$

$$\Delta b = a \Delta \epsilon = a(\epsilon - \epsilon_0) = (s/n)(\epsilon - \epsilon_0)$$

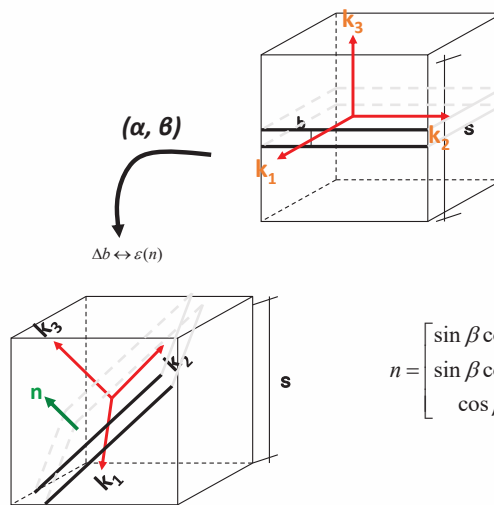
$$k = k_{matrix} + \frac{b^3}{12a} = k_{matrix} + \frac{(b_0 + a(\epsilon - \epsilon_0))^3}{12a}$$



PERMEABILITY ANISOTROPY



Relation to Embedded fracture model



$$n = \begin{bmatrix} \sin \beta \cos \alpha \\ \sin \beta \sin \alpha \\ \cos \beta \end{bmatrix}$$

Aperture variations using normal strain



MECHANICAL ANISOTROPY

- Transversal isotropic elastic behavior

$$\bullet \mathbf{D} = \begin{pmatrix} \mathbf{D}_{aa} & \mathbf{0}_{3 \times 3} \\ \mathbf{0}_{3 \times 3} & \mathbf{D}_{bb} \end{pmatrix}$$

$$\bullet \mathbf{D}_{aa} = \begin{pmatrix} \frac{1}{E_1} & -\frac{\nu_{21}}{E_2} & -\frac{\nu_{31}}{E_3} \\ -\frac{\nu_{12}}{E_1} & \frac{1}{E_2} & -\frac{\nu_{32}}{E_3} \\ -\frac{\nu_{13}}{E_1} & -\frac{\nu_{23}}{E_1} & \frac{1}{E_3} \end{pmatrix} \quad \text{or} \quad \mathbf{D}_{aa} = \begin{pmatrix} \frac{1}{E_1} & -\frac{\nu_{11}}{E_1} & -\frac{\nu_{31}}{E_3} \\ -\frac{\nu_{11}}{E_1} & \frac{1}{E_1} & -\frac{\nu_{31}}{E_3} \\ -\frac{\nu_{13}}{E_1} & -\frac{\nu_{13}}{E_1} & \frac{1}{E_3} \end{pmatrix}$$

$$\bullet \mathbf{D}_{bb} = \begin{pmatrix} \frac{1}{G_{23}} & 0 & 0 \\ 0 & \frac{1}{G_{31}} & 0 \\ 0 & 0 & \frac{1}{G_{12}} \end{pmatrix} \quad \text{or} \quad \mathbf{D}_{bb} = \begin{pmatrix} \frac{1}{G_{13}} & 0 & 0 \\ 0 & \frac{1}{G_{31}} & 0 \\ 0 & 0 & \frac{2(1+\nu_{11})}{E_1} \end{pmatrix}$$

PARAMETERS FOR TERTIARY MUDSTONE

Mechanical parameters
(Anisotropic Linear Elastic)
... mainly from Opalinus Clay

Parameter	Value
E_1 (MPa)	6000 MPa
ν_{11}	0.27
ν_{31}	0.27
E_3	3000 MPa
G_{13}	1200 MPa

Retention Curve (Van Genuchten)

Parameter	Value
P (MPa)	3.9
λ	0.128
Residual saturation, S_{rl}	0.0
Maximum saturation, S_{ls}	1.0

Element permeability parameters

Parameter	Value
k_{parallel} (m ²)	9.0×10^{-21}
$k_{\text{perpendicular}}$ (m ²)	4.0×10^{-21}
Reference porosity	0.261
Initial aperture, b_0 (m)	1.0×10^{-9}
Fracture spacing a (m)	5.0×10^{-3}
Maximum aperture, b_{max} (m)	3.0×10^{-7}
Threshold strain, ϵ_0	1.0×10^{-4}

+anisotropy angles in each case

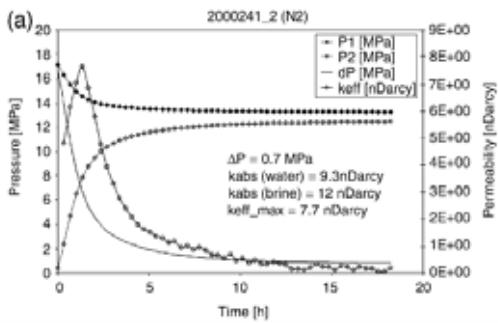
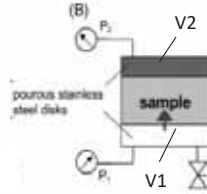
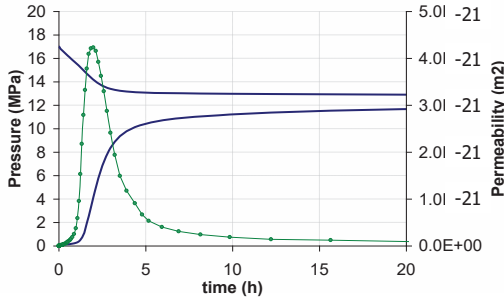
TEST1: ($\alpha = 0$), $\beta = 90$ bedding vertical

TEST2: ($\alpha = 0$), $\beta = 0$ bedding horizontal

Diffusion of dissolved gas

Parameter	Value
D (m ² /s)	5.45×10^{-10}

MODEL TEST1 RESULTS



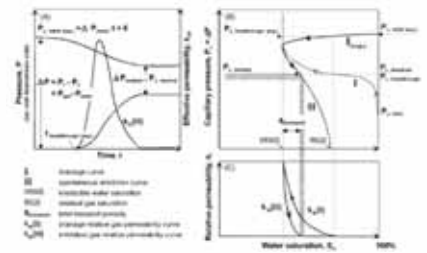
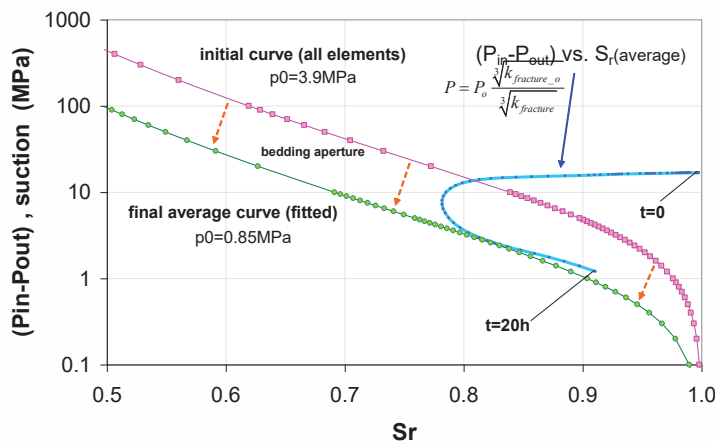
Considerations from pressure P1 decay

V1 reported in Hildebrand et al (2002) 2~3 cm³

V1 considered in model 6 cm³

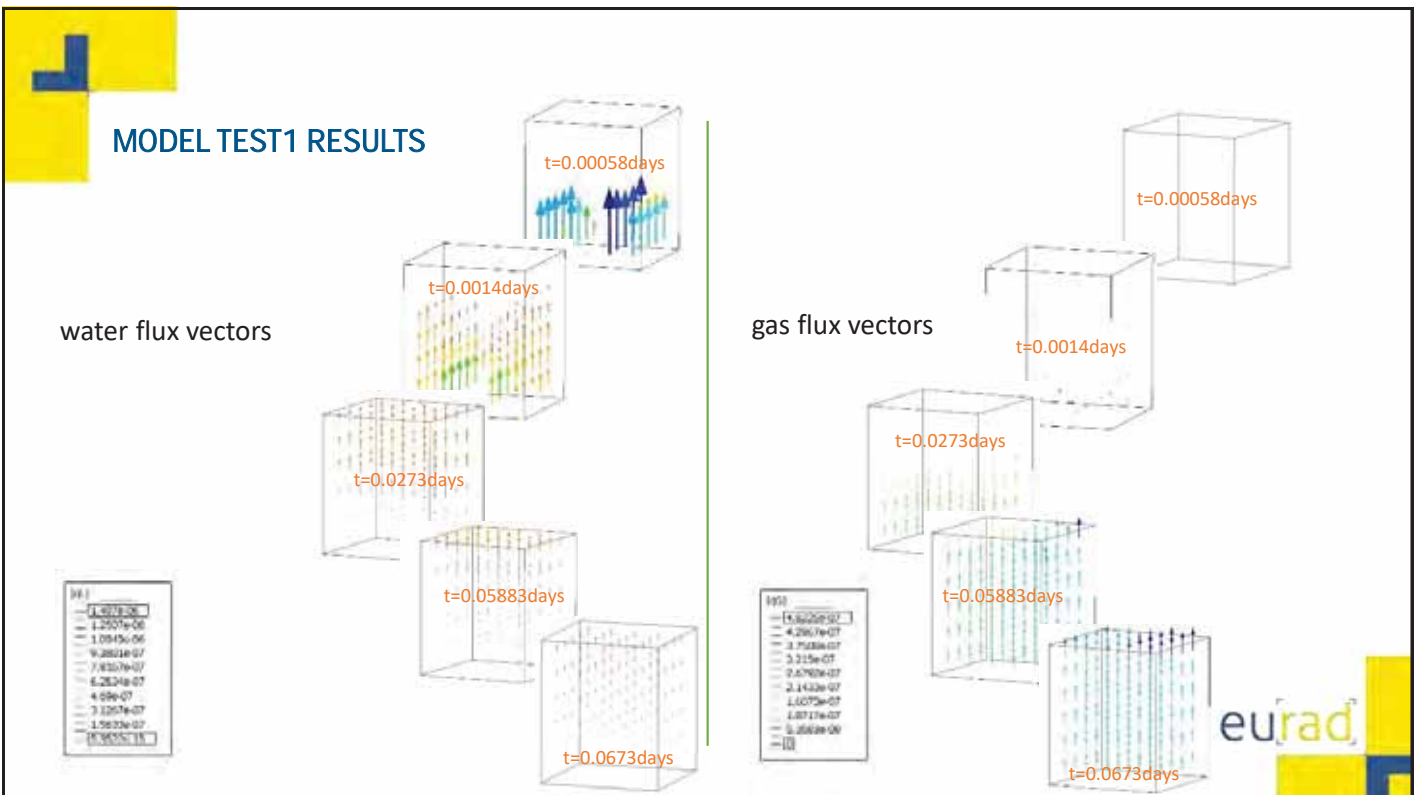
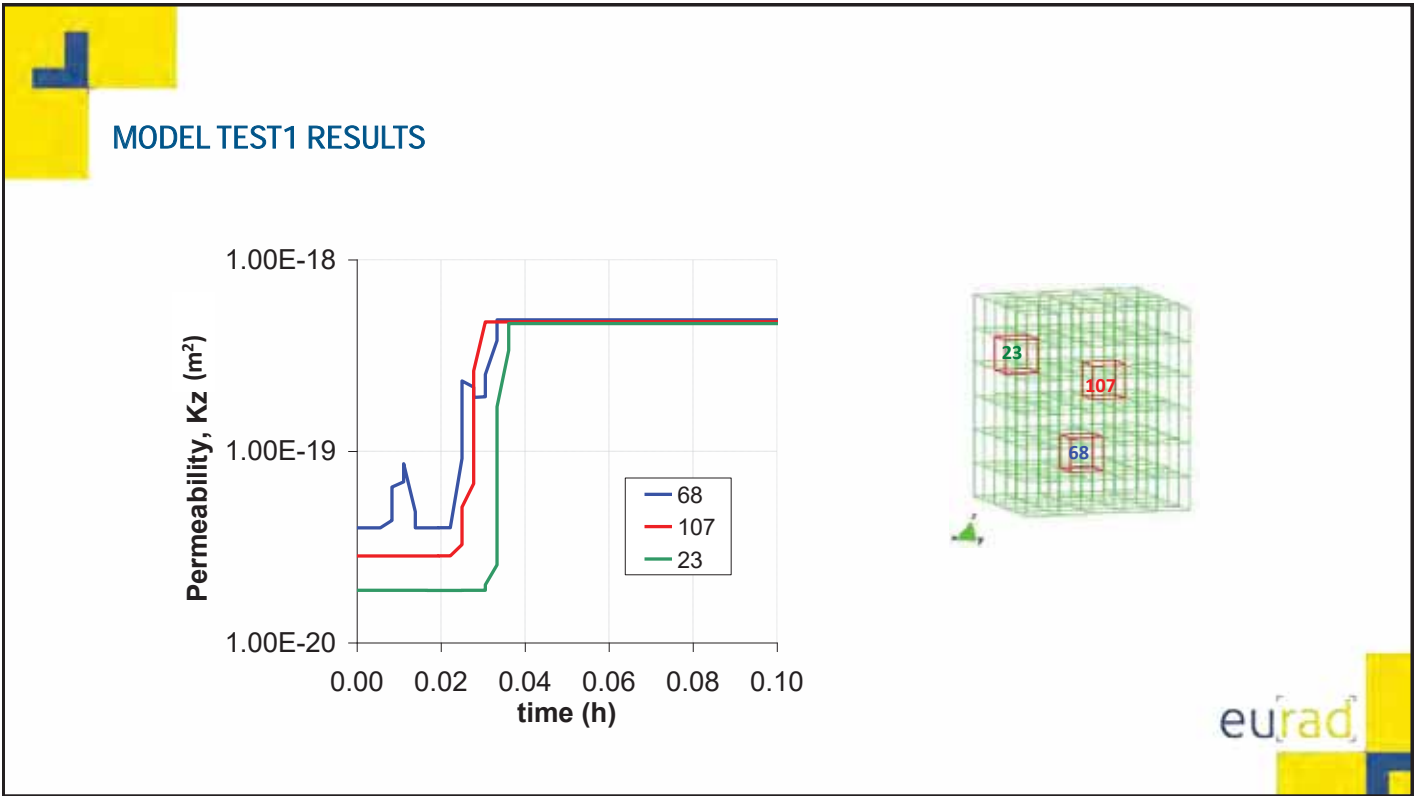


MODEL TEST1 RESULTS



Suction-Saturation average path does not correspond to any point in the sample





PARAMETERS FOR MUSTONE (TEST 3)

**Mechanical parameters
(Anisotropic Linear Elastic)**

... mainly from Opalinus Clay

Parameter	Value
E_1 (MPa)	6000
$\nu_1 = \nu_2$	0.27
E_2 (MPa)	3000
G_2 (MPa)	1200

Element permeability parameters

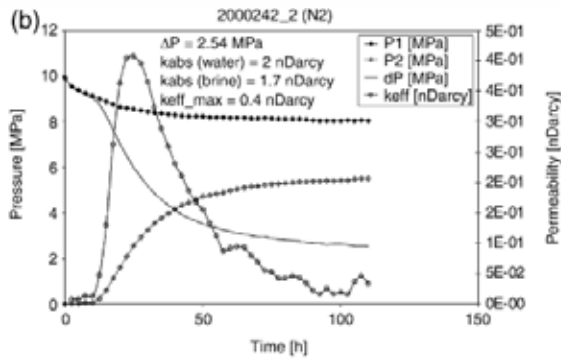
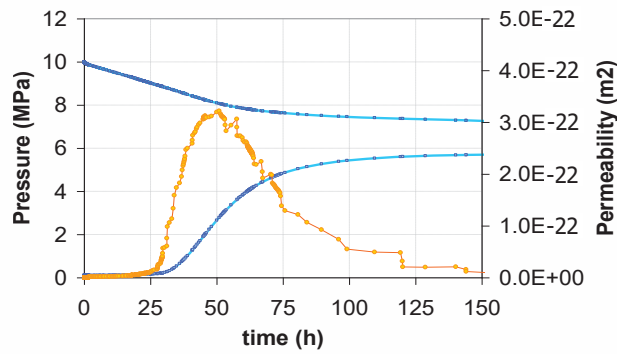
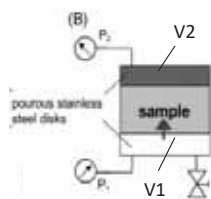
Parameter	Value
$k_{parallel}$ (m ²)	45.0x10 ⁻²¹
$k_{perpendicular}$ (m ²)	20.0x10 ⁻²¹
Reference porosity	0.299
Initial aperture, b_0 (m)	1.0x10 ⁻⁹
Fracture spacing a (m)	5.0x10 ⁻³
Maximum aperture, b_{max} (m)	5.0x10 ⁻⁷
Threshold strain, ϵ_0	2.0x10 ⁻⁴ 1.0x10 ⁻⁴

+anisotropy angles

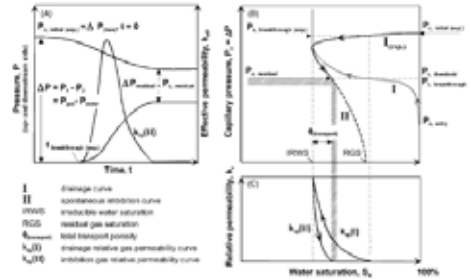
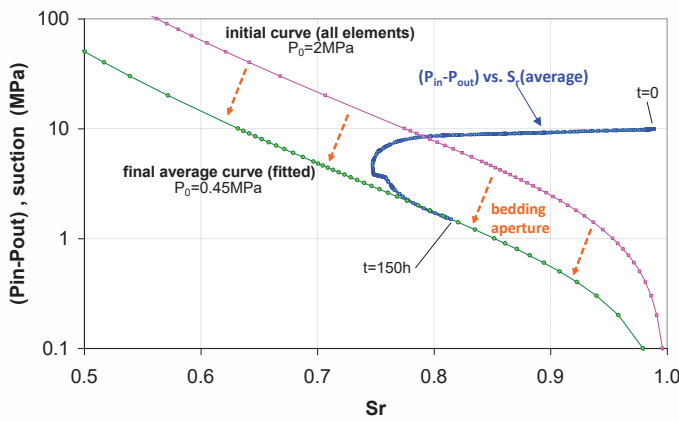
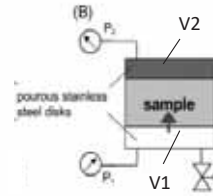
TEST3: ($\alpha = 0$), $\beta = 0$ bedding horizontal



MODEL TEST3 RESULTS



MODEL TEST3 RESULTS

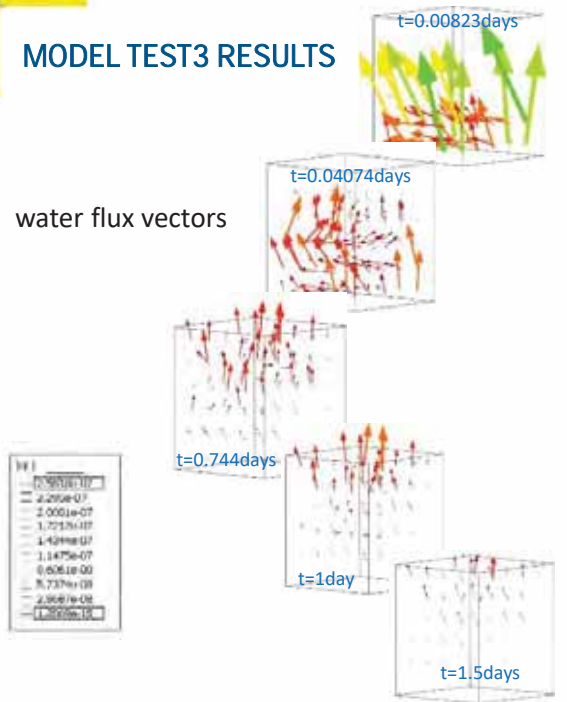


Suction-Saturation average path does not correspond to any point in the sample

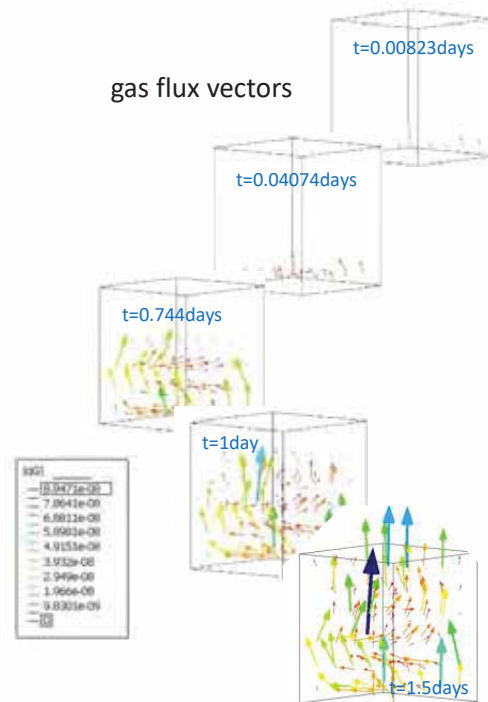


MODEL TEST3 RESULTS

water flux vectors



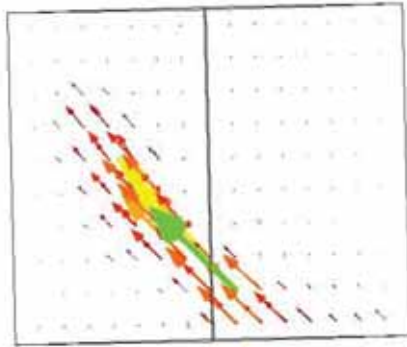
gas flux vectors



MODEL 45° RESULTS

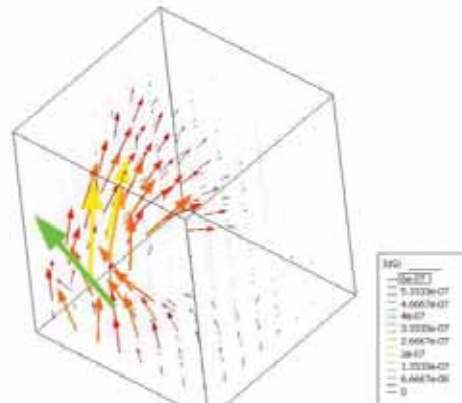
$$\alpha = \theta = 45^\circ$$

View **parallel** to bedding



step 1 16062
Display Vectors of q[G], [qG] factor 50000

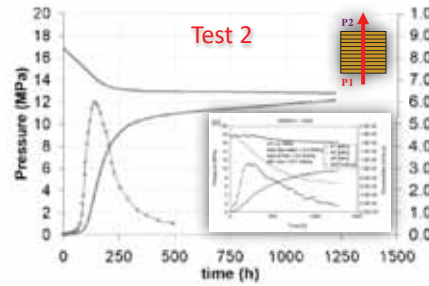
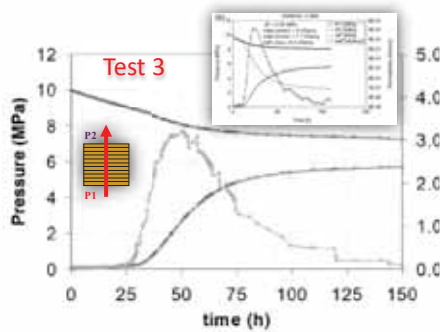
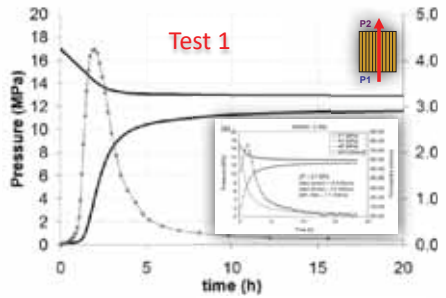
View **normal** to bedding



step 1 16062
Display Vectors of q[Z], [qZ] factor 50000

eurad

SUMMARY



The gas migration phenomena in stiff layered clays can be related to opening of preferential paths (bedding planes) coupled to conventional two phase flow through matrix pores.

At high net stresses (far from tensile stress states), gas can only flow through the sample after it has 'pushed out' part of the pore water.

The differential pressure ($P_{in} - P_{out}$) and the average saturation can be used to draw a path in the retention curve plane

eurad



CONTENTS

1. Fundamentals
2. Gas mixtures
3. Multiphase flow
4. Coupled deformation
5. Energy balance
6. Applications
7. Summary



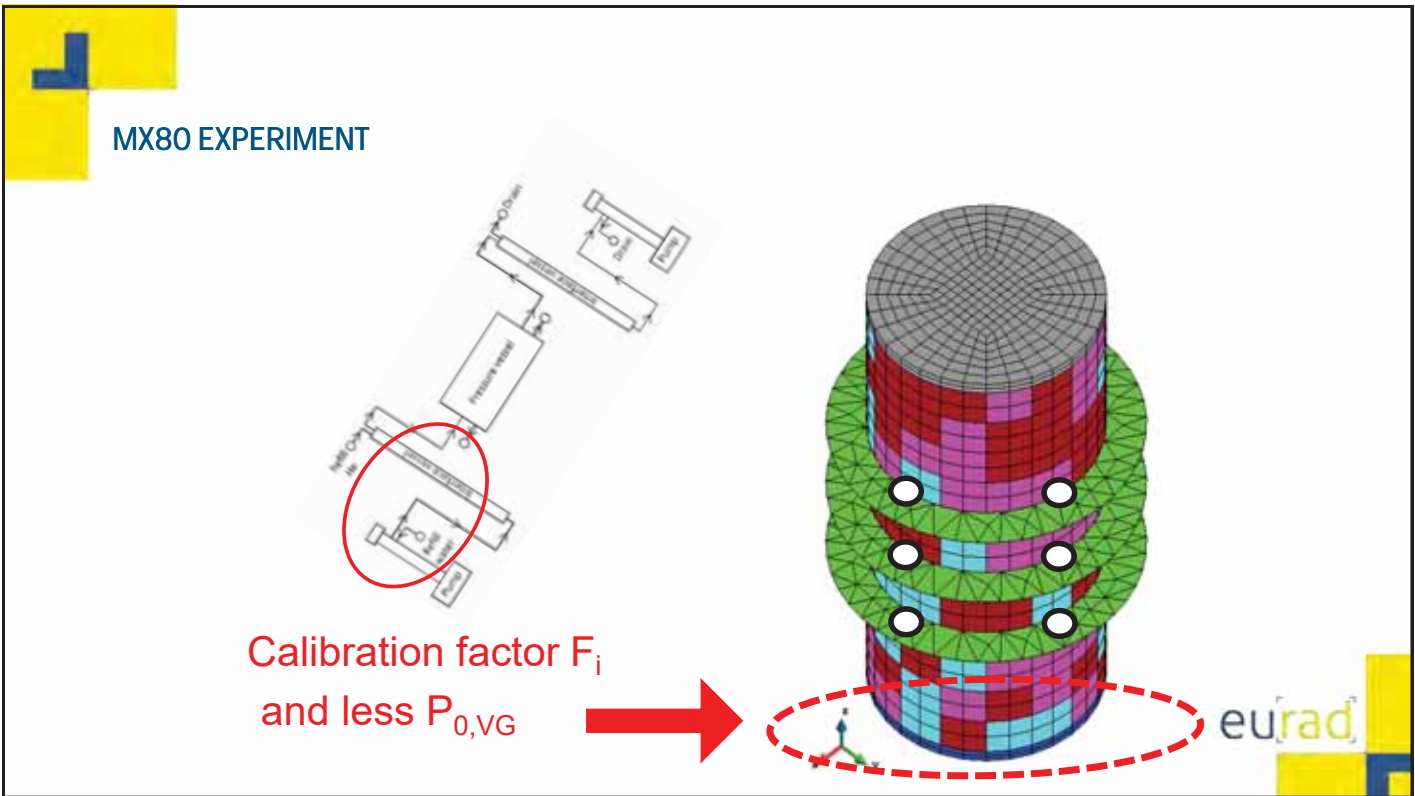
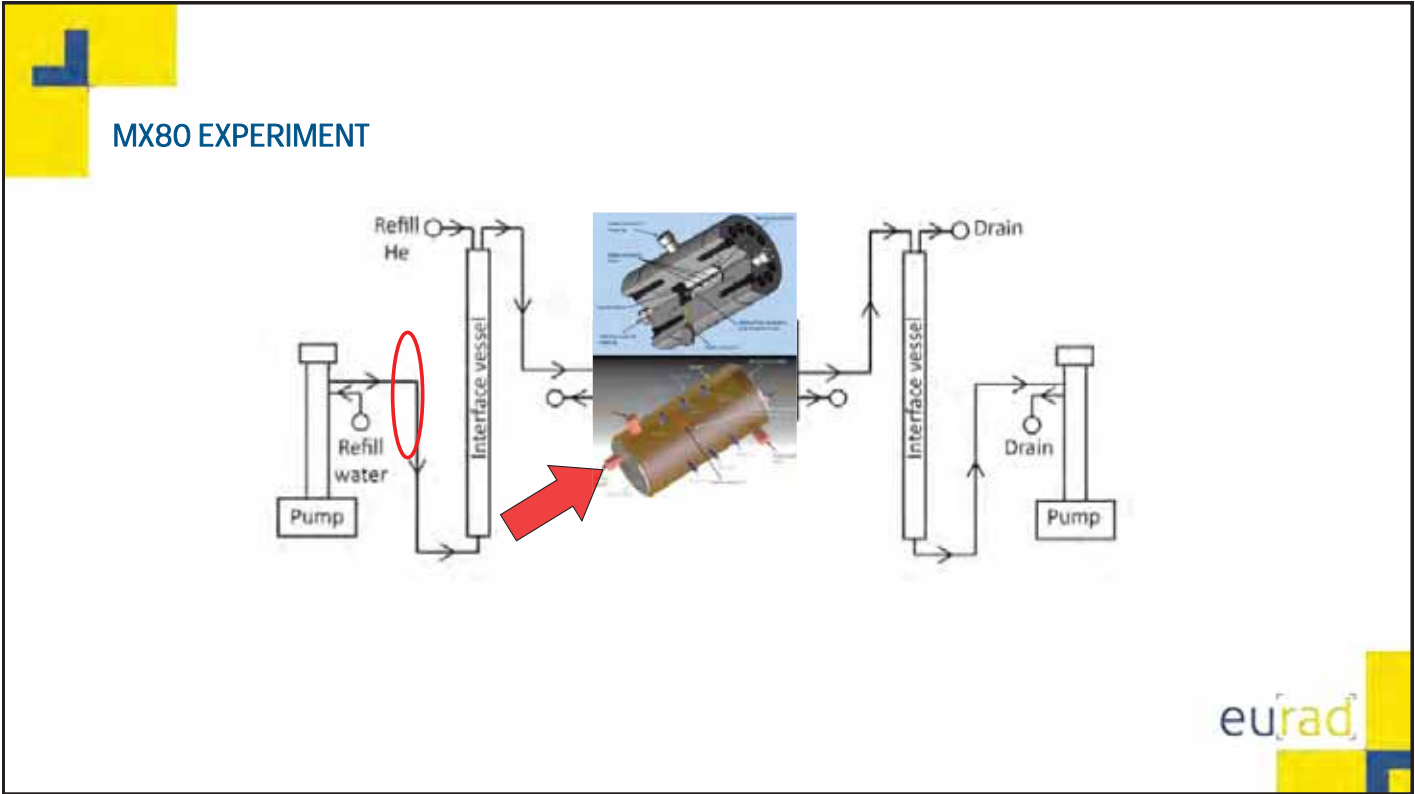

GAS TRANSFER THROUGH SATURATED CLAYEY MATERIALS

Task A: modelling Gas Injection Experiments (ENGINEER)

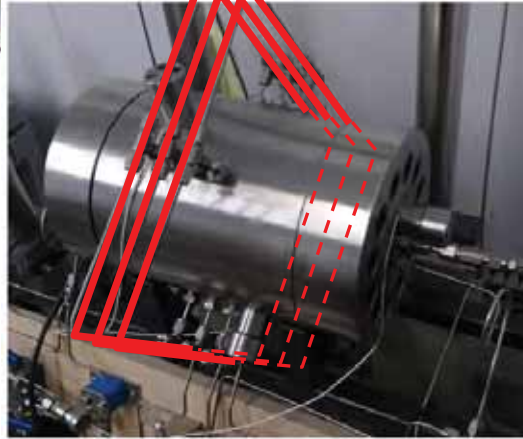
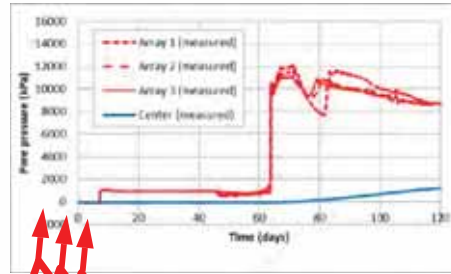
- Stage 0: Analysis of data, conceptual model and process model development
- **Stage 1A: 1D flow through saturated bentonite under constant volume boundary conditions (test Mx80-D)**
- Stage 1B (optional): 1D flow through saturated bentonite under isotropic boundary stress (test Mx80-4)
- **Stage 2A: spherical flow through saturated bentonite under a constant volume boundary condition (test Mx80-10)**
- Stage 2B (optional): spherical flow through saturated bentonite under a constant volume boundary condition (test Mx80-A)
- **Stage 3A (optional): Gas flow in natural material: triaxial test on Callovo-Oxfordian claystone**
- Stage 3B (optional): Gas flow in hydrated pellets under constant volume conditions

Damians, I.P., Olivella, S., and Gens, A.; 2019. Modelling a gas flow experiment in Mx80 bentonite. Proceedings of the XVII European Conference on Soil Mechanics and Geotechnical Engineering (XVII ECSMGE-2019), Geotechnical Engineering - Foundation of the future. Reykjavik, Iceland. 1st – 6th September 2019.



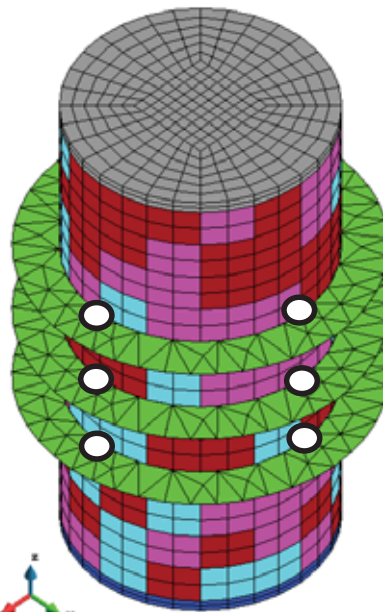
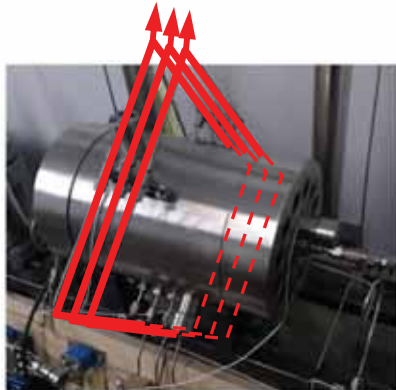



MX80 EXPERIMENT




eu_{rad}

MX80 EXPERIMENT



Volume connected to radial sensors.
Calibration of factor F_a

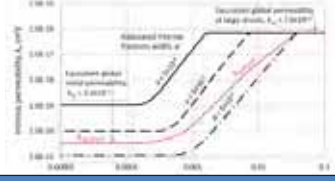
eu_{rad}



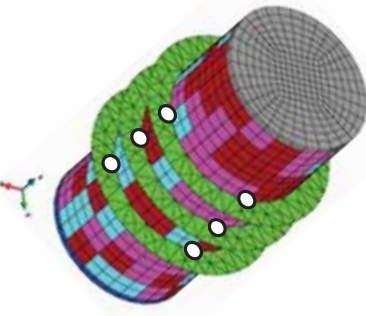
MX80 EXPERIMENT

EMBEDDED FRACTURE: CUBIC LAW + RELATIVE PERMEABILITY

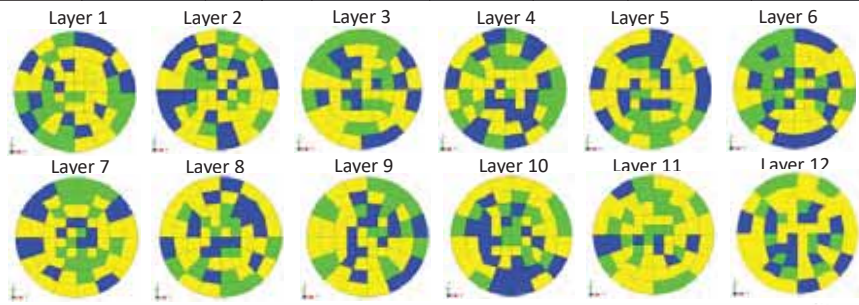
- Intrinsic permeability heterogeneous in 3 zones.
- Porosity set to 0.44
- $k_0 = \times 10^{-19} \times 10^{-20} \times 10^{-21} \text{ m}^2$ (resulting $k_{eq} = 3.3 \times 10^{-21} \text{ m}^2$)
- $P_0 = 10.8, 22.5, 48.6 \text{ MPa}$ with P_{00} at 10%
- Elastic modulus = 307 MPa and Poisson's ratio = 0.40




strain




Porosity	Intrinsic permeability	Water retention curve		Relative permeability γ	Embedded fractures definition parameters:				
		P_0	λ		a	b_0	b_{max}	ϵ_0	
0.44	1.0×10 ⁻¹⁹	10.8	0.45	$n_1 = 3$	5.0×10 ⁻⁴	9.5×10 ⁻⁹	7.5×10 ⁻⁷	0.01	
	1.0×10 ⁻²⁰	22.5			$n_{g_matrix} = 2$		5.0×10 ⁻⁵		3.5×10 ⁻⁷
	1.0×10 ⁻²¹	48.6			$n_{g_fracture} = 1$		5.0×10 ⁻⁶		1.5×10 ⁻⁹
-	m ²	MPa	-	n-power	m	m	m	%	



Layer 1 Layer 2 Layer 3 Layer 4 Layer 5 Layer 6
Layer 7 Layer 8 Layer 9 Layer 10 Layer 11 Layer 12





EMBEDDED FRACTURE: CUBIC LAW + RELATIVE PERMEABILITY

- Relative permeability as a function of saturation of matrix and saturation of fractures

$$\mathbf{q}_g = -\frac{k_{rg}\mathbf{k}}{\mu}(\nabla P_g + \rho_g g \nabla z)$$

- The generalized Darcy's law includes the product $k_{rg}\mathbf{k}$ which was calculated as:


$$k_{rg}\mathbf{k} = k_{rg}(\mathbf{k}_{matrix} + \mathbf{k}_{fractures}) = k_{rg}\left(\mathbf{k}_{matrix} + \mathbf{I} \frac{b^3}{12s}\right)$$

- In this case, relative permeability depends on the element degree of saturation which is calculated using the updated air entry value as described before. A model improvement consist in using a different relative permeability for fractures and matrix, i.e.:

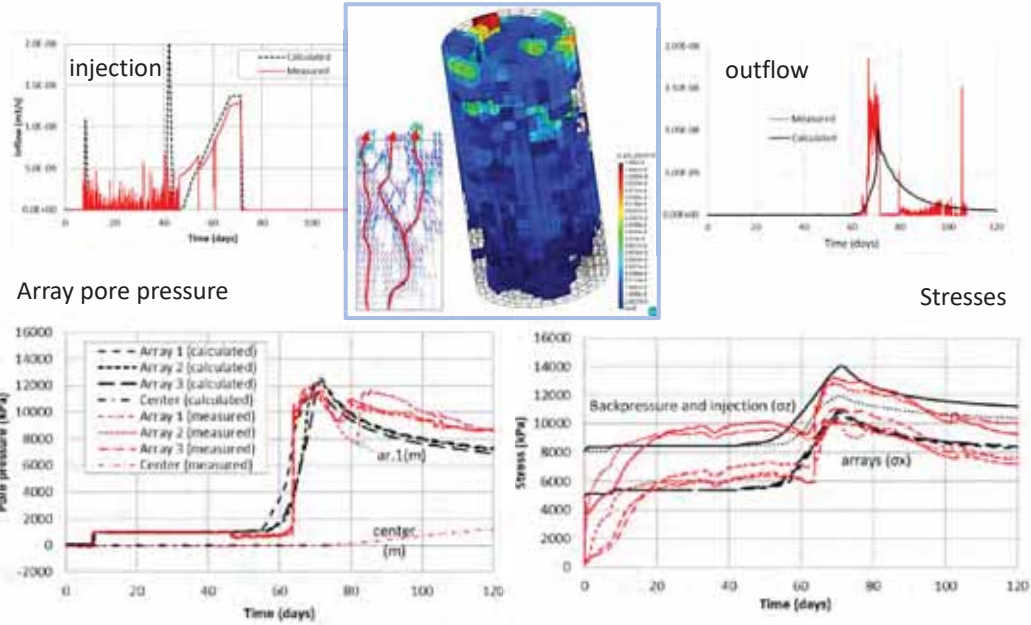
$$k_{rg}\mathbf{k} = \left((k_{rg})_{matrix} \mathbf{k}_{matrix} + (k_{rg})_{fractures} \mathbf{k}_{fractures} \right)$$

- In a first attempt, relative permeability of the matrix can be calculated as in the original models, while the relative permeability of the fractures can be set as 1 because the intrinsic permeability through the aperture will control the possibility for the gas to migrate.
- Implementation has been done considering the following:

$$(k_{rg})_{matrix} = S_g^n \quad \text{and} \quad (k_{rg})_{fractures} = S_g$$



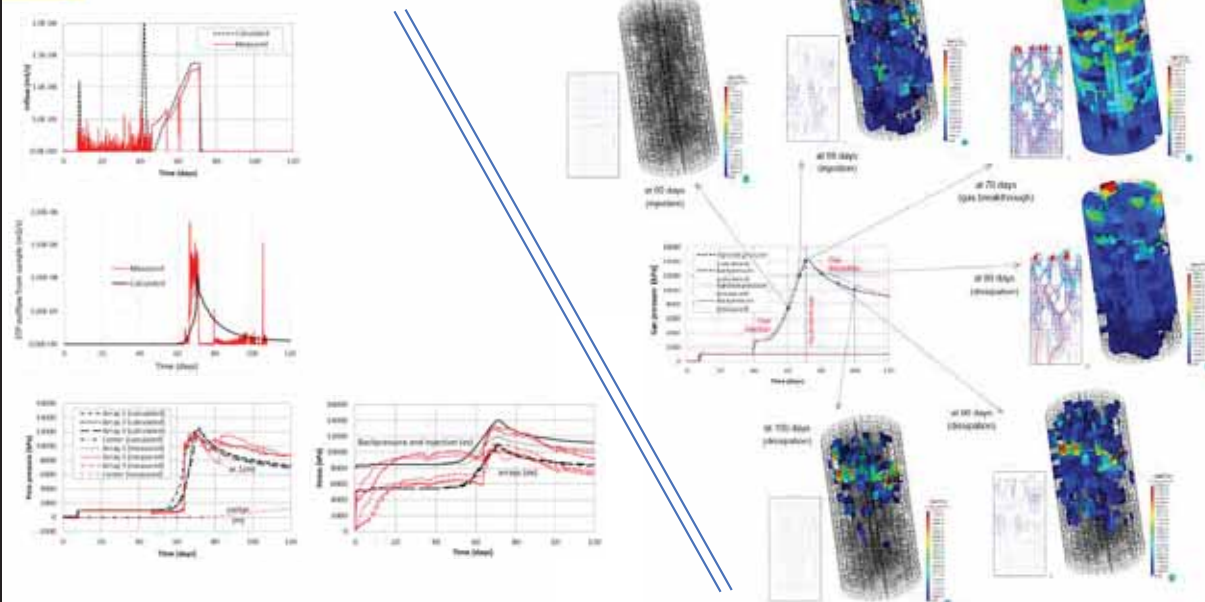
FINAL HM MODEL FOR STAGE 1A



eurad

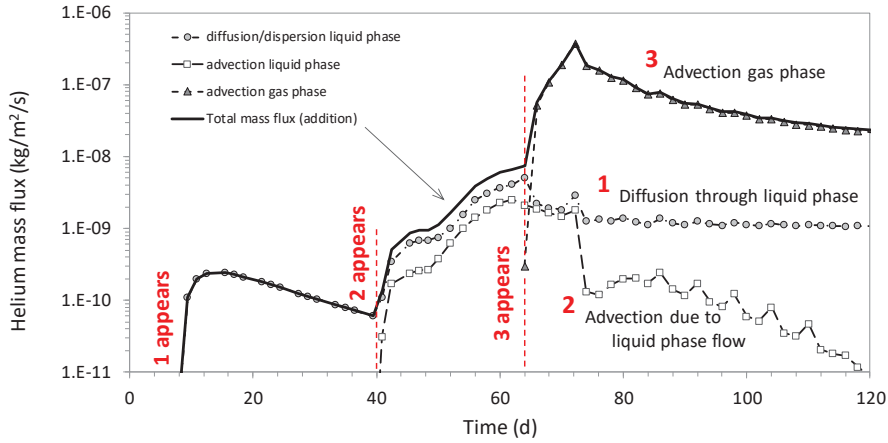
FINAL HM MODEL FOR STAGE 1A

Gas advection evolution and preferential gas paths generation



eurad

HELIUM FLUXES: DIFFUSIVE & ADVECTIVE

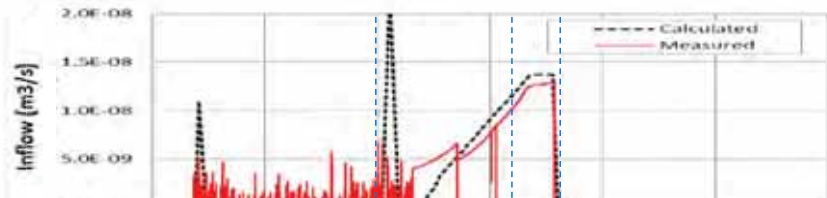
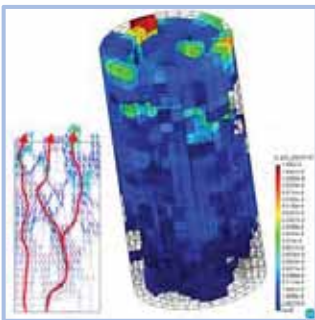


Complex flux combination:

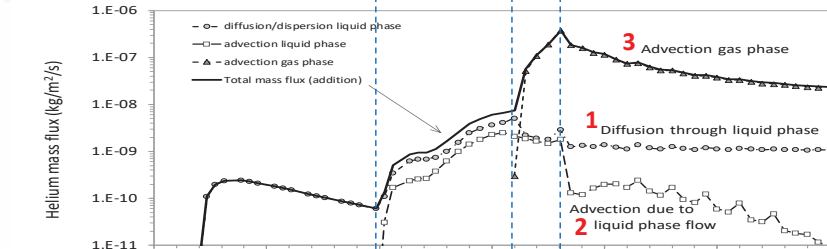
- from 10 to 40 days: dominated by **diffusion (1)** of Helium in water
- from 40 to 65 days: **combination** of diffusion/dispersion and liquid flux **advection (2)**
- from 65 to 121 days: dominated by **gas advective (3)** flux while liquid flux decays (and dispersion as well) and some diffusion remains



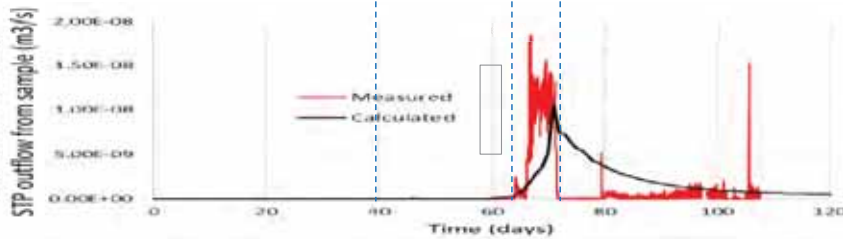
HELIUM FLUXES



Inflow
(into the system)

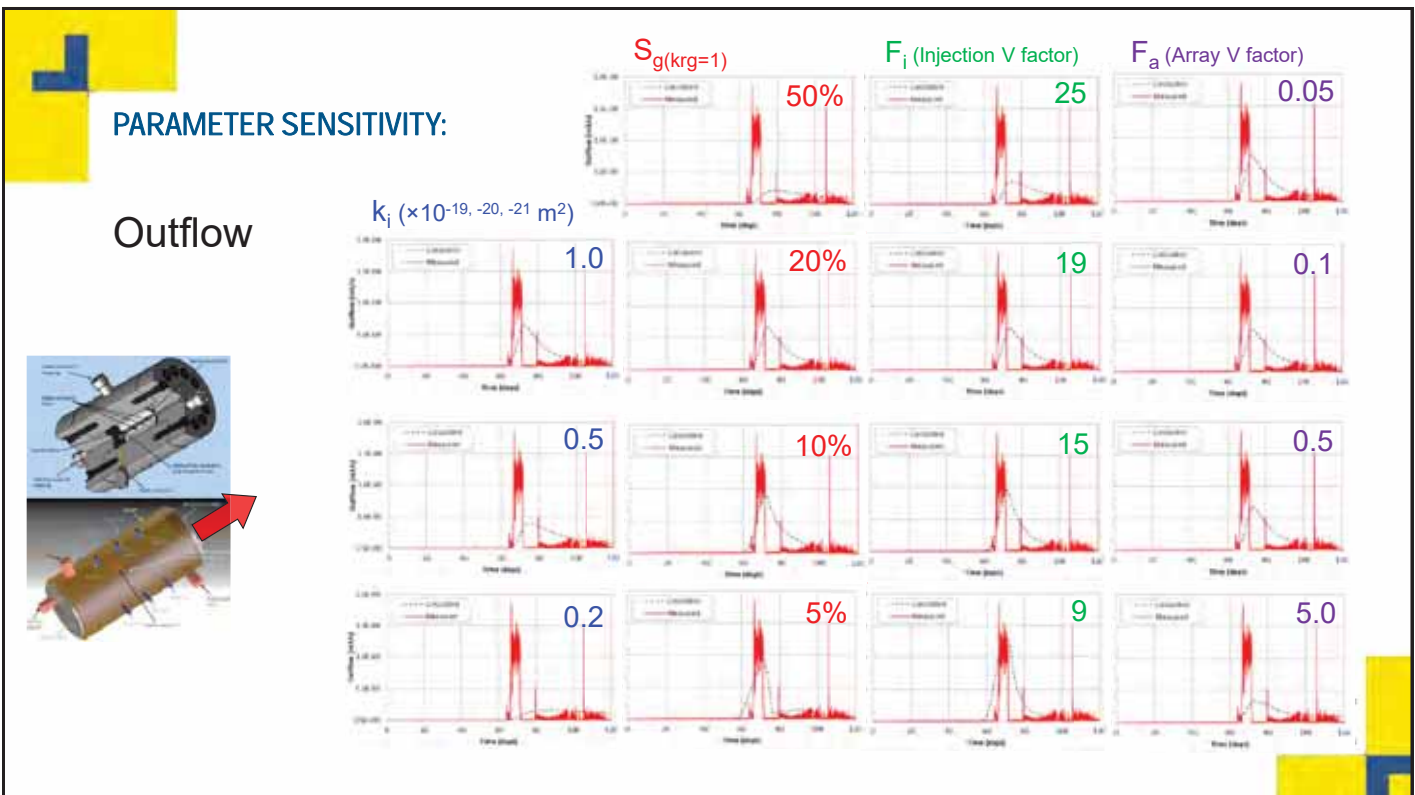
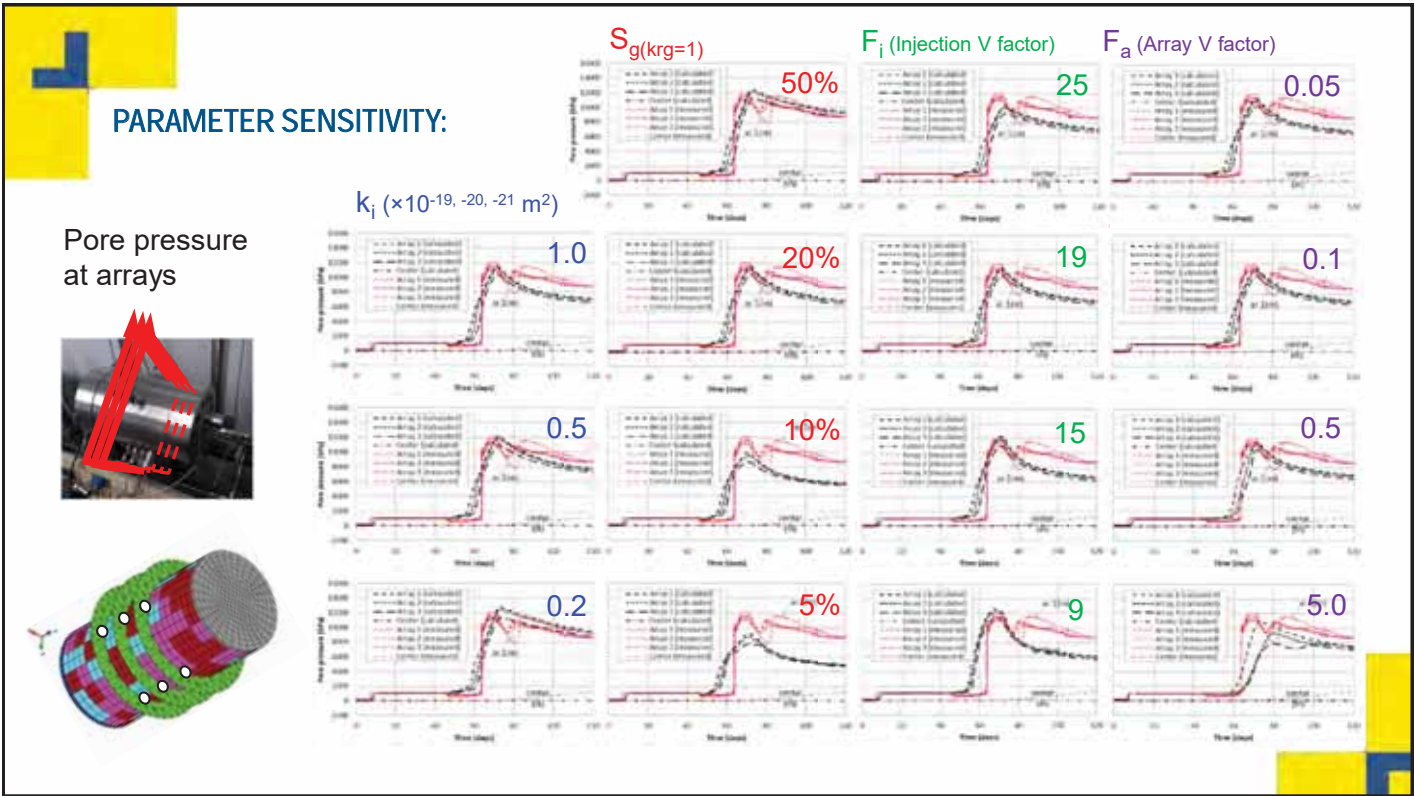


Mass
fluxes in
the sample

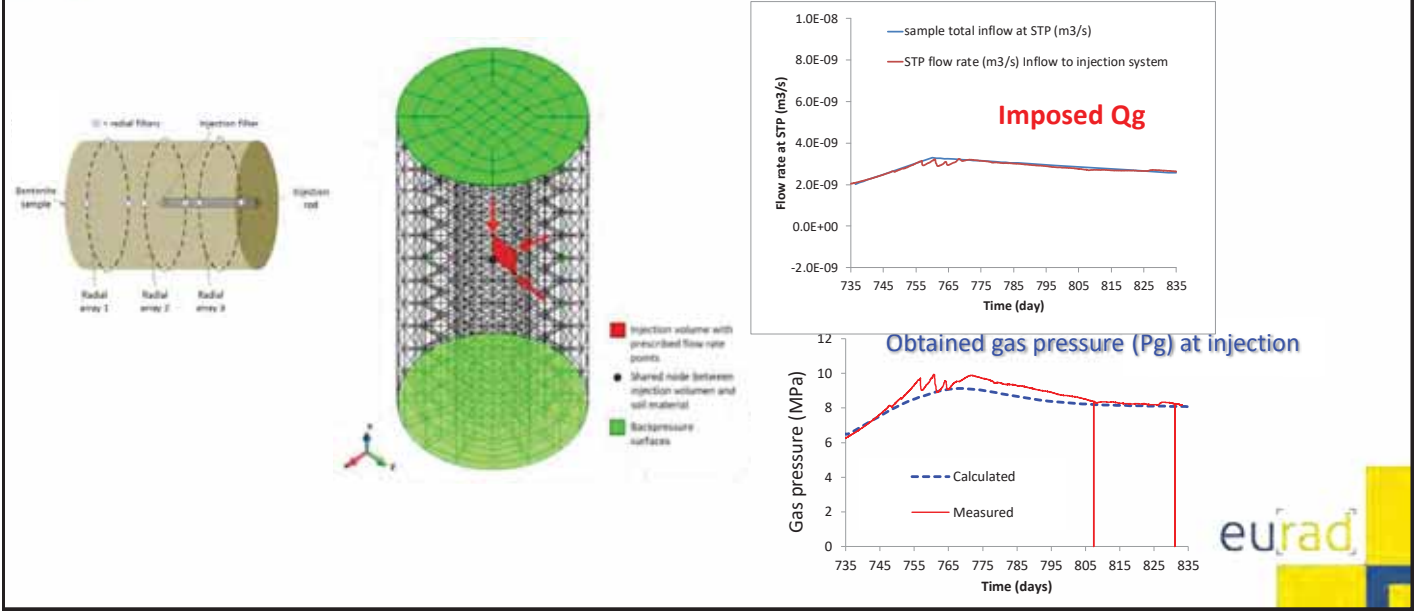


Outflow
(from the system)

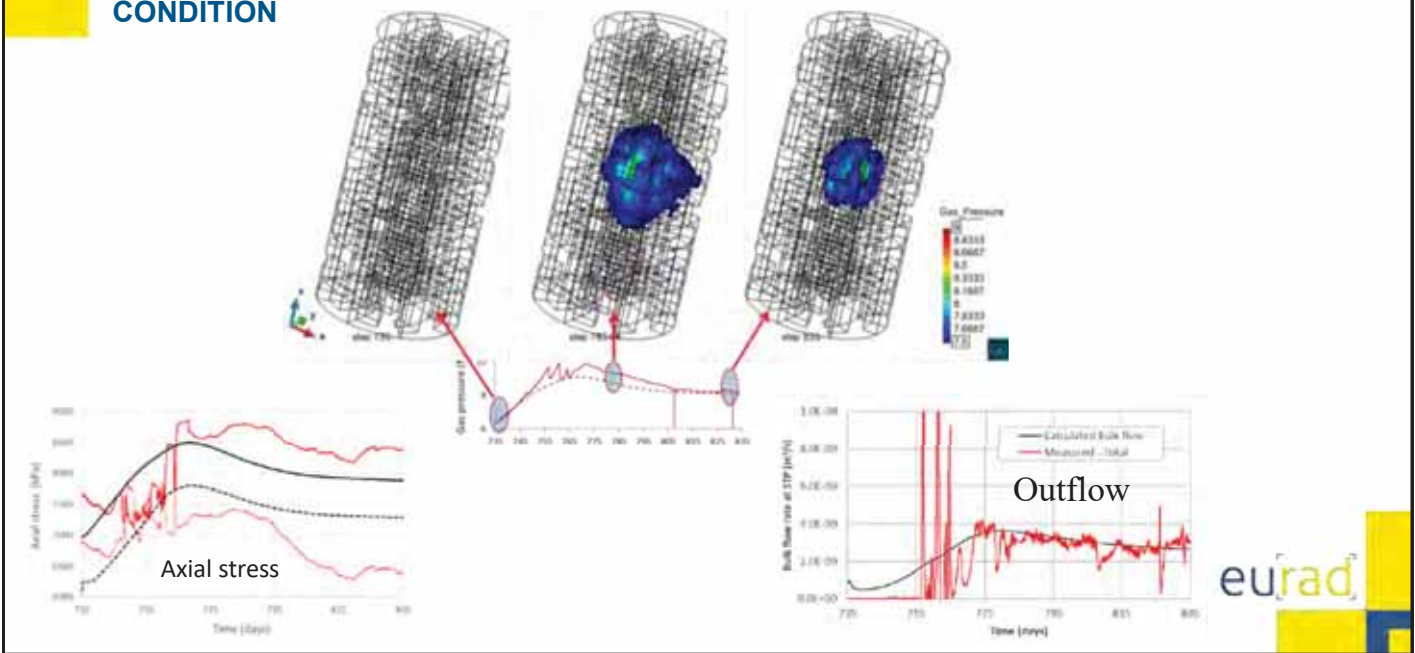




STAGE 2A: SPHERICAL FLOW UNDER A CONSTANT VOLUME BOUNDARY CONDITION



STAGE 2A: SPHERICAL FLOW UNDER A CONSTANT VOLUME BOUNDARY CONDITION



CONCLUDING REMARKS

- A single set of properties to model Stage 1A and 2A
- Additional volumes to represent injection system and arrays
- Injection flow rate prescribed as a target model condition
- Heterogeneity on intrinsic permeability and retention curve
- Embedded discontinuity model to simulate preferential path formation
- Relative permeability different for matrix and discontinuities



eu[rad]

CONTENTS

1. Fundamentals
2. Gas mixtures
3. Multiphase flow
4. Coupled deformation
5. Energy balance
6. Applications
7. Summary

eu[rad]

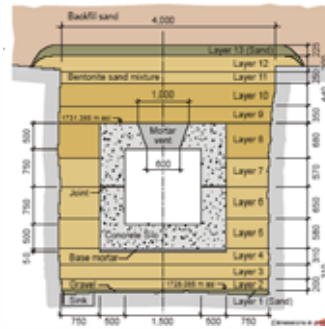
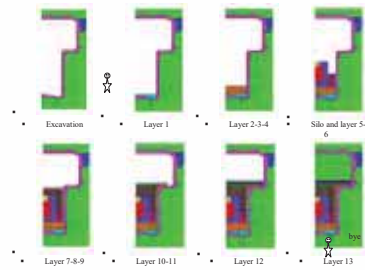
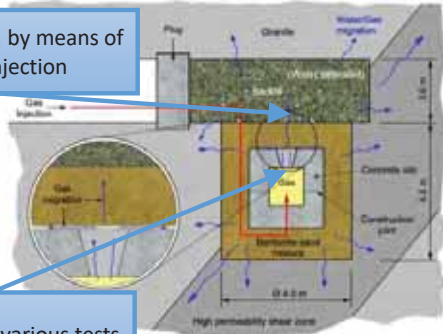
GAS FLOW. IN SITU EXPERIMENT AT GTS

Pressurization by means of water injection

Gas injection, various tests



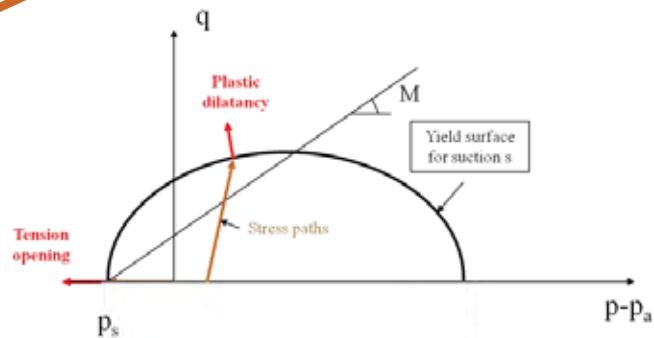
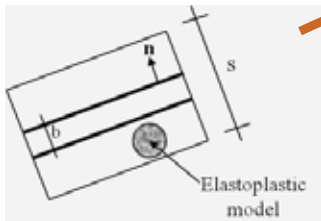
Olivella S. and E.E. Alonso, Gas flow through clay barriers, 2008, Geotechnique 58, No. 3, 157-176 [doi: 10.1680/geot.2008.58.3.157] GEOTECHNICAL RESEARCH MEDAL 2009



NORMAL DEFORMATIONS

- Model for damaged zone based on elastoplastic BBM
- Suction changes (drying-wetting) induces shrinkage/swelling
- Tensile strength depends on current suction

$$b = b_o + \Delta b \quad \text{and} \quad \Delta b = s \Delta \epsilon = s(\epsilon - \epsilon_o)$$



INTERFACE OPENING INDUCED BY PORE PRESSURE INCREASE

- Aperture changes are controlled by effective stress
- Interface opening is controlled by normal effective stresses
- If a confined material is permeable, no deformations take place as pore pressure is increased
- If a confined material is impermeable, interfaces tend to develop because of the compressibility of the buffer

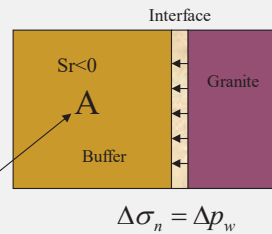
$$\sigma'_n = \sigma_n - \max(P_g, P_l) = \sigma_n - P$$

$$\Delta\sigma'_n = 0 = \Delta\sigma_n - \Delta P \Rightarrow$$

$$\Rightarrow \Delta\sigma_n = \Delta P$$

$$\Delta b \propto \Delta\epsilon_n \quad \Delta\epsilon_n \propto \Delta\sigma'_n$$

$$\begin{aligned} \Delta\sigma_A &= \Delta\sigma_n \\ \Delta p_{wA} &= 0 \\ \Delta\sigma'_A &= \Delta\sigma_n \end{aligned}$$



LARGE INTRINSIC PERMEABILITY VARIATIONS

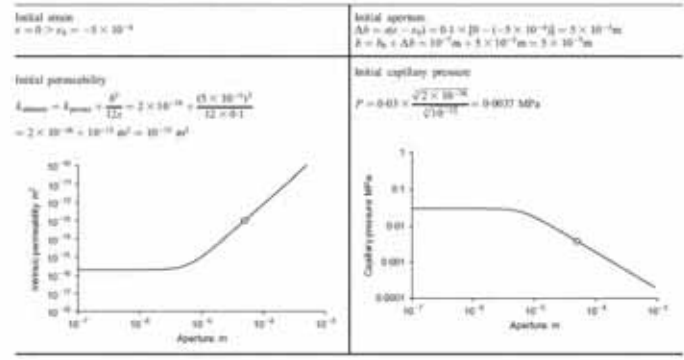
$$k_{element} = k_{fracture} \frac{b}{s} + k_{porous} \frac{s-b}{s} \cong \frac{b^3}{12s} + k_{porous}$$

$$P = P_o \frac{\sqrt[3]{k_{fracture-o}}}{\sqrt[3]{k_{fracture}}}$$

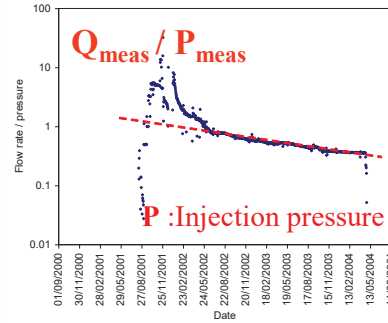
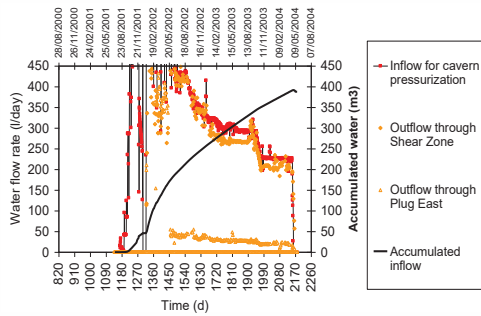
$$\begin{aligned} b &= b_o + \Delta b \\ \Delta b &= s\Delta\epsilon = s(\epsilon - \epsilon_o) \\ b &= b_o + s(\epsilon - \epsilon_o) \end{aligned}$$

$$s = a$$

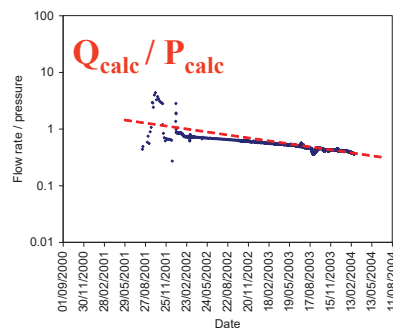
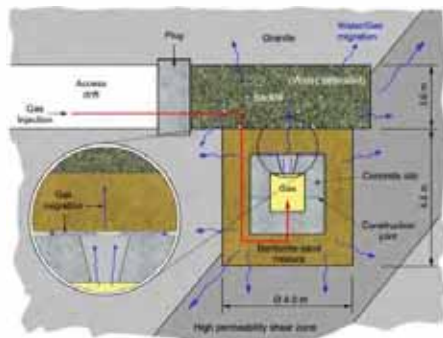
Table 4. Interface permeability and capillary pressure for GEM modelling



UPPER CAVITY PRESSURIZATION



Measured injected flow rate (l/d) divided by measured pressure (kPa) at PE/13/5/05

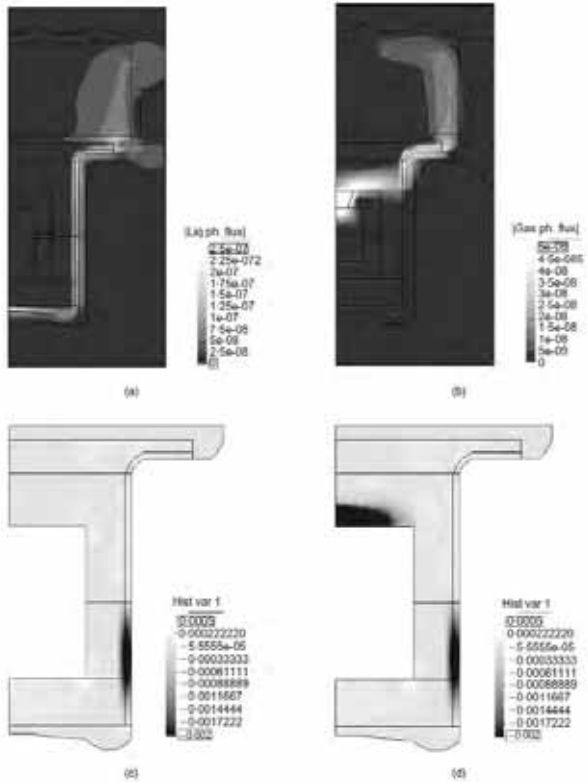


Calculated injected flow rate (l/d) divided by calculated pressure (kPa) at node 553

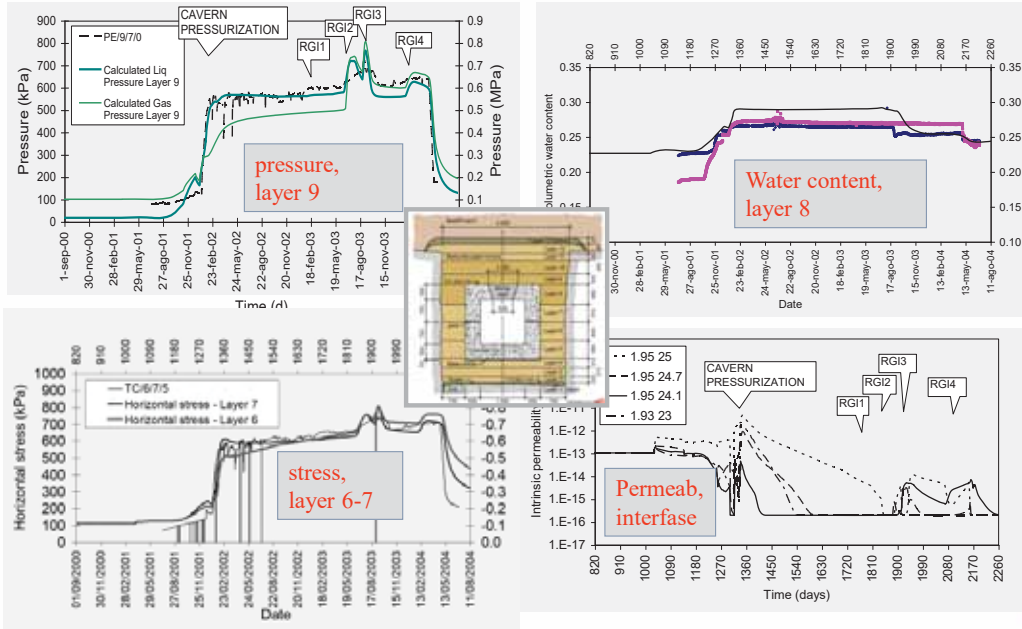


FLUXES AND DEFORMATIONS

- Calculated Water (left) and Gas (right) phase fluxes
- Zones that undergo irreversible deformations during Water (left) and Gas (right) injection



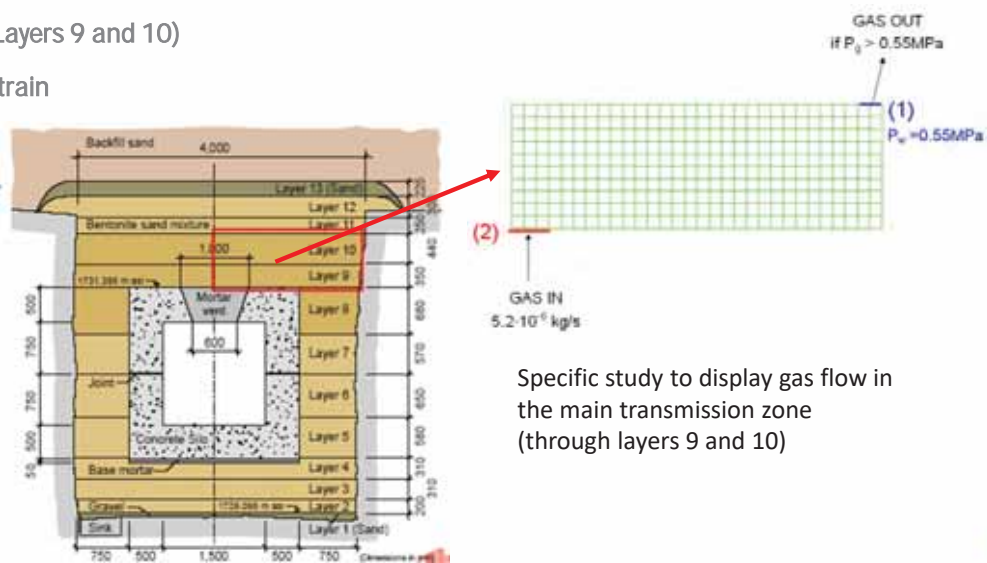
COMPARISON OF CALCULATED RESULTS AND MEASUREMENTS



eurad

GMT MAIN TRANSMISSION ZONE

- Mesh (Layers 9 and 10)
- Plane strain



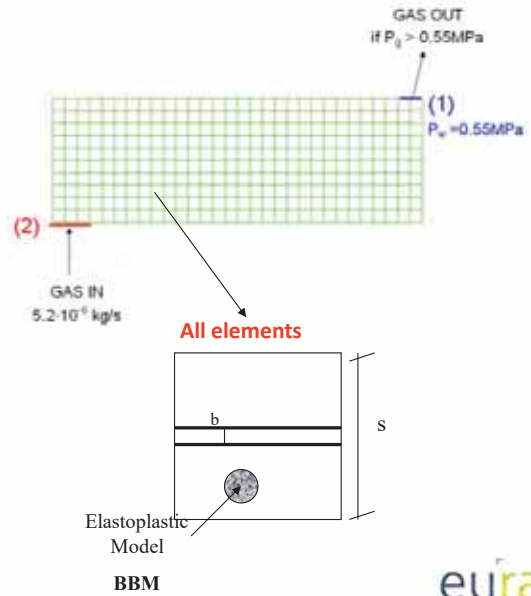
eurad

GMT MAIN TRANSMISSION ZONE

GMT
pressurization + RGI-3b gas injection stage

Analysis steps

time (days)	step	BC
0 – 1	initial	-
1 – 4	Pressuriz. ramp (0 to 0.55 MPa)	(1)
5 – 315 (- 4500)	Constant Pw (0.55 MPa)	(1)
315 – 318	Gas flux ramp (0 to 6.2e-5 kg/s)	(2)
318 – 4500	Constant gas flux (6.2e-5 kg/s)	(2)



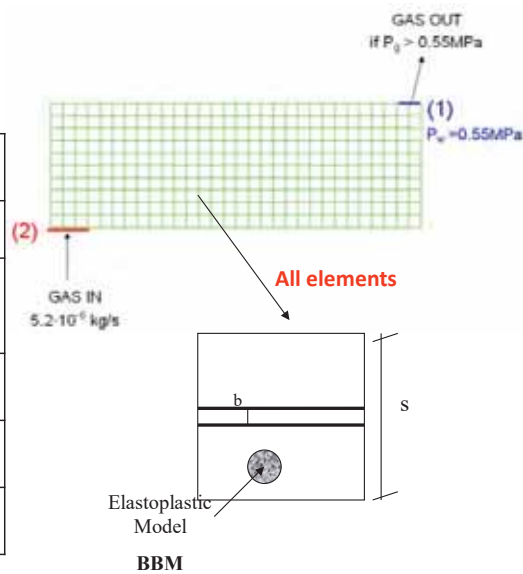
eurad

GMT Main transmission zone

GMT
pressurization + RGI-3b gas injection stage

Analysis steps

time (days)	step	BC
0-1	initial	-
1-4	Pressurization ramp (0-0.55MPa)	(1)
5-315 (-4500)	constant Pw (0.55MPa)	(1)
315-318	gas flux ramp (0-6.2e-5kg/s)	(2)
318-4500	constant gas flux (6.2e-5kg/s)	(2)



EMBEDDED FRACTURE PERMEABILITY

- Intrinsic fracture permeability (laminar flow):

$$k_{fracture} = \frac{b^2}{12}$$

- Equivalent fracture permeability:

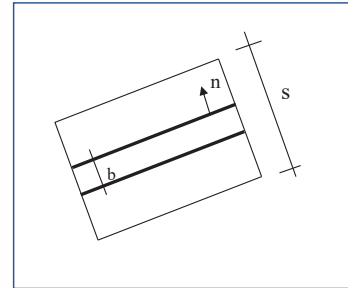
$$k_{equivalent} = k_{fracture} \frac{b}{s} = \frac{b^3}{12s} \quad (\text{Cubic Law})$$

- Equivalent element permeability:

$$k_{element} = k_{fracture} \frac{b}{s} + k_{matrix} \frac{s-b}{s} \cong \frac{b^3}{12s} + k_{matrix}$$

- Capillary air entry pressure:

$$P = P_o \frac{\sqrt[3]{k_{fracture_o}}}{\sqrt[3]{k_{fracture}}}$$



Aperture variations

$$b = b_o + \Delta b$$

$$\Delta b = s \Delta \epsilon = s(\epsilon - \epsilon_o)$$

Normal strain

Volumetric strain



GMT HETEROGENEOUS ANALYSIS

BBM parameters for S/B/Pb (Layers 9 and 10)

Parameter	Value
E (MPa)	50
ν	0.35
κ	0.0001
κ_s	0.001
λ (0)	0.049
r	7.0
β (MPa ⁻¹)	70
k	0.03
p_o^* (MPa)	0.267*
M	1.07
p_{s0}	0

Parameter	Value
k (m ²)	3.0x10 ⁻¹⁶
Reference porosity	0.3
Initial aperture, b_o (m)	1x10 ⁻⁷
Threshold strain, ϵ_o	1x10 ⁻³

*mean value



GMT HETEROGENEOUS ANALYSIS

Methodology to prepare the heterogenous field:

1. Random porosity field: Mean porosity $n = 0.3$ ($e_{mean} = 0.428$)

2. Compute $\varepsilon_v = -\frac{e - e_{mean}}{1 + e_{mean}}$

3. Obtain p_0^* (for BBM):

$$\frac{dp_0^*}{p_0^*} = \frac{1 + e_{mean}}{\lambda - \kappa} d\varepsilon_v \rightarrow p_0^* = p_{0mean}^* \exp\left(\frac{1 + e_{mean}}{\lambda - \kappa} \varepsilon_v\right)$$

n : porosity

p_0^* : pre-consolidation stress $p_{0mean}^* = 0.267$ MPa

k : initial matrix permeability

eurad

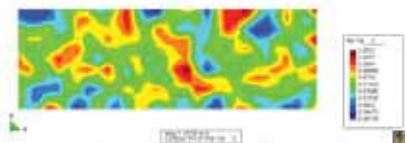
GMT HETEROGENEOUS ANALYSIS

- Initial Porosity. Uniform distribution, no spatial correlation. Porosity field: Var $\sim 1.0e-5$



- Initial field of $J_0^* = 3p_0^*$

$$p_{0mean}^* = 0.267 \text{ MPa}$$

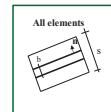


- Initial Permeability (log k)

$$b = b_0 + \Delta b \quad P = P_0 \sqrt[3]{\frac{k_{fracture, o}}{k_{fracture}}}$$

$$\Delta b = s \Delta \varepsilon = s(\varepsilon - \varepsilon_0)$$

$$k_{element} = k_{fracture} \frac{b}{s} + k_{matrix} \frac{s-b}{s} \cong \frac{b^3}{12s} + k_{matrix}$$

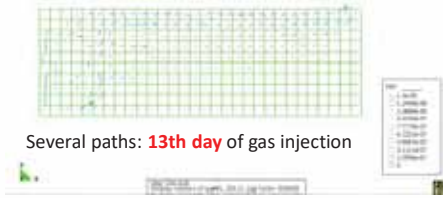


eurad

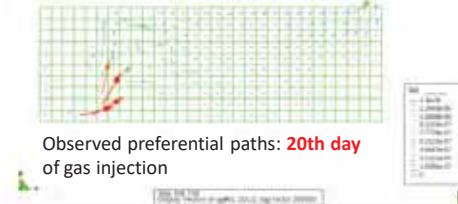
GMT HETEROGENEOUS ANALYSIS

Advective flow rate (m/s)

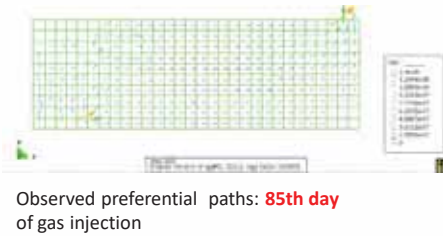
- GAS fluxes day 328



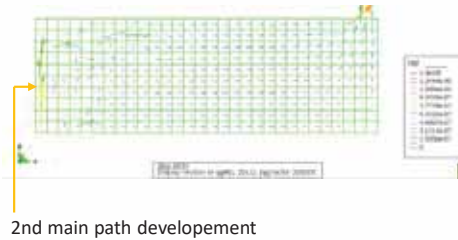
- GAS fluxes day 335



- GAS fluxes day 400



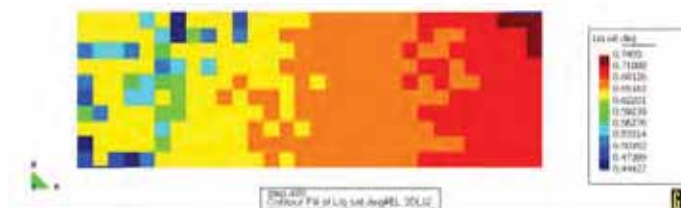
- GAS fluxes day 4500



eurad

GMT HETEROGENEOUS ANALYSIS

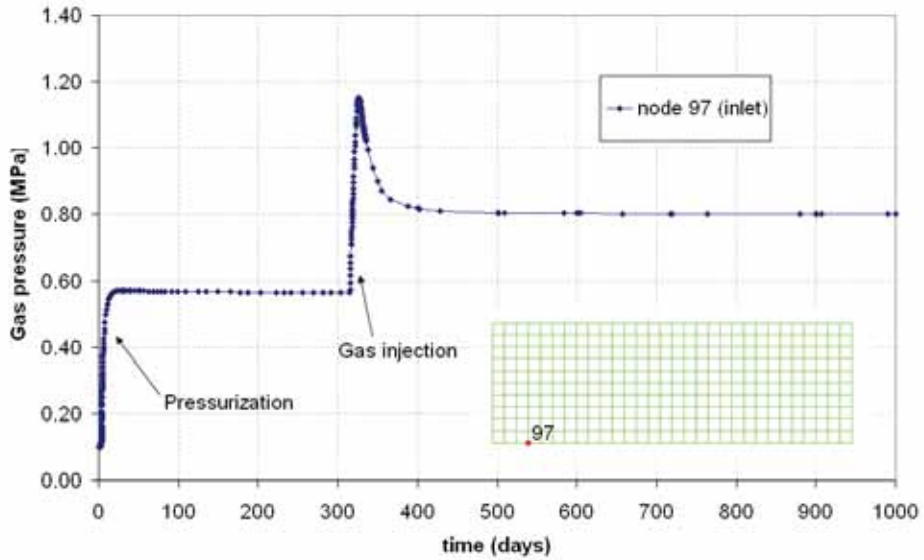
- Permeability (log k) and Degree of saturation: day 400
- Permeability increase. More than 2 orders of magnitude



eurad

GMT HETEROGENEOUS ANALYSIS

- Gas pressure evolution at inlet. (1):Water pressurization (2):Constant mass rate of gas injection

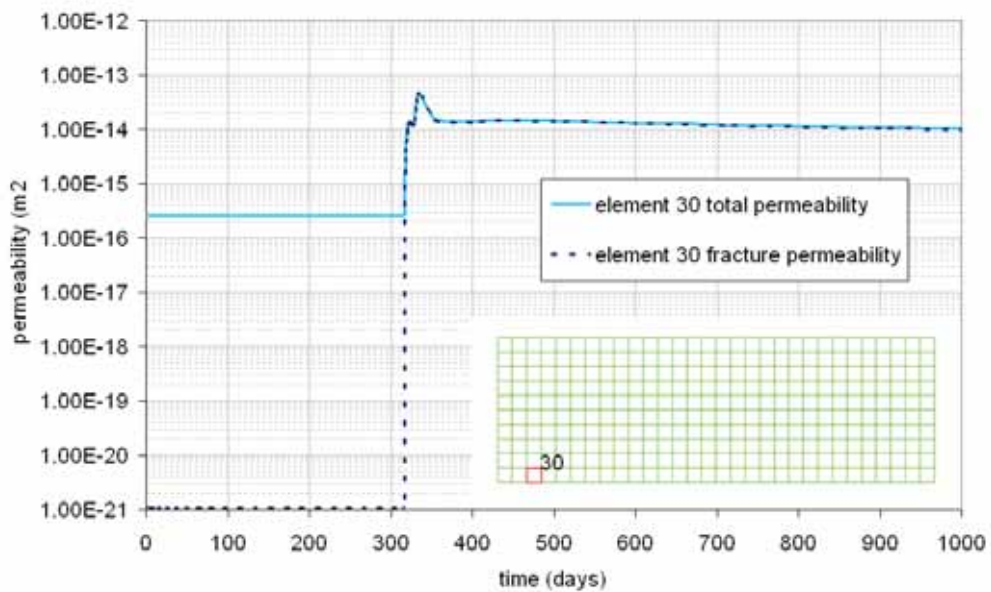


eurad

GMT HETEROGENEOUS ANALYSIS

Section 6: Applications

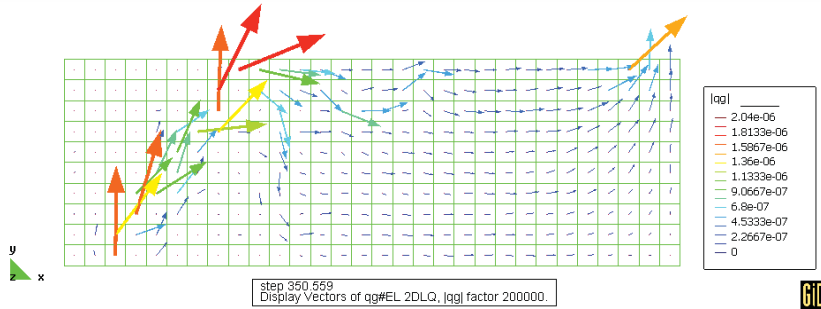
- Element permeability evolution



eurad

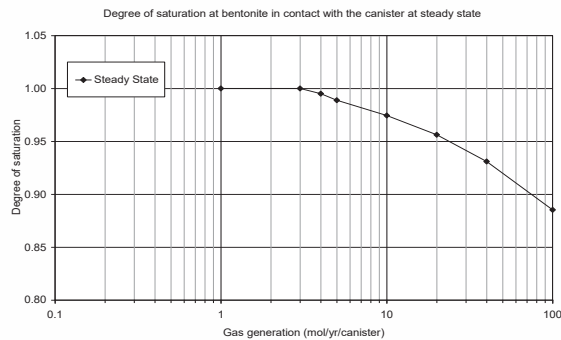
GMT HETEROGENEOUS ANALYSIS

- Preferential paths for SECOND simulation based on A different realization of the same random field
- GAS fluxes day 350



GAS GENERATION IN A REPOSITORY

- For a given repository scheme, the gas generation rate due to corrosion produces a certain condition of water distribution at steady state.
- A series of calculations were carried out for ANDRA
- In addition to gas generation rate, water consumption can be considered to affect the migration processes (oxidation of a metal consumes oxygen and produces hydrogen)





CONTENTS

1. Fundamentals
2. Gas mixtures
3. Multiphase flow
4. Coupled deformation
5. Energy balance
6. Applications
7. Summary



eurad



SUMMARY



- Gas migration in a repository is an issue to be investigated for the safety of a Spent Fuel Repository
- Gas generation in a SFR is due to corrosion of metals (oxygen is consumed and hydrogen generated)
- The transport processes are:
 - Diffusion/dispersion in the liquid phase
 - Advection as a two phase process in constant permeability porous media
 - Advection as a preferential path process in a deformable porous media
 - Gas diffusion/dispersion in the gas phase as a mixture of several components (usually neglected)
- The theoretical concepts have been described including Fundamentals, Gas mixtures, Multiphase flow, Coupled Deformation and Energy balance.
- Three applications have been presented:
 - Simulation of gas flow lab experiments in anisotropic clay rock
 - Simulation of gas flow lab experiments in bentonite
 - Simulation of gas flow in situ experiment in a scheme based on sand bentonite mixture



eurad



Appendix O. In situ thermo-hydro-mechanical experiment on poorly indurated clays (A. Dizier)




IN SITU THM TESTING AT HIGH TEMPERATURE

Poorly indurated clays (Boom Clay)

January 24, 2020 • Arnaud Dizier, Guangjing Chen, Jan Verstricht, Xiang-Ling Li and EURIDICE Team



The project leading to this application has received funding from the European Union's Horizon 2020 research and innovation programme under grant agreement n° 847593.



1



EIG EURIDICE

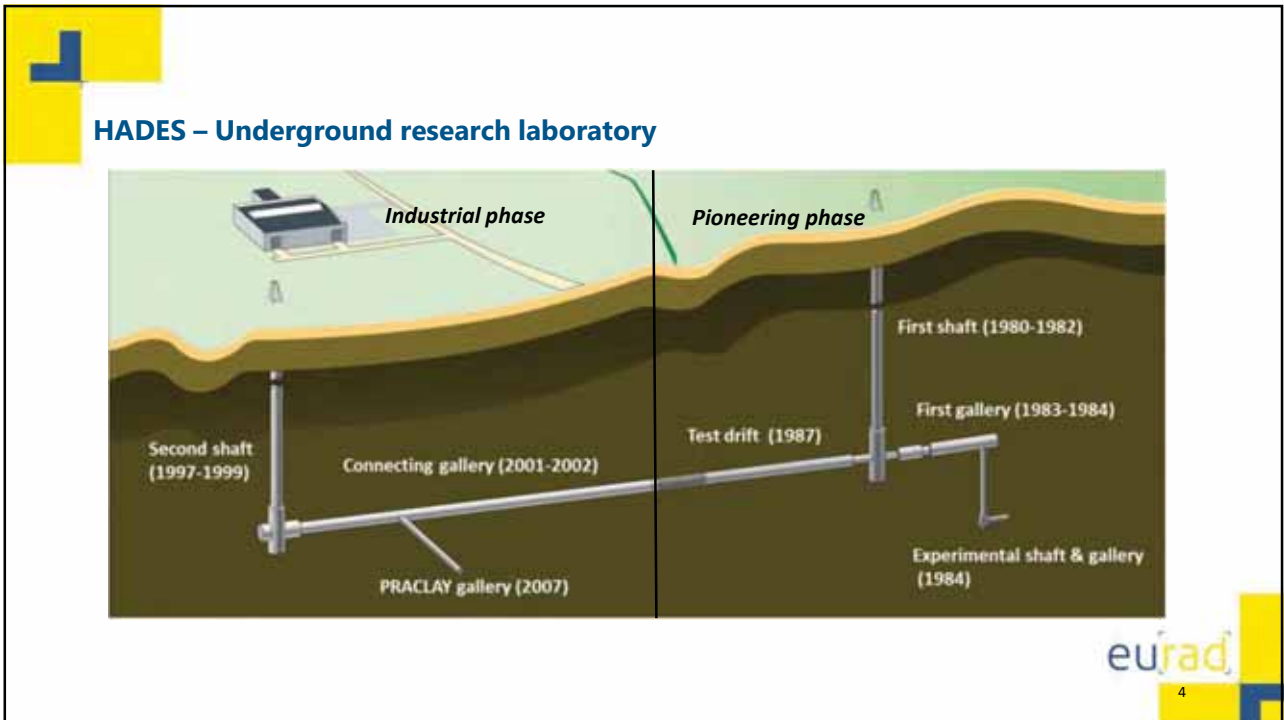
European Underground Research Infrastructure for Disposal of radioactive waste in Clay Environment



2



3



4

HADES – Underground research laboratory

Industrial phase (after 2000)



Pioneering phase (1980 – 1990)



eu|rad

5

5

CONTENT

- **General considerations on Boom Clay**
- **In situ thermo-hydro-mechanical testing**
 - **ATLAS heater test**
 - **Large scale PRACLAY heater test**

eu|rad

6

6

CONTENT

- **General considerations on Boom Clay**
- **In situ thermo-hydro-mechanical testing**
 - **ATLAS heater test**
 - **Large scale PRACLAY heater test**

eurad

7

7

BOOM CLAY: GEOLOGICAL CONTEXT

- **Boom Clay Formation: Rupelian, early Oligocene (± 30 Ma)**
 - **At the level of the laboratory : thickness of ~ 100 m, depth 185 – 287 m**



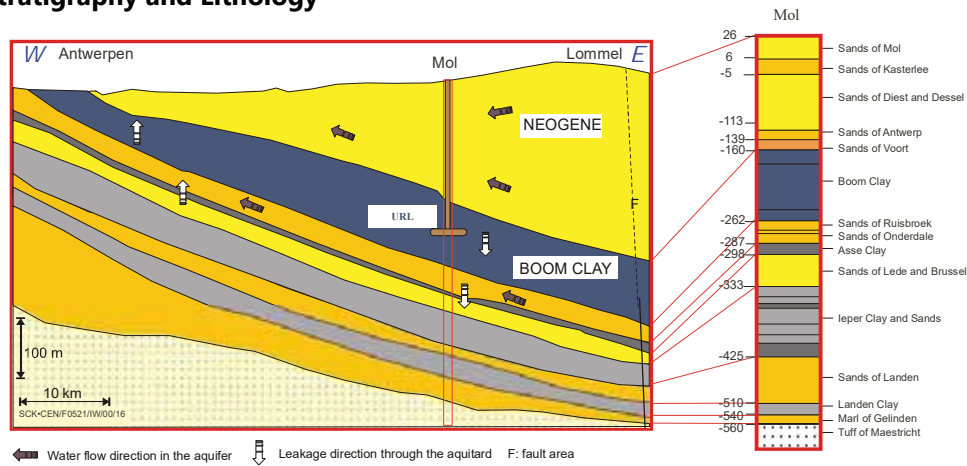
eurad

8

8

BOOM CLAY: GEOLOGICAL CONTEXT

- **Stratigraphy and Lithology**



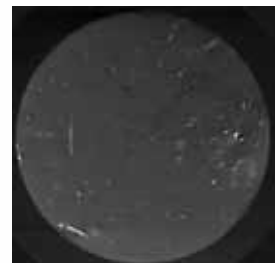
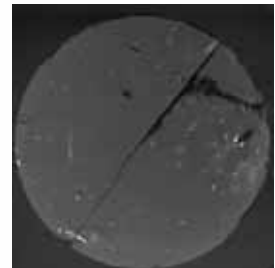
eurad

9

9

BOOM CLAY: POTENTIAL HOST ROCK ?

- **Boom Clay as a potential host rock for high level radioactive waste disposal**
 - **Geology: low seismic activities, no volcanic activities, no tectonic activities (uplift, faulting...)**
 - **Good hydrogeological conditions: very low hydraulic conductivity**
 - **Plastic clay, capacity of self-sealing/ self-healing**
 - **Good geochemical conditions for the sorption of the radionuclides on clay minerals**



eurad

10

10

BOOM CLAY: PHYSICAL CHARACTERISATION

Mineralogical composition [%]	De Craen et al., 2004
Clay minerals	30 – 60%
Illite	10 – 45%
Smectite + illite/smectite ML	10 – 30%
Kaolinite	5 – 20%
Chlorite	0 – 5%
Chlorite/smectite ML	0 – 5%
Quartz	15 – 20%
K-Feldspars	1 – 10%
Albite	1 – 10%
Carbonates	1 – 5%
Calcite	1 – 5%
Siderite	Present
Dolomite	Present
Ankerite	Present
Organic Carbon	1 – 5%
Others	
Glauconite, apatite, rutile, anatase, ilmenite,	Present
Zircon, monazite, xenotime	Present

eurad

11

11

BOOM CLAY: PHYSICAL CHARACTERISATION

- **Geotechnical properties:**
 - Porosity : 0.39
 - Soil density : 1900 - 2100 [kg/m³]
 - Plastic limit : 13 – 26.5 %
 - Liquid limit : 55 - 80 %
 - Water content : 20 – 30 wt% (dry weight)
- **Hydraulic characteristics:**
 - Hydraulic conductivity $K = 2 - 4 \cdot 10^{-12}$ m/s
- **Thermal characteristics:**
 - Thermal conductivity $\lambda = 1.35 - 1.7$ W.m⁻¹.K⁻¹

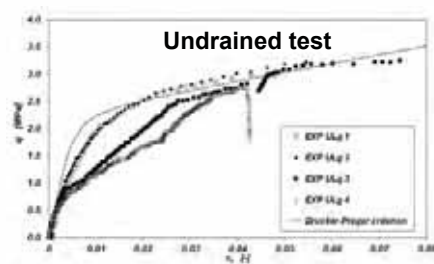
eurad

12

12

BOOM CLAY: PHYSICAL CHARACTERISATION

- **Geotechnical characteristics (Bernier et al., 2007)**
 - Poisson's coefficient ν' : 0.125
 - Young Modulus E' : 300 MPa
 - Cohesion c' : 300 kPa
 - Friction angle ϕ' : 18°
 - Dilatancy angle ψ' : 0° - 10°



CONTENT

- **General considerations on Boom Clay**
- **In situ thermo-hydro-mechanical testing**
 - ATLAS heater test
 - Large scale PRACLAY heater test

LONG HISTORY OF IN SITU TEMPERATURE TESTING

- **First test aiming at simulating a vitrified high level waste canister in a clay quarry in Terhagen before 1980**
- **In the underground research laboratory**
 - BACCHUS I, II (1988 - 1995)
 - CERBERUS (1985 - 1999)
 - CACTUS I, II (1990 - 1994)
 - ATLAS I, II, III, IV (1992 -...)
 - PRACLAY (2014-...)



eurad

15

15

CONTENT

- **General considerations on Boom Clay**
- **In situ thermo-hydro-mechanical testing**
 - **ATLAS heater test**
 - **Large scale PRACLAY heater test**

eurad

16

16

THM EXPERIMENTS IN HADES – ATLAS

- Small scale heater tests ATLAS I-II, III & IV
(Admissible Thermal Loading for Argillaceous Storage)

- Objectives:

➔ Validate and/or improve knowledge on Boom Clay THM behaviour by studying in-situ thermal properties and anisotropy

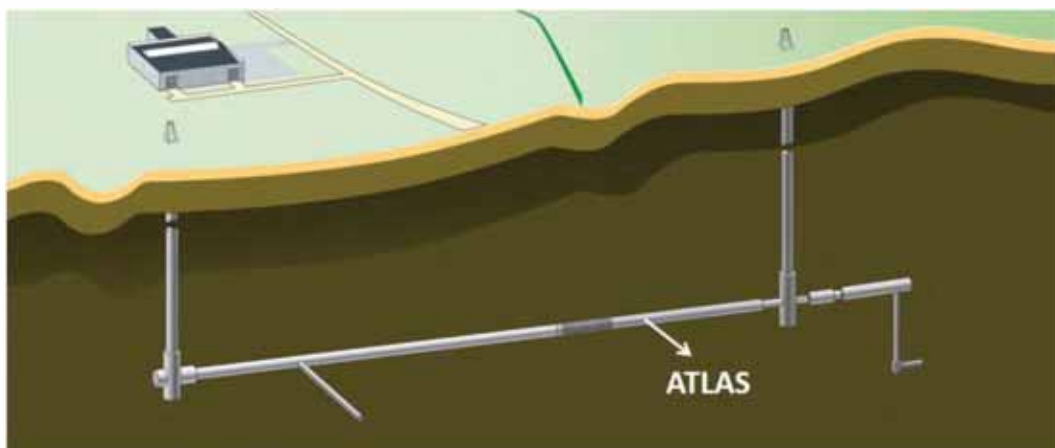
- Assess/ confirm the thermal properties of Boom Clay
 - Especially the thermal conductivity λ [W/(m·°C)]
- Investigate T→HM coupling in Boom Clay
 - A simple THM experiment
 - 1 Heater, several observation boreholes
 - Focus is only on the behaviour of the Boom Clay
 - No radioactive source (CERBERUS)
 - No backfill material (BACCHUS) or simulated Engineered Barrier System (EBS)

eurad

17

17

THM EXPERIMENTS IN HADES – ATLAS



eurad

18

18

THM EXPERIMENTS IN HADES – ATLAS

8 m 11 m
2.7 m

Test drift
Heater
Observation boreholes

Illustration ATLAS III experiment

1.5 m
2.7 m
1.3 m

euRad 19

19

THM EXPERIMENTS IN HADES – ATLAS

- **ATLAS instrumentation :**
 - Kulite pressure sensors on the heating probe
 - Piezometer filter
 - Flat-jacks and biaxial stressmeter

Central borehole with the heating probe

Illustration of a piezometer filter with twin tube connection

Illustration of an instrumented casing

Flat-jacks Biaxial Stressmeter

euRad 20

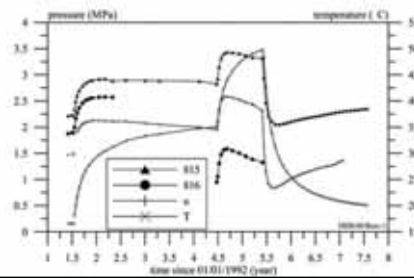
20

THM EXPERIMENTS IN HADES – ATLAS

• ATLAS heater tests: 4 tests in 2 stages

• ATLAS I-II

- 2 observation boreholes drilled in the same horizontal plane than the heater
- 3 years of heating at 112W/m (ATLAS I) + 1 year of heating at 225W/m (ATLAS II) (1993 – 1997). Cooling in one step.
- Limitations:
 - Relatively little instrumentation and low data acquisition rate (manual)
 - Sharp heating transients



eurad

21

21

THM EXPERIMENTS IN HADES – ATLAS

ATLAS heater tests: 4 tests in 2 stages

• ATLAS III & IV

- Additional boreholes (horizontal and inclined) + Additional T & p_w sensors
- Stepwise heating in 1 year: 0 → 50 → 112 → 175 W/m. Cooling in one step.
- Same heating strategy for ATLAS III (2007 – 2008) and ATLAS IV (2011 – 2012)
- Improvements:
 - High data acquisition rate
 - Investigation of thermal anisotropy

→ representative of far field

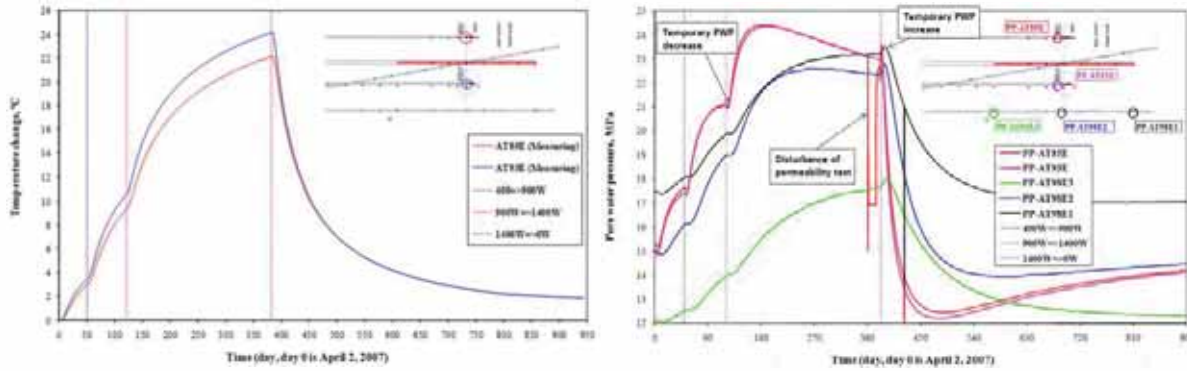
eurad

22

22

THM EXPERIMENTS IN HADES – ATLAS III

- ATLAS III: Temperature and pore water pressure evolution

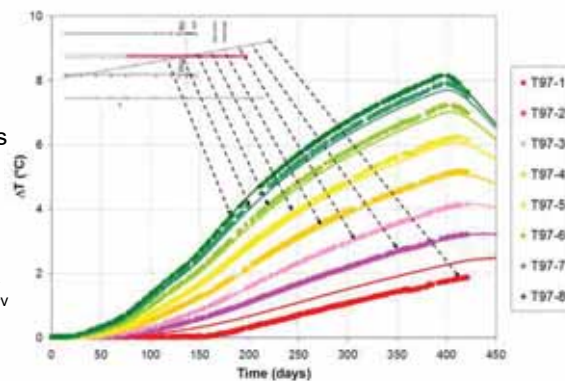


THM EXPERIMENTS IN HADES – ATLAS III

- ATLAS III: Temperature and pore water pressure evolution

Modelling (3D FEM)

- Anisotropic Thermo-hydro-poro-elastic model: transverse isotropic elasticity
- Heat transport (conduction)
- Model parameter values:
 - Consistent with previous studies
 - Limited optimisation except elastic moduli (far field)
 - Valid transverse anisotropy of intrinsic permeability: $K_h \approx 2 \times K_v$



THM EXPERIMENTS IN HADES – ATLAS III

- **ATLAS III: Temperature and pore water pressure evolution**

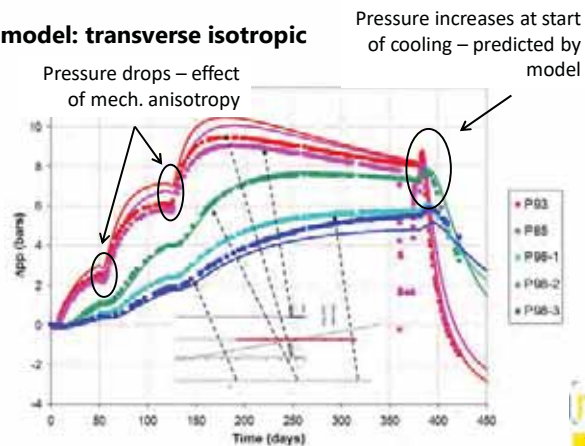
Modelling (3D FEM)

- **Anisotropic Thermo-hydro-poro-elastic model: transverse isotropic elasticity**

- **Heat transport (conduction)**

- **Model parameter values:**

- Consistent with previous studies
- Limited optimisation except elastic moduli (far field)
- Valid transverse anisotropy of intrinsic permeability: $K_h \approx 2 \times K_v$



rad
25

25

THM EXPERIMENTS IN HADES – ATLAS

- **Main learnings from ATLAS experiments on the far field Boom Clay behaviour**

- Anisotropic thermal conductivity of Boom Clay well estimated
- Importance of small strain stiffness characteristics in the far field and of the cross anisotropy in THM coupling
- Quite insignificant effect of thermo-plasticity in the far field

→ Validation of thermo-elastic model & THM parameters

- Predictive capability of modelling: temperature & pore water pressure evolutions of ATLAS III well captured by models
- ATLAS IV yields identical results to ATLAS III (no irreversible processes)

Limitations of the ATLAS experiments

- Small-scale → no information on pore water pressure and stress evolutions in the EDZ – near field

eurad
26

26

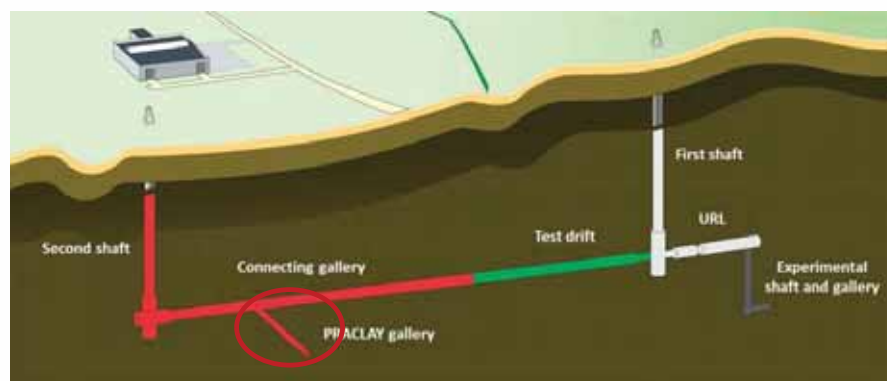
CONTENT

- General considerations on Boom Clay
- In situ thermo-hydro-mechanical testing
 - ATLAS heater test
 - Large scale PRACLAY heater test

27

THE LARGE-SCALE PRACLAY HEATER TEST

- The PRACLAY in – situ Experiment in URL HADES:
 - Demonstrating the feasibility of geological disposal of high-level radioactive waste in clay formation

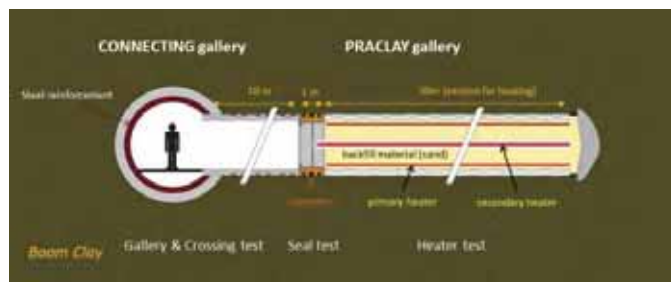


28

THE PRACLAY EXPERIMENT – OBJECTIVES AND DESIGN

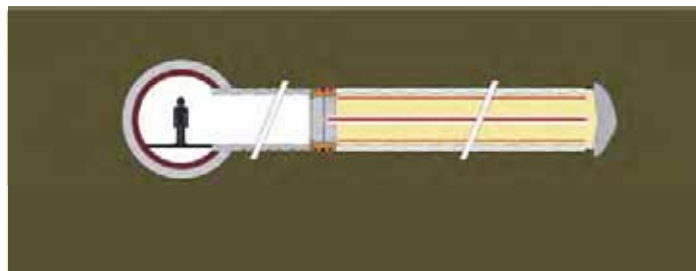
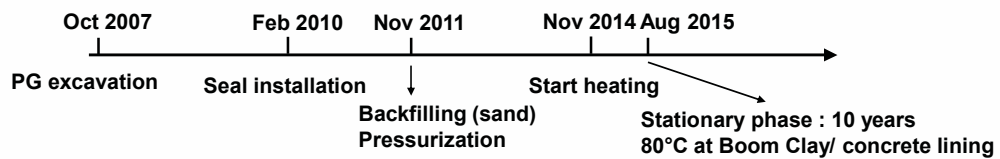
• The PRACLAY in – situ Experiment in URL HADES

- Gallery and Crossing test
 - Feasibility of constructing a gallery with industrial techniques
 - Feasibility of constructing a crossing between two galleries
- Seal test → Design and installation of the hydraulic seal
- Large scale-heater test → Simulate the heat-emitting high-level radioactive waste



29

THE PRACLAY EXPERIMENT - PHASES



euRad

30

30

PRACLAY GALLERY EXCAVATION

• excavation and gallery lining works (2007)

- Lining designed for geotechnical and thermal loads
- Segmental tunnel lining (wedge blocks technique, 8 segments and one key)
- Compressive materials



eurad

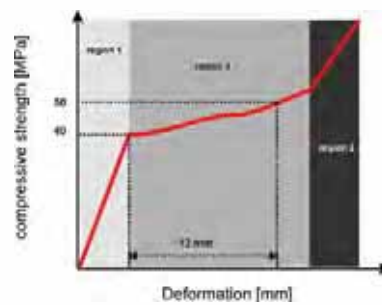
31

31

PRACLAY GALLERY EXCAVATION

• excavation works (2007)

- Installation of foam panels



eurad

32

32

PRACLAY GALLERY EXCAVATION

- **excavation works (2007)**
 - open-face tunnel boring machine
 - rotary erector



eurad

33

33

PRACLAY GALLERY EXCAVATION

- **excavation works (2007)**
 - Crossing with the installation of a steel reinforcement ring



eurad

34

34

PRACLAY GALLERY EXCAVATION



35

PRACLAY GALLERY EXCAVATION



36

PRACLAY GALLERY EXCAVATION



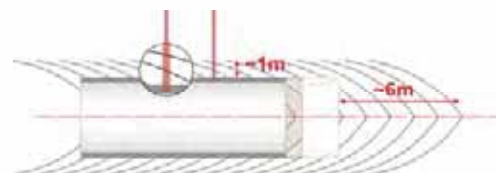
eu|rad

37

37

PRACLAY GALLERY EXCAVATION

Excavation induced fractures: gallery side-wall



Observations during the excavation
of the Connecting gallery

eu|rad

38

38

PRACLAY GALLERY EXCAVATION

- **excavation works (2007)**
 - Installation of a temporary lining for the hydraulic seal

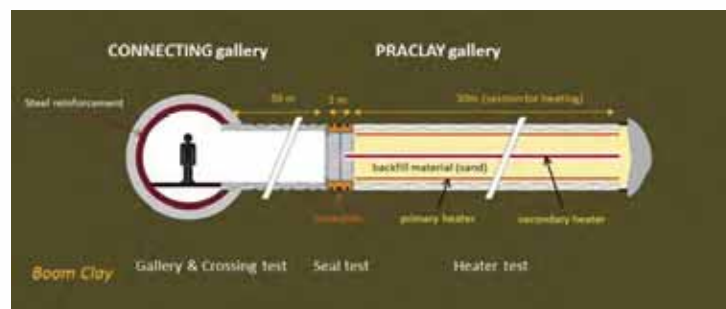
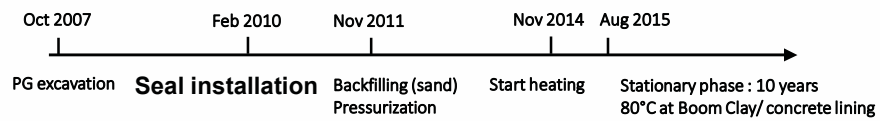


eurad

39

39

THE PRACLAY EXPERIMENT - PHASES



eurad

40

40

PRACLAY GALLERY – HYDRAULIC SEAL INSTALLATION



eu|rad

41

41

PRACLAY GALLERY – HEATER SYSTEM, BACKFILLING



eu|rad

42

42

THE PRACLAY EXPERIMENT – OBJECTIVES AND DESIGN

• The PRACLAY Heater Test – general objectives

- Examine the combined impact of hydro-mechanical disturbances caused by gallery construction and a large-scale thermal load on the Boom Clay due to heat-emitting high-level waste
 - Design independent
 - Conditions and dimensions that are representative for a real repository
 - Confirm and refine the already scientific bases
- To be sure that poorly indurated clay like the Boom Clay retains its ability to contain radioactive waste when it is heated
 - ✓ Low water permeability and no open fractures
 - ✓ Visco-elasto-plastic clay (Self-sealing properties)
 - ✓ High sorption capacities for radionuclides

euRad

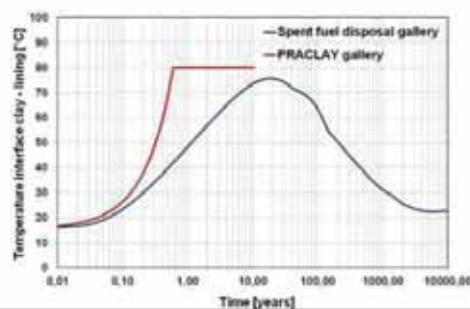
43

43

THE PRACLAY EXPERIMENT – OBJECTIVES AND DESIGN

• The PRACLAY Heater Test – design

- Thermal conditions
 - Temperature at gallery extrados = 80°C
 - Faster temperature increase
 - Heating during 10 years (or more)
 - Heated gallery section = 30 m (no gain in test representativeness by longer length)
- } More penalizing conditions



euRad

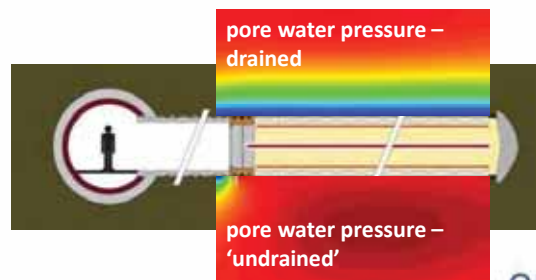
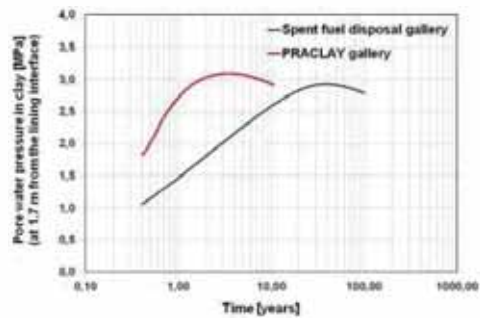
44

44

THE PRACLAY EXPERIMENT – OBJECTIVES AND DESIGN

- **The PRACLAY Heater Test – design**

- Hydraulic conditions
 - As much undrained as possible (more penalising : the higher the pore pressure build-up during heating, the higher the risk of damage/failure for host clay formation)



eurad

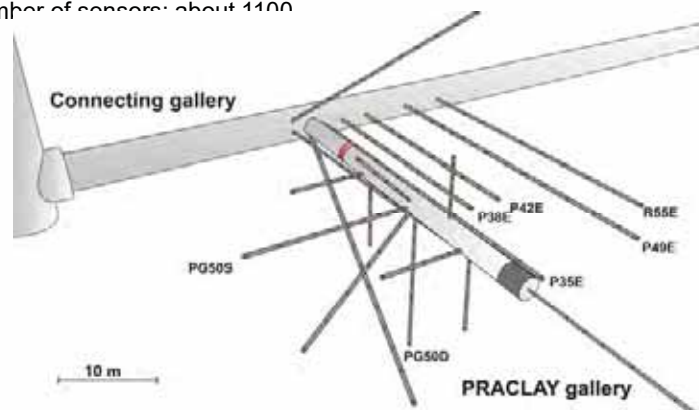
45

45

THE PRACLAY EXPERIMENT - MONITORING

- **Monitoring network: temperature, pore water pressure, stresses...**

- Number of sensors: about 1100



eurad

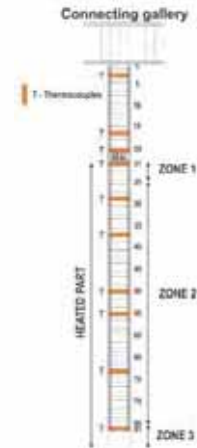
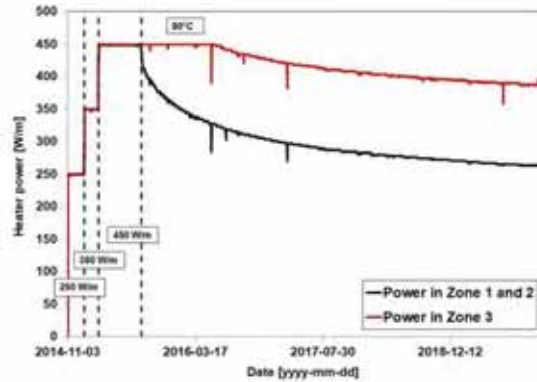
46

46

THE PRACLAY EXPERIMENT – HEATING

- **PRACLAY thermal loading plan:**

- 3 heating steps to reach 80°C at Boom Clay/ concrete lining interface
- 250 W/m representative from a real repository



eu^{rad}

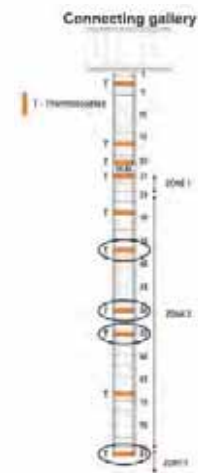
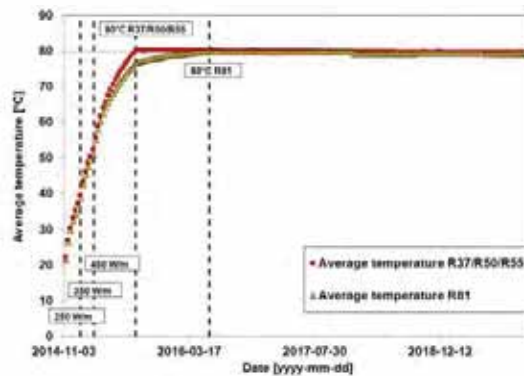
47

47

THE PRACLAY EXPERIMENT - HEATING

- **PRACLAY thermal loading plan:**

- Increase of the temperature in the concrete lining
- Current situation: 80°C at Boom Clay/ lining interface



eu^{rad}

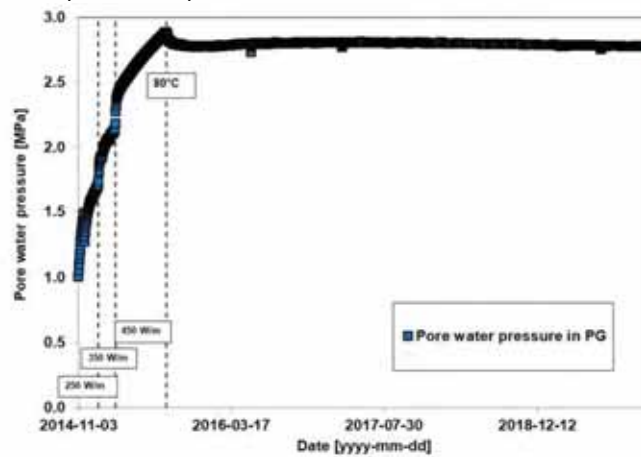
48

48

THE PRACLAY EXPERIMENT - HEATING

- **PRACLAY thermal loading plan:**

- Increase of the pore water pressure inside PG



Pressurization process:
Initial pore pressure in PG = 1 MPa

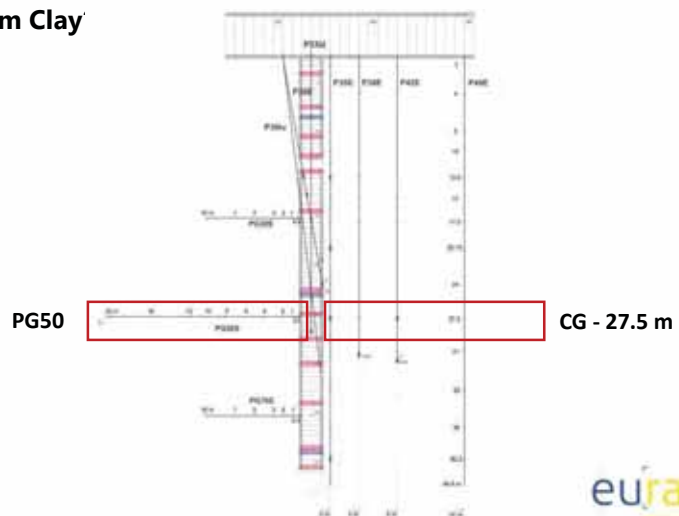
eurad

49

49

THE PRACLAY EXPERIMENT - OBSERVATIONS

- **What do we observe in the Boom Clay**



eurad

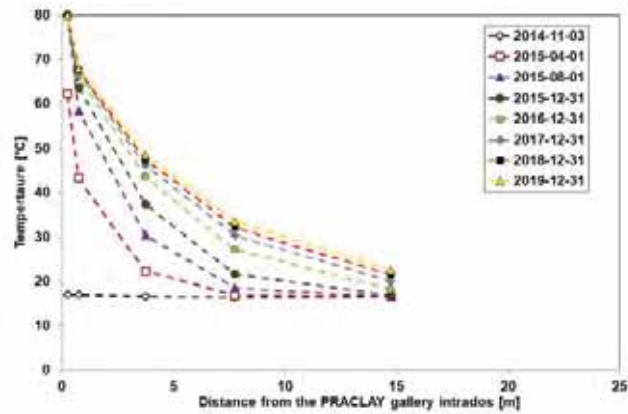
50

50

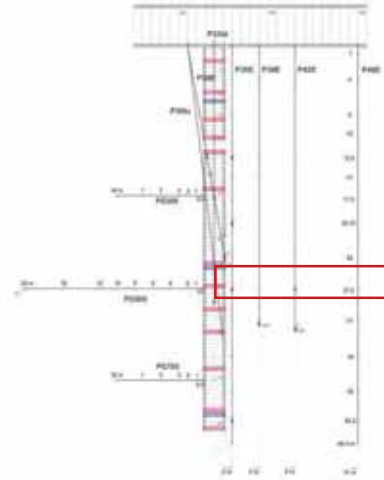
THE PRACLAY EXPERIMENT - OBSERVATIONS

- What do we observe in the Boom Clay?

- *Temperature* profiles in the clay (Horizontal profiles)



Extension of the thermally affected zone : > 16 m



euRad

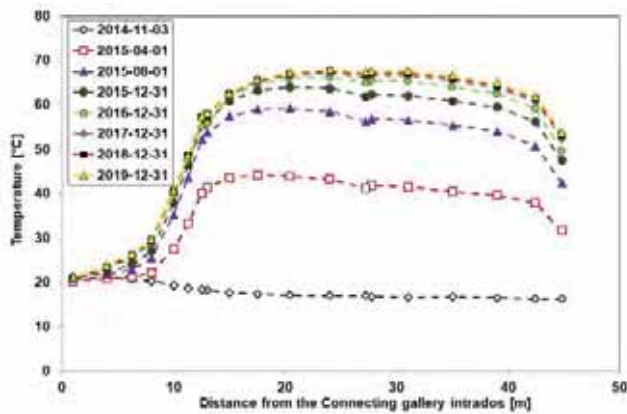
51

51

THE PRACLAY EXPERIMENT - OBSERVATIONS

- What do we observe in the Boom Clay?

- *Temperature* profiles in the clay (P35E)



euRad

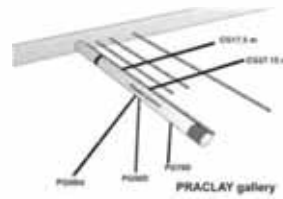
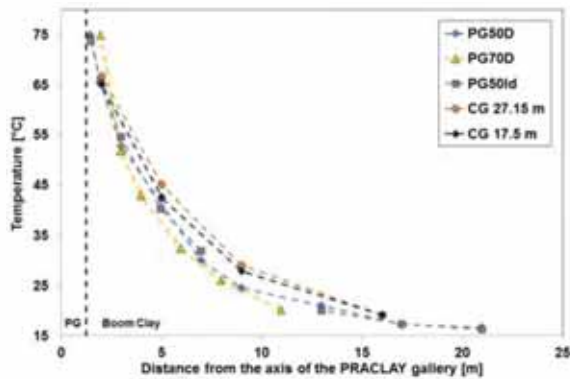
52

52

THE PRACLAY EXPERIMENT - OBSERVATIONS

• What do we observe in the Boom Clay?

- Temperature profiles in the clay (Vertical/ horizontal)



Extension of the thermally affected zone : > 16 m

eurad

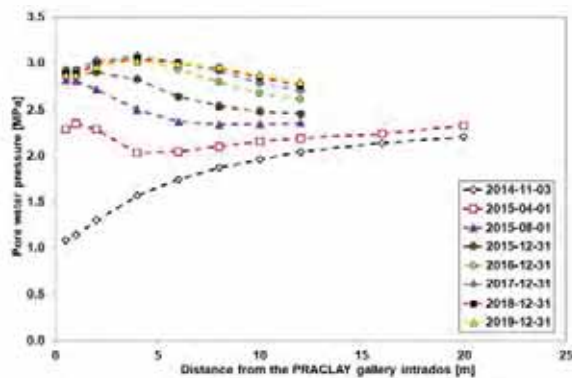
53

53

THE PRACLAY EXPERIMENT - OBSERVATIONS

• What do we observe in the Boom Clay?

- Pore water pressure profiles in the clay (Vertical plane, PG50D)



Extension of the hydraulic affected zone >16 m

eurad

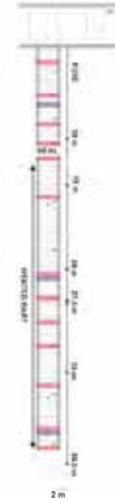
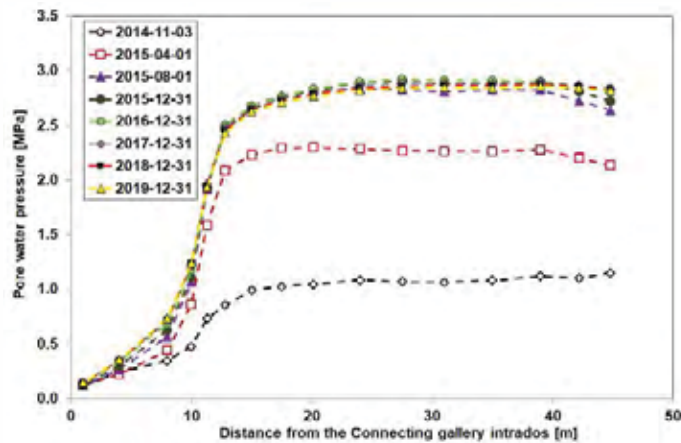
54

54

THE PRACLAY EXPERIMENT - OBSERVATIONS

• What do we observe in the Boom Clay?

- Pore water pressure profiles in the clay (P35E)



eurad

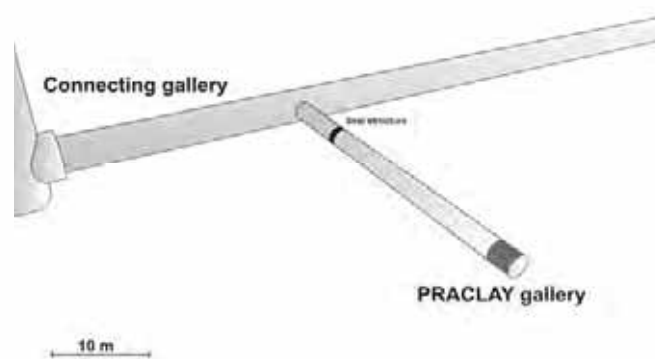
55

55

THE PRACLAY EXPERIMENT - OBSERVATIONS

• What do we observe in the seal ?

- Pore water pressure, total stress and displacement



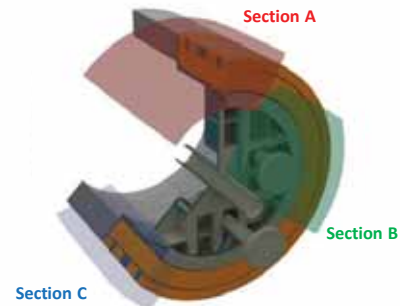
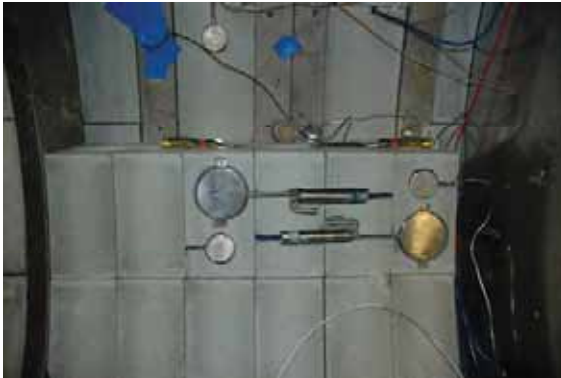
eurad

56

56

THE PRACLAY EXPERIMENT - OBSERVATIONS

- What do we observe in the seal?
 - Pore water pressure, total stress and displacement



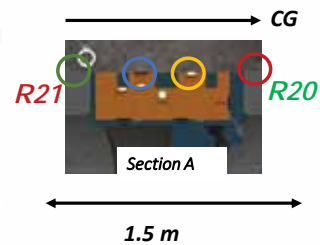
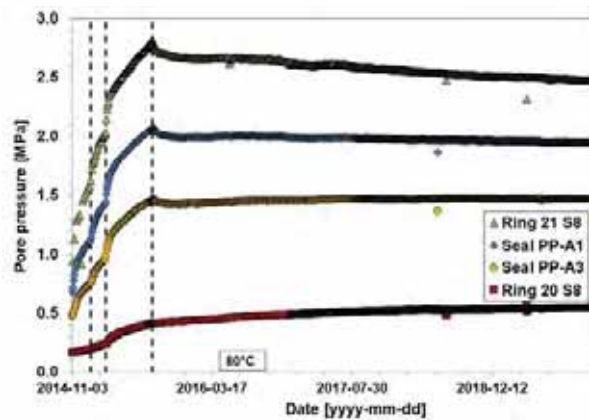
euRad

57

57

THE PRACLAY EXPERIMENT - OBSERVATIONS

- What do we observe in the seal?
 - Pore water pressure evolution at Boom Clay/ bentonite interface (Seal)



euRad

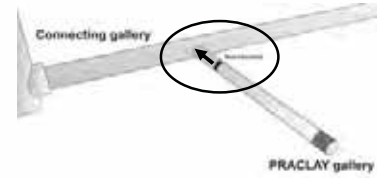
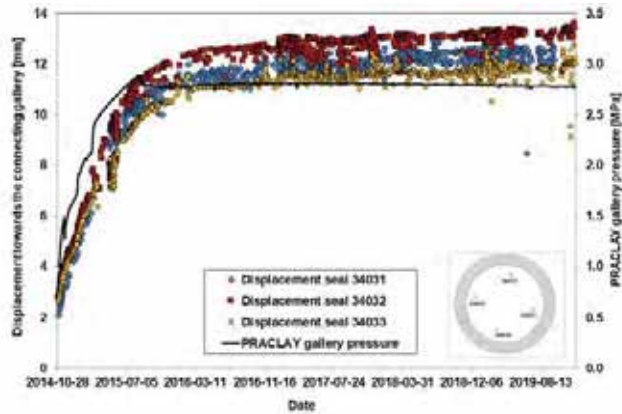
58

58

THE PRACLAY EXPERIMENT - OBSERVATIONS

- What do we observe in the seal/ concrete lining?

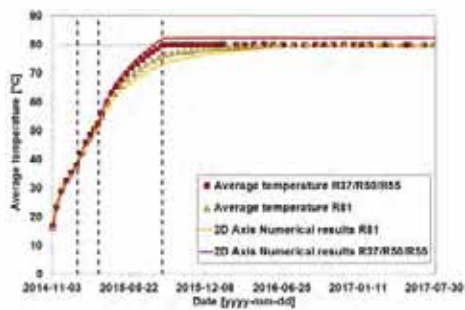
- Displacement of the SEAL towards the Connecting Gallery



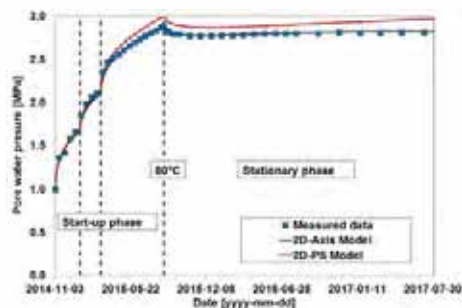
COMPARISON WITH NUMERICAL PREDICTIONS

- Numerical predictions:

- Modelling based on our knowledge (Concept, properties, parameters) before the switch-on of the heater test



Temperature evolution around the concrete lining (continuous line = modelling results)

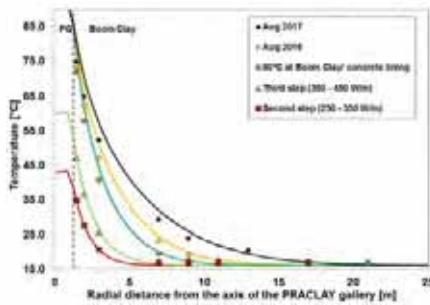


Pore water pressure in the PRACLAY gallery (continuous line = modelling results)

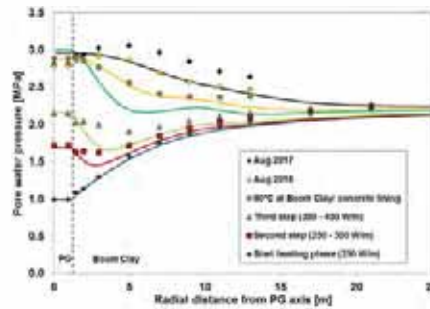
COMPARISON WITH NUMERICAL PREDICTIONS

• Numerical predictions:

- Modelling based on our knowledge (Concept, properties, parameters) before the switch-on of the heater test



Temperature profiles in the clay
(continuous line = modelling results)



Pore water pressure profiles in the clay
(continuous line = modelling results)

CONCLUSIONS

• In-situ THM experiments in poorly indurated clay (Boom Clay)

- Complementary work between the ATLAS and the large scale PRACLAY heater tests
- Large scale heater test:
 - No interruption of the heater system (good performance of the test set-up)
 - Boom Clay
 - ✓ Anisotropic responses, as expected (vertical vs horizontal profiles)
 - ✓ No indication of abrupt changes in pore water pressure nor large displacement
 - ✓ Up to now, the clay is able to sustain the thermal load
 - Seal fulfils its role as a hydraulic cut-off
 - Numerical predictions in good agreements with the observations
- Important information for simulating a geological disposal facility

Copyright © 2020 – EIG EURIDICE

PLEASE NOTE!

**This presentation contains data, information and formats for dedicated use ONLY and may not be copied, distributed or cited without the explicit permission of the EIG EURIDICE.
If this has been obtained, please reference it as a "personal communication. By courtesy of EIG EURIDICE".**

EIG EURIDICE

European Underground Research Infrastructure for Disposal of Nuclear Waste in Clay Environment

Boeretang 200 – BE-2400 MOL

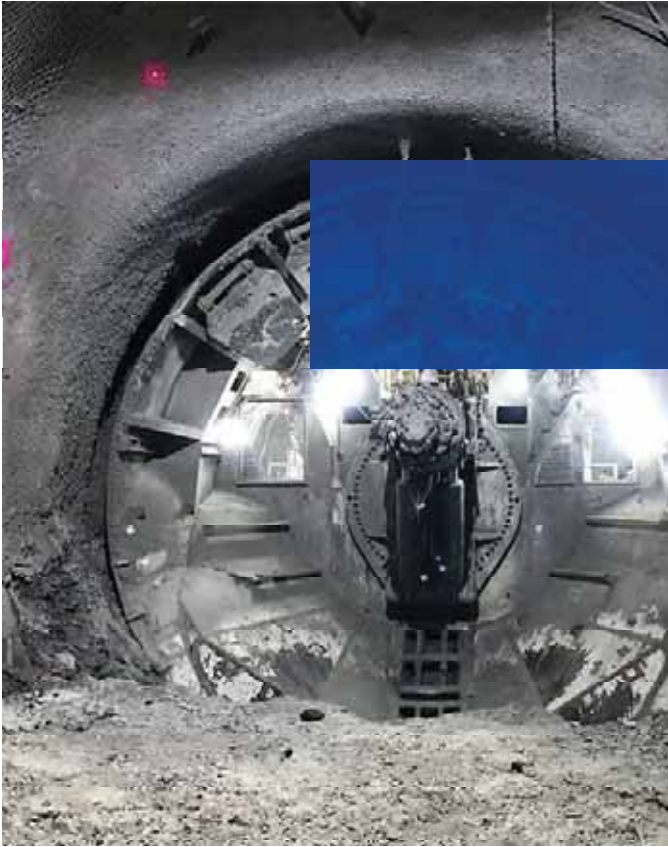


ESV EURIDICE GIE

eurad

63

Appendix P. In situ testing of gas transfer in clayey rocks (J. Talandier & R. de la Vaissière)



IN SITU TESTING OF GAS TRANSFER IN CLAYEY ROCKS

Rémi de La Vaissière, Jean Talandier

R & D division

EURAD School for Radioactive Waste Management (GAS & HITEC WPs)

Liège, 24th January 2020

Ce document est la propriété de l'Andra.
Il ne peut être reproduit ou communiqué sans son autorisation expresse et préalable.



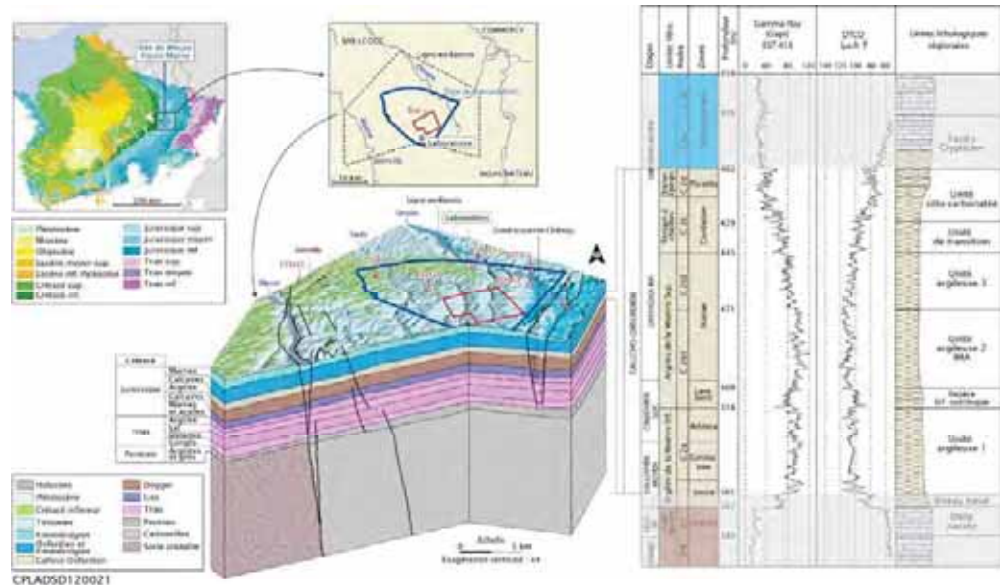
Context

ANDRA is the French national waste management organization

- its mission covers the management and disposal of radioactive waste

CIGEO project

- CIGEO project deals with High Level Waste and Intermediate Level and Long Life Waste
 - It is a **deep geological disposal project** which will be located in the eastern part of the Paris basin into a claystone :
 - The Callovo-Oxfordian "COx"

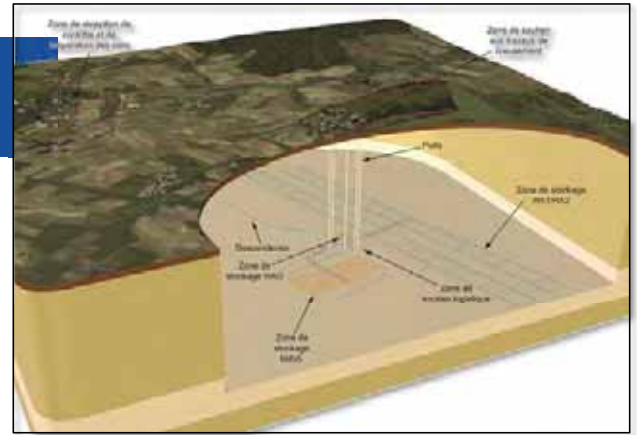


CIGEO project

Gas released into the repository

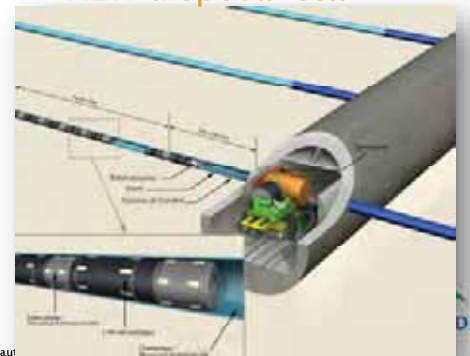
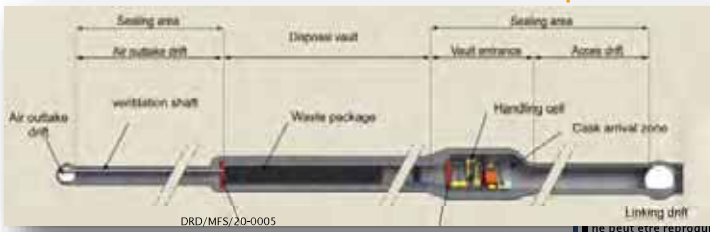
Gas production in a deep repository

- Underground facility will be composed of horizontal tunnels in the middle of the host clay layer
- Large quantity of iron (canisters, HLW lining, bolts, ...) will be present into the repository
 - Gas production (95 % of H₂) due to
 - anoxic corrosion of iron
 - radiolysis of the water present in/near the wastes
- A gas phase will form and accumulate if the rate of production exceeds the rate of release by different mechanisms



HLW disposal cell

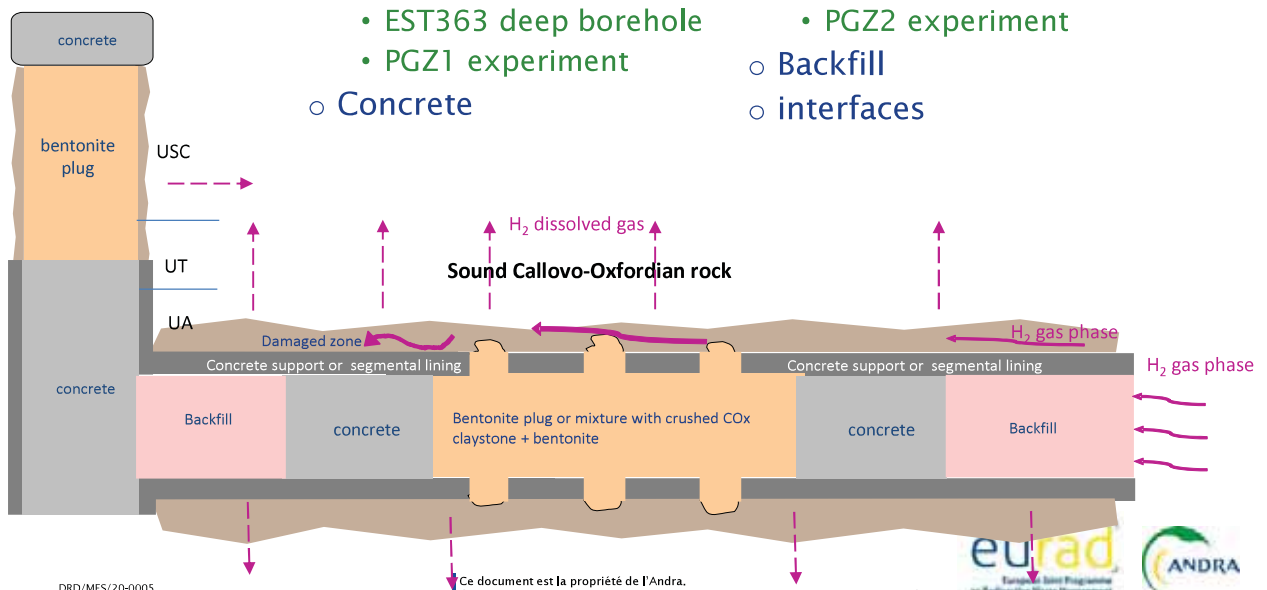
ILW disposal cell



Gas transfer during the post-closure phase

Schematic view of the disposal components

- COX claystone:
 - EST363 deep borehole
 - PGZ1 experiment
- Concrete
- Swelling clay
 - PGZ2 experiment
- Backfill
- interfaces



DRD/MFS/20-0005

Ce document est la propriété de l'Andra. Il ne peut être reproduit ou communiqué sans son autorisation expresse et préalable.



The Callovo-Oxfordian claystone

Main characteristics

Clay formation (URL)

- o Median depth \approx 490m
- o Thickness \approx 130 m

Very low horizontal hydraulic conductivity

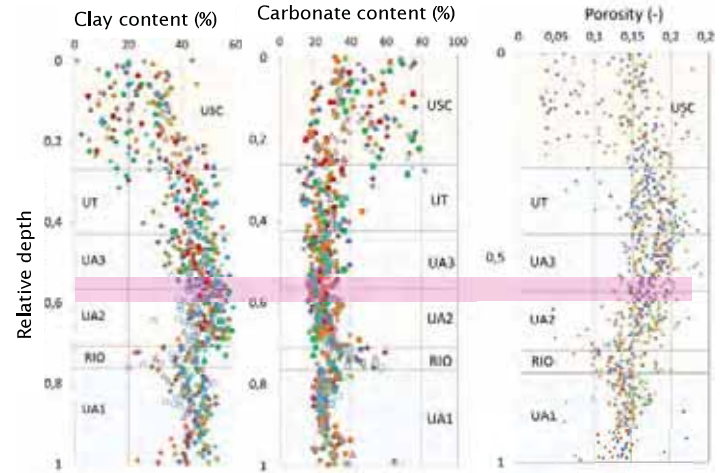
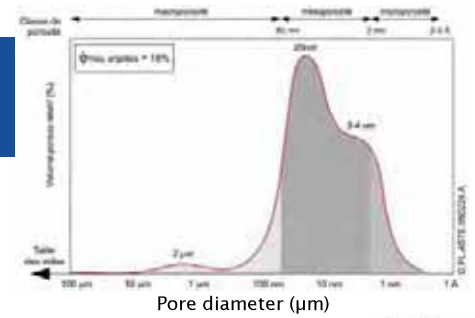
- o Geometrical mean: $3.3 \cdot 10^{-13}$ m/s
 - 95% confidence interval: $[4 \cdot 10^{-14} - 3 \cdot 10^{-12}]$ m/s

In-situ stresses in the middle of the COx layer

- o $\sigma_h \approx \sigma_v$
 - At 500 m depth, the minor stress is equal to \sim 12.5 MPa
- o $\sigma_H = 1.2$ to $1.3 \times \sigma_h$
 - the URL tunnels are excavated according to the direction of the horizontal stresses

Mean pore diameter : 10-30 nm

- o Young's Laplace equation gives a gas entry pressure of 6 MPa for a pore radius equals to 50 nm
 - What is the connected porous network for gas?



DRD/MFS/20-0005

Ce document est la propriété de la Direction des Ressources Humaines. Il ne peut être reproduit ou communiqué sans son autorisation expresse et préalable.

© 2014 Direction des Ressources Humaines

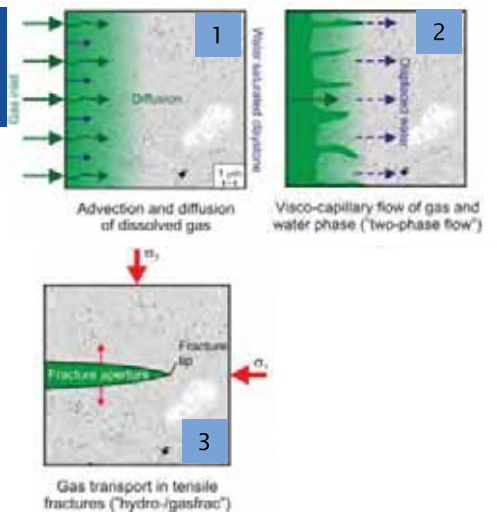
Gas transfer in porous media

Different mechanisms

For saturated porous medium, 3 gas migration mechanisms are usually described:

- increasing pressure ↓
1. migration by diffusion/advection as dissolved gas in the pore water
 2. visco-capillary flow or two phase flow:
 - When the gas pressure exceeds the gas entry pressure => simultaneous flow of the two immiscible fluids within the porous medium
 3. gas transport along macroscopic tensile fractures (gas-fracturing):
 - When the gas pressure exceeds the minimal principle stress and tensile strength of the rock

From Cuss et al. (2014)



Gas transfer in porous media

Different mechanisms

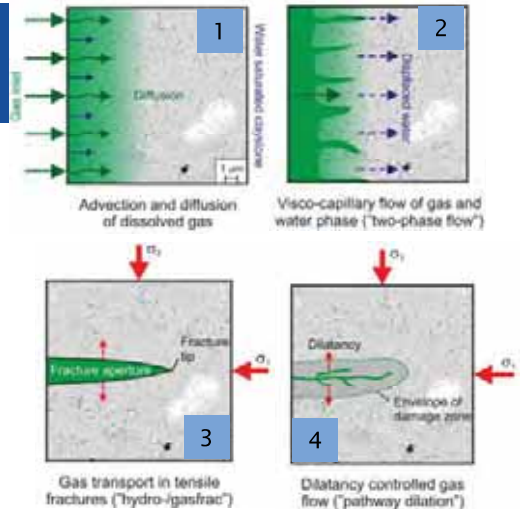
For saturated porous medium, 3 gas migration mechanisms are usually described :

1. migration by diffusion/advection as dissolved gas in the pore water
2. visco-capillary flow or two phase flow:
 - When the gas pressure exceeds the gas entry pressure => simultaneous flow of the two immiscible fluids within the porous medium
3. gas transport along macroscopic tensile fractures (gas-fracturing):
 - When the gas pressure exceeds the minimal principle stress and tensile strength of the rock

increasing pressure



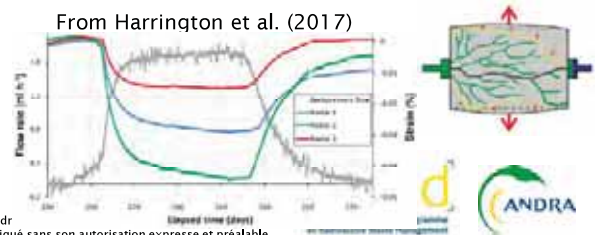
From Cuss et al. (2014)



For saturated porous clay-based media, an other gas migration mechanism has been described :

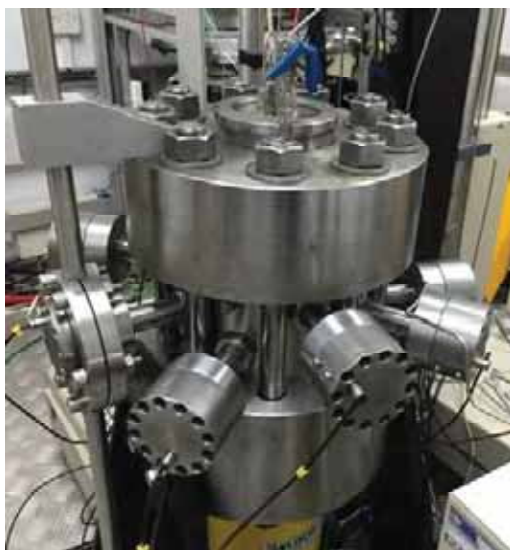
4. dilatant pathway ("dilatancy" or "microcracking")
 - appears for a pressure level lower than the fracturing pressure (Marschall et al., 2005)

From Harrington et al. (2017)



DRD/MFS/20-0005

Ce document est la propriété de l'Andra. Il ne peut être reproduit ou communiqué sans son autorisation expresse et préalable.



Gas injection test into COx

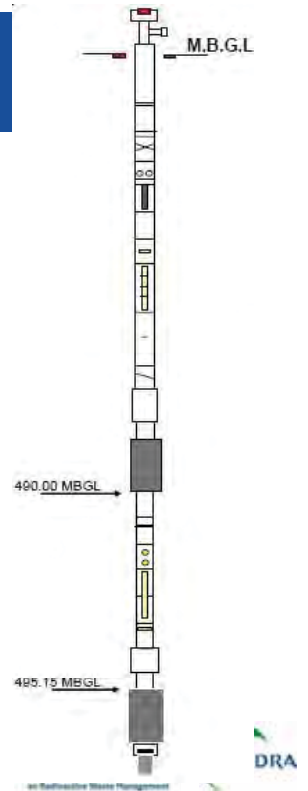
Deep borehole experiment

DRD/MFS/20-0005

Ce document est la propriété de l'Andra. Il ne peut être reproduit ou communiqué sans son autorisation expresse et préalable.

Gas injection test into CO_x claystone Deep borehole EST363

- Straddle packer tests between 490 to 495 m depth:
 - 5 m long interval with an interval volume of ~ 825 L
 - Gas tests performed in 2004
 - Gas tests were done with nitrogen

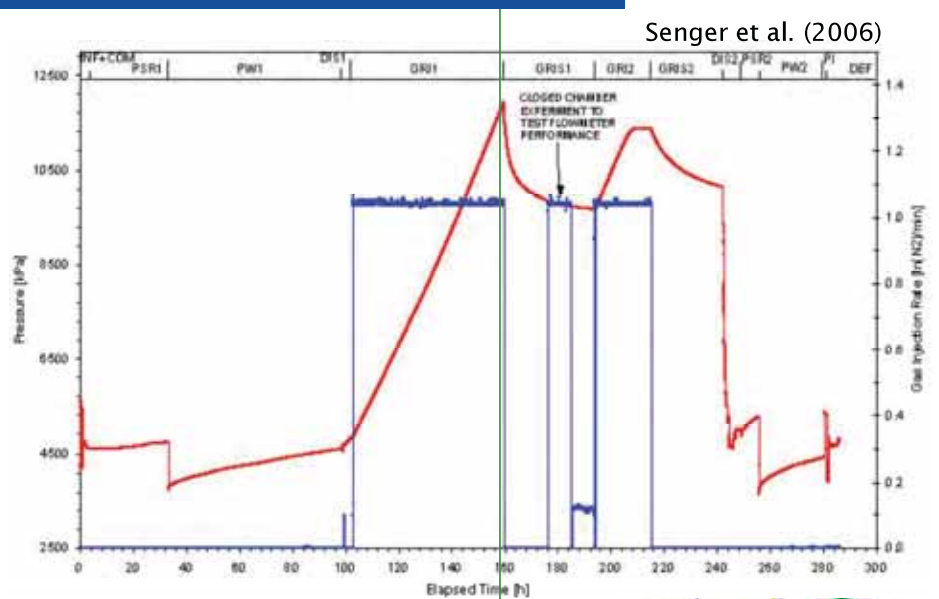


DRD/MFS/20-0005

Ce document est la propriété de l'Andra. Il ne peut être reproduit ou communiqué sans son autorisation expresse et préalable.

Gas injection test into CO_x claystone Deep borehole EST363

- Straddle packer tests between 490 to 495 m depth:
 - 5 m long interval with an interval volume of ~ 825 L
 - Gas tests performed in 2004
- Constant gas flow rate test at 1000 mLn/min
 - 2 injection steps GRI1 and GRI2



Senger et al. (2006)

DRD/MFS/20-0005

Ce document est la propriété de l'Andra. Il ne peut être reproduit ou communiqué sans son autorisation expresse et préalable.

Gas injection test into CO_x claystone Deep borehole EST363

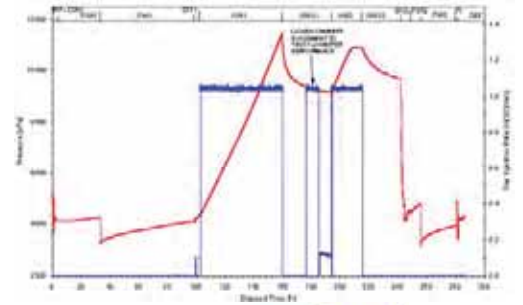
GRI1

- A gas fracture was created at about 11.9 MPa
 - Close to minimum stress estimation
 - The fracture is probably horizontal
- There is no flow into the rock
 - = entirely wellbore storage except at the end just prior to the fracture event

GRI2

- The fracture was re-opened at 11.3 MPa

During this deep borehole gas injection test, the percolation of gas into the rock was not clearly demonstrated



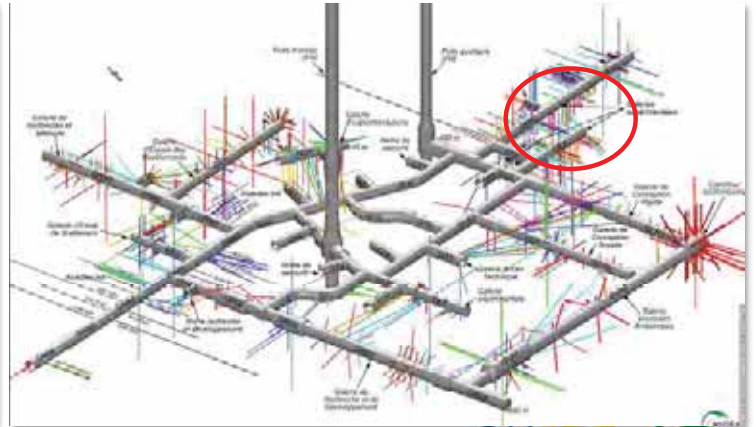
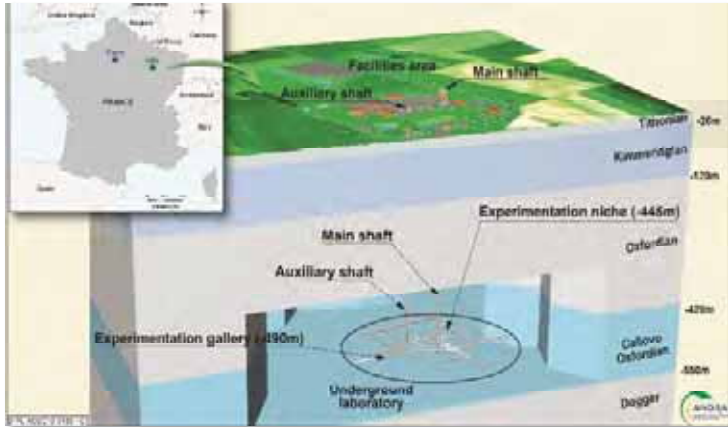
Gas injection test into CO_x

PGZ1 experiment

In-situ gas injection tests into CO_x PGZ1 experiment

« PGZ1 » is dedicated to identify gas migration mechanisms into CO_x claystone for different pressure levels

- it is located in the Andra's Underground Research Laboratory



DRD/MFS/20-0005

Ce document est la propriété de l'Andra.
Il ne peut être reproduit ou communiqué sans son autorisation expresse et préalable.

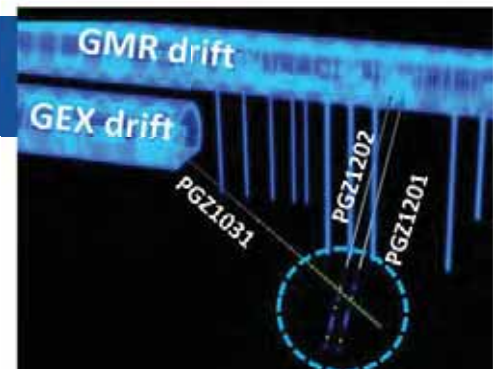


In-situ gas injection tests into CO_x PGZ1 layout

- Two boreholes PGZ1201 and PGZ1202 drilled from the GMR drift
 - aligned in parallel with 0.9 m separation and oriented parallel to sigma H
 - each equipped with a 3-fold packer system to monitor water/gas pressure in 3 intervals

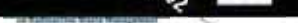


- One borehole PGZ1031 drilled from the GEX drift
 - the minimum vertical distance to PGZ1201 is 1.7 m
 - equipped with a multiple magnetic extensometers probe (MagX system[®]) to monitor axial deformation
- All equipment was installed in July 2009



DRD/MFS/20-0005

Ce document est la propriété de l'Andra.
Il ne peut être reproduit ou communiqué sans son autorisation expresse et préalable.

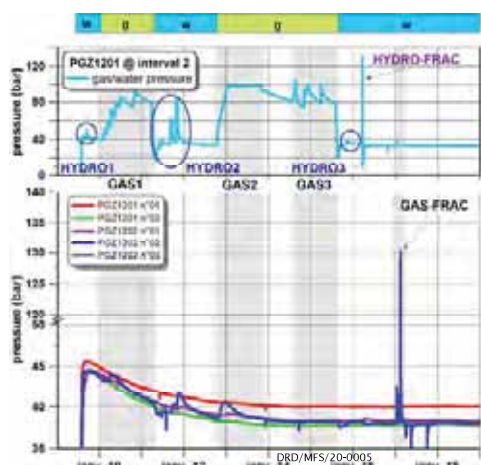


In-situ gas injection tests into COx

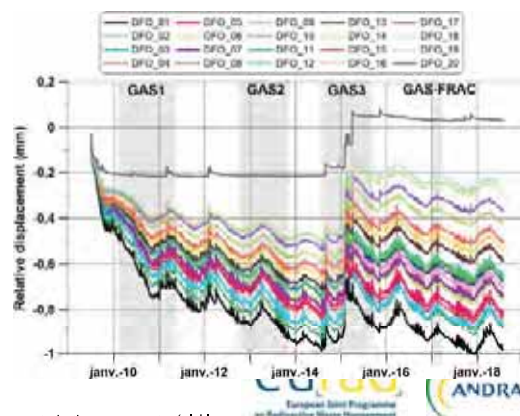
Overview water/gas injection sequence

10 years of water/gas pressure monitoring :

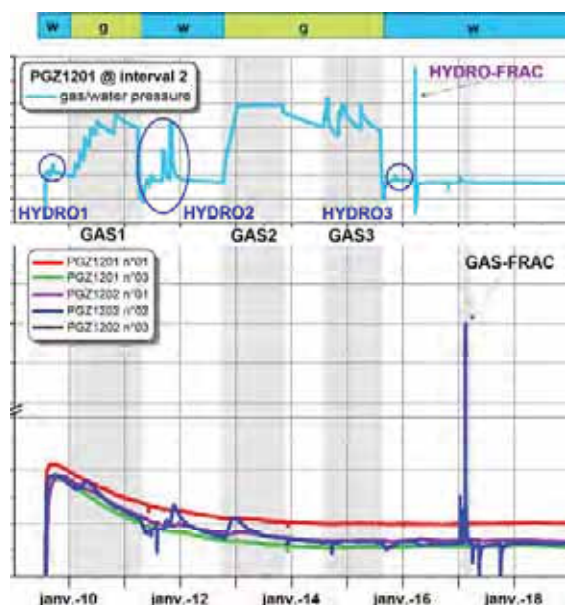
- Gas tests were done with nitrogen
- Water permeability tests (HYDROx) have been repeated in the middle interval of PGZ1201 borehole



relative displacement into PGZ1031 borehole



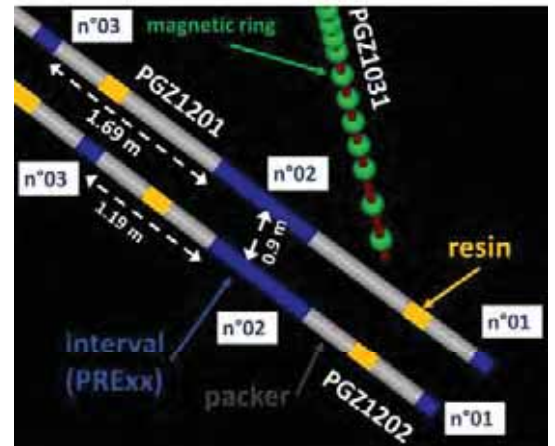
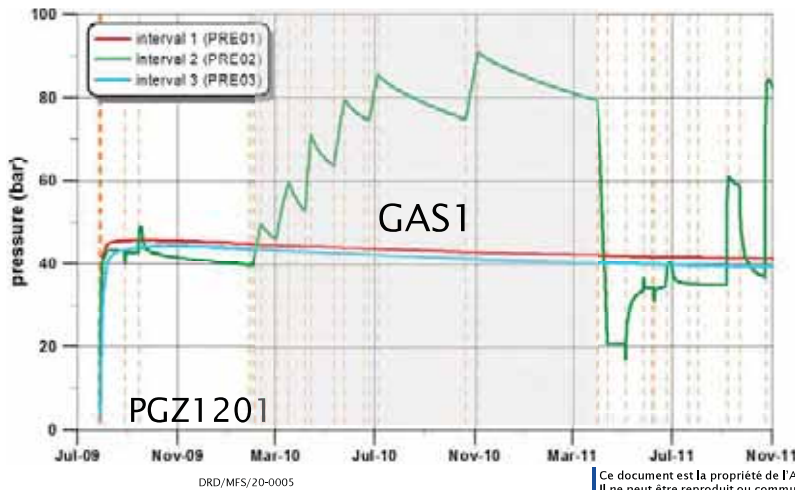
Ce document est la propriété de l'Andra.
Il ne peut être reproduit ou communiqué sans son autorisation expresse et préalable.



GAS1

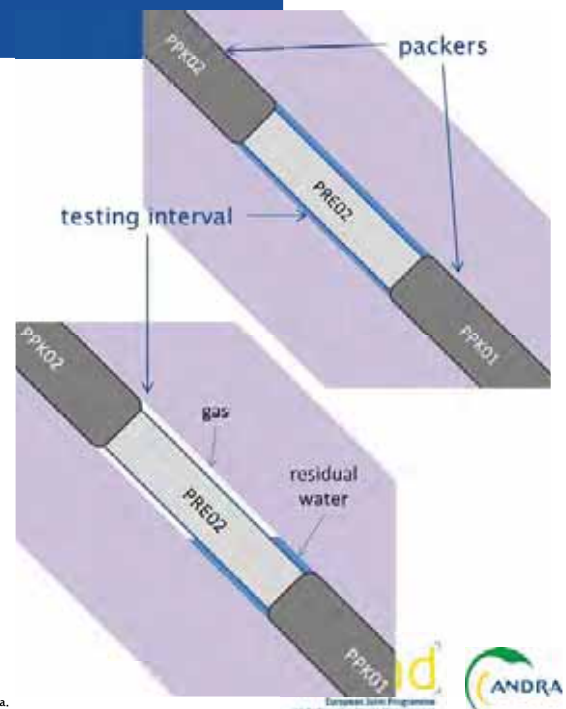
Main outcomes during GAS1 Classical two-phase flow model

- 6 constant gas flow steps (GR_{Ix}) followed by pressure recovery periods (GR_{ISx}):
 - maximal pressure = 9.1 MPa



Main outcomes during GAS1 Classical two-phase flow model

- At the beginning of the first injection step (GR_{I1}), the exact water volume of the interval 2 is unknown
 - creep
- Borehole is inclined => all water could not be removed during water-gas exchange
 - Residual water volume is unknown
- Calculation of dP at constant volume with ideal gas law and comparison with data and theoretical volume of the testing interval

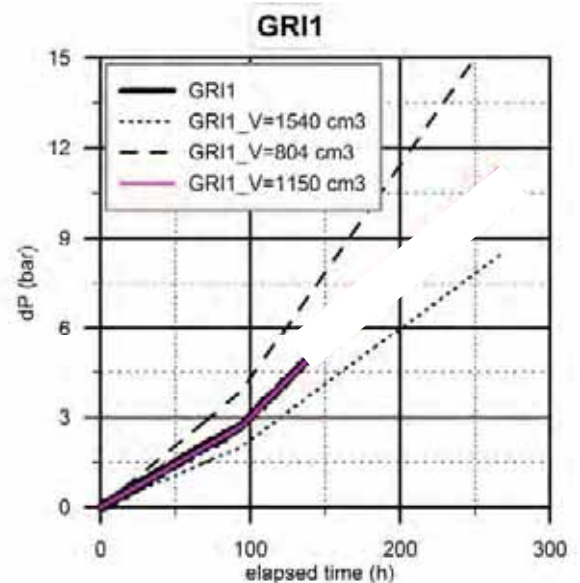


Main outcomes during GAS1 Classical two-phase flow model

- Ideal gas law: $dP = dn \times R \times T/V$
 - Gas volume is fixed a priori
 - Hypothesis:
 - Temperature is constant and homogeneous
 - Gas dissolution & diffusion are neglected
- To compare dP measured and dP calculated at constant volume

Results

- dP measured (bold line) is located between dP calculated for the 2 extrema volumes (804 and 1540 cm³)
 - Pink curve: dP_{best} fit for a volume equals to 1150 cm³
- Discrepancy after 170 h
 - Increasing gas volume = residual water is flushed out into the rock



DRD/MFS/20-0005

Ce document est la propriété de l'Andra.
Il ne peut être reproduit ou communiqué sans son autorisation expresse et préalable.

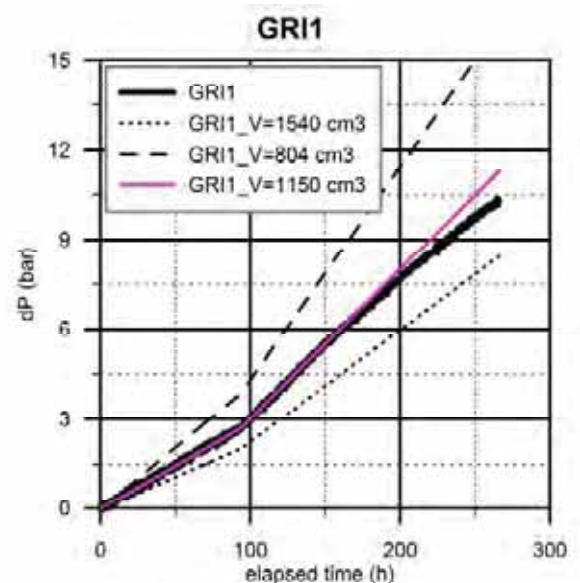


Main outcomes during GAS1 Classical two-phase flow model

- Ideal gas law: $dP = dn \times R \times T/V$
 - Gas volume is fixed a priori
 - Hypothesis:
 - Temperature is constant and homogeneous
 - Gas dissolution & diffusion are neglected
- To compare dP measured and dP calculated at constant volume

Results

- dP measured (bold line) is located between dP calculated for the 2 extrema volumes (804 and 1540 cm³)
 - Pink curve: dP_{best} fit for a volume equals to 1150 cm³
- Discrepancy after 170 h
 - Increasing gas volume = residual water is flushed out into the rock



DRD/MFS/20-0005

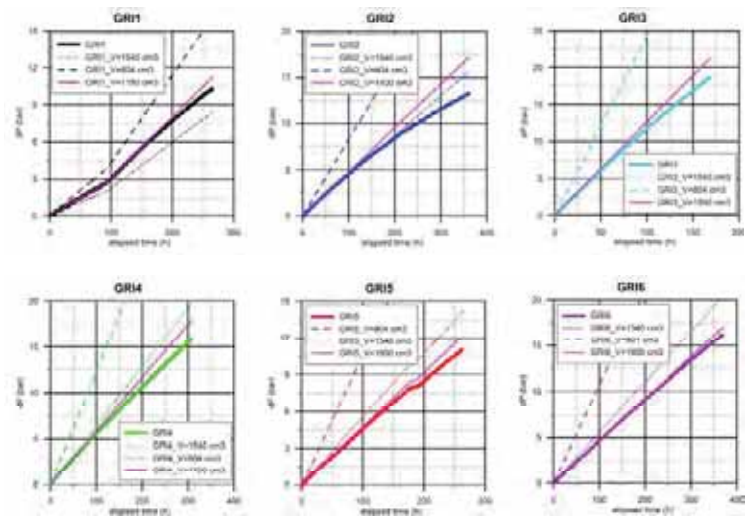
Ce document est la propriété de l'Andra.
Il ne peut être reproduit ou communiqué sans son autorisation expresse et préalable.



Main outcomes during GAS1 Classical two-phase flow model

o GRIx detailed data analysis

- During GRI1 to GRI3, data shows that the residual water is removed from the testing interval
- After GRI3, only gas can penetrate claystone
 - => maximal gas entry pressure ~ 2 MPa
- Can modeling reproduce data and validate this interpretation?



DRD/MFS/20-0005

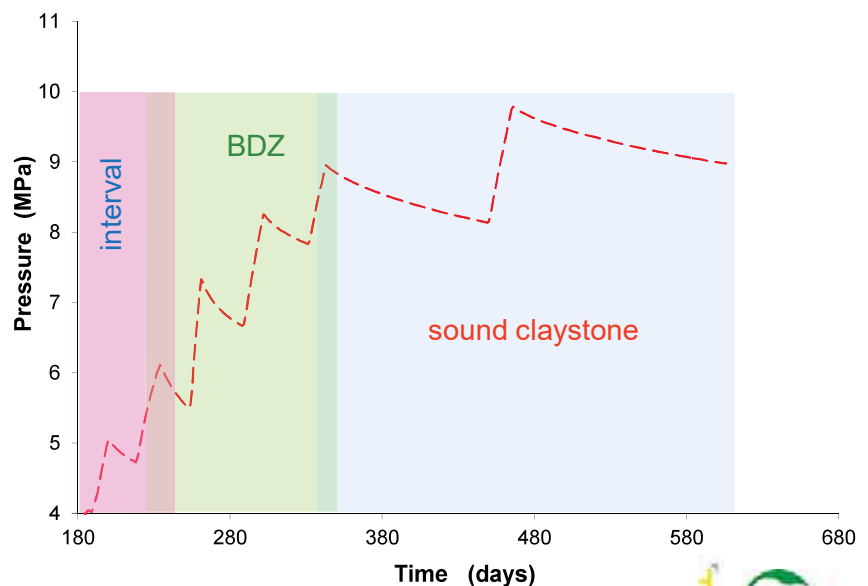
Ce document est la propriété de l'Andra.
Il ne peut être reproduit ou communiqué sans son autorisation expresse et préalable.



Main outcomes during GAS1 Classical two-phase flow model

o Classical two-phase flow model reproduced reasonably well observations

- Two separate zones with different gas entry pressure are required:
 - Inner zone corresponds to the Borehole Damage Zone with a very low gas entry pressure (≤ 2 MPa)
 - Outer zone corresponds to the sound claystone with a high gas entry pressure



DRD/MFS/20-0005

Ce document est la propriété de l'Andra.
Il ne peut être reproduit ou communiqué sans son autorisation expresse et préalable.

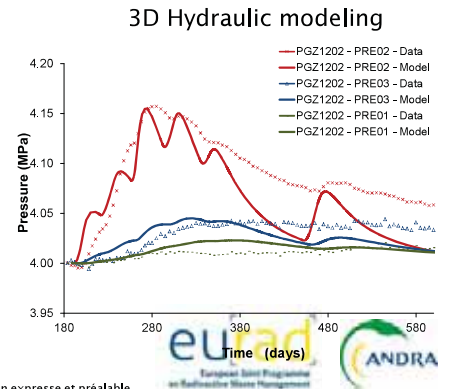
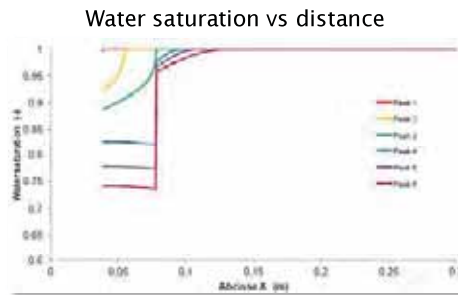
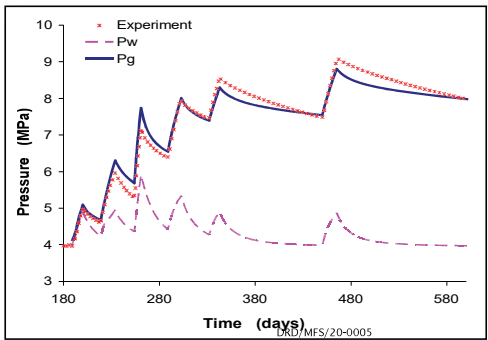


Main outcomes during GAS1

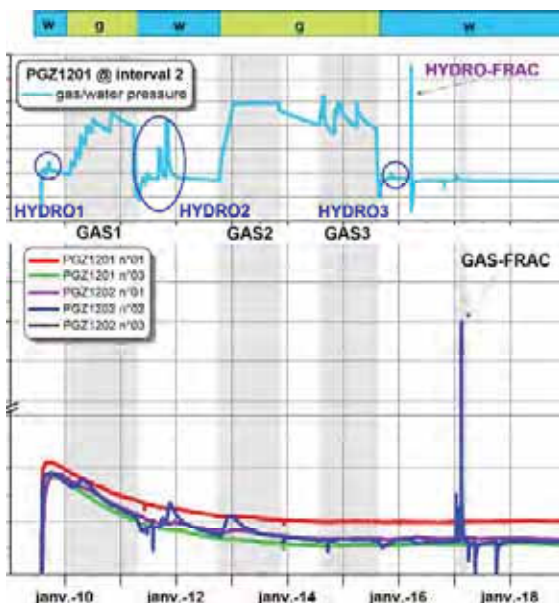
Classical two-phase flow model

- Classical two-phase flow model reproduced reasonably well observations
 - Two separate zones with different gas entry pressure are required:
 - Inner zone corresponds to the Borehole Damage Zone with a very low gas entry pressure (≤ 2 MPa)
 - Outer zone corresponds to the sound claystone with a high gas entry pressure

From de La Vaissière et al. (2014)



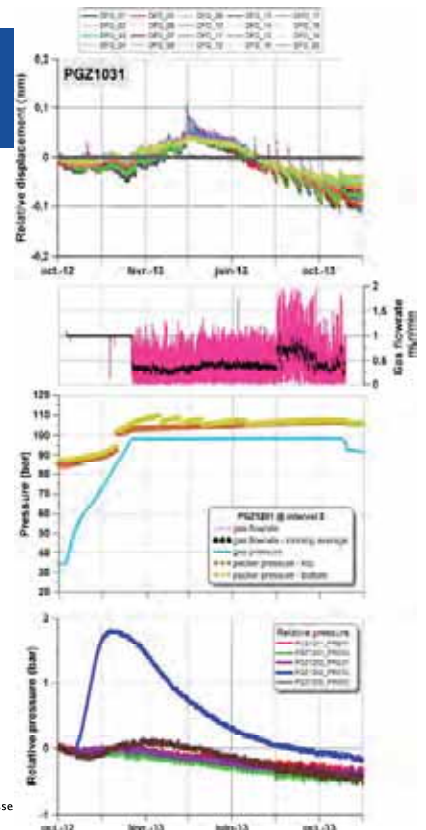
Ce document est la propriété de l'Andra. Il ne peut être reproduit ou communiqué sans son autorisation expresse et préalable.



GAS2

Main outcomes during GAS2 Pathway dilation?

- GAS2 is composed by:
 - a constant injection flow rate at 1 mLn/min during ~ 2.5 months to reach 9.8 MPa
 - Then, the gas pressure was kept constant during 9 months
 - Average gas outflow is constant ~ 0.3 - 0.4 mLn/min

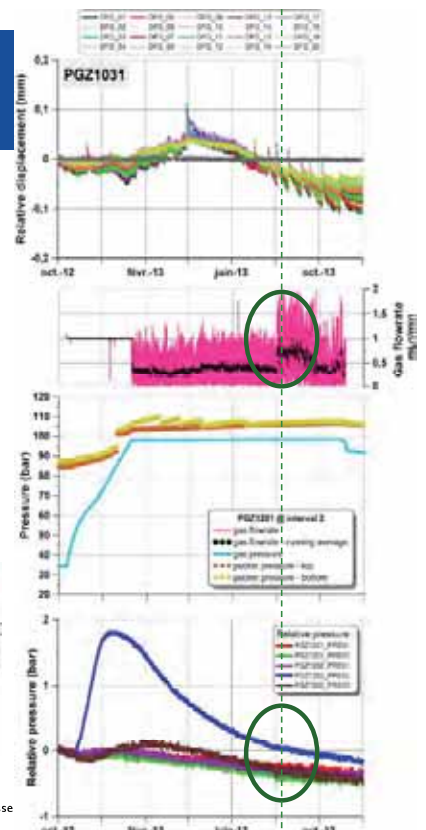


DRD/MFS/20-0005

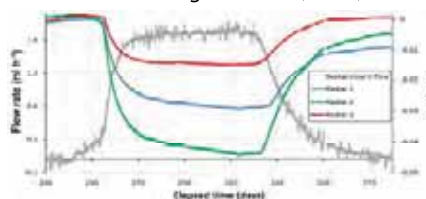
Ce document est la propriété de l'Andra.
Il ne peut être reproduit ou communiqué sans son autorisation expresse

Main outcomes during GAS2 Pathway dilation?

- An oscillation of the flow injection rate was observed in August 2013 during a constant pressure injection step at 9.8 MPa
 - Occurrence of dilatant pathway ?
 - or
 - suggest the genesis of a fracture that did not extend ?



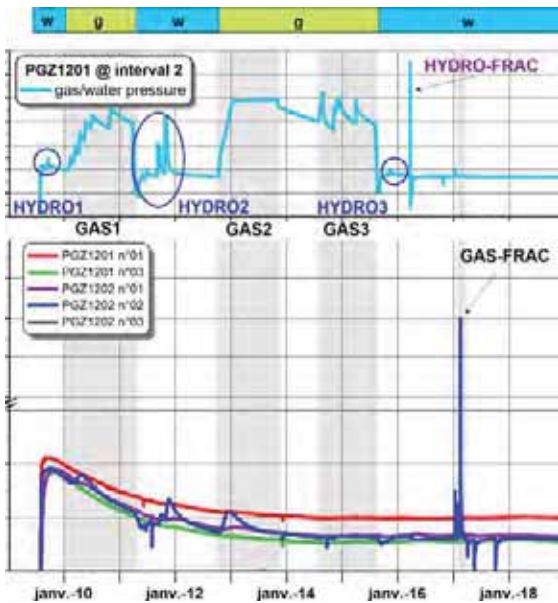
From Harrington et al. (2017)



DRD/MFS/20-0005

Ce document est la propriété de l'Andra.
Il ne peut être reproduit ou communiqué sans son autorisation expresse

GAS3



DRD/MFS/20-0005

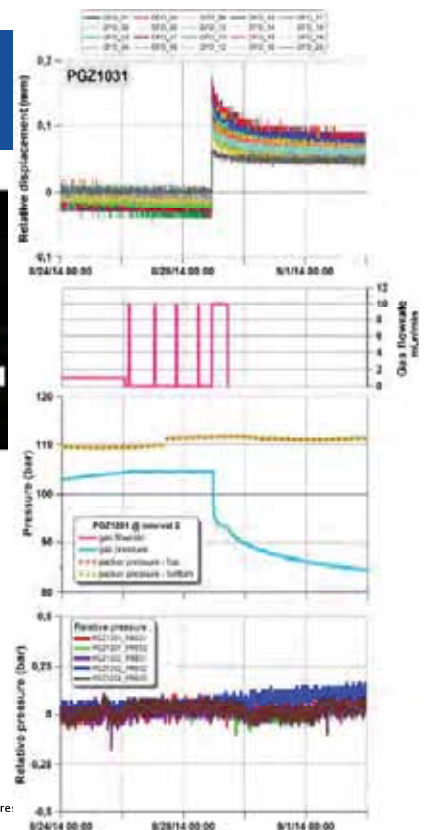
Ce document est la propriété de l'Andra. Il ne peut être reproduit ou communiqué sans son autorisation expresse et préalable.



Main outcomes during GAS3 Gas fracturing at different levels

During GAS3, 3 injection steps were conducted

- During step 1:
 - Injection at constant flow rate @ 1 mLn/min to reach 10.45 MPa during ~ 1 month
 - Then turned to a constant pressure injection phase at 10.45 MPa during 3 days
 - The flowmeter was operating in on/off mode between two set of pressures

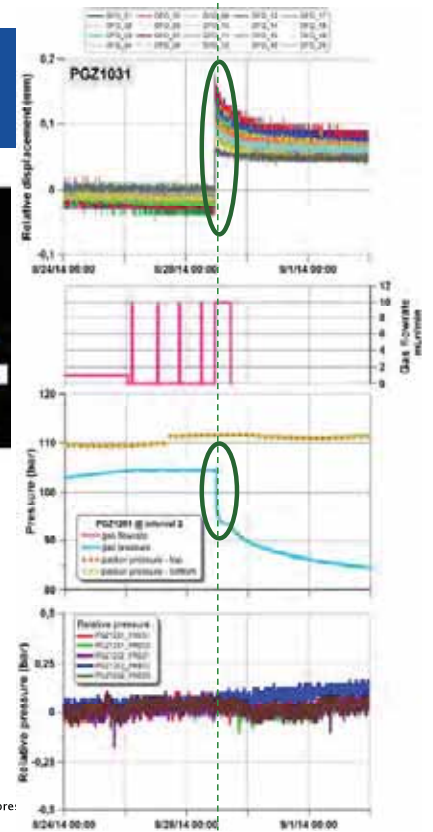


DRD/MFS/20-0005

Ce document est la propriété de l'Andra. Il ne peut être reproduit ou communiqué sans son autorisation expresse et préalable.

Main outcomes during GAS3 Gas fracturing at different levels

- A sudden gas breakthrough was observed during a constant pressure injection phase at 10.45 MPa
 - the gas pressure suddenly dropped in the test interval and the flow meter has reached its maximum value
 - and simultaneously
 - an overall rigid motion is detected on the extensometer string in borehole PGZ1031
- A gas fracture was created with a gas pressure value well below the minimum principal stress component (~ 12.5 MPa)

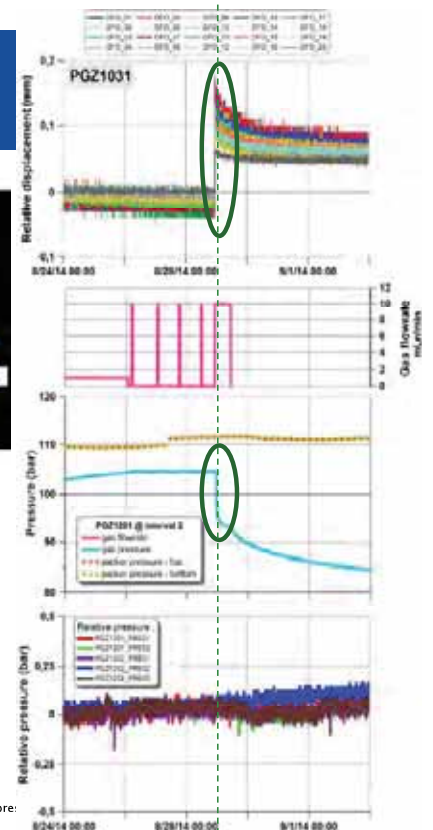


DRD/MFS/20-0005

Ce document est la propriété de l'Andra.
Il ne peut être reproduit ou communiqué sans son autorisation expresse.

Main outcomes during GAS3 Gas fracturing at different levels

- A sudden gas breakthrough was observed during a constant pressure injection phase at 10.45 MPa
 - the gas pressure suddenly dropped in the test interval and the flow meter has reached its maximum value
 - and simultaneously
 - an overall rigid motion is detected on the extensometer string in borehole PGZ1031
- A gas fracture was created with a gas pressure value well below the minimum principal stress component (~ 12.5 MPa)



It was not possible to locate the position of the fracture

DRD/MFS/20-0005

Ce document est la propriété de l'Andra.
Il ne peut être reproduit ou communiqué sans son autorisation expresse.

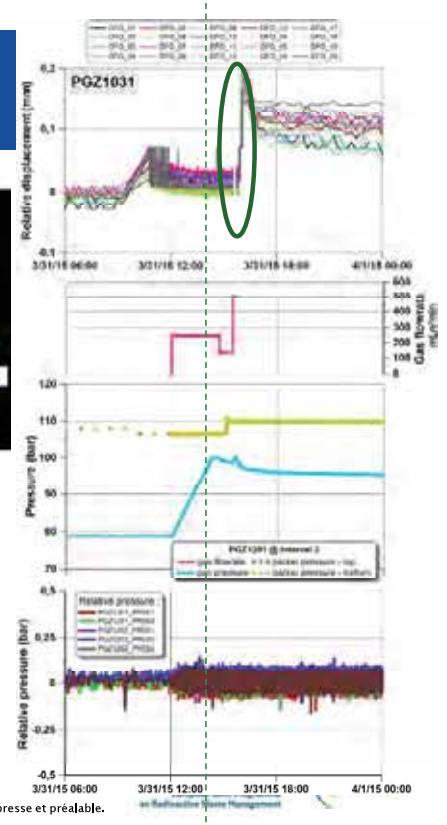
Main outcomes during GAS3 Gas fracturing at different levels

- During GAS3, a new gas injection steps was performed a few months later with a gas mixture (nitrogen + helium) and high gas flow rate
 - Helium is used as a gas tracer
 - Detection of helium is done on PGZ1031 head (extensometer borehole)
 - A maximal gas pressure is reached at 9.99 MPa
- During this test, no displacement was detected by the extensometer string
 - The recorded motion is due to human action

Helium was detected at the borehole head

DRD/MFS/20-0005

Ce document est la propriété de l'Andra.
Il ne peut être reproduit ou communiqué sans son autorisation expresse et préalable.



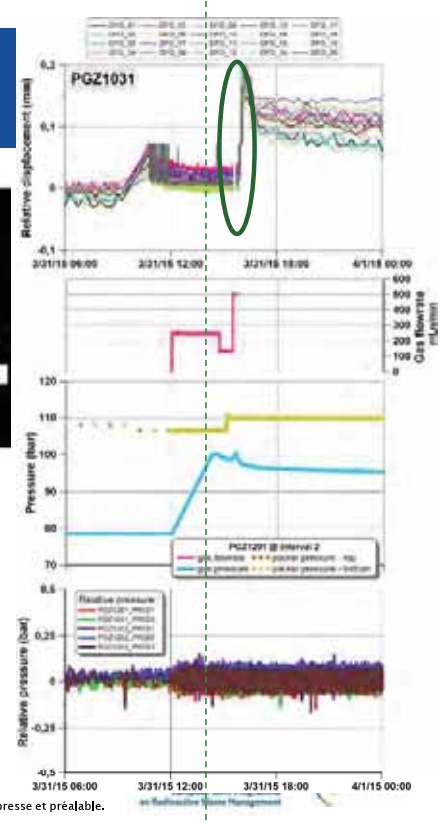
Main outcomes during GAS3 Gas fracturing at different levels

- During GAS3, a new gas injection steps was performed a few months later with a gas mixture (nitrogen + helium) and high as flow rate
 - Helium is used as a gas tracer
 - Detection of helium is done on PGZ1031 head (extensometer borehole)
 - A maximal gas pressure is reached at 9.99 MPa
- During this test, no displacement was detected by the extensometer string
 - The recorded motion is due to human action

Helium was detected at the borehole head

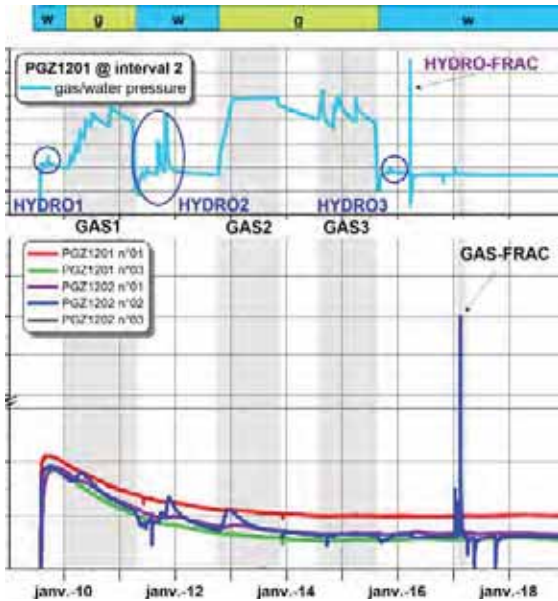
DRD/MFS/20-0005

Ce document est la propriété de l'Andra.
Il ne peut être reproduit ou communiqué sans son autorisation expresse et préalable.



This is evidence that a fracture was created in the rock

GAS-FRAC



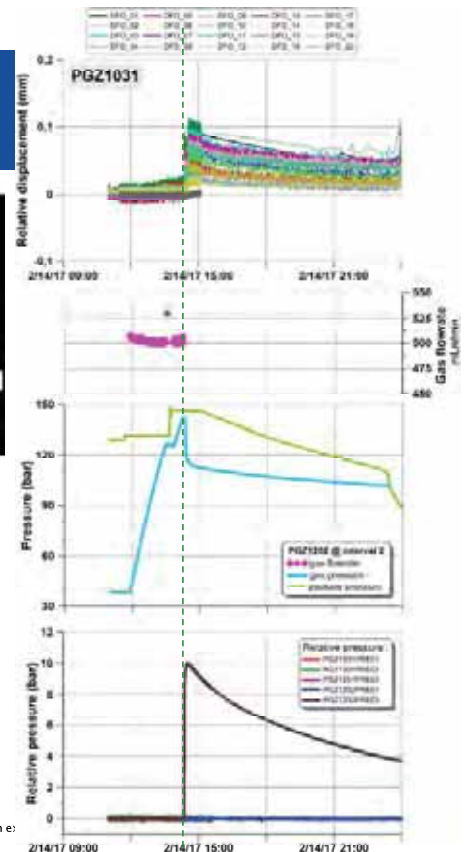
DRD/MFS/20-0005

Ce document est la propriété de l'Andra. Il ne peut être reproduit ou communiqué sans son autorisation expresse et préalable.



Main outcomes during GAS-FRAC Gas fracturing at different levels

- GAS-FRAC started with an injection at high constant flow rate @ 500 mLn/min that lasted about 2 hours
- The interval pressure reached progressively 14.18 MPa when the injection line was closed in order to monitor the pressure drop

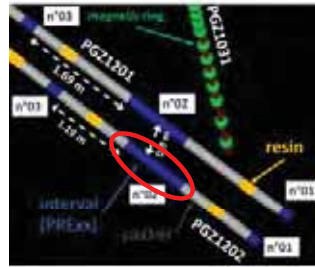


DRD/MFS/20-0005

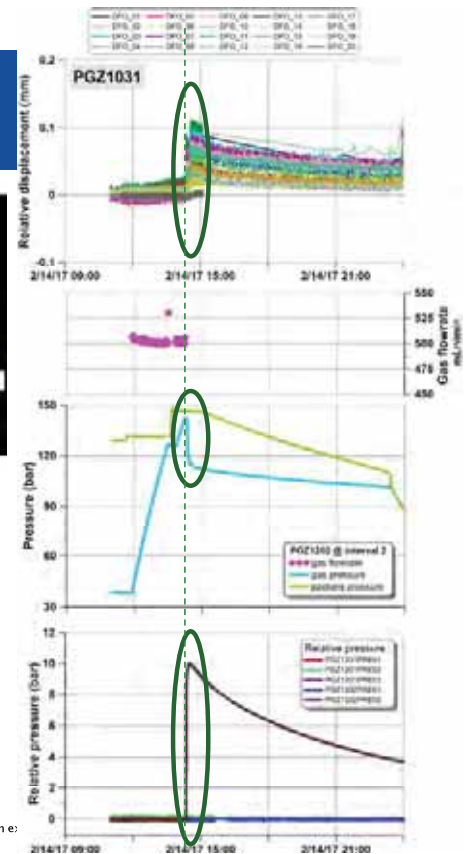
Ce document est la propriété de l'Andra. Il ne peut être reproduit ou communiqué sans son autorisation e:

Main outcomes during GAS-FRAC Gas fracturing at different levels

- GAS-FRAC started with an injection at high constant flow rate @ 500 mLn/min that lasted about 2 hours
- The interval pressure reached progressively 14.18 MPa when the injection line was closed in order to monitor the pressure drop
 - Six minutes after the injection line was closed a sudden pressure drop was observed with:
 - a simultaneous increase in pressure in the n°03 interval of the same borehole (PGZ1202)
 - a sudden differential displacements recorded by the PGZ1031 extensometer string
- A gas fracture was created with a gas pressure value well above the minimum principal stress component (~ 12.5 MPa)



One packer starts to leak : the testing program has been abandoned



DRD/MFS/20-0005

Ce document est la propriété de l'Andra.
Il ne peut être reproduit ou communiqué sans son autorisation e:

Gas fracturing process On-going analysis

de La Vaissière et al. (2019)

Gas-fracture threshold is depending on the kinetic of the fluid injection rate

Several aspects are being investigated to explain this phenomenon:

- Drained/undrained boundary condition
- Geometry of the cavity
- The stress applied by the packers

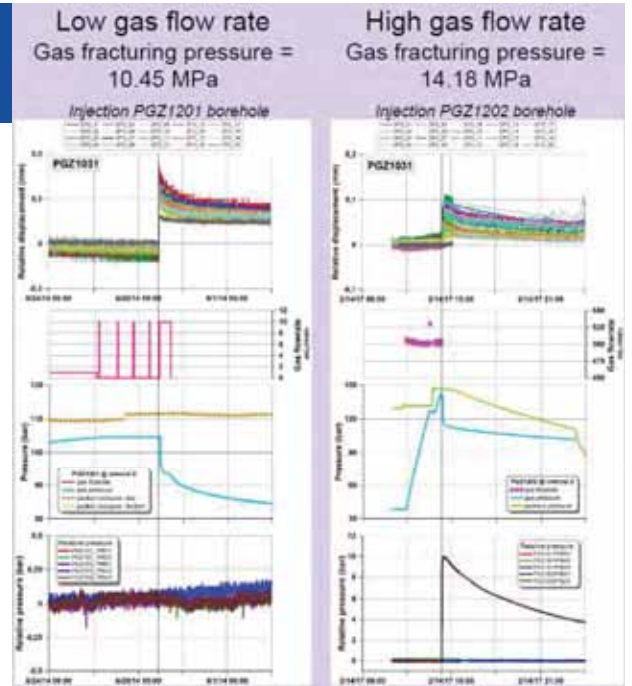
DRD/MFS/20-0005

Ce document est la propriété de l'Andra.
Il ne peut être reproduit ou communiqué sans son autorisation expresse et préalable.

Gas fracturing process Effective stress

Distribution of the effective stress surrounding the borehole :

- the distribution of the effective stress around the borehole is directly dependent on the kinetic of gas injection
 - High gas flow rate : the pore pressure boundary condition should be considered as undrained
 - Low gas flow rate : the effective stress is modified into the rock and the pore pressure boundary condition should be considered as drained



DRD/MFS/20-0005

Ce document est la propriété de l'Andra. Il ne peut être reproduit ou communiqué sans son autorisation expresse et préalable.



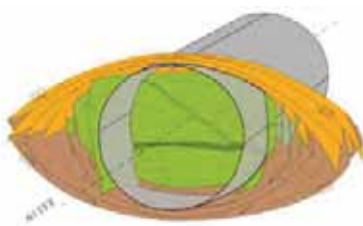
Gas fracturing process Geometry

Geometry of the cavity:

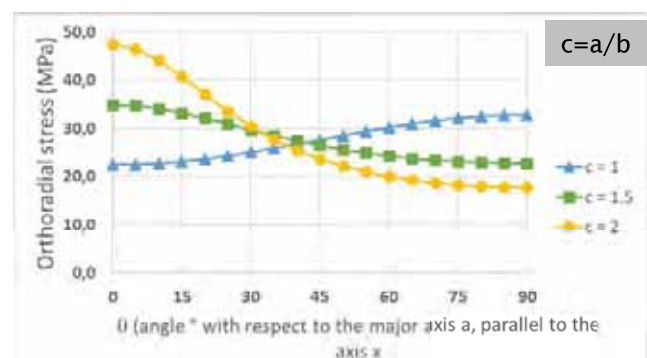
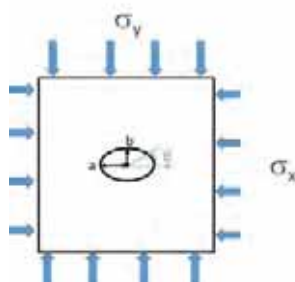
- the presence of ellipsoidal shape of a BDZ implies that the orthoradial stress component is minimal at the small axis

$$\text{Tangential stress component : } \sigma_{\theta\theta}(\theta) = \frac{\sigma_x[(c^2+2c)\sin^2\theta - \cos^2\theta] + \sigma_y[(1+2c)\cos^2\theta - c^2\sin^2\theta]}{c^2\sin^2\theta + \cos^2\theta}$$

From Armand et al. (2014)



Opening parallel to σ_H



DRD/MFS/20-0005

Ce document est la propriété de l'Andra. Il ne peut être reproduit ou communiqué sans son autorisation expresse et préalable.

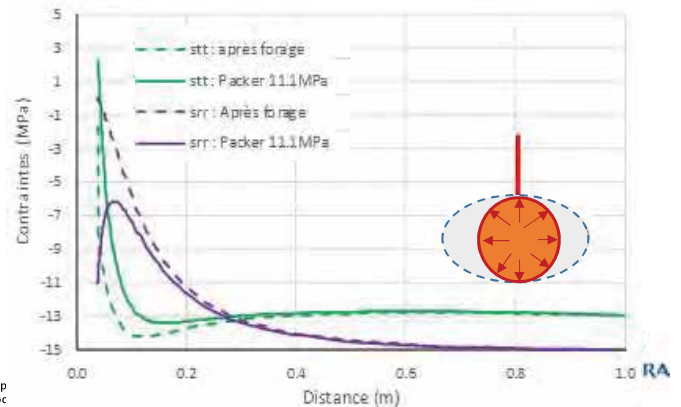


Gas fracturing process Packers

The stress applied by the packer:

- the pressure applied by the packer is always above the pressure into the interval
 - The figure represents the radial and orthoradial stresses calculated by a mechanical model at the small axis of the ellipse.
 - Two zones are considered in the model: a plastic zone corresponding to the damaged zone and an elastic zone for the rock

Orthoradial stress is positive (traction) but it becomes quickly negative with the distance to the borehole wall



DRD/MFS/20-0005

Ce document est la propriété de l'Andra.
Il ne peut être reproduit ou communiqué sans son autorisation expresse et préalable.

PGZ1 summary

Different gas injection tests at various flow rates (from 1 mLn/min to 500 mLn/min) have been conducted:

- GAS1 reveals that generalized Darcy's law allows for the correct modelling of measurements up to 9.1 MPa
 - Gas first percolates into BDZ and then starts to migrating into the sound claystone (with a high gas entry pressure above 4 MPa)
- GAS2 may suggest the occurrence of the pathway dilation phenomenon
- During GAS3 & GAS-FRAC, a relationship between gas flow rate and gas fracturing pressure is highlighted
 - The underlying processes are not yet fully understood
 - Analysis is underway
 - New boreholes and gas injection tests will be undertaken in the future

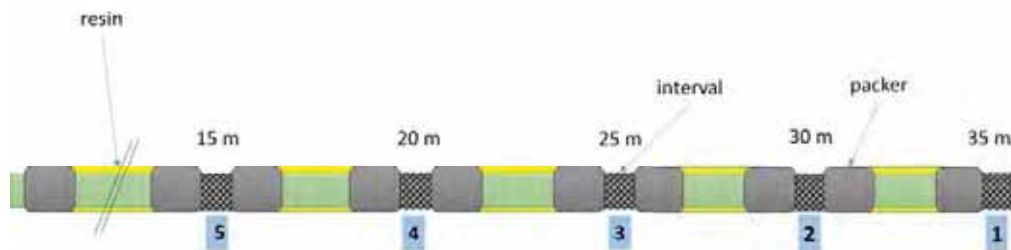
DRD/MFS/20-0005

Ce document est la propriété de l'Andra.
Il ne peut être reproduit ou communiqué sans son autorisation expresse et préalable.

New boreholes (PGZ3)

Two boreholes will be drilled to perform new gas injection test :

- ~ 35 m, horizontal and oriented parallel to σ_h and σ_H
- Equipped with multi-packers system with 5 intervals
- 2 gas injection sequences will be tested: fast and slow flow rate into two different intervals



Fast gas injection test

Slow gas injection test

eurad
European Joint Programme
on Radioactive Waste Management



DRD/MFS/20-0005

Ce document est la propriété de l'Andra.
Il ne peut être reproduit ou communiqué sans son autorisation expresse et préalable.

New boreholes (PGZ3)

Two boreholes will be drilled to perform new gas injection test :

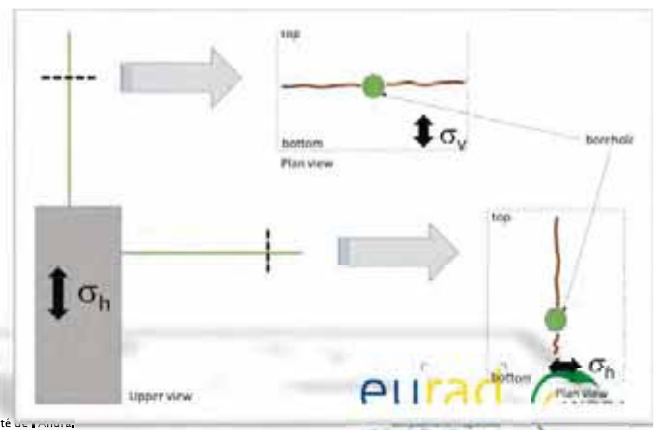
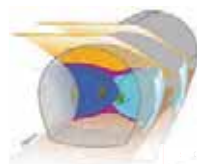
- ~ 35 m, horizontal and oriented parallel to σ_h and σ_H
- Equipped with multi-packers system with 5 intervals
- 2 gas injection sequences will be tested: fast and slow flow rate into two different intervals
 - Fast gas injection test : 2020
 - Slow gas injection test : 2020-2021
- Data will be available for modelers
 - GAS and DECOVALEX projects

Opening parallel to σ_H



DRD/MFS/20-0005

Opening parallel to σ_h



eurad
European Joint Programme
on Radioactive Waste Management



Ce document est la propriété de l'Andra.
Il ne peut être reproduit ou communiqué sans son autorisation expresse et préalable.



Gas injection test in swelling clay

PGZ2 experiment

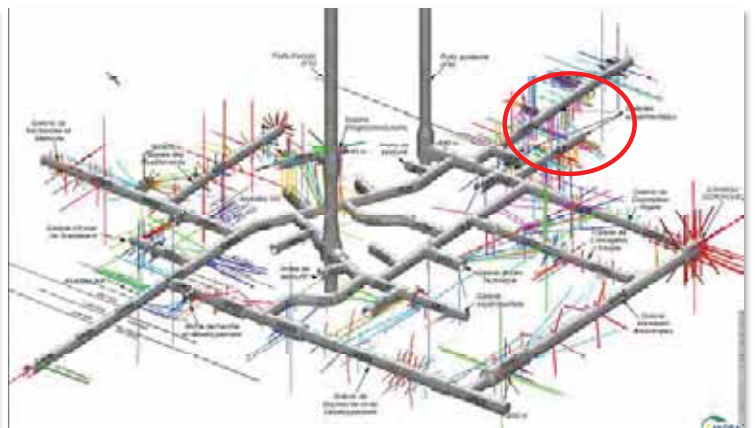
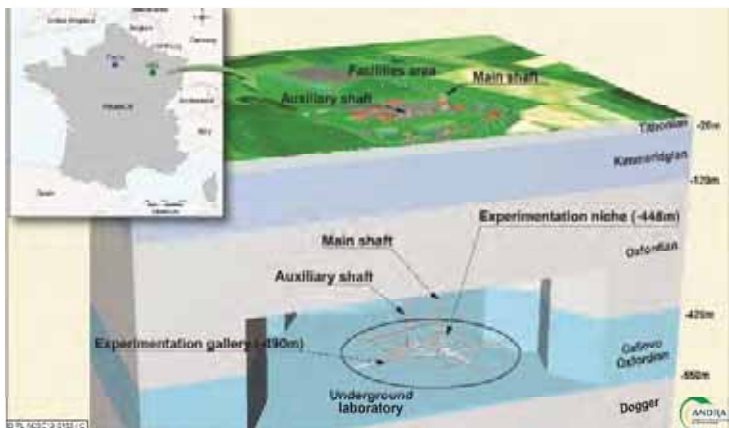
DRD/MFS/20-0005

Ce document est la propriété de l'Andra. Il ne peut être reproduit ou communiqué sans son autorisation expresse et préalable.



In-situ gas injection tests into bentonite PGZ2 experiment

- « PGZ2 » is dedicated to study :
 - Competition between gas production and bentonite resaturation,
 - Gas migration around and through the bentonite



DRD/MFS/20-0005

Ce document est la propriété de l'Andra. Il ne peut être reproduit ou communiqué sans son autorisation expresse et préalable.



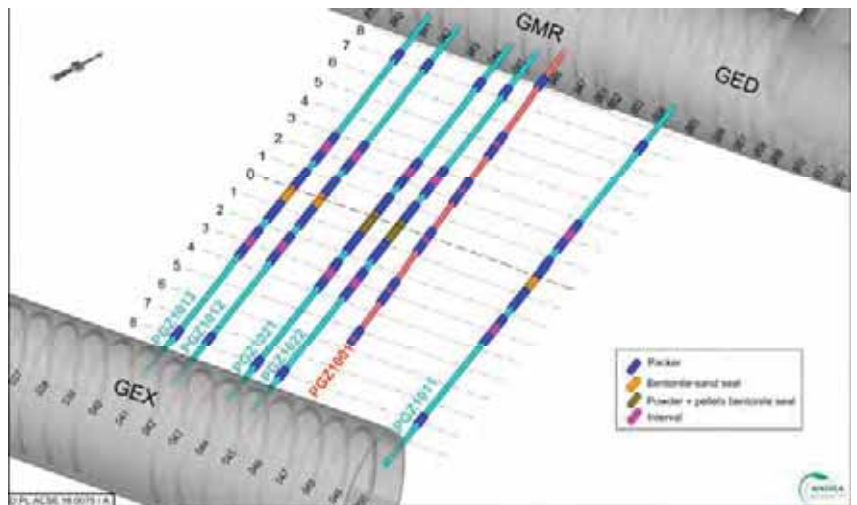
In-situ gas injection tests into bentonite Layout

Cores seals based on swelling clay (bentonite MX80) were set up in boreholes of 101 mm diameter between two drifts.

- This diameter limits the delay to get a full saturation of the seal
 - Natural hydration from CO_x

Different bentonite plug :

- Compacted bentonite (70%) + sand (30%)
 - PGZ1011-1012-1013
- Powder and pellets mixture
 - PGZ1021-1021



DRD/MFS/20-0005

Ce document est la propriété de l'Andra.
Il ne peut être reproduit ou communiqué sans son autorisation expresse et préalable.



In-situ gas injection tests into bentonite Layout

PGZ1001

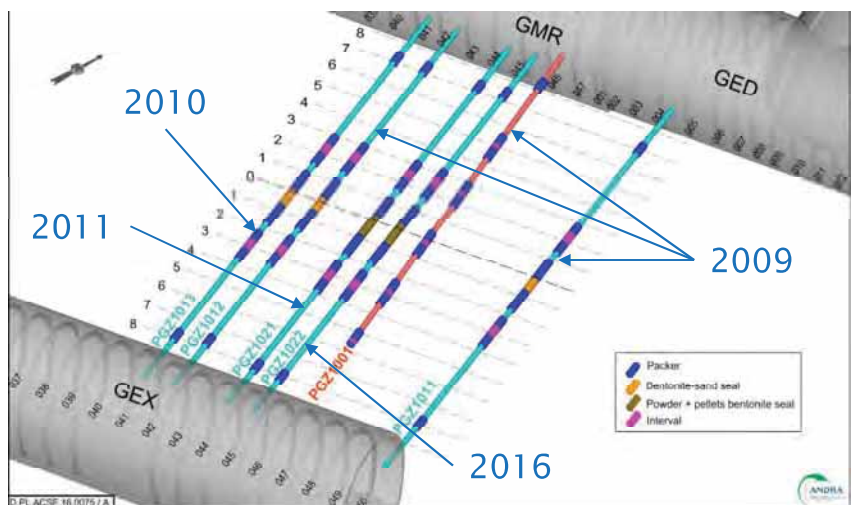
- Pore pressure profil between the two drifts

PGZ1011, PGZ1012 and PGZ1013

- PGZ1012 et PGZ1013
- PGZ1011
 - Gas injection
 - At different constant pressures during 70 days (october 2009 – january 2010)
 - Both faces of the seal

PGZ1021 and PGZ1022

- PGZ1021
 - Injection at constant flow rate
 - Only one side of the seal (GMR)
 - Directly after installation (april 2011) until december 2012
- PGZ1022



After full saturation, some gas interference tests have been done

DRD/MFS/20-0005

Ce document est la propriété de l'Andra.
Il ne peut être reproduit ou communiqué sans son autorisation expresse et préalable.





Gas injection test in swelling clay

Compacted bentonite + sand mixture

DRD/MFS/20-0005

Ce document est la propriété de l'Andra.
Il ne peut être reproduit ou communiqué sans son autorisation expresse et préalable.



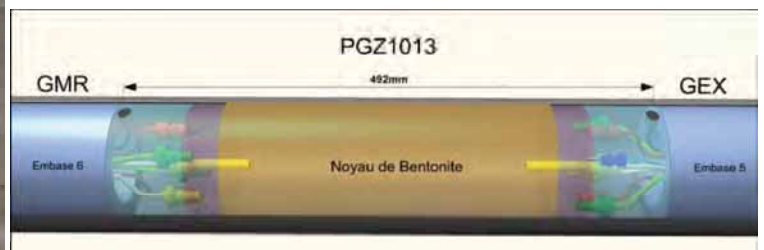
Characteristics of the compacted seals PGZ1011 to PGZ1013

Characteristics

- Bentonite (MX80) – sand (70% - 30% in mass)
- Target swelling pressure 7 MPa
 - Dry density of clay in the mixing ~ 2,06 g/cm³
 - Void annular => dry density of clay in-situ ~ 1,8 g/cm³

Sensors

- Interstitial pressure
- Total pressure
- Temperature



DRD/MFS/20-0005

Ce document est la propriété de l'Andra.
Il ne peut être reproduit ou communiqué sans son autorisation expresse et préalable.



Characteristics of the compacted seals PGZ1011 to PGZ1013

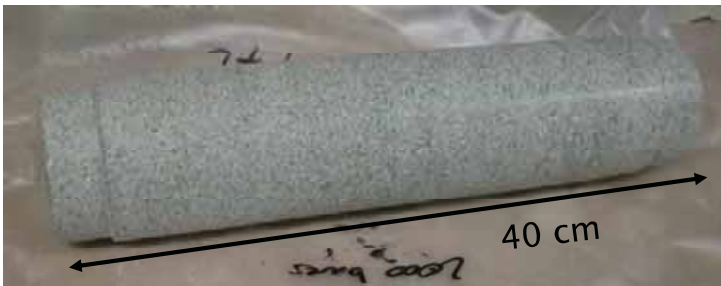


Characteristics

- CEA provided :
 - the compacted bentonite-sand plug
 - the sensors and the system surrounding the bentonite plug

Sensors

- Interstitial pressure
- Total pressure
- Temperature



Document est la propriété de l'Andra. Il ne peut être reproduit ou communiqué sans son autorisation expresse et préalable.

European Union Programme for Radioactive Waste Management

Installation of the plug into the borehole PGZ1011 to PGZ1013



After drilling the borehole between GEX and GMR drifts

- The first half-completion (provided by Solexperts) is inserted into the borehole from one drift until it exits on the other drift



DRD/MFS/20-0005

Document est la propriété de l'Andra. Il ne peut être reproduit ou communiqué sans son autorisation expresse et préalable.

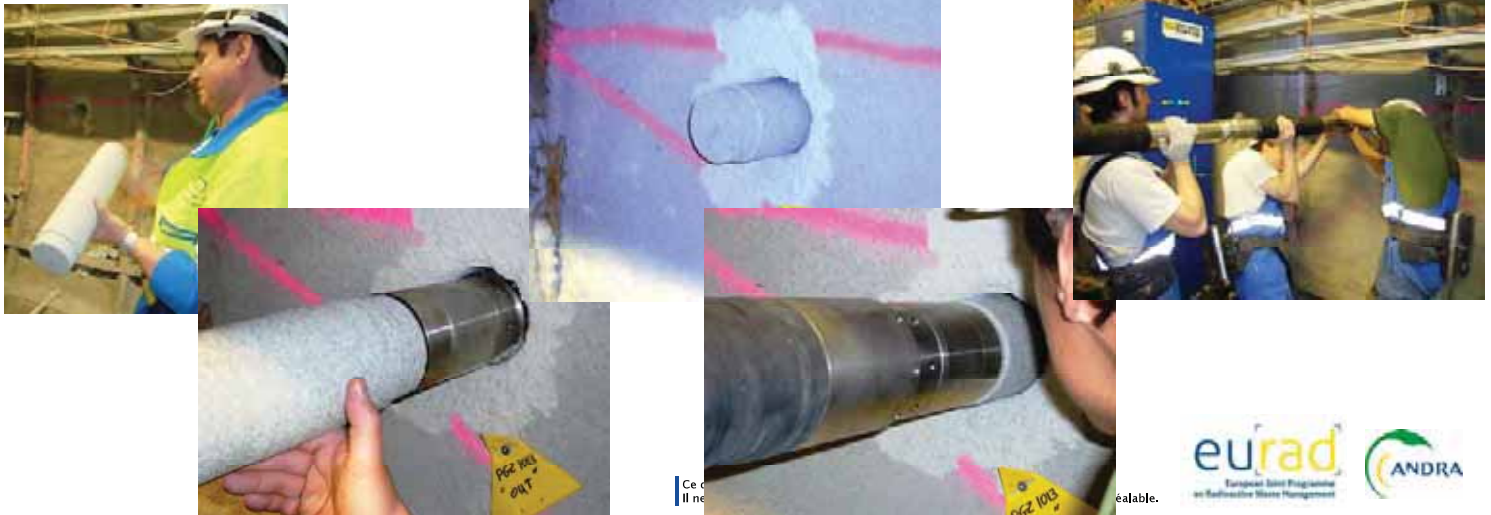
European Union Programme for Radioactive Waste Management

Installation of the plug into the borehole PGZ1011 to PGZ1013



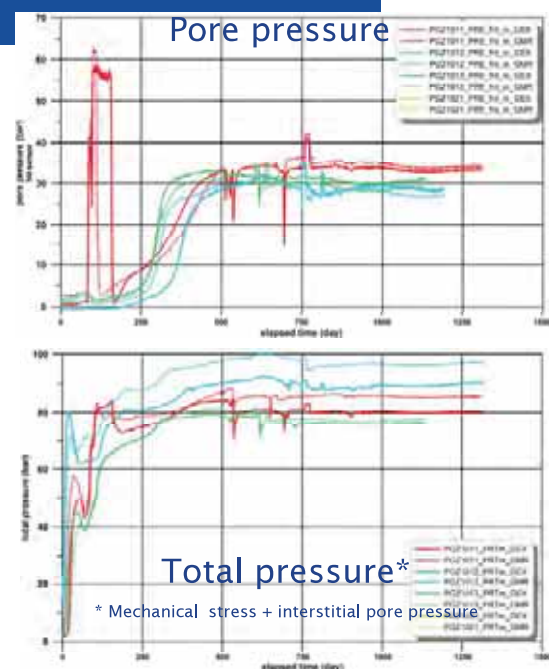
After drilling the borehole between GEX and GMR drifts

- Then the compacted bentonite plug is brought into contact with the sinter and the plug + second half of the completion are pushed into the borehole to the target distance



Results on compacted bentonite-sand mixture

- Hydration process
 - Full saturation (> 98%) reaches after 500-600 days
 - Complex transitory => structural effect due to the presence of void around the seal
 - Kinetic is slightly lower for PGZ1011 vs PGZ1012-1013
- Swelling pressure 4,5 < < 6,5 MPa
 - Lower than the target swelling pressure 7 MPa
 - Due to voids around seal which were much higher than expected
- Water hydraulic tests
 - Water permeability :1 to 5 10⁻¹³ m/s
 - During tests, no evidence of bypass at the interface between seal and claystone



* Mechanical stress + interstitial pore pressure



Gas interference test PGZ1013

The objective of this gas test is to evaluate the ability of gas to percolate along the interface between the rock and the bentonite plug

After full hydration, a gas interference test was done on PG1013 borehole

- First step, the water pressure was reduced on one side of the plug to create a pressure gradient along the plug
- Second step, gas is injected at different pressure at the opposite location
 - A gas mixture (nitrogen + helium) is used
 - Helium is detected in the extraction line



Swelling pressure = 4.5 to 5.5 MPa

DRD/MFS/20-0005

Ce document est la propriété de l'Andra. Il ne peut être reproduit ou communiqué sans son autorisation expresse et préalable.

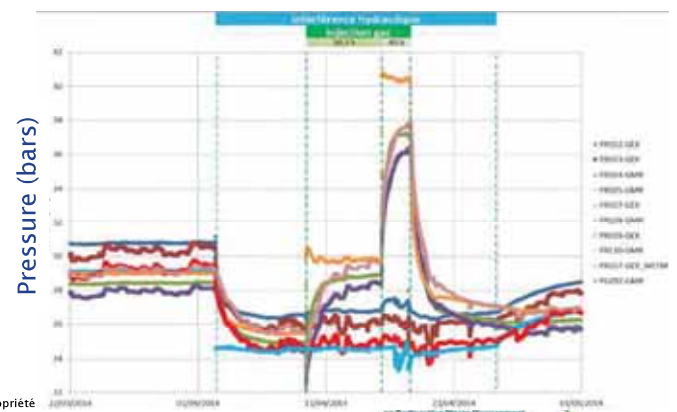
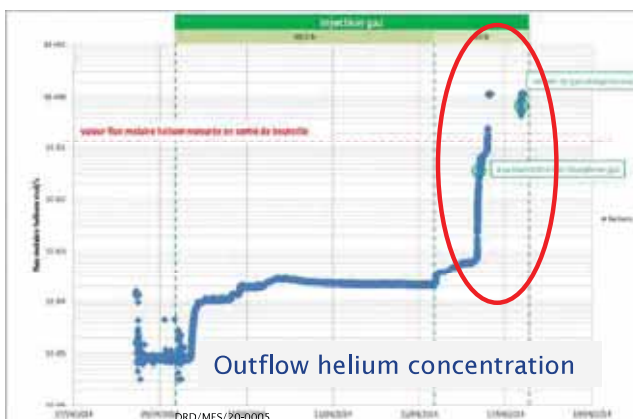
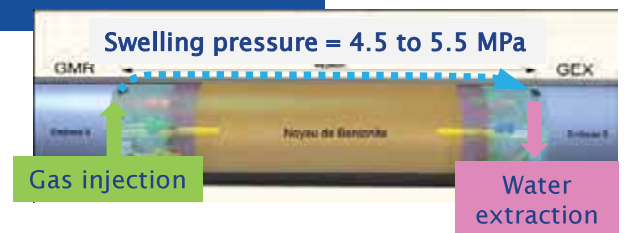


Gas interference test PGZ1013

Gas breakthrough with a small differential gas over pressure between 0.5 to 1.5 MPa

- Well below swelling pressure

Gas passage localized at the interface between plug/claystone or into the borehole damaged zone



Ce document est la propriété de l'Andra. Il ne peut être reproduit ou communiqué sans son autorisation expresse et préalable.

Gas transfer at interfaces

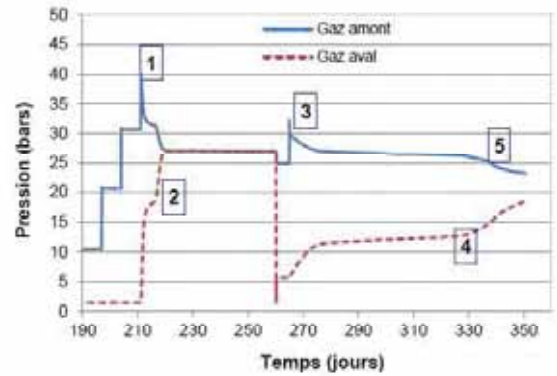
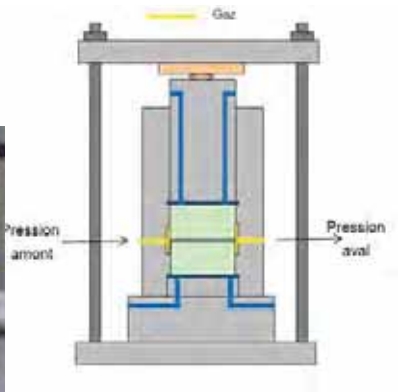
Laboratory tests



Gas injection test at interface between two blocks of bentonite

- Swelling pressure is 2.5 MPa
- Gas breakthrough pressure is 4 MPa : well above the swelling pressure !

Initial thickness ~3mm



DRD/MFS/20-0005

Ce document est la propriété de l'Andra. Il ne peut être reproduit ou communiqué sans son autorisation expresse et préalable.

European Joint Programme in Radioactive Waste Management



Gas injection test in swelling clay

Bentonite pellets and powder mixture

DRD/MFS/20-0005

Ce document est la propriété de l'Andra. Il ne peut être reproduit ou communiqué sans son autorisation expresse et préalable.



Characteristics of the powder and pellets mixture seals PGZ1021 and PGZ1022

Characteristics

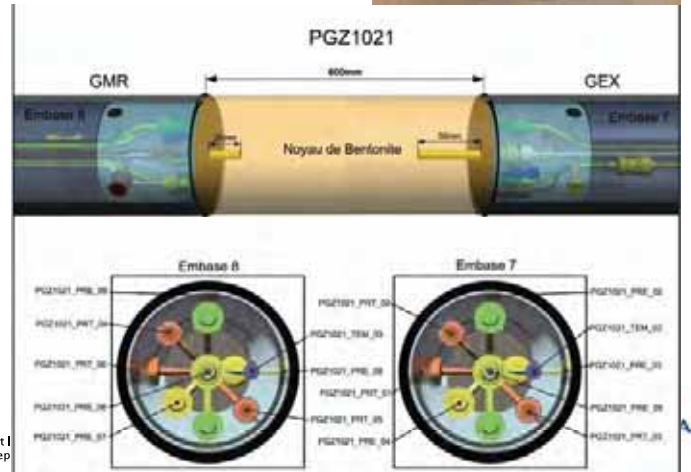
- Bentonite (MX80)
 - In mass, 68% pellets and 32% powder
- Dry density ?



Il ne peut être rep...

Sensors

- Interstitial pressure
- Total pressure
- Temperature

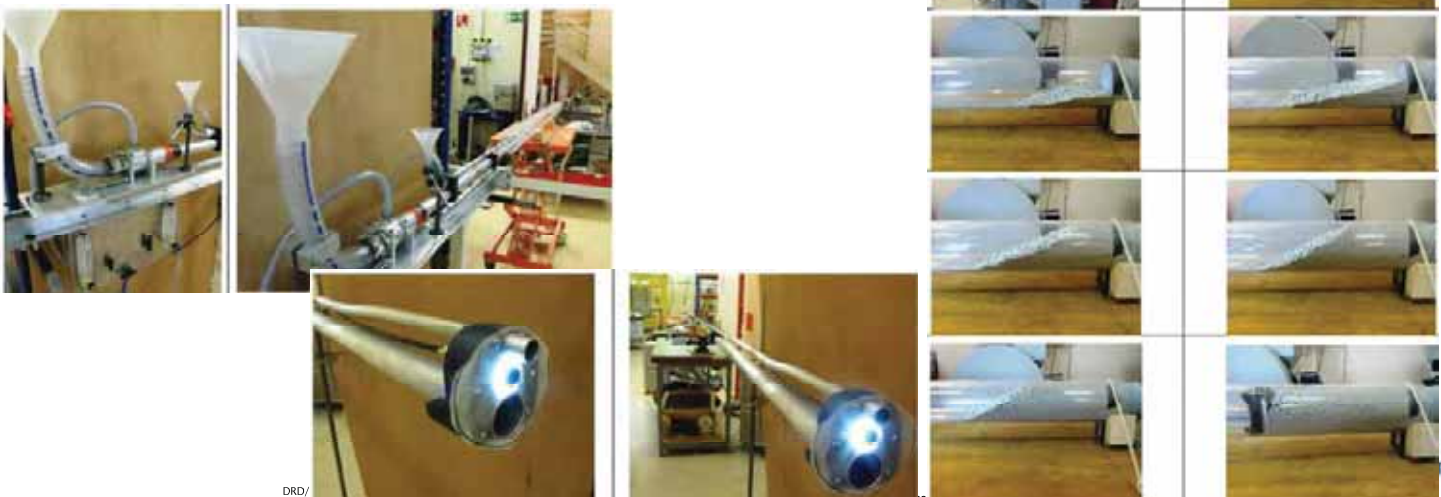


Powder and pellets mixture injection



The CEA has developed a specific tool to spray pellets and bentonite powder with compressed air in a borehole

- The talus formed is then compacted



DRD/

RA

Powder and pellets mixture injection



The CEA has developed a specific tool to spray pellets and bentonite powder with compressed air in a borehole

- The talus formed is then compacted



Il ne peut être reproduit ou communiqué sans son autorisation expresse et préalable.

In-situ injection powder and pellets mixture



The talus formed in the borehole is then compacted when the second half-completion is put in place (provided by Solexperts)



DRD/MFS/20-0005

Il ne peut être reproduit ou communiqué sans son autorisation expresse et préalable.

Estimation of the dry density of the mixture



The theoretical density is obtained as a function of the final length of the embankment, the radius of the borehole and the mass of material injected.

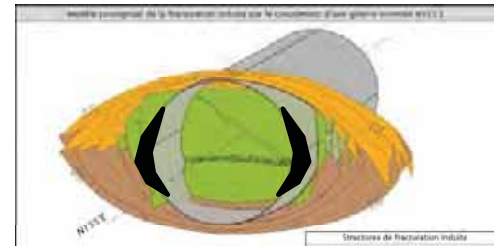
- The dry density was estimated at 1,54 – 1,55 (kg/m³) for the plugs in PGZ1021 and PGZ1022
 - Uncertainties about the density depend on the dispersion of the powder in the borehole (loss of mass) and the presence of breakouts (which increases the volume).



DRD/MFS/20-0005



Ce document est la propriété de l'Andra. Il ne peut être reproduit ou communiqué sans son autorisation expresse et préalable.



Breakouts are surface rock spalling that originate from part of the induced fracture network



Estimation of the dry density of the mixture

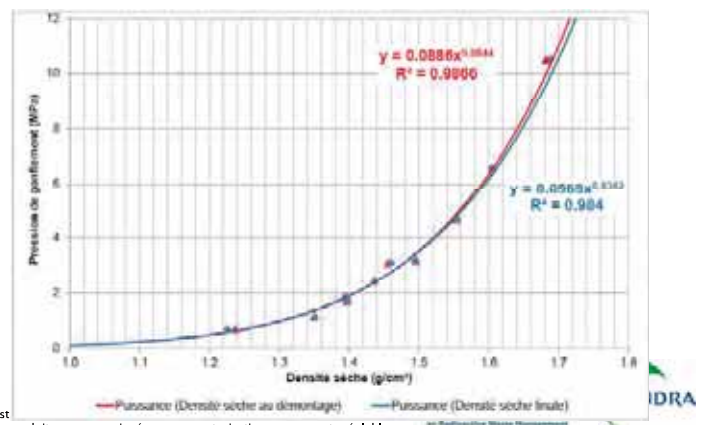


The theoretical density is obtained as a function of the final length of the embankment, the radius of the borehole and the mass of material injected.

- The dry density was estimated at 1,54 – 1,55 (g/m³) for the plugs in PGZ1021 and PGZ1022
 - Uncertainties about the density depend on the dispersion of the powder in the borehole (loss of mass) and the presence of breakouts (which increases the volume).
- Swelling pressure is estimated between 4 to 5 MPa
 - But total pressure sensor measures the pressure locally (strongly dependent from local density)



DRD/MFS/20-0005

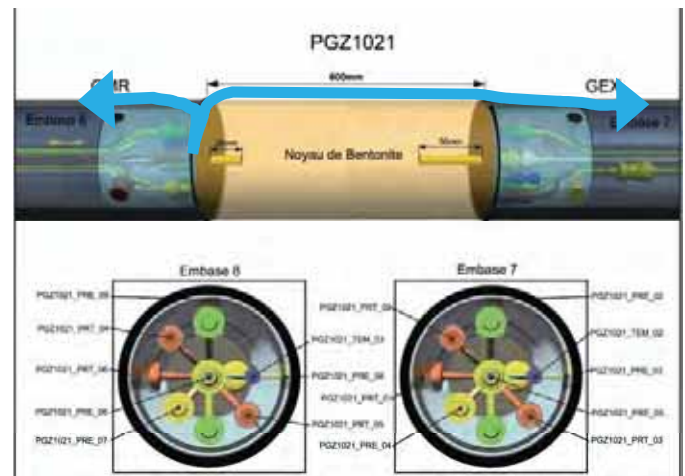


Ce document est la propriété de l'Andra. Il ne peut être reproduit ou communiqué sans son autorisation expresse et préalable.

Impact of gas injection during hydration PGZ1021

Directly after installation, gas (nitrogen) was injected at constant flow rate (~ 1 mLn/min at GMR side of the bentonite plug) during 20 months

- The gas pressure never rises
 - The gas could easily flow through the interfaces
 - packers-rock
 - bentonite-rock



DRD/MFS/20-0005

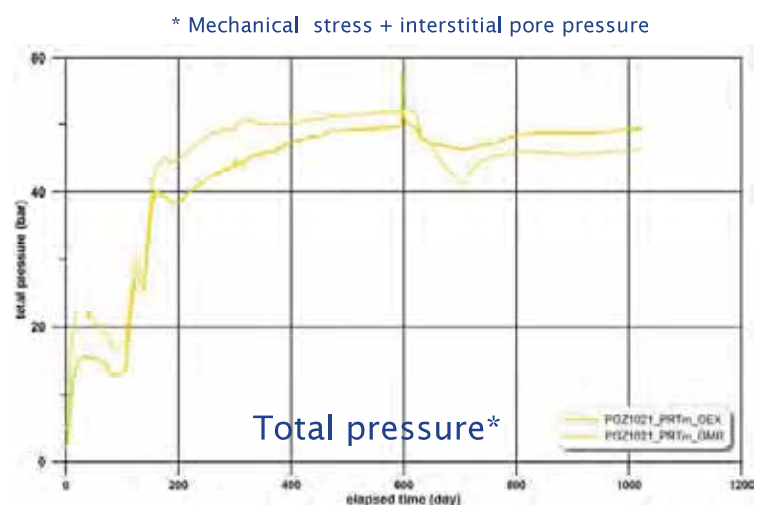
Ce document est la propriété de l'Andra.
Il ne peut être reproduit ou communiqué sans son autorisation expresse et préalable.



Impact of gas injection during hydration PGZ1021

Directly after installation, gas (nitrogen) was injected at constant flow rate (~ 1 mLn/min at GMR side of the bentonite plug) during 20 months

- The gas pressure never rises
 - The gas could easily flow through the interfaces
- The plug takes water from surrounding rock despite the long gas injection phase
 - Swelling pressure is closed to 2 MPa
 - Heterogeneity on swelling pressure: 2.1 MPa GMR side and 1.7 MPa GEX side



DRD/MFS/20-0005

Ce document est la propriété de l'Andra.
Il ne peut être reproduit ou communiqué sans son autorisation expresse et préalable.



Gas interference test PGZ1021

The objective of this gas test is to evaluate the ability of gas to percolate along the interface between the rock and the bentonite plug

After full hydration, a gas interference test was done on PG1021 borehole

- First step, the water pressure was reduced on one side of the plug to create a pressure gradient along the plug
- Second step, gas is injected at different pressure at the opposite location
 - A gas mixture (nitrogen + helium) is used
 - Helium is detected in the extraction line



DRD/MFS/20-0005

Ce document est la propriété de l'Andra. Il ne peut être reproduit ou communiqué sans son autorisation expresse et préalable.

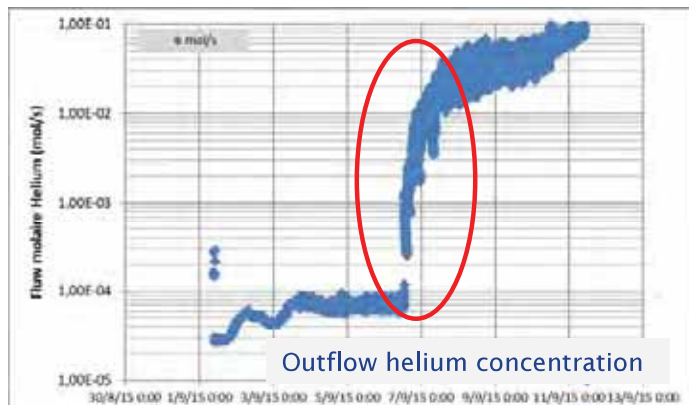


Gas interference test PGZ1021

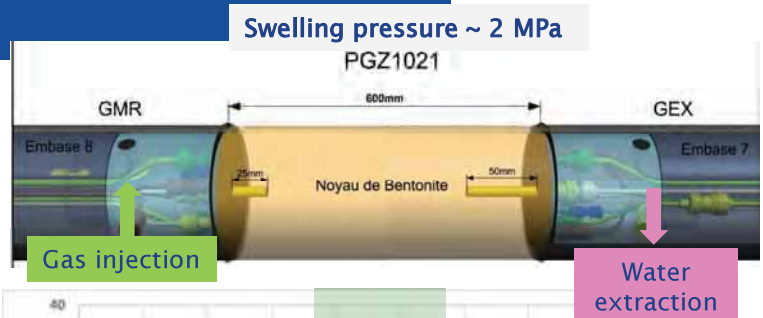
Gas breakthrough with a small differential gas over pressure between 0.5 to 1.5 MPa

- below swelling pressure

Gas passage localized at the interface between plug/claystone or into the borehole damaged zone



DRD/MFS/20-0005



Ce document est la propriété de l'Andra. Il ne peut être reproduit ou communiqué sans son autorisation expresse et préalable.



PGZ2 summary

Compacted bentonite-sand mixture plugs reach highest swelling pressure versus powder and pellets plugs

Gas injection tests carried out during hydration of the bentonite plugs does not prevent the natural resaturation of these plugs

- Only slower hydration kinetic is observed

After complete resaturation of the bentonite plugs, gas injection tests carried out at the plug-rock interface showed that the gas was able to percolate along the interface (or possibly into the damaged zone of the borehole) at a pressure **lower** than the swelling pressure

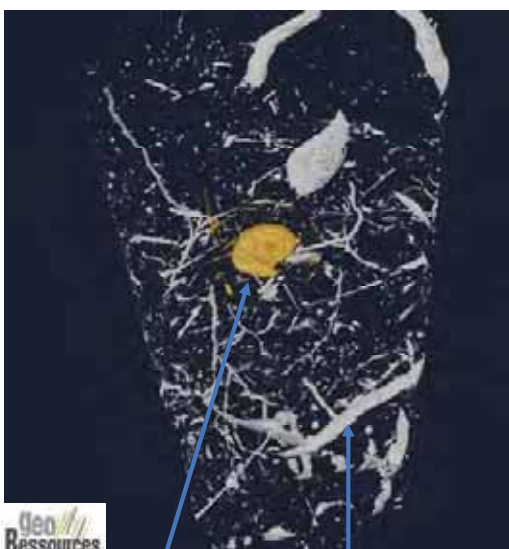
- In laboratory tests, gas injection tests performed in bentonite show that the gas breakthrough pressure is usually higher than the swelling pressure
- Important point regarding safety issues for a radioactive waste disposal because gas produced into the disposal will easily percolate along drifts and shafts

DRD/MFS/20-0005

Ce document est la propriété de l'Andra.
Il ne peut être reproduit ou communiqué sans son autorisation expresse et préalable.



X-ray tomography of COx sample



ammonite

bioturbation

DRD/MFS/20-0005

Thank you for your attention



The project leading to this application has received funding from the European Union's Horizon 2020 research and innovation programme under grant agreement n° 847593.

eurad
European Joint Programme
on Radioactive Waste Management



Ce document est la propriété de l'Andra.
Il ne peut être reproduit ou communiqué sans son autorisation expresse et préalable.

X-ray tomography of COx sample



ammonite

bioturbation

DRD/MFS/20-0005

References


- Armand, G. et al. (2014). Geometry and Properties of the Excavation Induced Fractures at the Meuse/Haute-Marne URL Drifts. *International Journal of Rock Mechanics and Mining Sciences* 27(1): 21-41
- Cuss, R. J. et al. (2014). Experimental observations of mechanical dilation at the onset of gas flow in Callovo-Oxfordian claystone. *Geological Society, London, Special Publications*, 400, 507-519
- de La Vaissière, R. et al. (2014). Gas injection test in the Callovo-Oxfordian claystone: data analysis and numerical modelling. *Geological Society, London, Special Publications*, 400, 427-441
- de La Vaissière, R., et al. (2019). From Two-Phase Flow to Gas Fracturing into Callovo-Oxfordian Claystone. ARMA. *Proceedings of the 53rd U.S. Rock Mechanics/Geomechanics Symposium*, 23-26 June, New York, USA
- de La Vaissière, R., et al. (2019). Effect of gas flow rate on gas fracturing in Callovo-Oxfordian claystone. *ISRM, Proceedings of the 14th International Congress on Rock Mechanics and Rock Engineering*, September 13-18, Foz do Iguaçu, Brazil
- Harrington, Jon F. et al. (2017). Gas transport properties through intact and fractured Callovo-Oxfordian mudstones. *Geological Society, London, Special Publications*, 454.
- Marschall, P. et al. (2005). Characterisation of Gas Transport Properties of the Opalinus Clay, a Potential Host Rock Formation for Radioactive Waste Disposal. *Oil & gas science & technology* 60 (1): 121-139.
- Senger, R. et al. (2006). Design and analysis of a gas threshold pressure test in a low-permeability clay formation at Andra's Underground Research Laboratory, Bure (FRANCE). *Proceedings, TOUGH Symposium 2006*, Lawrence Berkeley National Laboratory, Berkeley, California, May 15-17, USA

Ce document est la propriété de l'Andra.

Il ne peut être reproduit ou communiqué sans son autorisation expresse et préalable.



Appendix Q. In situ testing of gas transfer in crystalline rocks (P. Sellin)



IN SITU TESTING OF GAS TRANSFER


1 Crystalline rocks

2020-01-24 • Patrik Sellin

 The project leading to this application has received funding from the European Union's Horizon 2020 research and innovation programme under grant agreement n° 847593.

2020-01-24 EURAD Doctoral School 1

1



OVERVIEW

- **Background**
- **The Lasgit test**
 - Background
 - The location
 - Installation activities
 - Hydration
 - Gas injection tests
 - FCT
 - Decommissioning
- **Summary and conclusions**

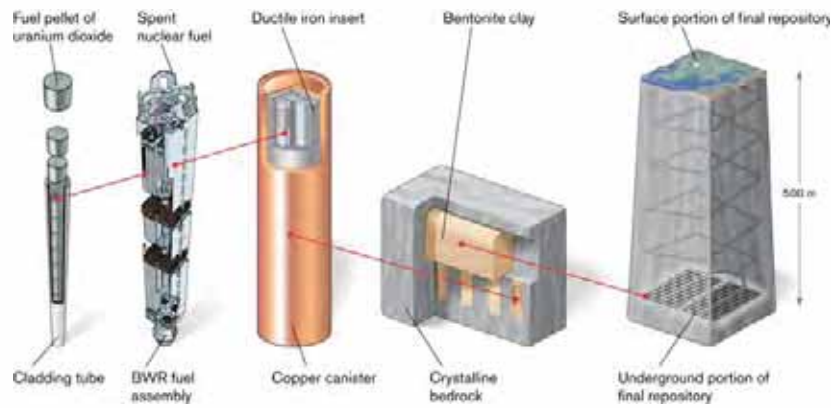


2020-01-24 EURAD Doctoral School 2

2

BACKGROUND

The KBS-3 concept (Sweden & Finland)



Primary safety function: Complete containment

Secondary safety function: Retardation

2020-01-24

EURAD Doctoral School

eurad

3

3

BACKGROUND

- **Transport of gas in the buffer can occur in two phases of the repository's evolution:**
 - Initially trapped air needs to escape
 - Hydrogen from corrosion of the steel insert – if the copper shell is damaged
- **Gas which is trapped in or by the buffer can escape by two principal mechanisms:**
 - Gas can be dissolved in the porewater and be removed by diffusion
 - In a gas phase, through a flow path

2020-01-24

EURAD Doctoral School

eurad

4

4

BACKGROUND - HISTORY

- **The iron insert was introduced in the early '90s**
- **Gas issue became important**
 - Especially in the case of manufacturing defects in the copper shell
- **Initial modelling and laboratory tests started 1992-1994**
 - Laboratory tests presented yesterday by Jon Harrington
- **RD&D 1998: "Special experiments are planned to determine how gas penetrates through a bentonite buffer"**
- **RD&D 2001: "There will not be time for any experiments on repository scale during the ensuing three-year period, which means that scale dependence will be a remaining uncertainty"**
 - SKI (regulator) review 2002: "need for experiments in different scales, including long-term tests in full scale"
- **RD&D 2004: "A clear conclusion from all projects in the area is that gas transport experiments on a larger, preferably full, scale are necessary. SKB has therefore decided to carry out a full-scale experiment in the Äspö HRL (Lasgit)"**
 - SKI (regulator) review 2002: "SKI is very positive to the decision about a full scale test"

2020-01-24

EURAD Doctoral School

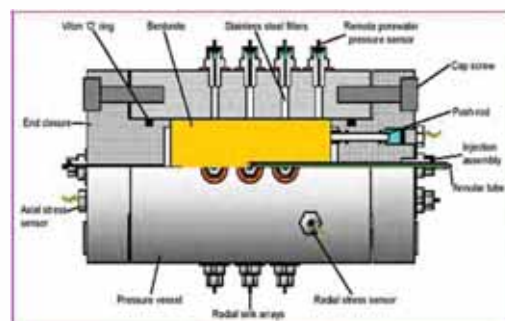
eurad

5

5

THE LASGIT TEST - BACKGROUND

- **A detailed study was initiated in ~1994 to examine the key variables controlling the entry and movement of corrosion gas in the bentonite**
- **Novel apparatus was designed and manufactured to allow the gas migration process to be investigated and quantified under simulated repository conditions**
- **Results showed gas flow was in pressure-induced pathways with conspicuous sensitivity to stress, porewater pressure and boundary conditions**



2020-01-24

EURAD Doctoral School

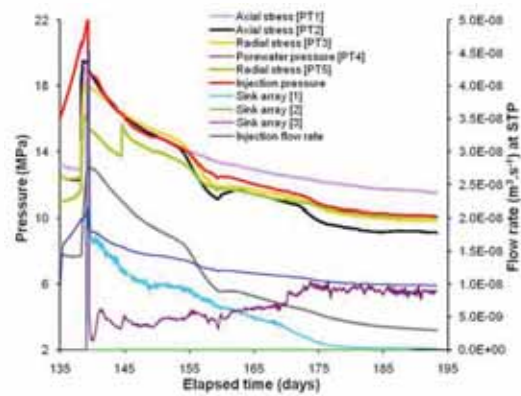
eurad

6

6

THE LASGIT TEST - BACKGROUND

- The knowledge was based on small-scale laboratory studies
- These diagnostic tests addressed specific issues relating to gas migration and its long-term effect on the hydro-mechanical performance of the buffer clay
- Laboratory studies have been used to develop process models to assess the likely implications of gas flow in a hard-rock repository system
- While significant improvements in our understanding of the gas-buffer system had been taken place, a number of important uncertainties remain
- **Central to these is the issue of scale and its effect on the mechanisms and process governing gas flow in compact bentonite**



2020-01-24

EURAD Doctoral School

eu rad

7

7

THE LASGIT TEST - BACKGROUND

- **Objectives of Lasgit are:**
 - To perform and interpret a series of large scale gas injection tests
 - Examine issues relating to up-scaling and its effect on gas movement and buffer performance
 - Provide information on the processes of hydration and gas migration
 - Provide high-quality test data to test/validate modelling approaches



2020-01-24

EURAD Doctoral School

eu rad

8

8

LOCATION



2020-01-24

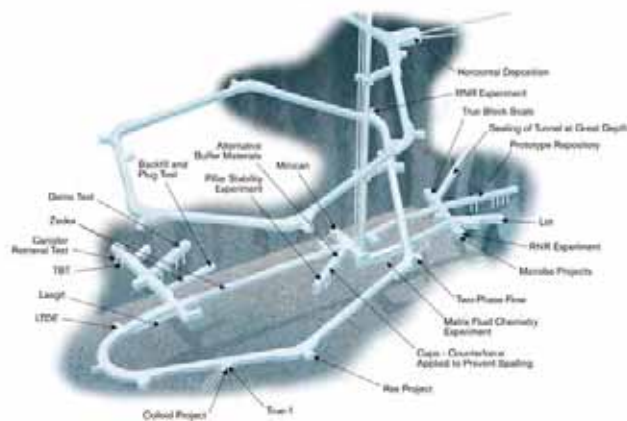
EURAD Doctoral School

eu|rad

9

9

LOCATION



2020-01-24

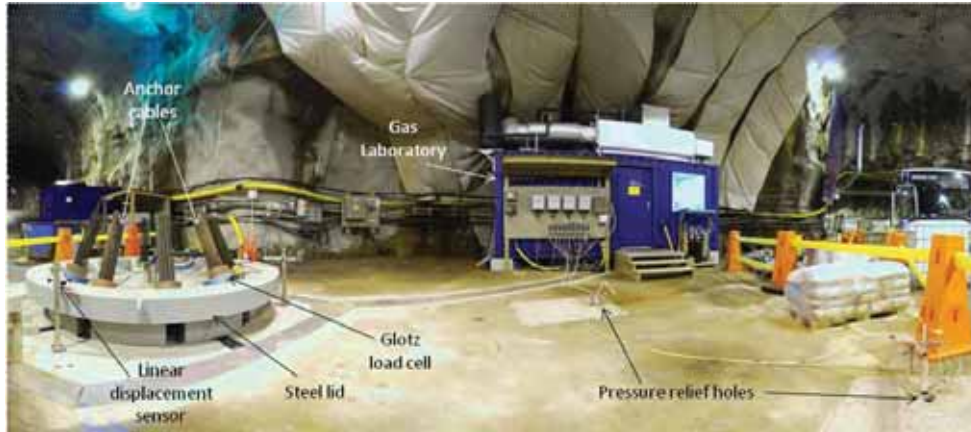
EURAD Doctoral School

eu|rad

10

10

THE LOCATION



2020-01-24

EURAD Doctoral School

euRad

11

11

THE DEPOSITION HOLE



2020-01-24

EURAD Doctoral School

euRad

12

12

INSTALLATION ACTIVITIES

- Geological Mapping of the Assembly Hall and deposition hole
- Inflow of water
- Manufacturing of buffer
- Preparation of canister
- Deposition hole instrumentation
- Gas laboratory
- Data acquisition
- Lid
- Gas injection equipment

2020-01-24

EURAD Doctoral School

eurad

13

13

GEOLOGICAL MAPPING OF THE ASSEMBLY HALL AND DEPOSITION HOLE

- The assembly hall constitutes of an enlarged part (higher and wider in about a 30m long section)
 - Geological mapping of tunnel roof, walls and parts of the floor
- The large deposition hole was drilled in 1999). The approximate depth of the hole is 8.5m and the diameter is 1.75m
- In the tunnel the geological mapping was made on paper. The orientations of structural features are obtained by compass readings
- The standard tunnel mapping is presented on a 2-D drawing where the tunnel walls have been unfolded to form a plane together with the tunnel roof
- The deposition holes are regarded as small tunnels

Rock type	Area m ²	% of mapped area (side walls, and roof, 809m ²)
Aspo diorite	752,37	93
Fine-grained granite	40,45	5
Greenstone	16,18	2
Total	809	100

Length interval in meters	Standard mapping of roof and walls, cut off about 1m	
	No of fractures	% of all the 132 fractures
1<2	9	7
2<3	21	16
3<4	14	11
4<5	15	11
5<6	12	9
6<7	9	7
7<8	9	7
8<9	10	8
9<10	4	3
10<15	23	17
15<20	4	3
20<25	2	1
Total	132	100

2020-01-24

EURAD Doctoral School

eurad

14

14

INFLOW OF WATER

- "External" water: 0.007-0.013 litres/minute
- "Internal water": 0.2 litres/minute
- Pressure drop tests or pulse tests performed in the anchor holes:
 - $K = 10^{-12} - 7 \cdot 10^{-10} \text{ m/s}$
- Gas leakage tests if there were any connections between the anchor holes themselves and the water filled Lasgit hole



2020-01-24

EURAD Doctoral School

eu|rad

15

15

MANUFACTURING OF BUFFER

Block No.	Water ratio (%)	Bulk density (kg/m ³)	Degree of saturation	Void ratio	Dry density (kg/m ³)
LASC1	26.5	2018.1	0.993	0.743	1594.9
LASC2	26.4	2015.2	0.986	0.743	1594.8
LASC3	26.2	2020.4	0.989	0.736	1601.2
LASC4	26.1	2017.4	0.984	0.738	1599.9
LASC5	26.8	2017.9	0.997	0.746	1592.0
LASC6	26.0	2020.9	0.986	0.733	1604.0
LASR1	22.5	2055.5	0.951	0.656	1678.6
LASR2	23.0	2050.2	0.958	0.668	1666.6
LASR3	22.6	2054.1	0.953	0.659	1675.2
LASR4	22.7	2059.6	0.962	0.656	1678.6
LASR5	23.3	2057.0	0.973	0.667	1668.0
LASR6	22.9	2059.7	0.965	0.658	1676.5
LASR7	23.6	2058.4	0.980	0.669	1665.5
LASR8	23.0	2050.8	0.957	0.667	1667.9
LASR9	22.6	2060.6	0.962	0.655	1680.2
LASR10	22.8	2054.1	0.957	0.661	1673.4
LASR11	22.7	2061.4	0.964	0.655	1679.9
LASR12	22.7	2061.1	0.964	0.655	1679.5



2020-01-24

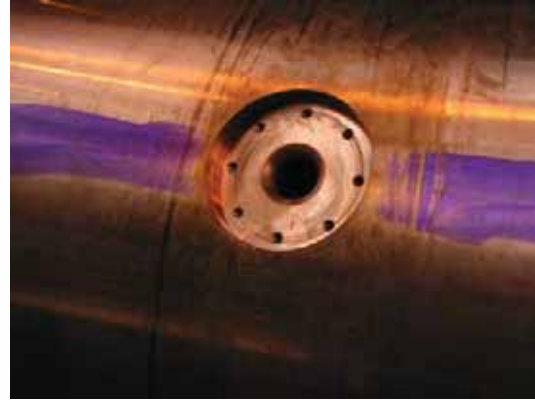
EURAD Doctoral School

eu|rad

16

16

CANISTER



2020-01-24

EURAD Doctoral School

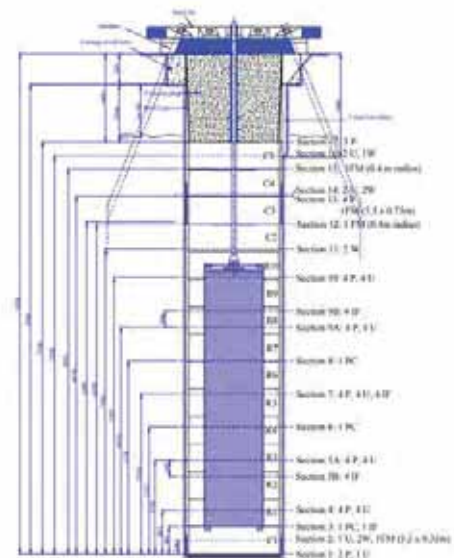
euRad

17

17

DEPOSITION HOLE INSTRUMENTATION

- Total pressure: 32 points
- Pore water pressure: 26 points
- Relative humidity: 7 points.
- In addition there will be measurements of plug and canister movements and also of the force in three of the anchors



2020-01-24

EURAD Doctoral School

euRad

18

18

GAS LABORATORY

- Hydration system
 - Hydraulic injection system
 - Gas injection system
 - Data acquisition system
 - Temperature control
-
- Calibration of instrumentation



2020-01-24

EURAD Doctoral School

eu^{rad}

19

19

DATA ACQUISITION

Area	Instrument	Manufacturer / supplier	Type
Laboratory	High pressure transducers	Hi-Pro	1000
	Low pressure transducers	Hi-Pro	1000
	Temperature sensor	RS Components?	K thermocouple
	Two-way servo valves	Hi-Pro	T5
	One-way servo valves	Hi-Pro	T1
	Oxygen level detector	BJ Industries	Series 310
	Web cam	TBG Solutions	-
Office	Thermocouple	-	K series
Downhole	4500-1X Total pressure cells	Geokon	4500-1X
	4500S Pore pressure cells	Geokon	4500S
	Thermocouple	-	-
	Global Force gauges	Global	-
	Stress Sensors mounted on canister	Sensotec	-
	Psychrometers	Wescor	-

2020-01-24

EURAD Doctoral School

eu^{rad}

20

20

LID

- **Restrict swelling of bentonite**
 - "Constant volume" conditions
- **Not deform or break during gas testing**
- **Minimize tension in anchor cables**
- **The lid was manufactured from carbon steel S 235 J2 G3 (SS 2172) with a thickness of 300 mm and a diameter of 2600 mm.**



2020-01-24

EURAD Doctoral School

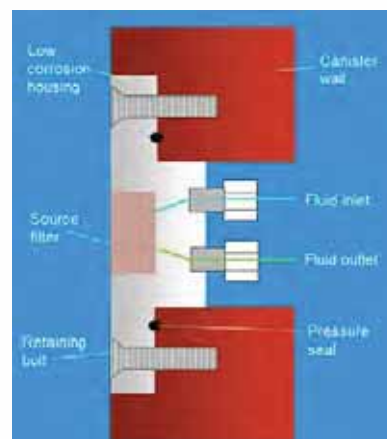
eurad

21

21

GAS INJECTION EQUIPMENT

- **To minimise corrosion each filter assembly are manufactured from bronze**
- **All fittings, pipe and valve work are selected for durability and low corrosion**
- **Each filter array is fitted with dual ports to facilitate the remove of test permeants**



2020-01-24

EURAD Doctoral School

eurad

22

22

LASGIT TESTING

- Hydration
- Gas injection tests
- FCT

2020-01-24

EURAD Doctoral School

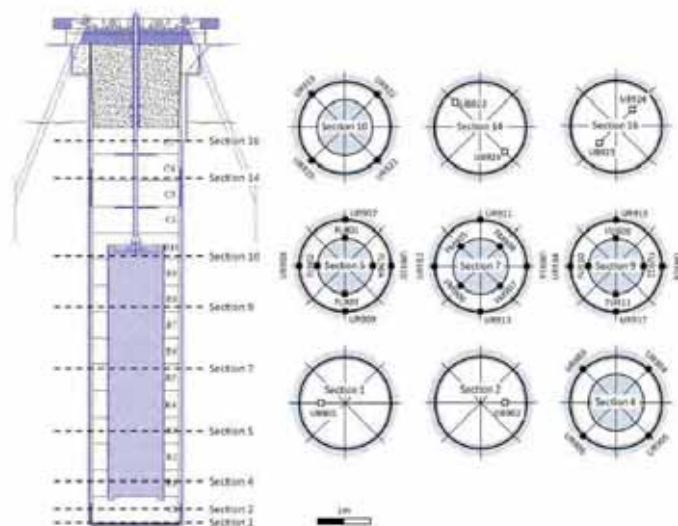
eu^{rad}

23

23

INSTRUMENTATION

- UB9xx = pore-pressure sensor within the bentonite buffer
- UR9xx = pore-pressure sensor at the rock wall
- FL90x = injection filter on the lower array
- FM90x = injection filter on the mid-plane array
- FU9xx = injection filter on the upper array
- Cx = bentonite block
- Rx = bentonite ring



2020-01-24

EURAD Doctoral School

eu^{rad}

24

24

HYDRATION

- Began on 1st February 2005 and was completed 25th May 2007
- P_w within the clay still low however P_w on the rock face exhibits a well defined asymptote
- Radial stress (rock wall) has increased significantly and continues to slowly evolve
- While non-uniformly distributed across the major axis of the hole, axial stress has also increased markedly and continues to evolve
- Suctions have decreased indicating progressive hydration of the clay
- Displacement data from the lid and canister indicate a dynamic, evolving system

The figure consists of six line graphs arranged in a 3x2 grid, all sharing an x-axis of 'Elapsed time (days)' from 0 to 2000.

- Top-left:** P_w in clay (kPa) vs. Elapsed time (days). Multiple lines show a slow, non-linear increase over time.
- Top-right:** P_w rock face (kPa) vs. Elapsed time (days). Lines show a rapid initial increase that levels off into a well-defined asymptote.
- Middle-left:** Radial stress (kPa) vs. Elapsed time (days). Lines show a steady, nearly linear increase over time.
- Middle-right:** Axial stress (kPa) vs. Elapsed time (days). Lines show a steady, nearly linear increase over time.
- Bottom-left:** Suction (kPa) vs. Elapsed time (days). Lines show a steady, nearly linear decrease over time.
- Bottom-right:** LID displacement (mm) vs. Elapsed time (days). Lines show a steady, nearly linear increase over time.

2020-01-24
EURAD Doctoral School
25

HYDRATION

- Average porewater pressure on the rock face at end of the stage was 1775 kPa
- Average radial stress on the rock face at the end of the stage was 4050 kPa
- Average axial stress within the clay at the end of the stage was 5155 kPa
- Average swelling pressure within the clay at the end of the stage was 2330 kPa
- Average radial and axial stress on the canister was 4640 kPa and 3630 kPa respectively

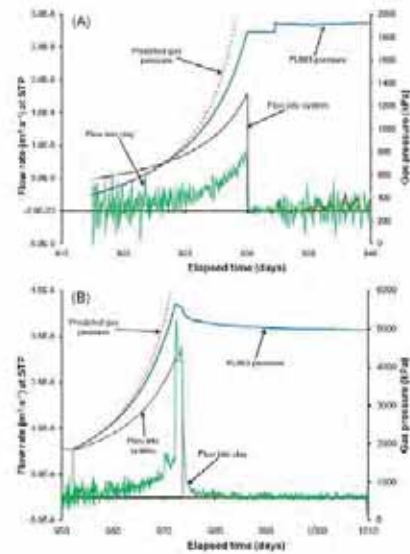
The figure contains four contour plots:

- Top-left:** Porewater pressure (rock face) at 601.00 days. A 2D plot with X (mm) and Z (mm) axes. Color scale ranges from 0 to 2000 kPa.
- Top-right:** Radial stress (rock face) at 601.00 days. A 2D plot with X (mm) and Z (mm) axes. Color scale ranges from 0 to 6000 kPa.
- Bottom-left:** Axial stress at 601.00 days. A circular plot with X (mm) and Y (mm) axes. Color scale ranges from 0 to 10000 kPa.
- Bottom-right:** Swelling pressure at 601.00 days. A 2D plot with X (mm) and Z (mm) axes. Color scale ranges from 0 to 10000 kPa.

2020-01-24
EURAD Doctoral School
26

GAS TEST 1

- Flow into the clay is calculated using a combination of weighted moving average and time moving average (mean)
- For plot (A) the departure between measured and predicted gas pressure is symptomatic of gas penetration of the buffer.
- In plot (B) the peak pressure response is symptomatic of the development of 'major' gas pathways within the buffer and is qualitatively similar in response to small-scale experiments



2020-01-24

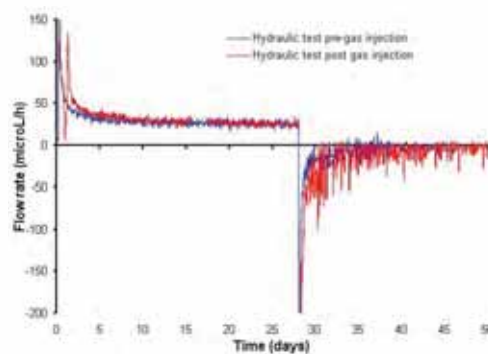
EURAD Doctoral School

eu^{rad}

27

27

GAS TEST 1 HYDRAULIC RESPONSE



- Visually data appears similar indicating nascent gas pathways appear to have no significant effect on the engineering performance of the buffer

2020-01-24

EURAD Doctoral School

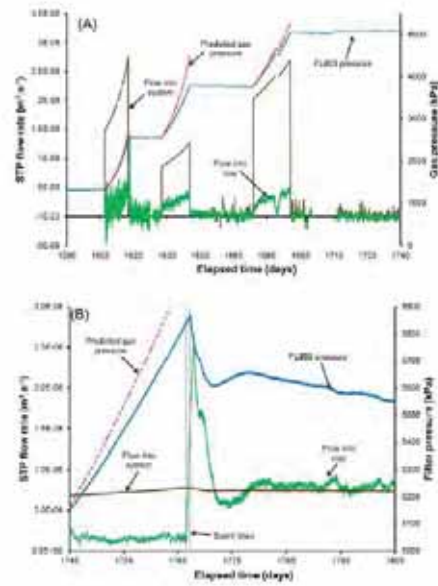
eu^{rad}

28

28

GAS TEST 2

- Inspection of plot (A) shows the reduction in flux into the clay during each constant pressure step.
- Plot (B) shows the 'major' gas entry event signified by the rapid increase in flux into the clay.
- This is followed by a well-defined negative flux transient which first under- and then over-shoots the injection flow rate into the system.
 - This is symptomatic of unstable gas pathways.



2020-01-24

EURAD Doctoral School

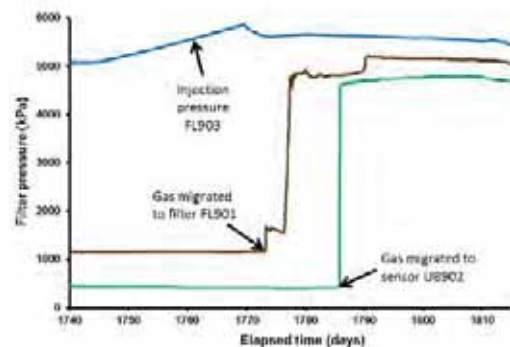
eu^{rad}

29

29

GAS TEST 2

- Prolonged gas injection in FL903
- As gas injection continued it resulted in an increase in pressure at FL901
- Pressure in sensor UB902 sometime later
- This shows that gas propagated to these locations and that the network of gas pathways continued to dynamically evolve following major gas entry



2020-01-24

EURAD Doctoral School

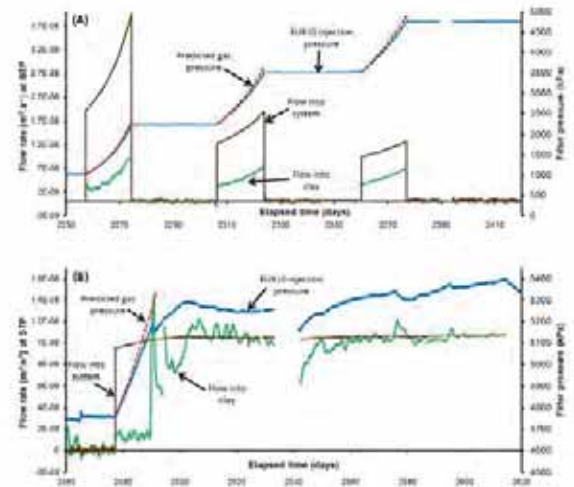
eu^{rad}

30

30

GAS TEST 3

- Inspection of plot (A) shows the reduction in flux into the clay during each constant pressure step
- Plot (B) shows the 'major' gas entry event signified by the rapid increase in flux into the clay
- This is followed by a secondary gas peak and an eventual transient which first under- and then over-shoots the injection flow rate into the system
 - This is symptomatic of unstable gas pathways.



2020-01-24

EURAD Doctoral School

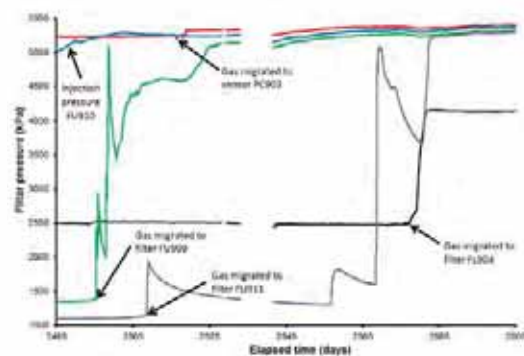
eu^{rad}

31

31

GAS TEST 3

- In order of first change, gas reached sensors FU909, FU911, PC903 and FL904
- The evolution of pressure shows that several gas pathways must have formed and that these continued to evolve spatially and temporally, even though the injection pressure was constant



2020-01-24

EURAD Doctoral School

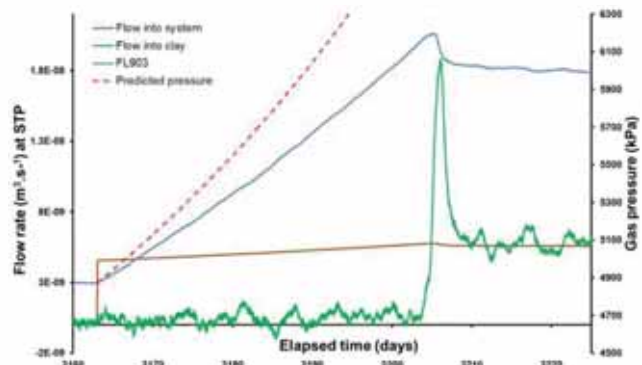
eu^{rad}

32

32

GAS TEST 4

- Peak pressure of 6.2, which was higher than in the earlier tests
- In general, very similar behaviour as the other tests



2020-01-24

EURAD Doctoral School

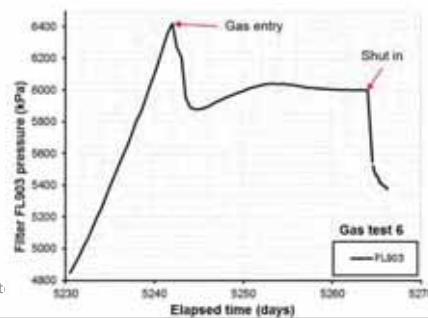
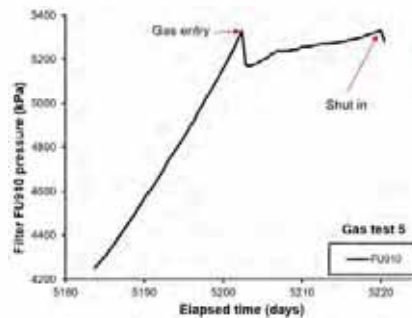
eu^{rad}

33

33

GAS TESTS 5 AND 6

- Prior to the final Full Canister Test repeat gas injection tests were conducted in filters FU910 and FL903
- Both tests consisted of:
 - Hydraulic, gas injection, repeat hydraulic
- Gas test 5 (FU910) [1]:
 - gas entry at 5,325 kPa
 - small drop in gas pressure of ~ 150 kPa
 - followed by increase in gas pressure
 - short shut-in conducted
- Gas test 6 (FL903) [2]:
 - Gas entry at 6,420 kPa
 - drop in gas pressure of ~ 550 kPa
 - followed by stabilisation of gas pressure
 - short shut-in suggesting plateau at around 5,200 kPa



2020-01-24

EURAD Doct

eu^{rad}

34

34

GAS ENTRY BEHAVIOUR

- Gas entry pressure has been increasing for filter FL903, but relatively constant in FU910 [1]
- Stresses have generally reached plateau or are decreasing since artificial hydration was stopped [2]
- Gas entry occurred when gas pressure was close to local stress [3]
 - Note: Local stress is taken as near-by sensors and may not truly represent the local stress state

[1] Gas entry pressure (kPa) vs Elapsed time (days). Legend: Filter FL903 (blue diamonds), Filter FU910 (red squares). Y-axis: 3200 to 14200. X-axis: 0 to 8000.

[3] Gas entry pressure (kPa) vs Estimate of local stress (kPa). Legend: Filter FU910 (red diamonds), Filter FL903 (blue squares), Unity (dotted line). Y-axis: 4000 to 7600. X-axis: 4000 to 7600.

[2] Average pressure (kPa) vs Elapsed time (days). Y-axis: 0 to 8000. X-axis: 0 to 5000.

2020-01-24
EURAD Doctoral School

35

35

FULL CANISTER TEST (FCT)

- **Fundamental question:** Does the volume of gas play a role on the post-entry behaviour?
- Full canister test involves pressurising the entire canister (available volume: 1.5 m³) and using a filter in the base of the canister [1]
- System modified utilising pallets of 12 cylinders of nitrogen [2]
- The mechanical deformation caused by the pressurisation of the canister resulted in a hydromechanical response in the buffer [3]
 - Result of slow drainage

[2] Photograph of the Full Canister Test (FCT) setup, showing the canister and associated equipment.

[1] Schematic diagram of the Full Canister Test (FCT) setup, showing the canister, filter, and sensor locations. A red arrow points to the 'FCT valve'.

[3] Radial stress (kPa) vs Elapsed time (days). Y-axis: 4400 to 6400. X-axis: 5263 to 5277. Legend: PR003, PR004, PR005, PR006, PR007, PR008, PR009, PR010, PR011, PR012, PR013, PR014, PR015, PR016, PR017, PR018, PR019, PR020, PR021, PR022.

EURAD Doctoral School

36

36

FCT – GAS ENTRY

- Two stage gas ramp conducted [1]
- Pressure raised to local stress and showed signs that water was being expelled from FCT filter
- Pressure held constant to allow water to drain
- Gas entry occurred around Day 5411
- Canister pressure began to decrease [2]
- The change in volume necessary to result in a reduced canister pressure can be calculated [3]
 - (Suggests more than 12 litres of pathways have formed)

[1]

2020-01-24
EURAD Doctoral School

37

GAS MOVEMENT (FCT)

- Gas migrated to UB902 [1,2]
 - Previously gas pressurised during Gas Test 3
- Moved upwards in the deposition hole to filter FL901
- UB902 and FL901 connected [2]
- Gas continuing to move but has not intercepted any other sensor

[2]

[1]

2020-01-24
EURAD Doctoral School

38

FUTURE

- Current plan is to close Äspö underground facility in 2024
- All projects need to be dismantled ahead
- Lasgit will be dismantled during 2020 according to current plan
- Dismantling of the installation
 - Sampling
 - Evaluation of parameters relevant for gas migration
 - Water content, dry density...



2020-01-24

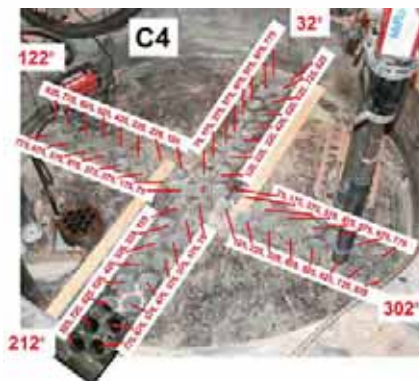
EURAD Doctoral School

eu^{rad}

39

39

DISMANTLING



2020-01-24

EURAD Doctoral School

eu^{rad}

40

40

SUMMARY

- Lasgit has been in operation for 15 years
- Seven gas injection tests have been performed (including FCT)
- The results are qualitatively similar to laboratory test results
- Entry/breakthrough pressures are generally close to total stress in the system
- No gas flow in the bentonite at constant pressure below the breakthrough pressure
- All observations suggest mechanisms of pathway propagation and dilatancy predominate
- Formation of gas pathways does not alter the hydraulic properties of the bentonite buffer
- An increased upstream volume (x1000) does not change the general behaviour of the process (preliminary)
- **Gas migration through a bentonite buffer does not jeopardize the properties of the barrier system**

2020-01-24

EURAD Doctoral School

eurad

41

41



2020-01-24

EURAD Doctoral School

eurad

42

42

Appendix R. In situ testing of EBS in crystalline rock (E. Bohner)



IN SITU TESTING OF EBS IN CRYSTALLINE ROCK

EURAD School for Radioactive Waste Management – GAS & HITEC
22-24 January 2020, Liege (Belgium)

Dr.-Ing. Edgar Bohner
VTT Technical Research Centre of Finland Ltd



The project leading to this application has received funding from the European Union's Horizon 2020 research and innovation programme under grant agreement n° 847593.

22-24 January

EURAD School for Radioactive Waste Management

1



OUTLINE



Nuclear energy in Finland



Nuclear waste management in Finland



Design and manufacturing of engineered barriers



In-situ demonstrations of EBS concepts and monitoring of EBS performance



Conclusions

22-24 January

EURAD School for Radioactive Waste Management

2



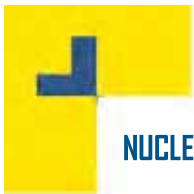


NUCLEAR ENERGY IN FINLAND

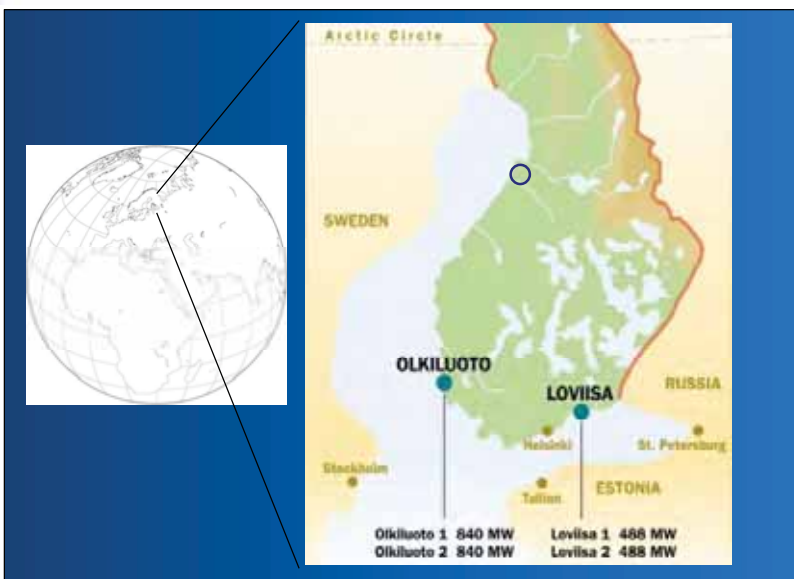


22-24 January

EURAD School for Radioactive Waste Management



NUCLEAR POWER PLANTS IN FINLAND



Four operational reactors (2 BWRs, 2 VVERs)

- Commissioned 1977-80
- Producing 70 TWh (2013)
- Operating at 92% energy capacity factor (world-leader efficiency)

Fifth reactor Olkiluoto 3 (1600 MW, EPR) under construction (2005-20xx)

Sixth reactor Hanhikivi I entering construction stage (CLA submitted June 2015)

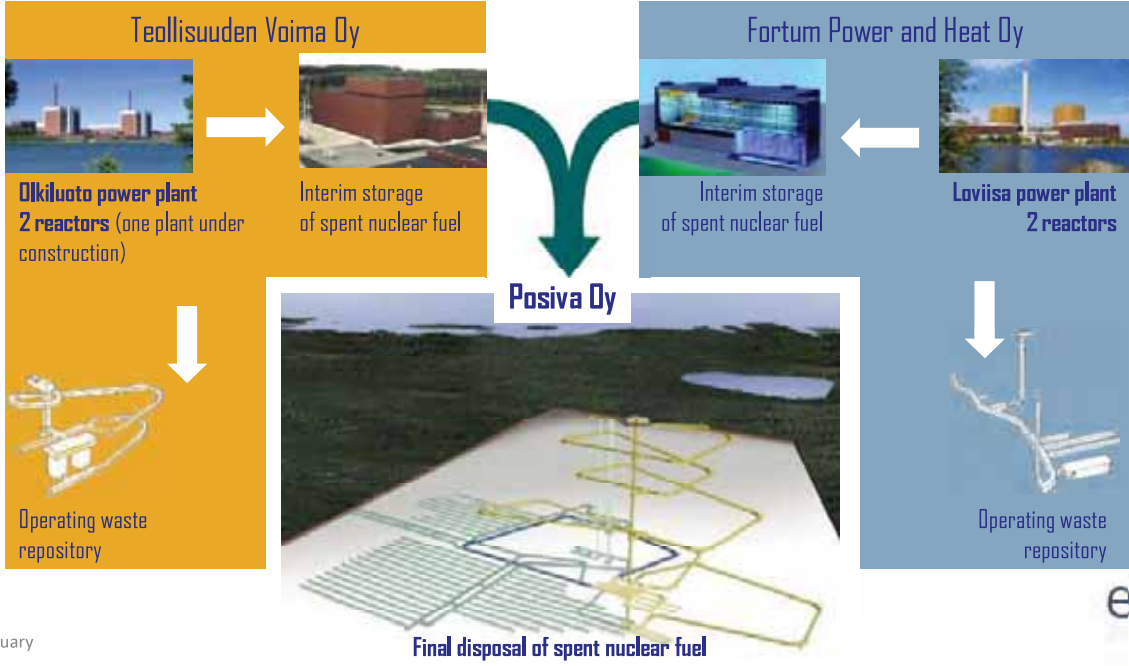
22-24 January

EURAD School for Radioactive Waste Management





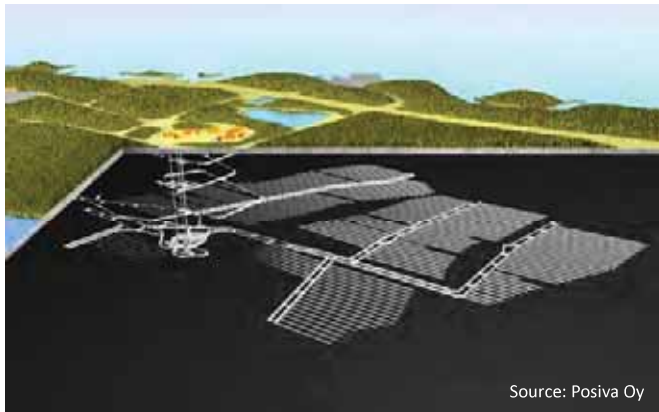
FINNISH NUCLEAR POWER AND WASTE ORGANISATION



22-24 January



NUCLEAR WASTE MANAGEMENT IN FINLAND



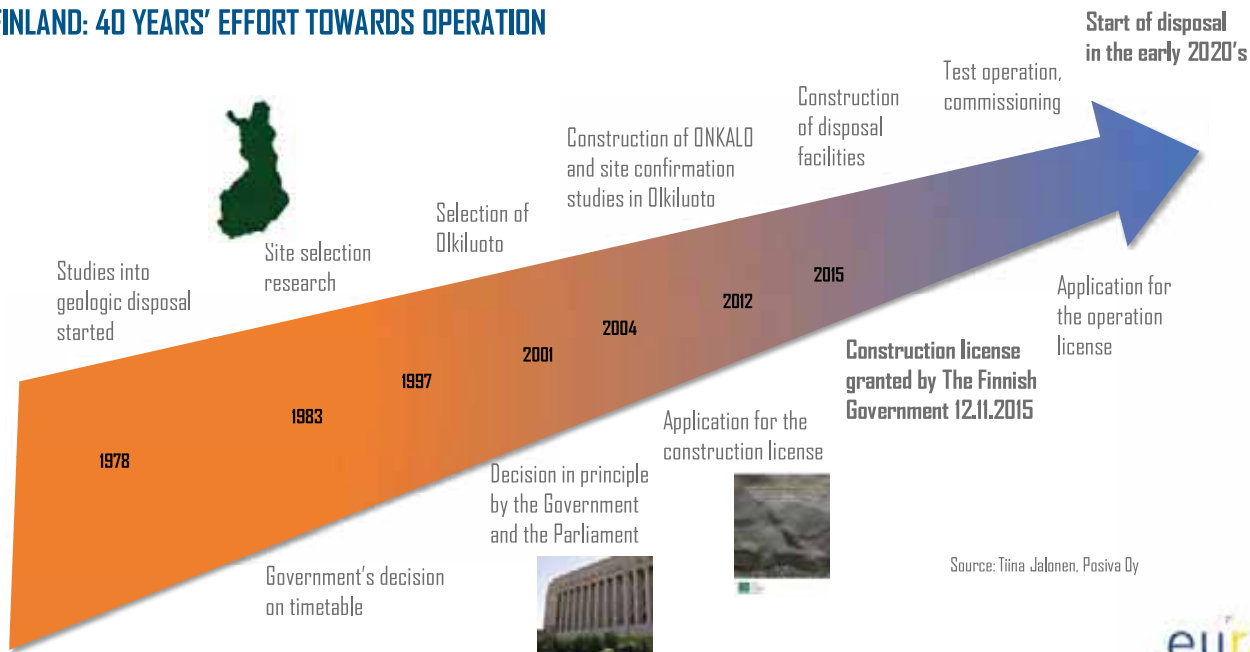
Source: Posiva Oy

Finnish Deep Geological Repository for High Level Waste

22-24 January



FINLAND: 40 YEARS' EFFORT TOWARDS OPERATION

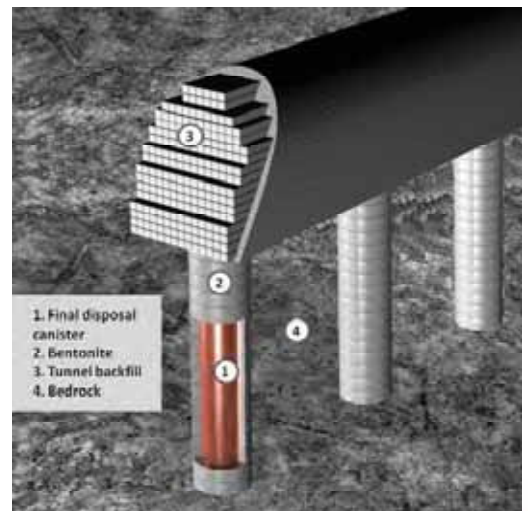


Source: Tiina Jalonen, Posiva Oy



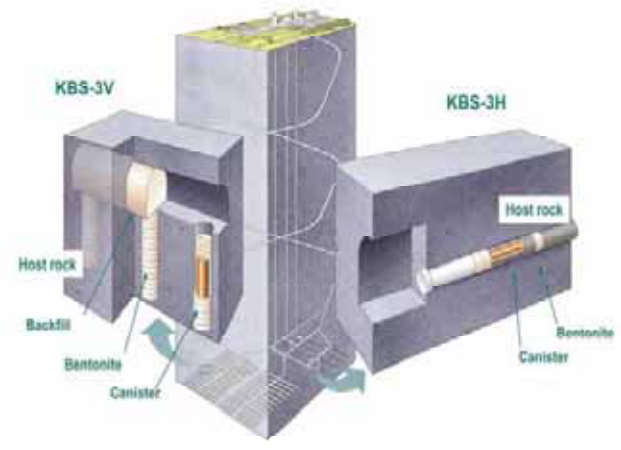
LONG TERM DISPOSAL OF HIGHLEVEL RADIOACTIVE WASTE

- International consensus that deep geological disposal on land is most appropriate way for isolating high level waste from entering the biosphere
- Barriers against movement of radionuclides are required
- Barriers include
 - waste form itself
 - corrosion resistant containers for encapsulation of waste (1)
 - special radionuclide- and groundwater-retarding materials around containers, i.e. buffer, backfill, plugs and seals (2),(3)
 - geological formation itself (4)





DESIGN AND MANUFACTURING OF ENGINEERED BARRIERS

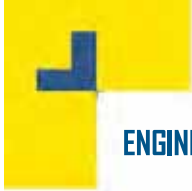


Source: SKB

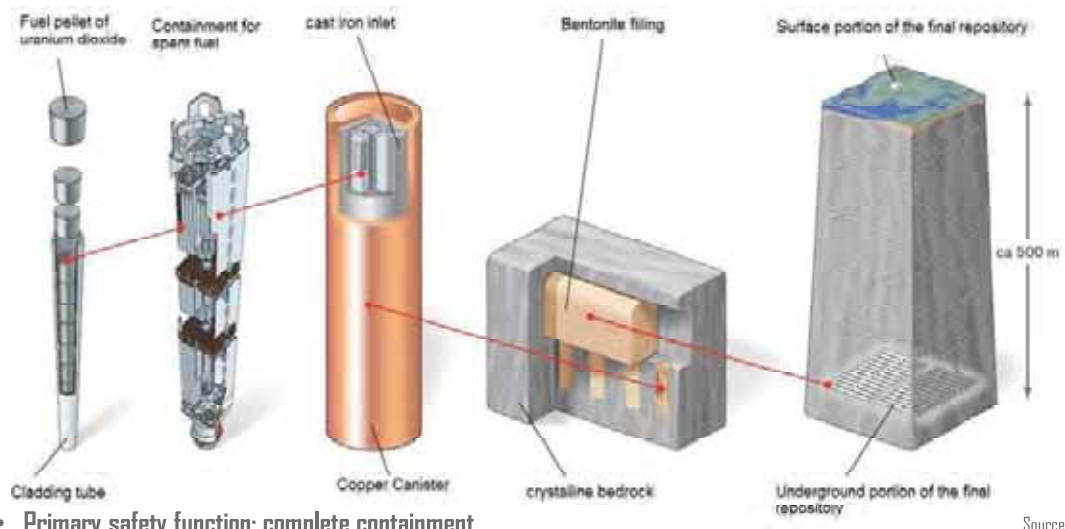


22-24 January

EURAD School for Radioactive Waste Management



ENGINEERED BARRIER SYSTEM (EBS) – KBS-3 CONCEPT



- Primary safety function: complete containment
- Secondary safety function: retardation
- Multi-barrier requirements: thermal-hydraulic-mechanical-(bio)chemical

Source: SKB

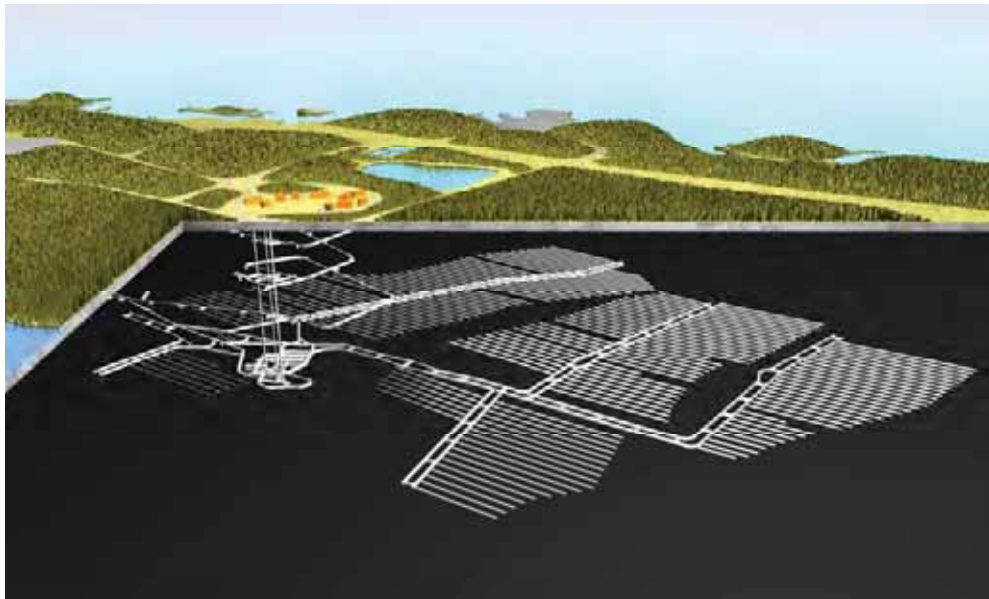


22-24 January

EURAD School for Radioactive Waste Management



REPOSITORY FOR SPENT NUCLEAR FUEL IN OIKILUOTO



SAFETY FUNCTIONS ASSIGNED TO EBS IN POSIVA'S REPOSITORY

Barrier	Safety functions
Canister	Ensure a prolonged period of containment of the spent fuel. This safety function rests first and foremost on the mechanical strength of the canister's cast iron insert and the corrosion resistance of the copper surrounding it.
Buffer	Contribute to mechanical, geochemical and hydrogeological conditions that are predictable and favorable to the canister. Protect canisters from external processes that could compromise the safety function of complete containment of the spent nuclear fuel and associated radionuclides. Limit and retard radionuclide releases in the event of canister failure.
Deposition tunnel backfill	Contribute to favorable and predictable mechanical, geochemical and hydrogeological conditions for the buffer and canisters. Limit and retard radionuclide releases in the possible event of canister failure. Contribute to the mechanical stability of the rock adjacent to the deposition tunnels.



EBS – BASIC REQUIREMENTS

- **Metal canister/container**
 - complete waste isolation
 - high corrosion resistance
- **Clay/bentonite buffer, backfill**
 - low permeability and hydraulic conductivity
 - self-sealing ability
 - maintaining thickness
 - physical and chemical longterm stability
 - minimise microbial activity
 - colloid filter
- **Concrete plugs and seals**
 - low permeability and diffusivity
 - chemical conditioning (low pH)



DISPOSAL CANISTER

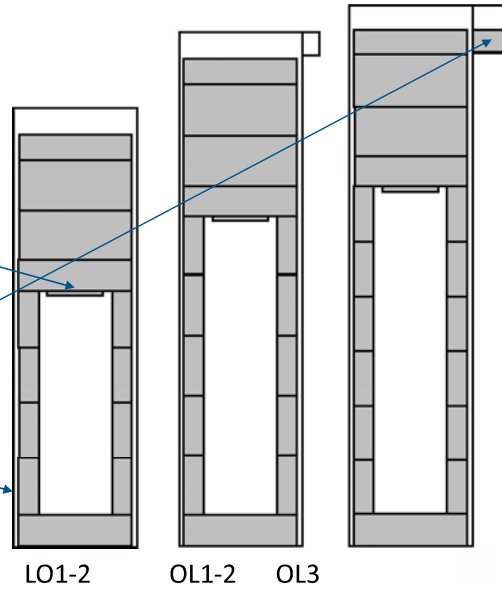
- **Oxygen free copper overpack for corrosion resistance**
 - Thickness 50 mm
 - Welding with Friction Stir Welding (FSW)
- **Nodular cast iron insert for mechanical strenght**
 - Three types
- **Design criteria to be set to ensure the integrity of the canister with NDE**
 - all the components, including copper overpack, lid and welds
 - NDE testing based on visual, Eddy current, ultrasonic, radiographic methods





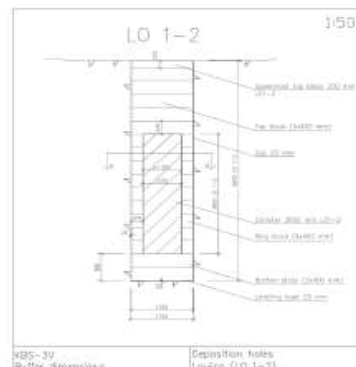
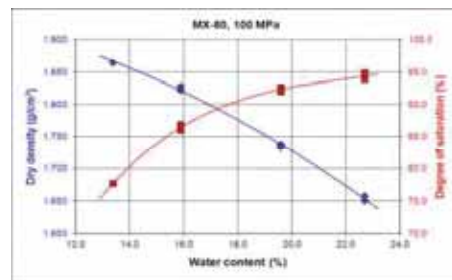
BUFFER DESIGN (POSIVA'S DESIGN 2012)

- Buffer consists of
 - 4 disks on top of the canister
 - a block in canister's recess
 - 4 to 6 ring blocks
 - a bottom block
 - for OL3 fuel also a chamfer block
 - gap between the block and rock surface are filled with bentonite pellets



BUFFER DESIGN (POSIVA'S DESIGN 2012)

- In the reference design
 - the target density of the saturated buffer is 2000 kg/m³
 - the allowable tolerance is ± 50 kg/m³
- This is achieved using (in installation phase)
 - ring shaped blocks with a nominal bulk density of 2050 kg/m³
 - disk blocks with a nominal bulk density of 1990 kg/m³
 - pellet filling with a loose density of 1075 kg/m³
 - the water content of 17% for all the buffer components



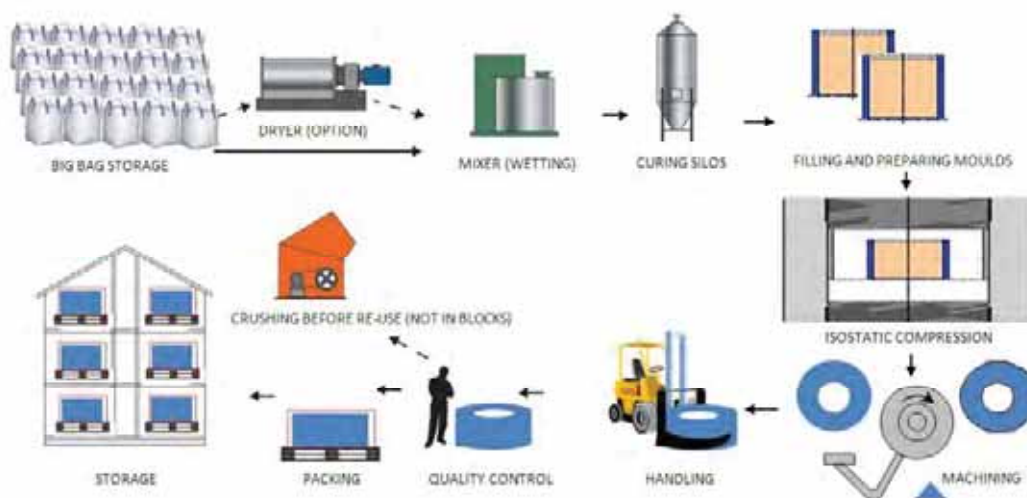


BUFFER COMPONENT MANUFACTURING

- Manufacturing technologies for bentonite blocks, rings and pellets
 - uniaxial compression
 - isostatic compression
 - roller compaction and extrusion of pellets
- Optimal component properties are achieved at varying material types, water contents, achievable densities and strengths to suit installation and operation



BUFFER AND PELLET PRODUCTION PROCESS AND QUALITY CONTROL





MOISTURE PROTECTION SYSTEMS AND COATINGS FOR QUALITY MANAGEMENT DURING EMPLACEMENT

- Protection of bentonite clay against water leakages and air humidity during installation phase
- Deposition hole liners and temporary thin-film coatings of bentonite components
- Bottom plate of buffer tower with integrated moisture protection liner with support rings, dewatering and alarm system
- Prototype solutions have been made and demonstrated at full-scale



BACKFILL DESIGN – REQUIREMENT HIERARCHY

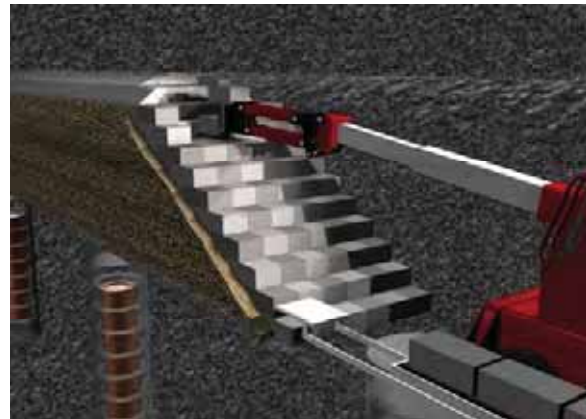
- Reference: Posiva-SKB Report 01 (2017)

Requirement level	Example for backfill
Safety function	Limit advective mass transfer
Performance target	Hydraulic conductivity $< 1 \times 10^{-10}$ m/s and swelling pressure > 0.1 MPa
Technical design requirement	Threshold dry density where the backfill material fulfills the performance target in certain site specific conditions.
Design specification	Specifications for the backfill design in order to reach the threshold dry density in the backfilled tunnel. For example, minimum dry density for the backfill blocks.



BACKFILL DESIGN AND PRODUCTION

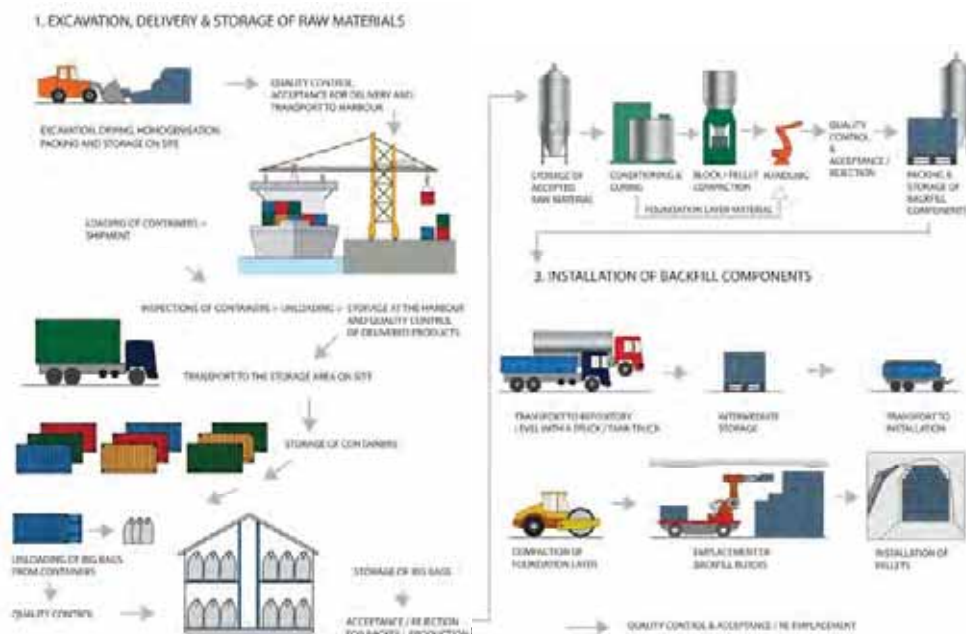
- Backfill concept is based on "block concept" with pre-compacted backfill blocks and bentonite pellets (Reference POSIVA 2012-18)
- Backfill blocks provide high average dry density for the backfill
- Automated and remote emplacement with a robot
- Full-scale test in 2018 in ONKALO



Source: Posiva Oy



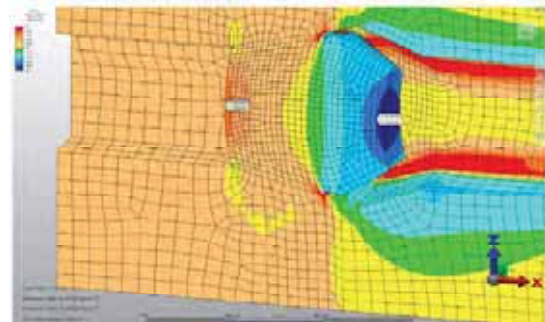
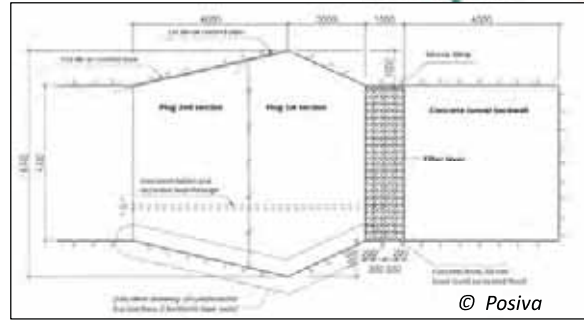
BACKFILL PRODUCTION PROCESS AND QUALITY CONTROL





CONCRETE PLUGS AND SEALS

- **Plug**
 - assures hydraulic isolation for operation phase (100 years)
 - keeps backfill in-place
 - withstands swelling and hydrostatic pressure
- **Concrete**
 - low heat, minimal shrinkage, highly flowable (like self-compacting concrete)
 - local materials (including long-term safety, not jeopardizing site)
 - target pH leachate < 11 (Ca:Si ratios)
 - high durability in saline groundwater
- **Rock**
 - no continuous or water conducting fractures
 - minimal EDZ



Posiva's Wedge Plug design (top) & water pressure simulations in FEM modeling (bottom)



IN-SITU DEMONSTRATIONS OF EBS CONCEPTS AND MONITORING OF EBS PERFORMANCE

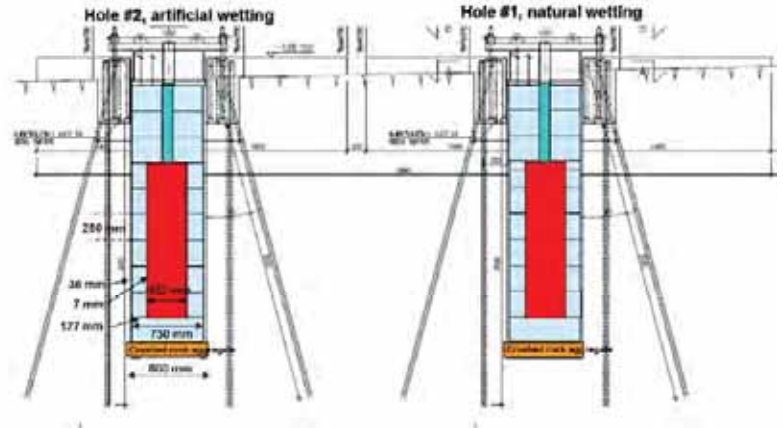




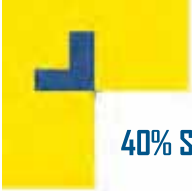
DESIGNING, COMMISSIONING AND MONITORING OF 40% SCALE BENTONITE BUFFER TEST

Project goals:

- To perform medium-scale tests in underground conditions
- Learn how to plan, build and monitor tests in a repository environment
- Get information about early phase processes of the bentonite buffer
 - distribution of heat
 - effect of artificial wetting
 - rate of saturation from gap at canister to middle of the buffer blocks
 - possible piping and erosion
 - buffer swelling and uplifting

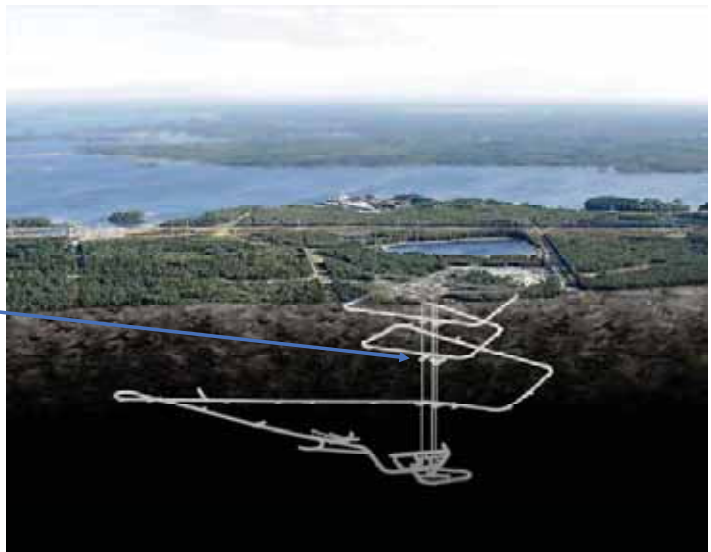


Source: Posiva Oy



40% SCALE BUFFER TEST – PROJECT SITE

- DNKALO, Posiva’s underground rock characterisation facility at Olkiluoto, Finland
- Test place:
 - 1475 m from entrance
 - 140 m underground



Source: Posiva Oy

40% SCALE BUFFER TEST – BASIC INFORMATION

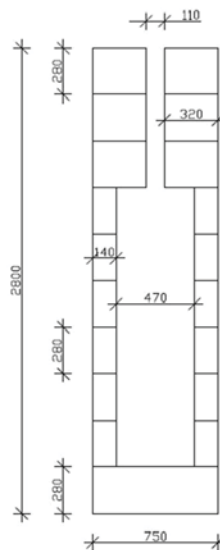
- **Two test holes**
 - 800 mm diameter
 - 3000 mm deep
 - 4 m from each other
- **Buffer blocks**
- **Gap filling pellets**
- **Heating canister**



Source: Posiva Oy

40% SCALE BUFFER TEST – DESIGNING BUFFER

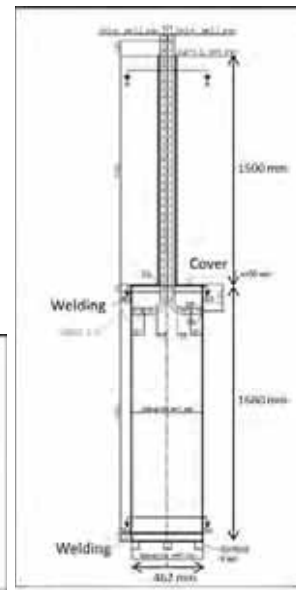
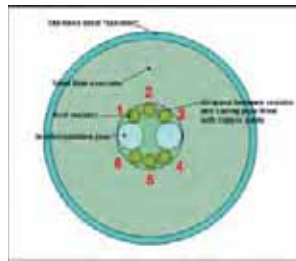
- **KBS-3V reference design based**
- **Buffer blocks**
 - MX-80 bentonite, 120 MPa isostatic, 17%
- **Pellets**
 - MX-80 bentonite, roller compacted, pillow shaped, 17%



Source: Posiva Oy

40% SCALE BUFFER TEST – DESIGNING HEATING CANISTER

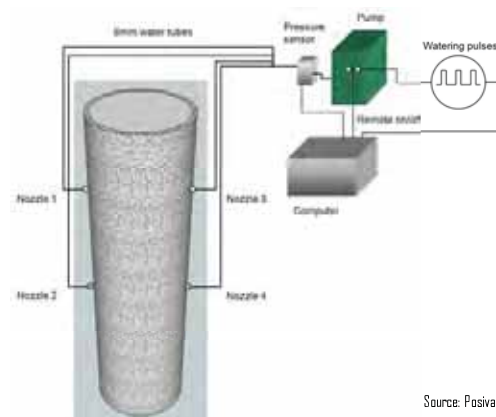
- To simulate heat generated by nuclear waste
- Surface temperature +90 °C
- 900 W heating power
 - 6 removable resistors
- Stainless steel 12 mm
 - 5 MPa compression
 - Filled with steel fiber concrete



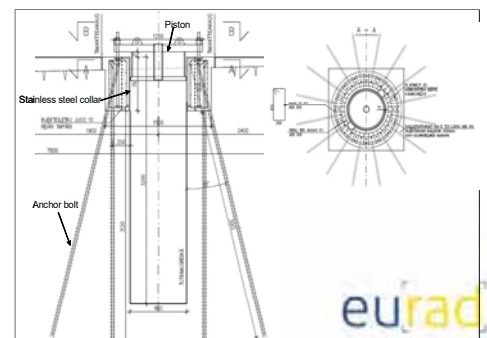
Source: Posiva Oy

40% SCALE BUFFER TEST – DESIGNING OTHER KEY COMPONENTS

- Piston-type lid & collar
- Anchoring, concrete slab
- Artificial wetting system



Source: Posiva Oy



40% SCALE BUFFER TEST - COMMISSIONING - SITE PREPARATION

- Concrete slab casting
- Two pilot holes, used later for instrumentation
- Test holes drilled with over-coring cutter
- EDZ removal
- Collar installation



22-24 January

EURAD School for Radioactive Waste Management

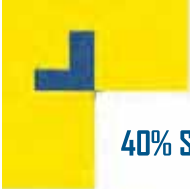
40% SCALE BUFFER TEST - COMMISSIONING - BUFFER INSTRUMENTATION AND ASSEMBLY

- Instrumentation done at VTT laboratory in Espoo, Finland
- Pre-assembled stacks
 - Sensors
 - Buffer
 - Heater



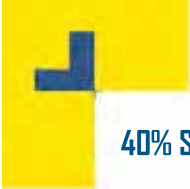
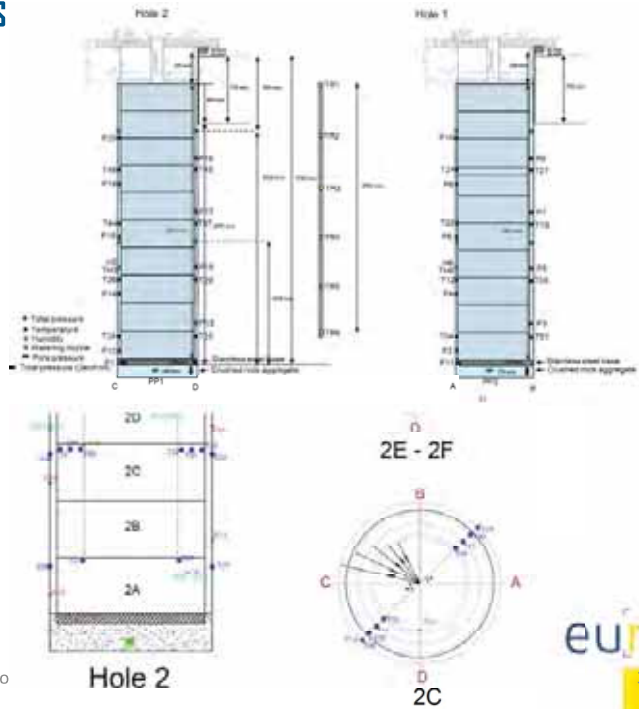
22-24 January

EURAD School for Radioactive Waste Management



40% SCALE BUFFER TEST - COMMISSIONING - SENSORS

- Sensor locations and quantities
- Instrumentation tubes:
 - Total pressure 20
 - Pore pressure 2
 - Temperature 22
 - Relative Humidity 2
- Bentonite blocks, canisters and pistons
 - Temperature 44
 - Relative Humidity 14
 - Force 8
 - Displacement 2



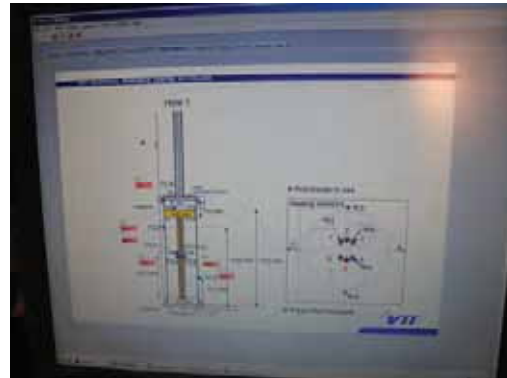
40% SCALE BUFFER TEST - COMMISSIONING - PLACEMENT

- Stacks were lowered to holes
- Gap filling pellets were installed
- Lid was secured and pre-tensioned



40% SCALE BUFFER TEST – COMMISSIONING – MONITORING

- Monitoring and heating were turned on in November 2011
- One hole was artificially wetted
 - Tracer compound
 - 100 liters
- Results of the tests are reported in
 - Hakola, I, Kivikoski, H, Löjja, M., Marjavaara, P.: Designing, Commissioning and Monitoring of 40% Scale Bentonite Buffer Test. Posiva Working Report 2015-08, May 2015 (available for download at www.Posiva.fi)



22-24 January

EURAD School for Radioactive Waste Management

eu[rad]

37

40% SCALE BUFFER TEST – CONCLUSIONS

- The overall performance of the test has been good
- The designed test solutions and concepts have proved to be robust
- The heating system has performed well
- The failure rate of pressure sensors has been high due to water leakage along and inside the cables
- Many disturbances caused by other constructions at the site
- The outcomes of the project are being used
 - to support the reference design work
 - for designing of planned full-scale ONKALO tests



22-24 January

EURAD School for Radioactive Waste Management

eu[rad]

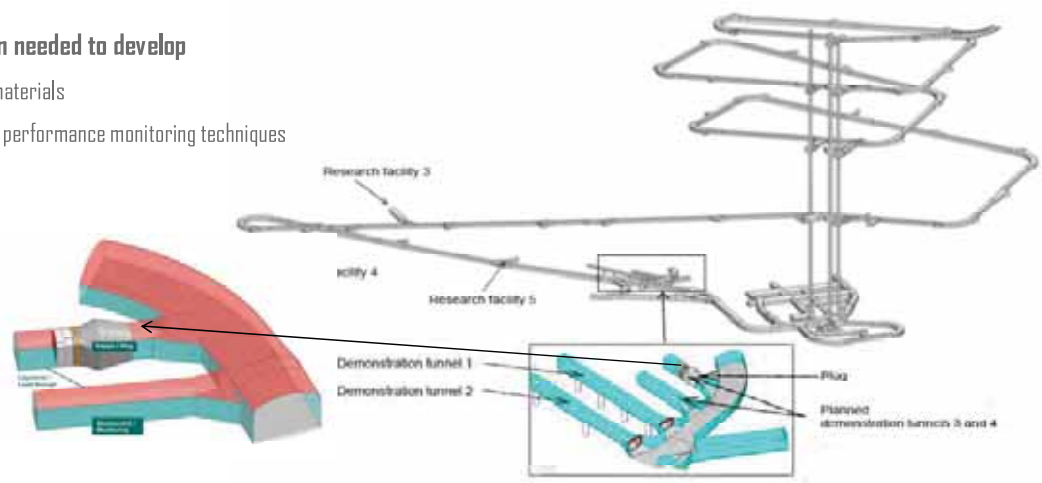
38



POPLU PROJECT – TUNNEL END PLUG IN ONKALO

- Posiva Oy together with VTT demonstrated the first full-scale construction and performance of EBS, with a deposition tunnel end plug (POPLU)
- The plug demonstration needed to develop
 - specialty concrete materials
 - instrumentation and performance monitoring techniques
- POPLU was part of the EU-project DOPAS

Source: DOPAS (@ Posiva)



22-24 January

EURAD School for Radioactive Waste Management



BACKGROUND: EU-DOPAS PROJECT FACTS

- Consortium of 14 Partners from 8 European countries, funded by EU FP7 Collaboration Program, Posiva Oy coordinator
- Duration: 4 years (September 2012 - August 2016)
- Total budget 15.8 M€, with EU contribution 8.7 M€
- Five sets of full-scale experiments, implemented in both under- or above-ground repository conditions
- See details at www.posiva.fi/en/dopas



© ANDRA



The research leading to these results has received funding from the European Atomic Energy Community's (Euratom) Seventh Framework Programme FP7/2007-2013, under Grant Agreement No. 323273 for the DOPAS project.

22-24 January





POPLU – CONCRETE RECIPE DEVELOPMENTS

- Background references: Sweden (SKB) recipe “B200”, Canadian (AECL) recipe, France (ANDRA) recipe – binary & ternary blends for low-pH
- Finland produced ~50 trial batches, with 10+ major changes to recipes
- Finalized 2 mix design options:
 - Binary mix binder composition (60% cement + 40% silica fume)
 - Ternary mix binder composition (38% cement + 32% silica+ 30% flyash)

	Final Ternary mix design	Final Binary mix design	B200 SKB with Finnish laboratory materials
CEM I 42,5 MH/SR/LA	105 kg/m ³	120 kg/m ³	120 kg/m ³
Silica	91 kg/m ³	80 kg/m ³	80 kg/m ³
Fly ash	84 kg/m ³	-	-
Quartz filler	114 kg/m ³	256 kg/m ³	-
Limestone filler	-	-	370 kg/m ³
Local aggregate	1840 kg/m ³	1805 kg/m ³	-
VTT laboratory aggregates			1600 kg/m ³
Effective water content	126 kg/m ³	125 kg/m ³	157 kg/m ³
Water/binder –ratio	0,45	0,60	0,79

22-24 Jan



POPLU – CONCRETE DEVELOPMENT: FINAL RECIPE PERFORMANCE OF HARDENED CONCRETE

	POPLU Target	POPLU Casting	POPLU Binary Lab	POPLU Ternary Lab	Sweden's DOMPLU “B200”	“Normal concrete”
Compressive strength, MPa @ 90 d	> 50	82.6	91.5	79.5	67.5	50
Split tensile strength, MPa	3.2	-	5.6	4.5	-	3.2
Modulus of elasticity, GPa	34	-	37.4	34.2	-	34
Autogenous shrinkage, mm/m	(min)	-	0.22	0.15	0.03	0.1
Drying shrinkage, mm/m	(min)	-	0.17	0.22	-	0.6
Water tightness, mm	max 50	2.1	4.0	5.0	5.3	25 - 50
Chloride diffusivity, m ² /s	(min)	-	2.1*10 ⁻¹²	2.8*10 ⁻¹²	-	10-20*10 ⁻¹²
pH of leachate at 90 days (reference/Groundwater)	< 11	- / 10.8	11.4 / 10.3	11.4 / 10.3	11.4 / 10.3	>12,5
Sulphate damage	(min)	-	none at 180d	none at 180d	-	-

22-24 January

EURAD School for Radioactive Waste Management





POPLU – CONCRETE DEVELOPMENT: FINAL RECIPE PERFORMANCE OF FRESH CONCRETE

- Slump flow: 630mm (0h), 590mm (1h), 490mm (2h), 300mm (3h).
- Slump: 260mm (0h), 260mm (1h), 240mm (2h), 180mm (3h).
- T50: 10,3s
- DIN flow: 550mm
- Air content: 0,60%
- Density: 2430 kg/m³
- Setting time: 14,5 h
- Comp.strength: 7,4 MPa (1d)
- Max. heat: 23,5h (semi-adiabatic)



DIN flow of Binary (FIN) mix design, SCC.

22-24 January

EURAD School for Radioactive Waste Management



POPLU – CONCRETE CASTING FIELD TESTS AND MOCK-UP

- After VTT laboratory mixture development and performance verification, the final binary and ternary recipes were re-produced in the ready-mix supplier's laboratory and then at their batch plant (Rudus Oy)
- Three on-site mock-up castings were done at Posiva's ONKALO repository, to verify mix design proportions and construction techniques (Rudus Oy and Hartela Oy)



22-24 January

EURAD School for Radioactive Waste Management





POPLU – CONCRETE CASTING OF PLUG

Example details

- start flushing pumping tubes at 8am
- 20 trucks à 4m³ each for delivery (Section #2), with 30 min route time, then underground
- Casting from 9am onwards, for 9-11 hours
- Final filling with 0.5 bar pressure for 30 min
- QC tests before leaving factory & when underground (fresh properties: slump, air, density, temperature)
- Preparing small samples for long-term QC + 2 x 1 m³ blocks (strength, water tightness, pH leachate)

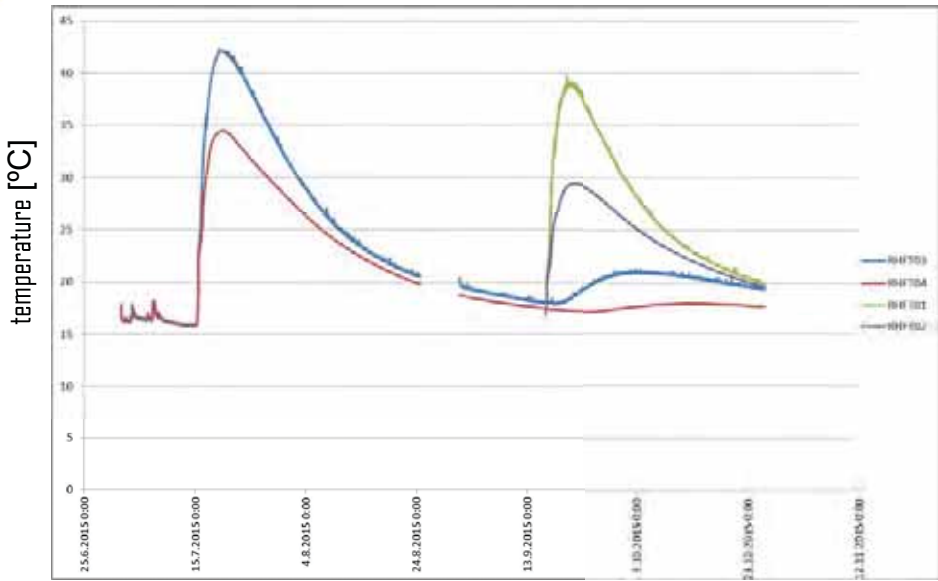


POPLU - CONCRETE PRODUCTION AND QUALITY CONTROL



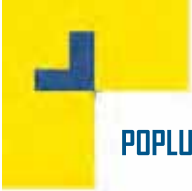


POPLU – CONCRETE TEMPERATURE DEVELOPMENT



Temperatures measured in central section, for 2 plug castings.

Requirement: concrete maximum temperature below 60°C.



POPLU – CONCLUSIONS OF CONCRETE DEVELOPMENT AND CASTING

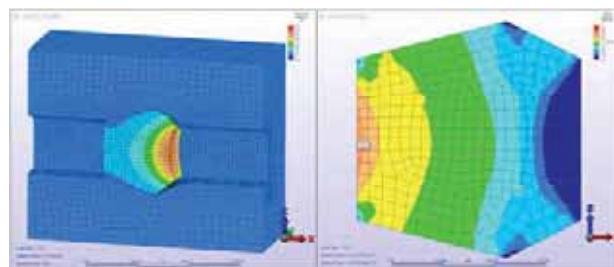
- Two new SCC mixtures were validated from lab-scale to full-scale field structures in Finland
- Developed eco-concrete recipes (105 kg/m³ cement, 0.45 w/b), low-heat, low-pH
- Fulfilled challenging underground environmental and construction demands
- Excellent balance of both early age (workability, stability) and long-term (shrinkage, permeability) requirements





POPLU - MONITORING SYSTEM

- A monitoring system for a full-scale demonstration based on 131 sensors was installed to the deposition tunnel end plug within the POPLU project
- A pressurization system allows for applying a hydrostatic water pressure up to 10 MPa (100 bar) in a filter layer behind the plug
- A leakage measurement system quantifies any seepage at the plug and in the nearby surrounding at the front face at the plug
- Sensors inside and around the concrete plug were selected to measure continuously during
 - concrete casting and grouting (pressure, displacement)
 - hydration process (temperature, RH, pressure)
 - pressurization phase (displacements, strain, pressure, RH, temperature)



Displacements (left) and principal stresses (right) in vertical direction due to hydraulic pressure on the back face of the plug

22-24 January

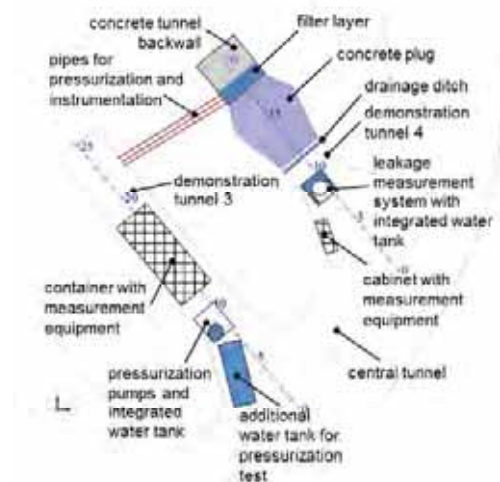
Source: DOPAS (© Posiva)



POPLU - REQUIREMENTS FOR THE INSTRUMENTATION SYSTEM

All sensors and wires need to be durable and robust to permanently operate without maintenance in a demanding environment:

- Corrosive environment for sensors and wires
 - inside tunnels RH is very high (close to 100%, constant plus temperatures)
 - inside concrete elevated temperature during hydration
 - pH < 12 due to low pH concrete (blend of cement, silica fume and fly ash)
 - presence of chloride and sulfate ions in groundwater
- High water pressure up to 10 MPa (100 bar)
- Long test duration (several years)



Horizontal section of demo tunnels 3 & 4 with concrete plug and locations of instrumentation equipment

22-24 January

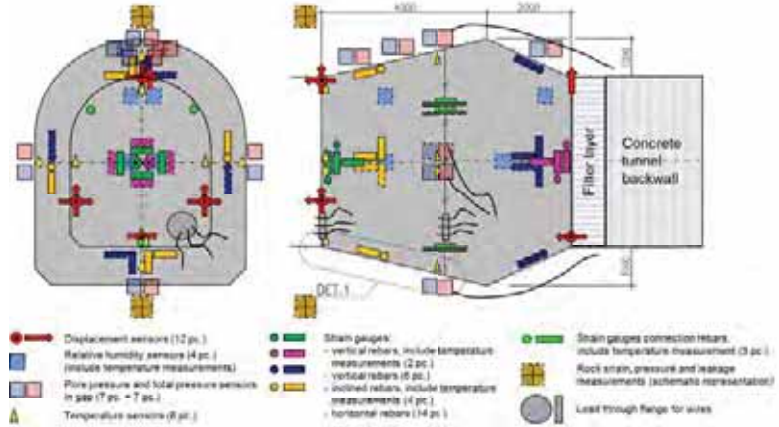
EURAD School for Radioactive Waste Management



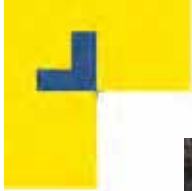
POPLU - MONITORING OF PLUG PERFORMANCE

- Performance monitoring included 131 sensors for accelerated pressurization test to 4.2 MPa (3 months → 100 years service life)
- Monitored leakage volumes, leachate quality, structural & near-field response (temperature, relative humidity, pressure, displacement, strains, chemical composition)
- Iteration of results back to improve requirements & design

Location and type of sensors installed in the concrete plug



22-24 January



POPLU - SENSOR INSTALLATION



Wire flange for sealing of cables passing between filter layer and plug section 1 during construction



Leakage box for interrupting potential water leakage along and inside the wires



Pressurization pipes mounted onto the concrete backwall surface and passing through a flange of the rock lead-through pipes



Installation of Teflon pipes into the rock lead-throughs



stainless steel tubes for hosting the sensor wires, mounted onto the filter layer wall





POPLU - SENSOR INSTALLATION



Total pressure sensor and pore pressure sensor on rock surface



Displacement sensors at the front face of the plug



Displacement sensors at the back face of the plug and specially designed sensor holder



relative humidity sensors (two difference types)



thermocouple



Three strain gauges on rebars in vertical, horizontal and perpendicular direction



POPLU - SENSOR INSTALLATION



Three cable flanges, which carry in total 51 sensor wires, photographed from inside (left) and outside (right) plug section 2

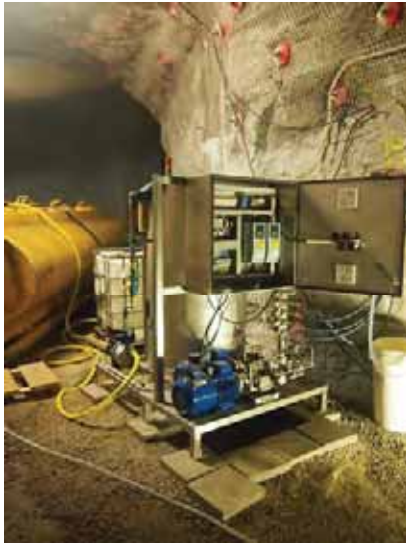


PVDF and stainless steel tubes, directing the pressure sensor cables to the cable flanges towards the filter layer (right side) and plug section 2 (left side)

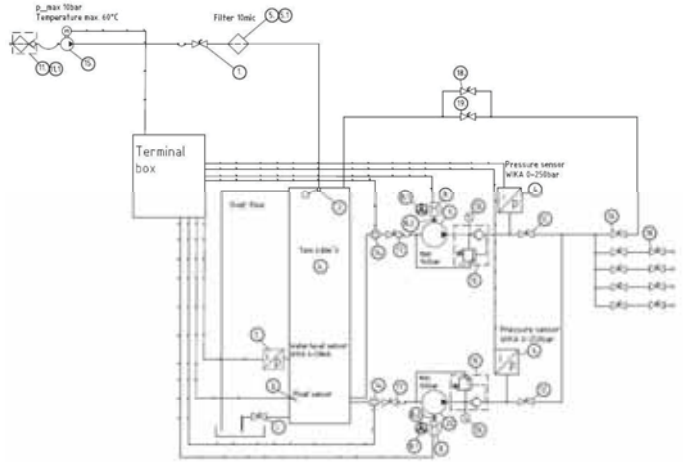




POPLU - PRESSURIZATION SYSTEM



Pressurization system and water supply tanks



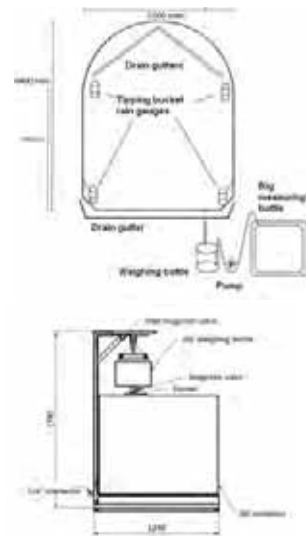
Pressurization system design (© Finfinet Oy)



POPLU - LEAKAGE MEASUREMENT SYSTEM



Leakage measurement system at front face of plug during pressurization test

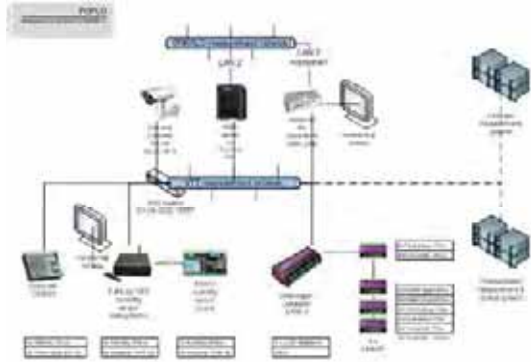


Schematic illustration of the design of the leakage measurement system. © VTT

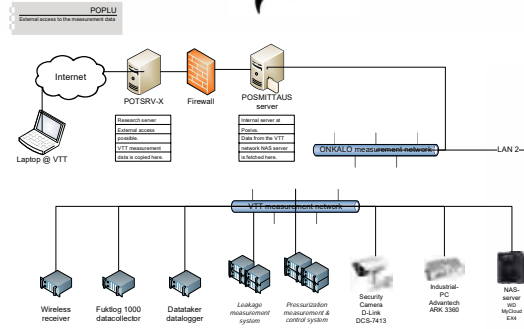




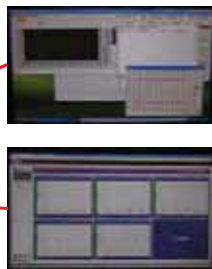
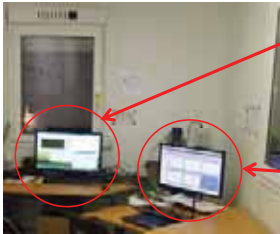
POPLU - DATA ACQUISITION SYSTEM



POPLU measuring and datalogging network layout



External access to the ONKALO measurement data

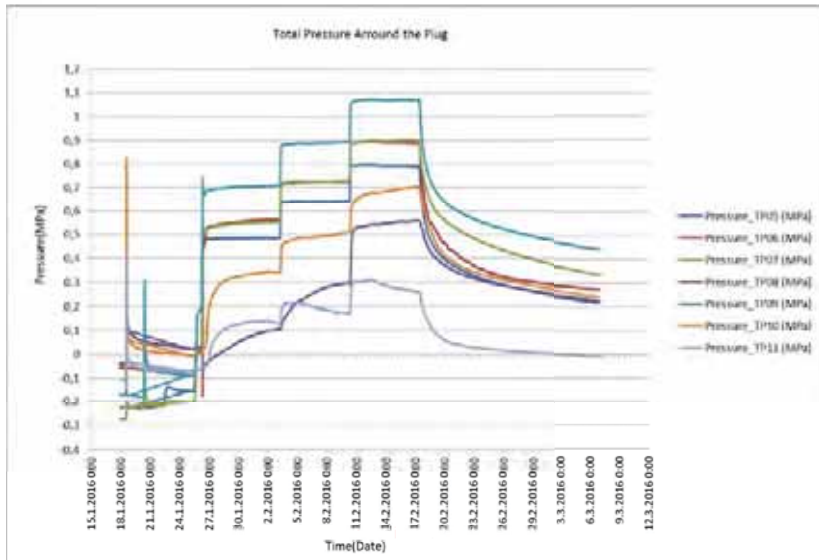


IT systems (left) as part of data acquisition system in measurement container in demo tunnel 3 (right)



POPLU - PLUG PERFORMANCE

- Slow pressurization (~1.4 MPa)
- Total pressure sensors around the plug



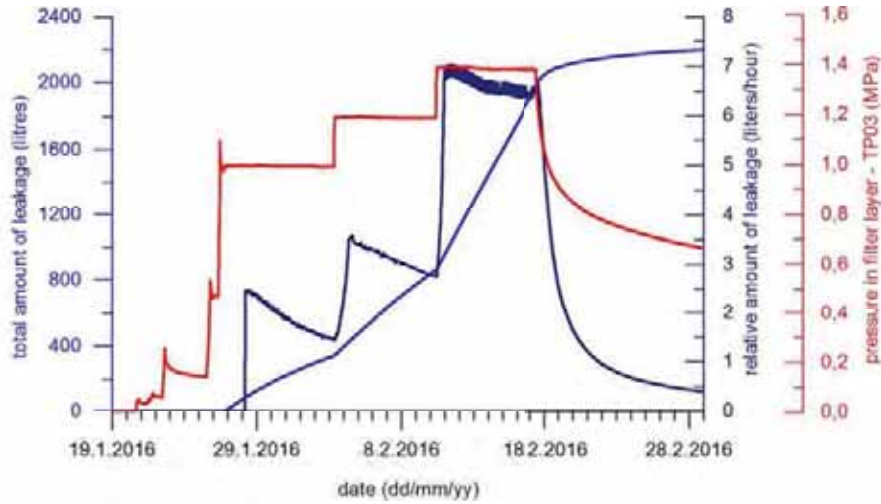
22-24 January





POPLU - PLUG PERFORMANCE

- Slow pressurization (~1.4 MPa)
 - Cumulative leakage, leakage rate and pressure in the filter layer (as measured by total pressure sensor TP03)

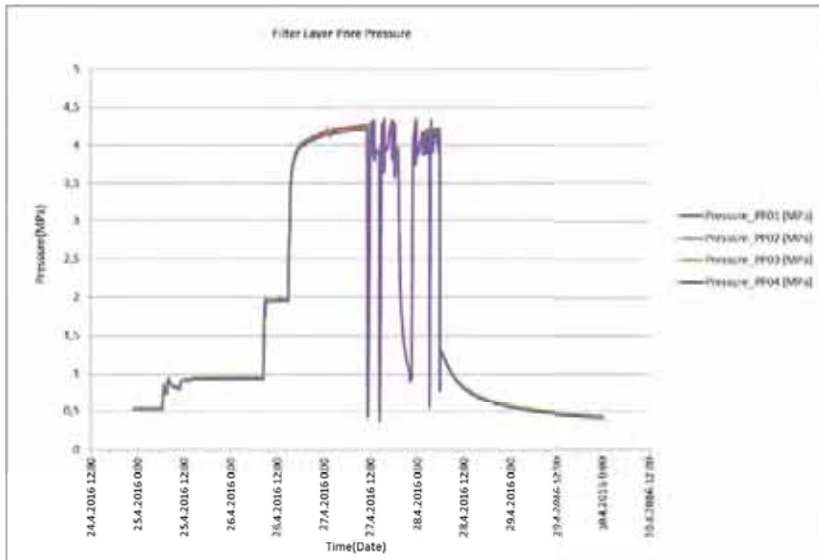


22-24 January



POPLU - PLUG PERFORMANCE

- Fast pressurization (~4.2 MPa)
 - Pore pressure sensors in filter layer



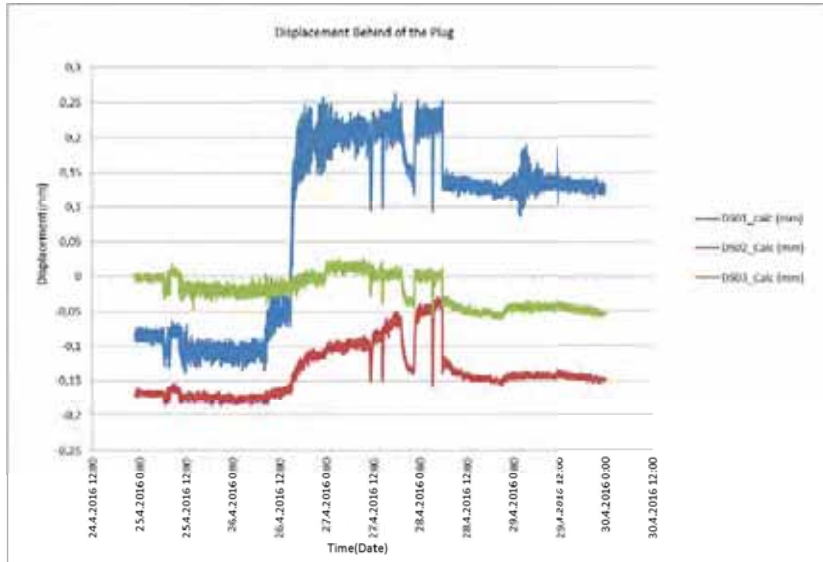
22-24 January





POPLU - PLUG PERFORMANCE

- Fast pressurization (~4.2 MPa)
 - Displacement sensors behind the plug



22-24 January



POPLU - PLUG PERFORMANCE ASSESSMENT

- Pressurisation system and leakage detection system components have performed very well
- Generally good performance of sensors, data collection, transfer and back-up systems
 - Systems provided reliable information during construction and casting activities as well as pressurization
 - Some strain gauges and relative humidity (RH) sensors have shown water running along cabling or sheltering tubes
 - Sensor failure or distortion of readings of several strain gauges and RH sensors during pressurization - pressure tests in pressure chamber prior installation (100 bars for 48 hours) were not sufficient for simulating conditions in plug
 - Incompatibility of some special temperature sensors with data logging system - change of data acquisition solution needed
 - Partly problems with signal disturbances/noise caused by electromagnetic fields as a result of pump operation or other activities in ONKALO (excavation, traffic, machines, etc.)

22-24 January

EURAD School for Radioactive Waste Management





POPLU – CONCLUSIONS

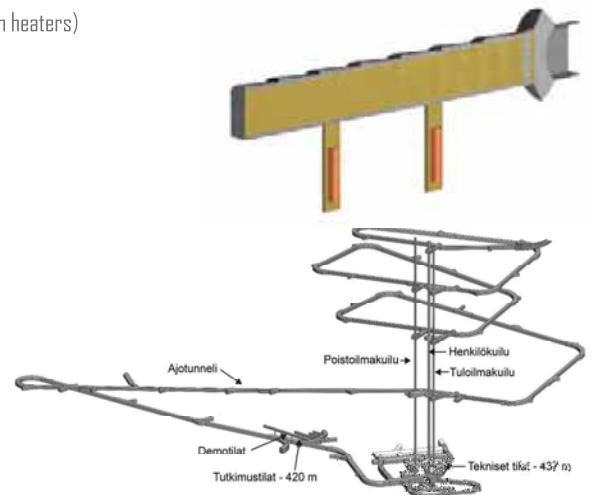
- Successful multi-scale approach to develop materials and systems for monitoring, pressurization system, leakage measurements and data management (lab→field)
- Results are used to demonstrate to Finland’s Nuclear Regulator Authorities the readiness for Operation
 - Reliable watertight and structurally-sound design that can be repeated (constructing 1 tunnel end plug per year for next 100 years in Finland)
- Unique repository tunnel end plug yields material and monitoring system solutions that can have applicability for other harsh environments, where high durability and very long service life is expected
- Led to new R&D via EU projects CEBAMA & Modern2020, as well as plans for wireless monitoring technology and borehole sealing technology



POSIVA’S LATEST DEMONSTRATION - FISST

Full-scale in situ system test in ONKALO demonstration area (-420m below surface)

- FISST is taking care of the needed modifications (for heating and instrumentation)
 - 2 canisters with insert (manufacturing tubes T88-89 joint project with SKB) – (with heaters)
 - 2 buffer (~50 tn buffer bentonite)
 - EH15 with segmented buffer
 - EH16 with full size blocks
 - ~50 meter backfill (~1400 tn of bentonite, ~9000 blocks & ~300 tn pellets)
- FISST will be implemented with existing Prototype machinery
 - KSAA (Canister installation machine)
 - BIM (Buffer installation machine)
 - TMA (Backfill material emplacement)
- The plug development and test chain
 - POPLU (wedge plug) → FISST (modified dome plug) → JOT (?)



Source: Posiva Oy



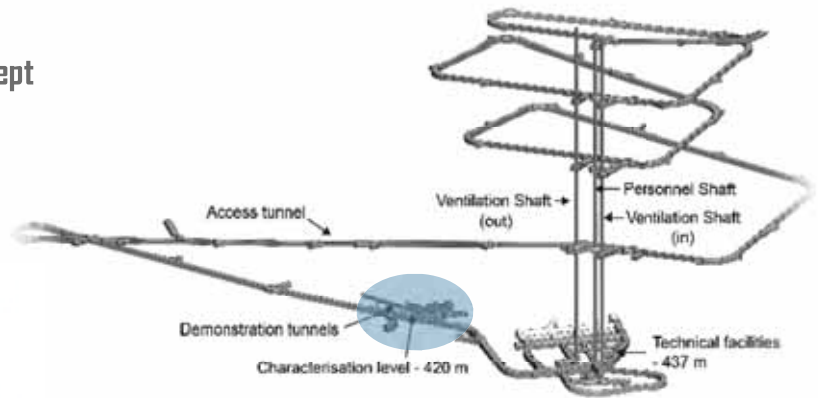
FISST

Full scale in situ system test, KBS-3V concept

- Includes all engineered barriers
 - Canister, Buffer, Backfill and Plug



22-24 January



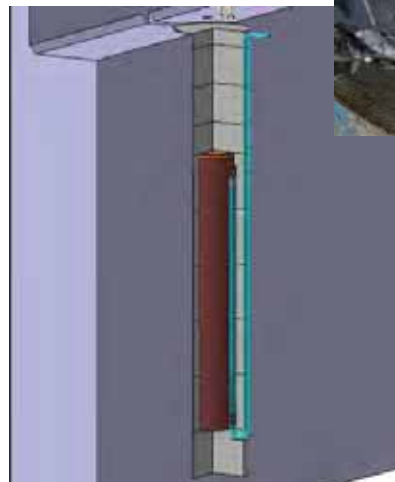
Source: Posiva Oy



FISST - INSTRUMENTATION

Test set up instrumented:

- Canister heat production
- Moisture distribution
- Pressure conditions in experimental hole (EH15 and EH16) and in the demonstration tunnel (DT2)
- Buffer/backfill interaction
- Gas sampling pipes behind the plug



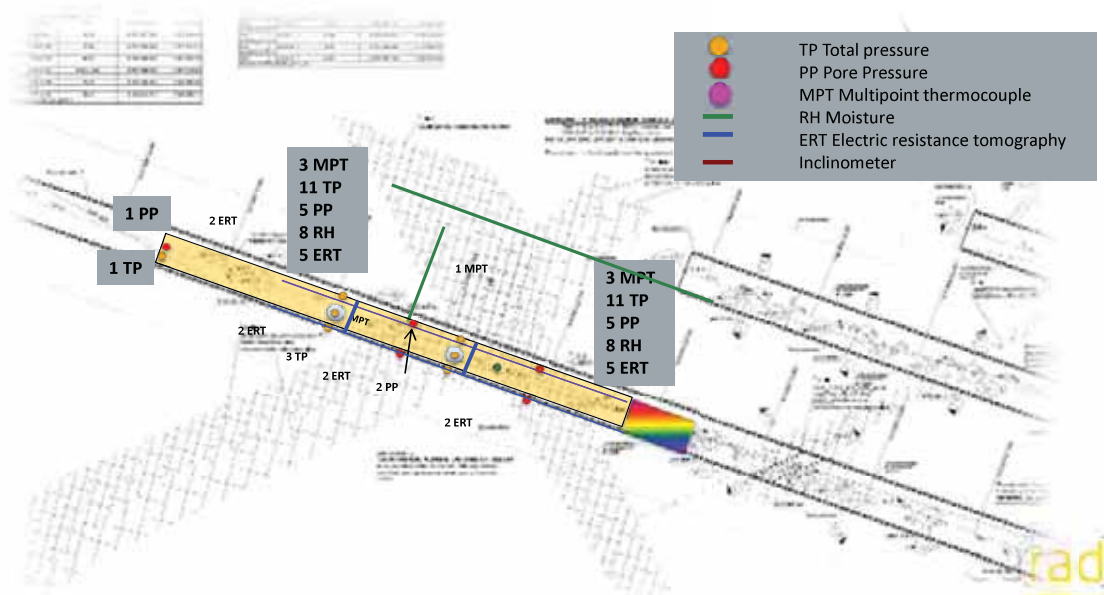
Source: Posiva Oy

22-24 January



FISST - INSTRUMENTATION

Top view of FISST demonstration area:



Source: Posiva Oy

22-24 January

EURAD School for Radioactive Waste Management



CONCLUSIONS



22-24 January

EURAD School for Radioactive Waste Management





R&D&I AS JOINT EFFORT

- Examples of recent VTT research financed by the EURATOM programme
 - DOPAS – Full-scale demonstration of plugs and seals (2012-2016), <http://www.posiva.fi/en/dopas>
 - CAST: Carbon-14 Source Term (2013-2018), <https://www.projectcast.eu/>
 - MIND: Microbes In Nuclear waste Disposal (2015-2019) <http://www.mind15.eu/>
 - CEBAMA – Cement-based materials, properties, evolution, barrier functions (2015-2019), <http://www.cebama.eu/>
 - MODERN2020 – Development and Demonstration of monitoring strategies and technologies for geological disposal (2015-2019), <http://www.modern2020.eu/>
 - BEACON – Bentonite Mechanical Evolution (2017-2021), <http://www.beacon-h2020.eu/>
 - EURAD: European Joint Programme on Radioactive Waste Management (2019-2023), <https://www.ejp-eurad.eu/>



CONCLUSIONS

- The Finnish final disposal of nuclear spent fuel is based on a system of multi-barriers, both natural and engineered
- Design, development, manufacturing and monitoring of the barriers is a successful approach which is based on scientific research, decision making, regulatory and implementer needs
- Technologies for a successful disposal exist and can often be transferred from other industries, like mining and construction. However, they need to be adapted and modified due to the long time scale and the high safety requirements
- Nuclear waste management in Finland is built on trust and transparency, which is a continuous process of communication between all stakeholders



CONTACTS



THANK YOU!

- Dr. Edgar Bohner
- Principal Scientist, Research Team Leader
- VTT Technical Research Centre of Finland Ltd
 - Email: edgar.bohner@vtt.fi
 - Cell: +358 40 196 9081
 - www.vtt.fi

- Johanna Hansen
- EU DOPAS Coordinator
 - Posiva Oy
- Email: Johanna.Hansen@Posiva.fi
- Cell: +358 50 532 0551
- www.posiva.fi

- Pasi Rantamäki
- FISST Project Manager
 - Posiva Oy
- Email: Pasi.Rantamaki@Posiva.fi
- Cell: +358 50 581 3613
- www.posiva.fi

